19 November 2010 | $10

Science

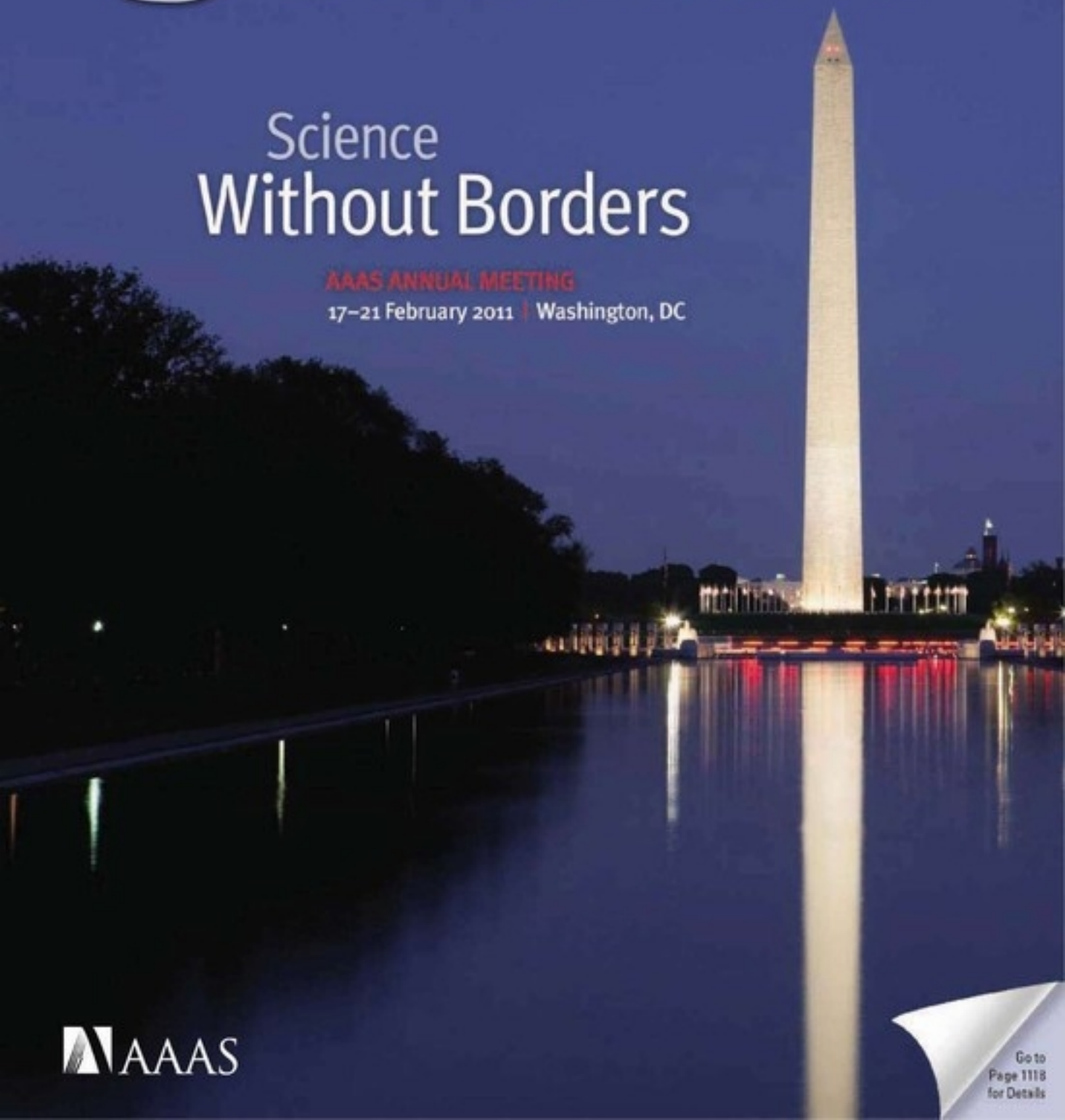

Science Without Borders

AAAS ANNUAL MEETING

17–21 February 2011 | Washington, DC

AAAS

Go to Page 1118 for Details

EDITORIAL

1021 A New Focus on Plant Sciences
Steven J. McCormick and Robert Tjian

NEWS OF THE WEEK

1028 Massive Cost Overrun to Webb Threatens Other NASA Missions
1029 Key Indicator of Ocean Health May Be Flawed
1030 GM Mosquito Trial Alarms Opponents, Strains Ties in Gates-Funded Project
1031 From *Science*'s Online Daily News Site
1032 Handful of U.S. Schools Claim Larger Share of Output
1033 New Spin on Solid Helium Bolsters Case for Bizarre Flow
>> Science *Express Report by H. Choi* et al.
1033 From the *Science* Policy Blog
1034 A World of Changes Prepares Subra Suresh to Tackle Change at NSF

NEWS FOCUS

1036 SCIENCE IN RUSSIA
Russian Science: Waking From Hibernation
University Research Should Compete With Russian Academy, Science Minister Argues
Uncertain Future for Academy's Biology Experiment
>> Science *Podcast*

LETTERS

1044 Time to Take Action on Climate Communication
T. E. Bowman et al.
Overbuilding: Doctoral Degree Surplus
R. L. Juliano
Overbuilding: Under Pressure
K. G. Mann
Overbuilding: Overhead Revisions
M. Wabl
Overbuilding: Boosting School Ratings
R. D. Burk
1047 CORRECTIONS AND CLARIFICATIONS
1047 TECHNICAL COMMENT ABSTRACTS

BOOKS *ET AL.*

1048 Biology's First Law
D. W. McShea and R. N. Brandon, reviewed by R. L. Millstein
1049 From Populations to Ecosystems
M. Loreau, reviewed by T. Fukami

POLICY FORUM

1052 Genetically Modified Salmon and Full Impact Assessment
M. D. Smith et al.

PERSPECTIVES

1054 Nanosilver Revisited Downstream
B. Nowack
1055 γ-Secretase and Human Disease
R. J. Kelleher III and J. Shen
>> *Brevia p. 1065*
1056 Magnetic Resonance and Microfluidics
M. Utz and J. Landers
>> *Report p. 1078*
1058 Topping Off a Multiscale Balancing Act
J. Lerman and B. O. Palsson
>> *Report p. 1099*
1059 π = Visual Cortex
K. D. Miller
>> *Report p. 1113*

REVIEW

1061 Plant and Animal Sensors of Conserved Microbial Signatures
P. C. Ronald and B. Beutler

CONTENTS continued >>

page 1036

page 1049

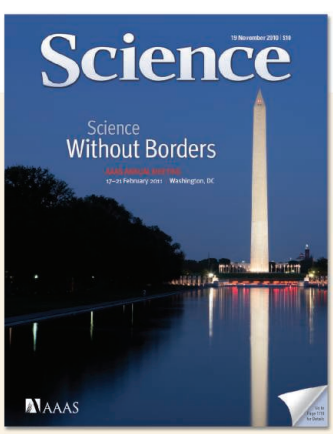

COVER

View of the Washington Monument in Washington, DC, site of the AAAS Annual Meeting, 17 to 21 February 2011. The meeting's theme—*Science Without Borders*—integrates the practice of science, in both research and teaching, which uses multidisciplinary approaches to problem-solving, crosses conventional borders, and takes into consideration the diversity of investigators and students. The preliminary program begins on page 1118.

Photo: iStockphoto.com/Sportstock

DEPARTMENTS

1019 This Week in *Science*
1022 Editors' Choice
1024 *Science* Staff
1027 Random Samples
1117 New Products
1118 AAAS Meeting Program
1128 *Science* Careers

Published by AAAS

BREVIA

1065 γ-Secretase Gene Mutations in Familial Acne Inversa
B. Wang et al.
Mutations causing a rare skin disease reveal a signaling pathway that is a drug target for Alzheimer's disease.
>> *Perspective p. 1055*

RESEARCH ARTICLE

1066 Structures of the CXCR4 Chemokine GPCR with Small-Molecule and Cyclic Peptide Antagonists
B. Wu et al.
Five crystal structures provide insight into chemokine and HIV-1 recognition.

REPORTS

1072 The Uncertainty Principle Determines the Nonlocality of Quantum Mechanics
J. Oppenheim and S. Wehner
The two central elements of quantum theory, once assumed to be distinct concepts, are shown to be linked.
>> Science *Podcast*

1075 Faster Interprotein Electron Transfer in a [Myoglobin, b_5] Complex with a Redesigned Interface
P. Xiong et al.
Faster electron transfer in a redesigned protein complex provides insights into the role of conformational distributions.

1078 Zooming In on Microscopic Flow by Remotely Detected MRI
V. S. Bajaj et al.
A magnetic resonance imaging system allows finer analysis of fluid flow.
>> *Perspective p. 1056*

1081 Probing the Ultimate Limit of Fiber-Optic Strain Sensing
G. Gagliardi et al.
The precisely spaced teeth of an optical frequency comb can be used as a highly accurate strain gauge.

1084 Loss of Carbon from the Deep Sea Since the Last Glacial Maximum
J. Yu et al.
Carbon loss from the ocean to the atmosphere and terrestrial biosphere occurred at different rates in the last deglaciation.

1088 Glacial Silicic Acid Concentrations in the Southern Ocean
M. J. Ellwood et al.
Silicon isotope distributions in sponges contain the signature of ocean nutrient distributions during the last glacial period.

1091 Structure of the Human Dopamine D3 Receptor in Complex with a D2/D3 Selective Antagonist
E. Y. T. Chien et al.
Discovery of a binding site in the extracellular domain of a dopamine receptor offers hope for more selective therapeutics.

1095 Mcl-1 Is Essential for Germinal Center Formation and B Cell Memory
I. Vikstrom et al.
A protein that inhibits apoptosis is essential for the survival of immune memory cells.

1099 Interdependence of Cell Growth and Gene Expression: Origins and Consequences
M. Scott et al.
Simple mathematical models describe the relationship between bacterial replication, cellular resources, and protein expression.
>> *Perspective p. 1058*

1102 Symbiotic Bacterium Modifies Aphid Body Color
T. Tsuchida et al.
Infection with a symbiotic bacterium leads to a spectacular phenotypic change in its host, making red aphids turn green.

1104 *PiggyBac* Transposon Mutagenesis: A Tool for Cancer Gene Discovery in Mice
R. Rad et al.
Mutations induced by a transposable element in mice can be used to identify cancer-causing genes.

1108 Calcium-Permeable AMPA Receptor Dynamics Mediate Fear Memory Erasure
R. L. Clem and R. L. Huganir
The subunit composition of AMPA receptors at lateral amygdala synapses changes after the acquisition of associative fear.

1113 Universality in the Evolution of Orientation Columns in the Visual Cortex
M. Kaschube et al.
Analysis of evolutionarily divergent species highlights constraint on brain structure imposed by self-organizing neural networks.
>> *Perspective p. 1059*

CONTENTS continued >>

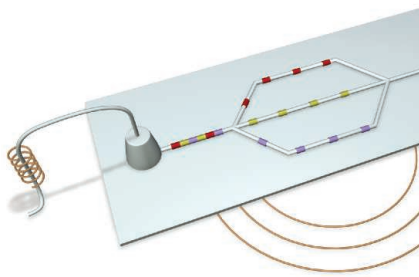

pages 1056 & 1078

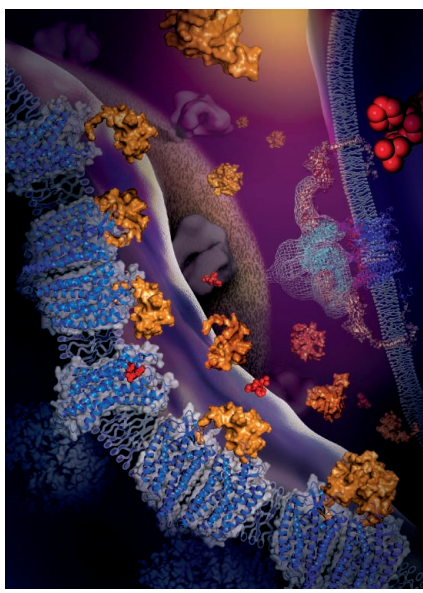

page 1066

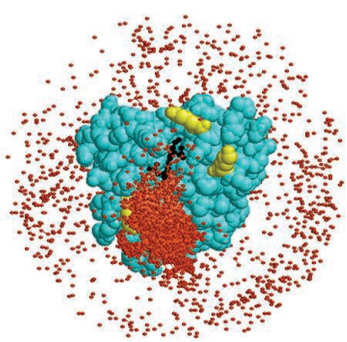

page 1075

CREDIT (MIDDLE IMAGE): YEKATERINA KADYSHEVSKAYA/STEVENS LABORATORY/THE SCRIPPS RESEARCH INSTITUTE

SCIENCEONLINE

SCIENCEXPRESS
www.sciencexpress.org

A Giant Planet Around a Metal-Poor Star of Extragalactic Origin
J. Setiawan et al.
A planet is observed to orbit a star whose properties are different from those of all other known planet-hosting stars.
10.1126/science.1193342

Evidence of Supersolidity in Rotating Solid Helium
H. Choi et al.
Measurements on rotating frozen helium support the formation of a quantum, or supersolid, phase.
10.1126/science.1196409
>> *News story p. 1033*

Plasticity of Animal Genome Architecture Unmasked by Rapid Evolution of a Pelagic Tunicate
F. Denoeud et al.
A metazoan genome departs from the organization that appears rigidly established in other animal phyla.
10.1126/science.1194167
>> Science *Podcast*

Glucose and Weight Control in Mice with a Designed Ghrelin O-Acyltransferase Inhibitor
B. P. Barnett et al.
A drug inhibiting the activation of ghrelin, a peptide that promotes weight gain, has beneficial metabolic effects in mice.
10.1126/science.1196154

Arabidopsis Type I Metacaspases Control Cell Death
N. S. Coll et al.
An ancient link between cell death control and innate immune receptor function has been discovered in plants.
10.1126/science.1194980

TECHNICALCOMMENTS

Comment on "Single-Crystal X-ray Structure of 1,3-Dimethylcyclobutadiene by Confinement in a Crystalline Matrix"
D. Scheschkewitz
Full text at www.sciencemag.org/cgi/content/full/330/6007/1047-c

Comment on "Single-Crystal X-ray Structure of 1,3-Dimethylcyclobutadiene by Confinement in a Crystalline Matrix"
I. V. Alabugin et al.
Full text at www.sciencemag.org/cgi/content/full/330/6007/1047-d

Response to Comments on "Single-Crystal X-ray Structure of 1,3-Dimethylcyclobutadiene by Confinement in a Crystalline Matrix"
Y.-M. Legrand et al.
Full text at www.sciencemag.org/cgi/content/full/330/6007/1047-e

SCIENCENOW
www.sciencenow.org
Highlights From Our Daily News Coverage

Can Google Predict the Stock Market?
New analysis shows a connection between search terms and stock market activity.

Large Size Didn't Keep Pterosaurs Grounded
Group argues that ancient reptiles flew just fine, despite their massive weight.

Neandertal Children Developed on the Fast Track
Tooth analysis suggests that our close cousins matured faster than we did.

SCIENCESIGNALING
www.sciencesignaling.org
The Signal Transduction Knowledge Environment

RESEARCH ARTICLE: Solution of the Structure of the TNF-TNFR2 Complex
Y. Mukai et al.
Structural differences in the binding of tumor necrosis factor to its two receptors may aid in the development of receptor-specific therapeutics.

RESEARCH ARTICLE: Activation of STIM1-Orai1 Involves an Intramolecular Switching Mechanism
M. K. Korzeniowski et al.

PERSPECTIVE: Calcium Signaling by STIM and Orai—Intimate Coupling Details Revealed
Y. Wang et al.
An intramolecular interaction within the protein STIM1 prevents untimely refilling of intracellular calcium stores.

PERSPECTIVE: Frizzled Signaling—Gα_o and Rab5 at the Crossroads of the Canonical and PCP Pathways?
D. Strutt and J.-P. Vincent
Rab5, a key effector of endocytosis, binds to Frizzled proteins and modulates their trafficking and signaling.

SCIENCECAREERS
www.sciencecareers.org/career_magazine
Free Career Resources for Scientists

SPECIAL SERIES ON RESEARCH INTEGRITY
Responsible Conduct of Research for Junior Researchers
E. Pain
In science, you have to be careful to be ethical.

Tooling Up: On Interview Day
D. Jensen
With the right attitude and actions, you can rise to the top on interview day.

SCIENCETRANSLATIONAL MEDICINE
www.sciencetranslationalmedicine.org
Integrating Medicine and Science

PERSPECTIVE: News from the Brain—The GPR124 Orphan Receptor Directs Brain-Specific Angiogenesis
E. Dejana and D. Nyqvist
A G protein–coupled receptor may represent a new therapeutic target for vascular pathologies in the central nervous system.

RESEARCH ARTICLE: Identification of Hematopoietic Stem Cell–Specific miRNAs Enables Gene Therapy of Globoid Cell Leukodystrophy
B. Gentner et al.
Hematopoietic stem cell–specific microRNAs regulate transgene expression in mice with a lysosomal storage disorder.

RESEARCH ARTICLE: Femtosecond Laser–Assisted Cataract Surgery with Integrated Optical Coherence Tomography
D. V. Palanker et al.
An image-guided, femtosecond laser creates accurate cuts in the eye to improve cataract surgery.

SCIENCEPODCAST
www.sciencemag.org/multimedia/podcast
Free Weekly Show

Download the 19 November *Science* Podcast to hear about science in Russia, animal genome plasticity, linking uncertainty with nonlocality in quantum mechanics, and more.

SCIENCEINSIDER
news.sciencemag.org/scienceinsider
Science Policy News and Analysis

SCIENCE (ISSN 0036-8075) is published weekly on Friday, except the last week in December, by the American Association for the Advancement of Science, 1200 New York Avenue, NW, Washington, DC 20005. Periodicals Mail postage (publication No. 484460) paid at Washington, DC, and additional mailing offices. The title SCIENCE is a registered trademark of the AAAS. Domestic individual membership and subscription (51 issues): $146 ($74 allocated to subscription). Domestic institutional subscription (51 issues): $910; Foreign postage extra: Mexico, Caribbean (surface mail) $55; other countries (air assist delivery) $85. First class, airmail, student, and emeritus rates on request. Canadian rates with GST available upon request, GST #1254 88122. Publications Mail Agreement Number 1069624. **Printed in the U.S.A.**

Change of address: Allow 4 weeks, giving old and new addresses and 8-digit account number. **Postmaster:** Send change of address to AAAS, P.O. Box 96178, Washington, DC 20090–6178. **Single-copy sales:** $10.00 current issue, $15.00 back issue prepaid includes surface postage; bulk rates on request. The identification code for *Science* is 0036-8075. *Science* is indexed in the *Reader's Guide to Periodical Literature* and in several specialized indexes.

AAAS
ADVANCING SCIENCE, SERVING SOCIETY

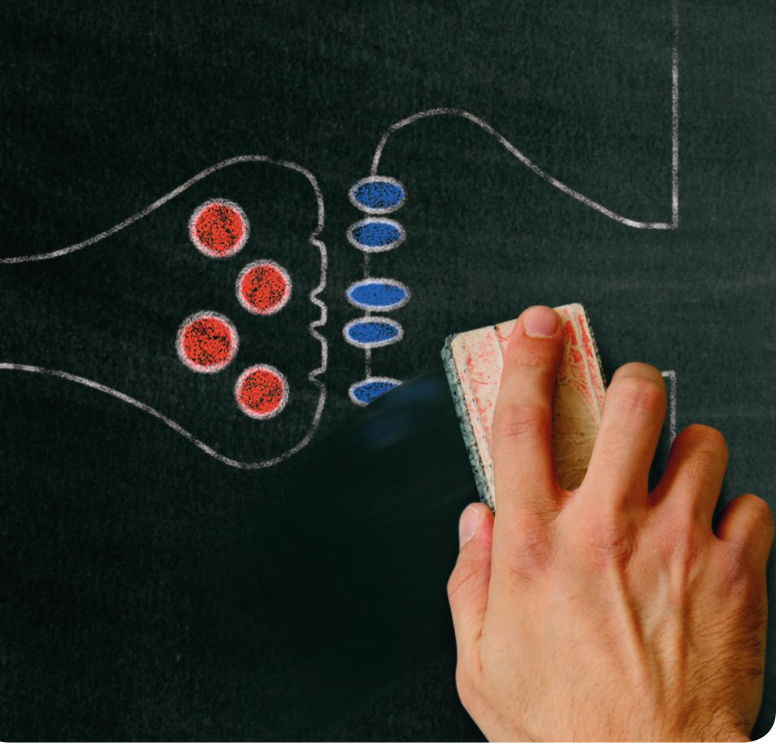

<< Wiping Out Memories

Inhibition of fear responses can be unexpectedly reversed even when a subject is perfectly safe. This can lead to inappropriate reactions to a fear-associated trigger, such as a bright light or loud noise. This type of reaction appears to underpin posttraumatic stress disorder, but there is little understanding of when training to inhibit fear may fail or succeed. Using a combination of electrophysiology and behavioral training in mice, **Clem and Huganir** (p. 1108, published online 28 October) observed that fear conditioning increased synaptic transmission by calcium-permeable AMPA receptors into the part of the brain that controls emotional responses (the amygdala). This effect lasted for about a week, during which the fearful memories could be erased if the animals were trained to reduce conditioned fear responses. Postmortem brain slices showed that the fear-induced synaptic changes also reversed, except in transgenic mice with a mutant subunit of the AMPA receptor.

Regulating Migration

The migration of cells around the body is an important factor in cancer development and the establishment of infection. Movement is induced by small proteins called chemokines, and so for a specific function, migration is controlled by a relevant chemokine binding to its respective receptor. This family of receptors is known as guanine (G) protein–coupled receptors, which span cell membranes to mediate between external signals from chemokines and internal mechanisms. The chemokine receptor CXCR4 is implicated in many types of cancer and in infection, and **Wu *et al.*** (p. 1066, published online 7 October; see the Report by **Chien *et al.***) report on a series of crystal structures obtained for CXCR4 bound to small molecules. In every case, the same homodimer structure was observed, suggesting that the interface is functionally relevant. These structures offer insights into the interactions between CXCR4 and its natural chemokine, as well as with the virus HIV-1.

Moving Carbon

During the last glacial maximum, approximately 23,000 years ago, both the atmosphere and the terrestrial biosphere contained much less carbon than in the immediately preindustrial era. The carbon must have been stored in the deep ocean, and the transfer of carbon to the air and land during deglaciation must have affected the carbonate chemistry and carbon isotopic composition of the sea. **Yu *et al.*** (p. 1084) estimated how deep-water carbonate concentrations changed over the course of the last deglaciation and combined their results with $^{13}C/^{12}C$ data to show that carbon released by the deep ocean between 17.5 and 14.5 thousand years ago mostly stayed in the atmosphere as CO_2, while between 14 and 10 thousand years ago, a substantial fraction was absorbed by the terrestrial biosphere.

Quantum Connection

A system that is quantum mechanically entangled with another distant system can be predicted by measuring the distant system. This form of "action-at-a-distance," or nonlocality, seemingly contradicts Heisenberg's uncertainty principle, which is one of the fundamental aspects of quantum mechanics. **Oppenheim and Wehner** (p. 1072) show that the degree of nonlocality in quantum mechanics is actually determined by the uncertainty principle. The unexpected connection between nonlocality and uncertainty holds true for other physical theories besides quantum mechanics.

Finely Tracking Flow

Magnetic resonance imaging (MRI) is in principle well-suited for tracking flow dynamics in microfluidic channels. However, multiple channels tend to be arrayed on much larger substrates, and MRI coils large enough to enclose the whole assembly do not have the sensitivity required to resolve an intimate picture of any one channel. **Bajaj *et al.*** (p. 1078, published online 7 October; see the Perspective by **Utz and Landers**) present an imaging protocol in which the spins of the fluid molecules in a microfluidic chip are first tagged by a conventionally sized coil and then analyzed downstream using a more sensitive and smaller coil through which the fluid flows incrementally after leaving the microfluidic device.

Enhanced Strain Sensitivity

The ability to measure tiny deformations in length is useful for many disciplines, from large-scale structural engineering to DNA analysis with optical tweezers. The most sensitive strain sensors are those using optical interferometers, which can detect small changes at the scale of visible wavelengths. Using an optical frequency comb to stabilize the output of a diode laser, and as a highly accurate ruler to determine small changes in length of an optic fiber sensor, **Gagliardi *et al.*** (p. 1081, published online 28 October) showed that sensitivity can be enhanced by several orders of magnitude. Such combined technology should provide for a new generation of high-performance sensors.

Silicon Leakage

Silicon is a major structural component of many marine organisms, whose chemistry is affected by oceanic nutrient distributions. To constrain nutrient changes since the last glacial period, **Ellwood *et al.*** (p. 1088, published online 21 October) measured the isotopic compositions of silicon obtained from the skeletons of deep-sea sponges found in deep cores from the Atlantic and Pacific sectors of the Southern Ocean and compared them to the silicon signatures in the skeletons of modern

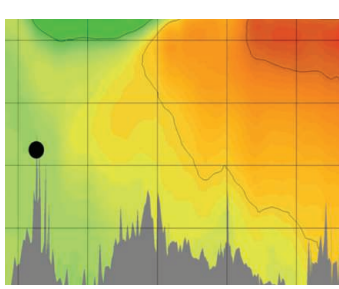

Continued on page 1020

CREDITS (TOP TO BOTTOM): CHRIS FUCCI/REAL CREATIVE ADVERTISING; ELLWOOD *ET AL.*

Continued from page 1019

sponges. The results indicate that nutrient redistribution, related to iron fertilization from dust deposition, boosted the growth of organisms that transferred silicon to mid-latitudes during the last glacial period.

Tweaking Dopamine Reception

Dopamine modulates many cognitive and emotional functions of the human brain by activating G protein–coupled receptors. Antipsychotic drugs that block two of the receptor subtypes are used to treat schizophrenia but have multiple side effects. **Chien *et al.*** (p. 1091; see the Research Article by **Wu *et al.***) resolved the crystal structure of one receptor in complex with a small-molecule inhibitor at 3.15 angstrom resolution. Homology modeling with other receptor subtypes might be a promising route to reveal potential structural differences that can be exploited in the design of selective therapeutic inhibitors having fewer side effects.

Germinal Center Survival

The humoral immune response, which comprises antibodies secreted by B lymphocytes, is critical for protection against pathogens. In response to infection, B lymphocytes proliferate and differentiate into antibody-producing effector cells. After an infection clears, a small number of cells persist as memory B cells; however, the survival signals that regulate effector and memory B lymphocyte generation are not well understood. To probe this question, **Vikstrom *et al***. (p. 1095, published online 7 October) deleted prosurvival genes in activated, antigen-specific B cells during a T lymphocyte–dependent immune response in mice. They found that a specific programmed cell death inhibitor, known as Mcl1, was required for the formation of germinal-center B cells (an effector cell population) and memory B cells but not for their maintenance. Dysregulation of the B cell responses mediated by Mcl1 may be a trigger for lymphomagenesis.

Turncoat Aphids

Aphid color has consequences for the fate of the wearer: Coccinellid beetles prefer to eat red ones and parasitoid wasps attack green ones. What might happen if aphids could change color and outwit their predators? **Tsuchida *et al.*** (p. 1102) have found that a subpopulation of the pea aphid can do this, but not without help from a previously unknown species of bacterium that lives intimately with the aphid as an endosymbiont and makes red aphids turn green. The bacterium interferes with host pigment biosynthesis—itself borrowed from fungi long ago in evolution—to stimulate blue-green pigment production as the aphid larva matures, turning the red nymph into a green adult. The ecological consequences of this about-turn of color have yet to be tested, but other studies have shown a variety of effects on aphid behavior mediated by endosymbionts in response to adaptation to different food plants, temperature tolerance, and predator avoidance.

Piggybacking on Cancer Genes

Transposons are mobile segments of DNA that can insert in or near important genes to cause mutations that disrupt gene function. **Rad *et al.*** (p. 1104, published online 14 October) adapted a mutagenic transposon called Piggybac, originally derived from a moth, into a tool for discovery of cancer-causing genes in mice. Mobilization of Piggybac in mice was associated with the development of leukemias and solid tumors. In many instances the causative mutations, which were identified by mapping the Piggybac integration sites, were within genes not previously implicated in cancer.

Orientation Columns

In the brain's visual cortex, certain neurons respond to vertical lines and others to horizontal lines, with a range in between. Such orientation of neurons tends to be organized in columns reflecting similar responses, and the columns are organized in pinwheels representing the range of responses. **Kaschube *et al*.** (p. 1113, published online 4 November; see the Perspective by **Miller**) looked at the organization of orientation columns in diverse placental mammals and discovered a similarity of organizational principles.

CREDIT: RYUICHI KOGA

Steven J. McCormick is president and a trustee of the Gordon and Betty Moore Foundation, Palo Alto, CA.

Robert Tjian is president of the Howard Hughes Medical Institute, Chevy Chase, MD.

A New Focus on Plant Sciences

PLANTS ARE ESSENTIAL TO THE SURVIVAL OF OUR PLANET—TO ITS ECOLOGY, BIODIVERSITY, and climate. They maintain human health by providing the basis for nutrition, shelter, clothing, and energy. The study of plants has yielded fundamental insights that have reshaped our understanding of the world and has enabled major human needs to be addressed. But the world population is expected to increase from six billion to nine billion people by the year 2050, challenging humanity to develop more efficient ways to harness plants for meeting growing global needs. Vigorous high-quality scientific research in the plant sciences will be crucial for the world's future. Yet basic plant science research has struggled to take root in the United States. For more than a decade, agricultural research writ large has received only 2% of total federal spending on R&D. Federal support for fundamental plant science research has been even less: The amount awarded on a competitive basis to academic and research institutions constitutes only about 2% of extramural spending for life sciences research ($382 million out of $17 billion in 2005).

Why is plant science not a federal research priority? For one thing, the United States has benefited from robust private-sector investment focused on crop plants, with the Monsanto Company alone investing $1.098 billion in R&D in 2009. The U.S. Department of Agriculture (USDA), with its broad mandate for applied research that emphasizes crops and animals, has only a modest program of plant research grants. Other USDA research funds are directed to agricultural experiment stations at state land-grant universities, which tend to deal with more local agricultural problems.

The Biology Directorate within the U.S. National Science Foundation funds broad areas of research outside the biomedical sciences but currently has no programs dedicated to fundamental plant biology. The National Institutes of Health, which funds the vast majority of life sciences research in the United States, has for the most part viewed plant science as the responsibility of other agencies, despite the fact that corn (maize) and thale cress (*Arabidopsis thaliana*) are excellent model organisms for basic biomedical research. Indeed, many fundamental biological processes that regulate human physiology have been clarified by studying analogous processes in plants. For example, it was basic plant biology research that revealed how small regulatory RNA molecules can ratchet up or dial down gene activity in response to different environments.

But there are some signs that U.S. plant science may receive more emphasis in the decade ahead. An outstanding plant scientist, Roger Beachy, now serves as director of the National Institute of Food and Agriculture, a new organization that will provide competitively awarded research grants. The 2009 U.S. National Academies report *A New Biology for the 21st Century* has called explicit attention to the role that fundamental plant science must play to address major societal challenges. And our two nongovernmental organizations—the Howard Hughes Medical Institute and the Gordon and Betty Moore Foundation—have recently taken steps to encourage this shift in national priorities. We are holding a competition to identify 15 outstanding plant scientists at institutions across the United States who will receive 5-year awards based solely on individual scientific excellence. These scientists are expected to have an outsized impact in many fields of basic plant biology and to span a broad spectrum of disciplines.

The United Kingdom, France, Germany, Brazil, India, and China are countries that have or are making serious research commitments that balance the needs of applied and basic plant sciences research. The United States should be among them. We have created this new effort to serve as a clarion call to the private, nonprofit, and government sectors at a time of great challenge, for both our nation and our planet. **– Steven J. McCormick and Robert Tjian**

10.1126/science.1198153

Published by AAAS

EDITED BY KRISTEN MUELLER AND JAKE YESTON

ASTRONOMY

Merging in the Dust

Gas-rich and intensely luminous, distant submillimeter galaxies (so termed for their emission wavelength, not their spatial extent) form stars at very high rates. It has been suggested that interactions between the galaxies power the emission, but most studies so far have been marred by the presence of dust, which can obscure or produce misleading signs of interaction. To circumvent this problem, Engel *et al.* analyzed high-resolution observations of CO emission lines from 12 submillimeter galaxies, 4 of which were newly observed. The CO lines trace the molecular gas that fuels star formation, and their observation is not affected by the presence of dust. Of the 12 galaxies analyzed, 5 were double systems, consisting of two galaxies engaged in the early stages of interaction; the remaining 7 either showed signs of being at an intermediate stage of merging or were compact galaxies, plausibly the end result of two galaxies coalescing into one. These results indicate that most submillimeter galaxies, if not all, are the product of interactions and mergers of galaxies. — MJC

Astrophys. J. **724**, 233 (2010).

BIOPHYSICS

Spiral Enhancement

When light strikes tiny metal particles, it can excite electrons at their surfaces along a pathway termed a plasmon resonance. Recently this phenomenon has been put to use to enhance Raman scattering by molecules in the vicinity of the particles, often by a factor of a billion or more. Hendry *et al.* explore a distinct application of plasmon excitation, in which they assemble mirror-image arrays of gold particles that possess a spiral sort of two-dimensional chirality, and as a result interact differently with left and right circularly polarized light. They then deposit chiral proteins onto the surfaces and examine the associated perturbations to circularly polarized plasmon excitation of left- versus right-handed particles (validated by control experiments with achiral particles of similar size and shape). They find that proteins with β-sheet motifs induce significantly greater shifts to one array's resonances over its counterpart's, whereas those with α helices induce little dissymmetry. Moreover, the effective refractive index shifts extracted from the β-sheet measurements are roughly a millionfold higher than those associated with differential circularly polarized light scattering by the biomolecules in solution. Though the detailed mechanism underlying the effect remains under study, the authors posit that quadrupolar interactions between the proteins and chiral optical fields at the surface play a key role. — JSY

Nat. Nanotechnol. **5**, 10.1038/NNANO.2010.209 (2010).

PHARMACOLOGY

Switching Drugs

Despite the long list of side effects that accompany many medications, most people still take their medicine. Perhaps this is because we know there is so much variation in drug effectiveness and side effects among individuals that we hope we will experience the benefits of the drug and be spared the side effects. Although such variation is well known, why is it so? Morris *et al*. sought to answer this question by comparing the spatial expression pattern of genes encoding 49 common drug targets found in the brain, in several inbred strains of mice. Many of the genes examined encode neuropsychiatric drug targets. Over 15,000 brain sections representing 203 regions of the brain were analyzed. Differences between strains occurred largely at the level of specific cell classes; for example, among neuronal subsets. Over half of the targets showed some type of interstrain variation in which brain structures they were expressed. When expression was examined across strains, strains that were more closely related showed more similar expression patterns. Gene expression in areas of the brain involved in autonomic functions, such as the hypothalamus, brainstem, and medulla, was very conserved. In contrast, the forebrain region, cortex, and hippocampus, which are involved in cognition, learning, and memory, showed the greatest interstrain expression variation. Whether such variation in gene expression also occurs in humans, and whether it influences the variation seen in the therapeutic effectiveness of drugs, still needs to be examined. — BAP

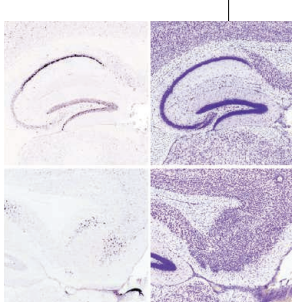

CREDITS (TOP TO BOTTOM): NASA/CXC/M.WEISS; MORRIS *ET AL., PROC. NATL. ACAD. SCI. U.S.A.* **107**, 19049 (2010)

Proc. Natl. Acad. Sci. U.S.A. **107**, 19049 (2010).

EVOLUTION

Who Needs Sex?

Despite the advantages conferred by mixing one's genes through sexual reproduction, many organisms, including plants, fungi, and animals, reproduce asexually. Asexual species are generally assumed to be evolutionary dead ends, however, because of the lack of genetic recombination and accumu-

Published by AAAS

lation of mutations. As such, they are expected to reach extinction rapidly, which may explain their relative rarity. Stöck *et al*. examined the evolutionary history of the asexual Amazon Molly, a fish thought to have arisen through hybridization of two parental species. Crosses of their putative ancestors failed to recapitulate the asexual phenotype. A survey of nuclear and mitochondrial loci within the asexual lineages showed considerable genetic variation and suggested a monophyletic origin, which indicates that the Amazon Molly originated from a single, or very small number, of founders. These results suggest that asexual fish species may be rare not because of the deleterious effects of asexuality but rather because the genomic conditions under which they can arise are rare. — LMZ

Mol. Ecol. 10.1111/j.1365-294X.2010.04869.x (2010).

PSYCHOLOGY

What's Left Undone Lingers On

Multitasking has a long history in computer operating systems, from the 1960s when programs were executed in batches on mainframes to refinements implemented on personal computers a quarter century ago. Swapping resources from one task to another is easy if they are independent, but doing so efficiently when resources need to be shared is more challenging. Fortunately, computers don't seem to experience the kind of interference described by Masicampo and Baumeister. They demonstrate that humans suffer from a hangover due to unfulfilled goals: When people were primed to strive for honesty as a goal and then required to write about an episode in which they had acted dishonestly, the induced sense of incompleteness negatively affected their ability to solve anagrams, a task that relies on fluid intelligence. Neither the prime alone nor the recounting of the episode sufficed, and people who had been primed but then wrote about someone else's dishonesty were not similarly afflicted. Furthermore, the unfulfilled goal, though detectable with implicit measures of activation, did not rise to the level of reportable or conscious awareness. — GJC

J. Exp. Soc. Psychol. 10.1016/j.jesp.2010.10.011 (2010).

MICROBIOLOGY

Aiding the Enemy

Paradoxically, some microbial infections get a boost from host immune responses. A group of worm parasites called filarial nematodes, which cause river blindness and elephantiasis, adapt their development to maximize reproductive success in response to specialized host immune cells called polynuclear eosinophils. Babayan *et al.* have found that even the most vigorous eosinophil response is rarely completely protective, and in fact seems to invigorate the worms to reproduce earlier in their life cycle with larger numbers of offspring. The problem lies in current strategies for experimental vaccine development, which rely on the same eosinophil responses that send the reproductive signals to the parasite. Hence, seeking to develop an antifilarial vaccine that does not provide sterilizing immunity may not result in public health benefit. — CA

PLoS Biol. **8**, e1000525 (2010).

APPLIED PHYSICS

Blast Assessments

Shrapnel is not the only danger posed by bombs. The exposure of soldiers to blast waves from explosive devices may, like the repeated blows to the head inflicted on boxers in the ring, result in traumatic brain injury that is not always immediately perceptible or diagnosed. As in the case of the punch-drunk boxer, continual exposures of this sort can lead to serious damage in the long term. Cullen *et al.* have devised a simple method based on the blast-induced change in color of a photonic crystal to provide a quantitative measure of blast exposure. The photonic crystal—similar in structure to an opal, with its material disrupted by a periodic array of holes—shimmers with a signature set of colors indicative of its particular periodic structure. The authors lithographically fabricated crystalline strips, which could be attached to helmets and other clothing, from chemically robust resins stable to temperatures as high as 300°C. Exposure to the shockwaves of an explosion distorts the structure and the color of these photonic crystal sensor strips. Calibration of the color change to blast strength can then provide an instant assessment of blast exposure and the subsequent need for precautions or medical intervention that may otherwise be overlooked. — ISO

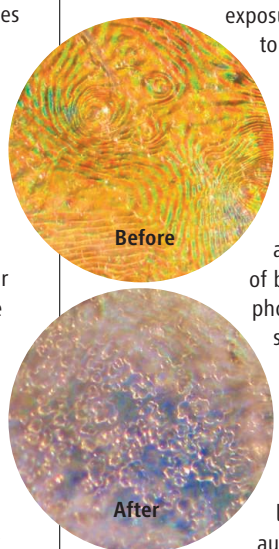

CREDIT: CULLEN *ET AL.*, *NEUROIMAGE* 10.1016/J.NEUROIMAGE.2010.10.076 (2010)

NeuroImage 10.1016/j.neuroimage.2010.10.076 (2010).

Published by AAAS

www.sciencemag.org

Science

1200 New York Avenue, NW
Washington, DC 20005
Editorial: 202-326-6550, FAX 202-289-7562
News: 202-326-6581, FAX 202-371-9227
Bateman House, 82-88 Hills Road
Cambridge, UK CB2 1LQ
+44 (0) 1223 326500, FAX +44 (0) 1223 326501

Subscription Services For change of address, missing issues, new orders and renewals, and payment questions: 866-434-AAAS (2227) or 202-326-6417, FAX 202-842-1065. Mailing addresses: AAAS, P.O. Box 96178, Washington, DC 20090-6178 or AAAS Member Services, 1200 New York Avenue, NW, Washington, DC 20005

Institutional Site Licenses please call 202-326-6755 for any questions or information

Reprints: Author Inquiries 800-635-7181
Commercial Inquiries 803-359-4578

Permissions 202-326-7074, FAX 202-682-0816

Member Benefits AAAS/Barnes&Noble.com bookstore www.aaas.org/bn; AAAS Online Store www.apisource.com/aaas/ code MKB6; AAAS Travels: Betchart Expeditions 800-252-4910; Apple Store www.apple.com/eppstore/aaas; Bank of America MasterCard 1-800-833-6262 priority code FAA3YU; Cold Spring Harbor Laboratory Press Publications www.cshlpress.com/affiliates/aaas.htm; GEICO Auto Insurance www.geico.com/landingpage/go51.htm?logo=17624; Hertz 800-654-2200 CDP#343457; Office Depot https://bsd.officedepot.com/portalLogin.do; Seabury & Smith Life Insurance 800-424-9883; Subaru VIP Program 202-326-6417; VIP Moving Services www.vipmayflower.com/domestic/index.html; Other Benefits: AAAS Member Services 202-326-6417 or www.aaasmember.org.

science_editors@aaas.org	(for general editorial queries)
science_letters@aaas.org	(for queries about letters)
science_reviews@aaas.org	(for returning manuscript reviews)
science_bookrevs@aaas.org	(for book review queries)

Published by the American Association for the Advancement of Science (AAAS), *Science* serves its readers as a forum for the presentation and discussion of important issues related to the advancement of science, including the presentation of minority or conflicting points of view, rather than by publishing only material on which a consensus has been reached. Accordingly, all articles published in *Science*—including editorials, news and comment, and book reviews—are signed and reflect the individual views of the authors and not official points of view adopted by AAAS or the institutions with which the authors are affiliated.

AAAS was founded in 1848 and incorporated in 1874. Its mission is to advance science, engineering, and innovation throughout the world for the benefit of all people. The goals of the association are to: enhance communication among scientists, engineers, and the public; promote and defend the integrity of science and its use; strengthen support for the science and technology enterprise; provide a voice for science on societal issues; promote the responsible use of science in public policy; strengthen and diversify the science and technology workforce; foster education in science and technology for everyone; increase public engagement with science and technology; and advance international cooperation in science.

Information for Authors
See pages 352 and 353 of the 15 January 2010 issue or access www.sciencemag.org/about/authors

Mummies for Medicine

Most med students dissect cadavers, not mummies. Now Swiss researchers plan to use ancient DNA to attack some of the modern world's most pressing medical problems. They're part of a small but growing movement to unravel the mysteries of disease from a surprising new angle: evolution.

Officially launched in late October, the University of Zurich's new Centre for Evolutionary Medicine will investigate both how diseases evolve and how humans become vulnerable to them. Some of their biggest questions involve changes in human anatomy, says the center's director, Frank Rühli, such as whether an increasingly sedentary lifestyle may have weakened spinal columns, causing back pain. They'll also take DNA from ancient remains, such as Egyptian mummies (see photo), to compare genomes of ancient pathogens with those of modern ones—a valuable tool for detecting how fast diseases evolve and how environmental changes can affect them. Knowing how maladies flourish, says Rühli, will give scientists a much better idea of how to combat them.

With 11 researchers in Zurich and some 20 local and international collaborators, Rühli says the center will be larger than any other institute in the burgeoning field. He hopes its clinical—rather than theoretical—approach will help convince skeptics that an evolutionary perspective could have practical value. "We all think that biological evolution has stopped," he says. But when anatomy can change in just a few decades, "that's not true."

CREDITS (TOP TO BOTTOM): P. PRISTER; DEPARTMENT OF BIORESOURCE ENGINEERING/MCGILL UNIVERSITY; INSET: THINKSTOCKPHOTOS.COM; LDA SACHSEN-ANHALT

THEY SAID IT

"Given the swimming pools of booze I've guzzled over the years—not to mention all of the cocaine, morphine, sleeping pills, cough syrup, LSD, Rohypnol… you name it—there's really no plausible medical reason why I should still be alive. Maybe my DNA could say why."

—Rock star Ozzy Osbourne, explaining in a column in *The Sunday Times* why he let a company sequence his genome.

High-Grade Hog

It may be "the other white meat," but to find out which cuts of pork are the juiciest, food scientists are looking at all the colors in the spectrum.

Last week, researchers at McGill University in Montreal, Canada, announced their invention of a machine that uses spectroscopy—the same technique used to examine the molecular makeup of faraway stars and planets—to assess pork quality. The meat's texture, color, and moisture content all affect the wavelengths of light reflecting off its surface. Now the scientists have discovered how to parse that data to quickly assess whether the meat is tender or tough, fatty or lean.

That allows pork producers to market their meat more accurately to the right customers, says lead researcher and bioengineer Michael Ngadi. For instance, Japan likes pigging out on more marbled, fattier meat, whereas Americans usually want leaner meat. Pork spectroscopy can also help regulatory agencies monitor whether pork producers keep their meat as lean as they claim, Ngadi says.

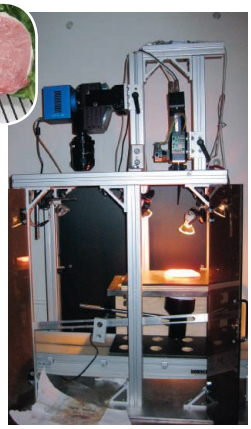

Steve Larsen, director of pork safety at the National Pork Board in Des Moines, says the technique's value lies in its ability to quickly analyze color, texture, and moisture content with only one device. "We don't yet have one machine that does all three," he says.

The researchers are negotiating with several pork producers to develop their technique for industrial use. The technology can be used to analyze other meats, as well as eggs, says Ngadi. "We will be seeing more and more of this technology," he says. "We just happen to be one of its early users."

Europe's First Farmers

Skilled migrants—or perhaps invaders—from what is now Turkey, Syria, Iraq, and surrounding countries ignited the agricultural revolution in Europe some 10,000 years ago, according to a new analysis of DNA from German skeletons up to 7300 years old.

Some scholars previously thought European hunter-gatherers could have learned farming from neighbors in the Near East, where agriculture originated. But 22 skeletons from a graveyard in central Germany tell a different story. Researchers led by Wolfgang Haak of the University of Adelaide in Australia compared DNA sequences of the 22 ancient farmers with those of 55 different modern populations from Europe and countries in the Near East. Their results, published online in *PLoS Biology* on 9 November, suggest not mere technology transfer, but migration. "The lineage of the European farmers stretched back to the Near East," says Haak.

Peter Bellwood of the Australian National University in Canberra, an archaeologist not part of the research team, says the conclusions mirror much of what many archaeologists and linguists already suspect about migrations in the European Neolithic period. And powered by a larger food supply, early agricultural societies worldwide would have experienced population booms that could have fueled expansion. Such rapid growth "was clearly of tremendous significance in underpinning these migrations."

GM mosquito release creates a buzz 1030

NSF's new director 1034

SPACE SCIENCE

Massive Cost Overrun to Webb Threatens Other NASA Missions

A project intended to revolutionize astronomy now threatens to derail NASA's entire space sciences program. An independent panel reported last week that overruns on the James Webb Space Telescope (JWST) could reach $1.7 billion, bringing its total cost to as much as $6.8 billion. NASA officials and the U.S. astronomy community are now scrambling to find a way out of the mess, which could defer the telescope's launch for up to 3 years, to 2017.

The stinging indictment of NASA management practices could not have come at a more awkward moment. Republicans promised last week to scale back government spending when they take over the House of Representatives in January (*Science*, 12 November, p. 896). Congress and the White House remain deadlocked over what to do with the U.S. human space flight program once the last space shuttle is retired sometime next year. And earlier this fall, a National Research Council (NRC) panel laid out an ambitious plan for U.S. astronomy (*Science*, 20 August, p. 894) that may prove a pipe dream given JWST's fiscal woes.

"I'm shocked by how big [the overrun] is," says astrophysicist Roger Blandford of Stanford University in Palo Alto, California, who chaired the NRC committee that produced the Astro2020 report. "And the impact could be severe." The overrun is $700 million more than NASA now spends each year on all astronomy projects. At particular risk is the Wide-Field Infra-Red Survey Telescope (WFIRST), the committee's top priority. This telescope would examine dark energy and exoplanets and conduct galactic surveys. But its fate is now uncertain given the size and scope of JWST's troubles.

Conceived in the late 1990s as a successor to the Hubble Space Telescope, JWST is designed to unfold a 6.5-meter mirror once it arrives at a gravitationally stable point 1.5 million km from Earth. It will beam back images of the earliest stars and galaxies, giving astronomers their first look at the cosmic dawn.

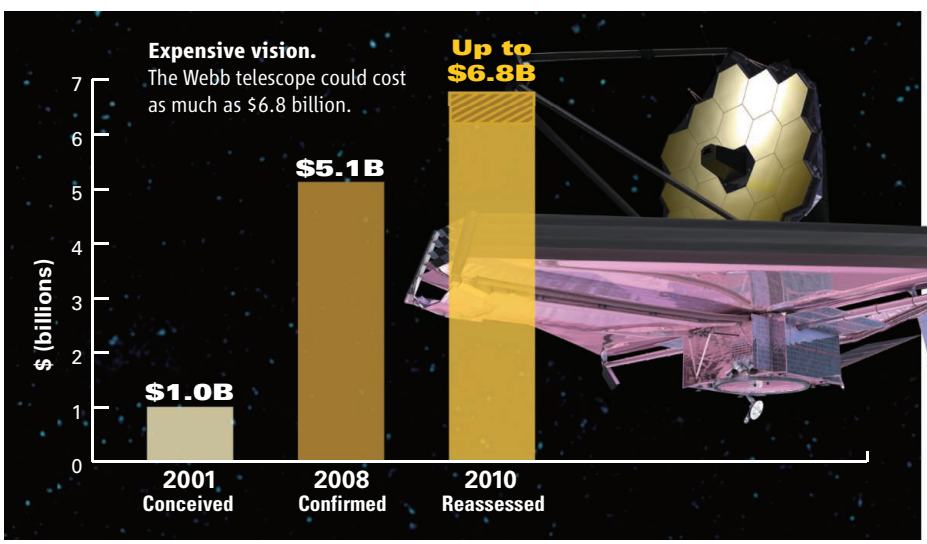

Rising costs are nothing new for NASA projects. But JWST, NASA's most ambitious science project to date, may turn out to be one of its biggest fiscal blunders. In 2001, its estimated price tag was $1 billion. In 2008, NASA confirmed it as a project with a cost of $5.1 billion and a launch date of 2014. This summer, after NASA requested additional funding, Senator Barbara Mikulski (D–MD), chair of a panel that oversees the NASA budget, asked for an independent review.

Led by John Casani of NASA's Jet Propulsion Laboratory in Pasadena, California, the review found that even in the most optimistic scenario, NASA would not be able to launch the telescope until September 2015. And that deadline would require an additional $200 million for the project in each of the fiscal years 2011 and 2012. That would put the total cost somewhere between $6.2 billion and $6.8 billion.

In a teleconference with reporters last week, Casani said NASA officials should shoulder the blame. "The fundamental root cause is that at the time of confirmation of the project [in 2008], the budget that NASA was presented with was basically flawed," he said. It "understated the requirements of the project." And NASA headquarters failed to identify the errors in the budgeting, Casani said.

"We had done a diligent job in assembling the numbers," says John Mather, senior project scientist for JWST at NASA's Goddard Space Flight Center in Greenbelt, Maryland, which developed the project's budget. "But we have to admit that it didn't work out."

Christopher Scolese, NASA's associate administrator, says NASA headquarters "didn't have the people" to perform the crosschecks and analyses that were required to confirm the budget. To avoid more surprises, the agency has agreed to a series of management changes recommended by the Casani panel, including a new program office for JWST at headquarters.

NASA has already spent $3 billion on the telescope, making it unlikely that the project will be canceled. However, congressional staffers and NASA officials say that a full rescue by Congress is equally unlikely. "We have to work with the Administration and Congress to see what flexibilities we do have," says Scolese. But he doubts that "we're going to find $200 million" more in 2011.

That means NASA may have to rethink other projects and consider cuts elsewhere in the science program. One option, which it followed after overruns in the Mars program, would be to merge WFIRST with a dark-energy observatory called Euclid that is on the drawing board of the European Space Agency (ESA). Next June, ESA intends to choose

CREDITS: NASA, CASANI REPORT

Published by AAAS

Special Report:
Slow recovery for Russian science
1036

from among three projects, including Euclid. Roger Bonnet, former ESA science chief and now director of the International Space Science Institute in Bern, says a single cooperative astronomy program between NASA and ESA might make sense. Blandford agrees: "We've got to examine all the options."

However, becoming a junior partner on an ESA mission is not an appealing prospect for U.S. astronomers. "The U.S. has had a strong history of leadership in the burgeoning fields of dark energy and exoplanet studies, and I think it would be a mistake to not continue to be leaders in those areas," says Adam Riess, an astrophysicist at Johns Hopkins University in Baltimore, Maryland.

The Casani report did find JWST to be on solid ground technically, giving astronomers hope that the telescope will eventually make it into space. Heidi Hammel, an astronomer at the Space Science Institute in Boulder, Colorado, notes that Hubble had similar overruns before its 1990 launch. "It proved the absolute workhorse for the broader community," she notes. "JWST is going to be that kind of tool, too." **–ANDREW LAWLER AND YUDHIJIT BHATTACHARJEE**

MARINE ECOLOGY

Key Indicator of Ocean Health May Be Flawed

The most widely used metric of how marine ecosystems are faring worldwide can't be trusted, according to a controversial new analysis of fisheries data. If so, then policymakers could be left without a global picture of whether reforms to fisheries management are working. But not everyone agrees with the conclusion.

The metric is the mean trophic level (MTL) of fish being caught, an indicator based on rank in the food web, which is commonly thought to provide a rough measure of the diversity and integrity of ocean food webs. But in a paper in this week's issue of *Nature*, a team led by Trevor Branch of the University of Washington, Seattle, concludes that the underlying data—seafood reported caught—don't reveal ecosystem health in most cases. "This widely used metric doesn't measure what we think it's measuring," says Branch. The analysis also challenges an influential interpretation of decreasing MTL—and the way fishing affects marine ecosystems.

This interpretation made headlines in 1998, when Daniel Pauly, a marine biologist at the University of British Columbia, Vancouver, and his colleagues highlighted an alarming decrease in MTL of marine species since 1950. They took trophic levels of each species, calculated from what it eats, and then averaged these levels for all species caught worldwide. The team argued that fishing vessels had been sequentially depleting top predators like cod and tuna, then working their way down the food chain, a process that reduces biodiversity and can perturb an ecosystem. This phenomenon, dubbed "fishing down the food web," threw a spotlight on the impact of industrialized fisheries and led to grim predictions of "jellyfish and plankton stew."

The big advantage of catch data is their wide geographic coverage. Fisheries scientists, however, have long pointed out problems with reported catches. The data are murky because they reflect not only what's living in the ecosystem but also the type of fishing gear used and the economics of fishing, for example—factors that can complicate interpretations of the abundance and diversity of fish in the ecosystem.

Branch and his colleagues decided to conduct a comprehensive comparison of catch data with two other sources of data, trawl surveys and stock assessments, which are scientific estimates of abundance within ecosystems. Relying on a recent compilation of surveys and assessments, they calculated trends in global MTL from each. Because catch data yielded a different trend, Branch argues that they aren't a reliable gauge of the state of marine ecosystems worldwide.

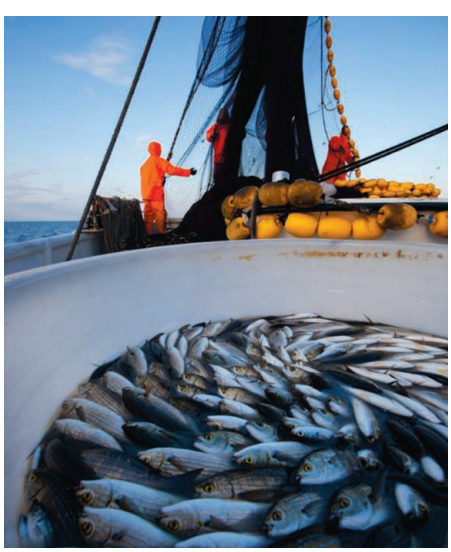

What's the catch? Data collected from fishing vessels may not reveal ecosystem health.

CREDIT: ISTOCKPHOTO.COM

Branch's analysis also suggests that humans may not be fishing down the food web after all. In their analysis of catch data, Branch's group found that all trophic levels—from American oysters to bigeye tuna—are being caught in ever-increasing amounts. Although the catch data don't reveal how ecosystems are faring, Branch says they hint at a more optimistic future—one in which higher-level predators aren't wiped out, even if they and all other parts of the food web are scarcer than before.

Pauly says the Branch team's analysis is misleading. He argues that catch data, when pooled globally, must be corrected for the size of the area being fished, which increased dramatically from 1950 to the 1980s as fleets expanded into the high seas and the Southern Ocean. In addition, the trawl surveys and stock assessments are limited in scope and don't reveal what's going on worldwide. Pauly also points out that large, long-lived predators are particularly vulnerable to overfishing.

Branch maintains his conclusions are valid. He recommends that researchers focus not on MTL from catch data but on trends in abundance from trawl surveys and stock assessments. Joseph Powers of Louisiana State University, Baton Rouge, agrees, but he sees value in keeping an eye on MTL from catch data all the same. "Even with biases," he says, "it's still telling you that things are changing and maybe you need to investigate what's causing those changes." **–ERIK STOKSTAD**

Published by AAAS

SCIENCE AND SOCIETY

GM Mosquito Trial Alarms Opponents, Strains Ties in Gates-Funded Project

For about a decade, scientists have debated how and when to carry out the first test release of transgenic mosquitoes designed to fight human disease—a landmark study they imagined might trigger fierce resistance from opponents of genetic engineering. A stream of papers and reports has argued that a release of any genetically modified (GM) mosquito should be preceded by years of careful groundwork, including an exhaustive public debate to win the hearts and minds of the local population.

But now, it turns out that with little public debate, a company released such mosquitoes a year ago in a fiscal paradise in the Caribbean, where they have been flying under the world's radar screen until last week. At a press conference in London on 11 November, British company Oxitec announced that it carried out the world's first small trial with transgenic *Aedes aegypti* mosquitoes in Grand Cayman in the fall of 2009, followed by a larger study there last summer. Oxitec chief scientist Luke Alphey also presented the unpublished results—which he declared a "complete success"—at a meeting of the American Society of Tropical Medicine and Hygiene in Atlanta a week earlier.

The announcement has taken aback opponents of GM mosquitoes and surprised many researchers in the field of genetic control of insect vectors. And some say that staying mum was a strategic mistake that provides critics with fresh ammunition. "I don't think they did themselves a favor," says Bart Knols, a medical entomologist at the University of Amsterdam in the Netherlands. "This could well trigger a backlash."

"I would completely reject any notion that this was done secretively."

—LUKE ALPHEY, CHIEF SCIENTIFIC OFFICER, OXITEC

Nor does the trial sit well with the collaborators in a big international project, in which Oxitec is a key member, to develop and test GM mosquitoes. The program, funded by a $19.7 million grant from the Bill & Melinda Gates Foundation and led by Anthony James of the University of California, Irvine, has spent years preparing a study site in the Mexican state of Chiapas, where it is testing another strain of Oxitec mosquitoes in cage studies. The project, one of Gates's Grand Challenges in Global Health, would "never" release GM mosquitoes the way Oxitec has now done in Grand Cayman, says James.

Oxitec has received $5 million from the Gates program, but the Grand Cayman trial is not part of that. "As a private company, they can push their own agenda," says James, even though this could possibly hurt the field as a whole. "It's a difficult situation," he says. "I would completely reject any notion that this was done secretively," says Alphey, who notes that the trial was well-known within the island's population of 50,000, "but just not picked up internationally."

Few deny that in the race to develop disease-fighting mosquitoes, Oxitec has an impressive lead. Its key idea, pioneered by Alphey while at the University of Oxford in the 1990s, is to release massive numbers of lab-bred male mosquitoes equipped with a gene that kills any offspring in the larval or pupal stage. When the males mate with females of a natural population, there are no progeny—and if the transgenic males mate more often than the natural ones, the mosquito population will dwindle or even collapse. (And because male mosquitoes don't bite, their release does not increase the risk of disease transmission to humans.)

Oxitec sees a key market in *Ae. aegypti*, the vector for dengue, a painful and sometimes fatal viral infection for which no drugs or vaccines exist. Many middle- and high-income countries already invest heavily in traditional mosquito-control measures to fight dengue, but the results are unimpressive—so an alternative is welcome. Alphey says the first small field study, designed to test whether the males can compete with their natural counterparts, was done on Grand Cayman in November and December of 2009. It was followed by a larger study, between May and October of this year, in which the insects' population-suppressing powers were also gauged. During that period, the team flooded about 16 hectares in the town of East End with transgenic males, about 10 for every naturally occurring wild male. By August, there were about 80% fewer mosquitoes around than in a comparable control area.

For the trial, Oxitec has worked with the Mosquito Research and Control Unit (MRCU) of the Cayman Islands, an overseas territory of the United Kingdom. The trial abided by the rules of the territory's new biosafety bill that has yet to become law, Alphey says. There were no town hall meetings or public debates because the government of the Cayman Islands didn't deem them necessary. But MRCU sent information about the study to local newspapers, Alphey says, and its 50 employees attended a lunch meeting about the project from which information filtered out to the rest of the island as well. MRCU, which could not be reached for comment, also posted a promotional video about the project on YouTube, but the clip does not mention

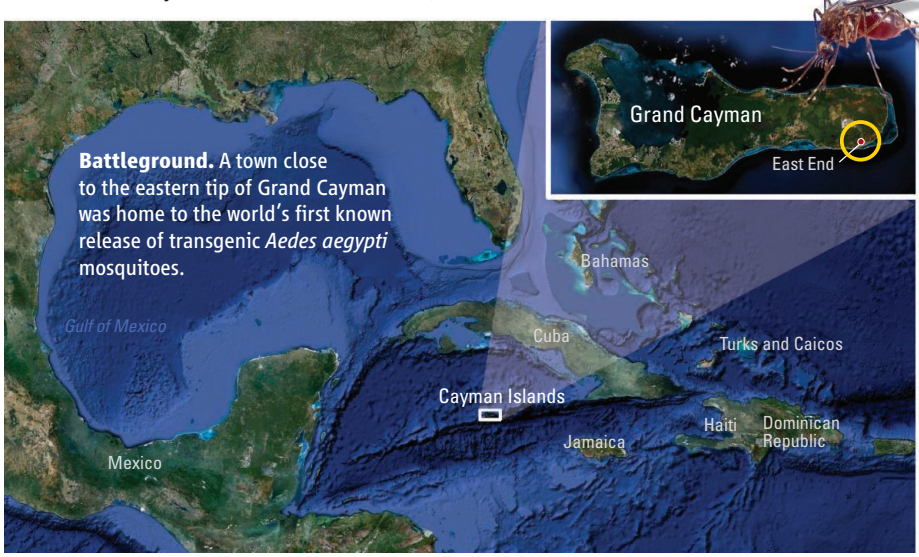

Battleground. A town close to the eastern tip of Grand Cayman was home to the world's first known release of transgenic *Aedes aegypti* mosquitoes.

CREDITS: (TOP) HADYN PARRY/OXITEC LTD.; (BOTTOM, PHOTO) ARS/USDA; GOOGLE MAPS

Published by AAAS

Enjoy your flight. The release of transgenic males led to an 80% reduction in the size of the local population, says Alphey.

that the mosquitoes are transgenic.

That's quite a contrast to the process the Grand Challenges project researchers used to select and prepare a site for a possible future release of Oxitec mosquitoes in Mexico. Currently, the mosquitoes are still being tested in cages, but even for that step the researchers spent years diligently consulting with local citizen groups, academics, regulators, and farmers. "We think that is the most ethical way to introduce a new technology like this," says James Lavery, a bioethicist at St. Michael's Hospital in Toronto, Canada, who works as a consultant for the project.

The World Health Organization (WHO) is still drafting guidelines for the release of transgenic mosquitoes, a process that will take at least three more months, says Yeya Touré, manager of innovative vector control interventions at WHO. Touré says he knew of the trial in Grand Cayman, and that he is not aware of any wrongdoing by Oxitec.

But environmental groups, taken by surprise, are lamenting what they see as a lack of openness. "If these mosquitoes are completely safe, then why the hush-hush?" says Gurmit Singh, chair of the Centre for Environment, Technology and Development in Malaysia, where Oxitec hopes to start a field trial soon as well. James—who also takes issue with Alphey's press conference to announce unpublished results—says it would be "unfortunate" if Oxitec's release in the Caribbean soured the climate for GM mosquitoes in general. Despite their differences, the collaborators are still on speaking terms, he stresses.

Not everybody thinks the release is such a big deal. Oxitec's transgenic mosquitoes are programmed not to have viable offspring, which makes it extremely unlikely that any newly introduced genes would spread, says medical entomologist Willem Takken of Wageningen University in the Netherlands. The company's technology is just a modern version of the so-called sterile insect technique (SIT), he says, in which massive numbers of male insects are sterilized by bombarding them with radiation and then released. Half a century old, SIT has been used safely and with great success against a range of agricultural pests (*Science*, 20 July 2007, p. 312).

Stickier issues arise with different strategies that don't try to reduce natural populations to zero but replace them with new ones unable to transmit disease, says John Marshall of Imperial College London. To achieve that, researchers try to find genes that make insects resistant to infection and make these genes spread through the entire population. That approach, which so far has proved elusive, is fraught with ethical and regulatory problems because its explicit goal is to spread genes far and wide.

Ethics and communication strategy aside, researchers say the results of the trial, if they hold up under peer review, are encouraging. Oxitec's technique offers the promise of an environmentally friendly way to reduce mosquito populations and, thus, to control disease, says Marcelo Jacobs-Lorena of Johns Hopkins University in Baltimore, Maryland. It also has an edge over insecticides because it's hard to see how mosquito populations could develop resistance to suicide genes. He thinks the stealthy trial will have a positive impact on the field: "There's too much caution and too much fear of the unknown. This study may help surmount that."

–MARTIN ENSERINK

CREDITS (TOP TO BOTTOM): ANDY MCKEMEY/OXITEC LTD.; THINKSTOCK.COM

ScienceNOW

From *Science*'s Online Daily News Site

Can Google Predict the Stock Market?

Whoever figures out how to predict the stock market will get rich quick. Unfortunately, the market's ups and downs ultimately depend on the choices of a massive number of people—and you don't know what they're thinking about before they decide to buy or sell a stock. Then again, maybe Google knows. A team of scientists writing in *Philosophical Transactions of the Royal Society A* has shown a strong correlation between queries submitted to the Internet search giant and the weekly fluctuations in stock trading.
http://scim.ag/Google-stocks

Physicists Create Black Hole 'Light' in Lab

Thirty-six years ago, Stephen Hawking, the famed British theoretical physicist, predicted that black holes—from which no light should escape—could, paradoxically, emit light. No one has ever observed this "Hawking radiation," but now, physicists report in *Physical Review Letters* that they've created something very much like it in the lab.
http://scim.ag/hawking-light

Whales Get Sunburns, Too

In these ozone-depleted times, most of us reach for a T-shirt or a bottle of sunscreen to protect us from the sun's ultraviolet radiation. Whales don't have those luxuries—and they're paying the price. In *Proceedings of the Royal Society B*, researchers report numerous cases of sunburned and blistered skin on whales in the wild, sparking concern that the thinned ozone layer may be causing skin cancer in these animals.
http://scim.ag/whales-burn

Read the full postings, comments, and more at **http://news.sciencemag.org/sciencenow**.

Published by AAAS

RESEARCH METRICS

Handful of U.S. Schools Claim Larger Share of Output

Quality attracts quality in academic research. But is that the best way to achieve economic prosperity?

A new analysis of the U.S. research base by Thomson Reuters points to an increasing concentration of academic research. The report, the latest in a series of such assessments of individual countries, examines both the share of scientific papers written by researchers at a particular institution and the impact of those papers, as measured by the average number of citations per publication.

Two dozen universities hold a combined 42% share of the overall U.S. output for the years 2005 to '09, the report finds (see first table). That's up from 31% during the 1981–85 period. That increased concentration has occurred at the same time the size of the overall pie has doubled, to roughly 1.6 million papers. Harvard University tops both lists, with a 4.2 share of that output, and its margin over second-place University of Michigan has widened in the past 30 years. The 61 U.S. members of the Association of American Universities (AAU) claim an outsized 56% share, up eight points.

Similarly, 19 universities received 47% of all citations to U.S. papers for 2005 to '09 (see second table). Papers from the Massachusetts Institute of Technology, which has been ranked first or second during the past 3 decades, have more than twice the impact as the world average. In addition, a handful of universities have maintained their dominance: Only six universities have held one of the top five places in the impact rankings since the 1980s.

PUBLICATION OUTPUT

Total papers 1981–1985	Share U.S. (%) 1981–1985	Institution	Total papers 2005–2009	Share U.S. (%) 2005–2009
469,201	48.5	AAU	905,522	56.1
25,630	2.65	Harvard University	68,146	4.22
13,071	1.35	University of Michigan System	33,084	2.05
10,567	1.09	Johns Hopkins University	31,503	1.95
16,941	1.75	University of California, Los Angeles	31,108	1.93
12,841	1.33	University of Washington System	30,320	1.88
13,366	1.38	Stanford University	28,318	1.75
10,248	1.06	University of California, San Diego	27,265	1.69
15,176	1.57	University of California, Berkeley	27,021	1.67
11,646	1.20	University of Pennsylvania	26,579	1.65
10,691	1.10	Columbia University	26,427	1.64
10,219	1.06	University of Maryland System	25,844	1.60
14,419	1.49	University of Minnesota System	25,497	1.58
13,919	1.44	University of Wisconsin, Madison	24,553	1.52
14,222	1.47	Cornell University	23,483	1.45
10,166	1.05	University of Florida	23,226	1.44
7,483	0.77	University of Pittsburgh	22,457	1.39
9,490	0.98	University of California, Davis	22,362	1.38
7,880	0.81	Duke University	21,954	1.36
8,715	0.90	Penn State University System	21,689	1.34
11,150	1.15	Yale University	21,676	1.34
8,792	0.91	Ohio State University	21,380	1.32
8,889	0.92	University of Colorado System	21,066	1.30
10,027	1.04	University of California, San Francisco	20,691	1.28
11,651	1.20	MIT	20,609	1.28
6,975	0.72	Texas A&M University System	19,432	1.20

CITATION OUTPUT

Institution	1981–85	1993–97	2005–09
MIT	2.14	2.16	2.28
Caltech	2.13	2.02	2.18
Princeton University	2.19	2.07	2.11
University of California, Santa Barbara	1.75	2.28	2.04
Stanford University	2.05	2.08	1.96
Harvard University	1.98	2.14	1.94
University of California, Berkeley	1.79	1.77	1.92
University of Colorado, Boulder	1.67	1.65	1.86
University of Chicago	1.98	1.92	1.85
University of Washington System	1.78	1.76	1.82
University of Pennsylvania	1.62	1.73	1.77
University of California, San Francisco	1.86	1.89	1.76
Johns Hopkins University	1.69	1.85	1.74
Columbia University	1.70	1.83	1.74
University of California, Los Angeles	1.62	1.61	1.74
Northwestern University	1.62	1.69	1.73
Boston University	1.35	1.59	1.71
Yale University	1.91	1.89	1.71
University of Rochester	1.46	1.60	1.71
U.S. UNIVERSITY average	1.37	1.40	1.37

The report also documents the growth by Asian and European nations in overall research productivity. It notes that the 27-member European Union surpassed the United States in 1995 and remains ahead, and that the Asian-Pacific countries did likewise for the first time in 2008 as part of their explosive growth (see first figure). It also finds that U.S. scientists work disproportionately in the health and social sciences when compared with the rest of the world (see second figure).

"In the United States you see a concentration by field, as well as by geography," says Jonathan Adams, co-author of the new report, who quickly adds, "I'm not saying it's a problem." But the report ends with this provocative question: Are the economic challenges facing the United States "best answered by such concentration, or does its response to the challenge of agile knowledge economies elsewhere in the world require an equally innovative response supported by a more pervasive network of U.S. institutions that draw on the talent spread across the 50 states?"

–JEFFREY MERVIS

GLOBAL OUTPUT

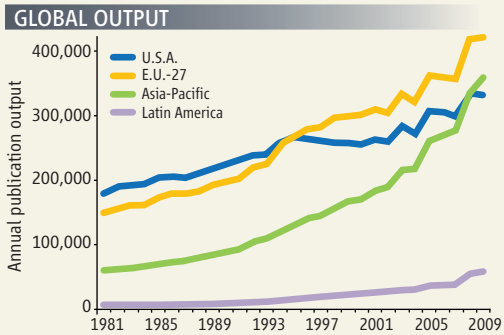

RESEARCH FOOTPRINT®

SOURCE: GLOBAL RESEARCH REPORT, USA © 2010 THOMSON REUTERS

Published by AAAS

CONDENSED-MATTER PHYSICS

New Spin on Solid Helium Bolsters Case for Bizarre Flow

For 6 years, physicists have debated whether solidified helium can flow like the thinnest liquid in a bizarre phenomenon known as "supersolidity." In fact, just 5 months ago one experimenter reported that a softening of the crystalline helium may explain the apparent signs of the strange resistance-free flow. Now, a team from South Korea and Japan reports online in *Science* this week (www.sciencemag.org/cgi/content/abstract/science.1196409) on a new experiment that strongly supports the presence of flow by literally putting a new spin on the original experiment. "If the experiment stands up, … then it's pretty close to a smoking gun" for supersolidity, says John Beamish, a physicist at the University of Alberta in Edmonton, Canada.

The first signs of supersolidity emerged in 2004 in experiments by Moses Chan of Pennsylvania State University, University Park, and Eunseong Kim, now at the Korea Advanced Institute of Science and Technology in Daejeon, South Korea. They fashioned a small can atop a metal shaft and filled it with the isotope helium-4 chilled and pressurized to solidify it. They then set the can twisting back and forth on the shaft.

The frequency of the "torsional oscillator" depended on the amount of mass moving in the can. As the temperature of the helium dipped below 0.2 kelvin, the frequency shot up. That suggested that some helium atoms were letting go of their neighbors and standing still as the rest of the helium moved. To do that, they would have to flow through the helium without resistance. Such "superfluid" flow occurs in liquid helium, and some theorists had speculated it might exist in solid helium, too.

However, similar experiments soon suggested that to flow, a helium crystal must be riddled with defects and imperfections. Other studies revealed that in the same temperature range, solid helium's stiffness changes. And in June in *Physical Review Letters*, John Reppy of Cornell University reported data that suggested that instead of twisting faster at lower temperatures because of flow, an oscillator actually twists slower at higher temperature as the defect-ridden helium softens (*Science*, 2 July, p. 20).

Now, Kim, Kimitoshi Kono of Japan's research institute RIKEN in Wako, and colleagues have performed a torsional oscillator experiment in a specialized refrigerator, or "cryostat," in which they can spin the whole experiment at speeds up to a revolution per second. Working in Kono's lab, they found that as the rate of rotation increased, the shift in the frequency that supposedly tracks the resistance-free flow decreased and eventually vanished.

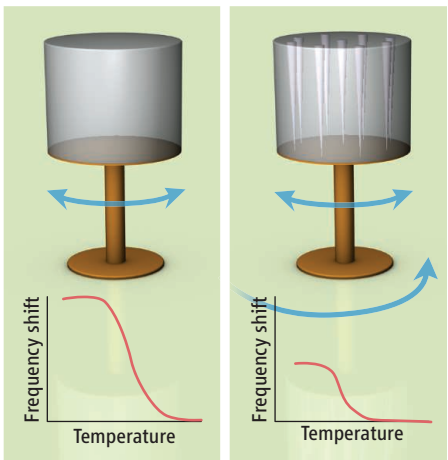

Spin out. Rotation reduces the frequency shift signaling resistance-free flow.

That's what should happen if the flow is real. Thanks to quantum mechanics, a superfluid abhors rotation. Spin a bucket of superfluid liquid helium, and the liquid will sprout tiny whirlpools called "vortices" spinning to counteract the rotation. Put a torsional oscillator in a spinning fridge, and vortices will tie up the superfluid, leaving less to stand still and reducing the frequency shift seen as superfluid flow sets in. Kim's result suggests that rotation stirs up vortices in solid helium, too, says Sébastien Balibar, a physicist at the École Normale Supérieure in Paris.

Measurements taken simultaneously showed that rotation did not affect the helium's stiffness, Balibar says, so changes in stiffness cannot explain the results. "The objection of John Reppy is ruled out," he says. However, Reppy counters that Kim and colleagues measure the stiffness of helium sequestered in a special channel across their can and that measurements there may not reveal what's going on elsewhere in the solid.

Does this prove supersolidity exists? Kim is cautious, noting that his team has not directly observed vortices. Still, he says, "I can't find a way to explain the experiment with a nonsupersolid scenario." It may be tough for others to find one, too. **–ADRIAN CHO**

ILLUSTRATION: P. HUEY/*SCIENCE*

*Science*Insider

From the *Science* Policy Blog

A panel has criticized a risk assessment by the U.S. government of a planned lab in Kansas to study the world's most **dangerous animal pathogens.** It says more information is needed on the potential economic impact of the accidental release of highly contagious pathogens. http://scim.ag/NBAF-risk

The **world's supply of oil** is increasingly in the hands of OPEC nations, according to a new report from the International Energy Agency that says production from non-OPEC nations has flattened. http://scim.ag/opec-dominance

Last month, Senator Charles Grassley (R–IA) complained about certain trips by **National Cancer Institute** scientists that were paid for by nonfederal sources. *Science*Insider analyzed records for some of the trips and found that many were to give talks sponsored by domestic universities or scientific societies. http://scim.ag/NCI_trips

Scientists on the **Spirit Mars Rover** team fear that the plucky robot has finally died after 6 years of exploration. Wind could still blow dust off its panels, says team leader Steve Squyres of Cornell University, so "we listen, [but] it could be a long wait." http://scim.ag/Spirit_phonehome

A bipartisan deficit panel has called for making permanent the U.S. **research and development tax credit**. It's an exception to the slew of spending cuts and removal of tax breaks that characterize the interim report from the chairs, who must release the final recommendations by 1 December. http://scim.ag/rd_taxcut

Advocates for indigenous people have managed to get a 100-person **scientific expedition to a remote area of Paraguay postponed**. Critics of the journey, sponsored by the Natural History Museum in London and coordinated with local tribes, feared the trip could spread diseases to indigenous people or lead to violent exchanges. http://scim.ag/paraguay_trip

For 2010 election coverage and more science policy news, visit **http://news.sciencemag.org/scienceinsider**.

NEWSMAKER INTERVIEW: SUBRA SURESH

A World of Changes Prepares Subra Suresh to Tackle Change at NSF

To understand how far Subra Suresh has come since growing up in the south of India, consider this:

In 1977, the 21-year-old Suresh took his first trip on an airplane. The flight took him from Madras (now Chennai), India, to Ames, Iowa, where he began a graduate program in engineering at Iowa State University. Thirty-three years later, in his first week as director of the U.S. National Science Foundation (NSF), Suresh twice flew halfway around the world—to a meeting of national funding agencies in Belgium and to Hawaii for an event that gave him the chance to meet with a powerful U.S. senator—and within 36 hours he was back in his 12th-floor office at NSF headquarters in Arlington, Virginia.

As the first Asian-American to lead NSF, Suresh's own story is part of the rise to prominence of scientists from that region. The older of two children in a lower-middle-class family, Suresh began first grade at the age of 4 after his mother, who still lives in Chennai, decided that having two kids at home "was too much to handle." He scored high enough on the grueling national entrance exams to be admitted to one of the top-rated Indian Institute of Technology (IIT) campuses, making him the first in his family to attend university. After graduating from IIT Madras with a degree in mechanical engineering, he chose Iowa State in large part because it agreed to waive his application fee. Throughout his graduate education, which culminated in a doctoral degree from the Massachusetts Institute of Technology (MIT), Suresh wrote weekly letters to his mother because the cost of a phone call—$4 per minute ($14 in today's dollars)—was prohibitive.

Three decades later he had become dean of MIT's School of Engineering, a member of the U.S. National Academy of Engineering, and co-founder of a company created to commercialize one of his discoveries. But you might not know it by listening to Suresh, a trim, soft-spoken 54-year-old man of medium height. "Subra isn't bombastic and doesn't brag about how great he is, but he's pretty sharp," says Karl Gschneidner, a retired professor of engineering at Iowa State who still runs an active research program. "He was one of the best students I ever had," he adds, pulling out his grade book for the class that Suresh took in 1977 and in which, not surprisingly, he earned an A. Asked what it takes to ace his course, Gschneidner says: "Knowing a hell of a lot, and answering problems the right way."

Suresh will need to draw upon those traits—and much more—to succeed as NSF director. On the plus side, he joins an agency held in high regard by the White House and Congress: On 18 October, his first day on the job, he attended the first-ever White House science fair and received a shout-out from President Barack Obama. Obama has promised a 10-year doubling of NSF's 2008 budget of $6 billion, in line with a 2007 law—the America COMPETES ACT—that would expand federal support for basic research and science education at NSF and three other agencies. The bill enjoyed broad, bipartisan support and grew out of a 2005 National Academies' report, *Rising Above the Gathering Storm*, that had been embraced by the Bush Administration. One of the first actions by congressional Democrats after taking power in January 2007 was to match the president's request for an 8% increase to NSF's research programs in a supplemental funding bill that froze the budgets of most federal agencies.

But the political and fiscal climate has changed dramatically since those heady days. This spring, a reauthorization of the 2007 COMPETES Act became mired in a partisan debate over its overall cost and the new federal programs it would create, and a shrunken version passed the House of Representatives with only 17 of a potential 177 Republican votes. The president has requested a 7% increase in NSF's 2011 budget, but few expect it to survive the final version of an annual spending bill that may be approved next month by the lame-duck Congress. A resurgent Republican party, which will control the House when the next Congress convenes in January, ran on a pledge to roll back federal spending to 2008 levels as part of an effort to reduce this year's $1.3 trillion budget deficit.

Even NSF's $3 billion windfall, part of the $787 billion American Recovery and Reinvestment Act passed in February 2009, could have a downside. No House Republican voted for the stimulus package, and observers worry that academic researchers will face the same "Where are the jobs?" question leveled at the entire stimulus pack-

"We're starting internal discussions on how to cope with the worst case [budget] scenario, which would be flat funding or worse. The community felt that long overdue support for basic science is something that's critically needed. But we also need to manage those expectations over the next few years."
—SUBRA SURESH*



CREDITS: © SAM KITTNER/KITTNER.COM

*In a 10 November 2010 interview with *Science*.

Published by AAAS

age, which critics view as a waste of taxpayer dollars. Then there's the unavoidable budget cliff facing scientists who received 2-year stimulus money and who next year will be seeking continued support for their projects from NSF's regular budget.

How will a new director, NSF's 13th since it was founded in 1950, fare in such a politically charged climate? "He brings his knowledge and passion for research, along with a very creative and broad view of science and technology as an administrator," says Thomas Magnanti, who hired Suresh as chair of MIT's department of materials science and engineering. In 2007, Suresh succeeded Magnanti as dean of engineering. "He's got to take those skills and apply them to working with the entire scientific community, as well as Congress and the Administration," says Magnanti, who last year was named founding president of the Singapore University of Technology and Design.

Last week, in his first public interview since taking office, Suresh indicated that he's already begun to do exactly that. Even before his Senate confirmation in September to the 6-year post, Suresh began asking colleagues about the myriad issues that he will face at NSF. In the few weeks since becoming director, he told *Science*, he's begun to "calibrate" those opinions with the 1500 scientists and engineers who manage NSF's programs and now work for him. The goal, he says, is to find "low-hanging fruit, … ideas that we can start to implement within a few months, with the existing budget."

He's careful not to overpromise. But he clearly feels that some changes are warranted. "Individually, each may look small and insignificant," Suresh explains. "But together, they could have a huge impact on the morale and efficiency of the organization."

One example of a possible early change is a tweak to NSF's peer-review system. A modest step, he says, would be a pilot project using modern communications tools to overcome obstacles in scheduling panel meetings or on-site visits for pending proposals. "I'd like to find a way to tap the best experts in the world," he says, "rather than just settling for whoever is available that week."

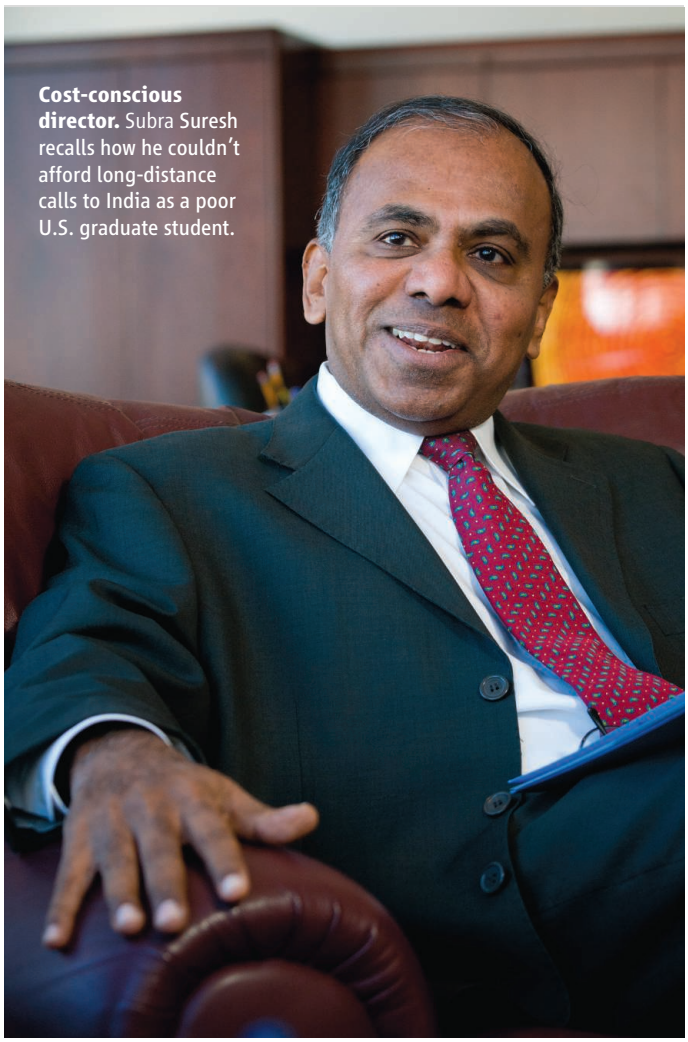

Cost-conscious director. Subra Suresh recalls how he couldn't afford long-distance calls to India as a poor U.S. graduate student.

CREDIT: © SAM KITTNER/KITTNER.COM

A more significant step that Suresh signaled he might be weighing is a reassessment of NSF's requirement that investigators describe the "broader impacts" of their grant proposal. That second criterion (scientific merit is the first) has been a thorn in the side of many researchers, who complain that it's unrealistic for NSF to expect them to devote time to, say, improving science education, raising public literacy, or increasing the number of minorities or women in science and engineering while they carry out their research. Suresh hinted that he'd like to give grantees some wriggle room.

"I think the spirit of the broader impacts criterion is good," he explained. "But the question is, on whom do you place the burden? A large program has multiple entities that can ensure or follow through on the broader impact. But an individual investigator, especially a young investigator, may not have the opportunity or resources to demonstrate broader impacts. So the question is whether you can put the requirement not just on the individual but on a program that includes a collection of individuals. Perhaps you could also have some accountability by the institution itself."

Another issue on Suresh's mind is what he called "the leaky pipeline" that drains the U.S. scientific enterprise of talent at every level, from undergraduates through senior academics. "I hope to be able to say something more about that before long," he told *Science*. These and other ideas were on the agenda of a 2-day retreat Suresh held last week with senior NSF managers.

Although Suresh says that he still has a lot to learn about how NSF operates, he's already plenty savvy about ducking questions on sensitive topics with political ramifications. For example, he declined to say whether he favors changes in programs aimed at a broader geographic distribution of limited NSF dollars, a popular cause within Congress that some scientists believe waters down the quality of NSF's portfolio. He said, "I'm not sufficiently up to speed" on NSF's proposal in this year's budget to combine several programs serving underrepresented minority college students, which the House and an important Senate panel have told NSF to drop. Finding the proper balance in NSF's portfolio between grants to individual investigators and large centers and between funding research and infrastructure, another perennial topic among academic leaders, is a problem "with multiple dimensions," he noted. All the elements are worth "nurturing," he added.

Suresh says he's looking forward to discussing these and other issues with the National Science Board, the 24-member presidentially appointed body that sets NSF's general policies. The board, which has 10 seats unfilled because the White House has yet to nominate replacements for members who have completed their 6-year terms, can also help him rally support for any proposed major changes. And it's a good bet there will be some.

"MIT was a visible position," says Suresh. "But this job gives you a chance to have an impact not just at one institution but across institutions, and potentially around the world. I'm looking forward to the challenge."

–JEFFREY MERVIS

Published by AAAS

Russian Science: Waking From Hibernation

Russian science has moved beyond survival mode and is trying to recapture its research glory. But as the government backs universities and applied research, what does the future hold for the Russian Academy of Sciences?

LATE LAST MONTH, RUSSIA'S MINISTRY OF Education and Science announced the first results of a novel attempt to revitalize science in the country's universities. It had offered "megagrants" of up to $5 million to attract top researchers from around the world to set up new labs at Russian universities. The first 40 successful applicants included some big names: 1998 medicine Nobelist Ferid Murad of the University of Texas, Houston, and mathematician Stanislav Smirnov of the University of Geneva, Switzerland, the 2010 Fields Medal winner. "This could build a very good bridge between France and Russia in this area," says another winner, Gérard Mourou, director of the Laboratory of Applied Optics in Palaiseau, France, and a pioneer of ultrahigh-intensity lasers.

How much the megagrant winners can boost Russian science remains an open question, however. Foreign winners are only required to spend one-third of each year in Russia, acknowledges Andrei Fursenko, Russia's minister of education and science (see p. 1038). "Four months is too low a commitment for this money," says Alexei Khokhlov, vice-rector of Moscow State University.

And the program notably failed to lure two big fish: this year's winners of the Nobel Prize in physics, Andre Geim and Konstantin Novoselov. The discoverers of graphene were both born and educated in Russia but are now working at the University of Manchester in the United Kingdom.

Online
sciencemag.org
Podcast interview with author Daniel Clery.

Indeed, the Nobel Prize announcement last month generated much debate in Russia about why many of the country's best and brightest scientists—tens of thousands of whom fled abroad during the economic crises of the 1990s—are still now gracing foreign universities and their work benefiting other economies. "I was never interested myself" in the Russian megagrants, says Geim. "It's difficult to run two labs efficiently."

Russian science has come a long way since Geim and Novoselov left in the 1990s, a time when some researchers moonlighted as taxi drivers to earn enough to eat. Salaries have slowly risen, and around the mid-2000s, the government—acknowledging that Russia couldn't live off its natural resources forever—launched programs to boost research-led industries such as nanotechnology. Russian researchers at home and abroad have welcomed such programs but complain that the government continues to provide inadequate funding for basic research and has failed to institute needed reforms—particularly in the Russian Academy of Sciences (RAS), which, they maintain, clings to its Soviet-era privileges and hierarchies while supporting large numbers of unproductive institutes and researchers.

Some have been trying to get RAS to

Published by AAAS

Brave new world. The Russian government wants more research to be done in universities, such as Moscow State University (*left*).

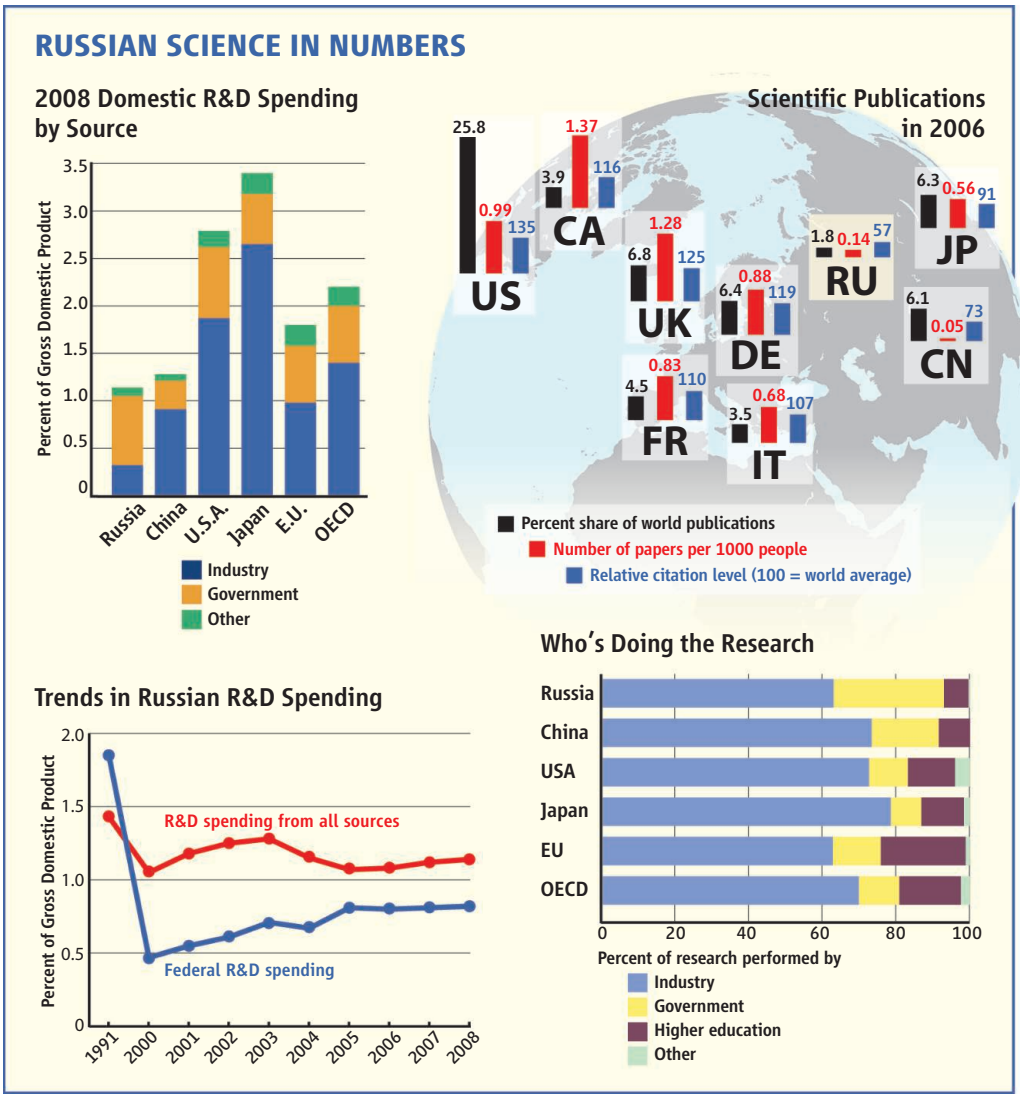

employ transparent, peer-reviewed funding to promote the best and most active researchers. And the government countered its critics this year with a string of programs to encourage more research in Russia's universities, outside the control of RAS. But while Russian scientists have been generally supportive of such efforts, they are reserving judgment on whether it will be enough to preserve what is good in Russian science. "Those at the top are trying to do their best to restore science in Russia. But it always gets muddled, and corruption is endemic," says Geim.

Slow recovery

At the height of the Soviet Union, science was prestigious. RAS, which carried out most basic research, was well-funded and ran hundreds of institutes. More research was done in science cities scattered across the vast expanse of the Soviet Union, often geared to military applications. And each centrally controlled industry had a generous budget for R&D that funded more institutes. "In Soviet times a scientific career was *the* career; all the best people went there. If you take the best and brightest, you should do very well," says economist Sergei Guriev of Moscow's New Economic School. Fursenko says there was a joke in Soviet times: "What is science? A method to satisfy your curiosity at the government's expense." In 1990, just before it collapsed, the Soviet Union employed almost 2 million scientists, engineers, and technicians at more than 4600 institutes.

Four years later, when *Science* published a special issue on Russian research (*Science*, 27 May 1994, p. 1259), many once-bustling laboratories were empty, dark, and inactive. Researchers couldn't afford reagents, consumables such as liquid nitrogen, or even electricity to run their experiments. The UNK, a huge particle accelerator at the Institute for High Energy Physics in Protvino, which was meant to rival those at CERN and the Fermi National Accelerator Laboratory, lay unfinished with 5 kilometers of its 21-kilometer tunnel still undug and warehouses full of magnets. At Gatchina near St. Petersburg, construction of the PIK reactor, a source of high-intensity neutrons for materials research, physics, and chemistry, had stalled with only 75% of the project completed.

Researchers' salaries were no longer enough to live on and so, with restrictions on travel eased, many fled to jobs abroad—including Geim and Novoselov. Official statistics say 25,000 scientists emigrated between 1989 and 2004, but independent estimates suggest more than 80,000 left in the early 1990s alone. Many researchers who remained left science altogether.

A fortunate few managed to find other sources of funding, such as by partnering with labs abroad or winning research contracts from international corporations. Other funders sprang up, including financier George Soros's International Science Foundation. In an initial challenge to RAS's authority, the government created the Russian Foundation for Basic Research (RFBR), which funded proposals chosen by peer review, but its resources

Staying put. 2010 physics Nobelists Andre Geim (*left*) and Konstantin Novoselov are resisting the pull to return to their birthplace.

CREDITS: (SOURCES, TOP LEFT) OECD; (TOP RIGHT) THOMSON REUTERS/NIFU STEP; (BOTTOM LEFT) MINISTRY OF EDUCATION AND SCIENCE OF THE RUSSIAN FEDERATION; (BOTTOM RIGHT) OECD; (PHOTO) RUSSELL HART/UNIVERSITY OF MANCHESTER

Published by AAAS

were slim. Throughout that decade, the main goal of scientists was survival rather than research productivity.

After 2000, as the economy began to strengthen, the plight of researchers gradually improved. The government slowly increased salaries: RAS researchers now earn five or six times what they did a decade ago. "It's not enough, but compared with a few years ago it's at least acceptable. It's higher than the average salary in Russia," says Fursenko.

As if waking from hibernation, Russian science started to come to life. The government provided money to complete the PIK reactor, which is now almost ready to power up for the first time. "Financing has only been provided for the 'bare' reactor, not for the instrument program. So we are trying to get money to do this work," says Valery Fedorov, director of neutron research at the Petersburg Nuclear Physics Institute. The UNK accelerator remains unfinished, but researchers at Protvino have stayed afloat working on smaller scale experiments and collaborating with CERN in Europe as well as with Brookhaven and Fermi national labs in the United States.

JINR, one of Russia's most prominent labs and a world-leading center for nuclear physics, also began to spread its wings. "After the end of the Soviet Union, the first 12 years were a very hard time for the institute. Our budget was small and it was not paid" by the government, says Mikhail Itkis, JINR's acting director. During this period, there were no upgrades of equipment, no new facilities—the lab just held on to what it had, Itkis says. International support kept the lab going. Set up as a Soviet response to CERN in the 1950s, JINR has 18 member nations from across the old Soviet bloc and they stayed on board, even though some are now members of NATO and the European Union. "They helped us survive," Itkis says.

"It's very hard to attack anything [in Russia] that is a totem of the Soviet system."

—SERGEI GURIEV, NEW ECONOMIC SCHOOL

In 2000, newly elected President Vladimir Putin acknowledged the importance of the lab with a law giving it special status and tax-free land. JINR was soon receiving its full budget again, but it was not much to work with: In 2005, it was budgeted just $37 million for an institute with 5000 staff members. JINR that year asked all of its members to increase their contributions by 20% and then to continue ramping them up until they reached a total of $200 million by 2016. Members agreed and have kept their promise. Next year's budget will total $100 million. The institute now has new facilities under construction, others being upgraded, and has won fame for the synthesis of new superheavy elements, nine in total. "We can't be the world leader in all areas of physical science, but in some areas we must be. That's our policy," Itkis says.

Bridging the gap

At the beginning of Putin's second administration in 2004, when Fursenko was appointed to

INTERVIEW: ANDREI FURSENKO

University Research Should Compete With Russian Academy, Science Minister Argues

The collapse of the Soviet Union led to hard times for Russian research, but the administrations of Vladimir Putin and Dmitry Medvedev have been trying to prioritize science again. The government has invested billions in nanotechnology through a state corporation called Rusnano and is developing a high-tech hothouse in the Moscow suburb of Skolkovo. But it has had to struggle against significant legacies: industries that are more interested in exploiting natural resources than developing new products; a fiercely independent Russian Academy of Sciences (RAS) that's resistant to change; and a university system more geared to churning out large numbers of graduates than carrying out research.

Minister of Education and Science Andrei Fursenko met with *Science* at the ministry's imposing Tverskaya Street headquarters in September to discuss how Russia plans to reinvigorate its research base. The interview, conducted before Russia announced the initial winners of its new university-based research grants (see main text, p. 1036), has been edited for brevity and clarity. **–DANIEL CLERY**

Q: What's the status of your new program to attract top international researchers to set up groups at Russian universities?

A.F.: We have more than 500 proposals—300 from Russian citizens, around 170 from foreign citizens, and a few tens from researchers with dual nationality. We have had to make some compromises: We had hoped that the scientists would spend half the year in Russia, but after discussions with overseas universities [where some applicants work], we have reduced that to 4 months, a semester.

We're now in the process of selection, and it's our first experience of this in Russia. Every proposal is examined by four experts in that field, two Russian and two foreign. If their opinions diverge, then we get another two experts. The opinions are then sent to a grant council of distinguished Russian scientists, academicians mainly—people with a recognized stature in different areas and a serious international reputation. The council members are approved by the government.

Q: This program specifically targets research money at Russian universities. Is it your policy to move toward a "research university" model?

A.F.: There are a few reasons behind this move towards universities. The first is the need for a really competitive environment in Russian science. The Russian Academy of Sciences is much stronger than any other institutions. Even after the last 20 years, it has no real competition.

Secondly, you have to build a scientific environment in a place where there are more young people: the universities. There are some good links between the RAS and universities, but to improve the participation of young people [in research], you have to improve their scientific environment.

And thirdly, a professor not involved in scientific inquiry is not a real professor. A university with no research is not a real university. We have to select carefully the leading research universities and support them.

We are engaged in a process of very serious reconstruction of higher education. We had a competition for the new status of "national research university." We had a competition for funds for innovative infrastructure for universities and for joint research projects with industry. This is absolutely a new approach for Russia.

Q: In a letter to President Medvedev last year, émigré Russian scientists described basic research in the country as "catastrophic" and warned of a "looming collapse." Is Russia neglecting basic research?

CREDIT: COURTESY NEW ECONOMIC SCHOOL

Published by AAAS

Out with the old? The Russian Academy of Sciences has embraced modern architecture but not modern funding methods.

his current position, the Russian government began to address the gap between research and the country's economy. The Soviet system of applied science institutes that served the military and key industries had collapsed. There was no mechanism for translating scientific advances into usable products or processes for industry. "Industry is not interested: They're quite happy with what they have. Initiatives that promote interaction are very important," says Khokhlov.

In 2007, the government bet big on nanotechnology. It founded the Russian Nanotechnology Corporation (Rusnano), arming it with $6 billion to spend and the goal of creating a $30 billion industry by 2015. Rusnano distributes most of that money as grants to companies to help commercialize nanotech products, but research institutes have also claimed a slice of the pie. The Kurchatov Institute in Moscow, the country's premier nuclear energy lab, recast its synchrotron x-ray source as the Kurchatov Center for Synchrotron Radiation and Nanotechnology. JINR is creating a new International Innovation Center for Nanotechnology, with $33 million from Rusnano. And in July, RAS and Rusnano announced the Center for Technology Transfer with just over half its $2 million budget coming from Rusnano.

Despite the gold rush, some researchers are doubtful about the government's "nanotechnology fever," as one scientist called it. Rusnano "is not really funding research. It's commercialization," says Guriev.

Yet more skepticism is reserved for the government's Skolkovo project, an attempt to create a Silicon Valley–style technology hothouse on the outskirts of Moscow. Launched 6 months ago, the project's aim is to bring together 12,000 researchers and businesspeople, focusing on government priorities—energy, IT, telecommunications, biomedicine, and nuclear technology. The Kurchatov Institute and Moscow State University are already linked to the project, as are numerous non-Russian companies, including Boeing.

A.F.: I wouldn't say that basic research in Russia in general are "catastrophic," and I think some Russian scientists doing world-class research will support me. But obviously the Soviet Union gave much more in this area. Huge manpower was devoted to basic research, and those scientists are now spread around the world. That approach produced good results in a totalitarian regime, but it's not appropriate in a democracy. Now when I talk to RAS colleagues, I tell them that it's taxpayers' money, [and] we have to explain why it is better to spend it on research and what research is needed.

It's a very complicated problem, how to distribute money. We are introducing new mechanisms to support basic research. Only a small part of the RAS's programs, for example, the molecular and cell biology program, is now competitively funded. Then there is the Russian Foundation for Basic Research, a successful grant-distributing institution. During the worldwide economic problems, there was limited money, and other ministries wanted to contract [RFBR]. But it is safe for this year and next. But [basic science funding] can't all be competitive. Some money has to go to the most distinguished institutions and researchers.

Q: The government's nanotechnology initiative seems to be trying to create a whole new industry in a few years. How is it progressing?

A.F.: Russia has some background in nanotechnology. Material science and instrumentation were both strong in the Soviet Union.

Rusnano is a new institution, independent from government and independent of the budget process. It may not be the best way to do it, but it's a new tool for Russians, and we have to reconstruct our applied research. We're creating new centers of attraction. Because of the demand for ideas, it is providing motivation for researchers and young people. Interest among young people in research is increasing. Ten years ago, students thought those studying science were losers. Now that's changed.

Q: And is the Skolkovo center also an attempt to foster innovation by bringing research and industry together?

A.F.: We need to simultaneously push innovation in Russia and get existing bodies to improve. We need real competition. Skolkovo is a new challenge for young people and existing structures. They will have a benchmark in Skolkovo. If it works, it can be used more widely, replicated elsewhere.

Q: How do you see Russian science developing in the future?

A.F.: Both basic and applied research as systems need to be more diverse, with a greater degree of competition. In basic research, we need more international cooperation. I'd like to see two or three leading international research centers in Russia. And we need greater integration between research and education, not only in moving research closer to higher education but in making greater use of RAS researchers in training master's students as well as Ph.D.s and postdocs. The academy should be involved in this.

CREDITS (TOP TO BOTTOM): BORIS KAVASHKIN/ITAR-TASS/NEWSCOM; ROMAN KRUCHININ/ ITAR-TASS/NEWSCOM

Published by AAAS

"Skolkovo is very strange," says Vyacheslav Strelkov of the Kurchatov Institute. "There are many scientific centers in Russia. Why put money into this new place? Our buildings are empty." The project is causing concern at JINR, too. Directly opposite JINR, on the banks of the broad Volga River, is one of the "free economic zones" granted to the institute by the 2000 law formalizing its status. These are meant to be tax-free science parks where high-tech companies can set up shop and interact with JINR. It remains almost empty; JINR researchers suspect that companies are waiting to see how Skolkovo pans out.

Back to basics

The government's emphasis on applied science has thrown its treatment of basic research into stark relief. "They simply do not understand how the basic science creates innovations and believe that [all] basic research should result in something useful," says Georgii Georgiev of the RAS Institute of Gene Biology. The slighting of basic research was brought to worldwide attention a year ago when more than 200 émigré Russian researchers sent a letter to President Dmitry Medvedev alerting him to the "catastrophic conditions of fundamental science" in Russia and warning of its "coming collapse." The signatories called for increased funding, integrating Russian science into the worldwide community, financial transparency, and international standards of quality assessment allied with competitive grants.

More warning bells were sounded early this year in a report from Thomson Reuters, which showed a slump in international publications by Russian scientists since the end of the Soviet Union (*Science*, 5 February, p. 631). Russia peaked at 29,000 papers in 1994 but was down to 22,000 by 2006—a period during which countries such as China and India dramatically increased their production of sci-

"Preserving the status quo, or making cosmetic changes, is not a practical position."

—ALEXEI KHOKHLOV, MOSCOW STATE UNIVERSITY

Uncertain Future for Academy's Biology Experiment

Ask anyone familiar with the Russian Academy of Sciences (RAS) how the organization can be reformed so that it funds the best researchers, rather than those with the best connections, and the discussion quickly turns to the efforts of Georgii Georgiev. The former director of the Institute of Gene Biology in Moscow, Georgiev founded and runs the academy's Molecular and Cell Biology (MCB) program. Since 2003, MCB has awarded grants to groups based on their scientific track record, and it has provided the chosen research teams with enough freedom and money to pursue what they deem interesting. Georgiev is "trying to establish an open and transparent system," says molecular biologist Peter Becker of the University of Munich in Germany, who has peer reviewed for the program.

The MCB program is widely recognized to have raised the quality of Russia's research in molecular and cell biology. But it is something of a radical experiment for the conservative RAS, and it has faced opposition from within the academy. Its 2010 budget was slashed from about $8 million to $6 million, ostensibly because of government spending cuts. "It's a clear sign that [the RAS leadership] don't like it, which is bad news for everyone," says economist Sergei Guriev of Moscow's New Economic School.

When a research group applies for funds from MCB, the assessment starts with a look at the impact factors of papers the group has published in international journals over the previous 5 years. The results are weighted depending on how great the group's contribution to the paper was. About 25 top groups are chosen in this way in each 5-year funding round, and the leaders of those research teams then review other applications. They look for measures of quality in addition to the group's publication record. "The aim was not to miss some important research not adequately published for some reason and to evaluate projects in applied research," Georgiev says. The program supports about 100 groups for 5 years with a maximum award of $130,000 per year.

"To improve science in Russia, … [we must] perform an audit of all research groups to support the productive ones and to close the dead ones."

—GEORGII GEORGIEV, RAS INSTITUTE OF GENE BIOLOGY

Between 2003 and 2009, the 100 groups chosen in the first funding round published 2000 papers in international peer-reviewed journals, including *Cell, Genes & Development,* and *Nature*—an impressive rate in an academy in which many researchers don't publish in international journals at all. According to Georgiev, the program is open to Russian émigrés, and it has encouraged some to return to Russia.

Many would like to see MCB's approach extended to other areas of RAS. "It should be duplicated" throughout the academy, says Anna Piotrovskaya, director of the Dynasty Foundation, a private funder that stepped in to support 50 young researchers when MCB funding was cut this year. "It would change significantly the atmosphere in the academy," says physicist Alexei Khokhlov, vice-rector of Moscow State University, who is also an academician at RAS. "Many academicians, including myself, proposed it several times, but I'm not so sure all members would agree with me."

The RAS presidium originally set up similar programs in 16 different fields back in 2003, but MCB is the only one that really took hold, in part because of Georgiev's fervent belief in its approach. "The RAS should … show the ability to change. It has to increase the amount of transparent competitive funding and to perform an audit of all research groups," he says.

Yet when the government cut the RAS budget by 10% this year, Georgiev says, the MCB program "was reduced more strongly by the RAS" than other programs. Researchers in Russia, and elsewhere, are hoping this is just a temporary setback. "Georgiev needs international support to make a point against the establishment. It's an uphill battle," says Becker.

–D.C.

CREDITS (TOP TO BOTTOM): ELENA LISJANSKAYA; IGNAT SOLOVEY/STRF

Published by AAAS

entific papers. In the 5 years from 2004 to 2008, Russia produced just 2.6% of all the world's published papers, less than China (8.4%), Canada (4.7%), and Australia (3.0%).

"This is a delicate question for us. It's a cultural issue," says Fursenko. Some Russian researchers publish only in Russian-language journals out of a sense of national pride. Fursenko says the decline in publications tracked by Thomson Reuters reflects a division between Russian researchers who publish in international journals and those who think this is beneath them—or just can't be bothered.

Tough love. Prime Minister Vladimir Putin spells out the future to the presidium of the Russian Academy of Sciences in May this year.

Indeed, many in RAS are hostile to international journals and attempts to quantify research productivity based on them. Science "is an ephemeral thing; it's hard to evaluate it. That's why certain contrivances were introduced," Mikhail Kovalchuk, director of the Kurchatov Institute, said at a Moscow press conference in September. "The creation of the citation index, of a journal's impact factor, was a strong commercial project from which people earned billions of dollars. … There's enormous money and national interests behind it. … That's why we must make our own rating system and not impose alien ones."

The government has begun to address the health of basic research by boosting science at universities rather than at RAS. Under the Soviet system, universities were primarily teaching institutions and they generally lacked research facilities. Over the past year or so, the government has launched several programs to boost university science, including a new status of "national research university" (of which there are now 40, including Moscow State), a competition for infrastructure grants, and a fund for industry to sponsor research projects by university groups.

The flagship effort is the megagrants program to attract topflight researchers to set up in Russian universities. Fursenko says the awardees were selected according to international standards based on publications and research excellence, and almost 1000 experts—600 of them from outside Russia—were consulted. "It'll be interesting to see what happens with this project," says Moscow State's Khokhlov. "Ideologically, this is a new thing in Russia. I support this type of funding."

More than 500 researchers applied to the program. Among the 40 winners announced in October, 20 are Russians, 15 of them living abroad. There will be a call for a second round of grants later in the year. "It seems that the competition was more or less fair," says one of the winners, evolutionary biologist Alexey Kondrashov of the University of Michigan, Ann Arbor. "I know personally eight out of the 40 winners, and they are all serious scientists. … Thus, one can expect a beneficial impact [on Russian science]."

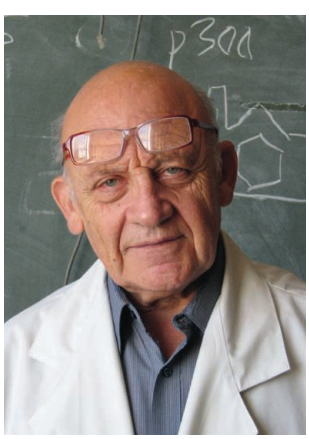

RAS should "allow young, active, ambitious Ph.D.s to take the positions of institute directors."

—EUGENE SVERDLOV, RAS INSTITUTE OF MOLECULAR GENETICS

An academic question

All this support for university research begs the question, what is the government doing about RAS? The academy still carries out the vast majority of Russia's basic research, but its 50,000 employees must struggle on with government funding of just $1.6 billion per year—less than $30,000 per person—to pay for salaries, equipment, and materials. (RAS does have other sources of funding, including rental income from land and buildings.)

To many outsiders, RAS is a relic of a bygone age. It retains a rigid hierarchical structure with all-powerful directors and presidium at its peak. Funding is handed down by influential academicians and institute directors. Reputations, rather than publications, are key. As a result, critics say, RAS continues to support a large number of unproductive researchers and institutes. "Too much depends on academic rank, and there is no transparency," says Khokhlov, who is himself an academician at RAS. "Once organized, labs exist forever. There is no procedure to close the old and open new. The system has to be more flexible."

So far, the government has not seriously interfered in the running of the academy, although the two have periodically fought over control of RAS's valuable real estate holdings. "The RAS is an independent body," says Fursenko. Still, in 2007 the government persuaded RAS to agree that any changes to its charter had to be approved by both a general meeting of RAS and the Russian government. Any new RAS director similarly now needs the approval of both bodies. "These changes were accepted by academy members as reasonable, since the academy is a state organization," says Eugene Sverdlov of the Institute of Molecular Genetics and an adviser to RAS.

In May this year, Vladimir Putin, now prime minister, addressed a general meeting of RAS and hinted at bigger changes on the horizon. "The Russian Academy of Sciences … cannot shy away from the modernization agenda," he said. "Internal transformations … in the system of the Russian Academy of Sciences are considered to be a matter of paramount importance. These will enable improved quality of R&D projects." If that wasn't clear enough, Putin drove home his point: "These plans should be implemented by identifying the leading institutions through open and transparent proposals, rather than by bureaucratic procedures or by the preference of an official."

Such statements make researchers who view RAS as a bastion of basic science in Russia nervous. "The RAS has enjoyed independence even in the most difficult

CREDITS (TOP TO BOTTOM): COURTESY PHOTOSERVICE OF THE GOVERNMENT OF THE RUSSIAN FEDERATION; RUDOLF POGOSYAN

Published by AAAS

Follow the money. The government lavishes funds on the planned Skolkovo Innovation Center (*above*), while the PIK neutron source (*left*) scrabbles for money to buy instruments.

times. Science cannot be administered too much; it needs independence to produce results," says Khokhlov.

Nevertheless, the majority of scientists who spoke with *Science* felt that RAS is in need of reform. For some, the most pressing problem is to clear out the dead wood. "To improve science in Russia, … [we must] perform an audit of all research groups to support the productive ones and to close the dead ones," says Georgiev. Sverdlov says that RAS had a rule that institute directors could serve no longer than 10 years and should retire at the age of 70, but the rule was abandoned in 2007. He urges his colleagues to adhere to the rule voluntarily. RAS should "allow young, active, ambitious Ph.D.s to take the positions of institute directors, provided that they are able to offer a long-term development program for the institute," he says.

Another model for changing RAS is its molecular and cell biology (MCB) program, one area of the academy's activities in which peer review is used to select the best projects and young researchers are given academic freedom (see sidebar, p. 1040). Yet, despite its many fans, RAS cut funding to the MCB program deeply this year.

A future dynasty?

There are few alternatives to RAS funding for Russia's researchers. RFBR remains a relatively small player. International funders have faded away. But perhaps as a sign of things to come, at least one of Russia's new superrich entrepreneurs has set up a private foundation to support research. In Soviet times, Dmitry Zimin worked on anti–ballistic missile systems. He later founded what became one of Russia's biggest telecommunications companies. In 2000, he sold off his interest in the company to devote himself to philanthropy and created the Dynasty Foundation. "The aim is to support young, talented people," says Dynasty Executive Director Anna Piotrovskaya.

Each year, Dynasty awards competitive 3-year grants to as many as 130 young theoretical physicists and mathematicians, allowing them to keep working in Russia. The disciplines were deliberately chosen as ones that didn't have high lab costs, but the foundation plans to move soon into biology, chemistry, and earth sciences. As well as supporting researchers, Dynasty gives grants every year to 500 high school science teachers, organizes public lectures, runs a popular science Web site, and supports the publication of popular science books. This year, when the MCB program's budget was cut, Dynasty helped with grants to 50 young biologists the program had identified. "We try not to work with the academy. Funds just disappear," Piotrovskaya says. The MCB program, she adds, "is the only program that is done transparently."

The past decade has seen definite progress in Russian science: Researchers get a living wage, there are pockets of excellent science, and, at least in applied research, the government is backing up words with funds. But for those eager for reform who are still battling against the structures and privileges of an outdated system, it must seem like waiting for a glacier to melt before the river underneath can flow again. "Sooner or later the majority of [RAS] members will understand that the only way to restore funding is through real changes. Preserving the status quo, or making cosmetic changes, is not a practical position," says Khokhlov.

Some, however, argue that reforming RAS is a lost cause. "It's very hard to attack anything [in Russia] that is a totem of the Soviet system," says Guriev. "We should leave the RAS as it is. Put all new money into research competitions (open to academicians as well), new structures, and the universities." Like many others, Guriev says competitively awarded funding is the key. "Once you decide you want to judge people by international academic publications and use international expertise, it becomes very transparent. It's not rocket science; others countries have done it."

"We try not to work with the academy. Funds just disappear."

—ANNA PIOTROVSKAYA, DYNASTY FOUNDATION

Others see a long struggle to regain the opportunities that have passed by Russian researchers. Says nuclear physicist Yuri Oganessian of JINR: "We've lost a generation. A gap exists. There was quite a long period when science was not a prestigious job. It's now coming back, but it takes time."

–DANIEL CLERY

With reporting by Jennifer Carpenter, Andrey Allakhverdov, and Vladimir Pokrovsky.

CREDITS (TOP TO BOTTOM): ITAR-TASS/NEWSCOM; DAVID ADJAYE/WIKIMEDIA COMMONS; COURTESY DYNASTY FOUNDATION

Published by AAAS

Overbuilding: Doctoral Degree Surplus

FINALLY AN INFLUENTIAL VOICE IN SCIENCE has spoken out against the short-sighted, self-destructive approach that many universities have adopted to expand their research facilities ("Overbuilding research capacity," B. Alberts, Editorial, 10 September, p. 1257). The use of NIH funds to build evermore research buildings and to hire evermore faculty members is clearly unsustainable. I would like to point out yet another aspect of "overbuilding": the heedless growth of graduate training in biomedical sciences, which is completely out of proportion with the real need for biomedical doctoral degrees.

The imbalance between biomedical Ph.D. production and the availability of research positions in academia and industry has been discussed many times (*1*–*3*). However, two recent developments make the problem more acute. First, the ongoing implosion of the U.S. pharmaceutical industry has led to the loss of thousands of research jobs (*4*, *5*). Second, the current chronic recession has led to a large increase in the number of young people entering graduate school (*6*), not necessarily because they are enthusiastic about science but because they have few other options. As a result, we are training too many students of uncertain quality. An effective solution to this problem would be to ban the support of graduate students on NIH research grants and to instead fund students exclusively through competitive individual or programmatic graduate fellowships.

CREDIT: ANJA HILD/ISTOCKPHOTO.COM

University leaders often seem to confuse quantity and quality. They want more grants, more buildings, more faculty, and more students. We need to substitute "better" for "more."

RUDY L. JULIANO

University of North Carolina Eshelman School of Pharmacy, Chapel Hill, NC 27599, USA. E-mail: arjay@med.unc.edu

References

1. *Nature* **457**, 635 (2009).
2. E. Marincola, F. Solomon, *Mol. Biol. Cell* **9**, 3003 (1998).
3. R. L. Juliano, G. S. Oxford, *Acad. Med*. **76**, 1005 (2001).
4. S. Pettypiece, A. Gerlin, "Pfizer may cut $3 billion in research with Wyeth deal (update3)," *Bloomberg* (15 October 2009); www.bloomberg.com/apps/news?pid=newsarchive&sid=aAh8pjthSok8.
5. L. M. Jarvis, *Chem. Eng. News* **88**, 5 (2010).
6. N. E. Bell, "Graduate enrollment and degrees: 1999 to 2009" (Council of Graduate Schools, Washington, DC, 2010); www.cgsnet.org/Default.aspx?tabid=57&mid=440&newsid440=116&.

Overbuilding: Under Pressure

THE EDITORIAL BY B. ALBERTS ("OVERBUILDING research capacity," 10 September, p. 1257) deals with the tangibles of personnel and space in the current university environment. I believe an equally important element is the loss of collegiality and commitment to education and service. My colleagues are under tremendous pressure to support their research infrastructure, including a major portion of their own salary. This pressure leads them to spend a substantial amount of their time and energy continuously applying for grant support. This creates a toxic, uncertain environment that is especially problematic for students, many of whom see academia as an unstable career choice.

KENNETH G. MANN

Department of Biochemistry, University of Vermont, Colchester, VT 05446, USA. E-mail: kenneth.mann@uvm.edu

Overbuilding: Overhead Revisions

IN HIS EDITORIAL "OVERBUILDING RESEARCH capacity" (10 September, p. 1257), B. Alberts discussed the counterintuitive management of overhead grant funding. I would like to suggest two additional changes to overhead policy. First, overhead should be a fixed percentage of grant dollars for all institutions, regardless of what the institution claims to require. This would minimize negotiations and would put an end to rewarding institutions with higher administrative costs. Second, the institution receiving a grant should be free to spend the overhead however it wants (within some general

Published by AAAS

legal constraints, of course). This would lower administrative costs for both the NIH and the recipient because there would be no need to audit how overhead is spent.

MATTHIAS WABL

Department of Microbiology and Immunology, University of California San Francisco, San Francisco, CA 94143–0414, USA. E-mail: mutator@ucsf.edu

Overbuilding: Boosting School Ratings

IN HIS EDITORIAL "OVERBUILDING RESEARCH capacity" (10 September, p. 1257), B. Alberts highlights how institutions evaluate their research capacity needs and acquire funding. One factor he omitted was school ratings. NIH dollars (as well as funding from other government entities such as the Department of Defense and the National Science Foundation) have become a benchmark for rating medical schools and research institutions. As a result, schools feel they must keep building in order to maintain their good ratings, which in turn attract donors. In addition to NIH's role in determining a rational and supportable biomedical infrastructure, new high-profile measures of success must be established that are not overly dependent on grant dollars.

ROBERT D. BURK

Albert Einstein College of Medicine, Bronx, NY 10461, USA. E-mail: robert.burk@einstein.yu.edu

CORRECTIONS AND CLARIFICATIONS

Research Articles: "Hemispheric aerosol vertical profiles: Anthropogenic impacts on optical depth and cloud nuclei" by A. Clarke and V. Kapustin (17 September, p. 1488). The lead author and article title of reference 2 were incorrect. The correct reference is as follows: 2. R. J. Charlson, J. Langner, H. Rodhe, *Nature* **348**, 22 (1990).

Perspectives: "Concentrating on solar electricity and fuels" by M. Roeb and H. Müller-Steinhagen (13 August, p. 773). In the third paragraph, the authors note that "By the end of this year,…groundbreaking for the construction of 2500 GW of CSP plants will have occurred in the United States." The correct figure is 2500 MW.

Letters: "Response" by S. M. Knowles to "Protect pharmaceutical innovation" by L. W. Musselwhite and J. Andrews (11 June, p. 1354). The response quoted a National Academies study that recommended extending the data exclusivity period to 12 to 14 years. The actual quote from the study was: "In the near term, the United States should adopt the European period of 10–11 years. However, research should be undertaken to determine whether this period is adequate, given the complexity and length of drug development today."

Reports: "Dark matter search results from the CDMS II experiment" by The CDMS II Collaboration (26 March, p. 1619). In the last sentence of the second paragraph, 10^{-6} should be 10^{6}.

TECHNICAL COMMENT ABSTRACTS

Comment on "Single-Crystal X-ray Structure of 1,3-Dimethylcyclobutadiene by Confinement in a Crystalline Matrix"

David Scheschkewitz

Legrand *et al*. (Reports, 16 July 2010, p. 299) reported on the photolytic reaction of an α-pyrone confined in a crystalline matrix. Their structural analysis invoked four products: activated precursor, isomeric Dewar β-lactone, and square and rectangular isomers of 1,3-dimethylcyclobutadiene. The reported x-ray data, however, suggest that all observed structures correspond to only one distinct species, the Dewar β-lactone.

Full text at www.sciencemag.org/cgi/content/full/330/6007/1047-c

Comment on "Single Crystal X-ray Structure of 1,3-Dimethylcyclobutadiene by Confinement in a Crystalline Matrix"

Igor V. Alabugin, Brian Gold, Michael Shatruk, Kirill Kovnir

Legrand *et al*. (Reports, 16 July 2010, p. 299) reported the experimental observation of square-planar and rectangular-bent geometries of 1,3-dimethylcyclobutadiene (Me_2CBD) confined within a crystalline matrix. However, we found no evidence for the Me_2CBD formation. We argue that the experimental x-ray density data are better attributed to the bicyclic β-lactone intermediate where carbon dioxide is covalently bound to cyclobutadiene.

Full text at www.sciencemag.org/cgi/content/full/330/6007/1047-d

Response to Comments on "Single-Crystal X-ray Structure of 1,3-Dimethylcyclobutadiene by Confinement in a Crystalline Matrix"

Yves-Marie Legrand, Arie van der Lee, Mihail Barboiu

Scheschkewitz and Alabugin *et al*. suggest that photolysis under confinement in a crystalline matrix of 4,6-dimethyl-α-pyrone does not yield the crystal structure of 1,3-dimethylcyclobutadiene (Me_2CBD) as we reported, but rather that of a 4,6-dimethyl-β-lactone intermediate. We provide arguments that the square-planar Me_2CBD^S/CO_2 complex and the rectangular-bent Me_2CBD^R molecule are stabilized under confinement by the guanidinium-sulfonate-calixarene host matrix used in our study.

Full text at www.sciencemag.org/cgi/content/full/330/6007/1047-e

Letters to the Editor

Letters (~300 words) discuss material published in *Science* in the previous 3 months or issues of general interest. They can be submitted through the Web (www.submit2science.org) or by regular mail (1200 New York Ave., NW, Washington, DC 20005, USA). Letters are not acknowledged upon receipt, nor are authors generally consulted before publication. Whether published in full or in part, letters are subject to editing for clarity and space.

Comment on "Single-Crystal X-ray Structure of 1,3-Dimethylcyclobutadiene by Confinement in a Crystalline Matrix"

David Scheschkewitz*

Legrand *et al*. (Reports, 16 July 2010, p. 299) reported on the photolytic reaction of an α-pyrone confined in a crystalline matrix. Their structural analysis invoked four products: activated precursor, isomeric Dewar β-lactone, and square and rectangular isomers of 1,3-dimethylcyclobutadiene. The reported x-ray data, however, suggest that all observed structures correspond to only one distinct species, the Dewar β-lactone.

The report by Legrand *et al*. (*1*) on the structure of 1,3-dimethylcyclobutadiene (Me_2CBD) in a crystalline guanidinium-sulfonate-calixarene (G_4C) matrix caught my attention, given a long-standing interest in phenomena associated with aromaticity and anti-aromaticity (*2*–*5*). The observation of the rectangular minimum and the square-planar transition state (or triplet state) of the highly reactive Me_2CBD as two distinguishable species inside the G_4C host promised major insights regarding the structure and bonding of cyclobutadiene, the archetypal anti-aromatic compound. Despite a recent report on bond length equalization in anti-aromatic pentaphenylborole (*6*), it was surprising that Me_2CBD in its square-planar form, that is, the bond-length–equalized triplet state [(*7*)], should be stable. Even more intriguingly, it was reported to coexist in close vicinity with a strongly bent CO_2 molecule, which had been retained in the G_4C host. Although hydrogen bonding to the guanidinium cations of G_4C may possibly affect the geometry of the CO_2 moiety, this seemed a rather remote possibility: In HF-CO_2 adducts, for instance, the CO_2 unit does not deviate from linearity (*8*). I therefore analyzed the x-ray diffraction studies reported by Legrand *et al*. in more depth.

Legrand *et al*. (*1*) interpreted the solid-state structures obtained after irradiation of a single crystal of 4,6-dimethyl-α-pyrone (Me_21) in a G_4C host (all species referred to hereafter are confined in G_4C) as due to the rearrangement of Me_21 via activated Me_21' to Dewar β-lactone Me_23. Further irradiation was claimed to result in decarboxylation of Me_23 to rectangular Me_2CBD^R and square-planar Me_2CBD^S (see Scheme 1). The relatively small carbon-oxygen distances between the CO_2 moiety and the CBD unit from 1.502 to 1.612 Å were attributed to van der Waals interactions even though they are fully in line with typical covalent single bonds. In particular, β-lactones exhibit C–O bonds of up to 1.553 Å (*9*). Notably, Legrand *et al*. do not discuss the even shorter distance of 1.41 Å between the carbon atoms of CO_2 and Me_2CBD^R after prolonged irradiation. I show here that the reported data are consistent with the photolytic formation and enantiomerization of Me_23 (*10*) without the need to invoke any other species (Scheme 1).

For the data obtained after the first irradiation of Me_21 (Fig. 1, A and B), Legrand *et al*. (*1*) applied a split model between Me_21 (50%) and a species referred to as Me_21' (50%), a more or less satisfactory description of the structure. Conversely, the split model including Me_2CBD^R-1 (22.7%) and Me_23 (77.3%) used for the data set obtained after a second period of irradiation (Fig. 1, C and D) is problematic. Atom C3 of Me_23 features a very large cigar-shaped ellipsoid that can only be due to two unmodeled positions of this atom. Its orientation toward the plane of the remaining ring atoms suggests that the use of a three-way split model including Me_21 could have resolved the issue. Therefore, the long C3–C6 distance in Me_23 (Fig. 2) is an artifact of this unresolved disorder involving Me_21, which has no C3–C6 bond at all. Because the main distinguishing feature between Me_21' and Me_23 is the C3–C6 bond length, it can be concluded that they both represent the Dewar β-lactone isomer. The shortening of the C2–C(3) and C3–C4 bonds of Me_23 is a typical librational effect of a large orthogonal displacement of an atom (cigar-shaped thermal ellipsoid) and thus an artifact.

There is also little topological difference between Me_2CBD^R-1 and Me_21'. The diagram in Fig. 2 shows barely significant deviations between the allegedly different compounds (<0.2 Å). To put these deviations into perspective, the two structures both assigned as Me_2CBD^R by Legrand *et al*. show C2–C3 bonds differing by 0.19 Å. Within the accuracy limits of the model, Me_2CBD^R-1 can therefore be regarded as the enantiomer of Me_21' (or Me_23).

The authors' interpretation of the third data set raises similar issues (Fig. 1, E and F). In this case, they applied a split model using Me_2CBD^R-2 (62.7%) and Me_2CBD^S (37.3%). Inspection of Me_2CBD^S confirms that it is almost identical to Me_21' (and thus with Me_23), now unperturbed due to the absence of the completely consumed starting material Me_21. Following the previous reasoning, Me_2CBD^R-2 is a somewhat distorted mirror image of Me_21' (and Me_23) as well.

Finally, the bond lengths of Me_2CBD^S shown in figure 4 in (*1*) are inconsistent with those deposited at the Cambridge Crystallographic Data Centre (CCSD 764868). Aside from the fact that

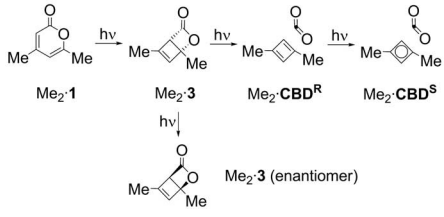

Scheme 1. Reaction proposed by Legrand *et al*. (*1*) (top) and reinterpretation presented here (bottom). The host, guanidinium-sulfonate-calixarene (G_4C), is not displayed.

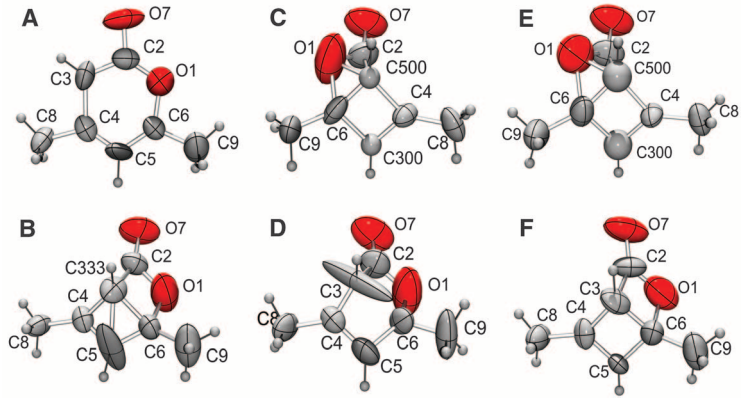

Fig. 1. Thermal ellipsoid plots of Me_21 (**A**), Me_21' (**B**), Me_2CBD^R-1 (**C**), Me_23 (**D**), Me_2CBD^R-2 (**E**), and Me_2CBD^S (**F**). Molecules are rotated to show topological similarities.

Imperial College London, Department of Chemistry, London SW7 2AZ, UK.

*To whom correspondence should be addressed. E-mail: d.scheschkewitz@imperial.ac.uk

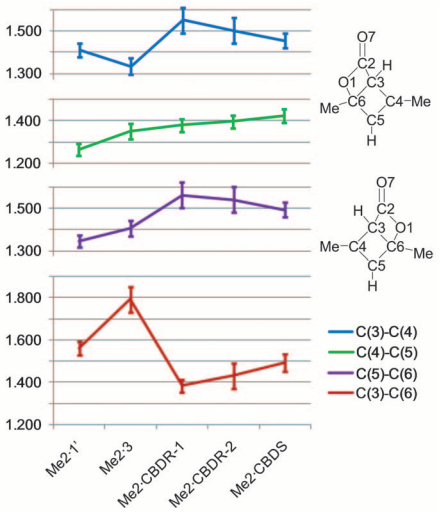

Fig. 2. Distances between endocyclic carbon atoms [data from CSD 764866 to 764868 (*1*)]. Error bars, 4 SD.

it is impossible to determine reliable bond lengths involving atom positions that are shared by two disordered molecules (C4 and C6), the bond lengths of Me_2CBD^S (Fig. 2) are not identical, but rather vary from 1.423 to 1.493 Å. The geometry of Me_2CBD^S is thus much closer to a rectangular arrangement than Legrand *et al.* (*1*) imply. Perhaps the strongest argument, however, is that the CO_2 moiety is hardly perturbed by the alleged changes of the CBD molecules. The carbon-oxygen bond lengths in all structures range from 1.319 to 1.347 Å for C2–O1 and from 1.163 to 1.178 Å for C2–O7, comparing favorably with the single (1.378 Å) and double bond (1.118 Å) of a bicyclic β-lactone closely related to $Me_2$3 (*11*).

In conclusion, Legrand *et al.* (*1*) are encouraged to thoroughly reinvestigate their crystallographic studies, maybe at lower temperatures. It can be anticipated that the formation of Dewar β-lactone, $Me_2$3, and its photolytically produced enantiomer will thus be confirmed rather than the presence of any cyclobutadiene derivative.

References and Notes

1. Y.-M. Legrand, A. van der Lee, M. Barboiu, *Science* **329**, 299 (2010).
2. K. Abersfelder, A. J. P. White, H. S. Rzepa, D. Scheschkewitz, *Science* **327**, 564 (2010).
3. M. Otto *et al.*, *Angew. Chem. Int. Ed.* **41**, 2275 (2002).
4. D. Scheschkewitz *et al.*, *Angew. Chem. Int. Ed.* **39**, 1272 (2000).
5. D. Scheschkewitz *et al.*, *Angew. Chem. Int. Ed.* **38**, 2936 (1999).
6. H. Braunschweig, I. Fernández, G. Frenking, T. Kupfer, *Angew. Chem. Int. Ed.* **47**, 1951 (2008).
7. O. Demel, K. R. Shamasundar, L. Kong, M. Nooijen, *J. Phys. Chem. A* **112**, 11895 (2008).
8. K. G. Tokhadze, A. I. Uspensky, Z. Mielke, Z. Latajka, H. Ratajczak, *J. Chem. Soc., Faraday Trans.* **92**, 3473 (1996).
9. J. Kaeobamrung, J. W. Bode, *Org. Lett.* **11**, 677 (2009).
10. G. Maier, H. P. Reisenauer, *Chem. Ber.* **114**, 3916 (1981).
11. J. Hegmann, M. Christl, K. Peters, E.-M. Peters, H. G. von Schnering, *Tetrahedron Lett.* **28**, 6429 (1987).
12. Financial support by the Aventis Foundation (Karl Winnacker fellowship) is gratefully acknowledged. I thank A. Berndt and W. Massa (Universität Marburg, Germany) for helpful discussions.

28 July 2010; accepted 25 October 2010
10.1126/science.1195752

Comment on "Single-Crystal X-ray Structure of 1,3-Dimethylcyclobutadiene by Confinement in a Crystalline Matrix"

Igor V. Alabugin,* Brian Gold, Michael Shatruk, Kirill Kovnir

Legrand *et al*. (Reports, 16 July 2010, p. 299) reported the experimental observation of square-planar and rectangular-bent geometries of 1,3-dimethylcyclobutadiene (Me_2CBD) confined within a crystalline matrix. However, we found no evidence for the Me_2CBD formation. We argue that the experimental x-ray density data are better attributed to the bicyclic β-lactone intermediate where carbon dioxide is covalently bound to cyclobutadiene.

Cyclobutadiene (CBD), the smallest neutral example of Hückel anti-aromaticity, has long been predicted to be a highly reactive species. Adding to the electronic instability is the ring strain created by the large deviation from the usual sp^2-trigonal geometry imposed by the four-membered ring. The shape and ground-state electron configuration of CBD were much debated until theoretical predictions converged on a rectangular singlet ground state rather than the Hückel's triplet, D_{4h} structure (*1*–*3*).

The challenge provided by anti-aromatic character and intrinsic instability of CBD inspired numerous experimental studies (*4*–*8*). The photochemical transformation of α-pyrone (*9*, *10*) (Scheme 1) confined within a matrix emerged as a promising route to this elusive molecule without protection provided by bulky substituents or transition metals (*11*).

Legrand *et al*. (*12*) redesigned Cram's approach (*13*) for trapping CBD in a hemicarcerand cage to the preparation of 1,3-dimethylcyclobutadiene (Me_2CBD) from 4,6-dimethyl-α-pyrone immobilized in a crystalline cavity of a host matrix at 175 K. Based on x-ray diffraction data, the authors suggested that the guest undergoes initial photochemical transformation into a 4,6-dimethyl-β-lactone Dewar intermediate (Scheme 1). Further irradiation was reported to push the reaction to completion via loss of CO_2 from the intermediate, thus "enabling the structure determination of 1,3-dimethylcyclobutadiene."

An exciting ramification is that these results would reveal direct x-ray structural information regarding CBD, "the Mona Lisa of organic chemistry" (*13*). Indeed, Legrand *et al*. reported the experimental observation of square-planar and rectangular-bent geometries in the host matrix (Fig. 1). The main part of the diffraction data (62.7%) for Me_2CBD was assigned to the square geometry (Me_2CBD^S), with the bent-rectangular form (Me_2CBD^R) being a minor component (37.3%). These preferences are opposite to theoretical predictions for an isolated CBD molecule (*1*–*3*), where the square form is expected to be a transition state between two Jahn-Teller distorted rectangles.

We were intrigued by this interpretation but identified a number of experimental inconsistencies. Initially, we were troubled by the unusually long (1.70 Å) C3–C6 bridge bond in the structure assigned to the bicyclic lactone. This value is only marginally lower than the longest known C–C bond (1.72 Å) (*14*, *15*) and deviates substantially from the theoretical value [1.55 Å, according to our density functional theory (DFT) calculations (*16*)]. There are large differences for other C–C bonds as well, e.g., $d_{C2\text{-}C3} = d_{C3\text{-}C4} =$ 1.37 Å versus 1.53 Å in theory. Even considering the effect imposed by the solid-state environment, the deviations are large enough to raise a concern about the accuracy of the results presented by Legrand *et al*. (*12*).

A stunning discrepancy, overlooked by Legrand *et al*. but obvious upon inspection of figure 4 in (*12*) (reproduced partially in Fig. 1 here) is that the "bystander" CO_2 molecule present in the cavity is strongly bent (119.9°)—a striking deviation from the textbook linear geometry but a good match for a trigonal planar carbon. According to the DFT calculations (*16*), such bending would cost ~75 kcal/mol, even without any additional structural distortions. Considering that one of the two C–O bonds in the reported x-ray geometry was shorter than the other (1.14 Å versus 1.34 Å), the overall penalty for the structural distortion from the optimal linear CO_2 increases to ~82 kcal/mol, a thermodynamic cost comparable in energy to a chemical bond.

Equally noteworthy are the very short distances between the CO_2 molecule and Me_2CBD: 1.50 and 1.61 Å. Legrand *et al*. attribute this finding to a "strong van der Waals contact" rather than to covalent bonding between the confined CO_2 and Me_2CBD^R molecules. This interpretation is questionable because the purported 1.50 Å C2–C3 van der Waals contact between Me_2CBD^S and CO_2 is shorter than the 1.56 Å C–C bond in Me_2CBD^R. Can a van der Waals contact really be shorter than a bond? The tabulated nonbonding van der Waals C–C and C–O contacts are 3.50 Å and 3.24 Å, respectively (*17*), both of them being substantially longer than the aforementioned "strong van der Waals" contacts.

On reexamination of the x-ray data of Legrand *et al*. (*12*), we found that the crystallographic results and their quality raise serious concerns about the conclusions drawn from them. A detailed assessment of the crystallographic work is given in the Supporting Online Material. Here, we will focus on the interpretation of structural parameters.

Figure 2 depicts the proposed bicyclic intermediate, along with alternative views of two components of the disordered Me_2CBD molecule, labeled according to Legrand *et al*. (*12*). It is immediately obvious that the C2–C3 bond length of 1.50(2) Å in Me_2CBD^S is comparable to those within the CBD unit. In Me_2CBD^R, this distance is even shorter, 1.41(3) Å, and three of the bonds in the CBD unit are longer than this value. The CO_2 and CBD units are thus almost certainly connected by a covalent C–C bond. In fact, the experimental x-ray density of Me_2CBD^S is better attributed to CO_2 covalently bound to CBD in a structure similar to the theoretically predicted geometry of the Dewar intermediate.

Why did CBD not form? We offer two possibilities: (i) free volume restrictions in the carcerand prevent the fragmentation or (ii) the bicyclic lactone is transparent in the 320- to 500-nm excitation range employed by the authors. It is known that the β-lactone intermediate only gives rise to CO_2 and CBD when irradiated with photons of

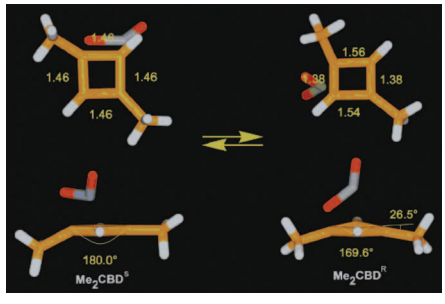

Fig. 1. Geometries of square (Me_2CDB^S) and rectangular-bent (Me_2CBD^R) dimethylcyclobutadiene from (*12*).

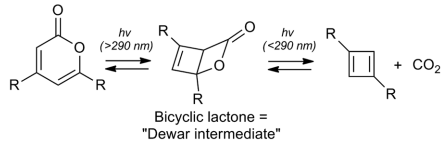

Scheme 1. Photochemical preparation of CBD derivatives from α-pyrone.

Department of Chemistry and Biochemistry, Florida State University, Tallahassee, FL 32306, USA.

*To whom correspondence should be addressed. E-mail: alabugin@chem.fsu.edu

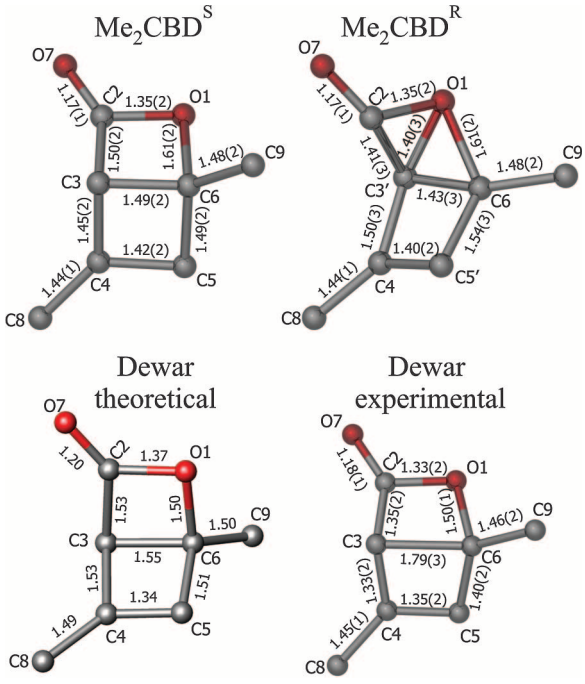

Fig. 2. Two components of crystallographic disorder of the guest molecule in the crystal structure of Me_2CBD (top) and theoretically calculated and experimentally suggested structure of the purported bicyclic intermediate (bottom). The bond lengths in Me_2CBD^S (top left) are very similar to those predicted theoretically for the Dewar intermediate (bottom left).

much higher energy (*18*) (Scheme 1). Interestingly, even in those cases, CO_2 is known to affect spectral properties of "free" CBD (*5*, *19*). Regrettably, we thus conclude that the crystallographic analysis of Me_2CBD remains an unsolved experimental challenge. The "Mona Lisa of organic chemistry" still smiles at us but keeps her secret.

References and Notes

1. J. L. Menke, E. V. Patterson, R. J. McMahon, *J. Phys. Chem. A* **114**, 6431 (2010).
2. A. Balková, R. J. Bartlett, *J. Chem. Phys.* **101**, 8972 (1994).
3. W. T. Borden, E. R. Davidson, P. Hart, *J. Am. Chem. Soc.* **100**, 388 (1978).
4. L. Watts, J. D. Fitzpatrick, R. Pettit, *J. Am. Chem. Soc.* **87**, 3253 (1965).
5. G. Maier, *Angew. Chem. Int. Ed. Engl.* **13**, 425 (1974).
6. T. Bally, S. Masamune, *Tetrahedron* **36**, 343 (1980).
7. B. R. Arnold, J. Michl, in *Kinetics and Spectroscopy of Carbenes and Biradicals*, M. S. Platz, Ed. (Plenum, New York, 1990), chap. 1.
8. D. W. Whitman, B. K. Carpenter, *J. Am. Chem. Soc.* **102**, 4272 (1980).
9. E. J. Corey, J. Streith, *J. Am. Chem. Soc.* **86**, 950 (1964).
10. M. Rosenblum, B. North, *J. Am. Chem. Soc.* **90**, 1060 (1968).
11. C. Y. Lin, A. Krantz, *J. Chem. Soc. Chem. Comm.* **1972**, 1111 (1972).
12. Y.-M. Legrand, A. van der Lee, M. Barboiu, *Science* **329**, 299 (2010).
13. D. J. Cram, M. E. Tanner, R. Thomas, *Angew. Chem. Int. Ed. Engl.* **30**, 1024 (1991).
14. F. Toda, *Eur. J. Org. Chem.* **2000**, 1377 (2000).
15. In the actual crystallographic information file provided as supporting information by Legrand *et al*. (*12*), this bond is even longer, 1.79(3) Å. Thus, there is also an obvious discrepancy between the values given in the text and those found in the crystal structure of the purported Dewar intermediate.
16. DFT calculations were performed at the B3LYP/6-31G** level of theory.
17. R. S. Rowland, R. Taylor, *J. Phys. Chem.* **100**, 7384 (1996).
18. O. L. Chapman, C. L. McIntosh, J. Pacansky, *J. Am. Chem. Soc.* **95**, 614 (1973).
19. R. G. S. Pong, B.-S. Huang, J. Laureni, A. Krantz, *J. Am. Chem. Soc.* **99**, 4153 (1977).

20. I.V.A. is funded in part by the National Science Foundation (CHE-0848686) and Petroleum Research Fund, administered by the American Chemical Society (Award 47590-AC4).

Supporting Online Material

www.sciencemag.org/cgi/content/full/330/6007/1047-d/DC1
SOM Text
Table S1

6 August 2010; accepted 25 October 2010
10.1126/science.1196188

Response to Comments on "Single-Crystal X-ray Structure of 1,3-Dimethylcyclobutadiene by Confinement in a Crystalline Matrix"

Yves-Marie Legrand, Arie van der Lee, Mihail Barboiu*

Scheschkewitz and Alabugin *et al*. suggest that photolysis under confinement in a crystalline matrix of 4,6-dimethyl-α-pyrone does not yield the crystal structure of 1,3-dimethylcyclobutadiene (Me_2CBD) as we reported, but rather that of a 4,6-dimethyl-β-lactone intermediate. We provide arguments that the square-planar Me_2CBD^S/CO_2 complex and the rectangular-bent Me_2CBD^R molecule are stabilized under confinement by the guanidinium-sulfonate-calixarene host matrix used in our study.

We recently reported the single-crystal x-ray structure of 1,3-dimethylcyclobutadiene synthesized within a guanidinium-sulfonate-calixarene (G_4C) crystalline matrix (*1*). Scheschkewitz (*2*) and Alabugin *et al*. (*3*) contend that our structures instead correspond with a bicyclic β-lactone intermediate. Our view on the importance of the quality of the x-ray data on structure resolution and the view of the Technical Comment authors coincide. In their comments, Scheschkewitz and Alabugin *et al*. consider our work as an unconvincing attempt, mainly due to the presumed poor quality of the experimental x-ray data. They fail, however, to place the crystallographic work in the particular context of highly advanced and challenging chemistry of unstable or reactive host-guest crystalline systems. A number of very comparable studies, albeit on other systems, have preceded our work (*4*–*7*), and the problems encountered are virtually the same as ours: resolved and unresolved disorder leading to results far from optimal data quality. Data and model quality are not expressed in a satisfactory way by just one or two numbers or parameters. Instead, a more or less complete set of parameters needs to be given to characterize the quality of data and model. Table S1 summarizes the different quality parameters for these very comparable studies (*1*, *4*–*7*) in the field of reactive host-guest crystalline systems. Our data are no worse than these studies, if not better, and in all cases the conclusion would be that the data warrants the structural model described in the paper. Our opinion is that all previous important contributions related to unstable molecules sequestered in porous crystals can reach their full potential.

The difficulties of experiments involving host-guest crystalline systems are related to the following factors: (i) in the case of nonreactive molecules (*4*, *5*), the multiple orientations of the guest in a host cavity induce disorder; (ii) in the case of reactional processes, inconsistent diffusion of the reagents or unequal distribution of the irradiation energy over the whole volume of the crystal also leads to disorder (*6*, *7*); and (iii) the preservation of the crystallinity of the host-matrix may be affected during the reactional process by a loss of water or solvent molecules. All these factors lead to what is called "poor" data quality. Data quality can indeed lead to alternative interpretations, as illustrated by the comments of Scheschkewitz (*2*) and Alabugin *et al*. (*3*). However, we show below that our interpretation is more likely.

Scheschkewitz and Alabugin *et al*. contest the atomistic interpretation we have derived from the electron density maps (*1*). Two general considerations are worth noting. First, an atomistic interpretation usually starts by assigning element types to the maxima observed in the phased electron density map. The electron density maps need subsequently to be interpreted in terms of a structurally logical interconnected set of bonds and angles, providing a full three-dimensional picture of unstable species as sequential snapshots of chemical reactions. It is indeed possible to get the desired structured model by using suitable restraints in the refinement, but this is not what we have done. Second, ab initio calculations and theoretical molecular models are highly valuable methods, but in order to be fairly compared with experimental data, they should be performed by considering the whole (crystalline host-matrix and guest molecule) as a unitary system, involving supplementary noncovalent interactions and supramolecular stabilization energies. This is very

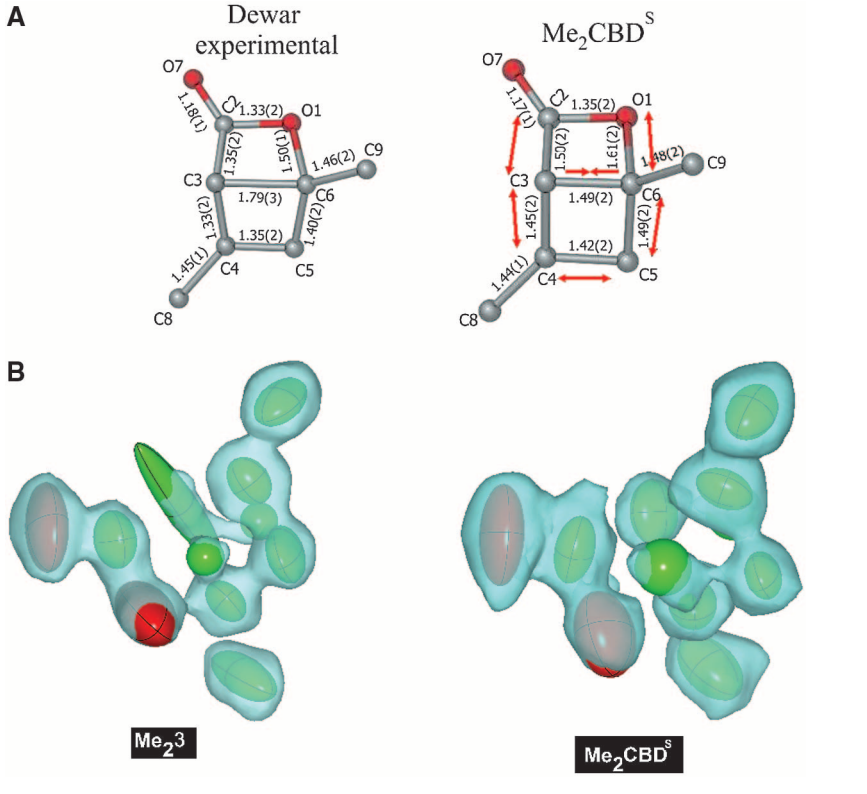

Fig. 1. (**A**) The bond lengths of Me_23 (left) and Me_2CBD^S (right) reproduced from Alabugin *et al*. (*3*). (**B**) Electron density maps for the x-ray crystal structure of Me_23 and Me_2CBD^S/CO_2 complex. Separate density maxima present on both sides of Me_23 and Me_2CBD^S correspond to conversion to Me_2CBD^R.

Adaptive Supramolecular Nanosystems Group, Institut Européen des Membranes, ENSCM-UMII-UMR-CNRS5635, Place Eugène Bataillon CC047, 34095 Montpellier Cedex 5, France.

*To whom correspondence should be addressed. E-mail: mihai.barboiu@iemm.univ-montp2.fr

difficult, and we have therefore limited ourselves to the analysis of the pure experimental data.

One of the most challenging aspects of our study (*1*) was to fit the appropriate host matrix with the active guest molecule, which underscores the importance of subtle noncovalent interactions for this kind of study. To be more precise, we were unsuccessful with cyclodextrine host systems or nonmethylated guest molecules until we imagined the {$G_4C \subset Me_21$} system. The G_4C host matrix offers a robust crystalline network, optimally immobilizing the 4,6-dimethyl-α-pyrone Me_21 molecule during the assembly of the crystal lattice (CCDC 764865). This fit is clearly almost optimal, considering that the guest Me_21 molecule is anchored via H-bonding and –CH-π interactions. Upon irradiation of $G_4C\{Me_21\}$, separate density maxima in the electronic density map were observed on both sides of the Me_21 ring (CCDC 764867), and the quality of the x-ray diffraction data set decreased, due to the appearance of resolved and nonresolved disorder within the crystal. Further irradiation induced conversion into $G_4C\{Me_23\&Me_2CBD^R\}$ (CCDC 764866). We agree that the bridging bond of 1.79 Å deviates substantially from the theoretical value. The cigar-shaped thermal ellipsoids for atom C3 in the structures of Me_21' and Me_23 could be real or indeed an artifact, as suggested by Scheschkewitz (*2*). Reexamination of the Fourier maps does not show separate maxima, but this does not mean per se that there is only one equilibrium site. Similar effects have been observed in (*7*). We only note that, if it really concerns dynamic disorder/thermal vibrations, the real C3–C6 distance (corrected for thermal motion effects) is even longer than that based on the distance between equilibrium sites (*8*). Based on the evolutive coherence between the different structures, we argue that the latter situation, that is, the one presented in (*7*), is the most likely one. Additionally, separate density maxima were detected on both sides of Me_23, corresponding to 22.7% conversion into Me_2CBD^R. Further irradiation led to the new geometry $G_4C\{Me_2CBD^S\&Me_2CBD^R\}$:$Me_2CBD^S/CO_2$ complex (62.7%) and Me_2CBD^R (37.3%) (CCDC 764868).

When unstable intermediates or products form in highly confined conditions, a complex random distribution of electron density maps inside the cavity is observed. Our experiments (*1*) resulted in the formation of a limited number of peaks showing specific relative geometrical positions into the cavity aligning along the sulfonate groups,

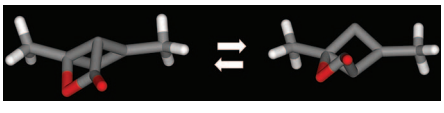

Fig. 2. Based on observed x-ray structures, the overall penalty for structural distortion during the enantiomerization reaction of Dewar-β-lactone as proposed by Scheschkewitz (*2*) is 212 kcal/mol (calculated in the gas phase).

as shown in fig. S2. Regarding the question of whether Me_23 transforms into the Me_2CBD^S/CO_2 complex, we argue that the latter complex, that is, the one presented in (*1*), is forming in such confined conditions. First, we observe two important geometrical tendencies when Me_23 transforms into Me_2CBD^S/CO_2: (i) the C2–C3 and C6–O1 bonds expand to 1.50 Å (1.54 Å after new refinements) and 1.61 Å, respectively, and (ii) the $C_3C_4C_5C_6$ ring tends toward a square geometry with a mean side length of 1.46 ± 0.04 Å. Another element showing the tendency of CO_2 to separate from CBD is the shape of the electronic clouds of the CO_2 atoms, which, in the Me_2CBD^S structure, are becoming oval and slightly bigger (Fig. 1B). Meanwhile, the electronic clouds of the $C_3C_4C_5C_6$ ring atoms are more localized. Linked by covalent bonds, the CO_2 and the $C_3C_4C_5C_6$ ring electronic clouds would be modified in a similar manner. Consequently, the CO_2 molecule is tending to leave the system, and simultaneously the $C_3C_4C_5C_6$ ring adopts a square geometry, different from the calculated and experimental trapezoidal geometry of the Dewar-β-lactone corresponding ring (Fig. 1A). Second, bending of CO_2 when interacting with other molecular units has previously been shown. The CO_2–IV phase structure confirms that at high pressure (a scenario not very different from confined conditions), CO_2 molecules are nonlinear (*9*). Interactions with metals (*10*) or metal ions (*11*), or ultraviolet photoreactions (*12*–*14*) can also produce bent states of CO_2. Third, Maier *et al.* (*15*) and Pong *et al.* (*16*) independently showed the tendency of cyclobutadiene to undergo strong association with ligands (including CO_2) constrained to remain in close proximity by a solid matrix. The model proposed by Pong *et al.* (*15*), based on asymmetric vibrational bands of a strongly interacting CO_2/cyclobutadiene system in which the CO_2 molecule bends in either a perpendicular or parallel manner relative to the plane of the cyclobutadiene, can unambiguously correlate with our experimental structure. Finally, under photoexcitation conditions, the formation of a bent CO_2 radical anion (*12*, *13*) in interaction with the Me_2CBD^S radical cation via strong ionic bonds—more in line with the observed C2–C3 and C6–O1 distances—seems reasonable because the host matrix is ionic and polar. We agree with Scheschkewitz (*2*) and Alabugin *et al.* (*3*) that much research remains to be done to experimentally characterize the Me_2CBD^S/CO_2 complex structure.

Regarding the Me_2CBD^R rectangular geometry, the CO_2 is perpendicularly oriented with respect to the $C_3C_4C_5C_6$ ring of Me_2CBD^S, and a proposed Dewar-β-lactone enantiomer Me_2CBD^R (*2*) does not fit with the distorted structure as presented in Fig. 2. Moreover, one might argue that the CO_2 molecule could not be in such vicinity with Me_2CBD^R and therefore is not present in the elementary cell where Me_2CBD^R is present, because of some fairly short distances as outlined in (*2*, *3*). Indeed, alternative refinements show that if the occupancy of the O7–C2–O1 part is refined freely, it drops down from 1.0 to 0.83, as compared with an occupation of 0.63 for Me_2CBD^S. Moreover, the coordinates and thermal parameter (U_{eq}) values of O7 and O1 are relatively high both in the initial model (both 0.14 $Å^2$) and the first alternative one (~0.11 $Å^2$). However, if the occupancy of the CO_2 part is constrained to be equal to the occupancy of Me_2CBD^S, it comes out at 0.73, with U_{eq} values of 0.09 $Å^2$ for O1 and O7, nearly equal to that of C3 (0.10 $Å^2$). Crystallographic agreement factors are very close to each other, but slightly lower for the first and second alternative models (R_F = 0.0797 and 0.0799, respectively) than for the initial model (R_F = 0.0809).

For a more lengthy discussion about the quality of the x-ray data questioned by Alabugin *et al.* (*3*) and more comments about table S1, see the Supporting Online Material of this Response.

In conclusion, we observed two distinct geometries: the square-planar Me_2CBD^S/CO_2 complex and the rectangular-bent Me_2CBD^R molecule, stabilized under confinement by the G_4C host matrix. We believe that the key to making additional progress in understanding the formation of CBD structures in confined conditions is to further improve the supramolecular design of the crystalline hosts and to develop new analytical capabilities. Reducing the uncertainty in CBD formation in the solid state under confined conditions will principally require the design of new complementary host-guest systems that reduce the disorder problem that has so far been an unavoidable challenge.

References

1. Y. M. Legrand, A. van der Lee, M. Barboiu, *Science* **329**, 299 (2010).
2. D. Scheschkewitz, *Science* **330**, 1047 (2010); www.sciencemag.org/cgi/content/full/330/6007/1047-c.
3. I. V. Alabugin, B. Gold, M. Shatruk, K. Kovnir, *Science* **330**, 1047 (2010); www.sciencemag.org/cgi/content/full/330/6007/1047-d.
4. D. Normile, B. Breiner, K. Rissanen, J. R. Nitchke, *Science* **324**, 169 (2009).
5. I. A. Riddell, M. M. J. Smulders, J. K. Clegg, J. R. Nitschke, *Chem. Commun. (Camb.)* (2010).
6. A. J. Blake *et al.*, *Nature Chem.* **2**, 688 (2010).
7. T. Kawamichi, T. Haneda, M. Kawano, M. Fujita, *Nature* **461**, 633 (2009).
8. W. R. Busing, H. A. Levy, *Acta Crystallogr.* **17**, 142 (1964).
9. J. H. Park *et al.*, *Phys. Rev. B* **68**, 014107 (2003).
10. H. J. Freund, R. P. Mesmer, *Surf. Sci.* **172**, 1 (1986).
11. T. A. Hanna, A. M. Baranger, R. G. Bergman, *J. Am. Chem. Soc.* **117**, 11363 (1995).
12. R. D. Richardson, B. K. Carpenter, *J. Am. Chem. Soc.* **130**, 3169 (2008).
13. M. Chiesa, E. Giamello, *Chem. Eur. J.* **13**, 1261 (2007).
14. M. Y. Zhang, B. K. Carpenter, F. W. Mclafferty, *J. Am. Chem. Soc.* **113**, 9499 (1991).
15. G. Maier, H.-G. Hartan, T. Sayrac, *Angew. Chem. Int. Ed. Engl.* **15**, 226 (1976).
16. R. G. S. Pong, B. S. Huang, J. Laureni, A. Krantz, *J. Am. Chem. Soc.* **99**, 4153 (1977).

Supporting Online Material

www.sciencemag.org/cgi/content/full/330/6007/1047-e/DC1
SOM Text
Figs. S1 to S3
Table S1

30 August 2010; accepted 26 October 2010
10.1126/science.1195846

EVOLUTION

A Law by Any Other Name Would Smell as Sweet

Roberta L. Millstein

Biology's First Law
The Tendency for Diversity and Complexity to Increase in Evolutionary Systems
by Daniel W. McShea and Robert N. Brandon
University of Chicago Press, Chicago, 2010. 184 pp. $55, £35.50. ISBN 9780226562254. Paper, $20, £13. ISBN 9780226562261.

The laws of physics are sufficiently well known that they have permeated popular culture. This is especially true of Newton's laws of motion: Everyone has heard that "an object in motion will stay in motion unless an external force acts on it" (Newton's first law) and "for every action, there is an equal and opposite reaction" (Newton's third law). Even $F = ma$ (Newton's second law) is fairly well known. But what of the laws of biology? Does biology even have any laws?

Biologists and philosophers of biology have been debating this question for decades. Some take the position that biology lacks laws—that the contingency of evolutionary processes means that biological entities and processes are not lawlike. Others argue that it does have laws, e.g., the principle of natural selection itself.

Biologist Daniel McShea and philosopher of biology Robert Brandon dive into this debate with their provocative *Biology's First Law: The Tendency for Diversity and Complexity to Increase in Evolutionary Systems*. McShea and Brandon (both at Duke University) boldly contend that they have uncovered a "zero-force law" for biology that is analogous to Newton's first law (also called "the law of inertia"). The basic idea behind their proposed "Zero-Force Evolutionary Law" (ZFEL) can be understood through one of the thought experiments they describe in the book. Imagine a yard containing a number of trees, and imagine that the wind blows from each point of the compass with equal probability. Come autumn, the result will be an increase in the dispersal of the leaves over time. This, they suggest, is a zero-force state because there are no directional forces acting on the leaves. Yet there is a change over time (unlike the phenomenon described by the law of inertia in physics)—the leaves that were originally clustered about the trees become more dispersed. And if an evolutionary system is similarly in a zero-force state, it too will experience an increase in divergence over time. More formally:

> ZFEL (special formulation): In any evolutionary system in which there is variation and heredity, in the absence of natural selection, other forces, and constraints acting on diversity or complexity, diversity and complexity will increase on average.

If the leaves were not free to blow in any direction—say, for example, they were to encounter a barrier such as a garage—there would still be a tendency for the leaves to disperse. However, because of the constraint, their dispersal may not in fact increase. This gives rise to an alternate formulation of the ZFEL:

> ZFEL (general formulation): In any evolutionary system in which there is variation and heredity, there is a tendency for diversity and complexity to increase, one that is always present but may be opposed or augmented by natural selection, other forces, or constraints acting on diversity or complexity.

McShea and Brandon devote the book to clarifying the terms contained in the ZFEL (complexity, for instance, is used in a fairly nonstandard way), describing numerous empirical studies that they claim provide evidence supporting their law, and discussing some of the law's implications for various issues in biology and the philosophy of biology. They insist that the ZFEL requires a "gestalt shift" in the way we think about evolutionary biology: Although we have believed that it is change that is in need of explanation, the ZFEL reveals that change is the default state. At every level of the biological hierarchy for which there is heritable variation (genes, organelles, organisms, species, etc.), it is stasis that requires explanation.

Two questions arise, however: Is the ZFEL a law at all? And if it is, is it actually a zero-force law? With respect to the first question, there has been considerable debate in the philosophy of science over the nature of scientific laws. But we can set those complexities aside because McShea and Brandon use a fairly traditional conception of scientific law: an empirical generalization that is true everywhere and always. They have no doubt described a universal generalization; it is in the claim that the law is empirical that a problem arises. As the authors themselves note, the basic idea behind the ZFEL arises from probability theory. Take a set of particles and let them all begin at position zero. At each successive unit of time, let each particle have an equal probability of increasing or decreasing its position by one. The longer the period of time, the more divergent the particles will be from one another on average.

That divergence will increase under these conditions is well known, but why is it an empirical claim about the world? The authors say that it isn't true by definition that divergence will increase, and it is certainly not logically impossible for divergence to decrease. Thus, the generalization is empirical. And yet, by this characterization of "empirical," the "law of large numbers" is empirical and the claim that if we toss a fair coin a large number of times the percentage of heads will approach 50% is empirical. This is at best a very weak notion of "empirical"; the generalization certainly does not seem to be mak-

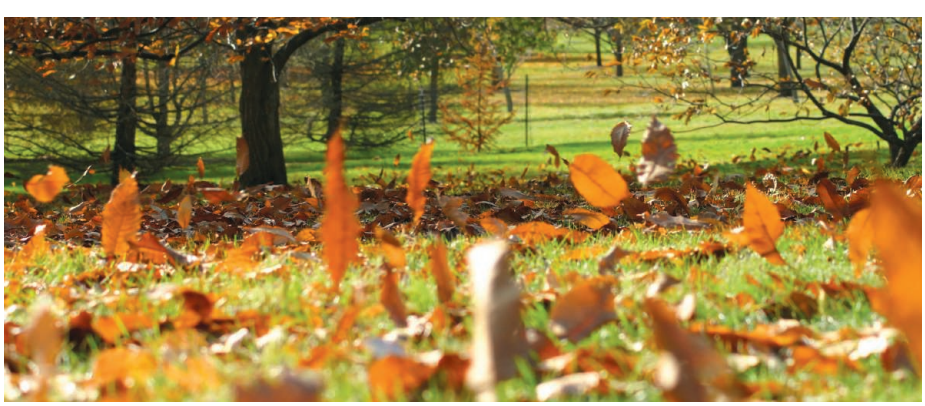

CREDIT: JODY DINGLE/ISTOCKPHOTO.COM

Dispersing leaves. A thought experiment for a zero-force state.

The reviewer is at the Department of Philosophy, University of California, Davis, One Shields Avenue, Davis, CA 95616, USA. E-mail: RLMillstein@ucdavis.edu

Published by AAAS

ing a substantive claim about the world in the same way that the law of inertia does. It can be proven mathematically; it does not need to be tested.

Even granting McShea and Brandon's claim that the ZFEL is a law, the question remains whether it is a zero-force law. Recall the leaf-blowing thought experiment. Is that really a zero-force state? We might have taken the wind to constitute a force acting on the leaves, but the authors seem to suggest that we should not count it as a force because it is not directional. This appears to me to be splitting hairs: If not a force in that technical sense, the wind is surely a cause, one that influences the various locations of the leaves. (And in the book McShea and Brandon give every reason to think they would see the wind as a cause.) In the ZFEL, new variation arising randomly plays the role of the wind. To cite one of the authors' many examples, if we had a number of populations of the same species in different environments, each undergoing natural selection in different ways, there would be a tendency (in the absence of constraints) for the populations to diverge from one another. The variations introduced into each population from the different selection pressures would be "random with respect to each other" and thus satisfy that criterion of the ZFEL. But surely these are different causes acting, with the unsurprising result that different effects occur. It is not clear why these causes would be any different in status from the causes acting in a situation where each population were in a similar environment, each undergoing natural selection in a similar way. There is no reason to think that the situation where the populations are undergoing natural selection in different ways is more fundamental, or more of a "zero-force" state, than the situation in which they are undergoing natural selection in the same way. And once we acknowledge that, it becomes even more unclear why certain causes (namely, random variation and heredity) are considered to be an omnipresent background, whereas other causes are picked out as constraints or forces acting against a "spontaneous" (McShea and Brandon's term) tendency.

What happens, then, if (in spite of its name) the ZFEL isn't really a zero-force law at all? The authors' generalization loses some of its rhetorical punch, perhaps, but punch isn't everything. There is a very interesting question lurking beneath the rhetoric of zero-force law (and, sadly, it risks being overshadowed by that rhetoric): Considering every level of the biological hierarchy, how prevalent are biological systems that satisfy the assumptions of the ZFEL—namely, heredity and random variation—with or without constraints or countervailing forces? If the answer turns out to be "most" or even "many," then McShea and Brandon will have drawn our attention to a widely applicable generalization that was known in particular cases without us necessarily having seen the forest for the trees. And even if the answer turns out to be "few," it still means that in each case we will have to consider whether we need to invoke special explanations for observed increases in diversity over time. A generalization does not have be a zero-force law, or a law at all, in order to be important, useful, and informative.

10.1126/science.1197366

From Populations to Ecosystems
Theoretical Foundations for a New Ecological Synthesis
by Michel Loreau
Princeton University Press, Princeton, NJ, 2010. 316 pp. $99.50, £69.95. ISBN 9780691122694. Paper, $45, £30.95. ISBN 9780691122700. Monographs in Population Biology, 46.

ECOLOGY

Why a Grand Unified Theory Is Neither Feasible nor Desirable

Tadashi Fukami

Ecology as a scientific discipline struggles with the dilemma of generality versus specificity. Robert MacArthur, a founder of modern ecology, reminded us that "Science should be general in its principles" (*1*). But many researchers, presumably including MacArthur himself, have been drawn to the discipline because of a fascination with the diversity of organisms and ecosystems. We love to learn the unique details of ecological phenomena. Of course, a widely recognized problem of working with a specific focus is that it prevents us from seeing the grand scheme of how nature works, which can in turn limit our understanding of details.

This problem is relevant not only to organisms or ecosystems but also to specific subdisciplines, each concerned with a particular

The reviewer is at the Department of Biology, Stanford University, Stanford, CA 94305, USA. E-mail: fukamit@stanford.edu

Bridging subdisciplines. Loreau offers a theoretical framework for linking population biology, community ecology, and ecosystem analysis.

level of biological organization (from populations to communities to ecosystems). It presents a challenge to the many who are searching for overarching principles that would meld the subfields. Attempts to develop unified general theories have proliferated in the ecological literature in recent years. But how general is general enough? If the utility of a general theory is determined by its level of generality, then the more general the better—with the ultimate goal being the formation of a single overarching ecological theory. However, the attendant simplification that comes with generalization forces us to ignore the very details about organisms and ecosystems that drew us to ecology in the first place.

A recent addition to the Monographs in Population Biology series [which began in 1967 with a contribution from MacArthur and E. O. Wilson (*2*)] powerfully presents one solution to this persistent dilemma. In *From Populations to Ecosystems: Theoretical Foundations for a New Ecological Synthesis*, Michel Loreau argues that an effective way forward is to give up building a single unified theory of ecology altogether. Loreau (a theoretical ecologist at McGill University) believes that "a monolithic unified theory of ecology is neither feasible nor desirable." As an alternative approach, he advocates theoretical merging of closely related, yet separately developed subdisciplines.

The merging (or bridge-laying) Loreau advocates involves translating different "languages" used in the mathematical models developed separately in various subdisciplines into a common language so that the subfields can talk to one another. Although this approach does not yield a truly unified theory, it helps, Loreau argues, to "generate new principles, perspectives, and questions at the interface between different subdisciplines and thereby contribute to the emergence of a new ecological synthesis that transcends traditional boundaries." Taking this tack, one gets a sense that the problem with specialization in subdisciplines can be solved by theoretical bridging without having to trade specificity for generality.

An elegant example of the author's approach can be seen in the work conducted by him and his colleagues over the past decade or so that merges two major subdisciplines of ecology, community ecology and ecosystem ecology. Loreau devotes much of the book to recounting this body of research. He starts by summarizing essential elements of the mathematical models developed in the two subdisciplines. He then discusses how the two sets of models, though developed separately and with apparently distinct sets of equations, can be merged by basing the two on a common currency: the mass and energy budgets of individual organisms. Once this translation is accomplished, new models that simultaneously consider the composition of coexisting species (the focus of traditional community ecology) and the flow of materials through functional compartments of ecosystems (the focus of traditional ecosystem ecology) can be built and analyzed. These allow one to study reciprocal influences between species composition and material flows in the ecosystem.

As Loreau acknowledges, his is not the first book to advocate this type of theoretical merging. In particular, the approach he presents resembles that laid out in an influential 1992 book by Donald DeAngelis (*3*). What makes Loreau's contribution novel and creative is his successful application of the merging approach to understanding the functional consequences of biodiversity loss, the topic that has received perhaps greater attention than any other ecological issue over the past two decades because of its broad social implications. Loreau's theoretical work has subsequently stimulated empirical investigation of community assembly as a fundamental process underlying the relationship between biodiversity and ecosystem functioning over both ecological (*4*) and evolutionary (*5*) time scales. Although more empirical evidence is needed, Loreau also discusses how similar types of theoretical merging can be useful for linking spatial ecology and evolutionary ecology with the now integrated community-ecosystem ecology. Looking further ahead, he suggests linking ecology more tightly to stoichiometry, genomics, and economics as future research directions that can benefit from more theoretical bridging.

For those readers who expect a truly unified theory of ecology from such ambitious words as "theoretical foundations" and "new ecological synthesis" used in its title, *From Populations to Ecosystems* may be disappointing. Certainly, although not pursued in the book, the ongoing search for greater unified theories should be continued, as it can help us see similarities among disparate systems and levels of organization. It seems likely, however, that ecology is inherently not a discipline in which a single general theory can be developed (*6*), a characteristic that leaves the apparent generality-specificity dilemma unresolved. In this light, Loreau's book demonstrates a valuable approach that eliminates the dilemma to a large extent, opening up exciting new avenues of research.

References

1. R. H. MacArthur, *Geographical Ecology* (Princeton Univ. Press, Princeton, NJ, 1972).
2. R. H. MacArthur, E. O. Wilson, *The Theory of Island Biogeography* (Princeton Univ. Press, Princeton, NJ, 1967).
3. D. L. DeAngelis, *Dynamics of Nutrient Cycling and Food Webs* (Chapman and Hall, London, 1992).
4. T. Fukami *et al.*, *Ecol. Lett.* **13**, 675 (2010).
5. P. A. Venail *et al.*, *Nature* **452**, 210 (2008).
6. D. Simberloff, *Am. Nat.* **163**, 787 (2004).

10.1126/science.1197441

FOOD SAFETY

Genetically Modified Salmon and Full Impact Assessment

Health and environmental impacts of GM salmon hinge on aggregate market size, which current regulatory processes ignore.

Martin D. Smith,[1,2]* Frank Asche,[3] Atle G. Guttormsen,[4] Jonathan B. Wiener[1,5,6]

As the U.S. Food and Drug Administration (FDA) considers approving a genetically modified (GM) Atlantic salmon (*Salmo salar*), it faces fundamental questions of risk analysis and impact assessment. The GM salmon—whose genome contains an inserted growth gene from Pacific chinook salmon (*Oncorhynchus tshawytscha*) and a switch-on gene from ocean pout (*Zoarces americanus*)—would be the first transgenic animal approved for human consumption in the United States (*1*, *2*). But the mechanism for its approval, FDA's new animal drug application (NADA) process (*2*), narrowly examines only the risks of each GM salmon compared with a non-GM salmon (*2*, *3*). This approach fails to acknowledge that the new product's attributes may affect total production and consumption of salmon. This potentially excludes major human health and environmental impacts, both benefits and risks. Regulators need to consider the full scope of such impacts in risk analyses to avoid unintended consequences (*4*), yet FDA does not consider ancillary benefits and risks from salmon market expansion (*2*, *3*), a result of what may be an overly narrow interpretation of statutes.

Alternatively, if FDA currently lacks the statutory authority to evaluate the full impacts of growth in the salmon market, then Congress should grant FDA the authority to evaluate these broader impacts of food innovations and should provide funding to build the necessary capacity. Because the approval of GM salmon will set an important precedent for GM animals intended for human consumption, it is essential to establish an approval process that assesses the full portfolio of impacts to ensure that such decisions serve society's best interests.

[1]Nicholas School of the Environment, Duke University, Durham, NC 27708, USA. [2]Department of Economics, Duke University, Durham, NC 27708, USA. [3]Department of Industrial Economics, University of Stavanger, 4036 Stavanger, Norway. [4]Department of Economics and Resource Management, Norwegian University of Life Sciences, 1432 Aas, Norway. [5]School of Law and Sanford School of Public Policy, Duke University, Durham, NC 27708, USA. [6]Resources for the Future, Washington, DC 20036, USA.

*Author for correspondence: E-mail: marsmith@duke.edu

"Materially Equivalent" Assessment

Aqua Bounty Technologies, the developer of the product, claims that its AquAdvantage Salmon is different from "standard" Atlantic salmon in two ways: It grows faster and it requires less feed to grow (*5*). FDA is evaluating these claims and whether each GM salmon is "materially equivalent" to a non-GM salmon (*2*, *3*). Health risks are quantified by comparing the nutritional profile of a GM salmon to a non-GM salmon and screening for known toxins and allergens (*2*).

Although comparing health information for GM and non-GM salmon is essential, quantifying risks in this manner implicitly (and implausibly) assumes that the new product will simply replace the old one in the market and that the new product leads to no changes in aggregate market prices and quantities. In fact, the consequences of small differences in the nutritional and health profiles (if any) of one GM salmon compared with one non-GM salmon could be dwarfed by the public health benefits from substantial growth in the salmon market and from the eating of more salmon in place of other proteins such as beef.

Market Transformation and Public Health

The AquAdvantage Salmon could lower the costs of production by reducing the amount of feed and other inputs needed to produce one salmon. Declining costs from technological innovation have led to increased salmon production (*6*, *7*), so much so that, despite increased demand from rising incomes, real salmon prices (i.e., adjusted for inflation) have declined [Supporting Online Material (SOM), see the figure]. U.S. per capita salmon consumption doubled between 1994 and 2004 (1.1 to 2.2 pounds/year or 0.5 to 1 kg/year) (*8*), even as real prices for substitute animal proteins like beef fell (SOM). Salmon prices fell faster than beef prices from 1981 to 2009. Because changes in relative price [e.g., salmon relative to beef (SOM)] drive changing patterns in animal protein consumption (*9*), these trends augur future market growth if GM salmon lowers production costs.

For adults, overall health benefits exceed health risks from consuming fish (*4*, *10*). Of the 10 most frequently consumed fish in the United States, salmon has the highest levels of omega-3 fatty acids, which are thought to reduce coronary heart disease (*9*, *10*). For American adults who currently eat no fish, consumption of just one serving of salmon per week can reduce risk of coronary death by 36% (*10*) (SOM). Omega-3s are also essential for fetal brain development (*11*). Thus, if GM salmon expands the aggregate salmon market, more consumers will eat more

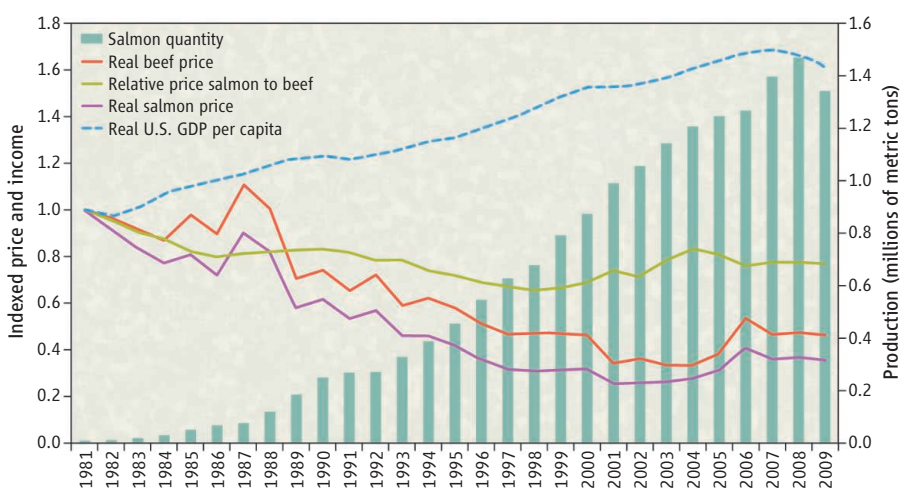

Prices, income, and salmon production. The real price (adjusted for inflation) of salmon and the relative price of salmon to beef have decreased as salmon production and real income have increased. Prices and GDP indexed to 1981 values. See SOM for details.

Published by AAAS

salmon and less of other proteins that are lower in omega-3 fatty acids, which would improve public health. GM salmon could put fresh salmon in reach as a protein source for low-income households susceptible to conditions linked to poor nutrition (*12*) (SOM).

If Congress wants FDA to promote healthier diets, lowering the price of healthy choices could be crucial. GM salmon could thus be not only the first transgenic animal approved for human consumption, but also the first GM food for which the price decrease from technological innovation itself promotes health benefits from increased consumption.

Environmental Impacts

FDA's focus on evaluating one GM fish with respect to one non-GM fish also presents an incomplete picture of aggregate environmental risks and benefits. FDA, like any federal agency, has a mandate to assess environmental impacts of its actions under the National Environmental Policy Act (NEPA) (*13*, *14*). Environmental concerns about salmon farming, which would increase in an expanded market, include local pollution from waste effluents, disease, and potentially increased pressure on wild fish stocks that provide sources of feed for salmon (*15*, *16*).

But potential impacts of escaped GM salmon on wild salmon (through either gene transfer or ecological competition) have dominated the discussion (*1*, *17*). Because Atlantic salmon was only recently domesticated, gene transfer to its wild cousins appears plausible. The current NADA for AquAdvantage Salmon applies to only two particular facilities, from which the escape risks appear minimal (*3*, *5*). Expanding production to other facilities (and increasing supply) could increase the risk of escape, but would also require FDA approval of an amended NADA (*3*).

The NADA for AquAdvantage Salmon neglects potential impacts of market expansion on the global commons that support the fish meal and/or fish oil trade as inputs (i.e., feed) to salmon farming. If each GM salmon substitutes for just one non-GM farmed salmon, as FDA's evaluation assumes, then waste effluent and pressure on wild sources of fish meal and oil would decline because the GM salmon require less feed to grow than do non-GM salmon (*5*). But if introducing GM salmon expands the aggregate market enough to compensate for the reduction of fish meal and oil input per salmon with the new technology, then demand for fish meal and oil will increase. The environmental risks of this increase are debatable (*6*, *18*). Salmon farming currently consumes 40% of world fish oil production. Commercial feed uses about 3 kg of wild fish to produce 1 kg of salmon. Although the ratio has decreased over time, the technology to produce feed without ingredients from fatty fish that only exist in the wild is not available (*19*).

The extent to which salmon market growth would pressure wild stocks (the inputs to salmon farming) will hinge on how well institutions manage these stocks (*20*). If well managed, increased demand will increase returns to fisheries; but if stocks are not well managed, demand growth will exacerbate overfishing (*20*, *21*). Changes in product markets can lead to unintended environmental impacts in input markets. For example, policies to promote ethanol, intended to reduce air pollution and greenhouse gas (GHG) emissions from automobiles, may induce land use changes (to grow inputs for ethanol production) that release even greater GHG emissions (*22*). When environmental or health externalities of a new technology or policy depend on market size, a full impact assessment can help to avoid unintended consequences.

FDA Mandate and Congressional Action

FDA's mandate is to determine whether a new animal drug is "safe" (*23*) and to examine its environmental impacts (*13*, *14*). The term "safe" is not defined in the statutes, which use it in reference to "health of man or animal" and "cumulative effect on man or animal" (*24*, *25*). FDA is applying a narrow analysis of "safety" in which it compares a portion of GM fish to an equivalent portion of non-GM fish (*2*, *3*). This narrow focus may derive from FDA's decision to treat GM fish as an animal drug rather than as a food; aggregate exposure to a drug is substantially shaped by disease incidence, whereas aggregate exposure to a food is driven more by market prices. Congress could facilitate broader analysis by giving FDA resources to better integrate biology and economics.

To expand its scope, FDA could broadly interpret the terms "safe" and "health" to include the overall safety of the new fish in the consumer's diet (compared with other foods that the new fish would replace, such as beef) and the overall public health effects of the new fish supply. A broader FDA interpretation of the ambiguous term "safe" could be upheld by the courts under longstanding doctrines of administrative law (*26*). If FDA declines to broaden its interpretation, or if it did so and the courts demurred, then Congress should amend the statute to empower and fund FDA to conduct a full impact assessment. Meanwhile, NEPA mandates FDA to assess the significant environmental impacts from market expansion that it is currently ignoring (*13*).

A narrow definition of "safe" that does not consider aggregate market size ignores the reality that people need to eat some form of protein and may choose to eat more of a new product if it costs less. Instead of focusing on the safety of food taken one portion at a time (or whether it was produced with molecular GM techniques versus classic breeding methods), a more useful approach would be to evaluate whether society is better off overall with the new product on the market than without it (*4*). Although FDA's narrow analysis might lead it to a decision that promotes the overall best interests of the public anyway, sound decision-making in this and future cases warrants a broader analysis of the full set of important consequences.

FDA ultimately will need to decide on the scope of broader impacts to assess by weighing the benefits of more information against the costs of doing more analysis and delaying the decision. In the case of GM salmon, a reasonable compromise would be to use existing studies to develop scenarios of market growth and the resulting broader human health and environmental impacts.

References and Notes

1. A. Pollack, *New York Times*, 25 June 2010, p. A1.
2. Center for Veterinary Medicine (CVM), FDA, *Guidance for Industry: Regulation of Genetically Engineered Animals Containing Heritable Recombinant DNA Constructs* (Report 187, CVM, Rockville, MD, 2009).
3. Veterinary Medicine Advisory Committee (VMAC), CVM, FDA, "VMAC Briefing Packet for AquAdvantage Salmon" (CVM, Rockville, MD, 2010).
4. J. D. Graham, J. B. Wiener, *Risk vs. Risk: Tradeoffs in Protecting Health and the Environment* (Harvard Univ. Press, Cambridge, MA, 1995).
5. AquaBounty Technologies, Inc., "Environmental Assessment for AquAdvantage Salmon" (AquaBounty Technologies, Waltham, MA, 2010).
6. F. Asche, *Mar. Resour. Econ.* **23**, 507 (2008).
7. A. G. Guttormsen, *Mar. Resour. Econ.* **17**, 91 (2002).
8. Food and Nutrition Board, Institute of Medicine, *Seafood Choices: Balancing Benefits and Risks* (National Academies Press, Washington, DC, 2007).
9. J. A. Chalfant, J. M. Alston, *J. Polit. Econ.* **96**, 391 (1988).
10. D. Mozaffarian, E. B. Rimm, *JAMA* **296**, 1885 (2006).
11. J. R. Hibbeln *et al.*, *Lancet* **369**, 578 (2007).
12. L. McLaren, *Epidemiol. Rev.* **29**, 29 (2007).
13. 42 U.S. Code (USC) §4332(2)(C).
14. 21 USC §379o.
15. R. L. Naylor *et al.*, *Nature* **405**, 1017 (2000).
16. S. Tveterås, *Mar. Resour. Econ.* **17**, 121 (2002).
17. W. M. Muir, *EMBO Rep.* **5**, 654 (2004).
18. R. L. Naylor *et al.*, *Proc. Natl. Acad. Sci. U.S.A.* **106**, 18040 (2009).
19. A. G. J. Tacon, M. Metian, *Aquaculture* **285**, 146 (2008).
20. M. D. Smith *et al.*, *Science* **327**, 784 (2010).
21. J. E. Wilen, *Bull. Mar. Sci.* **78**, 529 (2006).
22. T. Searchinger *et al.*, *Science* **319**, 1238 (2008).
23. 21 USC §360b(d)(1)(B).
24. 21 USC §321(u).
25. 21 USC §360b(d)(2).
26. *Chevron* v. *NRDC*, 467 U.S. 837 (1984).

27. The authors thank R. Perez for research assistance.

Supporting Online Material

www.sciencemag.org/cgi/content/full/330/6007/1052/DC1

10.1126/science.1197769

CHEMISTRY

Nanosilver Revisited Downstream

Wastewater treatment converts potentially toxic nanosilver particles into more benign silver sulfide nanoparticles.

Bernd Nowack

Hundreds of consumer products are on the market that contain metallic silver nanoparticles. Given the potential toxicity of silver, these engineered nanoparticles are currently under intense scrutiny by environmental and occupational scientists (*1*) and regulators (*2*). The reason for this interest is that the physical and chemical properties of particles in the nanorange (from about 1 to 100 nm) can be different from larger particles or dissolved compounds, and it is not yet clear whether these different properties also require a new and more rigorous human and environmental risk assessment compared with their larger counterparts. In a recent article, Kim *et al*. (*3*) reported the discovery and identification of silver sulfide (Ag_2S) nanoparticles in sewage sludge. This finding provides some insight into the fate of silver that had been introduced in various forms into the environment.

Kim *et al*. found that silver is present in sewage sludge as nanoparticles of the α phase of silver sulfide (α-Ag_2S), a phase found in nature as the mineral acanthite. Most of the silver that enters a wastewater treatment plant is removed during treatment, and it has been recognized that sulfide plays an important role in the removal of silver (*4*). Silver enters wastewater from a variety of sources, both industrial (e.g., photographic and electronic industries) and from consumer products. Textiles containing nanosilver release silver into the wash water as the dissolved ions and as coarse particles, as well as in nanoparticle form (*5*, *6*). Silver may also be discharged into wastewater as silver chloride precipitates (*7*).

Initial studies showed that silver nanoparticles are efficiently removed from wastewater (more than 90%) and thus accumulate in the sludge (*8*). A recent study modeled concentrations of nanosilver from engineered products entering the environment based on the life cycles of these products and predicted that silver nanoparticles could be expected at concentrations of tens of nanograms per liter in natural waters (*9*). Kim *et al*. did not investigate the discharged treated water, so the form and concentration of silver present in the effluent water remains an open question. It can be expected that a certain fraction of silver will be bound to small flocs (aggregations of suspended particles) that are not retained during clarification and will contain α-Ag_2S. Further investigations would be needed to determine whether surface modifications and coatings of engineered nanosilver make it more mobile and resistant to transformation reaction and produce less α-Ag_2S formation.

A recent assessment of European silver flows into the environment (*4*) came to the conclusion that currently biocidal uses of silver (including silver nanoparticles, as well as silver in other forms, such as ionic silver) make up not more than 15% of the total silver flow into wastewater. If the situation is similar in the United States (where Kim *et al*. conducted their study), most of the Ag_2S nanoparticles in the biosolid sample that was investigated were formed from non-nanoparticulate silver. The results of Kim *et al*. suggest that dissolved silver, silver chloride precipitates, or metallic silver nanoparticles are transformed during wastewater treatment into Ag_2S nanoparticles that are retained in the sludge. Thus, even in the absence of introduced silver nanoparticles, wastewater treatment plants are efficient producers of silver nanoparticles, albeit of another mineralogical form than the metallic silver nanoparticles produced by industry.

If the formation of α-Ag_2S nanoparticles from all forms of silver constitutes the standard case for wastewater treatment plants, the environmental risk assessment of silver and nanosilver would be simplified greatly. Silver is one of the most toxic metals to microorganisms and is also quite harmful to many other ecologically relevant species (*1*), but the speciation of silver strongly affects its toxicity. Silver bound to sulfur or organic ligands

Empa, Swiss Federal Laboratories for Materials Science and Technology, CH-9014 St. Gallen, Switzerland. E-mail: nowack@empa.ch

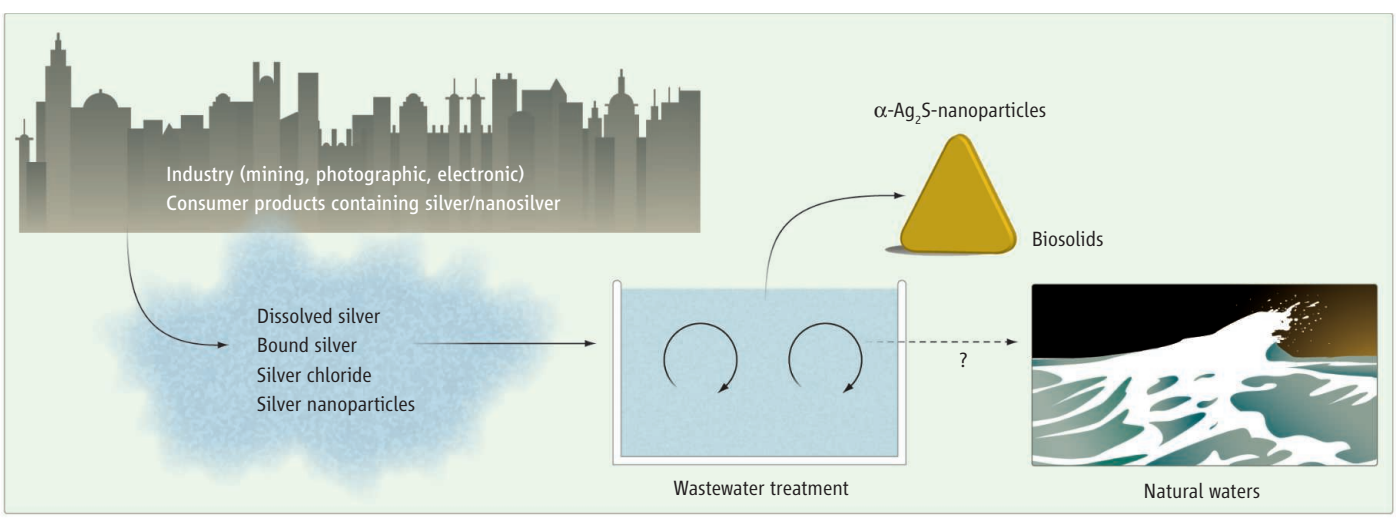

CREDIT: P. HUEY/*SCIENCE*

Silver trails. Silver enters the environment from a variety of sources (industrial and consumer products) in different forms (as ions, nanoparticles, and coarser particles, and as compounds, such as silver chloride). The work of Kim *et al*. now suggests that all the different forms of silver are transformed into the mineral α-Ag_2S during wastewater treatment. It remains open whether and in which form silver is present in the effluent.

Published by AAAS

is many orders of magnitude less toxic than the free silver ion (*4*, *10*). α-Ag_2S is one of the most insoluble silver minerals known, whereas metallic silver nanoparticles are an efficient source of silver ions in natural waters (*11*). If the majority of the silver is present as α-Ag_2S in sludge or in the effluent from the treatment plant, then its toxicity cannot be evaluated using data obtained in studies with either dissolved silver or metallic silver nanoparticles. From an environmental point of view, the use of nanosilver in consumer products would not be different from all other silver forms and would probably not constitute a problem for natural systems. It remains to be investigated, however, what the further fate of α-Ag_2S is in natural waters and whether it is transformed back to other silver forms.

References

1. S. W. P. Wijnhoven *et al.*, *Nanotoxicology* **3**, 109 (2009).
2. T. Faunce, A. Watal, *Nanomedicine* **5**, 617 (2010).
3. B. Kim *et al.*, *Environ. Sci. Technol.* **44**, 7509 (2010).
4. S. A. Blaser *et al.*, *Sci. Total Environ.* **390**, 396 (2008).
5. T. M. Benn, P. Westerhoff, *Environ. Sci. Technol.* **42**, 4133 (2008).
6. L. Geranio *et al.*, *Environ. Sci. Technol.* **43**, 8113 (2009).
7. C. A. Impellitteri, T. M. Tolaymat, K. G. Scheckel, *J. Environ. Qual.* **38**, 1528 (2009).
8. K. Tiede *et al.*, *J. Anal. At. Spectrom.* **25**, 1149 (2010).
9. F. Gottschalk, T. Sonderer, R. W. Scholz, B. Nowack, *Environ. Sci. Technol.* **43**, 9216 (2009).
10. O. Choi *et al.*, *Water Res.* **43**, 1879 (2009).
11. J. Liu, R. H. Hurt, *Environ. Sci. Technol.* **44**, 2169 (2010).

10.1126/science.1198074

GENETICS

γ-Secretase and Human Disease

The role of an enzyme in disease pathogenesis extends beyond Alzheimer's disease to a skin disorder.

Raymond J. Kelleher III[1,2] and Jie Shen[2,3]

The suspected culprit in Alzheimer's disease has been γ-secretase, an enzyme that cleaves type I transmembrane proteins. It processes amyloid precursor protein (APP), generating the β-amyloid (Aβ) peptides that give rise to the characteristic brain plaques of Alzheimer's disease patients. Presenilin is the presumptive catalytic subunit of γ-secretase, and mutations in the *PSEN1* and *PSEN2* genes that encode this subunit are the most common cause of familial Alzheimer's disease. On page 1065 of this issue, Wang *et al*. (*1*) report that mutations in *PSEN1* are also associated with a severe skin disorder, acne inversa. Mutations in genes encoding two other subunits of γ-secretase are also linked to this severe skin condition. The finding raises questions about the function of γ-secretase in human diseases, with implications for the development of therapeutics.

A key unresolved question is whether *PSEN* mutations cause familial Alzheimer's disease through loss of presenilin function and/or through increased production of longer Aβ peptides (*2*, *3*). *PSEN* mutations in familial Alzheimer's disease are almost exclusively missense, and the absence of nonsense or frameshift mutations argues against haploinsufficiency (only a single functional copy of a gene) and favors a disease mechanism based on gain of function by the mutant protein. However, the distribution of pathogenic mutations throughout the *PSEN* coding sequence is most compatible with a loss of protein function. Indeed, *PSEN* mutations that cause familial Alzheimer's disease impair the proteolytic activity of the mutant protein (*2*), and inactivation of presenilins in the adult mouse brain causes neurodegeneration (*4*), whereas Aβ overproduction does not (*5*). In addition, γ-secretase inhibitors can mimic the effects of pathogenic *PSEN* mutations on APP processing, which suggests that overproduction of longer Aβ is a manifestation of partial loss of presenilin function (*2*).

Wang *et al*. reveal that mutations in *PSEN1*, as well as in the *PSENEN* and *NCSTN* genes that encode the PEN2 and nicastrin subunits of γ-secretase, respectively, cause acne inversa. Six different mutations in these three genes were identified in six families with dominant transmission of a rare atypical form of acne inversa. Remarkably, all of the mutations segregated with the disease with complete penetrance despite the genetic heterogeneity among the families. Because all of the mutations are predicted to inactivate protein function, haploinsufficiency of these genes appears to lead to acne inversa. This is consistent with mouse studies showing that γ-secretase deficiency produces follicular hyperkeratosis (*6*, *7*), the initiating event in acne inversa. Similar disorders are observed in mice with skin-specific inactivation of the *Notch1* gene, which encodes another transmembrane protein cleaved by γ-secretase. This suggests that Notch1 is the enzyme's relevant substrate in acne inversa (*8*).

What do these findings from a disparate clinical disorder tell us about familial Alzheimer's disease? The major implication is that inactivating and missense mutations

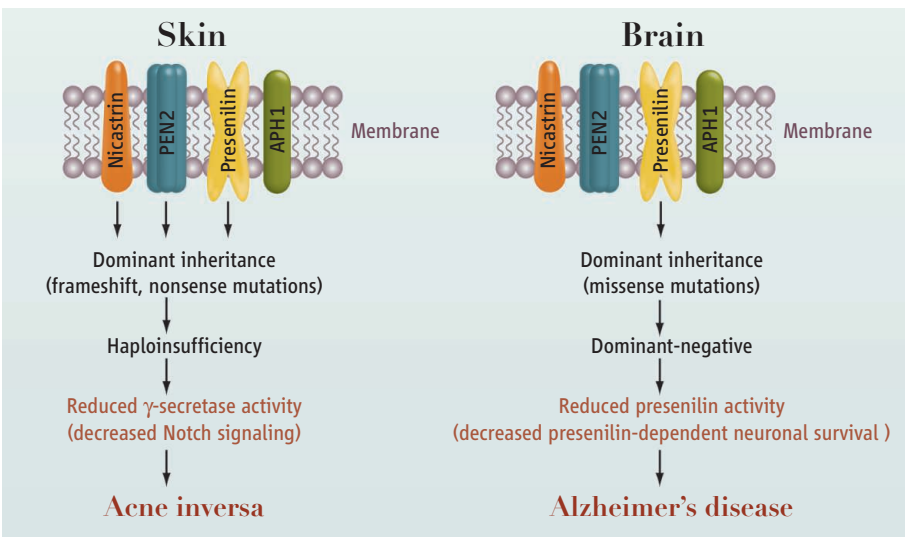

Mutations and mechanisms. Dominant inactivating mutations in presenilin-1, nicastrin, and PEN2 cause acne inversa as a result of haploinsufficiency. Dominant missense mutations in presenilins-1 and -2 confer a loss of protein function and may cause Alzheimer's disease through a dominant-negative mechanism.

[1]Center for Human Genetic Research, Massachusetts General Hospital, Boston, MA 02114, USA. [2]Department of Neurology, Harvard Medical School, Boston, MA 02115, USA. [3]Center for Neurologic Diseases, Brigham and Women's Hospital, Boston, MA 02115, USA. E-mail: kelleher@helix.mgh.harvard.edu

CREDIT: N. KEVITYAGALA/*SCIENCE*

is many orders of magnitude less toxic than the free silver ion (*4*, *10*). α-Ag_2S is one of the most insoluble silver minerals known, whereas metallic silver nanoparticles are an efficient source of silver ions in natural waters (*11*). If the majority of the silver is present as α-Ag_2S in sludge or in the effluent from the treatment plant, then its toxicity cannot be evaluated using data obtained in studies with either dissolved silver or metallic silver nanoparticles. From an environmental point of view, the use of nanosilver in consumer products would not be different from all other silver forms and would probably not constitute a problem for natural systems. It remains to be investigated, however, what the further fate of α-Ag_2S is in natural waters and whether it is transformed back to other silver forms.

References

1. S. W. P. Wijnhoven *et al.*, *Nanotoxicology* **3**, 109 (2009).
2. T. Faunce, A. Watal, *Nanomedicine* **5**, 617 (2010).
3. B. Kim *et al.*, *Environ. Sci. Technol.* **44**, 7509 (2010).
4. S. A. Blaser *et al.*, *Sci. Total Environ.* **390**, 396 (2008).
5. T. M. Benn, P. Westerhoff, *Environ. Sci. Technol.* **42**, 4133 (2008).
6. L. Geranio *et al.*, *Environ. Sci. Technol.* **43**, 8113 (2009).
7. C. A. Impellitteri, T. M. Tolaymat, K. G. Scheckel, *J. Environ. Qual.* **38**, 1528 (2009).
8. K. Tiede *et al.*, *J. Anal. At. Spectrom.* **25**, 1149 (2010).
9. F. Gottschalk, T. Sonderer, R. W. Scholz, B. Nowack, *Environ. Sci. Technol.* **43**, 9216 (2009).
10. O. Choi *et al.*, *Water Res.* **43**, 1879 (2009).
11. J. Liu, R. H. Hurt, *Environ. Sci. Technol.* **44**, 2169 (2010).

10.1126/science.1198074

GENETICS

γ-Secretase and Human Disease

The role of an enzyme in disease pathogenesis extends beyond Alzheimer's disease to a skin disorder.

Raymond J. Kelleher III[1,2] and Jie Shen[2,3]

The suspected culprit in Alzheimer's disease has been γ-secretase, an enzyme that cleaves type I transmembrane proteins. It processes amyloid precursor protein (APP), generating the β-amyloid (Aβ) peptides that give rise to the characteristic brain plaques of Alzheimer's disease patients. Presenilin is the presumptive catalytic subunit of γ-secretase, and mutations in the *PSEN1* and *PSEN2* genes that encode this subunit are the most common cause of familial Alzheimer's disease. On page 1065 of this issue, Wang *et al*. (*1*) report that mutations in *PSEN1* are also associated with a severe skin disorder, acne inversa. Mutations in genes encoding two other subunits of γ-secretase are also linked to this severe skin condition. The finding raises questions about the function of γ-secretase in human diseases, with implications for the development of therapeutics.

A key unresolved question is whether *PSEN* mutations cause familial Alzheimer's disease through loss of presenilin function and/or through increased production of longer Aβ peptides (*2*, *3*). *PSEN* mutations in familial Alzheimer's disease are almost exclusively missense, and the absence of nonsense or frameshift mutations argues against haploinsufficiency (only a single functional copy of a gene) and favors a disease mechanism based on gain of function by the mutant protein. However, the distribution of pathogenic mutations throughout the *PSEN* coding sequence is most compatible with a loss of protein function. Indeed, *PSEN* mutations that cause familial Alzheimer's disease impair the proteolytic activity of the mutant protein (*2*), and inactivation of presenilins in the adult mouse brain causes neurodegeneration (*4*), whereas Aβ overproduction does not (*5*). In addition, γ-secretase inhibitors can mimic the effects of pathogenic *PSEN* mutations on APP processing, which suggests that overproduction of longer Aβ is a manifestation of partial loss of presenilin function (*2*).

Wang *et al*. reveal that mutations in *PSEN1*, as well as in the *PSENEN* and *NCSTN* genes that encode the PEN2 and nicastrin subunits of γ-secretase, respectively, cause acne inversa. Six different mutations in these three genes were identified in six families with dominant transmission of a rare atypical form of acne inversa. Remarkably, all of the mutations segregated with the disease with complete penetrance despite the genetic heterogeneity among the families. Because all of the mutations are predicted to inactivate protein function, haploinsufficiency of these genes appears to lead to acne inversa. This is consistent with mouse studies showing that γ-secretase deficiency produces follicular hyperkeratosis (*6*, *7*), the initiating event in acne inversa. Similar disorders are observed in mice with skin-specific inactivation of the *Notch1* gene, which encodes another transmembrane protein cleaved by γ-secretase. This suggests that Notch1 is the enzyme's relevant substrate in acne inversa (*8*).

What do these findings from a disparate clinical disorder tell us about familial Alzheimer's disease? The major implication is that inactivating and missense mutations

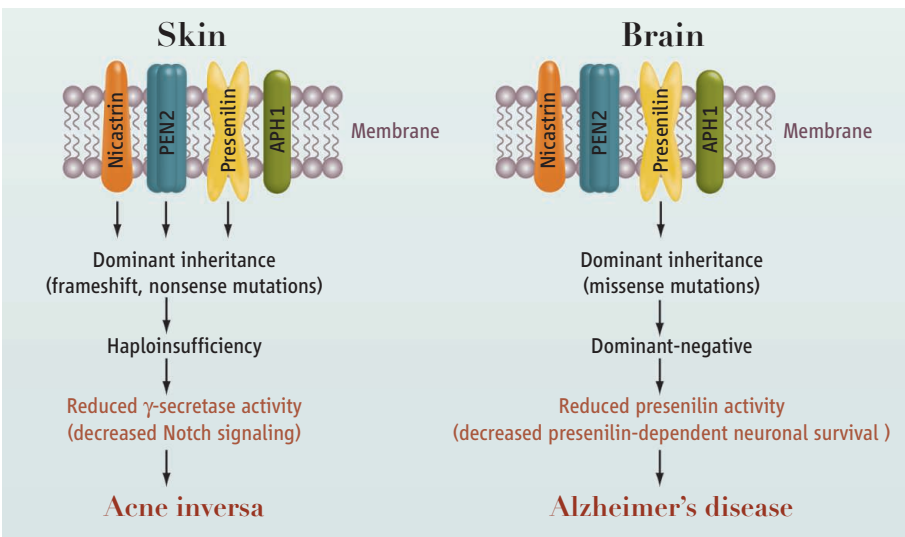

Mutations and mechanisms. Dominant inactivating mutations in presenilin-1, nicastrin, and PEN2 cause acne inversa as a result of haploinsufficiency. Dominant missense mutations in presenilins-1 and -2 confer a loss of protein function and may cause Alzheimer's disease through a dominant-negative mechanism.

[1]Center for Human Genetic Research, Massachusetts General Hospital, Boston, MA 02114, USA. [2]Department of Neurology, Harvard Medical School, Boston, MA 02115, USA. [3]Center for Neurologic Diseases, Brigham and Women's Hospital, Boston, MA 02115, USA. E-mail: kelleher@helix.mgh.harvard.edu

CREDIT: N. KEVITYAGALA/*SCIENCE*

in *PSEN1* produce different clinical phenotypes, hinting at different disease mechanisms. Although Notch1 appears to be the relevant substrate for γ-secretase in acne inversa, it is unclear whether Notch1 is involved in presenilin-dependent neuronal survival in the aging brain. The absence of dementia in the families with acne inversa also indicates that *PSEN1* haploinsufficiency is unlikely to cause familial Alzheimer's disease, although the acne inversa–affected family transmitting the *PSEN1* mutation includes just four affected individuals, and delayed onset and/or subtle signs of dementia cannot be excluded.

Conversely, Wang *et al*. note that acne inversa has not been reported in association with Alzheimer's disease, which is surprising given the 1 to 4% prevalence of acne inversa in the general population (*9*). Moreover, some *PSEN1* mutations in familial Alzheimer's disease cause a complete loss of Notch1 processing in cultured cells (*10*), which would be expected to mimic the phenotypic effects of the *PSEN1* mutation in familial acne inversa. In addition, loss of a single *Psen1* allele in mice does not produce skin disorders, which occur only with more severe reductions of presenilin expression. These inconsistencies raise the possibility that loss-of-function mutations in *PSEN1* may not always produce acne inversa with full penetrance, and that genetic modifiers may contribute to the development of acne inversa in the reported families.

Although *PSEN* mutations in familial Alzheimer's disease impair protein function, the missense nature of these mutations suggests that expression of the mutant protein is necessary to produce the disease. *PSEN* mutations could enhance production of longer Aβ by decreasing the proteolytic efficiency of the mutant protein (*11*). This model, however, is not compatible with the inability of presenilins bearing some pathogenic mutations to generate Aβ (*12*). Alternatively, mutant presenilin could influence the activity of wild-type presenilin in a dominant-negative manner (*2*). Such a "gain of negative function" model would reconcile the dominant inheritance of *PSEN* mutations with their deleterious effects on protein function. That presenilin is the only γ-secretase subunit targeted by mutations in familial Alzheimer's disease further suggests that γ-secretase–independent functions of presenilins may be important in disease pathogenesis. Presenilins are required for synaptic function and neuronal survival in the adult brain (*4*, *13*), establishing important links to neural processes perturbed in Alzheimer's disease, but the effector mechanisms mediating these essential activities are presently unclear.

A large-scale phase III clinical trial of a γ-secretase inhibitor (semagacestat) in Alzheimer's disease was halted because the drug worsened cognition and increased the risk of skin cancer (*14*). Mouse studies suggest that these adverse effects may be attributed to specific inhibition of γ-secretase rather than to nonspecific effects. The dementia and neurodegeneration caused by presenilin inactivation in the mouse brain predicted that γ-secretase inhibition might exacerbate the clinical features of Alzheimer's disease (*4*). In addition, reduced γ-secretase and Notch1 activity in mice causes a high frequency of skin cancer, demonstrating that γ-secretase is a tumor suppressor in skin (*6*–*8*). It remains to be seen whether the adverse effects of γ-secretase inhibitors include acne inversa.

The findings by Wang *et al*. should spur efforts to dissect the role of γ-secretase in acne inversa, and to examine patients with acne inversa and familial Alzheimer's disease more closely for evidence of subtle overlap in the clinical features. Better understanding of the molecular mechanisms by which presenilin and γ-secretase dysfunction leads to these disparate conditions will also bolster efforts to devise safe and effective disease-modifying therapies.

References

1. B. Wang *et al*., *Science* **330**, 1065 (2010).
2. J. Shen, R. J. Kelleher III, *Proc. Natl. Acad. Sci. U.S.A.* **104**, 403 (2007).
3. J. Hardy, D. J. Selkoe, *Science* **297**, 353 (2002).
4. C. A. Saura *et al*., *Neuron* **42**, 23 (2004).
5. M. C. Irizarry *et al*., *J. Neurosci.* **17**, 7053 (1997).
6. X. Xia *et al*., *Proc. Natl. Acad. Sci. U.S.A.* **98**, 10863 (2001).
7. T. Li *et al*., *J. Biol. Chem.* **282**, 32264 (2007).
8. M. Nicolas *et al*., *Nat. Genet.* **33**, 416 (2003).
9. F. W. Danby, L. J. Margesson, *Dermatol. Clin.* **28**, 779 (2010).
10. W. Song *et al*., *Proc. Natl. Acad. Sci. U.S.A.* **96**, 6959 (1999).
11. M. S. Wolfe, *EMBO Rep.* **8**, 136 (2007).
12. E. A. Heilig, W. Xia, J. Shen, R. J. Kelleher III, *J. Biol. Chem.* **285**, 22350 (2010).
13. C. Zhang *et al*., *Nature* **460**, 632 (2009).
14. http://newsroom.lilly.com/releasedetail.cfm?releaseID=499794, accessed on 10 October 2010.

10.1126/science.1198668

CHEMISTRY

Magnetic Resonance and Microfluidics

Marcel Utz[1,2] and James Landers[2,1]

The inner workings of microscale "lab-on-a-chip" devices can be revealed by nuclear magnetic resonance measurements on their exiting fluid flows.

Magnetic resonance imaging (MRI) is a well-established clinical tool that is routinely used to locate cartilage or ligament damage, cancerous lesions, and blood vessel occlusions; when combined with magnetic resonance spectroscopy (MRS), it can even map brain function. The image contrast in MRI instruments comes from the change in orientation of the rotational axis (precession) of atomic nuclei in a magnetic field, and can be adjusted to selectively image tissues on the basis of oxygen content, diffusivity, flow velocity, and other properties. Microfluidic "lab-on-a-chip" (LOC) devices represent an emerging technology with potential applications in medical diagnostics. These devices flow samples (which often consist of suspensions of cells) and reagents through miniaturized chemical reactors, and are typically fabricated via lithographic methods similar to those used in microelectronics. Although in principle, MRI should be the ideal tool for monitoring reactions on LOC devices, in practice this turns out to be notoriously difficult because of limitations in sensitivity and resolution. On page 1078 of this issue, Bajaj *et al*. (*1*) present an ingenious method that allows sensitive MRI measurements on an LOC device by recording magnetic resonance signals from the spent fluid that exits the device.

In MRI, the spatial position of a spin can be inferred from changes in its precession frequency. The sample is placed in a magnetic field that has a gradient in one direction. The nuclear spins are excited by radio-frequency pulses, and the resulting Larmor precession induces a signal in a receiver coil surrounding the sample. The field gradient causes the precession frequency of each spin to depend on its location. The experiment is repeated

[1]Department of Chemistry, University of Virginia, Charlottesville, VA 22904, USA. [2]Department of Mechanical and Aerospace Engineering, University of Virginia, Charlottesville, VA 22904, USA. E-mail: mu3q@virginia.edu; jpl5e@virginia.edu

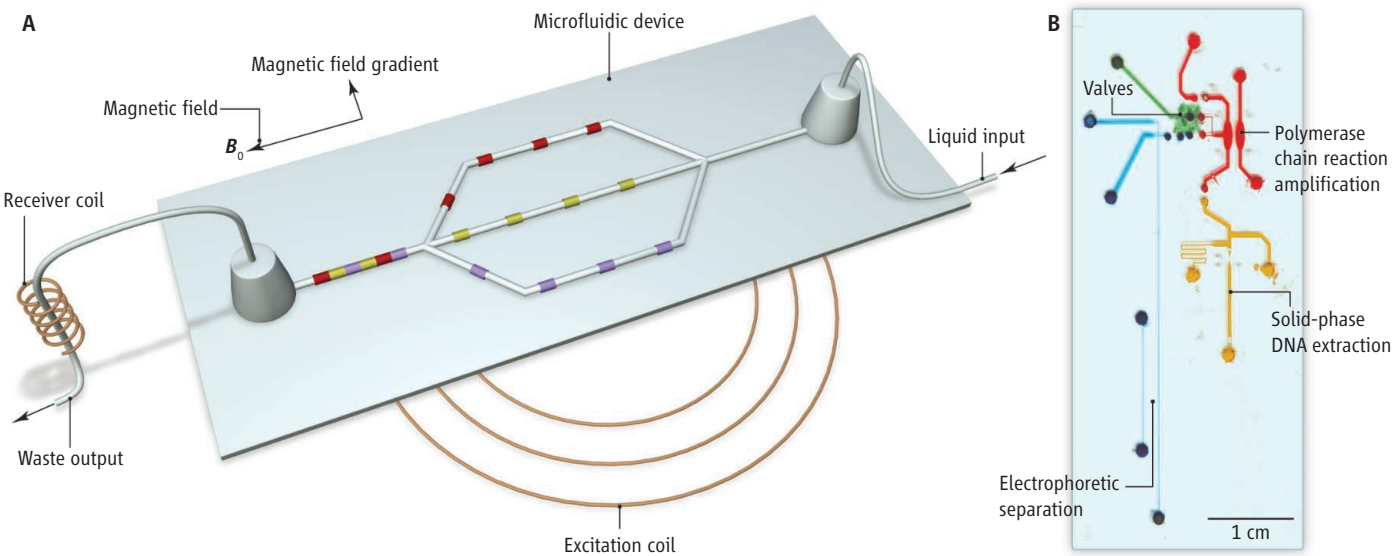

The answers flow out in the end. (**A**) Principles of remote detection of processes inside microfluidic devices with MRI are illustrated. Spin precession is induced in the entire chip by means of the excitation coil. Liquid is pumped through the microfluidic chip. Volume packets flowing through different channels in the network precess at different frequencies because of a gradient in the magnetic field (represented by red, green, and violet colors in the channels). The phase angle acquired in this precession is converted into a modulation of the spin polarization, which is long-lived. The labeled volume packets are then transported to the receiver coil, where the information is read out. (**B**) The photo shows an integrated microfluidic chip for genomics that analyzes short tandem repeats.

with a field gradient of different magnitude and direction, and an image is obtained by Fourier transformation of the resulting data set. Special pulse-excitation protocols can encode additional parameters, such as velocity and diffusivity.

Microfluidic LOC devices consist of networks of channels, chambers, and valves with features that range in size from hundreds of nanometers to a few millimeters (*2*–*4*). Compared with benchtop methods, LOCs require very small volumes of samples and reagents, and create a closed system that minimizes the risk of contamination. Complex analytical methods can be brought directly into the hands of forensic, environmental, and other scientists, as well as primary medical care providers, even in remote locations far from sophisticated laboratory facilities.

The key processes that occur within an LOC—fluid convection (flow), diffusion, separation, and chemical reactions—can all be monitored with MRI and MRS, even simultaneously. Other flow quantification methods, such as optical particle tracking, perturb the system and provide no chemical information. Because MRI uses the atomic nuclei as "spies" to convey information about the chemical and transport processes, it causes no such perturbation. Unfortunately, MRS and MRI both suffer from low sensitivity. A sample contained within the small internal structures of an LOC device poses a challenge because the strength of the induced signal per spin decreases as the coil size is increased to accommodate the device.

Past endeavors to combine magnetic resonance with microfluidic systems have resorted to miniaturized receiver coils (*5*–*8*) or microstrip lines (*9*, *10*) that focus the sensitivity on the available sample volume. This approach has led to "hyphenated" techniques, such as liquid chromatography–magnetic resonance (*11*). By integrating planar microcoils onto the chip (*6*–*8*), the products of on-chip reactions and separations can be quantified by MRS. The coils can be coupled wirelessly to the MRS receiver so that data can be collected without needing physical connections, by simply inserting the chip into the MRI scanner (*7*, *8*). However, the operation of the microfluidic system as a whole cannot be observed through such focused receivers, because it is impractical to envelop each pertinent feature with a separate microcoil.

Bajaj *et al*. have circumvented the dilemma between receiver sensitivity and size. As in conventional MRI, they used magnetic-field gradients to encode position and velocity, exciting nuclear precession with a large radio-frequency coil that surrounds the entire LOC. However, leveraging a development by the Pines group several years ago (*12*) to study the flow of gases in porous media (*13*), the frequency is measured only after the polarized nuclei have been washed out of the LOC along with the surrounding fluid, into an exit microcapillary wound with a small receiver coil (see the figure, panel A). With the resulting optimum sensitivity, transport processes in microfluidic systems can be observed directly that would otherwise have been inaccessible.

In a sense, this approach is similar to a recently proposed method (*14*) that injects dyes into different parts of the chip, which are then detected by absorbance spectroscopy from a common exit port; instead of dyes, the more elegant MRI approach by Bajaj *et al*. uses nuclear spin states as tracers. The only requirement for investigating an LOC in this way is that the spins are transported to the observation coil within the spin-lattice relaxation time, usually several seconds. It should be possible to study most LOCs, given typical pumping speeds and small device length scales. Obviously, such measurements require fluidic connections to the chip while it is in the MRI scanner to ensure continued flow. This restriction notwithstanding, it is exciting that the broad arsenal of MRI techniques is now available to study chemical reactions, separation, convection, and diffusion processes in LOC devices.

An example of an LOC that could be examined—a genomic analysis chip that integrates cell lysis, DNA purification, polymerase chain reaction amplification, and electrophoretic separation (*3*)—is shown in panel B of the figure. It contains a host of elements that rely on complex transport and separation processes (indicated by the arrows), which could, in principle, be studied by MRI.

With the work of Bajaj *et al*., it now seems justified to hope that MRI will be able to do

CREDIT (PANEL A): P. HUEY/*SCIENCE*

Published by AAAS

for the development of microfluidic LOCs what it has done for medical diagnostics, by providing a generally applicable, powerful, and flexible tool to study a complex chemical and biological system without perturbing its operation.

References

1. V. S. Bajaj, J. Paulsen, E. Harel, A. Pines, *Science* **330**, 1078 (2010).
2. T. Thorsen *et al.*, *Science* **298**, 580 (2002).
3. C. J. Easley *et al.*, *Proc. Natl. Acad. Sci. U.S.A.* **103**, 19272 (2006).
4. R. G. Blazej, P. Kumaresan, R. A. Mathies, *Proc. Natl. Acad. Sci. U.S.A.* **103**, 7240 (2006).
5. D. L. Olson, T. L. Peck, A. G. Webb, R. L. Magin, J. V. Sweedler, *Science* **270**, 1967 (1995).
6. C. Massin *et al.*, *J. Magn. Reson.* **164**, 242 (2003).
7. M. Utz, R. Monazami, *J. Magn. Reson.* **198**, 132 (2009).
8. M. Utz, K. Wang, in *Proceedings of the 13th International Conference on Miniaturized Systems for Chemistry and Life Sciences (μTAS 2009)*, Jeju, Korea, 1 to 5 November, 2009, T. S. Kim *et al.*, Eds. (Chemical and Biological Microsystems Society, San Diego, 2009), p. 1656.
9. H. G. Krojanski, J. Lambert, Y. Gerikalan, D. Suter, R. Hergenröder, *Anal. Chem.* **80**, 8668 (2008).
10. J. Bart, J. W. Janssen, P. J. van Bentum, A. P. Kentgens, J. G. Gardeniers, *J. Magn. Reson.* **201**, 175 (2009).
11. K. Albert, Ed., *On-line LC-NMR and Related Techniques* (Wiley, Chichester, UK, 2002).
12. J. Granwehr, E. Harel, S. Han, S. Garcia, A. Pines, *Phys. Rev. Lett.* **95**, 07553 (2004).
13. C. Hilty *et al.*, *Proc. Natl. Acad. Sci. U.S.A.* **102**, 14960 (2005).
14. D. C. Leslie *et al.*, *Lab Chip* **10**, 1960 (2010).

10.1126/science.1198402

MICROBIOLOGY

Topping Off a Multiscale Balancing Act

Quantitative predictions of the relationship between cell growth and gene expression have been made and validated in *Escherichia coli*.

Joshua Lerman and Bernhard O. Palsson

The genotype-phenotype relationship is fundamental to biology. Finding general, underlying rules that govern the complex relationship between gene expression and cell growth, however, has proven a challenge. On page 1099 of this issue, Scott *et al*. (*1*) offer empirical "growth laws" that correlate the growth rates of bacteria with how they allocate resources to protein synthesis and metabolic functions.

The genotype-phenotype relationship in microbes can be conceptualized as a five-layer hierarchical model (see the figure). A cell faces myriad constraints on its function at all layers (*2*, *3*). At the whole-cell level, it may be difficult to determine the constraints that govern cellular functions on a mechanistic basis, but they can be identified from empirical observation. Microbiologists pursued this approach in the 1950s and 1960s, resulting in empirical parameters such as the growth and nongrowth maintenance coefficients (*4*) and yield coefficients that are widely used in the bioprocessing literature (*5*).

Scott *et al*. expand on the whole-cell empirical approach by means of an insightful combination of targeted experimentation and mathematical analysis. Using *Escherichia coli* cells grown under a variety of conditions, they first confirmed a previously established correlation between growth rate and the ribosomal content of the cell (ribosomes assemble proteins from amino acids). Next, they used mutant strains to show that the proportionality constant between ribosomal content and growth rate depends on the overall rate at which the cell incorporates amino acids into protein. To achieve a small increase in growth rate, mutant strains that incorporate amino acids slowly must dedicate more resources to ribosome production than their more rapidly synthesizing counterparts.

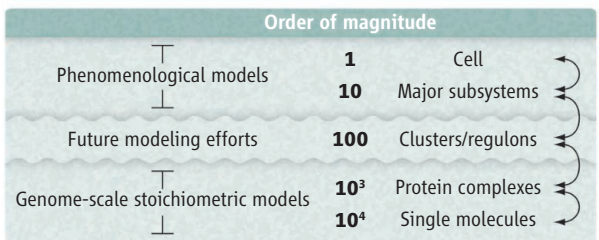

The microbial genotype-phenotype relationship. Bacterial cell growth and gene expression are linked through a hierarchy that extends from tens of thousands of molecules to a single cell. Each layer in the hierarchy imposes constraints on adjacent layers (arrows, right). At the top, empirical models can predict the relative levels of proteins belonging to major subsystems within a cell (e.g., metabolism, macromolecular synthesis). At the bottom, genome-scale models can make predictions by accounting for all single molecules and protein complexes. A future modeling challenge is to characterize the functionality of the ~100 coordinately expressed clusters of protein complexes and to determine the evolutionary pressures leading to regulon formation (middle layer).

The authors then subjected cells growing in different nutritional environments to increasing concentrations of an antibiotic that disables ribosomal function. Another striking correlation emerged: As the concentration of the antibiotic increased, translation capacity and growth dropped linearly toward zero, and there was a corresponding linear increase in the fraction of the proteome dedicated to ribosomes. Finally, chemical composition data taken from cells close to the no-growth point suggested that there is a hard upper bound on the fraction of the proteome that can be dedicated to ribosomes and related proteins; it is capped at around 0.55, independent of growth conditions.

Given these findings, and given that the cell's regulatory efforts enforce a balance between metabolism and macromolecular synthesis, the authors reasoned that they could mathematically describe proteome resource allocation using only three variables: R, P, and Q, where R represents the growth rate–dependent fraction of the proteome that is dedicated to macromolecular synthesis, P represents the growth rate–dependent fraction of the proteome dedicated to everything else, and Q represents the growth rate–independent (or housekeeping) fraction. This grouping of proteins into three categories is able to relate R, P, and Q in quantitative terms without any adjustable parameters, and without requiring detailed knowledge of the underlying regulatory circuits. Surprisingly, Q-class proteins occupy a substantial fraction of the proteome (50%).

The authors evaluated the predictive potential of these empirical equations through a series of experiments. They exploited the empirical relationships between proteome fractions to (i) validate the predicted constrained positive linear relationship between the abundance of P-class proteins and growth rate in a fixed nutritional environment, and (ii) mathematically characterize cells forced to express unnecessary (or useless) protein.

This work comes on the heels of parallel developments at lower levels of the hierarchy shown in the figure. The availability of

Department of Bioengineering, University of California, San Diego, La Jolla, CA 92093, USA. E-mail: palsson@ucsd.edu

full genome sequences in the mid-1990s led to the construction of genome-scale metabolic models that were able to recapitulate optimal growth phenotypes (*6*). The reconstruction of the entire protein synthesis machinery (*7*) moved us up a notch in the hierarchy, enabling the description of the optimal ribosomal content as a function of growth rate (the starting point for Scott *et al*.). At the systems biology level, "omics" data sets have led to an understanding of how optimal network properties form (*8*, *9*). At this level, a combination of inference methods (*10*) and bottom-up reconstructions has proved productive (*11*). Decomposing network functionality into coordinately expressed gene clusters, and determining the degree of flexibility within and among these clusters (in terms of expression levels), could complete our understanding of the hierarchy, now that we have the top-level relationships developed by Scott *et al*.

Taken together, these developments lead to a multiscale understanding of the genotype-phenotype relationships underlying metabolism and growth in microbes. At all levels, model structures must be developed in order to adequately capture constraints and allow for optimization subject to these constraints (*12*). Cementing these levels into a coherent multiscale framework is a challenge facing the field. Experiments that enable bacteria to rapidly evolve in controlled laboratory settings are a way to interrogate this relationship further, as they produce optimal growth phenotypes (*13*, *14*). The genetic basis for such changes in phenotype can now be determined through whole-genome resequencing, followed by allelic replacement to identify causal mutations (*15*). Clearly, an exciting era is ahead of us, in which a combination of in silico and experimental approaches promises to continue the development of mechanistic and principled genotype-phenotype relationships that are akin to the development of fundamental physical laws a century ago. If successful, such development will move microbiology into a fundamentally new realm.

References

1. M. Scott, C. W. Gunderson, E. M. Mateescu, Z. Zhang, T. Hwa, *Science* **330**, 1099 (2010).
2. B. Palsson, *Nat. Biotechnol.* **18**, 1147 (2000).
3. F. Jacob, *Science* **196**, 1161 (1977).
4. S. J. Pirt, *Proc. R. Soc. London Ser. B* **163**, 224 (1965).
5. J. E. Bailey, D. F. Ollis, *Biochemical Engineering Fundamentals* (McGraw-Hill, New York, ed. 2, 1906).
6. J. S. Edwards, R. U. Ibarra, B. O. Palsson, *Nat. Biotechnol.* **19**, 125 (2001).
7. I. Thiele, N. Jamshidi, R. M. Fleming, B. Ø. Palsson, *PLOS Comput. Biol.* **5**, e1000312 (2009).
8. R. Bonneau *et al*., *Cell* **131**, 1354 (2007).
9. N. E. Lewis *et al*., *Mol. Syst. Biol.* **6**, 390 (2010).
10. R. De Smet, K. Marchal, *Nat. Rev. Microbiol.* **8**, 717 (2010).
11. M. J. Herrgård, B. S. Lee, V. Portnoy, B. Ø. Palsson, *Genome Res.* **16**, 627 (2006).
12. N. D. Price, J. L. Reed, B. O. Palsson, *Nat. Rev. Microbiol.* **2**, 886 (2004).
13. R. U. Ibarra, J. S. Edwards, B. O. Palsson, *Nature* **420**, 186 (2002).
14. B. Teusink, A. Wiersma, L. Jacobs, R. A. Notebaart, E. J. Smid, *PLOS Comput. Biol.* **5**, e1000410 (2009).
15. C. D. Herring *et al*., *Nat. Genet.* **38**, 1406 (2006).

10.1126/science.1199353

NEUROSCIENCE

π = Visual Cortex

Three distantly-related mammals share a brain architecture characterized by a density of π

Kenneth D. Miller

Archimedes, the great scientist of ancient Greece, performed the first systematic calculation of the value of π, the ratio of a circle's circumference to its diameter. Twenty-three centuries later, scientists continue to be delighted by π's appearance in new and unexpected areas of science. The latest is perhaps the most surprising: On page 1113 of this issue, Kaschube *et al*. (*1*) show that three distantly-related mammals share a common organizing scheme for neurons in the brain's visual cortex characterized by a density closely approaching 3.14 (π). The result offers insight into the development and evolution of the visual cortex, and strongly suggests that key architectural features are self-organized rather than genetically hard-wired.

The cerebral cortex is a thin, six-layer sheet of neurons. A long-standing model system for cortical studies is the primary visual cortex (V1), the first piece of cortex to receive visual input (*2*). Neurons in V1 are highly selective for the spatial orientation of a light/dark edge; some prefer (respond best to) vertical edges, whereas others prefer horizontal or diagonal lines. Preferred orientation exhibits what is called "columnar" organization: The neurons beneath any given spot on the cortical sheet, across the layers, prefer the same orientation. Imaging techniques allow researchers to visualize the arrangement, or "map," of preferred orientations across the cortical sheet (see the figure). These orientation maps have a quasi-periodic structure: Preferred orientations change continuously across the sheet, repeating every millimeter or so. The local distance between repeats is the local "map period" (λ). The maps also contain "pinwheels"— points at which all preferred orientations converge. There has long been debate over the degree to which these features reflect detailed genetic programming or self-organization based on general rules that guide the growth and decay of synapses (*3*, *4*).

To explore this question, Kaschube *et al*. compared, with unprecedented quantitative precision, the density and arrangement of pinwheels in three mammals: the galago, a primate; a tree shrew, a close primate relative; and a distantly related carnivore, the ferret. This precise measurement of pinwheel distribution required considerable advances. Measurement "noise" corrupts maps, and existing methods to "smooth" the noise also smooth away, or hide, real pinwheels. The authors found filters that solve this problem. They also used wavelet-based methods that they had previously developed to precisely measure the local map period (*5*), and they gained precision by analyzing an unprecedented number of maps (more than 100) and pinwheels (roughly 10,000).

They found strong evidence of a common design. Most strikingly, the mean density of pinwheels per λ^2 was within 1% of π for all three species. The grand average was 3.14, with a 95% confidence interval of 3.08 to 3.20 ($\pi \pm 2\%$). Does a density of π just follow from the periodic map structure? To test this, they "phase-randomized" measured maps, creating maps that precisely retained the measured periodic structure but were otherwise random (see the figure). These maps had much higher pinwheel densities (mean 3.50), which suggests that π is a special property of the maps found in brains.

Why should the pinwheel density be π? Kaschube *et al*. have a beautiful theoretical answer. For many years, the senior author, Fred Wolf, and his group have been constructing a theory of orientation map development that builds on mathematical methods devel-

Center for Theoretical Neuroscience, Department of Neuroscience, Kavli Institute for Brain Science, College of Physicians and Surgeons, Columbia University, New York, NY 10032–2695, USA. E-mail: ken@neurotheory.columbia.edu

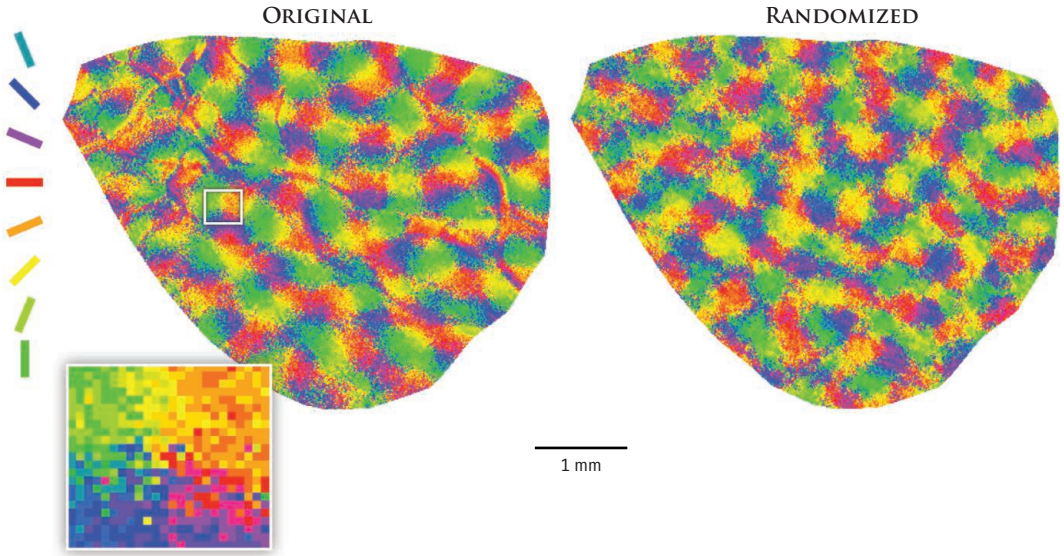

Pinwheels and π. Colors on an orientation map from a galago visual cortex (**left**) indicate preferred orientations of neurons (lines, far left). Orientations change roughly periodically, cycling from red to red with fairly regular spacing. (Colored lines across the map are blood vessel artifacts.) Pinwheels (inset) form where all orientations meet. Real maps have mean pinwheel density close to π. A phase randomized version of the same map (**right**) has a higher density, suggesting that a pinwheel density approaching π is a self-organized feature of the visual cortex.

oped in physics for studying pattern formation (*6*). These methods allow division of models into "universality classes," such that all models in a class share the same set of possible outcomes (e.g., the same set of possible orientation maps) when a certain "control parameter" is small. Wolf and his colleagues assumed, as in many previous models of orientation maps (*7*), that each site in the two-dimensional cortical sheet is characterized by two variables: an orientation preference and selectivity. These variables then develop through mutual interactions; for example, a site preferring vertical might nudge its neighbors toward the same preference. They assumed that these interactions respect basic symmetries; for example, the interactions between a site and its surrounding sites should have the same form no matter where the site is on the cortical sheet. Finally, they allowed for long-range interactions (between sites more than a map period apart), based on the presence in V1 of long-range connections between neurons. In the mature animal, these connections link cells of similar preferred orientation (*8*), and their basic structure is present before orientation maps develop (*9*, *10*). They showed that all models that share the basic symmetries they assumed, and also have long-range suppressive interactions, form a universality class that generates maps with pinwheel densities closely approaching π (*11*). ["Suppressive" means that a site preferring vertical tends to push connected sites away from vertical; this is consistent with the largely suppressive effects that V1's long-range connections have on neural activity (*8*).] The suppressive long-range interactions are key to stabilizing pinwheels, which otherwise largely disappear during development. The theoretical framework strictly applies only when the control parameter is small, but in numerical simulations of a particular biologically plausible model in the class, Kaschube *et al*. found that the conclusions apply more broadly. Thus, a large and very plausible class of self-organizing models predict—independent of model details and with no tunable parameters—the precise structures that Kaschube *et al*. found across distant species.

The universality of self-organizing behavior provides a simple and compelling explanation for the arrival of widely divergent evolutionary lines at this common design. Rodents and lagomorphs, which separated from the primate/shrew line long after carnivores, lack orientation maps (their V1 neurons are orientation selective, but preferred orientation varies apparently randomly from cell to cell) (*12*–*14*). Thus, maps either independently evolved at least twice, or arose once and were lost in the rodent/lagomorph lines. The common ancestor of primates and carnivores had small brains with little neocortex (*15*). If this ancestor's V1 had maps, they likely would have contained only a small number of "hypercolumns" (regions of area λ^2). How did the common design either evolve twice, or persist in distant lines through substantial changes in V1, including an expansion to hundreds or thousands of hypercolumns? The universality of self-organization provides a simple answer; it is very difficult to think of a plausible alternative.

There is still much to be determined. This theoretical framework applies to maps containing power (a measure of signal strength) at only a single spatial period, and must be extended to incorporate the fact that real maps contain power over a broader range of periods. In addition, circuit development is determined by rules governing the growth and decay of thousands of synapses impinging on each neuron. How does this complexity yield a high-level description in terms of interactions between just two variables per cell (orientation preference and selectivity)? Experimentally, it will be fascinating to fill in the evolutionary tree of orientation maps and the common design. A definitive experiment, not yet technically feasible, would be to specifically eliminate the long-range connections during brain development and see whether maps with low pinwheel density develop, as theory predicts. Despite some caveats, the parameter-free prediction of π and its experimental verification to 2% precision will stand as landmarks of theoretical biology, as well as tremendous spurs to our thinking about cortical evolution and development.

References

1. M. Kaschube *et al*., *Science* **330**, 1113 (2010); 10.1126/science.1194869.
2. D. H. Hubel, T. N. Wiesel, *Brain and Visual Perception: The Story of a 25-Year Collaboration* (Oxford Univ. Press, New York, 2004).
3. K. D. Miller, E. Erwin, A. Kayser, *J. Neurobiol.* **41**, 44 (1999).
4. A. D. Huberman, M. B. Feller, B. Chapman, *Annu. Rev. Neurosci.* **31**, 479 (2008).
5. M. Kaschube, F. Wolf, T. Geisel, S. Löwel, *J. Neurosci.* **22**, 7206 (2002).
6. M. C. Cross, P. C. Hohenberg, *Rev. Mod. Phys.* **65**, 851 (1993).
7. N. V. Swindale, *Network* **7**, 161 (1996).
8. A. Angelucci, P. C. Bressloff, *Prog. Brain Res.* **154**, 93 (2006).
9. E. M. Callaway, L. C. Katz, *J. Neurosci.* **10**, 1134 (1990).
10. E. S. Ruthazer, M. P. Stryker, *J. Neurosci.* **15**, 7253 (1996).
11. M. Kaschube, M. Schnabel, F. Wolf, *N. J. Phys.* **10**, 015009 (2008).
12. S. D. Van Hooser, J. A. Heimel, S. Chung, S. B. Nelson, L. J. Toth, *J. Neurosci.* **25**, 19 (2005).
13. S. D. Van Hooser, *Neuroscientist* **13**, 639 (2007).
14. K. Ohki, S. Chung, Y. H. Ch'ng, P. Kara, R. C. Reid, *Nature* **433**, 597 (2005).
15. J. H. Kaas, *Evolutionary Neuroscience*, J. H. Kaas, Ed. (Elsevier, London, 2009), pp. 523–544.

10.1126/science.1198857

Plant and Animal Sensors of Conserved Microbial Signatures

Pamela C. Ronald[1,2,3]* and Bruce Beutler[4]

The last common ancestor of plants and animals may have lived 1 billion years ago. Plants and animals have occasionally exchanged genes but, for the most part, have countered selective pressures independently. Microbes (bacteria, eukaryotes, and viruses) were omnipresent threats, influencing the direction of multicellular evolution. Receptors that detect molecular signatures of infectious organisms mediate awareness of nonself and are integral to host defense in plants and animals alike. The discoveries leading to elucidation of these receptors and their ligands followed a similar logical and methodological pathway in both plant and animal research.

The mechanisms of plant and animal defense against microbes have historically been presumed to be separate and distinct (fig. S1). Beginning around the 1870s, studies of animal responses to infection revealed the existence of both "natural" or innate immunity, which involved the cells and molecules mediating host inflammatory responses, and adaptive immunity, which permitted the generation of cellular receptors with immense diversity and exquisite specificity for foreign macromolecules of almost any kind. Lacking phagocytes, lymphocytes, antibodies, and many other parts of the animal armamentarium, it seemed that the plant response to disease must use a fundamentally different strategy.

However, discoveries over the past 15 years demonstrate that the mechanisms that allow plants and animals to resist infection show impressive structural and strategic similarity (Fig. 1). Remarkably, the elucidation of these mechanisms followed a common approach involving a concerted attack on the same basic questions: What molecules are recognized by the host as signatures of infection? What receptors mediate recognition? These questions were ultimately answered by classical genetic studies.

Host Receptors that Recognize Microbial Signature Molecules

In biological systems, recognition implies the existence of one or more specific receptors that sense a molecular change in the environment and transduce this change at the cellular level, eliciting a response.

Plant host defense. Plant biology led the way in the discovery of proteins that directly sense infection. As in studies of interactions between lipopolysaccharide (LPS) and Toll-like receptor 4 (TLR4) (described below), genetic data preceded and accurately predicted physical evidence of receptor:ligand interaction. In 1946, Flor, working with the rust disease of flax, proposed the "gene-for-gene hypothesis" based on genetic analyses of variation within host and pathogen populations: When corresponding pathogen avirulence (*avr*) and host resistance (*R*) genes are present in each organism, recognition occurs and defense responses are activated, limiting infection (*1*). Flor's model presumed that specific sensors for microbial molecules, termed elicitors, or avr gene products, were present in immunocompetent hosts.

An intense hunt began in the 1980s to identify the genes encoding these receptors and their corresponding elicitors. Biochemists used innovative cell culture bioassays to monitor early responses of plant cells to diverse microbial molecules (*2*). They identified specific binding sites for elicitors on intact plant cells and on isolated plasma membranes, suggesting the presence of specific host receptors. However, as in mammalian systems, attempts to purify these receptors were unsuccessful.

In the 1990s, an avalanche of genetic experiments led to the isolation of the first *R* genes from multiple plant species. These discoveries established that diverse molecules and mechanisms govern the resistance phenotypes described by Flor and that the resistance response was more complex than previously realized. Some scientists predicted that certain *R* gene products might in fact be equivalent to the receptors that the biochemists were seeking (*2*). However, many plant biologists saw elicitor perception as a field of its own, little overlapping with the field of gene-for-gene resistance. One reason for this philosophical divergence was that many *R* genes conferred resistance to specific races of pathogens carrying *avr* genes thought to be highly variable, whereas elicitors were thought to be more broadly conserved. Isolation of diverse classes of *R* genes allowed direct testing of these disparate views.

Many *R* genes were shown to encode NLRs [nucleotide-binding domain, leucine-rich repeat (LRR)–containing intracellular proteins]. Others encoded kinase domains or receptor-like proteins, lacking kinases. Some R proteins were later shown to directly or indirectly perceive highly variable *avr* gene products, which are secreted directly into the plant cell through bacterial type III secretion systems (TTSS). One *R* gene, *Xa21* (*Xanthomonas* resistance 21), is of special interest in the context of this review, not only because it was predicted to recognize a conserved microbial determinant common to most if not all *X. oryzae* pv. *oryzae* (*Xoo*) strains, a property not previously noted in studies of most other *R* genes, but also because of its distinctive structure: a receptor kinase with LRRs in the extracellular domain (*3*). The cytoplasmic domain of XA21 belongs to the non–arginine-aspartate (non-RD) subclass of kinases. In contrast to RD kinases that carry a conserved arginine immediately preceding the catalytic aspartate, non-RD kinases typically carry a cysteine or glycine in place of the arginine. The non-RD domain was later shown to be a hallmark of kinases associated with early signaling events in both plant and animal innate immunity (*4*). LRR kinases that function in development fall into the RD class.

The predicted structure of XA21 immediately suggested a mechanism of action, in which the extracellular domain would engage a microbial elicitor leading to signal transduction by the cytoplasmic domain (Fig. 1). However, the structure of XA21 gave no clue as to nature of the microbially derived molecule, which was not isolated for another 14 years. We now know that XA21 binds to a highly conserved type I secreted peptide called $AxY^{S}22$ and that sulfation is critical for recognition (*5*).

The availability of the finished *Arabidopsis* and rice genome sequences (representative species of the two major classes of flowering plants, monocots and dicots) revealed that *Xa21* represented a large class of predicted host sensors with non-RD kinase domains. These include 35 proteins encoded in the *Arabidopsis* genome and 328 proteins encoded in the rice genome (*4*). Among these are the *Arabidopsis* proteins FLS2 and EFR (Ef-Tu receptor) and the rice proteins XA26, Pid2, and XA21 (Fig. 1).

The discovery of FLS2 in 2000, also by positional cloning and transgenic complementation of a null genetic background, was of particular importance to plant biologists because it was the first demonstration that a plant host sensor could directly bind a conserved microbial signature [see Supporting Online Material (SOM)]. Boller and colleagues showed that bacterial flagellin, or derivatives of the conserved flg22 epitope present in its N-terminal region, could elicit defense responses in *Arabidopsis* seedlings carrying the FLS2 receptor. With the discovery in 2001 that TLR5 served as the animal receptor

[1]Department of Plant Pathology, University of California, Davis, CA 95616, USA. [2]Joint Bioenergy Institute, Emeryville, CA 94710, USA. [3]Department of Plant Molecular Systems Biotechnology and Crop Biotech Institute, Kyung Hee University, Yongin 446-701, Korea. [4]Department of Genetics, Scripps Research Institute, 10550 North Torrey Pines Road, La Jolla, CA 92037, USA.

*To whom correspondence should be addressed. E-mail: pcronald@ucdavis.edu

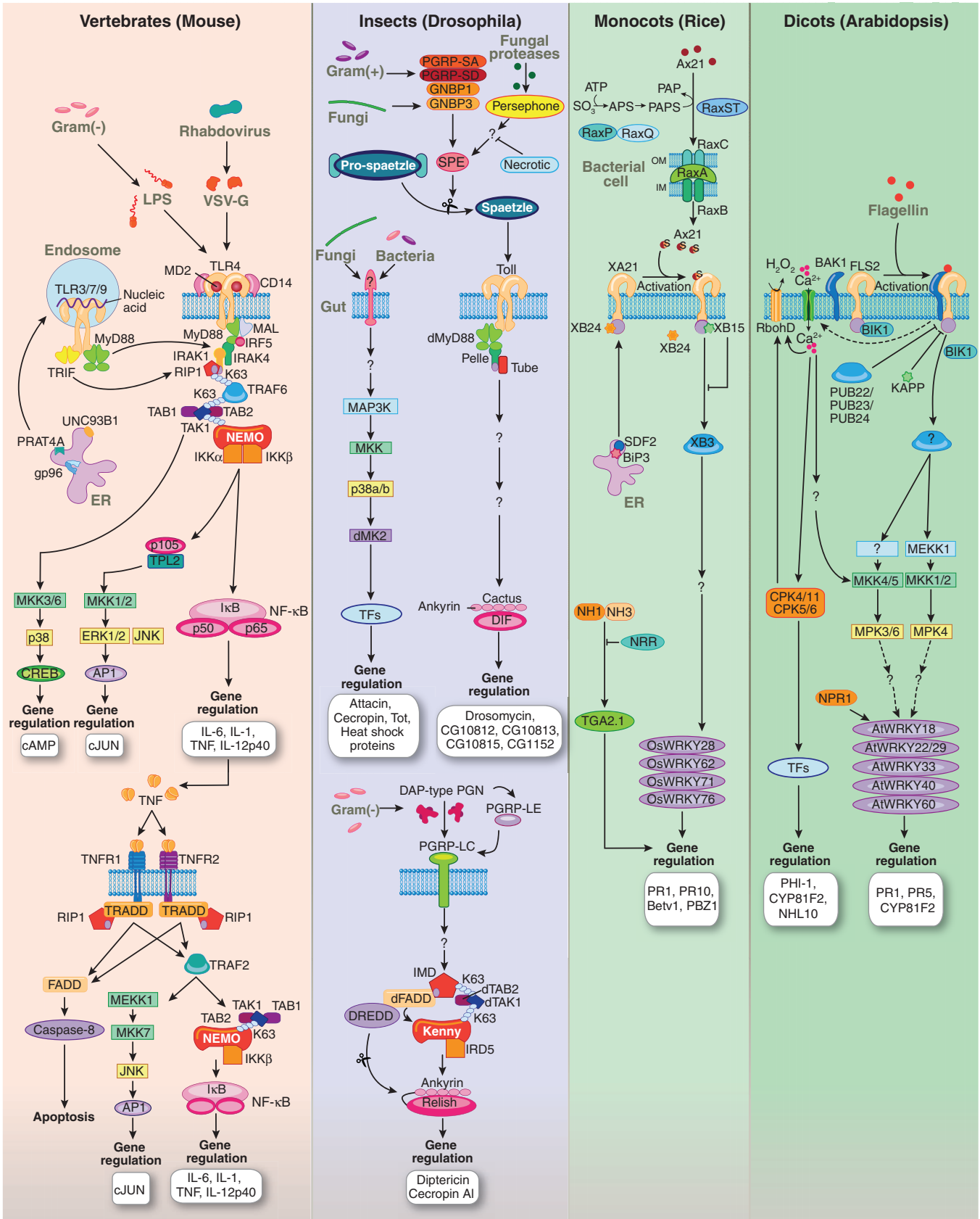

Fig. 1. Host-sensor mediated immune pathways in plants and animals. The pathways depicted are for mouse, fruit fly, rice, and *Arabidopsis*. (See SOM for details.)

for flagellin (*6*), a clear, irrefutable picture emerged: Plants and animals use similar types of cell surface sensors to detect conserved microbial signatures. These host sensors are often called pattern recognition receptors (PRRs) because they recognize conserved microbial-associated molecular patterns (MAMPs).

With the demonstration that XA21 binds a highly conserved *Xoo*-derived peptide (*5*) and the discovery that a mutation in FLS2 rendered *Arabidopsis* susceptible to the bacterial pathogen *Pseudomonas syringae* (*7*), the plant biology community began to accept that some classically defined resistance genes such as *Xa21* encode receptors for microbial signatures and that FLS2 functions in host resistance (*8*). In addition to the well characterized XA21, FLS2, and EFR host sensors, several receptor-like proteins and receptor kinases have been shown or hypothesized to be involved in recognition of conserved microbial signatures (see SOM). Conversely, a number of conserved microbial signature molecules, including proteins, fatty acids, and oligosaccharides, have been identified from bacteria and oomycetes, but their receptors have not yet been identified.

Insect host defense. The last common ancestor of insects and mammals is believed to have lived 640 million years ago (Ma), not long after the divergence of plants and animals. Work in *Drosophila* established that Toll, originally known for its function in development and its ability to elicit a nuclear factor κB (NF-κB) response, is a key transducer of responses to fungal and Gram-positive bacterial infection (*9*). Like XA21, FLS2, and EFR, Toll carries LRRs in the predicted extracellular domain and signals through a non-RD kinase called Pelle (in the case of Toll, the kinase is not integral to the receptor). It also shares the Toll /interleukin-1 (IL-1) receptor (TIR) domain with several plant NLRs (fig. S2). Thus, the discovery of a role for Toll in the innate immune response provided a structural link between sensors used by plants and animals to detect infection.

Toll does not serve as a receptor for any known molecule of fungal origin, nor do eight of the nine Toll paralogs known in *Drosophila* (all of them save Toll itself) have any immune function whatsoever. Instead, Toll responds to Spaetzle, which is cleaved from an endogenous protein as a result of infection. This recognition leads to activation of Pelle and to signals that culminate in the production of antimicrobial peptides as well as hundreds of other proteins, most of unknown function (Fig. 1) (*9*).

A second sensing pathway in *Drosophila* detects Gram-negative bacteria. The Imd pathway shows striking similarities to the mammalian tumor necrosis factor (TNF) signaling pathway (Fig. 1) (*9*). Mammalian TLRs trigger TNF release, and TNF signals via a pair of receptors represented on most cells. Thus, two separate ancestral pathways may have been passed to insects but became fused together in mammals, or conversely, a single ancestral pathway was split in insects but retained intact in mammals. Notably, unlike its human counterpart receptor-interacting protein (RIP), *Drosophila* Imd lacks a kinase domain. To date, no kinases have been found to associate with the peptidoglycan receptor complex PGRP-LC, which operates as the transmembrane sensor for the Imd pathway.

The determination that Toll has an immune function in *Drosophila* immediately raised questions as to whether mammalian homologs, first reported in 1994 (*10*, *11*), might have a similar function. Although transfection-mediated overexpression of truncated, chimeric versions of one human TLR induced NF-κB activation in mammalian cells (*12*), no conclusions regarding the specificity of the receptor could be drawn on this basis; indeed it remained uncertain whether it responded to a microbial ligand, to an endogenous ligand, or was actually involved in infection at all. Unbiased genetic research revealed the actual function of this receptor and pointed to a specific role for TLRs in microbe sensing.

Mammalian host defense. In mammals, the identification of microbial inducers of innate immune responses, equivalent to the elicitors of the plant world, long preceded the discovery of the specific receptors that detect infection. The groundwork for receptor discovery was laid as early as the 1890s, when heat-stable molecules of microbial origin were shown to induce fever and shock in the mammalian host. Foremost among the inducers was endotoxin (LPS), represented in most Gram-negative bacteria (*13*). Widely known for its ability to induce septic shock, LPS is perhaps the most powerful elicitor of inflammation known in mammals but is not unique in a qualitative sense. Lipopeptides, double-stranded RNA, microbial DNA, flagellin, and other molecules of microbial origin elicit inflammatory responses similar to those provoked by LPS. The identification of the receptors for these molecules was the central challenge in the field of animal innate immunity.

In mammals, the cytokine response (and particularly TNF production) was taken as an indicator of a biological response to LPS. The existence of a nonredundant LPS receptor was strongly suggested by two spontaneous mouse mutations affecting a locus known as *Lps*. Both mutations rendered mice insensitive to LPS and highly susceptible to Gram-negative infection. The mutations were positionally cloned in 1998, revealing that these strains carried either a missense error in *Tlr4* or deletion of the entire locus (*14*). Genetic data predicted that LPS must directly interact with TLR4, in that certain isoforms of LPS were species-dependent in their stimulatory effects (*15*, *16*). Later TLR4 was found to contact LPS in conjunction with MD-2, a secreted host protein with a hydrophobic pocket into which most of the LPS lipid chains become inserted (*17*). An essential contribution to LPS sensing is also made by CD14, an LRR protein that facilitates engagement of LPS by the TLR4/MD-2 complex, and is absolutely required for the detection of highly glycosylated (smooth) LPS.

Twelve mouse TLRs and ten human TLRs are now recognized, and most respond to infection, each detecting a circumscribed collection of molecules of microbial origin. Mutations that abolish the function of individual TLRs cause selective susceptibility to a certain spectrum of microbes; mutations that prevent all TLR signaling cause severe and general immunodeficiency (*18*). Nucleic acid–sensing TLRs are positioned chiefly within endosomes; those that detect other components of microbes are located mainly at the cell surface, although they are subject to internalization, as are some plant sensors such as the *Arabidopsis* FLS2 receptor (*19*). TLRs lack kinase domains and signal via cytoplasmic TIR domains that recruit one or more adaptor proteins (MyD88, TICAM1, TRAM, or TIRAP) to propagate signaling (Fig. 1).

In addition to the TLRs, intracellular sensors of the retinoic acid-inducible gene I (RIG-I)–like helicase family (RIG-I, Mda5, and Lgp2) detect single- and double-stranded RNA and the 5′ triphosphate moiety of viral RNA. C-type lectins, including dectin-1 and DC-SIGN, as well as eIF2α kinases such as double-stranded RNA-dependent protein kinase (PKR) and general control nonderepressible 2 (GCN2) kinase, are known to sense microbial carbohydrates and viral nucleic acids, respectively. Inflammasomes also detect and respond to some pathogens and danger signals (among them asbestos, silica, and nigericin) often in a subsidiary, TLR-dependent manner. The cores of these inflammasomes are formed by intracellular proteins of the NOD-like receptor (NLR) family, including Nlrp1, Nlrp3, IPAF, and AIM2. NLR proteins mediate apoptotic and inflammatory responses. The NLR proteins are structurally similar to plant NLR proteins but do not carry TIR domains, which are apparently reserved for signaling by TLRs or IL-1, IL-18, or IL-33, either at the cell surface or within endosomes. In contrast to the animal NLR proteins, none of the plant NLRs has been demonstrated to bind conserved microbial signatures, nor do they associate with non-RD kinases, suggesting a distinct mode of activation for these proteins (*4*).

As discussed in recent reviews, successful pathogens have evolved countermeasures to host sensor-mediated immunity, for example, delivering inhibitors of the immune response directly into the plant cytoplasm via the TTSS (*8*). In animals, TTSS-mediated delivery of proteins with TIR domain structures is known (*20*). Poxviruses encode proteins with TIR domain facsimiles as well (*21*). These findings attest to the universal importance of the innate immune response apparatus and its efficacy in combating infection.

Comparisons Between Animals and Plants: What Two Billion Years of Evolution Has Changed and What It Hasn't

We now know that plants and animals respond to microbial signature molecules using analo-

gous regulatory modules, which likely came about as a consequence of convergent evolution (fig. S2) (*22*). For example, many plant, fly, and mammalian host sensors, including XA21, FLS2, EFR, Toll, and the TLRs, use the LRR domain as their ligand recognition and binding surface. LRR proteins are among the most avid binding reagents found in nature, used in both plants and animals for the engagement of proteins, lipids, glycans, and nucleic acids (*18*). Undoubtedly, the ability of LRRs to engage almost any type of molecule led to their selection as molecular building blocks in recombinatorial adaptive immune receptors in jawless fish (*23*), whereas other vertebrates used the immunoglobulin fold for the same purpose. The three-dimensional structures of several TLR extracellular domains (TLR3, TLR4, TLR2/6, and TLR1/2) suggest that all of these sensors share similar shapes (fig. S2).

Similarly, the non-RD kinase motif has been recruited by both plants and animals to transduce the innate immune response. Mutagenesis of the kinase domains of RIP1, RIP2, RIP4, IL-1 receptor-associated kinase (IRAK1), and XA21 demonstrate that kinase activity is at least partially dispensable for the innate immune response (see SOM). This is a departure from the conventional role of kinases in signaling, and in the cases of IRAK1, XA21, and RIP2, evidence suggests that these non-RD kinases function partly as phosphorylation-mediated scaffold proteins, as distinct from enzymes that mediate signaling through a phospho-relay cascade. Thus, it appears that plant and animal receptors that associate with non-RD kinases or carry the non-RD domain integral to the receptor serve as host sensors per se. In contrast, RD kinases regulate nonimmune responses or serve as coregulators of the non-RD host sensors and do not bind microbial signatures on their own.

In animals, the MyD88/IRAK1/IRAK4 complex associates with the RING finger ubiquitin ligase TNF receptor-associated factor 6 (TRAF6), which autoubiquitinates and also ubiquitinates other proteins to propagate TLR signaling. Similarly, XB3, a plant RING finger ubiquitin ligase, transduces XA21-mediated innate immunity (see SOM).

Plants do not have NF-κB–related transcription factors. Instead, the rice and *Arabidopsis* innate immune responses rely on WRKY-related transcription factors, which do not exist in animals. The WRKY motif is often accompanied by zinc finger and leucine zipper motifs, and as WRKY factor regulation is dependent on mitogen-activated protein kinase cascades in *Arabidopsis* (Fig. 1), WRKY and activator protein 1 (AP1) might be considered analogous.

Host sensor–mediated immune responses are essential for innate immunity in both plants and animals, but sustained or highly induced immune responses can be harmful. Thus, negative regulation of these pathways is critical. In animals, negative regulators act at multiple levels within TLR signaling cascades (*24*). Little is yet known about negative regulation of plant innate immunity, although one important class of negative regulators is the Ser/Thr protein phosphatase 2Cs (PP2Cs) (Fig. 1). Another important control of innate immune responses in both plants and animals is by endoplasmic reticulum (ER)–resident chaperones, which are required for TLR2, TLR4, TLR5, TLR7, TLR9, EFR, and XA21 biogenesis (Fig. 1).

Outlook

The lineages of humans and mice diverged 60 to 120 Ma, monocots and dicots about 170 to 235 Ma, insects and mammals >640 Ma, and plants and animals perhaps one billion years ago. If evolution is depicted as a tree, and extant species as terminal leaves on that tree, we must acknowledge that we have examined only a few of those leaves, gaining only a fragmentary impression of what is and what once was. As sequencing methodology advances, we will almost surely see that some species emphasize specific mechanisms of resistance to the relative exclusion of others. Witness *Drosophila* with its single immunologically active Toll receptor, *Arabidopsis* with its dozens of host sensors, and rice with its hundreds (*4*). Only recently, we were surprised to discover the independent evolution of a system of recombinatorial receptors mediating adaptive immunity in the jawless fishes (*25*) and the presence of a predicted microbial sensor in wheat with a structure that does not appear in rice (last common ancestor: a mere 50 to 70 Ma) (*26*). Many similar surprises likely await the examination of other "leaves."

In the future, researchers will increasingly focus on harnessing basic knowledge about host sensors to advance plant and animal health. A diverse array of conserved signatures from pathogenic microbes will likely be discovered. Many of these will almost certainly act as binding partners for the large class of predicted orphan host sensors present in agronomically important crops (*4*). Some will likely serve as new drug targets to control deadly groups of bacteria for which there are currently no effective treatments (*27*). Characterization of new host sensors will pave the way to interspecific and intergeneric transfer between plants of engineered receptors that confer resistance to a variety of pathogens. The effectiveness of this approach has already been demonstrated by the transfer of Xa21 and engineered derivatives to cultivated rice varieties (*3*), of a stripe rust resistance gene to cultivated wheat varieties (*26*), and of *Arabidopsis* EFR to tobacco and tomato (see SOM). In vertebrates as well, there may be room to engineer resistance. Adult chickens are remarkably indifferent to LPS. Would they be more sensitive to it and better able to resist Gram-negative infection if they expressed the mammalian version of TLR4? Are some microbes pathogenic to humans because they have managed to evade detection by human TLRs? Other manipulations may be imagined now that some of the essential building blocks of immunity have been elucidated.

References and Notes

1. H. H. Flor, *Annu. Rev. Phytopathol.* **9**, 275 (1971).
2. T. Boller, *Annu. Rev. Plant Physiol. Plant Mol. Biol.* **46**, 189 (1995).
3. W. Y. Song *et al.*, *Science* **270**, 1804 (1995).
4. C. Dardick, P. Ronald, *PLoS Pathog.* **2**, e2 (2006).
5. S. W. Lee *et al.*, *Science* **326**, 850 (2009).
6. F. Hayashi *et al.*, *Nature* **410**, 1099 (2001).
7. C. Zipfel *et al.*, *Nature* **428**, 764 (2004).
8. T. Boller, S. Y. He, *Science* **324**, 742 (2009).
9. D. Ferrandon, J. L. Imler, C. Hetru, J. A. Hoffmann, *Nat. Rev. Immunol.* **7**, 862 (2007).
10. N. Nomura *et al.*, *DNA Res.* **1**, 27 (1994).
11. T. Taguchi, J. L. Mitcham, S. K. Dower, J. E. Sims, J. R. Testa, *Genom.* **32**, 486 (1996).
12. R. Medzhitov, P. Preston-Hurlburt, C. A. Janeway Jr., *Nature* **388**, 394 (1997).
13. B. Beutler, E. T. Rietschel, *Nat. Rev. Immunol.* **3**, 169 (2003).
14. A. Poltorak *et al.*, *Science* **282**, 2085 (1998).
15. I. Smirnova, A. Poltorak, E. K. L. Chan, C. McBride, B. Beutler, *Genome Biol.* **1**, 1 (2000).
16. E. Lien *et al.*, *J. Clin. Invest.* **105**, 497 (2000).
17. H. M. Kim *et al.*, *Cell* **130**, 906 (2007).
18. B. A. Beutler, *Blood* **113**, 1399 (2009).
19. S. Robatzek, D. Chinchilla, T. Boller, *Genes Dev.* **20**, 537 (2006).
20. C. Cirl, T. Miethke, *Int. J. Med. Microbiol.* **300**, 396 (2010).
21. A. Bowie *et al.*, *Proc. Natl. Acad. Sci. U.S.A.* **97**, 10162 (2000).
22. F. M. Ausubel, *Nat. Immunol.* **6**, 973 (2005).
23. Z. Pancer *et al.*, *Nature* **430**, 174 (2004).
24. L. A. O'Neill, *Immunity* **29**, 12 (2008).
25. M. D. Cooper, M. N. Alder, *Cell* **124**, 815 (2006).
26. D. Fu *et al.*, *Science* **323**, 1357 (2009).
27. H. W. Boucher *et al.*, *Clin. Infect. Dis.* **48**, 1 (2009).
28. This paper is dedicated to Julius Rothstein (1830–1899) and his wife, Fanny Rothstein née Frank (1834–1911), the great, great grandparents and last common ancestors of the authors.

Supporting Online Material

www.sciencemag.org/cgi/content/full/330/6007/1061/DC1
SOM Text
Figs. S1 and S2
References

10.1126/science.1189468

γ-Secretase Gene Mutations in Familial Acne Inversa

Baoxi Wang,[1]* Wei Yang,[2]* Wen Wen,[3]* Jing Sun,[2]* Bin Su,[1]* Bo Liu,[4] Donglai Ma,[1] Dan Lv,[2] Yaran Wen,[2] Tao Qu,[1] Min Chen,[5] Miao Sun,[2] Yan Shen,[2,4]† Xue Zhang[2,3]†

Acne inversa (AI), also known as hidradenitis suppurativa, is a chronic inflammatory disease of hair follicles whose characteristic features include draining sinuses, painful skin abscesses, and disfiguring scars (*1*). The German philosopher Karl Marx is thought to have suffered from this skin condition (*2*). AI typically occurs after puberty and can be either familial or sporadic. Familial AI [Online Mendelian Inheritance in Man (OMIM) 142690] usually shows an autosomal-dominant inheritance pattern and appears to be genetically heterogeneous (*1*, *3*).

γ-Secretase is a transmembrane protease consisting of four essential protein subunits: one catalytic presenilin subunit and three cofactor subunits [presenilin enhancer 2 (PEN2), nicastrin (NCT), and anterior pharynx defective 1 (APH1)] (Fig. 1). It mediates intramembranous cleavage of various type I membrane proteins, including amyloid precursor protein and Notch (*4*). Genetic inactivation of γ-secretase in mouse skin produces epidermal and follicular abnormalities that are histopathologically similar to those observed in human AI and that arise through alterations in Notch signaling (*5*).

To investigate the genetic mechanisms underlying AI, we collected samples from six Han Chinese families with features of AI as well as additional skin lesions on back, face, nape, and waist (figs. S1 and S2). By means of a combined genome-wide linkage scan and haplotype analysis in two large four-generation families (families 1 and 2), we mapped an AI locus to an interval on chromosome 19q13 (*6*). The PEN2-coding *PSENEN* gene maps to this region. Sequence analysis of all *PSENEN* exons and introns in family 1 revealed a guanine deletion (c.66delG), producing a frameshift and premature termination codon (p.F23LfsX46) (Fig. 1 and fig. S3). In family 2, we identified a cytosine deletion (c.279delC) in *PSENEN*, causing a frameshift and delayed termination codon (p.F94SfsX51) (Fig. 1 and fig. S3). These two deletions were predicted to change the distal three-fourths and the functionally important C-terminal domain of PEN2, respectively (*7*). In families 3 to 6, we found a cytosine deletion (c.725delC, family 4) in *PSEN1*, the gene encoding presenilin 1, and different mutations in the NCT-coding *NCSTN* gene, including a guanine deletion (c.1752delG, family 3), a guanine-to-adenine transition at the invariant +1 position of the donor site of intron 13 (c.1551+1G>A, family 5), and a cytosine-to-thymine transition (c.349C>T, family 6) (Fig. 1 and fig. S3). The single-base deletion in *PSEN1* would result in a frameshift and premature termination codon (p.P242LfsX11) (Fig. 1). The three distinct *NCSTN* mutations were predicted to cause a frameshift and premature termination codon (p.E584DfsX44), an abnormal splicing event, and a nonsense mutation at codon 117 (p.R117X), respectively (Fig. 1). In each family, the independent heterozygous mutations were detected in all available affected individuals. None of the mutations were detected in chromosomes from 200 ethnically matched control individuals.

To study mRNA expression of the mutant alleles, we conducted reverse transcription polymerase chain reaction (RT-PCR) analysis by using peripheral lymphocytes available from the affected individuals of families 3 to 6. In the individuals carrying a frameshift or nonsense mutation in *PSEN1* or *NCSTN*, we observed a marked reduction in transcript expression from the mutant allele, suggesting that these mutations most likely cause nonsense-mediated mRNA decay and thus result in a complete loss of function (figs. S3 and S4). In the carrier of the splicing mutation in *NCSTN*, we confirmed the skipping of exon 13, leading to loss of 32 amino acid residues in the NCT protein (p.A486_T517del) (Fig. 1 and fig. S3).

Overall, our results establish haploinsufficiency of the γ-secretase component genes as the genetic basis for a subset of familial AI and implicate the γ-secretase–Notch pathway in the molecular pathogenesis of AI, making γ-secretase a promising target for anti-AI therapeutic drug development.

Our genetic findings also demonstrate that familial AI can be an allelic disorder of early-onset familial Alzheimer's disease (AD). It is well known that mutations in the two presenilin genes (*PSEN1* and *PSEN2*), but not the other γ-secretase component genes, cause early-onset familial AD and non-Alzheimer dementias (*4*, *8*). Notably, all the AD/dementia-causing *PSEN* mutations identified so far are missense or in-frame deletions or insertions (www.molgen.ua.ac.be/ADMutations), and no AD case has been reported to co-occur with AI. Of the 50 affected individuals we genotyped in our study families, 15 were age 50 or above. Interestingly, none of these individuals had symptoms of AD or dementias, although definitive exclusion of these diagnoses will require careful neurological evaluation of the patients.

If further studies confirm that familial AD and AI are mutually exclusive phenotypes in individuals with *PSEN1* mutations, then our findings suggest that *PSEN1* mutations may cause familial AD and AI through distinct mechanisms and that simple inactivation of a single *PSEN1* allele may not be sufficient to cause familial AD.

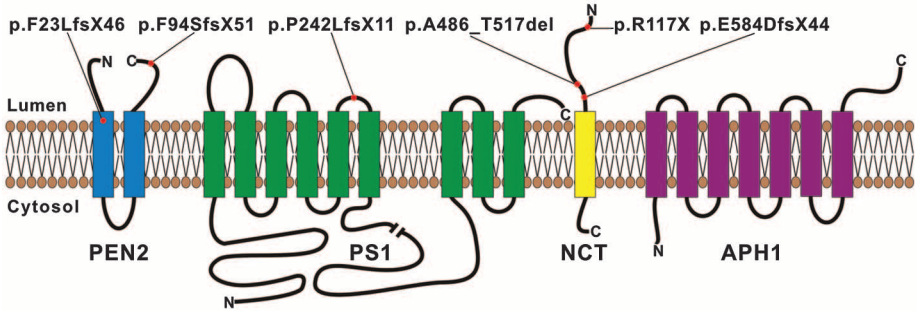

Fig. 1. Schematic diagram of the γ-secretase complex with a summary of acne inversa-associated mutations. Colored bars represent the transmembrane domains. Mutations are shown as red dots.

References and Notes

1. J. Revuz, *J. Eur. Acad. Dermatol. Venereol.* **23**, 985 (2009).
2. S. Shuster, *Br. J. Dermatol.* **158**, 1 (2008).
3. M. Gao *et al.*, *J. Invest. Dermatol.* **126**, 1302 (2006).
4. B. A. Bergmans, B. De Strooper, *Lancet Neurol.* **9**, 215 (2010).
5. Y. Pan *et al.*, *Dev. Cell* **7**, 731 (2004).
6. Materials and methods are available as supporting material on *Science* Online.
7. S. Prokop, C. Haass, H. Steiner, *J. Neurochem.* **94**, 57 (2005).
8. J. Shen, R. J. Kelleher 3rd, *Proc. Natl. Acad. Sci. U.S.A.* **104**, 403 (2007).

Supporting Online Material

www.sciencemag.org/cgi/content/full/science.1196284/DC1
Materials and Methods
SOM Text
Figs. S1 to S4
Tables S1 to S4
References

9 August 2010; accepted 28 September 2010
Published online 7 October 2010;
10.1126/science.1196284
Include this information when citing this paper.

[1]Peking Union Medical College Hospital, Chinese Academy of Medical Sciences–Peking Union Medical College (CAMS-PUMC), Beijing, China. [2]State Key Laboratory of Medical Molecular Biology, Institute of Basic Medical Sciences, CAMS-PUMC, Beijing, China. [3]China Medical University, Shenyang, China. [4]Chinese National Human Genome Center at Beijing, Beijing, China. [5]Institute of Dermatology, CAMS-PUMC, Nanjing, China.

*These authors contributed equally to this work.
†To whom correspondence should be addressed. E-mail: xuezhang@pumc.edu.cn (X.Z.); shen.yan@imicams.ac.cn (Y.S.)

Structures of the CXCR4 Chemokine GPCR with Small-Molecule and Cyclic Peptide Antagonists

Beili Wu,[1] Ellen Y. T. Chien,[1] Clifford D. Mol,[1] Gustavo Fenalti,[1] Wei Liu,[1] Vsevolod Katritch,[2] Ruben Abagyan,[2] Alexei Brooun,[3] Peter Wells,[3] F. Christopher Bi,[3] Damon J. Hamel,[2] Peter Kuhn,[1] Tracy M. Handel,[2] Vadim Cherezov,[1] Raymond C. Stevens[1]*

Chemokine receptors are critical regulators of cell migration in the context of immune surveillance, inflammation, and development. The G protein–coupled chemokine receptor CXCR4 is specifically implicated in cancer metastasis and HIV-1 infection. Here we report five independent crystal structures of CXCR4 bound to an antagonist small molecule IT1t and a cyclic peptide CVX15 at 2.5 to 3.2 angstrom resolution. All structures reveal a consistent homodimer with an interface including helices V and VI that may be involved in regulating signaling. The location and shape of the ligand-binding sites differ from other G protein–coupled receptors and are closer to the extracellular surface. These structures provide new clues about the interactions between CXCR4 and its natural ligand CXCL12, and with the HIV-1 glycoprotein gp120.

Chemokine receptors are G protein–coupled receptors (GPCRs) that, together with their small protein ligands, regulate the migration of many different cell types, most notably leukocytes (*1*–*3*). CXCR4, one of 19 known human chemokine receptors, is activated exclusively by the chemokine CXCL12 (also known as stromal cell–derived factor–1, SDF-1) and couples primarily through G_i proteins. Targeted deletion of CXCR4 or CXCL12 in mice confers embryonic lethality and leads to defects in vascular and CNS development, hematopoiesis, and cardiogenesis (*4*, *5*). CXCR4 has been associated with more than 23 types of cancers, where it promotes metastasis, angiogenesis, and tumor growth or survival (*6*–*10*). Furthermore, T-tropic HIV-1 uses CXCR4 as a co-receptor for viral entry into host cells (*11*). Thus, the discovery that endogenous CXCL12 inhibits HIV-1 entry suggested the therapeutic potential of targeting CXCR4 to block viral infection (*12*, *13*). Despite a wealth of data related to CXCR4 and GPCRs in general, many aspects of ligand binding and signaling are poorly understood at the molecular level. For instance, CXCR4 has a propensity to form hetero- and homooligomers (*14*, *15*), and such oligomerization could play a role in the allosteric regulation of CXCR4 signaling (*16*). Although structural understanding of GPCRs has benefited from a number of recent breakthroughs (*17*–*20*), coverage of the superfamily's phylogenetic tree is incomplete, and a structure of a GPCR that is activated by a protein ligand has not been reported.

Protein engineering, ligand selection, and structure determination. Here we report the crystal structures of human CXCR4 in complex with a small-molecule antagonist at 2.5 Å resolution and with a cyclic peptide inhibitor at 2.9 Å resolution. Three stabilized constructs (CXCR4-1, CXCR4-2, and CXCR4-3) (table S1) expressed in baculovirus-infected *Spodoptera frugiperda* (Sf9) insect cells were selected for structural studies on the basis of thermal stability, monodispersity, and lipid matrix diffusion. Similar to the previously determined high-resolution structures of the β_2-adrenergic receptor (β_2AR) (*17*, *21*) and A_{2A} adenosine receptor (A_{2A}AR) (*18*), the CXCR4 constructs contain a T4 lysozyme (T4L) fusion inserted between transmembrane (TM) helices V and VI at the cytoplasmic side of the receptor. In addition, all three constructs contain a thermostabilizing L125$^{3.41}$W mutation (*22*–*24*). The constructs differ in the precise T4L junction site, the position of the C-terminal truncation, as well as a T240$^{6.36}$P mutation in CXCR4-3, and required further stabilization with ligands to facilitate purification and crystallization. Two antagonists were selected for crystallization trials on the basis of ligand solubility, binding affinity, and induced protein thermostability (tables S2 and S3) and using a small, druglike, isothiourea derivative (IT1t) (*25*) and CVX15, a 16-residue cyclic peptide analog of the horseshoe crab peptide polyphemusin, which was previously characterized as an HIV-inhibiting and antimetastatic agent (*26*–*28*).

Before crystallization trials, the effects of the protein engineering on CXCR4 function were evaluated using radioligand-binding and calcium flux assays. CXCR4-WT (wild type) expressed in Sf9 cells binds a [^{3}H]bis(imidazolylmethyl) amine analog (BIMA) with an affinity similar to that of the same construct expressed in human embryonic kidney (HEK) 293 cells (dissociation constant, K_d = 3.5 ± 1.5 and 3.7 ± 1.4 nM, respectively). All other constructs expressed in Sf9 cells also show similar binding affinity to BIMA and IT1t (table S3). However, CXCR4-1 and CXCR4-2 display lower binding affinities for the CVX15 peptide compared with CXCR4-WT and CXCR4-3. Calcium flux assays demonstrated the expected result that these constructs do not activate G proteins (fig. S1), because of the T4L insertion in the third intracellular loop, which is critical for G protein interactions. Assays with the same constructs lacking T4L confirmed that the stabilizing L125$^{3.41}$W mutation, as well as the various C-terminal truncations, did not adversely affect calcium release, whereas the T240$^{6.36}$P mutation, which is present only in the CXCR4-3 construct, abolished signaling.

After extensive optimization of crystallization conditions in lipidic mesophase, five distinct crystal structures were obtained (table S4). CXCR4-1, CXCR4-2, and CXCR4-3 were cocrystallized with IT1t (two crystal structures for CXCR4-2); crystals

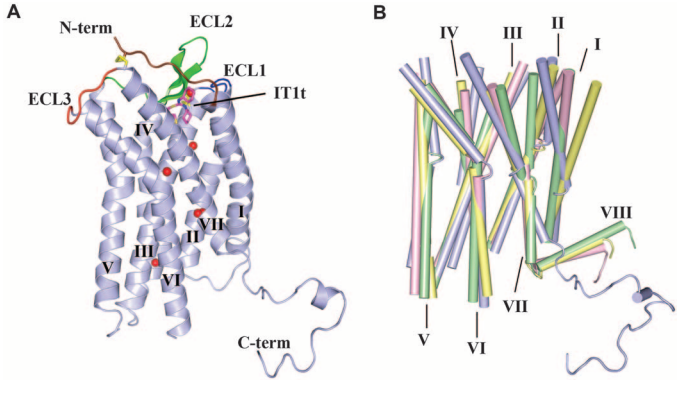

Fig. 1. Overall fold of the CXCR4-IT1t complex and comparison with other GPCR structures. (**A**) Overall fold of the CXCR4-2–IT1t. The receptor is colored blue. The N terminus, ECL1, ECL2, and ECL3 are highlighted in brown, blue, green, and red, respectively. The compound IT1t is shown in a magenta stick representation. The disulfide bonds are yellow. Conserved water molecules (*68*) are shown as red spheres. (**B**) Comparison of TM helices for CXCR4 (blue); β_2AR (PDB ID: 2RH1; yellow); A_{2A}AR (PDB ID: 3EML; green); and rhodopsin (PDB ID: 1U19; pink).

[1]Department of Molecular Biology, The Scripps Research Institute, 10550 North Torrey Pines Road, La Jolla, CA 92037, USA. [2]Skaggs School of Pharmacy and Pharmaceutical Sciences, and San Diego Supercomputer Center, University of California, San Diego, La Jolla, CA 92093, USA. [3]Pfizer Worldwide Research and Development, 10770 Science Center Drive, San Diego, CA 92121, USA.

*To whom correspondence should be addressed. E-mail: stevens@scripps.edu

of CXCR4-3 were also obtained with CVX15. Data collection and refinement statistics for all five crystal structures are shown in table S1 (*29*).

Overall architecture of CXCR4. The overall structure of CXCR4 bound to the small-molecule antagonist IT1t is conserved in all crystal structures with a Cα root mean square deviation (RMSD) in a TM bundle of less than 0.6 Å. Binding of the CVX15 cyclic antagonist peptide induced conformational differences relative to IT1t in the CXCR4-3/CVX15 structure (TM Cα RMSD of 0.9 Å). For clarity, we focus on the highest-resolution crystal structure of CXCR4-2/IT1t (2.5 Å, monomer A) for discussion of the CXCR4 structural features and comparison with other GPCR structures. The final model includes 293 residues (27 to 319) of the 352 residues of CXCR4 and residues 2 to 161 of T4L. The 26 N-terminal residues of CXCR4 did not have interpretable density and are presumed to be disordered. The main fold of CXCR4 consists of the canonical bundle of seven-TM α helices (Fig. 1A), which shows about the same level of structural divergence from seven-TM helical bundles of previously solved GPCR structures (Cα RMSDs ≈ 2.0 to 2.2 Å) (Fig. 1B). The most striking differences in the disposition of the TM helices of CXCR4 are the following: (i) The extracellular end of helix I is shifted toward the central axis of the receptor by 9 Å compared with β_2AR and by more than 3 Å compared with A_{2A}AR. (ii) Helix II makes a tighter helical turn at Pro92$^{2.58}$, resulting in ~120° rotation of its extracellular end compared with other GPCR structures (this rotation essentially introduces a one-residue gap in the sequence alignment that would result in wrong residues facing the ligand-binding pocket in a homology model that did not account for the rotation). (iii) Both intracellular and extracellular tips of helix IV in CXCR4 substantially deviate (~5 and ~3 Å, respectively) from their consensus positions in other GPCRs. (iv) The extracellular end of helix V in CXCR4 is about one turn longer. (v) Helix VI has a similar shape in all structures and is characterized by a sharp kink at the highly conserved residue, Pro254$^{6.50}$; however, its extracellular end is shifted by ~3 Å in CXCR4 relative to β_2AR and A_{2A}AR. Finally (vi), the extracellular end of helix VII in CXCR4 is two helical turns longer than in other GPCR structures. These two extra turns place Cys274$^{7.25}$ at the tip of helix VII in a strategic position to form a disulfide bond with Cys28 in the N-terminal region. Taken together, these multiple differences suggest that accurate homology modeling of even the CXCR4 TM bundle, let alone the entire structure, would be challenging.

The extracellular interface of CXCR4 consists of 34 N-terminal residues; extracellular loop 1 (ECL1, residues 100 to 104) linking helices II and III; ECL2 (residues 174 to 192) linking helices IV and V; and ECL3 (residues 267 to 273) linking helices VI and VII (Fig. 1A). Clear density starts at Pro27, adjacent to Cys28, which pins the base of the N-terminal segment to Cys274$^{7.25}$ at the tip of helix VII via a disulfide bond; these two cysteines are conserved in all chemokine receptors except CXCR5 and CXCR6 (fig. S2). Another disulfide links Cys109$^{3.25}$ with Cys186 of ECL2, which is the largest extracellular loop in CXCR4. Although ECL2 length, sequence, and secondary structure vary dramatically in GPCRs, the disulfide connecting ECL2 with the extracellular end of helix III is highly conserved in chemokine receptors and most other class A GPCRs. Both disulfide bonds at the extracellular side of CXCR4 are critical for ligand binding (*30*), and the crystal structure shows that they function by constraining ECL2 and the N-terminal segment (residues 27 to 34), which shapes the entrance to the ligand-binding pocket.

The intracellular side of CXCR4 contains intracellular loop 1 (ICL1, residues 65 to 71) linking

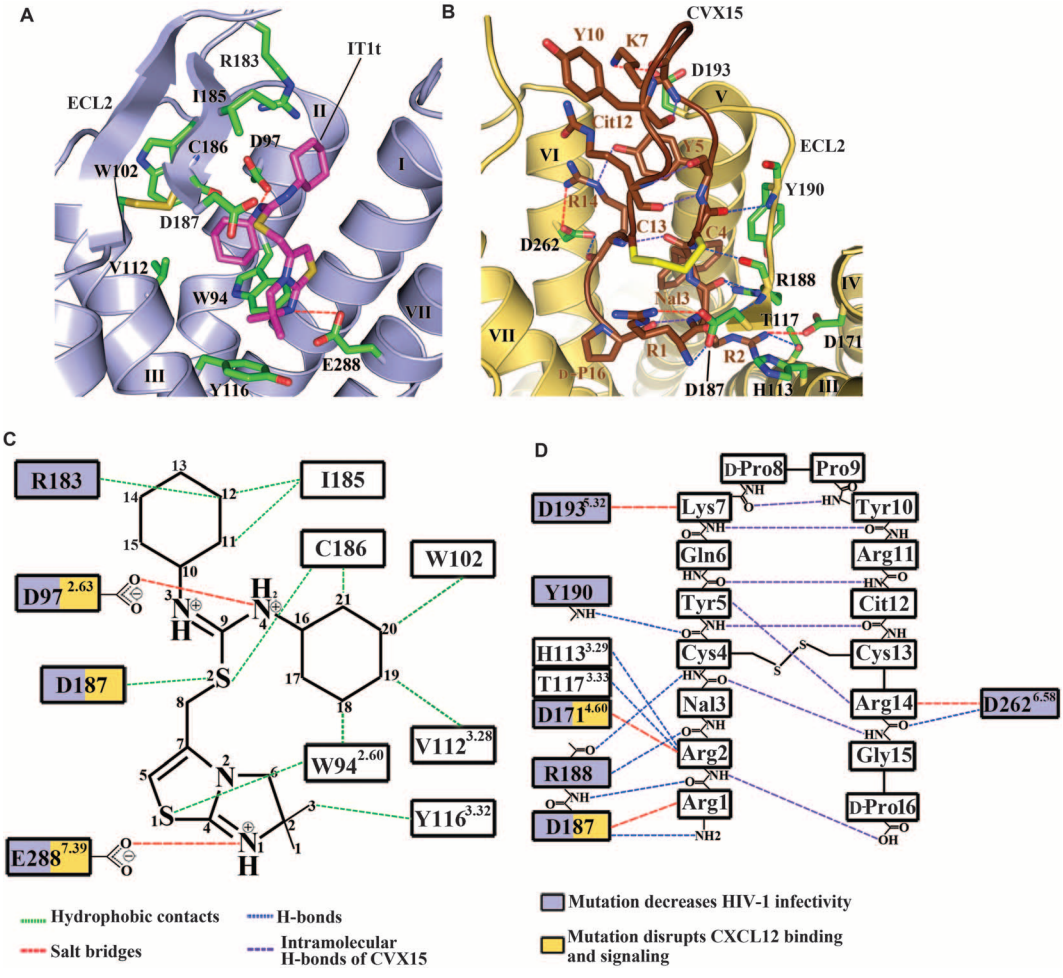

Fig. 2. CXCR4 ligand-binding cavities for the small molecule IT1t and the cyclic peptide CVX15. (**A**) CXCR4 ligand-binding cavity for the small molecule IT1t. IT1t (magenta) and the residues of the receptor (green) involved in the ligand interactions are shown in stick representation. Nitrogen atoms are blue and sulfur atoms are yellow. Key for dashed lines is shown below. Only the helices involved in the receptor-ligand interaction and part of ECL2 are shown. (**B**) CXCR4 ligand-binding cavity for the peptide CVX15. The residues of CVX15 (brown) and the residues of the receptor (green) involved in receptor-ligand polar interactions are shown in stick representation. The Cys4-Cys13 disulfide bridge in CVX15 is shown as a yellow stick. (**C**) Schematic representation of selected interactions between CXCR4 and IT1t in the ligand-binding pocket. Mutations reported to decrease HIV-1 infectivity and to disrupt CXCL12 binding and signaling are indicated with blue and yellow squares, respectively (*57*, *69*). (**D**) Schematic representation of selected interactions between CXCR4 and CVX15 in the ligand-binding pocket.

helices I and II; ICL2 (residues 140 to 144) linking helices III and IV; ICL3 (residues 225 to 230) linking helices V and VI; and the C terminus. ICL3 also contains T4L inserted between Ser229 and Lys230 and flanked by short linkers (GS-T4L-GS). Structural alignment of CXCR4 with high-resolution GPCR structures indicates that the intracellular half of the TM bundle is structurally more conserved (Cα RMSDs with β_2AR, A_{2A}AR, and rhodopsin are 1.8, 1.9, and 1.4 Å, respectively) than the extracellular half (2.6, 2.2, and 2.2 Å, respectively). Therefore, it comes as a surprise that in all five CXCR4 structures, helix VII is about one turn shorter at the intracellular side, ending just after the GPCR-conserved NPxxY motif, and that all structures lack the short α helix VIII (Fig. 1B). The C-terminal part of CXCR4 beyond Ala303$^{7.54}$ adopts an extended conformation and participates in a number of crystal contacts with the extracellular side of a symmetry-related molecule in the highest-resolution crystal structure, CXCR4-2–IT1t (fig. S4A). Because of its structural persistence and common α-helical sequence motif [F(RK)xx(FL)xxx(LF)], helix VIII was thought to be a regular structural element of all class A GPCRs. However, CXCR4 contains only a par-

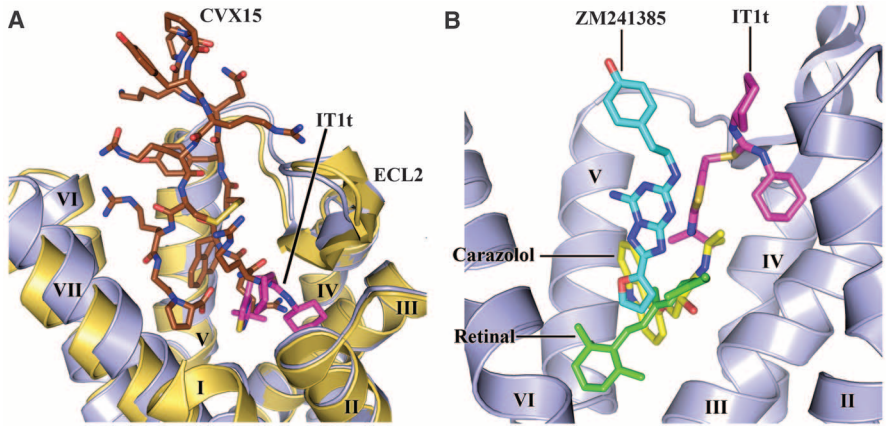

Fig. 3. CXCR4 ligand-binding modes and comparison with other GPCR structures. (**A**) Comparison of the ligand-binding modes for IT1t and CVX15. CXCR4 molecules in the CXCR4-2–IT1t and CXCR4-3–CVX15 complexes are colored blue and yellow, respectively. IT1t (magenta) and CVX15 (brown) are shown as sticks. (**B**) Comparison of the small-molecule ligand-binding modes for CXCR4, β_2AR (PDB ID: 2RH1), A_{2A}AR (PDB ID: 3EML), and rhodopsin (PDB ID: 1U19). Only CXCR4 helices are shown (blue). The ligands IT1t (for CXCR4, magenta), carazolol (for β_2AR, yellow), ZM241385 (for A_{2A}AR, cyan), and retinal (for rhodopsin, green) are shown in stick representation.

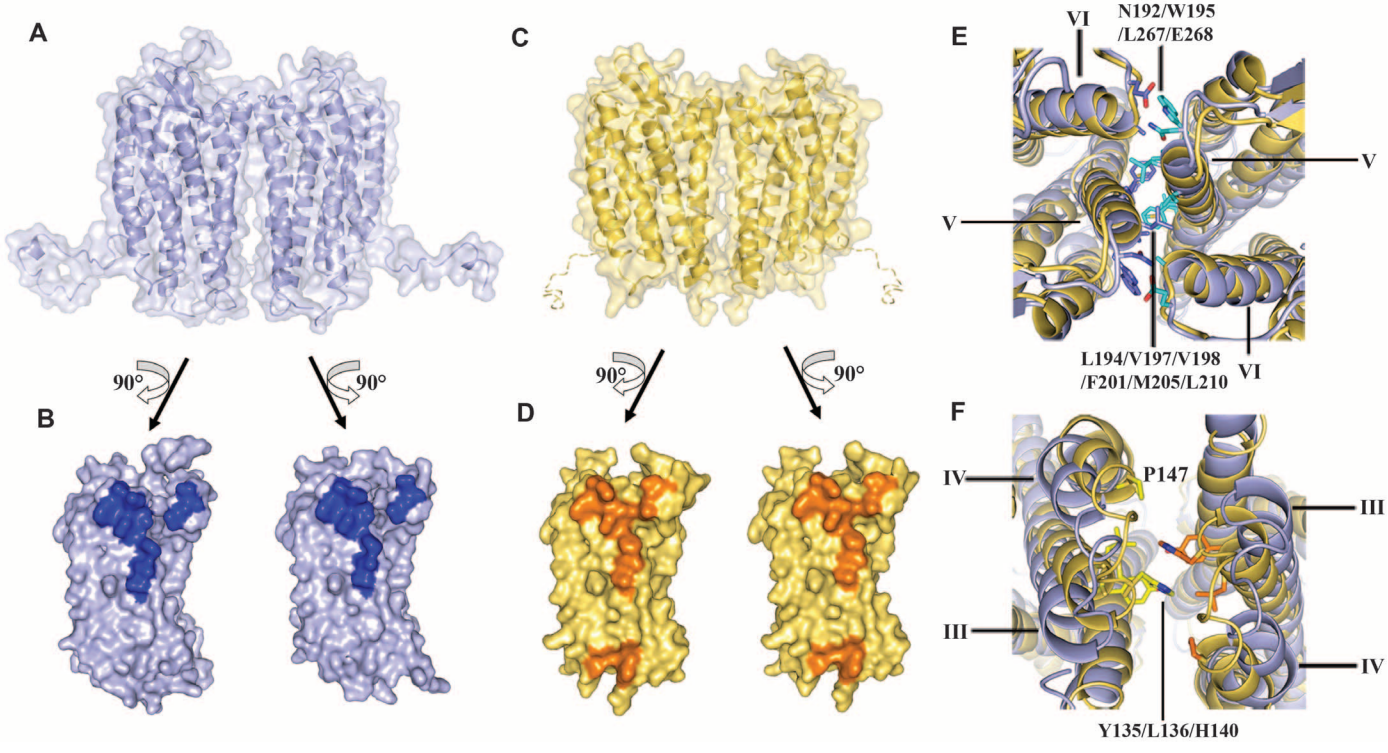

Fig. 4. Dimer interactions in CXCR4-2–IT1t and CXCR4-3–CVX15. (**A**) Molecular surface representation of the CXCR4 dimer in CXCR4-2–IT1t (blue). (**B**) Dimer interface in CXCR4-2–IT1t. The surface involved in dimerization is highlighted in dark blue. (**C**) Molecular surface representation of the CXCR4 dimer in CXCR4-3–CVX15 (yellow). A hypothetical path of the C terminus, which is not observed in the CXCR4-3–CVX15 structure, is shown as a dashed curve. (**D**) Dimer interface in CXCR4-3–CVX15. The surface involved in dimer interaction is highlighted in orange. (**E**) Top view of the extracellular side of the dimers. Two structures show similar interactions via helices V and VI. Residues of CXCR4-2–IT1t involved in the dimer interaction are shown in stick representation and are colored blue in molecule A, cyan in molecule B. (**F**) Bottom view of the intracellular side of the dimers. Contacts can only be observed at the intracellular tips of helices III and IV, and ICL2 in CXCR4-3–CVX15. The residues of CXCR4-3–CVX15 involved in the dimer interaction are shown in stick representation and are colored yellow and orange. These interactions are not present in the CXCR4–IT1t complex.

tially conserved motif FKxxAxxxL, and although it may be capable of forming an α helix under certain conditions, this helix would be less stable because of the replacement of Phe or Leu with Ala. In addition, CXCR4 lacks a putative palmitoylation site at the end of helix VIII, which anchors to the lipid membrane in many GPCRs.

Construct CXCR4-3 contains a T240$^{6.36}$P mutation near the intracellular side of helix VI, which results in retention of ligand-binding affinity but abolishes signaling (table S3 and fig. S1). Comparison of the CXCR4-3 structure with CXCR4-1 and CXCR4-2 reveals that the only effect of the T240$^{6.36}$P mutation is the disruption of a short section of helix VI between Gly231$^{6.27}$ and Pro240$^{6.36}$. Because helix VI is thought to be one of the major players in the signaling mechanism (*31*, *32*), disruption of its structure would likely affect G protein binding and activation. Thus, T240$^{6.36}$P represents a novel structure-based uncoupling mutation.

Molecular recognition of the small molecule IT1t and the cyclic CVX15 peptide by CXCR4. Strong electron density was observed for IT1t in the binding cavity of both subunits of the CXCR4 homodimer (fig. S3A). Compared with previous GPCR structures, the cavity is larger, more open, and located closer to the extracellular surface (Fig. 2, A and C; Fig. 3B; and table S5). The IT1t ligand occupies part of the pocket defined by side chains from helices I, II, III, and VII, but makes no contact with helices IV, V, and VI, in stark contrast to ligands in previous GPCR structures. The nitrogens of the symmetrical isothiourea group are both protonated with a net positive resonance charge; one of them (N4) forms a salt bridge (2.9 Å) with the Asp97$^{2.63}$ side chain. Note that the electron density does not preclude the existence of a very similar ligand conformation with a flipped thiourea group, in which the N3 nitrogen forms a salt bridge to Asp97$^{2.63}$, and the N4 nitrogen makes a polar interaction with main-chain carbonyl of Cys186 in ECL2. The importance of both nitrogens is supported by a reduction in binding affinity of ~100-fold upon methylation of one of them (*25*). Both cyclohexane rings fit into small subpockets and so make hydrophobic contacts with CXCR4. Connected by a short flexible linker, the imidazothiazole ring system is the only part of the ligand that contacts helix VII, in particular, by making a salt bridge (2.8 Å) between the protonated imidazothiazole N1 and Glu288$^{7.39}$ (*33*).

In the CXCR4-3–CVX15 complex, the bulky 16-residue ligand fills most of the binding-pocket volume (Fig. 2, B and D; fig. S3B; and table S5). The peptide forms a disulfide-stabilized (Cys4 to Cys13) β hairpin, with D-Pro8-Pro9 at the tip of the turn exposed to the extracellular milieu. The N-terminal part of the peptide backbone from Arg1 to Cys4 forms hydrogen bonds to CXCR4 backbone residues Asp187 to Tyr190 and so adds a partial third strand to the ECL2 β hairpin. The core-specific interactions are formed by two arginines at the peptide N terminus: Arg1 makes polar interactions with Asp187 (3.1 and 3.4 Å); Arg2 interacts with Thr117$^{3.33}$ (2.7 Å) and Asp171$^{4.60}$ (3.1 Å) and may form an additional hydrogen bond with His113$^{3.29}$ (3.1 Å), depending on its protonation state. The bulky naphthalene ring of Nal3 is anchored in a hydrophobic region bordered by helix V. Arg14 makes a salt bridge with Asp262$^{6.58}$ (3.5 Å) and an intramolecular hydrogen bond to the Tyr5 side chain, which in turn makes hydrophobic contacts with helix V side chains. Finally, the C-terminal D-proline is buried in the pocket next to the N terminus of the peptide and so makes a water-mediated interaction with the Asp288$^{7.39}$ side chain of CXCR4. The importance of the above interactions is supported by analyses of structure-activity relations of a series of CVX15 analogs (*26*).

The small-molecule and peptide ligand-binding sites substantially overlap (Fig. 3A). As CVX15 fills the entire pocket, some conformational variations between the two complexes are not surprising. CVX15 binding induces major deviations in the base of the receptor N terminus (residues 29 to 33), as well as a minor adjustment of extracellular tips of helices VI (~1.5 Å inward), VII (~1.5 Å tangential), and V (~0.5 Å outward). Major differences observed between binding of IT1t and CVX15 to CXCR4 compared with ligand-binding modes in β_2AR, A_{2A}AR, and rhodopsin (Fig. 3B) highlight the structural plasticity of GPCR binding sites.

Receptor dimerization. CXCR4 has been previously shown to homo- and heterodimerize, constitutively and upon ligand binding, by many different experimental methods (*14*, *15*, *34*–*40*). Although the functional importance of dimerization remains incompletely characterized, a considerable body of data suggests that it has important in vivo pharmacological effects. For example, WHIM syndrome (warts, hypogammaglobulinemia, infections, and myelokathexis syndrome) has been linked to mutations in the C terminus of CXCR4 and results in truncated variants that exhibit enhanced signaling and fail to desensitize and internalize upon CXCL12 stimulation. As a primarily heterozygous disease in which truncated CXCR4 is coexpressed with the wild-type receptor, dimerization has been proposed as the most likely mechanism to explain the dominance of mutant CXCR4 over the wild-type receptor (*41*, *42*). The structures presented here corroborate the concept of CXCR4 dimerization and define the dimer interface for a human GPCR with substantial buried surface area (850 Å^2). A similar, parallel, symmetric dimer of CXCR4 is observed in all five crystal structures (Fig. 4 and fig. S4), which suggests that these contacts represent a biologically relevant homodimer interface.

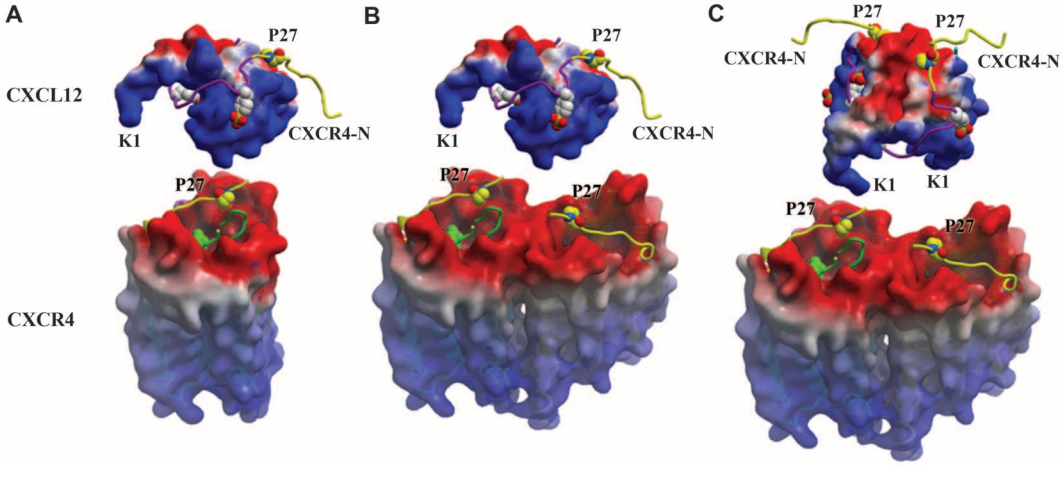

Fig. 5. Stoichiometry of possible CXCR4–CXCL12 binding or signaling complexes. No information on the orientation of CXCL12 with respect to CXCR4 is implied from the models presented. (**A**) Monomeric CXCR4 binding monomeric CXCL12, (**B**) dimeric CXCR4 binding monomeric CXCL12, (**C**) dimeric CXCR4 binding dimeric CXCL12 at either one or both orthosteric sites on each protomer. Alternatively, the 2:2 complex could involve two CXCL12 monomers binding dimeric CXCR4 (not shown). Both CXCR4 and CXCL12 surfaces are colored according to their electrostatic potential from red (negative) to blue (positive), highlighting the charge complementarity of these proteins. The portion of the CXCR4 N-terminal domain (CXCR4-N) present in both the CXCL12 complex (PDB ID: 2K05) and crystal structures of this study is colored yellow, while the remainder is purple (site 1). Pro27 and the three sulfotyrosines from the CXCR4 N terminus are represented with space-filling models. The CVX15 peptide (green ribbon) is shown in one CXCR4 receptor per panel and suggests the binding site for Lys1 and the rest of the flexible N-terminal region of CXCL12, which is critical for receptor activation (site 2). Figures were prepared using ICM software (www.Molsoft.com).

In dimers of CXCR4 bound to IT1t, the monomers interact only at the extracellular side of helices V and VI, leaving at least a 4 Å gap between the intracellular regions, which is presumably filled by lipids (Fig. 4, A and B, and table S6). Dimer association is driven mostly by hydrophobic interactions involving Leu194$^{5.33}$, Val197$^{5.36}$, Val198$^{5.37}$, Phe201$^{5.40}$, Met205$^{5.44}$, and Leu210$^{5.49}$ contacts. A substantial role is also played by a Trp195$^{5.34}$-Leu267$^{6.63}$ contact, which includes both side-chain stacking and a hydrogen bond from Trp195$^{5.34}$ (NE1) to the main-chain carbonyl oxygen of Leu267$^{6.63}$. Another specific polar interaction includes a hydrogen-bonding network between the side chains of Asn192 and Glu268 in opposing receptors, which also involves the main-chain carbonyl oxygens of Leu266$^{6.62}$ and Trp195$^{5.34}$. Pro191 in ECL2 likely plays a role in this network by stabilizing the Trp195$^{5.34}$ side-chain conformation. As these contacts persist throughout all five crystal structures, they are likely genuine, rather than artifacts of crystallization (Fig. 4E).

In addition, dimers of CXCR4 bound to CVX15 are stabilized by interactions at the intracellular ends of helices III and IV and at ICL2, controlled largely by hydrophobic interactions of Tyr135$^{3.51}$, Leu136$^{3.52}$, His140, and Pro147 side chains (~400 Å^2 buried) (Fig. 4, C, D, and F, and table S6). It appears that binding of the bulky CVX15 peptide induces a small tilt in the extracellular part of helix V, which brings the intracellular parts of opposing receptors into close contact. This type of ligand-induced conformational change could explain the cooperative binding observed with certain CXCR4 ligands, as well as the effects of allosteric modulators. Specifically, binding of a ligand to one receptor could induce a structural change in helix V of the second receptor, which could modify the ligand-binding affinity to the second receptor, resulting in either negative or positive cooperativity. Extending this concept to chemokine receptor heterodimers, CXCR4 has been reported to dimerize with CCR2 and CCR5, and both complexes show negative binding cooperativity with their ligands, not only in vitro but also in vivo (*37*, *39*), an observation that may have implications for drug efficacy.

The CXCR4 dimer is strikingly different from previous models of GPCR dimerization, which suggested contacts through either helix I or helices IV and V (*43*–*47*) and implied contacts throughout the length of the TM bundle. It is also notable that with the exception of Trp195$^{5.34}$ (conservation ~70%), little sequence conservation is found among chemokine receptors for the residues that constitute the dimerization site, even though many receptors have been shown to oligomerize (*40*). The specific nature of the interactions may facilitate the ability of CXCR4 to heterodimerize with other chemokine receptors (*37*, *39*, *48*), as well as GPCRs outside of the chemokine family (*49*), although one cannot discount the possibility that many modes of oligomerization may exist.

Implications for the two-site model of chemokine binding and complexes of CXCR4 with CXCL12 and gp120. The known structures of chemokines, including CXCL12, feature a disordered N-terminal domain that largely controls receptor signaling and is hypothesized to penetrate the receptor helical bundle (*50*, *51*). The chemokine N terminus is followed by a core globular domain, which is thought to bind to the receptor N terminus and ECLs, which form an interaction site that confers affinity and specificity (*52*). The separation of the binding and signaling functions has led to the so-called "two-site" model of receptor binding, with the chemokine core domain being the "site one" docking domain and the chemokine N terminus being the "site two" signaling trigger (*50*, *53*, *54*). The nuclear magnetic resonance (NMR) structure of CXCL12 in complex with a 38-residue, sulfotyrosine-containing peptide derived from the CXCR4 N terminus has been determined [Protein Data Bank (PDB) ID: 2K05] (*55*). This structure is thought to represent at least part of the "site one" complex and reveals important interactions between CXCL12 and residues, including three sulfated tyrosines, that are absent from the CXCR4 receptor structure.

The peptide and small-molecule complexes of CXCR4 identify the likely "site two" of the chemokine-signaling trigger. The IT1t compound and CVX15 peptide have both been characterized as competitive inhibitors of CXCL12, and many of the receptor-ligand contacts in the cocrystal structures presented are important for CXCL12 binding, including the acidic Asp187, Glu288$^{7.39}$, and Asp97$^{2.63}$ (Fig. 2) (*56*, *57*). The CVX15 peptide, rich in basic residues, may trace, to some extent, the path of the N-terminal signaling peptide of CXCL12 (KPVSLSYR), and the binding site of IT1t may point to the major anchor region for this domain. Furthermore, our preliminary modeling studies suggest that Lys1, the most critical residue in CXCL12 for receptor activation, could reach into the CXCR4 pocket and interact with one of these acidic residues (Fig. 5). The extensive binding site mapped out by the CVX15 peptide also clarifies how progressive shortening of the CXCL12 N terminus leads to a gradual loss of binding affinity (*50*). Taken together, these data suggest that the small molecule and cyclic peptide block ligand binding by acting as orthosteric competitors of the CXCL12 N-terminal signaling trigger, providing strong support for the two-site model of binding. Along these lines, a recent NMR study showed that the CXCR4 antagonist AMD3100 could displace the CXCL12 N terminus from the receptor without displacing the chemokine core domain (*58*).

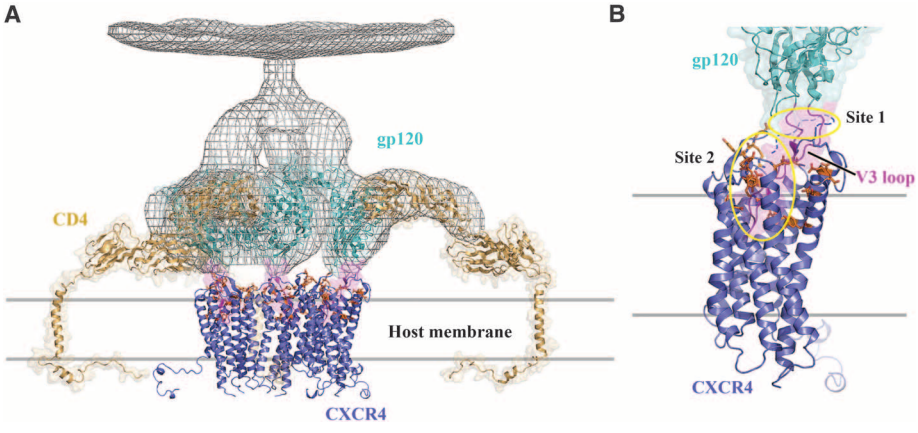

Fig. 6. Model of early stages of the HIV-1 entry process. (**A**) Viral entry begins with binding of envelope spikes consisting of a heterotrimer $(gp120)_3$ $(gp41)_3$ [wire, adapted from density map of gp120/CD4/17b Fab complex derived by cryo–electron tomography of intact HIV-1 spikes (*70*); PDB ID: 3DNO] to CD4 on the surface of host target cells. Glycoprotein gp120 (core structure, cyan, PDB ID: 2QAD) interacts with CD4 (tan, PDB ID: 1WIP and 2KLU). This interaction triggers conformational changes in gp120 that increase the exposure of the third variable loop V3 (magenta) and a region of gp120 between inner and outer domains. CCR5 or CXCR4 (blue) is then recruited as a co-receptor. The number of spikes involved in viral entry and the number of molecules of CD4 or CXCR4 binding to a single spike are unknown; here, three CD4 molecules are represented, which results in the close approach of gp120 molecules to the host cell membrane where the interaction with three CXCR4 molecules is depicted. (**B**) By analogy to a two-site model based on CCR5 (*65*), the N terminus of CXCR4 containing sulfotyrosines (site 1, circled in yellow) binds first to the base of the V3 loop, which induces further conformational changes in gp120 that enable V3 to bind to the extracellular side of CXCR4, primarily ECL2, ECL3, and the ligand-binding cavity (site 2, circled in yellow). CXCR4 residues previously shown to affect gp120 binding are shown as sticks with carbons colored in orange. A hypothetical path of the CXCR4 N terminus, which is not observed in the current structure, is shown as a blue dashed curve. Only CXCR4 monomers are shown for clarity, although dimers are also possible. Figures 1, 2, 3, 4, and 6 were prepared using PyMOL.

Chemokines are able to bind their receptors as monomers in order to activate cell migration (*59*). However, chemokine oligomers, including CXCL12, appear to be functional and to induce alternative signaling responses, such as cellular activation or signals to halt migration (*55*, *60*, *61*), which suggests the concept that these complexes dynamically change their stoichiometries and structures as part of their functional regulation. Given the oligomeric nature of CXCR4 and the complementary electrostatic surfaces of the ligand and receptor, one can envision CXCL12 binding the receptor as a 1:1, 1:2, or 2:2 ligand:receptor complex (Fig. 5). Additional experiments will be necessary to fully define the relevance and functional implications of different chemokine: receptor stoichiometries and structures. Nevertheless, the current CXCR4 structures are compatible with emerging concepts of signaling diversity induced by alternative binding modes of the ligands.

CXCR4 and the related CCR5 serve as co-receptors for HIV-1 viral particles, facilitating their entry into cells. Structures have been reported for the other key components of the entry complex, HIV-1 glycoproteins gp120 and gp41, and the host leukocyte glycoprotein receptor CD4 (*62*–*64*). The N termini of CXCR4 and CCR5, including sulfated tyrosine residues, have been implicated in gp120 binding, analogous to CXCL12 recognition (*65*). Other structural features critical to the interaction involve the gp120 V3 loop, which becomes exposed on CD4 binding (*66*) and then interacts with CXCR4 ECL2 and ECL3. The basic character of the protruding V3 loop along with acidic residues in the CXCR4 binding pocket have been reported to be important for HIV-1 infectivity (Fig. 2, C and D) (*57*, *67*), which suggests that the loop could also penetrate the pocket (Fig. 6). Thus, the CXCR4 structures suggest testable hypotheses regarding interaction of CXCR4 with its natural ligand and with HIV-1 gp120. The real challenge will be in understanding the dynamic changes in these complexes that result in signal transduction and viral fusion. As further details of these interactions are resolved, new opportunities for drug discovery efforts targeting specific functional states of the receptor will likely emerge.

References and Notes

1. M. Baggiolini, *Nature* **392**, 565 (1998).
2. B. Moser, M. Wolf, A. Walz, P. Loetscher, *Trends Immunol.* **25**, 75 (2004).
3. C. R. Mackay, *Nat. Immunol.* **2**, 95 (2001).
4. Q. Ma *et al.*, *Proc. Natl. Acad. Sci. U.S.A.* **95**, 9448 (1998).
5. Y. R. Zou, A. H. Kottmann, M. Kuroda, I. Taniuchi, D. R. Littman, *Nature* **393**, 595 (1998).
6. A. Müller *et al.*, *Nature* **410**, 50 (2001).
7. F. Balkwill, *Semin. Cancer Biol.* **14**, 171 (2004).
8. A. Zlotnik, *J. Pathol.* **215**, 211 (2008).
9. A. M. Fulton, *Curr. Oncol. Rep.* **11**, 125 (2009).
10. B. A. Teicher, S. P. Fricker, *Clin. Cancer Res.* **16**, 2927 (2010).
11. Y. Feng, C. C. Broder, P. E. Kennedy, E. A. Berger, *Science* **272**, 872 (1996).
12. C. C. Bleul *et al.*, *Nature* **382**, 829 (1996).
13. E. Oberlin *et al.*, *Nature* **382**, 833 (1996).
14. G. J. Babcock, M. Farzan, J. Sodroski, *J. Biol. Chem.* **278**, 3378 (2003).
15. Y. Percherancier *et al.*, *J. Biol. Chem.* **280**, 9895 (2005).
16. J. Wang, M. Norcross, *Drug Discov. Today* **13**, 625 (2008).
17. V. Cherezov *et al.*, *Science* **318**, 1258 (2007).
18. V. P. Jaakola *et al.*, *Science* **322**, 1211 (2008).
19. T. Warne *et al.*, *Nature* **454**, 486 (2008).
20. J. H. Park, P. Scheerer, K. P. Hofmann, H. W. Choe, O. P. Ernst, *Nature* **454**, 183 (2008).
21. M. A. Hanson *et al.*, *Structure* **16**, 897 (2008).
22. C. B. Roth, M. A. Hanson, R. C. Stevens, *J. Mol. Biol.* **376**, 1305 (2008).
23. In Ballesteros-Weinstein numbering, a single most-conserved residue among the class A GPCRs is designated *x*.50, where *x* is the transmembrane helix number. All other residues on that helix are numbered relative to this conserved position.
24. Single-letter abbreviations for the amino acid residues are as follows: A, Ala; C, Cys; D, Asp; E, Glu; F, Phe; G, Gly; H, His; I, Ile; K, Lys; L, Leu; M, Met; N, Asn; P, Pro; Q, Gln; R, Arg; S, Ser; T, Thr; V, Val; W, Trp; Y, Tyr; and x, any amino acid.
25. G. Thoma *et al.*, *J. Med. Chem.* **51**, 7915 (2008).
26. H. Tamamura *et al.*, *FEBS Lett.* **550**, 79 (2003).
27. S. J. DeMarco *et al.*, *Bioorg. Med. Chem.* **14**, 8396 (2006).
28. G. Moncunill *et al.*, *Mol. Pharmacol.* **73**, 1264 (2008).
29. Materials and methods are available as supporting material on *Science* Online.
30. H. Zhou, H. H. Tai, *Arch. Biochem. Biophys.* **373**, 211 (2000).
31. P. Scheerer *et al.*, *Nature* **455**, 497 (2008).
32. K. P. Hofmann *et al.*, *Trends Biochem. Sci.* **34**, 540 (2009).
33. Experimental measurement of the acidic dissociation constant, pK_a, by means of multiplexed capillary electrophoresis gave $pK_{a1} = 5.39$, $pK_{a2} = 7.89$, and $pK_{a3} = 9.92$, indicating that the conjugated acid of isothiourea N4 has a pK_a of 5.4, which is also consistent with the prediction ($pK_a = 4.84 \pm 0.60$) by pK_a database from ACD/Labs, and suggesting that N4 is unprotonated at the physiological condition of pH = 7.4. Crystallization of the CXCR4-2/IT1t complex was performed at pH 5.5, and the acidic microenvironment of $Glu288^{7.39}$ may further shift the equilibrium toward protonation.
34. A. J. Vila-Coro *et al.*, *FASEB J.* **13**, 1699 (1999).
35. K. E. Luker, M. Gupta, G. D. Luker, *FASEB J.* **23**, 823 (2009).
36. A. Levoye, K. Balabanian, F. Baleux, F. Bachelerie, B. Lagane, *Blood* **113**, 6085 (2009).
37. D. Sohy *et al.*, *J. Biol. Chem.* **284**, 31270 (2009).
38. J. Wang, L. He, C. A. Combs, G. Roderiquez, M. A. Norcross, *Mol. Cancer Ther.* **5**, 2474 (2006).
39. D. Sohy, M. Parmentier, J. Y. Springael, *J. Biol. Chem.* **282**, 30062 (2007).
40. C. L. Salanga, M. O'Hayre, T. Handel, *Cell. Mol. Life Sci.* **66**, 1370 (2009).
41. K. Balabanian *et al.*, *Blood* **105**, 2449 (2005).
42. B. Lagane *et al.*, *Blood* **112**, 34 (2008).
43. F. Fanelli, P. G. De Benedetti, *J. Comput. Aided Mol. Des.* **20**, 449 (2006).
44. M. Filizola, *Life Sci.* **86**, 590 (2010).
45. W. Nemoto, H. Toh, *Curr. Protein Pept. Sci.* **7**, 561 (2006).
46. P. H. Reggio, *AAPS J.* **8**, E322 (2006).
47. S. Vohra *et al.*, *Biochem. Soc. Trans.* **35**, 749 (2007).
48. N. Isik, D. Hereld, T. Jin, *PLoS ONE* **3**, e3424 (2008).
49. O. M. Pello *et al.*, *Eur. J. Immunol.* **38**, 537 (2008).
50. M. P. Crump *et al.*, *EMBO J.* **16**, 6996 (1997).
51. C. Dealwis *et al.*, *Proc. Natl. Acad. Sci. U.S.A.* **95**, 6941 (1998).
52. S. K. Gupta, K. Pillarisetti, R. A. Thomas, N. Aiyar, *Immunol. Lett.* **78**, 29 (2001).
53. I. Clark-Lewis *et al.*, *J. Leukoc. Biol.* **57**, 703 (1995).
54. T. N. Wells *et al.*, *J. Leukoc. Biol.* **59**, 53 (1996).
55. C. T. Veldkamp *et al.*, *Sci. Signal.* **1**, ra4 (2008).
56. A. Brelot *et al.*, *J. Virol.* **73**, 2576 (1999).
57. A. Brelot, N. Heveker, M. Montes, M. Alizon, *J. Biol. Chem.* **275**, 23736 (2000).
58. Y. Kofuku *et al.*, *J. Biol. Chem.* **284**, 35240 (2009).
59. C. D. Paavola *et al.*, *J. Biol. Chem.* **273**, 33157 (1998).
60. V. Appay, A. Brown, S. Cribbes, E. Randle, L. G. Czaplewski, *J. Biol. Chem.* **274**, 27505 (1999).
61. L. G. Czaplewski *et al.*, *J. Biol. Chem.* **274**, 16077 (1999).
62. R. Diskin, P. M. Marcovecchio, P. J. Bjorkman, *Nat. Struct. Mol. Biol.* **17**, 608 (2010).
63. M. Pancera *et al.*, *Proc. Natl. Acad. Sci. U.S.A.* **107**, 1166 (2010).
64. P. D. Kwong *et al.*, *Nature* **393**, 648 (1998).
65. C. C. Huang *et al.*, *Science* **317**, 1930 (2007).
66. C. C. Huang *et al.*, *Science* **310**, 1025 (2005).
67. B. J. Doranz *et al.*, *J. Virol.* **73**, 2752 (1999).
68. T. E. Angel, M. R. Chance, K. Palczewski, *Proc. Natl. Acad. Sci. U.S.A.* **106**, 8555 (2009).
69. S. Tian *et al.*, *J. Virol.* **79**, 12667 (2005).
70. J. Liu, A. Bartesaghi, M. J. Borgnia, G. Sapiro, S. Subramaniam, *Nature* **455**, 109 (2008).

71. This work was supported in part by the Protein Structure Initiative grant U54 GM074961 for structure production, NIH Roadmap Initiative grant P50 GM073197 for technology development, NIH grants R21 RR025336 and R21 AI087189 to V.C., and Pfizer. T.M.H. acknowledges support from NIH R01 AI037113 and R01 GM081763, D.J.H. from F32 GM083463, and R.A. from R01 GM071872. The authors thank J. Velasquez for help on molecular biology, T. Trinh and K. Allin for help on baculovirus expression, I. Wilson and D. Burton for careful review and scientific feedback on the manuscript, W. Schief for electron microscopy models of gp120-gp41-CD4 complex, G. W. Han for evaluating the structure quality and preparation for PDB submission, and A. Walker for assistance with manuscript preparation. The authors acknowledge E. La Chapelle on chemistry tool compound synthesis; A. Rane on radiolabeling of [^{3}H]BIMA; M. Cui for help developing [^{3}H]BIMA binding assay; Y. Zheng, The Ohio State University, and M. Caffrey, Trinity College (Dublin, Ireland), for the generous loan of the in meso robot [built with support from the National Institutes of Health (GM075915), the NSF (IIS0308078), and Science Foundation Ireland (02-IN1-B266)]; and J. Smith, R. Fischetti, and N. Sanishvili at the General Medicine and Cancer Institutes Collaborative Access Team (GM/CA-CAT) beamline at the Advanced Photon Source for assistance in development and use of the minibeam and beamtime. The GM/CA-CAT beamline (23-ID) is supported by the National Cancer Institute (Y1-CO-1020) and the National Institute of General Medical Sciences (Y1-GM-1104). R.C.S. is the founder and is a board member of Receptos, a biotech company focused on GPCR structure–based drug discovery. Transfer of IT1t, CVX15, and [^{3}H]BIMA will require a Material Transfer Agreement (MTA) with Pfizer, and transfer of all other constructs and biological materials requires an MTA with the Scripps Research Institute. Atomic coordinates and structure factors have been deposited in the Protein Data Bank with identification codes 3ODU (CXCR4-2–IT1t, $P2_1$), 3OE0 (CXCR4-3–CVX15, *C2*), 3OE8 (CXCR4-2–IT1t, *P1*), 3OE9 (CXCR4-3–IT1t, *P1*), and 3OE6 (CXCR4-1–IT1t, *I222*).

Supporting Online Material

www.sciencemag.org/cgi/content/full/science.1194396/DC1
Materials and Methods
Figs. S1 to S4
Tables S1 to S6
References

29 June 2010; accepted 2 September 2010
Published online 7 October 2010;
10.1126/science.1194396

The Uncertainty Principle Determines the Nonlocality of Quantum Mechanics

Jonathan Oppenheim[1]* and Stephanie Wehner[2,3]*

Two central concepts of quantum mechanics are Heisenberg's uncertainty principle and a subtle form of nonlocality that Einstein famously called "spooky action at a distance." These two fundamental features have thus far been distinct concepts. We show that they are inextricably and quantitatively linked: Quantum mechanics cannot be more nonlocal with measurements that respect the uncertainty principle. In fact, the link between uncertainty and nonlocality holds for all physical theories. More specifically, the degree of nonlocality of any theory is determined by two factors: the strength of the uncertainty principle and the strength of a property called "steering," which determines which states can be prepared at one location given a measurement at another.

A measurement allows us to gain information about the state of a physical system. For example, when measuring the position of a particle, the measurement outcomes correspond to possible locations. Whenever the state of the system is such that we can predict this position with certainty, then there is only one measurement outcome that can occur. Heisenberg (*1*) observed that quantum mechanics imposes strict restrictions on what we can hope to learn—there are incompatible measurements such as position and momentum whose results cannot be simultaneously predicted with certainty. These restrictions are known as uncertainty relations. For example, uncertainty relations tell us that if we were able to predict the momentum of a particle with certainty, then, when measuring its position, all measurement outcomes would occur with equal probability. That is, we would be completely uncertain about its location.

Nonlocality can be exhibited when measurements on two or more distant quantum systems are performed; that is, the outcomes can be correlated in a way that defies any local classical description (*2*). This is why we know that quantum theory will never be superseded by a local classical theory. Nonetheless, even quantum correlations are restricted to some extent: Measurement results cannot be correlated so strongly that they would allow signaling between two distant systems. However, quantum correlations are still weaker than what the no-signaling principle demands (*3*).

So why are quantum correlations strong enough to be nonlocal, yet not as strong as they could be? Is there a principle that determines the degree of this nonlocality? Information theory (*4*, *5*), communication complexity (*6*), and local quantum mechanics (*7*) provided us with some rationale for why limits on quantum theory may exist. But evidence suggests that many of these attempts provide only partial answers. Here, we take a very different approach and relate the limitations of nonlocal correlations to two inherent properties of any physical theory.

At the heart of quantum mechanics lies Heisenberg's uncertainty principle (*1*). Traditionally, uncertainty relations have been expressed in terms of commutators

$$\Delta A \Delta B \geq \frac{1}{2}|\langle\psi|[A, B]|\psi\rangle| \qquad (1)$$

with standard deviations $\Delta X = \sqrt{\langle\psi|X^2|\psi\rangle - \langle\psi|X|\psi\rangle^2}$ for $X \in \{A, B\}$. However, the more modern approach is to use entropic measures. Let $p(x^{(t)}|t)_\sigma$ denote the probability that we obtain outcome $x^{(t)}$ when performing a measurement labeled t when the system is prepared in the state σ. In quantum theory, σ is a density operator, whereas for a general physical theory, we assume that σ is simply an abstract representation of a state. The well-known Shannon entropy $H(t)_\sigma$ of the distribution over measurement outcomes of measurement t on a system in state σ is thus

$$H(t)_\sigma := -\sum_{x^{(t)}} p(x^{(t)}|t)_\sigma \log p(x^{(t)}|t)_\sigma \qquad (2)$$

In any uncertainty relation, we wish to compare outcome distributions for multiple measurements. In terms of entropies, such relations are of the form

$$\sum_t p(t) H(t)_\sigma \geq c_{\mathcal{T},\mathcal{D}} \qquad (3)$$

where $p(t)$ is any probability distribution over the set of measurements $\mathcal{T}$, and $c_{\mathcal{T},\mathcal{D}}$ is some positive constant determined by $\mathcal{T}$ and the distribution $\mathcal{D} = \{p(t)\}_t$. To see why Eq. 3 forms an uncertainty relation, note that whenever $c_{\mathcal{T},\mathcal{D}} > 0$ we cannot predict the outcome of at least one of the measurements t with certainty [i.e., $H(t)_\sigma > 0$]. Such relations have the great advantage that the lower bound $c_{\mathcal{T},\mathcal{D}}$ does not depend on the state σ (*8*). Instead, $c_{\mathcal{T},\mathcal{D}}$ depends only on the measurements and hence quantifies their inherent incompatibility. It has been shown that for two measurements, entropic uncertainty relations do in fact imply Heisenberg's uncertainty relation (*9*), providing us with a more general way of capturing uncertainty [see (*10*) for a survey].

One may consider many entropic measures instead of the Shannon entropy. For example, the min-entropy

$$H_\infty(t)_\sigma := -\log \max_{x^{(t)}} p(x^{(t)}|t)_\sigma \qquad (4)$$

used in (*8*) plays an important role in cryptography and provides a lower bound on $H(t)_\sigma$. Entropic functions are, however, a rather coarse way of measuring the uncertainty of a set of measurements, as they do not distinguish the uncertainty inherent in obtaining any combination of outcomes $x^{(t)}$ for different measurements t. It is thus useful to consider much more fine-grained uncertainty relations consisting of a series of inequalities, one for each combination of possible outcomes, which we write as a string $\mathbf{x} = (x^{(1)}, \ldots, x^{(n)}) \in \mathcal{B}^{\times n}$ with $n = |\mathcal{T}|$ (*11*). That is, for each $\mathbf{x}$, a set of measurements $\mathcal{T}$, and distribution $\mathcal{D} = \{p(t)\}_t$,

$$P^{\text{cert}}(\sigma;\mathbf{x}) := \sum_{t=1}^{n} p(t)\, p(x^{(t)}|t)_\sigma \leq \zeta_{\mathbf{x}}(\mathcal{T},\mathcal{D}) \qquad (5)$$

For a fixed set of measurements, the set of inequalities

$$U = \left\{ \sum_{t=1}^{n} p(t)\, p(x^{(t)}|t)_\sigma \leq \zeta_{\mathbf{x}} | \forall \mathbf{x} \in \mathcal{B}^{\times n} \right\} \qquad (6)$$

thus forms a fine-grained uncertainty relation, as it dictates that one cannot obtain a measurement outcome with certainty for all measurements simultaneously whenever $\zeta_{\mathbf{x}} < 1$. The values of $\zeta_{\mathbf{x}}$ thus confine the set of allowed probability distributions, and the measurements have uncertainty if $\zeta_{\mathbf{x}} < 1$ for all $\mathbf{x}$. To characterize the "amount of uncertainty" in a particular physical theory, we are thus interested in the values of

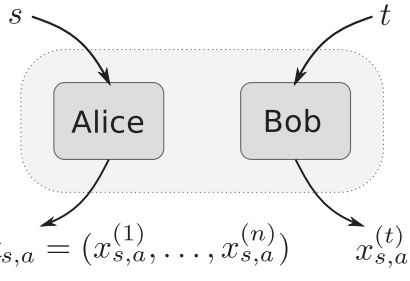

Fig. 1. Any game where, for every choice of settings s and t and answer a of Alice, there is only one correct answer b for Bob can be expressed using strings $\mathbf{x}_{s,a}$ such that $b = \mathbf{x}^{(t)}_{s,a}$ is the correct answer for Bob (*13*) for s and a. The game is equivalent to Alice outputting $\mathbf{x}_{s,a}$ and Bob outputting $\mathbf{x}^{(t)}_{s,a}$.

[1]DAMTP, University of Cambridge, Cambridge CB3 0WA, UK. [2]Institute for Quantum Information, California Institute of Technology, Pasadena, CA 91125, USA. [3]Centre for Quantum Technologies, National University of Singapore, 117543 Singapore.

*To whom correspondence should be addressed. E-mail: jono@damtp.cam.ac.uk (J.O.); wehner@nus.edu.sg (S.W.)

$$\zeta_{\mathbf{x}} = \max_{\sigma} \sum_{t=1}^{n} p(t)\, p(x^{(t)}|t)_{\sigma} \qquad (7)$$

where the maximization is taken over all states allowed on a particular system (for simplicity, we assume it can be attained in the theory considered). We will also refer to the state $\rho_{\mathbf{x}}$ that attains the maximum as a "maximally certain state." However, we will also be interested in the degree of uncertainty exhibited by measurements on a set of states Σ quantified by $\zeta_{\mathbf{x}}^{\Sigma}$ defined with the maximization in Eq. 7 taken over $\sigma \in \Sigma$. Fine-grained uncertainty relations are directly related to the entropic ones, and they have both a physical and an information-processing appeal (*12*).

As an example, consider the binary spin-½ observables Z and X. If we can obtain a particular outcome $x^{(Z)}$ given that we measured Z with certainty—that is, $p(x^{(Z)}|Z) = 1$—then the complementary observable must be completely uncertain, that is, $p(x^{(X)}|X) = ½$. If we choose which measurement to make with probability ½, then this notion of uncertainty is captured by the relations

$$\frac{1}{2}p(x^{(X)}|X) + \frac{1}{2}p(x^{(Z)}|Z) \leq \zeta_{\mathbf{x}} = \frac{1}{2} + \frac{1}{2\sqrt{2}}$$

$$\text{for all } \mathbf{x} = (x^{(X)}, x^{(Z)}) \in \{0,1\}^2 \qquad (8)$$

where the maximally certain states are given by the eigenstates of $(X + Z)/\sqrt{2}$ and $(X - Z)/\sqrt{2}$.

We now introduce the concept of nonlocal correlations. Instead of considering measurements on a single system, we consider measurements on two (or more) space-like separated systems traditionally named Alice and Bob. We use $t \in \mathcal{T}$ to label Bob's measurements, and $b \in \mathcal{B}$ to label his measurement outcomes. For Alice, we use $s \in \mathcal{S}$ to label her measurements, and $a \in \mathcal{A}$ to label her outcomes (*11*). When Alice and Bob perform measurements on a shared state σ_{AB}, the outcomes of their measurements can be correlated. Let $p(a,b|s,t)_{\sigma_{AB}}$ be the joint probability that they obtain outcomes a and b for measurements s and t. We can now again ask ourselves: What probability distributions are allowed?

Quantum mechanics as well as classical mechanics obeys the no-signaling principle, meaning that information cannot travel faster than light.

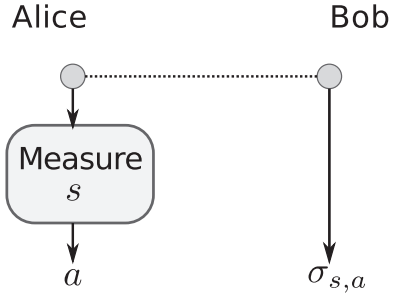

Fig. 2. When Alice performs a measurement labeled s and obtains outcome a with probability $p(a|s)$, she effectively prepares the state $\sigma_{s,a}$ on Bob's system. This is known as steering.

This means that the probability that Bob obtains outcome b when performing measurement t cannot depend on which measurement Alice chooses to perform (and vice versa). More formally, $\sum_a p(a,b|s,t)_{\sigma_{AB}} = p(b|t)_{\sigma_B}$ for all s, where $\sigma_B = \mathrm{tr}_A(\sigma_{AB})$. Curiously, however, this is not the only constraint imposed by quantum mechanics (*3*). Here we find that the uncertainty principle imposes the other limitation.

To do so, let us recall the concept of so-called Bell inequalities (*2*). These are most easily explained in their more modern form in terms of a game played between Alice and Bob. Let us choose questions $s \in \mathcal{S}$ and $t \in \mathcal{T}$ according to some distribution $p(s,t)$ and send them to Alice and Bob, respectively, where we take for simplicity $p(s,t) = p(s)p(t)$. The two players now return answers $a \in \mathcal{A}$ and $b \in \mathcal{B}$. Every game comes with a set of rules that determines whether a and b are winning answers given questions s and t. Again for simplicity, we thereby assume that for every s, t, and a, there exists exactly one winning answer b for Bob (and similarly for Alice). That is, for every setting s and outcome a of Alice, there is a string $\mathbf{x}_{s,a} = (x_{s,a}^{(1)}, \ldots, x_{s,a}^{(n)}) \in \mathcal{B}^{\times n}$ of length $n = |\mathcal{T}|$ that determines the correct answer $b = x_{s,a}^{(t)}$ for question t for Bob (Fig. 1). We say that s and a determine a "random-access coding" (*13*), meaning that Bob is not trying to learn the full string $\mathbf{x}_{s,a}$ but only the value of one entry. The case of non-unique games is a straightforward but cumbersome generalization.

As an example, the Clauser-Horne-Shimony-Holt (CHSH) inequality (*14*), one of the simplest Bell inequalities whose violation implies nonlocality, can be expressed as a game in which Alice and Bob receive binary questions $s,t \in \{0,1\}$ respectively, and similarly their answers $a,b \in \{0,1\}$ are single bits. Alice and Bob win the CHSH game if their answers satisfy $a \oplus b = s \cdot t$. We can label Alice's outcomes using string $\mathbf{x}_{s,a}$, and Bob's goal is to retrieve the tth element of this string. For $s = 0$, Bob will always need to give the same answer as Alice in order to win, and hence we have $\mathbf{x}_{0,0} = (0,0)$, and $\mathbf{x}_{0,1} = (1,1)$. For $s = 1$, Bob needs to give the same answer for $t = 0$, but the opposite answer if $t = 1$. That is, $\mathbf{x}_{1,0} = (0,1)$ and $\mathbf{x}_{1,1} = (1,0)$.

Alice and Bob may agree on any strategy ahead of time, but once the game starts, their physical distance prevents them from communicating. For any physical theory, such a strategy consists of a choice of shared state σ_{AB}, as well as measurements, where we may without loss of generality assume that the players perform a measurement depending on the question they receive and return the outcome of said measurement as their answer. For any particular strategy, we may hence write the probability that Alice and Bob win the game as

$$P^{\text{game}}(\mathcal{S},\mathcal{T},\sigma_{AB}) = \sum_{s,t} p(s,t) \sum_{a} p(a,b = x_{s,a}^{(t)}|s,t)_{\sigma_{AB}} \qquad (9)$$

To characterize what distributions are allowed, we are generally interested in the winning probability maximized over all possible strategies for Alice and Bob:

$$P_{\max}^{\text{game}} = \max_{\mathcal{S},\mathcal{T},\sigma_{AB}} P^{\text{game}}(\mathcal{S},\mathcal{T},\sigma_{AB}) \qquad (10)$$

which, in the case of quantum theory, we refer to as a Tsirelson's type bound for the game (*15*). For the CHSH inequality (*14*), we have $P_{\max}^{\text{game}} = 3/4$ classically, $P_{\max}^{\text{game}} = 1/2 + 1/(2\sqrt{2})$ quantum mechanically, and $P_{\max}^{\text{game}} = 1$ for a theory allowing any nonsignaling correlations. $P_{\max}^{\text{game}}$ quantifies the strength of nonlocality for any theory, with the understanding that a theory possesses genuine nonlocality when it differs from the value that can be achieved classically. However, the connection we will demonstrate between uncertainty relations and nonlocality holds even before the optimization.

The final concept we need in our discussion is steerability, which determines what states Alice can prepare on Bob's system remotely. Imagine that Alice and Bob share a state σ_{AB}, and consider the reduced state $\sigma_B = \mathrm{tr}_A(\sigma_{AB})$ on Bob's side. In quantum mechanics, as well as many other theories in which Bob's state space is a convex set $\mathcal{S}$, the state $\sigma_B \in \mathcal{S}$ can be decomposed in many different ways as a convex sum,

$$\sigma_B = \sum_a p(a|s)\sigma_{s,a} \text{ with } \sigma_{s,a} \in \mathcal{S} \qquad (11)$$

corresponding to an ensemble $\mathcal{E}_s = \{p(a|s), \sigma_{s,a}\}_a$. Schrödinger (*16*, *17*) noted that in quantum mechanics, for all s there exists a measurement on Alice's system that allows her to prepare $\mathcal{E}_s = \{p(a|s), \sigma_{s,a}\}_a$ on Bob's site (Fig. 2). That is, for measurement s, Bob's system will be in the state $\sigma_{s,a}$ with probability $p(a|s)$. Schrödinger called this steering to the ensemble $\mathcal{E}_s$, and it does not violate the no-signaling principle, because for each of Alice's settings, the state of Bob's system is the same once we average over Alice's measurement outcomes.

Even more, he observed that for any set of ensembles $\{\mathcal{E}_s\}_s$ that respect the no-signaling constraint (i.e., for which there exists a state σ_B such that Eq. 11 holds), we can in fact find a bipartite quantum state σ_{AB} and measurements that allow Alice to steer to such ensembles. We can imagine theories in which our ability to steer is more restricted, or perhaps even less restricted (some amount of signaling is permitted). Our notion of steering thus allows forms of steering not considered in quantum mechanics (*16*–*19*) or other restricted classes of theories (*20*). Our ability to steer, however, is a property of the set of ensembles we consider, and not a property of one single ensemble.

We are now in a position to derive the relation between how nonlocal a theory is and how uncertain it is. We may express the probability (Eq. 9) that Alice and Bob win the game by using a particular strategy (Fig. 1) as

$$P^{\text{game}}(\mathcal{S},\mathcal{T},\sigma_{AB}) = \sum_s p(s) \sum_a p(a|s) P^{\text{cert}}(\sigma_{s,a}; \mathbf{x}_{s,a}) \qquad (12)$$

where $\sigma_{s,a}$ is the reduced state of Bob's system for setting s and outcome a of Alice, and $p(t)$ in $P^{\text{cert}}(\cdot)$ is the probability distribution over Bob's questions $\mathcal{T}$ in the game. This immediately suggests that there is indeed a close connection between games and our fine-grained uncertainty relations. In particular, every game can be understood as giving rise to a set of uncertainty relations, and vice versa. It is also clear from Eq. 5 for Bob's choice of measurements $\mathcal{T}$ and distribution $\mathcal{D}$ over $\mathcal{T}$ that the strength of the uncertainty relations imposes an upper bound on the winning probability,

$$P^{\text{game}}(\mathcal{S},\mathcal{T},\sigma_{AB}) \leq \sum_s p(s)\sum_a p(a|s)\ \zeta_{\mathbf{x}_{s,a}}(\mathcal{T},\mathcal{D}) \leq \max_{\mathbf{x}_{s,a}} \zeta_{\mathbf{x}_{s,a}}(\mathcal{T},\mathcal{D}) \quad (13)$$

where we have made explicit the functional dependence of $\zeta_{\mathbf{x}_{s,a}}$ on the set of measurements. This seems curious given that we know from (*21*) that any two incompatible observables lead to a violation of the CHSH inequality, and that to achieve Tsirelson's bound Bob must measure maximally incompatible observables (*22*) that yield stringent uncertainty relations. However, from Eq. 13 we may be tempted to conclude that for any theory it would be in Bob's best interest to perform measurements that are very compatible and have weak uncertainty relations in the sense that the values $\zeta_{\mathbf{x}_{s,a}}$ can be very large. But can Alice prepare states $\sigma_{s,a}$ that attain $\zeta_{\mathbf{x}_{s,a}}$ for any choice of Bob's measurements?

The other important ingredient in understanding nonlocal games is thus steerability. We can think of Alice's part of the strategy $\mathcal{S}$, σ_{AB} as preparing the ensemble $\{p(a|s), \sigma_{s,a}\}_a$ on Bob's system whenever she receives question s. Thus, when considering the optimal strategy for nonlocal games, we want to maximize $P^{\text{game}}(\mathcal{S}, \mathcal{T}, \sigma_{AB})$ over all ensembles $\mathcal{E}_s = \{p(a|s), \sigma_{s,a}\}_a$ that Alice can steer to, and use the optimal measurements $\mathcal{T}_{\text{opt}}$ for Bob. That is,

$$P^{\text{game}}_{\max} = \max_{\{\mathcal{E}_s\}_s} \sum_s p(s)\sum_a p(a|s)\zeta^{\sigma_{s,a}}_{\mathbf{x}_{s,a}}(\mathcal{T}_{\text{opt}},\mathcal{D}) \quad (14)$$

and hence the probability that Alice and Bob win the game depends only on the strength of the uncertainty relations with respect to the sets of steerable states. To achieve the upper bound given by Eq. 13, Alice needs to be able to prepare the ensemble $\{p(a|s), \rho_{\mathbf{x}_{s,a}}\}_a$ of maximally certain states on Bob's system. In general, it is not clear that the maximally certain states for the measurements that are optimal for Bob in the game can be steered to.

It turns out that in quantum mechanics, this can be achieved in cases where we know the optimal strategy. For all XOR games (*23*)—that is, correlation inequalities for two outcome observables (which include CHSH as a special case)—as well as other games where the optimal measurements are known, we find that the states that are maximally certain can be steered to (*12*). The uncertainty relations for Bob's optimal measurements thus give a tight bound,

$$P^{\text{game}}_{\max} = \sum_s p(s)\sum_a p(a|s)\ \zeta_{\mathbf{x}_{s,a}}(\mathcal{T}_{\text{opt}},\mathcal{D}) \quad (15)$$

where we recall that $\zeta_{\mathbf{x}_{s,a}}$ is the bound given by the maximization over the full set of allowed states on Bob's system. It is an open question whether this holds for all games in quantum mechanics.

An important consequence of this is that any theory that allows Alice and Bob to win with a probability exceeding $P^{\text{game}}_{\max}$ requires measurements that do not respect the fine-grained uncertainty relations given by $\zeta_{\mathbf{x}_{s,a}}$ for the measurements used by Bob (the same argument can be made for Alice). Even more, it can lead to a violation of the corresponding min-entropic uncertainty relations (*12*). For example, if quantum mechanics were to violate CHSH using the same measurements for Bob, it would need to violate the min-entropic uncertainty relations (*8*). This relation holds even if Alice and Bob were to perform altogether different measurements when winning the game with a probability exceeding $P^{\text{game}}_{\max}$: For these new measurements, there exist analogous uncertainty relations on the set Σ of steerable states, and a higher winning probability thus always leads to a violation of such an uncertainty relation. Conversely, if a theory allows any states violating even one of these fine-grained uncertainty relations for Bob's (or Alice's) optimal measurements on the sets of steerable states, then Alice and Bob are able to violate the Tsirelson's type bound for the game.

Although the connection between nonlocality and uncertainty is more general, we examine the example of the CHSH inequality in detail to gain some intuition on how uncertainty relations of various theories determine the extent to which the theory can violate Tsirelson's bound (*12*). To briefly summarize, in quantum theory, Bob's optimal measurements are X and Z, which have uncertainty relations given by $\zeta_{\mathbf{x}_{s,a}} = 1/2 + 1/(2\sqrt{2})$ of Eq. 8. Thus, if Alice could steer to the maximally certain states for these measurements, they would be able to achieve a winning probability given by $P^{\text{game}}_{\max} = \zeta_{\mathbf{x}_{s,a}}$—that is, the degree of nonlocality would be determined by the uncertainty relation. This is the case. If Alice and Bob share the singlet state, then Alice can steer to the maximally certain states by measuring in the basis given by the eigenstates of $(X + Z)/\sqrt{2}$ or of $(X - Z)/\sqrt{2}$. For quantum mechanics, our ability to steer is only limited by the no-signaling principle, but we encounter strong uncertainty relations. On the other hand, for a local hidden variable theory, we can also have perfect steering, but only with an uncertainty relation given by $\zeta_{\mathbf{x}_{s,a}} = 3/4$, and thus we also have the degree of nonlocality given by $P^{\text{game}}_{\max} = 3/4$. This value of nonlocality is the same as deterministic classical mechanics, where we have no uncertainty relations on the full set of deterministic states but our abilities to steer to them are severely limited. In the other direction are theories that are maximally nonlocal, yet remain no-signaling (*3*). These have no uncertainty (i.e., $\zeta_{\mathbf{x}_{s,a}=1}$), but unlike in the classical world, we still have perfect steering, so they win the CHSH game with probability 1.

For any physical theory, we can thus consider the strength of nonlocal correlations to be a tradeoff between two aspects: steerability and uncertainty. In turn, the strength of nonlocality can determine the strength of uncertainty in measurements. However, it does not determine the strength of complementarity of measurements (*12*). The concepts of uncertainty and complementarity are usually linked, but we find that it is possible to have theories that are just as nonlocal and uncertain as quantum mechanics, but that have less complementarity. This suggests a rich structure relating these quantities.

References and Notes

1. W. Heisenberg, *Z. Phys.* **43**, 172 (1927).
2. J. S. Bell, *Physics* **1**, 195 (1965).
3. S. Popescu, D. Rohrlich, *Found. Phys.* **24**, 379 (1994).
4. G. V. Steeg, S. Wehner, *QIC* **9**, 801 (2009).
5. M. Pawłowski *et al.*, *Nature* **461**, 1101 (2009).
6. W. van Dam, http://arxiv.org/abs/quant-ph/0501159 (2005).
7. H. Barnum, S. Beigi, S. Boixo, M. B. Elliott, S. Wehner, *Phys. Rev. Lett.* **104**, 140401 (2010).
8. D. Deutsch, *Phys. Rev. Lett.* **50**, 631 (1983).
9. I. Białynicki-Birula, J. Mycielski, *Commun. Math. Phys.* **44**, 129 (1975).
10. S. Wehner, A. Winter, *N. J. Phys.* **12**, 025009 (2010).
11. Without loss of generality, we assume that each measurement has the same set of possible outcomes, because we may simply add additional outcomes that never occur.
12. See supporting material on *Science* Online.
13. S. Wehner, M. Christandl, A. C. Doherty, *Phys. Rev. A* **78**, 062112 (2008).
14. J. Clauser, M. Horne, A. Shimony, R. Holt, *Phys. Rev. Lett.* **23**, 880 (1969).
15. B. Cirel'son (Tsirelson), *Lett. Math. Phys.* **4**, 93 (1980).
16. E. Schrödinger, M. Born, *Proc. Camb. Philos. Soc.* **31**, 555 (1935).
17. E. Schrödinger, P. A. M. Dirac, *Proc. Camb. Philos. Soc.* **32**, 446 (1936).
18. H. M. Wiseman, S. J. Jones, A. C. Doherty, *Phys. Rev. Lett.* **98**, 140402 (2007).
19. S. J. Jones, H. M. Wiseman, A. C. Doherty, *Phys. Rev. A* **76**, 052116 (2007).
20. H. Barnum, C. Gaebler, A. Wilce, http://arxiv.org/abs/0912.5532 (2009).
21. M. M. Wolf, D. Perez-Garcia, C. Fernandez, *Phys. Rev. Lett.* **103**, 230402 (2009).
22. A. Peres, *Quantum Theory: Concepts and Methods* (Kluwer Academic, Dordrecht, Netherlands, 1993).
23. In an XOR game, the answers $a \in \{0,1\}$ and $b \in \{0,1\}$ of Alice and Bob, respectively, are single bits; whether Alice and Bob win or not depends only on the XOR of the answers $a \oplus b = a + b \bmod 2$.
24. The retrieval game used was discovered in collaboration with A. Doherty.

Supported by the Royal Society (J.O.) and by NSF grants PHY-04056720 and PHY-0803371, the National Research Foundation of Singapore, and the Singapore Ministry of Education (S.W.). Part of this work was done while J.O. was visiting California Institute of Technology, and while J.O. and S.W. were visiting the Kavli Institute for Theoretical Physics (Santa Barbara, CA), which is funded by NSF grant PHY-0551164.

Supporting Online Material

www.sciencemag.org/cgi/content/full/330/6007/1072/DC1
SOM Text
Figs. S1 to S4
References

10 May 2010; accepted 1 October 2010
10.1126/science.1192065

Faster Interprotein Electron Transfer in a [Myoglobin, b_5] Complex with a Redesigned Interface

Peng Xiong,[1,2] Judith M. Nocek,[1] Josh Vura-Weis,[1,3] Jenny V. Lockard,[1,3] Michael R. Wasielewski,[1,3]* Brian M. Hoffman[1]*

Direct measurements of electron transfer (ET) within a protein-protein complex with a redesigned interface formed by physiological partner proteins myoglobin (Mb) and cytochrome b_5 (b_5) reveal interprotein ET rates comparable to those observed within the photosynthetic reaction center. Brownian dynamics simulations show that Mb in which three surface acid residues are mutated to lysine binds b_5 in an ensemble of configurations distributed around a reactive most-probable structure. Correspondingly, charge-separation ET from a photoexcited singlet zinc porphyrin incorporated within Mb to the heme of b_5 and the follow-up charge-recombination exhibit distributed kinetics, with median rate constants, $k_f^s = 2.1 \times 10^9$ second^{-1} and $k_b^s = 4.3 \times 10^{10}$ second^{-1}, respectively. The latter approaches that for the initial step in photosynthetic charge separation, $k = 3.3 \times 10^{11}$ second^{-1}.

Ultrafast electron transfer (ET) has evolved within photosystems I and II (*1*) to occur on time scales of 10^{-11} to 10^{-12} s. Most biological redox processes involve long-range transfer of an electron or hole between redox centers separated by a noncovalent, dynamically fluctuating, protein-protein interface. These processes are many orders of magnitude slower, typically on time scales longer than 10^{-6} s (*2*–*5*). Here we report that redesigning the interface between the physiological ET partners, myoglobin (Mb) and cytochrome b_5 (b_5), leads to the fastest interprotein ET rate constants yet observed, with values that approach those occurring within the photosynthetic reaction centers. This ultrafast ET occurs within an interprotein ET photocycle (Fig. 1A) in which both charge separation and recombination exhibit distributed kinetics, in keeping with Brownian dynamics (BD) simulations (Fig. 1, B to D), which show that the complex exists as an ensemble of bound configurations. Relatively small overall differences among similar configurations within the ensemble lead to a broad distribution in their ET rate constants.

We recently described a strategy for redesigning the interface between weakly bound (dynamically docked) ET partner proteins, thereby enhancing and coupling both their binding and reactivity, by optimizing the placement of surface charges within the putative docking interface (*6*). We applied this strategy to the [Mb, b_5] complex and obtained a triple mutant, in which three acidic surface residues surrounding the Mb (horse) heme (Asp^{44}, Asp^{60}, and Glu^{85}) are replaced by Lys [Mb(+6)], that exhibits both strongly enhanced binding to b_5 (bovine) and intracomplex ET from the triplet state of Zn-deuteroporphyrin (ZnD)–substituted Mb to the Fe^{3+} b_5 heme (Fe^{3+}P). Intriguingly, variations in the apparent efficiency of intersystem crossing from the photoexcited ZnD singlet state (^{1}ZnD) to the ZnD triplet state (^{3}ZnD) during ET quenching titrations of ZnDMb(+6) by Fe^{3+} b_5 were interpreted as providing indirect evidence for extremely rapid intracomplex ET from ^{1}ZnD to the Fe^{3+}P of Fe^{3+} b_5, $k \sim 10^9$ s^{-1}. Here we report direct measurements of ultrafast interprotein ET across the noncovalent [Mb, b_5] interface through femtosecond transient absorption (fs-TA) measurements of the intracomplex photocycle (Fig. 1A) that begins when laser excitation generates the ^{1}ZnD state, which reacts by

[1]Department of Chemistry, Northwestern University, 2145 Sheridan Road, Evanston, IL 60208–3113, USA. [2]School of Life Science and Chemical Engineering, Huaiyin Institute of Technology, 1 East Meichen Road, Huaián, Jiangsu Province, China 223003. [3]Argonne-Northwestern Solar Energy Research (ANSER) Center, Northwestern University, Evanston, IL 60208–3113, USA.

*To whom correspondence should be addressed. E-mail: bmh@northwestern.edu

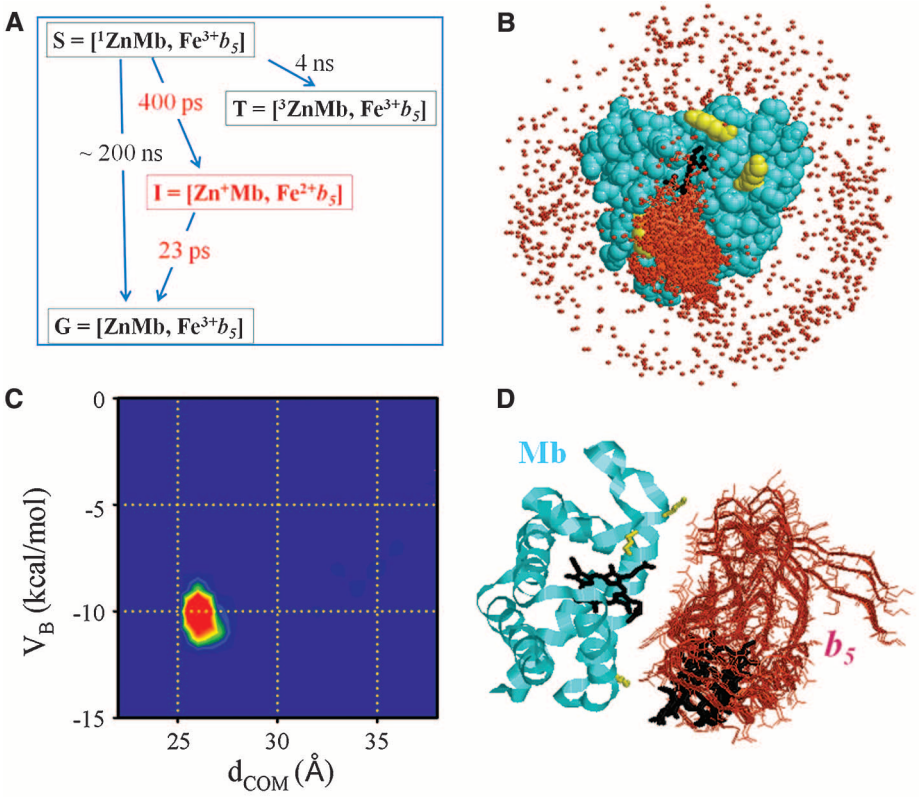

Fig. 1. ET photocycle and corresponding BD simulation for the docking of $Fe^{3+}b_5$ (red) onto Mb(+6) (cyan) (**A**) The vertical spacing between states corresponds roughly to their energetic difference (see **SI**). The labels correspond with "1/*e*" times for ET. Spatial distribution (**B**), contour plot (**C**), and four representative configurations (**D**) in the vicinity of the most-probable configuration as defined by Boltzmann weighting the electrostatic potential energies (V_B). Details: Center-of-mass (COM) reaction criterion (d = 39 Å) as described in (*6*); 10^4 trajectories; 293 K; μ = 18 mM; pH 7.0; mutation sites in yellow; the representative configurations are within ± 0.25 kcal/mol and ± 0.25 Å of the most-probable configuration.

^{1}ZnD → Fe^{3+}P ET to form the charge-separated intermediate, **I** = [ZnD^+Mb, $Fe^{2+}b_5$], and concludes with Fe^{2+} → ZnD^+ charge recombination. The photocycle energetics are given in the supporting online materials (SOM) (*7*).

The measurements use Mb(+6) reconstituted with Zn-deuteroheme dimethyl ester, with the heme neutralization having increased the Mb charge by an additional +2 [denoted ZnMb(+8)]. fs-TA experiments were performed with ZnMb(+8) by itself (fig. S1) (*7*) and with a sample in which more than 95% of the Mb is in the [ZnMb, $Fe^{3+}b_5$] complex (Fig. 2). The photoexcited isolated ^{1}ZnMb(+8) converts almost quantitatively (intersystem crossing yield ~ 98%) to ^{3}ZnMb(+8), with a time course (Fig. 3, left) that is well described at all wavelengths by the exponential decay of ^{1}ZnMb(+8) and the concomitant appearance of ^{3}ZnMb(+8) (Eq. 1),

$$\Delta A = A\ \exp(-{}^1k_D t) + B[1 - \exp(-{}^1k_D t)]$$
$$= [A - B]\ \exp(-{}^1k_D t) + B \qquad (1)$$

where $^1k_D = 2.5 \times 10^8\ s^{-1}$. The wavelength-dependent amplitude factor, A, corresponds to the zero-time excited singlet-ground state difference spectrum (fig. S1), B to the persistent triplet-ground difference spectrum, and thus $[A - B]$ to the ^{1}ZnMb-^{3}ZnMb difference (*8*).

Figure 2 displays representative transient absorption-difference spectra of the [ZnMb(+8), $Fe^{3+}b_5$] complex taken from 425 to 725 nm at delay times ranging from ~1 ps to ~4 ns. Focusing first on wavelengths λ < 525 nm, the initial difference spectrum corresponds to the ^{1}ZnMb-ground state difference, its most prominent feature being a maximum at 452 nm. With time, this maximum decreases in intensity and gradually blue-shifts toward 445 nm, the maximum of the ^{3}ZnMb-ground state difference (*8*, *9*). The decay of ^{1}ZnMb complexed by $Fe^{3+}b_5$ is like that for ^{1}ZnMb alone, in being homogeneous for λ < 530 nm. This similarity is seen more clearly in the inset, where the longest-time (~4 ns) absorbance difference has been subtracted from each trace, generating a ^{1}ZnMb-^{3}ZnMb difference spectrum that homogeneously decays to zero at the longest time. The decay after photoexcitation of ^{1}ZnMb in the complex is much faster than for ^{1}ZnMb alone, and it cannot be described by a single exponential. It can be fit by a biexponential (Fig. 3, blue) in which both decay constants are sharply increased by intracomplex ET ($k_{1f} = 1.1 \times 10^{10}\ s^{-1}$, $k_{2f} = 1.2 \times 10^9\ s^{-1}$; $f_1/f_2 = 3/4$). However, such a fit implies the presence of two distinct (classes of) configurations for the complex, whereas the BD simulations (Fig. 1) do not show such a bimodal clustering of "hits." Rather, the simulation yields an ensemble of BD hits that is smoothly distributed over a single region of the Mb surface in the vicinity of the heme (Fig. 1B). This is emphasized by a plot of these hits as a function of their Boltzmann-weighted calculated electrostatic binding energy (V_B) relative to the dissociated complex, and a parameter that reflects the b_5 location, the center-of-mass distance (d_{COM}) (Fig. 1C). This plot shows that the ensemble of hits is rather tightly distributed around a single most-probable maximum at an electrostatic energy of $V_B \sim -10$ kcal/mol, and center-of-mass distance of $d_{COM} \sim 26$ Å. Thus, although the biexponential function provides a satisfactory description of the decay of ^{1}ZnMb in complex with $Fe^{3+}b_5$, its use is not physically justified.

Careful consideration of the structures associated with the BD hits shows that even though the hits exhibit a narrow range of distances, there is a considerable distribution in the positioning of b_5 relative to Mb, and this should cause a distribution in ET rate constants. Figure 1D superimposes onto the coordinates of the "target" Mb the b_5 coordinates of four representative configurations from among 224 hits within ± 0.25 Å and ± 0.25 kcal/mol of the most-probable configuration. Focusing on the b_5 hemes (black)

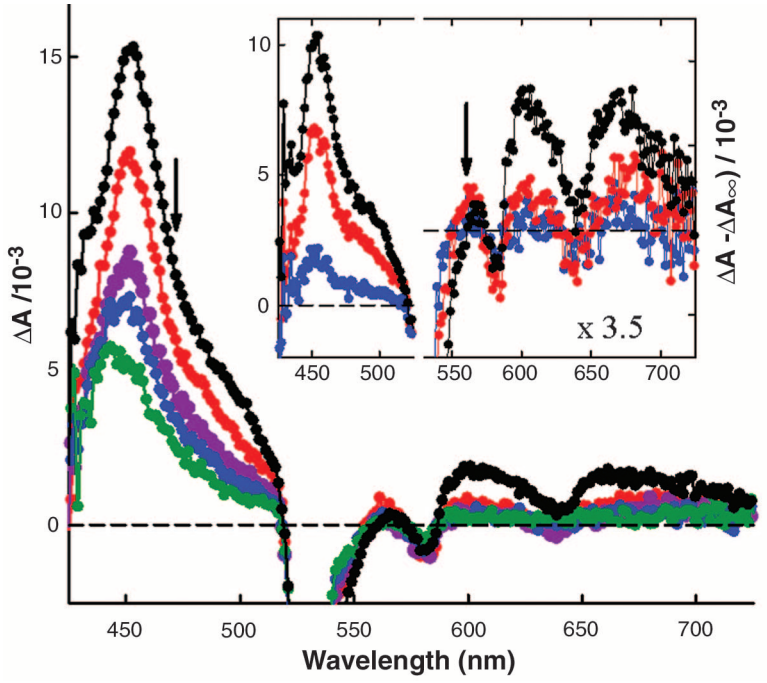

Fig. 2. fs-TA absorbance-difference measurements subsequent to photoexcitation of [ZnMb(+8), $Fe^{3+}b_5$]. Representative time-resolved spectra at delay times of 1.5 ps (black), 107 ps (red), 527 ps (purple), 1027 ps (blue), and ΔA_∞ = 3827 ps (green). (**Inset**) Redisplay of selected spectra after subtraction of the residual difference at t = 3.8 ns. Arrows refer to representative time slices shown in Fig. 3. Conditions: 0.1 mM ZnMb(+8), 0.2 mM $Fe^{3+}b_5$, 95% of Mb bound to b_5 ($K_a = 8.0 \times 10^5\ M^{-1}$); 10 mM potassium phosphate; pH 7.0; ambient temperature; 2 mm pathlength; fresh sample was used for each time point.

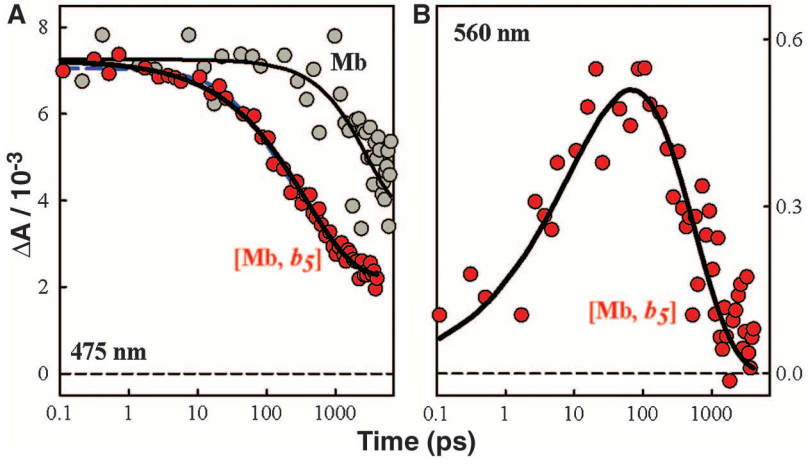

Fig. 3. Representative kinetic progress curves. (**A**) Traces at 475 nm for decay of ^{1}ZnMb(+8) (gray) and its complex with $Fe^{3+}b_5$ (red). ZnMb(+8) trace was fit with Eq. 1; trace for complex was fit with a biexponential function (blue) and Eq. 2 (black). (**B**) Progress curve for **I** obtained by averaging time slices between 556 and 563 nm. Trace was fit with Eq. 3 (black). $[\mathbf{I}]_{max}$ ~ 0.2 μM, on the basis of the maximum absorbance change and reported difference spectrum (*8*). Conditions: as in Fig. 2.

shows a substantial variation among their positions and orientations, even among these similarly bound configurations. The driving force for ET should vary little, if at all, among the different configurations, but the structural variations within the ensemble will produce wide variation in the ET pathways that cross the protein-protein interface, and the correspondingly large variations in the preexponential term will cause large variations in the ET rate constant (*10*). These variations will not be time-averaged during the decay because dynamic interconversion among the configurations of the complex must be slower than the ET time scale set by the ultrafast interprotein ET that we observe. As a result, the ET process involves an ensemble of static configurations, each with its own structure and its own ET rate constant, and one expects to observe distributed kinetics. ET will occur first in the complexes with the largest rate constant. As the more ET-active configurations progressively become depleted, the remaining complexes with a ^{1}ZnD will progressively have smaller ET rate constants. As a result, the effective rate constant will decrease in time as the reaction progresses.

Prompted by these considerations, the singlet decay traces from the short wavelength range also were fit with a distributed decay—a version of Eq. 1 with a "stretched exponential" (*11*)

$$\Delta A = [A - B]\ \exp[-(^1k_D t) - (k_f^s t)^n] + B \quad (2)$$

This function corresponds to a distribution in ET rate constants whose width varies inversely with n, but can equivalently be thought of in terms of an ET rate constant that decreases in time; the constant, k_f^s, which fixes the "1/e" time for ET, corresponds to the median ET rate constant for the distribution (*11*). The fits to Eq. 2 (Fig. 3A) give $k_f^s = 2.1(5) \times 10^9\ s^{-1}$ and a distribution parameter, $n = 0.57(5)$ (Table 1).

The homogeneous decay of the difference spectrum for wavelengths $\lambda < 525$ nm indicates that the charge-separated ET intermediate **I** either is not spectroscopically distinct in this wavelength range or does not accumulate to a level detectable at these wavelengths because the system displays "inverted kinetics." However, the results for $\lambda > 525$ nm confirm the formation of **I** and can be used to monitor the charge-recombination ET return to the ground state. The difference spectra in this range do not vary homogeneously in time (Fig. 2). This is best seen at ~560 nm, a ^{1}ZnD-ground isosbestic and a wavelength range where the difference spectrum is governed by absorbance changes associated with the $Fe^{2+}b_5/Fe^{3+}b_5$ redox change (*8*). One observes a difference maximum that grows with time and then decays (Fig. 2); the corresponding kinetic trace at this wavelength (Fig. 3B) clearly shows the appearance and loss of the [ZnD^+Mb, $Fe^{2+}b_5$] charge-separated intermediate as it is formed by excitation of ZnD to the ^{1}ZnD excited state, followed by ^{1}ZnD → Fe^{3+}P charge separation, and disappears by Fe^{2+}P → ZnD^+ charge recombination.

Following the above discussion, the time course for **I** is appropriately described by assuming a stretched exponential function for both the charge-separation and charge-recombination ET processes (Eq. 3) (*12*, *13*). Numerical solution to the differential equations for this model in Mathcad gives a progress curve equivalent to that of the heuristic distributed function

$$\Delta A = I\{\exp[-(^1k_D t) - (k_f^s t)^n] - \exp(-k_b^s t)^m]\} \quad (3)$$

The fit to the progress curve for **I** is excellent (Fig. 3B); fixing k_f^s and n as the values determined for the singlet ET progress curves gives $k_b^s = 4.3 \times 10^{10}\ s^{-1}$ ($m = 0.49$) as the median rate constant for charge recombination, roughly 20 times the k_f^s for charge separation (Table 1). The similarity of the distribution parameters for charge separation and recombination ET reactions ($n \approx m = 1/2$) is as expected because the ET reactions occur on a time scale that is short compared to the time scale for structural rearrangement of the individual reactive complexes. However, fits to the full photocycle with stretched exponentials would predict a maximum concentration of **I** roughly twice that determined from the observed maximum absorbance change and reported difference spectrum (*8*), an indication that the distribution in rate constants associated with the stretched exponentials (*11*) represents the ensemble of structures only imperfectly.

The striking nature of these results is highlighted by comparison to representative rate constants previously reported for ET across a protein interface, as well as to those for ET between redox sites within the reaction center of cyanobacteria, algae, and plants. The median rate constant for photoinitiated ^{1}ZnDMb → $Fe^{3+}b_5$ charge separation, k_f^s, is more than three times the rate constant for the fastest interprotein ET process previously reported, ^{1}Zn-cytochrome c (Cc) → cytochrome c oxidase (CcO) singlet-state ET, and the charge-recombination rate constant, $k_b^s = 4.3 \times 10^{10}\ s^{-1}$, is more than 60 times as large. In fact, this median interprotein rate constant is only roughly one-eighth the rate constant for the initial charge separation within the *Blastochloris viridis* photosynthetic reaction center (Table 1).

We examined features of the distribution in rate constants, $H(k_b^s)$, associated with the observed distribution parameter, $m = ½$ (*11*). The most-probable value for k_b^s is about one-fifth of the median value, yet almost one-fifth of the configurations have rate constants that match (or exceed) that for photosynthetic charge separation. Clearly, a substantial fraction of the ensemble of [Mb(+8), b_5] structures have extremely efficient ET pathways, although the pathways for many are poor.

The ^{3}ZnD that remains after the ^{1}ZnD photocyle is complete undergoes ^{3}ZnD → Fe^{3+}P ET within the complex (*6*). This charge separation is three orders of magnitude slower than for ^{1}ZnD, but still slightly faster than the corresponding process in other Zn-substituted protein ET pairs (Table 1). The driving force for ^{3}ZnD → Fe^{3+}P ET is less than for ^{1}ZnD → Fe^{3+}P, but considerations of the ET energetics suggest that this difference should make the ^{3}ZnD reaction faster, not slower (inverted region) (*7*). We suggest that the ^{3}ZnD reaction is so much slower because highly reactive configurations of the complex preferentially undergo ^{1}ZnD ET, and intersystem crossing to the triplet occurs only in configurations with much poorer ET pathways. As a result, ET from the triplet porphyrin presumably is gated by the dynamics of conformational interconversion to reactive conformations, and not controlled by the actual charge-separation process. Thus, the interface redesign strategy has created a complex that not only has unprece-

Table 1. Rate constants for interprotein and photosynthetic electron transfer. Cc, cytochrome c; CcO, cytochrome c oxidase; Pc, plastocyanin; P, bacteriochlorophyll special pair; (P)*, photoexcited P; B, bacteriochlorin; H, bacteriopheophytin; Q, quinone.

ET	[Donor, acceptor]	ET rate constant (s^{-1})		Reference
		Charge separation	Charge recombination	
Protein-protein	**[^{1}ZnMb(+8), $Fe^{3+}b_5$]**	**$2.1 \times 10^{9*}$**	**4.3×10^{10}†**	**This work**
	[^{1}ZnCc, Cu_A^{2+}CcO]	5.7×10^8	–	(*14*)
	[^{3}ZnMb(+6), $Fe^{3+}b_5$]	1.0×10^6	–	(*6*)
	[^{3}ZnCc, Cu_A^{2+}CcO]	4.5×10^5	–	(*14*)
	[^{3}ZnCc, Cu^{2+}Pc]	2.3×10^5	9.6×10^5	(*15*)
	[Fe^{2+}Cc(Ru39), Cu_A^{2+}CcO]	6.0×10^4		(*16*)
	[Reaction center (P^+), $Fe^{2+}Cc_2$]	1.0×10^6		(*17*)
Photosynthetic reaction center‡ (*Bl. viridis*)	[(P)*, B]	3.3×10^{11}		(*18*)
	[B^-, H]	1.1×10^{12}		
	[H^-, Q]	5.0×10^9		

*ET rate constant from stretched-exponential fit (Eq. 2, see text); biexponential fit, $k_{1f} = 1.1 \times 10^{10}\ s^{-1}$, $k_{2f} = 1.2 \times 10^9\ s^{-1}$. †ET rate constant from stretched-exponential fit (Eq. 3; see text).

dented rate constants for interprotein ET, but also reveals details of the conformational distributions and dynamics that underlie protein-protein binding and reaction.

References and Notes

1. R. E. Blankenship, *Molecular Mechanisms of Photosynthesis* (Blackwell Science, Oxford, ed. 1, 2002).
2. V. L. Davidson, *Acc. Chem. Res.* **41**, 730 (2008).
3. M. Prudêncio, M. Ubbink, *J. Mol. Recognit.* **17**, 524 (2004).
4. C. C. Page, C. C. Moser, P. L. Dutton, *Curr. Opin. Chem. Biol.* **7**, 551 (2003).
5. H. B. Gray, J. R. Winkler, *Proc. Natl. Acad. Sci. U.S.A.* **102**, 3534 (2005).
6. J. M. Nocek, A. K. Knutson, P. Xiong, N. Petlakh Co, B. M. Hoffman, *J. Am. Chem. Soc.* **132**, 6165 (2010).
7. See supporting materials on *Science* Online.
8. J. M. Nocek, B. P. Sishta, J. C. Cameron, A. G. Mauk, B. M. Hoffman, *J. Am. Chem. Soc.* **119**, 2146 (1997).
9. S. Papp, J. M. Vanderkooi, C. S. Owen, G. R. Holtom, C. M. Phillips, *Biophys. J.* **58**, 177 (1990).
10. D. N. Beratan *et al.*, *Acc. Chem. Res.* **42**, 1669 (2009).
11. M. N. Berberan-Santos, E. N. Bodunov, B. Valeur, *Chem. Phys.* **315**, 171 (2005).
12. D. Lukoyanov, B. M. Barney, D. R. Dean, L. C. Seefeldt, B. M. Hoffman, *Proc. Natl. Acad. Sci. U.S.A.* **104**, 1451 (2007).
13. J. M. Nocek *et al.*, *J. Am. Chem. Soc.* **113**, 6822 (1991).
14. J. R. Winkler, B. G. Malmström, H. B. Gray, *Biophys. Chem.* **54**, 199 (1995).
15. M. M. Ivković-Jensen *et al.*, *Biochemistry* **38**, 1589 (1999).
16. L. Geren, B. Durham, F. Millett, *Methods Enzymol.* **456**, 507 (2009).
17. X.-M. Gong, M. L. Paddock, M. Y. Okamura, *Biochemistry* **42**, 14492 (2003).
18. W. Zinth, J. Wachtveitl, *ChemPhysChem* **6**, 871 (2005).

19. Funding for this work was provided as follows: P.X., J.M.N., and B.M.H., the National Institute of Health (grant HL063203); J.V.-W., J.V.L., and M.R.W., as part of the ANSER Center, an Energy Frontier Research Center funded by U.S. Department of Energy, Office of Science, Office of Basic Energy Sciences (DE-SC0001059).

Supporting Online Material

www.sciencemag.org/cgi/content/full/330/6007/1075/DC1
Materials and Methods
SOM Text
Fig. S1
References

27 August 2010; accepted 8 October 2010
10.1126/science.1197054

Zooming In on Microscopic Flow by Remotely Detected MRI

Vikram S. Bajaj,* Jeffrey Paulsen, Elad Harel,† Alexander Pines*

Magnetic resonance imaging (MRI) can elucidate the interior structure of an optically opaque object in unparalleled detail but is ultimately limited by the need to enclose the object within a detection coil; acquiring the image with increasingly smaller pixels reduces the sensitivity, because each pixel occupies a proportionately smaller fraction of the detector's volume. We developed a technique that overcomes this limitation by means of remotely detected MRI. Images of fluids flowing in channel assemblies are encoded into the phase and intensity of the constituent molecules' nuclear magnetic resonance signals and then decoded by a volume-matched detector after the fluids flow out of the sample. In combination with compressive sampling, we thus obtain microscopic images of flow and velocity distributions ~10^6 times faster than is possible with conventional MRI on this hardware. Our results illustrate the facile integration of MRI with microfluidic assays and suggest generalizations to other systems involving microscopic flow.

In the hospital and laboratory alike, magnetic resonance imaging (MRI) routinely provides detailed information about the structure, fluid dynamics, and chemistry deep within opaque objects, organs, and materials. However, the conventional geometry of an MRI experiment severely limits its sensitivity for a ubiquitous class of applications, including cerebrovascular angiography and parallel microfluidic assays, in which the dimensions of the imaged objects are orders of magnitude larger than those of the fluid-containing channels they enclose. Because the signal in an inductive nuclear magnetic resonance (NMR) coil is proportional to the magnetic flux the coil encloses, the sensitivity of an NMR detector is optimized when the feature of interest completely fills the detector's active volume—a constraint that cannot be met for these systems. In addition, local magnetic field gradients at the interface of fluid and solid channel boundaries cause line broadening and exacerbate this loss of sensitivity. Both factors severely limit the accessible resolution—the ability to zoom in to see details of interest—in the MRI of microfluidic devices, porous materials, or biological fluid channels in the brain and other organs.

To sensitively image a microscopic feature of a flowing system, an NMR coil should ideally be embedded within the object such that it precisely encloses only the element of interest. Indeed, this approach has been adopted in microfluidic device studies: Multiple radio frequency–resonant structures have been fabricated directly on a chip, such that each detector is matched to the dimensions of the microchannel that fills it (*1*–*4*). However, this method will not easily scale to circuitous or highly parallel microfluidic geometries because it requires a separate and isolated resonant circuit and electronics for each detector in the array (*2*, *5*), and it additionally obscures the correlation between elements in the flow pathway. It cannot be integrated into existing microfluidic assays, nor can it be applied to microporous materials (*6*), microchromatography columns, or living systems, whose internal fluid channels are inherently inaccessible to a local detector.

We have developed a suitable alternative to this direct mode of NMR detection. Remote detection (*7*) is a generalization of multidimensional NMR (*8*) in which physical translation of the sample occurs before acquisition of the signal (see fig. S1). We have applied remote detection to gas flow in channels (*9*) and porous materials (*10*) and to time-resolved liquid flow (*11*). Here, we introduce a combination of methods that allow us to zoom in on the microscopic details of microfluidic flow dynamics in three spatial dimensions via the amplifying action of remote flow. These methods include fabrication of microsolenoid NMR probes with demountable microfluidic device holders; design of remote MRI sequences for spatial encoding in the presence of motion, as well as for velocimetric measurements; and compressive sampling algorithms for faster image encoding. This combination of remote MRI methods (Fig. 1) spectroscopically mimics the implantation of a coil around a microscopic feature of interest. The mechanism of remote detection is analogous to that of a magnetic recording tape on which complex data are first encoded and later read out by a single stationary detector as the tape advances.

Specifically, the macroscopic imaged structure (e.g., microfluidic chip) is enclosed by a conventional MRI coil, which we use only to encode information in the phase of the NMR signal of any analyte (solute or solvent) containing spin-½ nuclei, such as protons. We can use any Fourier phase-encoding pulse sequence without modification from the library of conventional MRI methods to encode the desired spatial, dynamic (*12*–*14*), or chemical information (fig. S3). However, instead of inefficiently detecting the result with the same coil, we next store the NMR phase information as long-lived longitudinal magnetization (intensity) that decays with the spin lattice relaxation time, which is usually several seconds for diamagnetic fluids such as water or organic solvents (fig. S4). Within that time, the encoded fluid flows to a detector whose volume is matched to the feature of interest (e.g., microfluidic channel), where the information encoded within it—a spectrum or an image—is read out as the fluid flows past. Our method does not require the encoded fluid packets to arrive at the detector in order; simple Fourier transformation yields both the encoded information and a correlated time-of-flight dimension that reflects the arrival of fluid packets at the detector. Most important, because

Materials Sciences Division, Lawrence Berkeley National Laboratory, Berkeley, CA 94720, USA, and Department of Chemistry, University of California, Berkeley, CA 94720, USA.

*To whom correspondence should be addressed. E-mail: vsbajaj@lbl.gov (V.S.B.); pines@berkeley.edu (A.P.)
†Present address: James Franck Institute, University of Chicago, Chicago, IL 60637, USA.

the volume of our single detector is matched to the size of the interesting features, remote detection allows us to zoom in on them while minimizing the sensitivity loss due to filling factor or susceptibility broadening. This setup provides a signal enhancement of 400 relative to conventional MRI for our geometry and in the experiments we present here (Figs. 2 and 3).

Further, because the Fourier image coefficients are stored and then read out indirectly, we benefit from tremendous flexibility in the way that they are digitally sampled. Indeed, most systems for which remote detection is likely to be useful are sparse in that their interesting features occupy a small fraction of the image field of view. Just as sparse electronic data can be compressed to a fraction of their normal volume, our images can be represented and sampled sparsely. Sparse or nonuniform sampling of the Fourier space is critically important in reducing the time required to acquire images with high resolution and high dimensionality. This is because a conventional MRI image comprises repetitions of an experiment whose parameters are serially incremented to encode each point in the multidimensional Fourier space. Its acquisition therefore requires a time proportional to the product of the number of points in each dimension. By using compressed sensing, now also introduced in clinical MRI (*15*), we further reduce acquisition times in remotely detected images by factors of 8 to 64 by sampling only a chosen subset of these points. Our implementation of compressed sensing relies on the sparse representation of images in the wavelet domain (*16*) and nonlinear reconstruction (fig. S5) (*17*). Combining sparse sampling with remote detection allows us to record images about 1 million times as quickly as in a conventional MRI experiment that might be recorded using the same imaging hardware [enhancement by a factor of ~1100 to 3200 gives ~$1000^2 = 10^6$ increase in speed (*17*)].

In the examples below, we enclose microfluidic devices (chip dimensions ~3 cm by 4 cm; microfluidic channels with rectangular cross section of 50 to 150 μm) with a commercially produced volume-encoding coil (40 mm × 40 mm cylinder) in an unmodified high-field MRI system. We subject them to magnetic field gradients (Fig. 1) that encode information about the spatial distribution of flow and its velocity in the spin degrees of freedom of water, although the method is generically applicable to any analyte. Our detector is a microsolenoid (250 μm × 0.5 mm) NMR probe connected to the outlet of the microfluidic device. We acquire NMR signals stroboscopically as the detector coil empties and fills with new encoded fluid. Accordingly, our scheme (Fig. 1B) uses gradient pulses that compensate for the deleterious effects of fluid motion during the encoding period or render the signal phase sensitive to the velocity alone while removing its dependence on position and acceleration (*13*, *18*) [hereafter called phase contrast (*17*)].

We thus explore the limits of resolution at commercially available gradient strengths, achieving a time resolution of 30 ms and spatial resolution of better than 15 μm, at flow rates approaching 100 cm/s. These measurements furthermore explicitly correlate two complementary descriptions of the flow field—the Lagrangian, in which the flow is parameterized in terms of fluid parcel trajectories and times of flight, and the Eulerian, in which the velocity is specified at each point in space—in three spatial dimensions. By contrast, optical measurements in the en face geometry typically require transparent samples and confocal arrangements to image concentration or velocity gradients in the perpendicular dimension. Our method, however, resolves only the components of the velocity field that are in steady state over the duration of the experiment; non–steady-state flow contributes a random phase and cannot be elucidated using this or other MRI-based techniques.

To validate our method, we applied remotely detected velocimetry to three microscale structures: a microcapillary (diameter 50 μm), a serpentine microfluidic mixer, and a constricted microchannel. In the first case, it is well known that the pressure-driven flow of water should produce a parabolic axial velocity profile due to the vanishing relative velocity of viscous liquids at solid boundaries. This expected distribution is indeed revealed by two-dimensional sections of axial velocity–encoded images (Fig. 2, A and B). These high-resolution (15 μm) experiments also illustrate several unique features of remotely detected velocimetry. Beyond revealing expected correlations between time of flight and local velocity, the data demonstrate how the image appearance depends predictably on this time of flight to the detector, in the sense that faster-moving components arrive at earlier times of flight. Further, because the velocity varies continuously, each voxel contains a distribution of velocities that are measured as a geometric average in phase contrast measurements, but are separated here by a Lagrangian time-of-flight parameter (fig. S3). Alternatively, the true velocity distribution can also be measured by Fourier velocity methods (see below), in which the velocity-encoding gradient is stepped through a series of values to generate a conjugate Fourier dimension that encodes the velocity distribution.

Next, we applied our velocimetry method to flow in a serpentine microfluidic mixer (Fig. 2 and movies S1 and S2), in which the encoded transverse velocity, orthogonal to the overall axis of flow, changes in sign as the channel winds back and forth. Finally, we investigated flow in a constricted microchannel—an important geometry

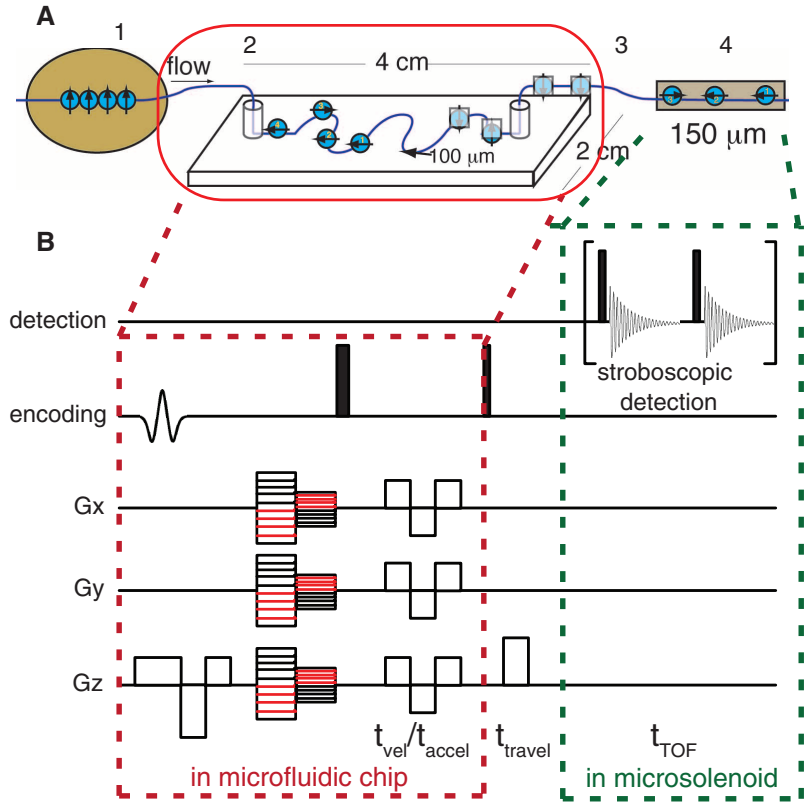

Fig. 1. Remotely detected MRI. (**A**) Spins in fluid analytes are polarized (1) in an MRI magnet and then encoded (2) in an MRI volume coil with switchable gradients (encircled in red). Information is stored (3) as the fluid travels to an optimized microsolenoid detector (4), where it is detected (still in the MRI magnet). (**B**) MRI pulse sequence. After slice selection, information is encoded into the phase of the NMR signal by magnetic field gradients (*Gx*, *Gy*, *Gz*) and stored by a $\pi/2$ pulse for travel to the detector, where it is detected stroboscopically. t_{vel} and t_{accel}, times over which velocity- or acceleration-phase encoding is performed; t_{travel}, travel time from chip to microsolenoid; t_{TOF}, time for travel of a fluid packet from chip to detector.

because many microfluidic elements, including valves and connectors, incorporate discontinuous changes in the channel boundary. We examined accelerating water flow through the constriction with 20-μm resolution (first using conventional, not compressed, sampling to validate the method). The data in Fig. 3A and movie S3 clearly resolve both the faster components of the flow and those that are retarded by the constriction and arrive later. Further, multidimensional velocity images with three spatial dimensions (Fig. 3B), acquired with compressed sensing, illustrate that flow near the constriction appears dispersive at this spatial resolution. Indeed, fine Fourier sampling of the velocity dimension (Fig. 3C) reveals a broad velocity distribution for voxels near the constriction, and, because these measurements simultaneously elucidate flow in the Lagrangian picture, the time-of-flight dispersion curves (Fig. 3D) for spins that transit this voxel similarly reveal correlated information about the dispersion.

Our approach thus addresses two important problems in microfluidics. Microfluidics promises to miniaturize laboratory-scale chemistry so that it can be conducted in parallel and in portable devices (*19*–*22*). However, critically lacking for the design of new devices (as well as for parallel assays in existing ones) is a nonperturbing tool to probe both microscale chemistry and flow dynamics (*23*). Although NMR spectra contain specific chemical information and MRI delivers information about flow distributions, neither is generically suitable for microfluidic applications in its conventional incarnation (*24*). Remote detection is a method by which a single generic NMR-MRI detector can easily be coupled to any microfluidic geometry without modification. Nonetheless, microfluidic remote detection has a number of limitations. It is applicable only to analytes that are themselves NMR-active or can be detected indirectly by contrast agents or other sensors. Moreover, the residence time of the analytes in the device after encoding must be less than that required for the spins to relax to thermal equilibrium polarization (T_1 relaxation). For example, if a remotely detected microfluidic assay requires an incubation period longer than T_1, it will have to be conducted first with the flow arrested, to be followed by MRI encoding of the result and transport to the remote detector within a time shorter than T_1.

This method also has potential applications beyond microfluidics. Microsolenoid NMR detectors routinely achieve picomolar mass sensitivity (*1*). Thus, without specialized hardware, our method can now be applied to flow in microporous materials and, with detection of chemical shifts (*11*), to high-throughput studies of combinatorial chemistry, cellular metabolism, and small-molecule screening. Next, its application to analogous flow structures in vivo may enable sensitive localized spectroscopy—and possibly imaging—of microvasculature in the brain, kidneys, and liver with catheter microcoils or surface coil detectors and blood as the encoding fluid, particularly if slowly relaxing hyperpolarized substances, such as ^{13}C polarized by dynamic nuclear polarization or optically polarized ^{129}Xe, are used as the encoding medium. Finally, remote detection, in separating the polarization, encoding, and detection steps of an experiment, permits the separate optimization of each. We therefore anticipate that this technology, in combination with sensitive NMR chemical sensors (*5*, *25*) and microfabricated NMR detectors (*26*) based on optical magnetic field sensors that operate at low magnetic fields (*27*), will be central to the construction of low-cost NMR devices for highly parallel analytical, biomedical, and clinical applications (*28*).

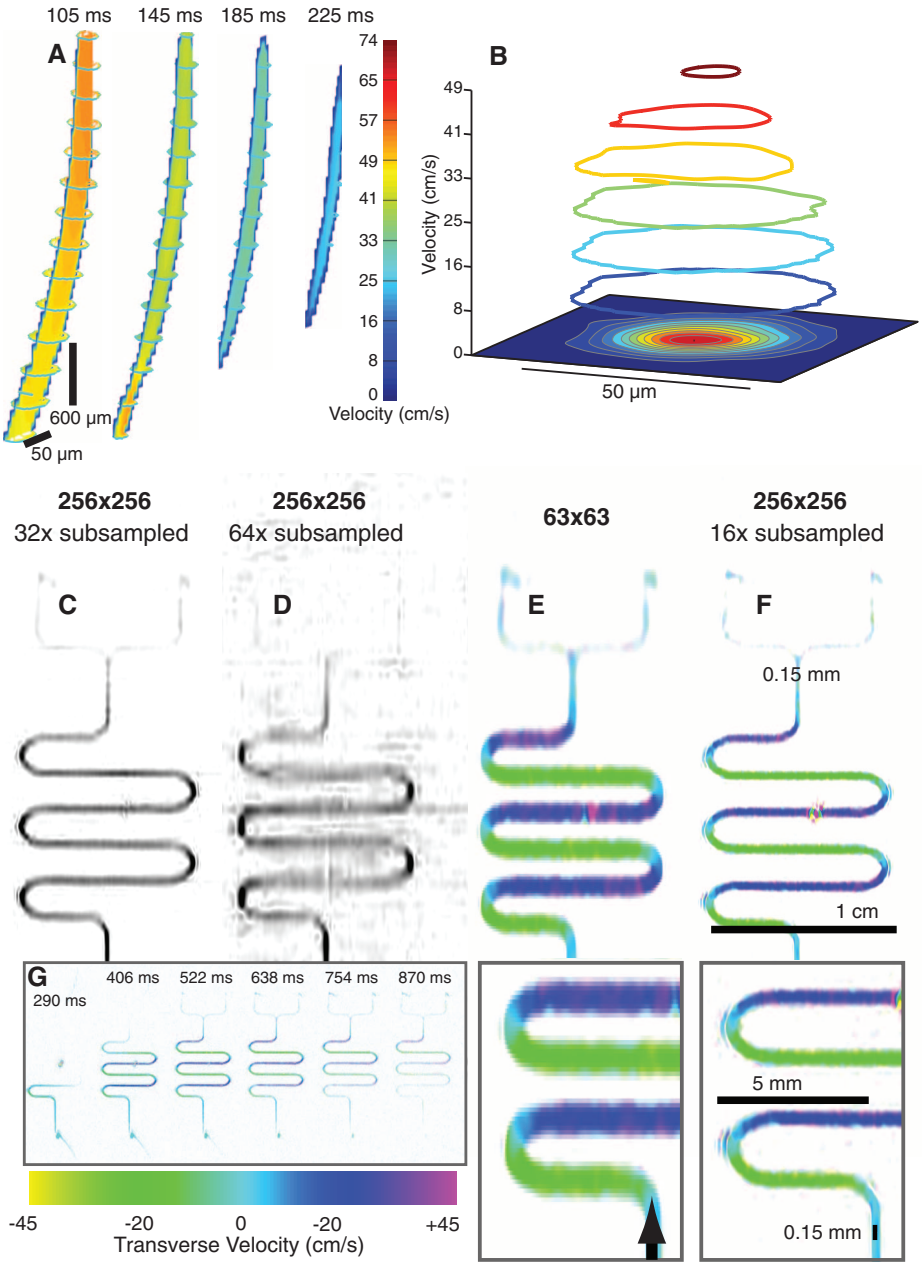

Fig. 2. Images of flow in microfluidic devices. (**A**) Three-dimensional [15 (*X*) × 15 (*Y*) × 15 (*Z*) points] velocity-encoded images of flow through a microcapillary. Each image represents the segments of the flow that arrived with the indicated time of flight (TOF). The 3D contours are drawn at the outer surface of the image (capillary boundary). The colored surface within the 3D capillary indicates the velocity in a plane through the center of the capillary. (**B**) A two-dimensional velocity image cross-section [15 (*X*) × 15 (*Y*) points] illustrating parabolic velocity profile in the capillary. (**C** to **G**) Images of flow in a microfluidic serpentine mixer, demonstrating the use of compressed sensing. (C) Image [256 (*X*) × 256 (*Y*) pixels] acquired with 32× subsampling. (D) As in (C), but with 64× subsampling. (E) Velocimetric MRI image (63 × 63 pixels) of flow in which the transverse velocity has been encoded. (F) A higher-resolution (256 × 256 pixels) velocimetric image, acquired in the same amount of time as the image in (E) with 16× subsampling. (G) Selected images showing flow pattern as a function of TOF (note: actual time resolution was 50 ms; see movies S1 and S2).

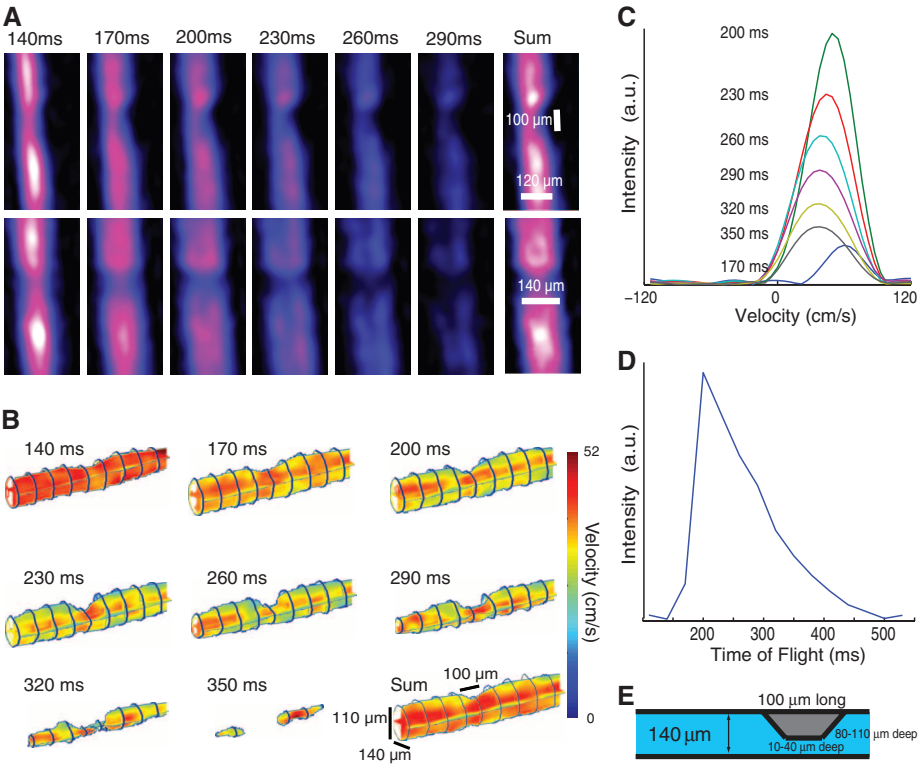

Fig. 3. Accelerating flow in a microfluidic constriction. (**A**) Two-dimensional images (63 × 15 points, *XZ* and *YZ* plane; constriction in *X*) show the high resolution (20 μm) achieved by motion-compensated spatial encoding. The progression reveals fast and slow components of the flow dynamics (see movie S3). The sum is over all TOFs. (**B**) Axial velocity–encoded images [16 (*X*) × 16 (*Y*) × 64 (*Z*)] acquired with 8× subsampling, illustrating acceleration near the constriction and the correlation of velocity and TOF. (**C** and **D**) Around the constriction, flow is dispersive at this spatial resolution; velocity distributions measured at different TOFs (C) reveal fast and slow components, as does the TOF dispersion curve (D). (**E**) Schematic of the constricted microfluidic channel.

References and Notes

1. D. L. Olson, T. L. Peck, A. G. Webb, R. L. Magin, J. V. Sweedler, *Science* **270**, 1967 (1995).
2. Y. Maguire, I. L. Chuang, S. G. Zhang, N. Gershenfeld, *Proc. Natl. Acad. Sci. U.S.A.* **104**, 9198 (2007).
3. C. Massin *et al.*, *J. Magn. Reson.* **164**, 242 (2003).
4. H. Wensink *et al.*, *Lab Chip* **5**, 280 (2005).
5. H. Lee, E. Sun, D. Ham, R. Weissleder, *Nat. Med.* **14**, 869 (2008).
6. Y.-Q. Song, H. Cho, T. Hopper, A. E. Pomerantz, P. Z. Sun, *J. Chem. Phys.* **128**, 052212 (2008).
7. A. J. Moulé *et al.*, *Proc. Natl. Acad. Sci. U.S.A.* **100**, 9122 (2003).
8. J. Jeener, B. H. Meier, P. Bachmann, R. R. Ernst, *J. Chem. Phys.* **71**, 4546 (1979).
9. C. Hilty *et al.*, *Proc. Natl. Acad. Sci. U.S.A.* **102**, 14960 (2005).
10. J. Granwehr *et al.*, *Magn. Reson. Imaging* **25**, 449 (2007).
11. E. Harel, A. Pines, *J. Magn. Reson.* **193**, 199 (2008).
12. E. Fukushima, *Annu. Rev. Fluid Mech.* **31**, 95 (1999).
13. P. T. Callaghan, *Principles of Nuclear Magnetic Resonance Microscopy* (Clarendon, Oxford, 1991).
14. D. G. Cory, A. N. Garroway, *Magn. Reson. Med.* **14**, 435 (1990).
15. M. Lustig, D. Donoho, J. M. Pauly, *Magn. Reson. Med.* **58**, 1182 (2007).
16. D. L. Donoho, *IEEE Trans. Inform. Theory* **52**, 1289 (2006).
17. See supporting material on *Science* Online.
18. J. M. Pope, S. Yao, *Concepts Magn. Reson.* **5**, 281 (1993).
19. G. M. Whitesides, *Nature* **442**, 368 (2006).
20. H. Wu, A. Wheeler, R. N. Zare, *Proc. Natl. Acad. Sci. U.S.A.* **101**, 12809 (2004).
21. C. Monat, P. Domachuk, B. J. Eggleton, *Nat. Photonics* **1**, 106 (2007).
22. S. Koster, E. Verpoorte, *Lab Chip* **7**, 1394 (2007).
23. A. J. deMello, *Nature* **442**, 394 (2006).
24. A. M. Wolters, D. A. Jayawickrama, J. V. Sweedler, *Curr. Opin. Chem. Biol.* **6**, 711 (2002).
25. L. Schröder, T. J. Lowery, C. Hilty, D. E. Wemmer, A. Pines, *Science* **314**, 446 (2006).
26. M. P. Ledbetter *et al.*, *Proc. Natl. Acad. Sci. U.S.A.* **105**, 2286 (2008).
27. J. M. Taylor *et al.*, *Nat. Phys.* **4**, 810 (2008).
28. P. Yager *et al.*, *Nature* **442**, 412 (2006).

29. We thank D. Wemmer for his careful reading of the manuscript and L.-S. Bouchard for helpful discussions. Supported by the U.S. Department of Energy, Office of Basic Energy Sciences, Division of Materials Sciences and Engineering under contract DE-AC02-05CH11231 (V.S.B., J.P., E.H., A.P.). We thank the Agilent Foundation for its generous and unrestricted gift. The Lawrence Berkeley National Laboratory has applied for a patent on aspects of this method. The authors declare no competing interests. **Author contributions:** V.S.B., J.P., E.H., and A.P. designed the experiments. V.S.B., J.P., and E.H. performed the experiments. V.S.B. and J.P. analyzed the data and wrote the paper.

Supporting Online Material

www.sciencemag.org/cgi/content/full/science.1192313/DC1
Materials and Methods
Figs. S1 to S6
Movies S1 to S3
References

14 May 2010; accepted 21 September 2010
Published online 7 October 2010;
10.1126/science.1192313

Probing the Ultimate Limit of Fiber-Optic Strain Sensing

G. Gagliardi,[1]* M. Salza,[1] S. Avino,[1] P. Ferraro,[1] P. De Natale[2]

The measurement of relative displacements and deformations is important in many fields such as structural engineering, aerospace, geophysics, and nanotechnology. Optical-fiber sensors have become key tools for strain measurements, with sensitivity limits ranging between 10^{-9} and $10^{-6}\varepsilon$ hertz $(\mathrm{Hz})^{-1/2}$ (where ε is the fractional length change). We report on strain measurements at the $10^{-13}\varepsilon$-$\mathrm{Hz}^{-1/2}$ level using a fiber Bragg-grating resonator with a diode-laser source that is stabilized against a quartz-disciplined optical frequency comb, thus approaching detection limits set by thermodynamic phase fluctuations in the fiber. This scheme may provide a route to a new generation of strain sensors that is entirely based on fiber-optic systems, which are aimed at measuring fundamental physical quantities; for example, in gyroscopes, accelerometers, and gravity experiments.

Optical sensors and interferometers are widely used for high-sensitivity strain measurements. Gravitational-wave, long-baseline interferometers are the most sensitive strain detectors developed to date, with impressively low detection limits on the order of $10^{-22}\varepsilon$ $\mathrm{Hz}^{-1/2}$ (where ε is the fractional length change), from a few tens of hertz up to the kilohertz range (*1*). However, these detectors are extremely complex and cumbersome, with a length of several kilometers. Smaller–length scale (centimeter) optical-fiber sensors are widespread tools for static and dynamic local-deformation monitoring inside mechanical structures and materials, in environments as diverse as ocean depths, geothermal wells (*2*), and aircrafts (*3*). Strain sensitivities ranging between 10^{-9} and $10^{-6}\varepsilon$ $\mathrm{Hz}^{-1/2}$ are presently feasible with the use of standard telecommunication fiber technology (*4*). Higher strain resolutions have been demonstrated with passive fiber-optic resonators using frequency-stabilized lasers (*5*, *6*)

[1]Consiglio Nazionale delle Ricerche–Istituto Nazionale di Ottica (INO) and European Laboratory for Non-Linear Spectroscopy (LENS), Comprensorio "A. Olivetti," Via Campi Flegrei 34, I-80078 Pozzuoli (Naples), Italy. [2]Consiglio Nazionale delle Ricerche–INO and LENS, Largo E. Fermi 6, I-50125 Firenze, Italy.

*To whom the correspondence should be addressed. E-mail: gianluca.gagliardi@ino.it

achieving $p\varepsilon$ and sub-$p\varepsilon$ levels (1 pε = $10^{-12}\varepsilon$). Most of these approaches are rewarding for strain signals in the acoustic and ultrasonic frequency ranges. On the contrary, for slow-changing phenomena, strain sensing can be very challenging, as it must contend with laser frequency instabilities and drifts that degrade the signal-to-noise ratio. Nonetheless, a sensor capable of tracking very slow deformations with high resolution and accuracy would be of primary importance in several applications, including telescope control (*7*), inertial sensing (*8*), seismic monitoring (*9*), and nanotechnology (*10*). Quasi-static interrogation techniques may have an impact in wavelength-encoded chemical sensing; for instance, with opto-acoustic resonators (*11*) and optical microcavities (*12*). Attempts toward laser noise suppression for fiber sensing that rely on easily available atomic and molecular transitions (*13*, *14*), as well as free-space cavities and interferometers (*5*, *15*), have been made in the past few years. Optical frequency comb (OFC) synthesizers provide an absolute frequency (wavelength) grid with a previously unachieved level of stability from the extreme ultraviolet to the mid-infrared (*16*). OFCs originate from short, mode-locked laser pulses that are equally time-spaced by a radio-frequency clock, and combs are now commercially available in compact fiber-based arrangements (*16*). OFCs have been proposed as light sources for interferometers aimed at accurate distance and displacement determinations (*17*), as they can guarantee the traceability of displacements to an absolute time standard (*18*).

The ultimate performance of most fiber-optic systems is hampered by thermally induced phase noise (*19*). The physical problem is similar to Johnson's noise in electrical circuits, and it can be treated in a way analogous to Nyquist theory by starting from thermal equilibrium energy fluctuations. This is the case for long-fiber interferometers and Sagnac gyroscopes (*20*, *21*). The same noise appears in the low-frequency spectrum of fiber lasers (*22*). This issue has been extensively investigated, both theoretically and experimentally, over the past decades, and different models have been proposed (*23*) but never tested in the infrasonic region (1 mHz to 20 Hz).

We demonstrate strain measurements using a fiber Bragg-grating (FBG) resonator sensor by means of a laser that is stabilized against an OFC. The OFC provides a phase-coherent link between the laser and a radio-frequency oscillator referenced to the primary time standard, leading to an interrogation system that is almost free of laser frequency noise. The response of our sensor is approaching the thermally induced noise limit (*23*). In the experimental setup (Fig. 1), an extended-cavity diode laser emitting ~1560 nm is phase-locked to the nearest comb tooth with a frequency offset given by a 30-MHz local oscillator [further details in (*24*)]. The comb repetition rate and carrier-envelope offset frequency are phase-locked to a 10-MHz oven-controlled quartz oscillator (OCXO) (*24*). We adopted a Pound-Drever-Hall (PDH) scheme to lock the laser to the FBG resonator [reference S3 in (*24*)]. Actually, two secondary carriers (SCs) are created by phase modulation from a tunable synthesizer. A typical PDH signal is thus obtained for the SCs and sent to a servo that drives the synthesizer to frequency-lock one of them to a cavity mode. Hence, active interrogation of the sensor is carried out by the SC, adding only a negligible noise from the synthesizer, whereas the laser carrier remains phase-locked to the OFC. Strain readout is taken from the locking servo signal.

Mechanical perturbations in the intracavity fiber are seen as proportional changes of the resonance frequency position and translated into SC frequency changes by the locking loop. To estimate the strain resolution, we caused a known deformation in the sensor by applying a voltage to the piezoelectric actuator (PZT). We then carried out a careful calibration of the PZT displacement by using the PDH linear slope as a frequency-to-strain transducer (*25*). Figure 2 shows a measurement performed in the time domain for an excitation of $2n\varepsilon_{rms}$ at 0.1 Hz (1 ne = $10^{-9}\varepsilon$, and ε_{rms} is the root mean square fractional length change). The data on the vertical axis were obtained by frequency counting the SC shift with a 12-digit precision counter linked to the OCXO and are expressed as absolute optical frequency variations [via eq. 1 in (*24*)]. The time-domain frequency counts are proportional to the slow deformation, as they contain information on frequency changes of the cavity resonance with respect to the OFC, and can be directly back-traced to the OCXO. The laser serves as a secondary length standard that is directly compared to the fiber cavity optical path length during strain measurements. The plot exhibits a clean sinusoidal signal with a weak, superimposed modulation at a lower frequency (~10 mHz), which can be attributed to the torsion-oscillation resonance of the insulation pendulum. A slow change of the center frequency, caused by temperature drifts in the fiber, is barely visible. However, the root mean square value of the oscillation amplitude in Fig. 2 is consistent with that expected from the PZT voltage

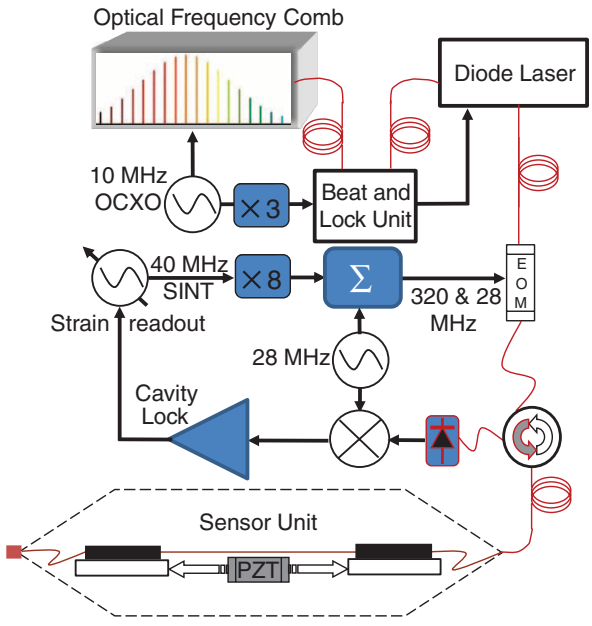

Fig. 1. Experimental setup. The system is composed of a sensor unit, a diode laser, an OFC with a reference oscillator (OCXO), and a laser-comb phase-lock unit. All optical units are connected by optical fibers. The sensing element is a Fabry-Pérot fiber resonator formed by two identical single-mode 99% FBG reflectors, placed at a relative distance L = 130 mm along an acrylic-coated silica fiber. A PZT is used to modulate the cavity length. The resonator is thermally and acoustically shielded from the environment. A seismic insulation in the horizontal and vertical planes, at frequencies above 0.7 Hz, is provided with a latex-cord pendulum suspension. SINT, synthesizer; EOM, electro-optic modulator.

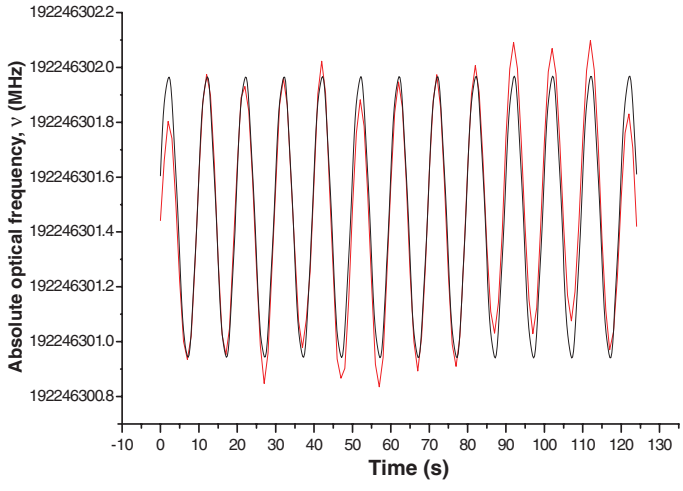

Fig. 2. Direct absolute frequency measurements of the SC frequency are performed by a precision counter (red line) referred to the OCXO when a slow deformation is applied ($2n\varepsilon_{rms}$ at 100 mHz). A sinusoidal fit to the experimental values is also represented (black line).

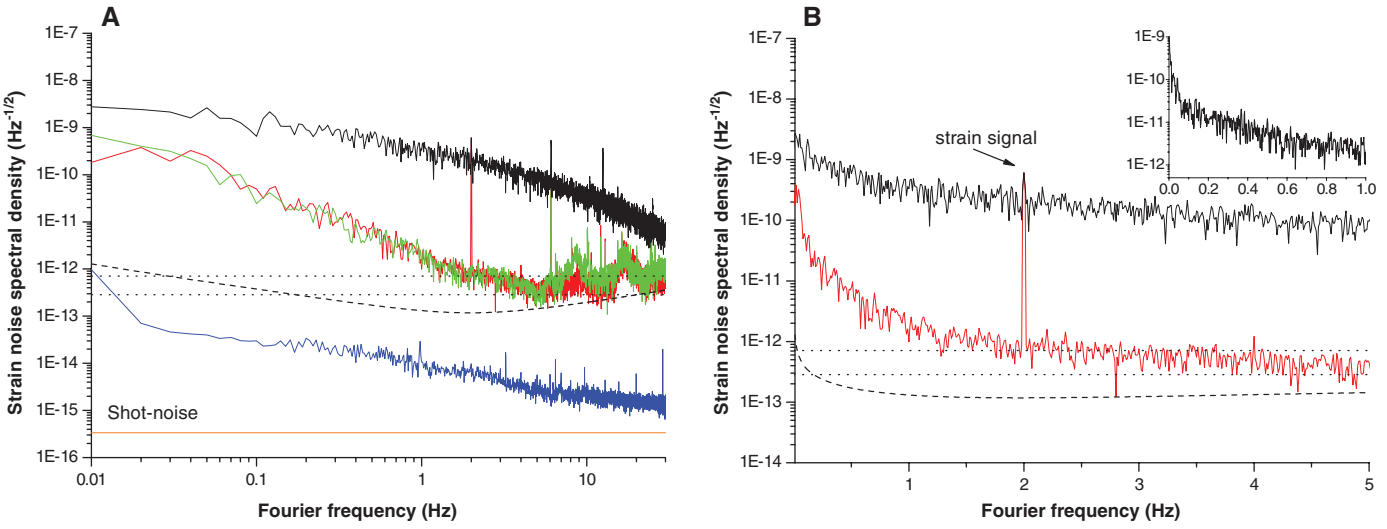

Fig. 3. (**A**) Strain spectrum recorded when the laser is locked to the OFC (red line) and in the free-running condition (black) with a 2-Hz signal for strain calibration. The green trace is recorded when no strain is applied, whereas the dotted lines represent the thermodynamic noise range predicted in (*23*). The blue and orange lines correspond to the measured dark electronic noise and the theoretical shot noise (200-μW power), respectively. The dashed curve represents the strain-noise spectral density derived from the measured OCXO phase noise. (**B**) Same recording as in (A), shown on a magnified horizontal scale to point out the signal enhancement deriving from comb stabilization (55 dB around 1 to 2 Hz). (Inset) A higher-resolution spectrum (acquisition time = 1500 s) shows the strain noise below 1 Hz.

and confirms the correctness of the low-frequency calibration procedure.

Based on the measured response, we applied a sinusoidal displacement of $61p\varepsilon_{rms}$ to the 130-mm intracavity fiber and assessed the strain resolution via a fast Fourier transform of the servo output. The resulting strain-noise spectral density curves in the infrasonic range are shown in Fig. 3A with a superimposed perturbation at 2 Hz for voltage-to-strain conversion. From the average noise floor in Fig. 3B, a lower bound of $550f\varepsilon_{rms}/\sqrt{Hz}$ around 2 Hz can be observed, with a minimum of $350f\varepsilon_{rms}/\sqrt{Hz}$ at 5 Hz (1 fε = 10^{-15}ε). The noise level is still 60 dB higher than the expected shot-noise–limited resolution (*5*) and is 40 dB above the measured electronic background. A recording with a narrower-resolution bandwidth in the low-frequency region is shown in the inset of Fig. 3B, illustrating a detection limit of $20p\varepsilon_{rms}/\sqrt{Hz}$ and $10p\varepsilon_{rms}/\sqrt{Hz}$ at 50 mHz and 200 mHz, respectively. It is worth noting the dramatic improvement resulting from laser frequency stabilization to the OFC, with a 40- to 60-dB enhancement in the frequency range between 0.1 and 10 Hz. In Fig. 3B, the strain-noise contribution from the OFC reference oscillator is also shown. When the laser is locked to the comb, a mere multiplication of the OCXO phase noise up to the optical domain [× N, where N is defined in (*24*)] yields a level of $120f\varepsilon/\sqrt{Hz}$ at 2 Hz. This suggests that the actual resolution, around 1 Hz, is ~15 dB above that predicted from oscillator-induced laser-frequency noise.

We have also experimentally compared the previous strain spectrum with that obtained when the comb is driven by an oscillator that has a phase noise of –80 dB/Hz at 2 Hz; i.e., at least 40 dB above the OCXO level. A degradation of only 20 to 25 dB could be appreciated from the strain-noise spectrum (fig. S1), which confirms that the dominant noise does not originate within the OFC. This implies that the system is still not limited by the locked laser stability. When light is transmitted through the fiber, the medium itself imposes a spectrum of refractive index (phase) fluctuations that affects the minimum detectable strain (*19*). A complete theoretical model for finite-cladding fibers provides the phase-noise spectral density and also contains an analytical expression for the low-frequency behavior (*23*). According to this model, the low-frequency noise spectrum should be nearly flat. Apparently, a reliable estimate of this noise level is seriously affected by the uncertainty of the involved parameters (*22*, *26*), though the correctness of the model has never been tested for frequencies below 250 Hz (*20*, *27*), where thermal effects can be more relevant. Particularly, the insulating boundary conditions of the fiber may influence the thermal response because they reflect on the heat dissipation, as already established for fiber lasers (*22*). In Fig. 3, A and B, two thermal-noise curves are simulated with the use of an effective fiber length $L_{eff} = 2FL/\pi$, with Finesse F = 110 (L is the resonator length). These curves correspond to the extreme cases calculated with the fiber thermo-optic and thermal-expansion coefficients available from the literature (*19*, *22*, *28*). We observe that the data obtained in this investigation exhibit a nonflat spectrum with a plateau of $312 \pm 13f\varepsilon/\sqrt{Hz}$ (from a least-squares fitting of the noise baseline). This value is fully consistent with the predicted thermal-noise range above 1 Hz (Fig. 3). The OCXO phase noise is well below the thermal-induced, refractive-index noise floor from 0.2 to 10 Hz, which thereby represents the real limitation to strain resolution. Therefore, the broad spectral features from 10 to 30 Hz are most likely caused by mechanical coupling of thermodynamic noise to the resonator.

At very low frequencies (below 1 Hz), noise increases slowly with a $1/f$ dependence. Although a seismic noise contribution is likely in low-frequency strain monitoring, it should decay approximately with $1/f^2$ (*29*). Alternatively, this noise roll-up

Fig. 4. Strain spectrum at acoustic frequencies with a calibration signal at 1.5 kHz and thermodynamic noise curves (dotted lines). The three sharp peaks at lower frequencies are due to 50-Hz line voltage coupling to the electronics. The central broad feature can be attributed to acoustic resonances of the laser cavity mount or the OFC.

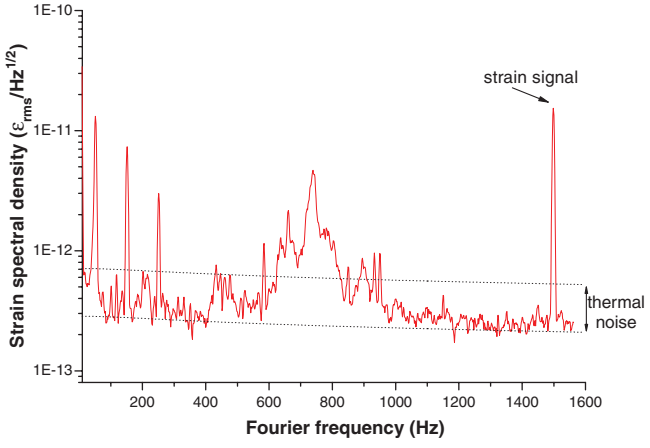

could be attributed to the OCXO phase noise, but the scaling law must be different, as shown by the dashed curve in Fig. 3A. Excess thermally induced fluctuations due to insulating boundary conditions (fiber acrylic buffer) could be responsible for this unexpected response (*22*). Moving toward lower frequencies (inset in Fig. 3B), below 0.1 Hz, a seismic contribution starts to be evident. The noise spectrum recorded from 10 to 1600 Hz (Fig. 4) indicates the resolution in the case of acoustic-strain detection. On these time scales, the laser-emission spectrum is narrowed down to the comb-tooth linewidth by the phase lock (fig. S2). Again, the noise level of this investigation approaches the thermodynamic noise with a minimum of $220 f\varepsilon_{rms}/\sqrt{Hz}$ around 1.5 kHz.

At present, the system strain resolution is limited by thermally induced phase fluctuations in the fiber, and this limit has been experimentally identified via the dramatic noise reduction resulting from laser phase-lock to the OFC. A more quantitative understanding of thermally induced phase noise can be performed with the use of fiber-optic cavities with different lengths and materials in well-controlled thermodynamic conditions.

References and Notes

1. D. Reitze, *Nat. Photonics* **2**, 582 (2008).
2. M. Niklès, F. Ravet, *Nat. Photonics* **4**, 431 (2010).
3. M. Jones, *Nat. Photonics* **2**, 153 (2008).
4. Y. J. Rao, *Meas. Sci. Technol.* **8**, 355 (1997).
5. J. H. Chow, D. E. McClelland, M. B. Gray, I. C. M. Littler, *Opt. Lett.* **30**, 1923 (2005).
6. G. Gagliardi, S. De Nicola, P. Ferraro, P. De Natale, *Opt. Express* **15**, 3715 (2007).
7. D. G. MacMynowski, *Appl. Opt.* **48**, 2105 (2009).
8. T. T. Y. Lam, G. Gagliardi, M. Salza, J. H. Chow, P. De Natale, *Meas. Sci. Technol.* **21**, 094010 (2010).
9. G. A. Cranch *et al.*, *IEEE Photon. Technol. Lett.* **15**, 1579 (2003).
10. Y. Bitou, *Precis. Eng.* **33**, 187 (2009).
11. L. Su, S. R. Elliott, *Opt. Lett.* **35**, 1212 (2010).
12. F. Vollmer, S. Arnold, *Nat. Methods* **5**, 591 (2008).
13. A. Arie, B. Lissak, M. Tur, *J. Lightwave Technol.* **17**, 1849 (1999).
14. T. T. Y. Lam *et al.*, *Appl. Opt.* **49**, 4029 (2010).
15. T. T. Y. Lam, J. H. Chow, C. M. Mow-Lowry, D. E. McClelland, I. C. M. Littler, *IEEE Sens. J.* **9**, 983 (2009).
16. P. Maddaloni, P. Cancio, P. De Natale, *Meas. Sci. Technol.* **20**, 052001 (2009).
17. P. Balling, P. Kren, P. Masika, S. A. van den Berg, *Opt. Express* **17**, 9300 (2009).
18. Y. Bitou, *Opt. Lett.* **34**, 1540 (2009).
19. W. H. Glenn, *IEEE J. Quantum Electron.* **25**, 1218 (1989).
20. S. Knudsen, A. B. Tveten, A. Dandridge, *IEEE Photon. Technol. Lett.* **7**, 90 (1995).
21. R. P. Moeller, W. K. Burns, *Opt. Lett.* **21**, 171 (1996).
22. S. Foster, A. Tikhomirov, M. Milnes, *IEEE J. Quantum Electron.* **43**, 378 (2007).
23. K. H. Wanser, *Electron. Lett.* **28**, 53 (1992).
24. Materials and methods are available as supporting material on *Science* Online.
25. J. H. Chow, I. C. M. Littler, G. de Vine, D. E. McClelland, M. B. Gray, *J. Lightwave Technol.* **23**, 1881 (2005).
26. E. Rønnekleiv, *Opt. Fiber Technol.* **7**, 206 (2001).
27. K. H. Wanser, A. D. Kersey, A. Dandridge, *Opt. Photonics News* **4**, 37 (1993).
28. S. Chang *et al.*, *Chin. J. Phys.* **38**, 437 (2000).
29. D. C. Agnew, *Rev. Geophys.* **24**, 579 (1986).

30. We thank M. Prevedelli, A. Arie, M. De Rosa, and J. H. Chow for helpful discussions. Technical assistance on the electronic setup was provided by R. Abbate, who passed away in September 2008. We thank Avanex Corp. (San Donato, Milan, Italy) for kindly providing part of the equipment. This experiment was partly funded by Ente Cassa di Risparmio di Firenze.

Supporting Online Material

www.sciencemag.org/cgi/content/full/science.1195818/DC1
Materials and Methods
Figs. S1 and S2
References

29 July 2010; accepted 19 October 2010
Published online 28 October 2010;
10.1126/science.1195818

Loss of Carbon from the Deep Sea Since the Last Glacial Maximum

Jimin Yu,[1]* Wally S. Broecker,[1] Harry Elderfield,[2] Zhangdong Jin,[3] Jerry McManus,[1] Fei Zhang[3]

Deep-ocean carbonate ion concentrations ($[CO_3^{2-}]$) and carbon isotopic ratios ($\delta^{13}C$) place important constraints on past redistributions of carbon in the ocean-land-atmosphere system and hence provide clues to the causes of atmospheric CO_2 concentration changes. However, existing deep-sea $[CO_3^{2-}]$ reconstructions conflict with one another, complicating paleoceanographic interpretations. Here, we present deep-sea $[CO_3^{2-}]$ for five cores from the three major oceans quantified using benthic foraminiferal boron/calcium ratios since the last glacial period. Combined benthic $\delta^{13}C$ and $[CO_3^{2-}]$ results indicate that deep-sea-released CO_2 during the early deglacial period (17.5 to 14.5 thousand years ago) was preferentially stored in the atmosphere, whereas during the late deglacial period (14 to 10 thousand years ago), besides contributing to the contemporary atmospheric CO_2 rise, a substantial portion of CO_2 released from oceans was absorbed by the terrestrial biosphere.

Past atmospheric CO_2 concentrations recorded in ice cores and deep-ocean $\delta^{13}C$ recorded in benthic foraminiferal carbonates indicate that the amounts of carbon stored in atmosphere and terrestrial biosphere during the Last Glacial Maximum (LGM) [24 to 18 thousand years ago (ka)] were considerably smaller, by roughly 200 Pg (1 Pg = 10^{15} g) and 500 Pg, respectively, than those during preindustrial times (*1*, *2*). On glacial-interglacial time scales, carbon lost from these sources during ice ages must have been stored in the deep ocean (*3*), the largest reservoir of the ocean-land-atmosphere system. Transfer of this substantial amount of carbon back to the atmosphere and land during deglacial periods would inevitably cause perturbations of the deep-ocean carbonate system, including deep-ocean $[CO_3^{2-}]$ and $\delta^{13}C$. Therefore, deep-ocean $[CO_3^{2-}]$ and $\delta^{13}C$ records should provide insights into carbon reorganizations among different reservoirs of the ocean-land-atmosphere system.

Efforts have been made to reconstruct past $[CO_3^{2-}]$ of the ocean's interior using various proxies (*4*–*8*). Each of these approaches has complications specific to the assumptions underlying its methodology. Existing reconstructions are mostly qualitative and limited to low resolutions or Holocene-LGM time slices for restricted regions and, as a consequence, results are still in dispute (*9*). Extensive core-top calibration (*9*) shows that benthic foraminiferal boron/calcium (B/Ca) ratios serve as a quantitative proxy for deep-ocean $[CO_3^{2-}]$ reconstructions. Although the mechanism for the benthic B/Ca relationship with deep-water $[CO_3^{2-}]$ is not yet well understood, subsequent down-core studies (*10*, *11*) strongly support the core-top empirical calibration. Here, we present benthic foraminiferal B/Ca-derived deep-sea $[CO_3^{2-}]$ records for five cores from the three major oceans that are capable of resolving millennial time-scale changes during the past 50,000 years (Fig. 1 and fig. S1). We measured B/Ca in epifaunal benthic foraminifera *Cibicidoides wuellerstorfi*. B/Ca ratios were converted to seawater $[CO_3^{2-}]$ based on the 1.14 μmol/mol per μmol/kg sensitivity obtained from a global core-top calibration (*9*). Replicates of a consistency standard and samples show an average uncertainty (1 SD) of ±4 μmol/mol in B/Ca, corresponding to an error of ±3.5 μmol/kg in seawater $[CO_3^{2-}]$. Detailed information for materials and methods is described in the supporting online material (SOM) (*12*).

In the Caribbean Basin, glacial deep-water $[CO_3^{2-}]$ in site VM28-122 (*10*) was 27 to 34 μmol/kg higher than that during the late Holocene (Table 1 and Fig. 1A). The decreased glacial weight percent of calcium carbonate (%$CaCO_3$) (Fig. 1A) in this core is thus not caused by intensified dissolution but is due to other reasons, such as dilution by terrestrial detritus. By contrast, deep-ocean $[CO_3^{2-}]$ in site BOFS 8K (*11*) located at 4-km water depth in the polar North Atlantic exhibits an opposite pattern, displaying low values during the last glacial period and high values during the Holocene, reminiscent of the typical Atlantic-type %$CaCO_3$ variation (Fig. 1B) (*13*). Glacial-interglacial changes are relatively small in deep-water $[CO_3^{2-}]$ for Indo-Pacific records (Fig.

[1]Lamont-Doherty Earth Observatory of Columbia University, 61 Route 9W/Post Office Box 1000, Palisades, NY 10964–8000, USA. [2]The Godwin Laboratory for Palaeoclimate Research, Department of Earth Sciences, University of Cambridge, Downing Street, Cambridge CB2 3EQ, UK. [3]State Key Laboratory of Loess and Quaternary Geology, Institute of Earth Environment, Chinese Academy of Sciences, Xi'an, 710075, China.

*To whom correspondence should be addressed. E-mail: jiminyu@ldeo.columbia.edu

1C-E). Relative to the late Holocene, the $[CO_3^{2-}]$ in site WIND 28K from the southwestern Indian Ocean was elevated during the mid-marine isotope stage (MIS) 3 and LGM and showed a clear deglacial peak at 14 to 10 ka (Table 1 and Figs. 1C and 2G), a variation similar to the Indo-Pacific %$CaCO_3$ pattern (Fig. 1C) (*13*, *14*). Past deep-ocean $[CO_3^{2-}]$ varied differently for cores located at two water depths at Ontong Java Plateau (OJP) in the western equatorial Pacific. Site MW91-9 GGC15 (GGC15 hereafter) at 2.3-km water depth shows little change in deep-water $[CO_3^{2-}]$ during the past 50,000 years (Fig. 1D), consistent with estimates from %$CaCO_3$ (Fig. 1D) and shell weight changes (*5*). Lower deep-ocean $[CO_3^{2-}]$ is observed during 30 to 20 ka in site MW91-9 GGC48 (GGC48 hereafter) located at 3.4-km water depth (Fig. 1E). A deglacial peak is obvious in this core, but the decline of $[CO_3^{2-}]$ is only ~5 μmol/kg during the past 10,000 years (Table 1 and Fig. 2I). The decreased $[CO_3^{2-}]$ during the LGM in GGC48 is supported by %$CaCO_3$ (Fig. 1E), shell weight, size index (fig. S5) (*5*), and Zn/Ca ratios (*7*).

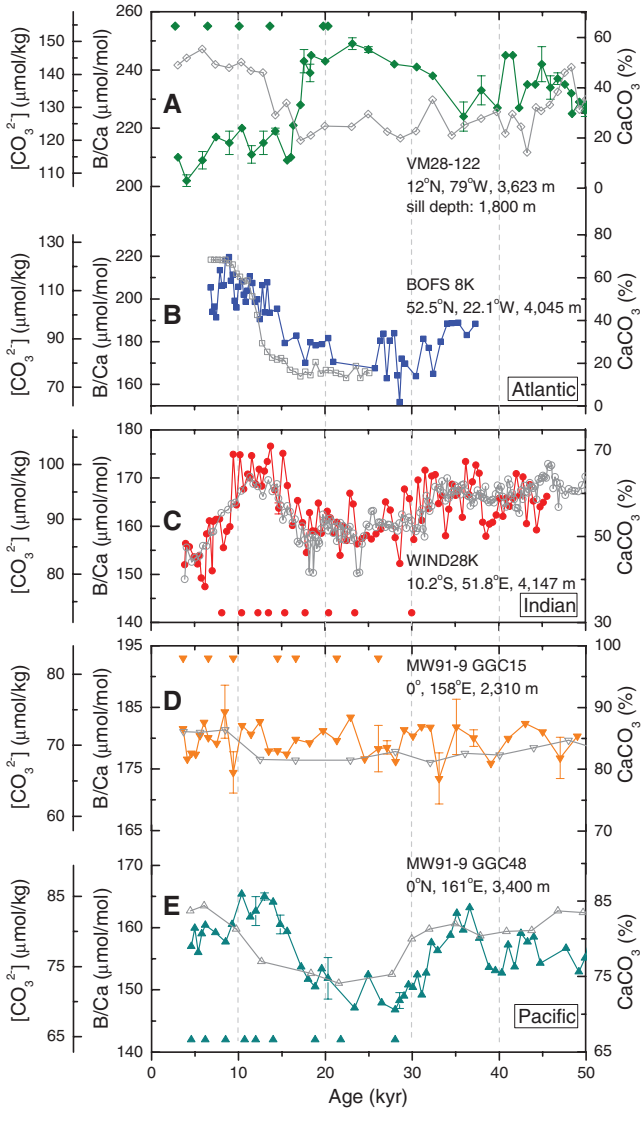

Fig. 1. Deep-ocean $[CO_3^{2-}]$ (solid symbols) compared with sediment %$CaCO_3$ (empty symbols) during the past 50,000 years. (**A**) VM28-122 (*10*). (**B**) BOFS 8K (*11*). (**C**) WIND 28K. (**D**) MW91-9 GGC15. (**E**) MW91-9 GGC48. Deep-sea $[CO_3^{2-}]$ was calculated from B/Ca measured in *C. wuellerstorfi* using a sensitivity of 1.14 μmol/mol per μmol/kg (*9*). Error bars in (A) and [(C) to (E)] represent SD of replicate measurements from the same depth interval. Symbols along the *x* axis indicate ^{14}C dates (table S1). See SOM for materials and methods.

At the LGM, atmospheric CO_2 concentration was about 90 parts per million in volume (ppmv) lower than the preindustrial value (*15*) (Fig. 2N). Assuming equilibrium between surface oceans and atmosphere and because of the generally inverse relationship of seawater CO_2 content and $[CO_3^{2-}]$, preformed surface seawater $[CO_3^{2-}]$ would have been elevated by ~60 μmol/kg during the LGM (*10*). In contrast to large increases in surface values, our results show that changes in deep-water $[CO_3^{2-}]$ are much smaller and in the opposite direction at some locations. Relative to the late Holocene, deep-water $[CO_3^{2-}]$ at the LGM was elevated by 34 μmol/kg in the upper North Atlantic Deep Water (NADW) (site VM28-122) and decreased by 18 μmol/kg in the lower NADW (site BOFS 8K) (Table 1 and Fig. 2, A and E). Between the LGM and the late Holocene, changes in deep-water $[CO_3^{2-}]$ are <6 μmol/kg for cores from the Indo-Pacific (Table 1 and Fig. 2, G and I), similar to that (<5 μmol/kg) inferred from foraminiferal assemblage (*4*). The generally small changes in deep-ocean $[CO_3^{2-}]$ may point to sea-floor carbonates as an effective buffer of deep-ocean pH on the glacial-interglacial time scales (*4*).

Compared to the LGM, atmospheric CO_2 during MIS 3 was higher (*15*), and a lower preformed sur-

Table 1. Reconstructed deep-ocean $[CO_3^{2-}]$ during four time intervals for cores from the North Atlantic, Indian, and equatorial Pacific Oceans.

Core	Location	Deep-water $[CO_3^{2-}]$ (μmol/kg)			
	(Latitude, longitude, water depth)	Late Holocene (0–5 ka)	Deglacial peak (10–14 ka)	LGM (18–24 ka)	Mid MIS3 (36–45 ka)
VM28-122	12°N, 79°W, 3623 m (1800 m)*	111 ± 4 (2)†	120 ± 4 (3)	145 ± 4 (4)	138 ± 6 (8)
BOFS 8K	52.5°N, 22.1°W, 4045 m	105 ± 8 (5)	108 ± 5 (14)	87 ± 4 (5)	94 ± 3 (2)
WIND 28K	10.2°S, 51.8°E, 4147 m	84 ± 2 (4)	99 ± 3 (11)	89 ± 3 (16)	93 ± 4 (23)
MW91-9 GGC15	0, 158°E, 2310 m	70 ± 2 (3)	72 ± 2 (4)	72 ± 2 (4)	72 ± 2 (5)
MW91-9 GGC48	0, 161°E, 3400 m	79 ± 2 (2)	84 ± 2 (7)	73 ± 3 (5)	78 ± 3 (11)
		Changes relative to the late Holocene (μmol/kg)			
VM28-122 (Intermediate North Atlantic)			9 ± 6	34 ± 6	27 ± 7
BOFS 8K (Deep North Atlantic)			3 ± 9	−18 ± 9	−11 ± 9
WIND 28K (Abyssal Indo-Pacific)			15 ± 4	5 ± 3	9 ± 4
MW91-9 GGC15 (Intermediate equatorial Pacific)			2 ± 3	2 ± 3	2 ± 3
MW91-9 GGC48 (West equatorial Pacific at 3.4 km)			5 ± 3	−6 ± 4	−1 ± 4

*Sill depth. †Number of samples used to calculate averages. Errors represent 1 SD of all samples during the time intervals of interest.

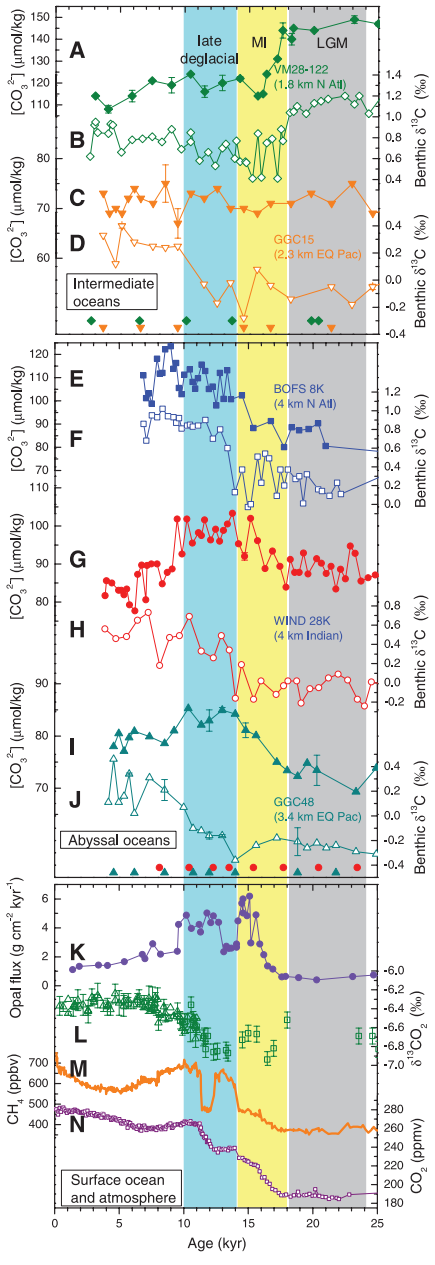

Fig. 2. Records of deep-ocean $[CO_3^{2-}]$ and benthic $\delta^{13}C$ compared with surface Southern Ocean and atmospheric records during the past 25,000 years. (**A** and **B**) VM28-122 (*10*) from the Caribbean Sea. (**C** and **D**) MW91-9 GGC15 at OJP from the equatorial Pacific. (**E** and **F**) BOFS 8K (*11*) from the North Atlantic. (**G** and **H**) WIND 28K from the Indian. (**I** and **J**) MW91-9 GGC48 at OJP from the equatorial Pacific. (**K**) Upwelling intensity in the Southern Ocean (*22*). (**L**) $\delta^{13}C$ of atmospheric CO_2 [triangles, (*31*); squares, (*32*)]. (**M**) Atmospheric CH_4 (*27*). (**N**) Atmospheric CO_2 (*15*). Shaded bars indicate the LGM (18 to 24 ka), early deglacial or MI (17.5 to 14.5 ka), and late deglacial (14 to 10 ka). In (A) to (J), error bars stand for SD of replicate measurements. Solid and empty symbols are for $[CO_3^{2-}]$ and $\delta^{13}C$, respectively. Symbols along the *x* axis indicate ^{14}C dates (table S1). $\delta^{13}C = [(^{13}C/^{12}C)_{sample}/(^{13}C/^{12}C)_{standard} - 1] \times 1000‰$; the reported values correspond to the Pee Dee belemnite standard. See Table 1 for core locations.

face $[CO_3^{2-}]$ would be expected. The slightly low $[CO_3^{2-}]$ in the Caribbean Basin during MIS 3 (Fig. 1A) possibly reflects such a decreased preformed value. Relatively high $[CO_3^{2-}]$ in BOFS 8K, WIND 28K, and GGC48 during MIS 3 (Fig. 1, B, C, and E) may indicate decreased dissolved inorganic carbon (DIC) at these locations, which is suggested by elevated benthic $\delta^{13}C$ in these cores (fig. S6).

Glacial-interglacial changes in nonconservative properties such as $[CO_3^{2-}]$ and $\delta^{13}C$ can arise from changes in inventories of various reservoirs, preformed values, rates and pathways of circulation, mixing of different water masses, and carbonate compensation. To fully constrain their respective contributions to changes in $[CO_3^{2-}]$ and $\delta^{13}C$, extensive records for various regions are needed. We selected the five cores at key locations to study the first-order carbonate chemistry histories of major deep-water masses. Limited by the number of records, we can only speculate about the most likely reasons to explain our results. Because of the shallow sill depth of the Caribbean Basin (1.8 km), the $[CO_3^{2-}]$ for VM28-122 reflects that of upper NADW. This water was rapidly ventilated, as suggested by high benthic $\delta^{13}C$ (Fig. 2B) and small benthic-planktonic age difference during the LGM and late Holocene in this core (*16*). Thus, the higher glacial $[CO_3^{2-}]$ of the Caribbean Basin partially reflects elevated preformed surface values in the North Atlantic. Core WIND 28K is currently bathed in the deep water formed in the Southern Ocean that is further transported to the abyssal Pacific (fig. S1). We interpret changes in $[CO_3^{2-}]$ recorded by this core as reflecting those of southern-sourced water in the past. The positive gradient in $[CO_3^{2-}]$ between the northern- and southern-sourced deep waters observed today has been maintained throughout the past 50,000 years (Fig. 1A, C). The significantly lower glacial $[CO_3^{2-}]$ at BOFS 8K (Fig. 1B) is consistent with a greater northern penetration of southern-sourced waters into the deep North Atlantic, as indicated by other proxies (*8*, *11*, *17*). Circulation changes also occurred in the Pacific (*18*–*20*). Today, deep-water chemistry at 2- to 3-km water depth of the equatorial Pacific is only slightly influenced by the North Pacific Deep Water (NPDW) (*21*) that is located at ~1-km water depth in the North Pacific with the lowest $[CO_3^{2-}]$ in the world oceans (fig. S1). The influence from glacial NPDW would be greater because this water mass is thought to have deepened to ~3-km water depth during the LGM (*18*, *19*). Thus, lower glacial $[CO_3^{2-}]$ at GGC48 (Fig. 1E) is consistent with such a depth shift associated with NPDW. The unchanged $[CO_3^{2-}]$ overlying GGC15 (Fig. 1D) may indicate a different mixing ratio of glacial NPDW with southern-sourced deep waters, an additional influence from a glacial intermediate water mass located above ~2 km (*18*, *20*), and/or carbonate compensation. Our current data set provides insufficient information to quantify their respective effects at GGC15. Nonetheless, our results show that circulation changes have imposed strong influences on deep-water $[CO_3^{2-}]$ variations not only in the Atlantic but also in the Pacific.

Because they reflect different aspects of the carbonate system, deep-water $[CO_3^{2-}]$ and $\delta^{13}C$ together provide insights into carbon redistribution among ocean, atmosphere, and terrestrial biosphere. During the early deglacial period [known as the Mystery Interval (MI)], three cores from abyssal oceans show clear increases of 10 to 18 μmol/kg in $[CO_3^{2-}]$ (Fig. 2, E, G, and I), concurrent with a sharp drop of intermediate water $[CO_3^{2-}]$ in the North Atlantic (Fig. 2A) and a rapid rise in atmospheric CO_2 (Fig. 2N) (*15*). The decrease in $[CO_3^{2-}]$ observed at VM28-122 may reflect that of surface preformed values in response to rising atmospheric CO_2 (Fig. 2N) and/or an incursion of southern-sourced low-$[CO_3^{2-}]$ to the intermediate North Atlantic as indicated by decreased benthic $\delta^{13}C$ (Fig. 2B). Although limited in number of records, the increases of deep-water $[CO_3^{2-}]$ occurred in cores widely distributed in the three major oceans. This indicates transfer of CO_2 from a sizable volume of deep oceans into intermediate water depths and atmosphere (Fig. 3A). Proxy data (*22*) suggest that CO_2 release during the MI was linked to intensified upwelling in the Southern Ocean (Fig. 2K) driven by a

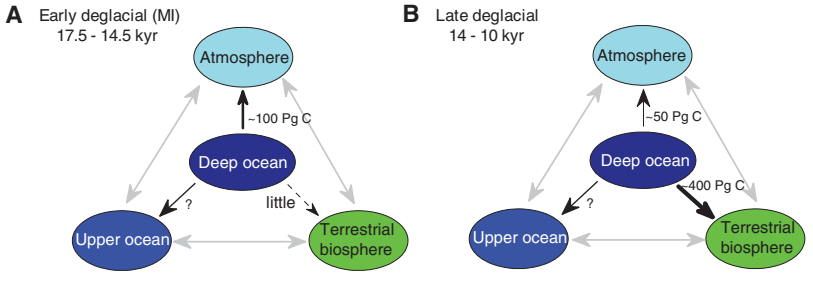

Fig. 3. Summary diagram of carbon reorganization between deep ocean (>~3 km), upper ocean (<~2 km), land biosphere, and atmosphere during the early (**A**) and late (**B**) deglacial periods. Double arrows indicate carbon exchange between reservoirs, and single arrows indicate net flux (indicated by numbers and line thicknesses), not pathways, of carbon from one reservoir to another. During the early deglacial (17.5 to 14.5 ka), transfer of carbon from the deep ocean to the atmosphere may be linked to intensified upwelling in the Southern Ocean (*22*). During the late deglacial (14 to 10 ka), carbonate compensation might play an additional role in release of carbon from deep oceans. The net flux of ~400 Pg carbon from deep ocean to terrestrial biosphere was through sequestration of atmospheric CO_2 by forest.

southward shift of the Southern Hemisphere westerlies. A ~10 μmol/kg increase in [CO_3^{2-}] is observed in WIND 28K and GGC48 from the Indo-Pacific Oceans (Table 1 and Fig. 2, G and I). This is an underestimation of the [CO_3^{2-}] rise caused by carbon release for two reasons. First, once deep-water [CO_3^{2-}] deviates from the steady-state value, carbonate compensation kicks in and tends to bring [CO_3^{2-}] to its initial value (*23*), a process to reduce the initial [CO_3^{2-}] increase. Second, bioturbation would attenuate amplitude of climate signals, especially for Pacific cores (*12*). Because elevated deep-ocean [CO_3^{2-}] promotes carbonate preservation on the sea floor and removes alkalinity from oceans, the [CO_3^{2-}] rise must reflect a decrease in DIC. A 10-μmol/kg increase in [CO_3^{2-}] would require a loss of ~20 μmol/kg in DIC of deep waters (fig. S7). If these deep waters make up 30% of the global oceans in volume, the amount of carbon that escaped from these sources would be ~98 Pg. Given uncertainties with our calculation (*12*), the estimated carbon loss from deep oceans during the MI is comparable to ~105 Pg carbon needed for a 50-ppmv rise in atmospheric CO_2 during the MI (Fig. 2N) (*15*). The close match of carbon fluxes between deep-ocean release and the atmospheric CO_2 rise makes unlikely a notable increase in terrestrial biosphere during the MI. This is consistent with benthic foraminiferal $\delta^{13}C$ and land records (*24*, *25*). The preferential uptake of light ^{12}C by the terrestrial biosphere should lead to an increase in oceanic $\delta^{13}C$. A dynamic vegetation model study suggests a large increase of global terrestrial carbon storage by ~350 Pg (*26*), which would drive up deep-ocean $\delta^{13}C$ by ~0.2 per mil (‰). However, no clear trend is observed in benthic $\delta^{13}C$ during the MI (Fig. 2, D, F, H, and J). The lag of $\delta^{13}C$ rise to [CO_3^{2-}] increase is not an artifact of bioturbation because (i) the abundances of *C. wuellerstorfi* in these cores are roughly constant during the last deglacial period (fig. S3), (ii) the lag is observed in all three cores with various sedimentation rates and thus likely reflects a real climate signal, and (iii) bioturbation would equally influence benthic B/Ca and $\delta^{13}C$ from the same samples and minimally compromise their relative timing. During the MI, the small rise in atmospheric CH_4 (Fig. 2M) indicates only modest expansion of wetland areas at low latitudes (*27*). Speleothem and pollen records suggest that climate was characterized by dry/cold conditions in southern Europe and East Asia (*24*, *25*) and that steppe vegetation dominated the land biomass in southern Europe (*28*). Therefore, based on deep-water [CO_3^{2-}] and benthic $\delta^{13}C$ results, we conclude that CO_2 released from abyssal oceans during the MI remained in the atmosphere as opposed to being used for reforestation (Fig. 3A).

Compared with the MI, the late deglacial (14 to 10 ka) witnessed a smaller rise in atmospheric CO_2 (Fig. 2N). However, almost three-quarters of the LGM-to-Holocene shifts in benthic $\delta^{13}C$ [0.3 to 0.4‰, corresponding to ~500 Pg carbon (*1*)] and in atmospheric $\delta^{13}CO_2$ occurred during the late deglacial (Fig. 2, F, H, J, and L). At that time, the climate in East Asia and southern Europe was warmer and wetter (*24*, *25*), and vegetation in southern Europe was dominated by forest biomass (*28*). These changes indicate substantial growth of terrestrial biosphere from 14 to 10 ka, in contrast to the limited, even negligible, growth during the MI. Therefore, despite only a 25-ppmv rise in atmospheric CO_2 (Fig. 2N), the high demand for carbon by land biosphere growth may suggest a greater oceanic CO_2 release during the late deglacial than during the MI (Fig. 3B).

The associated carbon removal from deep oceans alone would be expected to drive up deep-water [CO_3^{2-}] by decreasing DIC in deep oceans. However, during the late deglacial, only a small [CO_3^{2-}] increase was observed in BOFS 8K (Fig. 2E), which was more likely caused by a reduced influence of low-[CO_3^{2-}] southern-sourced waters (*29*). In our deep Indo-Pacific records, we observe no rise in deep-water [CO_3^{2-}] but wide [CO_3^{2-}] peaks during the late deglacial (Fig. 2, G and I). One explanation for the absence of a rise in deep Indo-Pacific [CO_3^{2-}] is deep-ocean carbonate compensation. The transient rise in deep-sea [CO_3^{2-}] due to carbon release caused by processes like intensified upwelling in the Southern Ocean (*22*) would upset the oceanic alkalinity balance between riverine input and marine burial. On a time scale of ~5000 years (*23*), carbonate compensation serves as a negative feedback tending to bring deep-sea [CO_3^{2-}] back to the initial steady-state value. The initially increased deep-water [CO_3^{2-}] would promote the preservation and burial of carbonate on the sea floor. Because carbonate preservation is most sensitive to deep-sea [CO_3^{2-}] changes at around the depth of lysocline, the carbonate compensation effect may be most easily detected in our deep Indo-Pacific cores. At shallow depths (VM28-122 and GGC15), its effect may be overwhelmed by other influences, such as changes in circulation and preformed values. Improved carbonate preservation from 14 to 10 ka is clear in WIND 28K (Fig. 1C), the Cape Basin (~34°S, ~5°E, Atlantic) (*13*), and other locations in the Southern Ocean (*30*). Carbonate burial removes alkalinity from oceans and leads to a decrease in seawater [CO_3^{2-}]. Thus, the late deglacial [CO_3^{2-}] plateau might suggest a strong carbonate compensation effect to counteract any rise in deep-water [CO_3^{2-}] driven by initial CO_2 degassing. By reducing the whole oceanic alkalinity, carbonate compensation doubles the amount of CO_2 release (*23*) that is caused by the initial disturbance. During the Bølling-Allerød (14.5 to 12.9 ka), the strength of upwelling in the Southern Ocean was weakened when atmospheric CO_2 stopped rising (Fig. 2, K and N). However, the large increase in atmospheric CH_4 (Fig. 2M) suggests expansion of low-latitude wetland areas during this period (*27*). We infer that carbonate compensation played an important role in oceanic release of CO_2 that was needed for land biosphere growth and atmospheric CO_2 rise during the late deglacial, particularly during the Bølling-Allerød period.

Our results suggest that variations in the interactions among the oceanic, sedimentary, atmospheric, and terrestrial carbon reservoirs have played an important and continuing role in defining the observed changes in deep-ocean chemistry and atmospheric CO_2 since the last ice age. The timing and amplitude of our deep-ocean [CO_3^{2-}] and benthic $\delta^{13}C$ records offer constraints for models designed to quantify the mechanisms on past atmospheric CO_2 changes.

References and Notes

1. M. I. Bird, J. Lloyd, G. D. Farquhar, *Nature* **371**, 566 (1994).
2. D. M. Sigman, E. A. Boyle, *Nature* **407**, 859 (2000).
3. W. Broecker, *Prog. Oceanogr.* **11**, 151 (1982).
4. D. M. Anderson, D. Archer, *Nature* **416**, 70 (2002).
5. W. S. Broecker, E. Clark, *Science* **294**, 2152 (2001).
6. A. Sanyal, N. G. Hemming, G. N. Hanson, W. S. Broecker, *Nature* **373**, 234 (1995).
7. T. M. Marchitto, J. Lynch-Stieglitz, S. R. Hemming, *Earth Planet. Sci. Lett.* **231**, 317 (2005).
8. T. M. Marchitto, D. W. Oppo, W. B. Curry, *Paleoceanography* **17**, 1038 (2002).
9. J. M. Yu, H. Elderfield, *Earth Planet. Sci. Lett.* **258**, 73 (2007).
10. J. M. Yu, G. L. Foster, H. Elderfield, W. S. Broecker, E. Clark, *Earth Planet. Sci. Lett.* **293**, 114 (2010).
11. J. M. Yu, H. Elderfield, A. Piotrowski, *Earth Planet. Sci. Lett.* **271**, 209 (2008).
12. Materials and methods are available as supporting material on *Science* Online.
13. D. A. Hodell, C. D. Charles, F. J. Sierro, *Earth Planet. Sci. Lett.* **192**, 109 (2001).
14. J. W. Farrell, W. L. Prell, *Paleoceanography* **4**, 447 (1989).
15. D. Lüthi *et al.*, *Nature* **453**, 379 (2008).
16. W. S. Broecker, E. Clark, *Geochem. Geophys. Geosyst.* **3**, 1021 (2002).
17. W. B. Curry, D. Oppo, *Paleoceanography* **20**, PA1017 (2005).
18. K. Matsumoto, T. Oba, J. Lynch-Stieglitz, H. Yamamoto, *Quat. Sci. Rev.* **21**, 1693 (2002).
19. L. Keigwin, *Paleoceanography* **13**, 323 (1998).
20. J. C. Herguera, E. Jansen, W. H. Berger, *Paleoceanography* **7**, 273 (1992).
21. W. J. Schmitz, *On the World Ocean Circulation: Volume II. The Pacific and Indian Ocean: A Global Update* (Woods Hole Oceanographic Institution, Woods Hole, MA, 1996).
22. R. F. Anderson *et al.*, *Science* **323**, 1443 (2009).
23. W. S. Broecker, T. H. Peng, *Global Biogeochem. Cycles* **1**, 15 (1987).
24. D. Fleitmann *et al.*, *Geophys. Res. Lett.* **36**, L19707 (2009).
25. Y. J. Wang *et al.*, *Science* **294**, 2345 (2001).
26. J. O. Kaplan, I. C. Prentice, W. Knorr, P. J. Valdes, *Geophys. Res. Lett.* **29**, 2074 (2002).
27. E. Monnin *et al.*, *Science* **291**, 112 (2001).
28. J. M. R. Allen *et al.*, *Nature* **400**, 740 (1999).
29. J. F. McManus, R. Francois, J.-M. Gherardi, L. D. Keigwin, S. Brown-Leger, *Nature* **428**, 834 (2004).
30. W. R. Howard, W. L. Prell, *Paleoceanography* **9**, 453 (1994).
31. J. Elsig *et al.*, *Nature* **461**, 507 (2009).
32. H. J. Smith, H. Fischer, M. Wahlen, D. Mastroianni, B. Deck, *Nature* **400**, 248 (1999).

33. We thank N. McCave and D. McCorckle for providing core materials used in this study; P. deMenocal, P. Tomascak, B. Hönisch, X. Wang, and B. Yan for assistance with laboratory work; and three anonymous reviewers for their constructive comments. This research is funded by Lamont-Doherty Postdoctoral Fellowship (J.Y.), NSF, National Oceanic and Atmospheric Administration, Comer Education Foundation, National Natural Science Foundation of China, and U.K. Natural Environment Research Council. This is LDEO contribution 7412.

Supporting Online Material

www.sciencemag.org/cgi/content/full/330/6007/1084/DC1
Materials and Methods
Figs. S1 to S7
Table S1
References

3 June 2010; accepted 18 October 2010
10.1126/science.1193221

Glacial Silicic Acid Concentrations in the Southern Ocean

Michael J. Ellwood,[1]* Martin Wille,[1]† William Maher[2]

Reconstruction of nutrient concentrations in the deep Southern Ocean has produced conflicting results. The cadmium/calcium (Cd/Ca) data set suggests little change in nutrient concentrations during the last glacial period, whereas the carbon isotope data set suggests that nutrient concentrations were higher. We determined the silicon isotope composition of sponge spicules from the Atlantic and Pacific sectors of the Southern Ocean and found higher silicic acid concentrations in the Pacific sector during the last glacial period. We propose that this increase results from changes in the stoichiometric uptake of silicic acid relative to nitrate and phosphate by diatoms, thus facilitating a redistribution of nutrients across the Pacific and Southern Oceans. Our results are consistent with the global Cd/Ca data set and support the silicic acid leakage hypothesis.

The distribution of nutrients in the deep ocean is affected by deep ocean circulation processes. In the modern ocean, "conveyor belt"–type circulation resulting from deep-water production in the North Atlantic transports regenerated nutrients out of the Atlantic through to the Pacific via the Southern Ocean. Consequently, the Southern Ocean plays a key role in facilitating deep-water communication between the Atlantic and the Pacific Oceans. The modern Southern Ocean also plays a pivotal role in determining the air-sea balance of CO_2 and global biological production through the formation of mode, intermediate, and deep waters, which also facilitate nutrient exchange between ocean basins. However, the distributions of key nutrients, silicic acid and nitrate/phosphate, in the surface and deep Southern Ocean are dissimilar (Fig. 1A). In Southern Ocean surface waters, diatoms preferentially remove silicic acid, compared with nitrate and phosphate, as a consequence of iron limitation (*1*, *2*), resulting in the depletion of silicic acid in the main thermocline (200 to 1000 m) but enrichment at depth (>1500 m) after opal dissolution (*1*, *3*–*5*). In contrast, phosphate and nitrate concentrations in the surface and deep Southern Ocean are high and relatively homogeneous south of ~45°S (Fig. 1A) (*5*).

The reconstruction of nutrient distributions during glacial times has proven controversial (*6*–*8*). Nutrient reconstructions based on benthic foraminifera Cd/Ca data indicate minimal change in deep-water nutrient concentrations in the South Atlantic and a slight decline in concentrations in the southeast Indian Ocean (*6*, *9*), implying that there has been a steady supply of northern component water flowing out of the Atlantic into the Southern Ocean. Contrastingly, nutrient reconstructions based on benthic foraminifera carbon isotope ($\delta^{13}C$) data suggest an increase in deep-water nutrient concentrations from the South Atlantic on into the southeast Indian Ocean (*6*–*9*), along with an increase in the age of deep waters (*10*). In the South Pacific, the change in $\delta^{13}C$ deep-water values is somewhat muted, but they still imply higher nutrient concentrations compared with those of the present day (*11*–*13*). Overall, the $\delta^{13}C$ results imply that there was a reduction in northern component water flowing out of the Atlantic into the Southern Ocean (*14*).

Here, we evaluate the relative distribution of silicic acid within the deep Southern Ocean across the past 150 thousand years (ky), with the use of the silicon isotope ($\delta^{30}Si$) composition of sponge spicules isolated from two deep-water cores located in the Pacific (core E33-22: 54.92°S, 120°W, 2743 m) and Atlantic [Ocean Drilling Program 177 (ODP177) site 1089: 40.94°S, 09.89°E, 4620 m] sectors of the Southern Ocean.

Silicon isotope $\left[\delta^{30}Si = \{[(^{30}Si/^{28}Si)_{sample}/(^{30}Si/^{28}Si)_{standard}] - 1\} \times 10^3\right]$ studies indicate that $\delta^{30}Si$ fractionation occurs during sponge-spicule formation (*15*–*17*) and is coupled to the silicic

[1]Research School of Earth Sciences, The Australian National University, Canberra, ACT 0200, Australia. [2]Institute for Applied Ecology, Faculty of Applied Science, University of Canberra, Canberra, ACT 2601, Australia.

*To whom correspondence should be addressed. E-mail: michael.ellwood@anu.edu.au

†Present address: Institute of Geoscience, University of Tübingen, 72074 Tübingen, Germany.

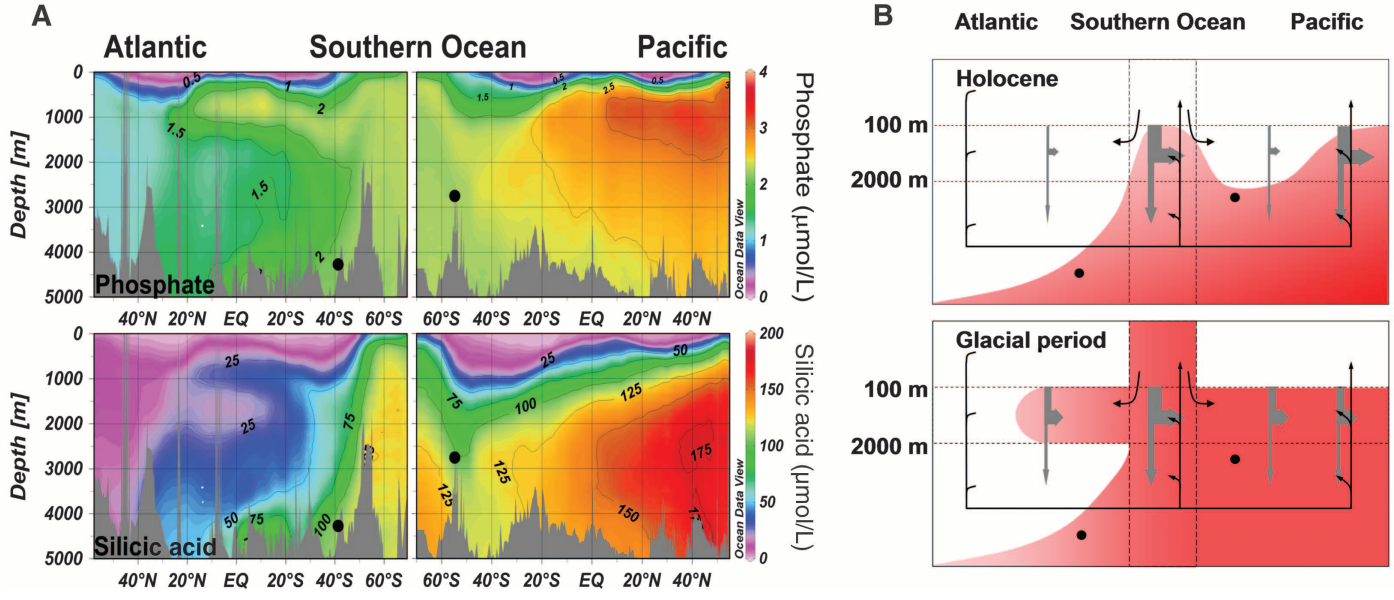

Fig. 1. Meridional sections of phosphate and silicic acid concentration. (**A**) Atlantic and Pacific Ocean sections of phosphate (top) and silicic acid (bottom) concentrations extending into the Southern Ocean. Data were obtained from the electronic version of the World Ocean Circulation Experiment (http://odv.awi.de). Black dots represent core sites ODP177 site 1089 (40.94°S; 4620 m, Atlantic sector) and E33-22 (54.92°S; 2743 m, Pacific sector). EQ, equator. (**B**) Cartoon of the silicic acid meridional section for the modern and the glacial ocean; the redder the color, the higher the silicic acid concentration. For the glacial ocean, the distribution of silicic acid becomes more "phosphate-like," with higher concentrations at shallower depths in the Southern Ocean and a reduction in the meridional silicic acid concentration gradient across the Pacific basin. Black lines represent modern water flows; gray arrows indicate the export of diatom opal to the oceans' interior. These cartoons are based on a conceptual model presented by Sarmiento *et al.* (*5*).

acid concentration of the water in which the sponges grow. In addition, sponge silica becomes progressively depleted in ^{30}Si, relative to ^{28}Si, when the seawater concentration of silicic acid increases (*15*, *17*). Silicon isotope sponge records for ODP177 site 1089 and E33-22 are shown in Fig. 2 (*18*). For ODP177 site 1089, $\delta^{30}Si$ values are within the range of –0.5 to –1.6 per mil (‰) and do not show long-term secular changes. $\delta^{30}Si$ values for the Last Glacial Maximum [20 to 25 thousand years ago (ka)] and the penultimate interglacial-glacial transition are comparable to present-day values, suggesting that silicic acid concentrations in the south Atlantic have remained relatively constant over the past 150 ky. This trend is consistent with other $\delta^{30}Si$ sponge and Cd/Ca data for this region (*6*, *15*, *19*). Both the $\delta^{30}Si$ and Cd/Ca results conflict with the $\delta^{13}C$ data for this region, which suggests that deep-water nutrients levels were higher during glacial periods (Fig. 2) (*8*).

In contrast, during the deglacial transition (10 to 15 ka), $\delta^{30}Si$ values for ODP177 site 1089 are lower by ~0.5‰, which translates into an increase in silicic acid concentration (Fig. 3). This increase coincides with an increase in opal accumulation at core site TN057-13PC (fig. S2), which is located further south at 53.2°S (*20*), and with the age of surface and deep waters (*11*). This change in the $\delta^{30}Si$ sponge record, however, is not a direct result of changes in diatom opal accumulation locally near ODP177 site 1089; the nearby core TN057-21PC (41.1°S, 7.8°E, 4981 m) shows a decline in diatom abundance from 15 to 22 ka (*21*). Thus, the change in the $\delta^{30}Si$ sponge record during this period probably reflects a decline in northern component deep water and an increase in southern component water ventilating this site during the deglacial transition (*20*).

Counterbalancing the ODP177 site 1089 $\delta^{30}Si$ sponge record is the record from E33-22. For this core, $\delta^{30}Si$ values during the Holocene, early parts of marine isotope stages (MISs) 3 and 4, MIS 5d, and the penultimate glacial period are comparable to Atlantic values (Fig. 2). However, during MIS 2, the latter part of MIS 3, and MIS 5e, $\delta^{30}Si$ values are ~1 to 2‰ lower (i.e., lighter) than Atlantic values, which equates to a higher silicic acid concentration of ~40 μmol L^{-1}. The $\delta^{30}Si$ excursion at the onset of MIS 5e also coincides with the penultimate deglacial transition, where changes in the $\delta^{30}Si$ and germanium:silicon (Ge:Si) records for the surface ocean also occur (fig S4). The abundance of negative $\delta^{30}Si$ values during this transition period reflects a bathing of the site with silicic acid–enriched water (*18*). During the deglacial transition (10 to 15 ka), $\delta^{30}Si$ sponge values increase toward the early Holocene value of –1.3‰ and are similar to Atlantic sector values for this time period (Fig. 3). Like ODP177 site 1089, the E33-22 $\delta^{30}Si$ sponge record is not majorly influenced by changes in diatom opal accumulation (*22*).

The main caveat associated with interpreting our $\delta^{30}Si$ sponge records is the possible influence of secular changes in the silicic acid inventory of the global ocean (*18*). Modeling suggests that changes in the global silicic acid inventory have little influence on the overall $\delta^{30}Si$ composition of seawater, unless the global inventory is reduced to half of its present-day value (figs. S5 and S6 and table S3) (*23*).

We also evaluated this caveat with the use of Ge:Si sponge records obtained for E33-22

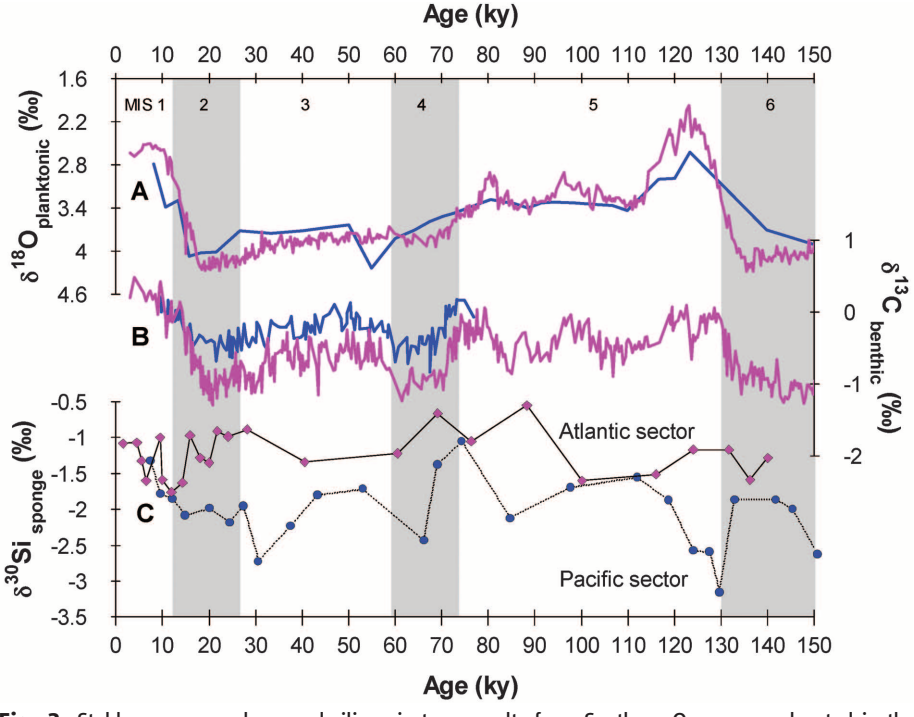

Fig. 2. Stable oxygen, carbon, and silicon isotope results from Southern Ocean cores located in the Pacific (E33-22, E11-2) and the Atlantic (ODP177 site 1089) sectors. (**A**) Planktonic $\delta^{18}O$ results are for *Globigerina bulloides* (ODP177 site 1089, purple line) *(29) and Neogloboquadrina pachyderma* (E33-22, blue line) (*13*). (**B**) Benthic $\delta^{13}C$ results are for *Cibicidoides* (ODP177 site 1089, purple line, and E11-2, 56°S; 115°W; 3109 m, Pacific sector, blue line) (*7*, *29*). (**C**) Silicon isotope results for sponge spicules isolated from E33-22 (blue circles) and ODP177 site 1089 (purple diamonds).

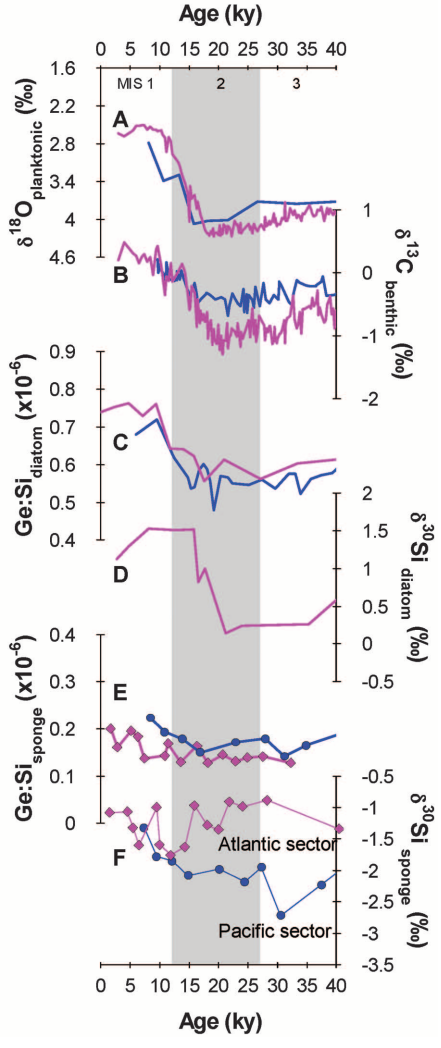

Fig. 3. Comparison of isotope and trace element records from the Southern Ocean covering the past 40 ky. (**A**) Stable $\delta^{18}O$ isotope records for planktonic foraminifera (blue line, Pacific sector; purple line, Atlantic sector) (*13*, *29*). (**B**) Stable $\delta^{13}C$ isotope records for benthic foraminifera (blue line, Pacific sector; purple line, Atlantic sector) (*7*, *13*, *29*). (**C**) Diatom Ge:Si records for cores in the Atlantic (RC13-259; 53°53′S, 04°56′W, purple line) (*30*) and Pacific (E17-9; 63°05′S, 135°07′W, blue line) (*30*) sectors of the Southern Ocean. (**D**) Diatom $\delta^{30}Si$ record for core RC13-259 (*1*). (**E**) Sponge Ge:Si records for core E33-22 (blue circles, Pacific sector) and ODP177 drill site 1089 (purple diamonds, Atlantic sector). (**F**) Sponge $\delta^{30}Si$ records for core E33-22 (blue circles, Pacific sector) and ODP177 drill site 1089 (purple diamonds, Atlantic sector).

and ODP177 site 1089 and by combining these with the diatom Ge:Si records published for the Pacific and Atlantic sectors of the Southern Ocean (Fig. 3). Because the Ge:Si ratio of diatom opal appears to be a faithful record of the seawater Ge:Si ratio, with little opal-seawater fractionation occurring at high silicic acid concentrations (*24*), it can be used to monitor changes in the seawater Ge:Si ratio over time. In contrast, there is major Ge:Si fractionation within deep-sea sponge silica (*25*), with fractionation being related to changes in the silicic acid concentration of seawater and the Ge:Si ratio of seawater. Close inspection of sponge Ge:Si records from ODP177 site 1089 and E33-22 shows a general decline in ratios from Holocene values near 0.2×10^{-6} to ~0.15×10^{-6} during glacial times (Fig. 3). Correspondingly, Southern Ocean diatom Ge:Si records from these two regions also show a coherent reduction from modern values of ~0.76×10^{-6} to 0.55×10^{-6} during glacial times (Fig. 3). Such a reduction in both the diatom and sponge Ge:Si records requires a global oceanic reduction in the germanium inventory by ~20 Gmol, an increase in the silicon inventory by ~36 Pmol, or some combination of both. Modeling of both the sponge and the diatom Ge:Si records using a 10-box model indicates that the main cause for the decline in these records probably results from a change in both the global germanium and silicon inventories during the last glacial period (fig. S7 and table S4) (*18*). However, such changes in either the germanium or silicic acid inventories cannot explain the divergence seen in the two δ^{30}Si sponge records during MIS 2 (Fig. 3F). These changes result from regional changes in the concentration of silicic acid associated with changes in opal production and, hence, opal regeneration in the deep ocean and changes in deep ocean circulation.

The silicic acid leakage hypothesis (SALH) purports that, during the last glacial period, the distribution of nutrients in the surface and deep Southern Ocean was different as a result of iron fertilization of surface waters via increased dust deposition (*1*). Under this scenario, iron fertilization is believed to have reduced silicic acid use in Southern Ocean waters, relative to nitrate and phosphate, thereby allowing the silicic acid concentration of Southern Ocean surface waters to increase and for some of that silicic acid to "leak" out of the Southern Ocean to lower latitudes (*2*, *4*, *18*). Based on the SALH, the distribution of silicic acid in the surface ocean during the last glacial period is likely to have been similar to that of nitrate and phosphate (Fig. 1B). Thus, the glacial increase in silicic acid concentration for core E33-22 probably resulted from two processes: (i) an increase in the global silicic acid inventory associated with changes in surface ocean use and (ii) a reduced meridional silicic acid concentration gradient across the Pacific basin as silicic acid becomes more phosphate-like in its distribution (Fig. 1B).

Our modeling results suggest that a reduction in silicic acid use in surface waters during the last glacial period, associated with iron fertilization from increased dust deposition, leads to an increase in global silicic acid inventory by 6 to 19% and is dependent on whether changes are restricted to just the surface Southern Ocean or to the global surface ocean (Fig. 4 and table S3) (*18*). These changes in the silicic acid inventory are associated with changes in opal production and sedimentation and are also reflected in the diatom δ^{30}Si records from high and low latitudes (Fig. 4) (*26*, *27*). However, changes in the silicic acid inventory are not directly reflected in the diatom and sponge Ge:Si records, because a redistribution of silicic acid also leads to a redistribution of germanium (fig. S7 and table S4).

The meridional redistribution of silicic acid across the Pacific Ocean is also consistent with benthic foraminifera δ^{13}C records from the South Tasman Rise (*11*) and the Chatham Rise (*12*), suggesting that Southern Ocean mid- to deep waters (depths of 1500 to 3500 m) were more "Pacific-like," indicating an increased southward extension of Pacific Deep Water into the Southern Ocean (*11*, *12*). The Cd/Ca data from the northwest and eastern equatorial Pacific Ocean provide supporting evidence for this idea (*9*), with the Holocene-glacial decline in Cd/Ca foraminifera ratios in the Northwest Pacific consistent with a reduction in the meridional nutrient gradient across the Pacific Ocean. Contrastingly, the Cd/Ca foraminifera data from the deep Southern Ocean suggest that glacial phosphate and nitrate concentrations were similar or slightly lower compared with those of the present day (*6*, *9*), which is also compatible with the SALH and our δ^{30}Si sponge results from the Atlantic sector of the Southern Ocean (Fig. 3).

Our results show that the glacial concentration of silicic acid in the Atlantic sector of the Southern Ocean was comparable to present-day levels, whereas silicic acid concentrations in the Pacific sector were higher. Such heterogeneity within the Southern Ocean suggests that the glacial contribution of deep water feeding into the Southern Ocean from the Atlantic was comparable to that of the present day, whereas ventilation in the Pacific sector was reduced through either an increased southward extension of Pacific Deep Water or a reduction in deep-water ventilation; both states are compatible with the mid-climate state of reduced Antarctic overturning (*28*). Detailed investigations of the δ^{30}Si composition of sponges from across the Pacific should refine estimates for the redistribution of silicic acid across this basin associated with changes in deep-water ventilation.

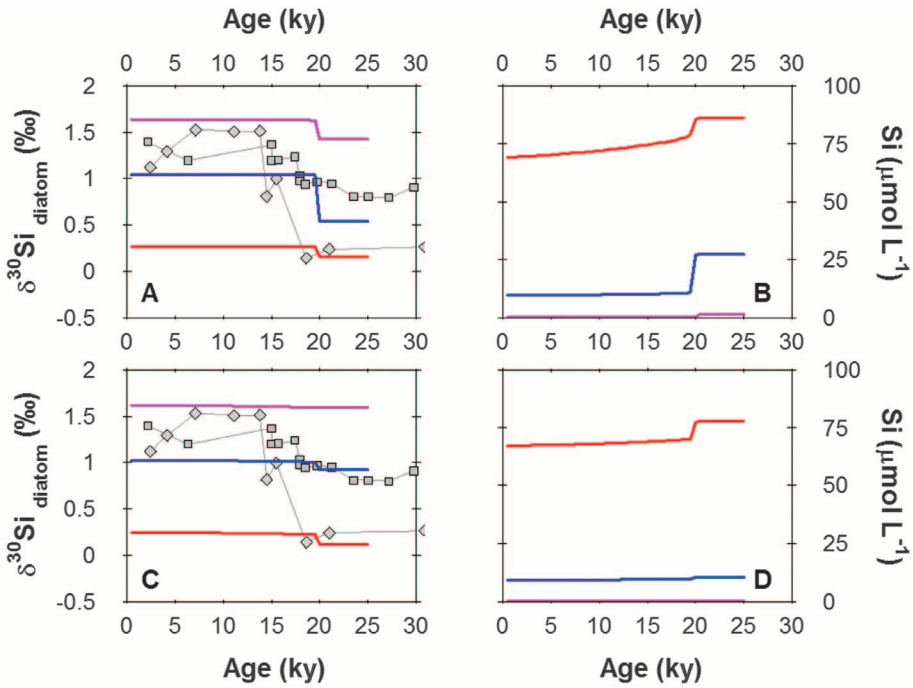

Fig. 4. Glacial-interglacial changes in δ^{30}Si composition of diatoms from the Southern Ocean and the eastern equatorial Pacific, along with model results. (**A**) Silicon isotope composition of Southern Ocean (diamonds) (*1*) and eastern equatorial Pacific (squares) (*27*) diatoms, along with modeled δ^{30}Si diatom opal results versus time for the surface Antarctic (red curve), the intermediate Indo-Pacific (blue curve), and the surface Pacific (purple curve). In the model, an instantaneous change in silicic acid use in all surface boxes was initiated at 20 ky (table S3) (*18*). (**B**) Modeled silicic acid concentrations associated with an instantaneous change in silicic acid use initiated in all surface boxes at 20 ky. (**C**) Silicon isotope composition of Southern Ocean (diamonds) (*1*) and eastern equatorial Pacific (squares) (*27*) diatoms, along with modeled δ^{30}Si diatom opal results versus time for the surface Antarctic (red curve), the intermediate Indo-Pacific (blue curve), and the surface Pacific (purple curve). In the model, an instantaneous change in silicic acid use in only the surface Antarctic boxes was initiated at 20 ky (table S3) (*18*). (**D**) Modeled silicic acid concentrations associated with an instantaneous change in silicic acid use initiated in the surface Antarctic box at 20 ky.

References and Notes

1. M. A. Brzezinski *et al.*, *Geophys. Res. Lett.* **29**, 1564 (2002).
2. K. Matsumoto, J. L. Sarmiento, M. A. Brzezinski, *Global Biogeochem. Cycles* **16**, 1031 (2002).
3. S. Takeda, *Nature* **393**, 774 (1998).
4. J. L. Sarmiento, N. Gruber, M. A. Brzezinski, J. P. Dunne, *Nature* **427**, 56 (2004).
5. J. L. Sarmiento *et al.*, *Global Biogeochem. Cycles* **21**, GB1S90 (2007).
6. Y. Rosenthal, E. A. Boyle, L. Labeyrie, *Paleoceanography* **12**, 787 (1997).
7. U. S. Ninnemann, C. D. Charles, *Earth Planet. Sci. Lett.* **201**, 383 (2002).
8. D. A. Hodell, K. A. Venz, C. D. Charles, U. S. Ninnemann, *Geochem. Geophys. Geosyst.* **4**, 1004 (2003).
9. E. A. Boyle, *Annu. Rev. Earth Planet. Sci.* **20**, 245 (1992).
10. L. C. Skinner, S. Fallon, C. Waelbroeck, E. Michel, S. Barker, *Science* **328**, 1147 (2010).
11. A. D. Moy, W. R. Howard, M. K. Gagan, *J. Quat. Sci.* **21**, 763 (2006).
12. I. N. McCave, L. Carter, I. R. Hall, *Quat. Sci. Rev.* **27**, 1886 (2008).
13. U. S. Ninnemann, C. D. Charles, *Paleoceanography* **12**, 560 (1997).
14. A. M. Piotrowski, S. L. Goldstein, S. R. Hemming, R. G. Fairbanks, *Earth Planet. Sci. Lett.* **225**, 205 (2004).
15. K. R. Hendry, R. B. Georg, R. E. M. Rickaby, L. F. Robinson, A. N. Halliday, *Earth Planet. Sci. Lett.* **292**, 290 (2010).
16. C. L. de la Rocha, M. A. Brzezinski, M. J. DeNiro, *Geochim. Cosmochim. Acta* **61**, 5051 (1997).
17. M. Wille *et al.*, *Earth Planet. Sci. Lett.* **292**, 281 (2010).
18. See the supporting online material available on *Science* Online.
19. D. W. Lea, *Paleoceanography* **10**, 733 (1995).
20. R. F. Anderson *et al.*, *Science* **323**, 1443 (2009).
21. S. Barker *et al.*, *Nature* **457**, 1097 (2009).
22. Z. Chase, R. F. Anderson, M. Q. Fleisher, P. W. Kubik, *Deep Sea Res. Part II Top. Stud. Oceanogr.* **50**, 799 (2003).
23. R. B. Georg, A. J. West, A. R. Basu, A. N. Halliday, *Earth Planet. Sci. Lett.* **283**, 67 (2009).
24. P. N. Froelich *et al.*, *Paleoceanography* **7**, 739 (1992).
25. M. J. Ellwood, M. Kelly, W. A. Maher, P. De Deckker, *Earth Planet. Sci. Lett.* **243**, 749 (2006).
26. C. L. De La Rocha, M. A. Brzezinski, M. J. DeNiro, A. Shemesh, *Nature* **395**, 680 (1998).
27. L. E. Pichevin *et al.*, *Nature* **459**, 1114 (2009).
28. D. M. Sigman, M. P. Hain, G. H. Haug, *Nature* **466**, 47 (2010).
29. D. A. Hodell *et al.*, in *Proceedings of the Ocean Drilling Program, Scientific Results Volume*, R. Gersonde, D. A. Hodell, P. Blum, Eds. (Ocean Drilling Program, College Station, TX, 2002), vol. 177.
30. R. A. Mortlock *et al.*, *Nature* **351**, 220 (1991).

31. We acknowledge the Antarctic Research Facility at Florida State University for E33-22 core samples and the Ocean Drilling Program for ODP177 site 1089 core samples. This research was supported with funds from the Australian Research Council (grants DP0770820 and DP0771519). This manuscript benefited from the thoughtful comments of two anonymous reviewers.

Supporting Online Material

www.sciencemag.org/cgi/content/full/science.1194614/DC1
Materials and Methods
SOM Text
Figs. S1 to S7
Tables S1 to S4
References

2 July 2010; accepted 28 September 2010
Published online 21 October 2010;
10.1126/science.1194614

Structure of the Human Dopamine D3 Receptor in Complex with a D2/D3 Selective Antagonist

Ellen Y. T. Chien,[1] Wei Liu,[1] Qiang Zhao,[1] Vsevolod Katritch,[2] Gye Won Han,[1] Michael A. Hanson,[3] Lei Shi,[4] Amy Hauck Newman,[5] Jonathan A. Javitch,[6] Vadim Cherezov,[1] Raymond C. Stevens[1]*

Dopamine modulates movement, cognition, and emotion through activation of dopamine G protein–coupled receptors in the brain. The crystal structure of the human dopamine D3 receptor (D3R) in complex with the small molecule D2R/D3R-specific antagonist eticlopride reveals important features of the ligand binding pocket and extracellular loops. On the intracellular side of the receptor, a locked conformation of the ionic lock and two distinctly different conformations of intracellular loop 2 are observed. Docking of R-22, a D3R-selective antagonist, reveals an extracellular extension of the eticlopride binding site that comprises a second binding pocket for the aryl amide of R-22, which differs between the highly homologous D2R and D3R. This difference provides direction to the design of D3R-selective agents for treating drug abuse and other neuropsychiatric indications.

Dopamine is an essential neurotransmitter in the central nervous system and exerts its effects through activation of five distinct dopamine receptor subtypes that belong to the G protein–coupled receptor (GPCR) superfamily. The receptors have been classified into two subfamilies, D1-like and D2-like, on the basis of their sequence and pharmacological similarities (*1*). The D1-like receptors (D1R and D5R) couple to stimulatory G-protein α subunits ($G_{s/olf}$), activating adenyl cyclase, whereas D2-like receptors (D2R, D3R, and D4R) couple to inhibitory G-protein α subunits ($G_{i/o}$), inhibiting adenyl cyclase. The high degree of sequence identity (*2*, *3*) within the transmembrane (TM) helices between D2R and D3R (78%), and more importantly, the near-identity of the residues inferred to form the binding site in these receptors (*4*), have created a formidable challenge to developing D3R-selective compounds with drug-like physicochemical properties (*3*, *5*). Antipsychotic drugs that block both D2R and D3R are used clinically to treat schizophrenia, but these agents can produce multiple side effects that can limit their tolerability. It has been hypothesized that selective targeting of the individual D2-like receptor subtypes might produce fewer side effects (*6*). Through extensive medicinal chemistry efforts, D3R-preferential antagonists and partial agonists (e.g., SB 277011A, NGB 2904, BP 897; see fig. S1) have been developed and shown to attenuate drug-seeking behaviors in animal models of relapse, without associated motor effects, supporting D3R blockade as a plausible target for therapeutic discovery (*7*–*11*) particularly for substance abuse (*12*). However, even the best D3R-preferential compounds are still highly lipophilic and display poor bioavailability or predicted toxicity that has precluded clinical trials. To better understand dopamine receptors and the molecular basis for pharmacological specificity within the dopamine receptors, we have determined the crystal structure of the human D3R in complex with eticlopride, a potent D2R/D3R antagonist (*13*, *14*).

To crystallize the D3R, we modified it by introducing a point mutation in the transmembrane domain [Leu119$^{3.41}$Trp (*15*)] to enhance thermal stability (*16*), and replacing most of the third cytoplasmic loop (ICL3) (Arg222 to Arg318) with T4-lysozyme (D3R-T4L) (*17*). Further stabilization of the receptor was achieved by purifying with the antagonist eticlopride, which conferred the highest thermostability compared with five other ligands (*18*) (table S2). The engineered receptor retained near-native ligand binding properties (table S3) and crystallized from a lipidic mesophase in an orthorhombic space group. Diffraction data were anisotropic, extending to 2.9 Å in the *c** direction and 3.6 Å in the *a** direction. Overall, the structure was determined at 3.15 Å and included all data up to 2.9 Å where an improvement in map quality was observed (see fig. S8 and table S1). The structure was determined with two receptors arranged in an antiparallel orientation in the asymmetric unit of the crystal (fig. S2). Both copies of the receptor are very similar [root mean square deviation of 0.6 Å for the seven-TM bundle] and will be treated identically in the discussion

[1]Department of Molecular Biology, The Scripps Research Institute, 10550 North Torrey Pines Road, La Jolla, CA 92037, USA. [2]Skaggs School of Pharmacy and Pharmaceutical Sciences, and San Diego Supercomputer Center, University of California, San Diego, La Jolla, CA 92093, USA. [3]Receptos, 10835 Road to the Cure, Suite 205, San Diego, CA 92121, USA. [4]Department of Physiology and Biophysics and HRH Prince Alwaleed Bin Talal Bin Abdulaziz Alsaud Institute for Computational Biomedicine, Weill Cornell Medical College, Cornell University, 1300 York Avenue, New York, NY 10021, USA. [5]Medicinal Chemistry Section, National Institute on Drug Abuse–Intramural Research Program, Baltimore, MD 21224, USA. [6]Center for Molecular Recognition and Departments of Psychiatry and Pharmacology, Columbia University College of Physicians and Surgeons, 630 West 168th, New York, NY 10032, USA.

*To whom correspondence should be addressed. E-mail: stevens@scripps.edu

except where noted otherwise. The N-terminal 31 residues are not included in the deposited structure as they do not have interpretable density. The main fold of the D3R consists of the canonical seven-TM bundle of α helices (Fig. 1A), which resembles previously solved GPCR structures (*19*–*22*). Subtleties in the orientations of these helices, as well as differences in the intracellular and extracellular portions of the receptor, confer the pharmacological and biochemical properties unique to the D3R.

The extracellular region in general is characterized by high sequence diversity among the GPCR family, which translates into high structural diversity in terms of the presence of varied secondary-structure elements and the presentation of individual amino acids in the binding pocket (*23*, *24*). In the D2R and D3R, for instance, the second extracellular loop (ECL2) is much shorter than in the β-adrenergic receptors (βARs) and lacks the helical secondary structure. The portion of ECL2 in D3R (residues 182 to 185) that contributes to the ligand binding pocket is quite similar to that in the βARs in both spatial positioning relative to bound ligand, and in the presentation of side chains in the ligand binding pocket. In the D3R, a disulfide bond is formed between Cys355 and Cys358 in ECL3 in addition to the canonical disulfide bond bridging ECL2 (Cys181) and helix III (Cys103$^{3.25}$) (*25*). Comparison of the D3R structure to the β_2AR structure reveals small shifts in the helical bundle; for example, the extracellular tips of helices VI and VII are tilted by ~3 Å and ~2 Å, respectively (Fig. 1B), whereas the extracellular tips of helices III and V are about 3.5 Å closer to each other in the D3R as compared with the β_2AR structure. The latter shift can be explained by the fact that a segment of ECL2 connecting the tips of helixes V and III through a C181-Cys103$^{3.25}$ disulfide bond in D3R and other D2-like receptors is one amino acid shorter than in β_2AR and D1-like dopamine receptors (see fig. S4, B and D).

A common feature thought to be important in many class A GPCRs is the ionic lock—a salt bridge between the charged Arg$^{3.50}$ in the conserved "D[E]RY" motif and Asp/Glu$^{6.30}$ at the cytoplasmic side of helices III and VI. This interaction is observed in all of the inactive rhodopsin crystal structures (Fig. 2A) (*26*, *27*) and has been implicated through mutagenesis as a major factor in stabilizing the receptors in the inactive conformation (*28*, *29*). Despite the presence of residues capable of forming this interaction, the ionic lock has not been found in any of the other GPCR crystal structures published to date (*19*–*22*) (Fig. 2, C to E). The absence of this interaction is puzzling given its presumed importance and has been thought to be partly attributable to the inclusion of the T4L fusion protein within ICL3, which may induce a non-native helical conformation within this region. However, the presence of an intact ionic lock in both molecules in the D3R structure establishes the possibility of forming this interaction in the presence of T4L (Fig. 2B). The propensity for formation of the ionic lock, therefore, may indicate different distributions of conformational states in different receptors that may have direct implications for basal signaling activities. Differences between the two molecules observed in the crystallographic asymmetric unit may highlight particular areas of conformational flexibility in receptor structure. In chain A, ICL2 forms a 2.5 turn α helix that runs parallel to the membrane (Fig. 1A). The observation of this α

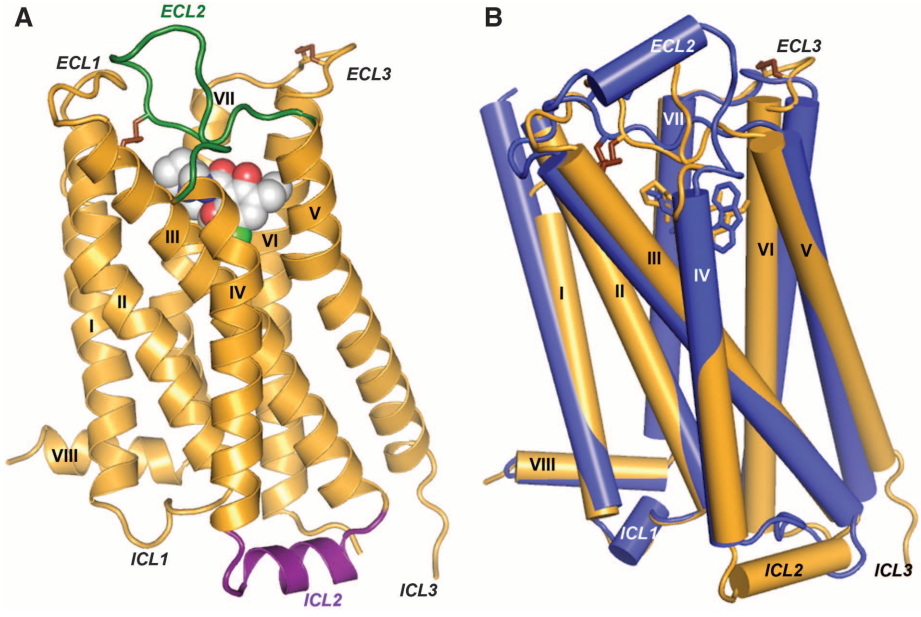

Fig. 1. Overall D3R structure with eticlopride and comparison with β_2AR structure. (**A**) A model of the D3R with the bound ligand eticlopride in space-filling representation; ECL2 is shown in green, ICL2 in purple, and disulfide bonds in brown (conformation of chain A shown). (**B**) Comparison of the TM domains of D3R (brown) and β_2AR (blue; PDB ID: 2RH1).

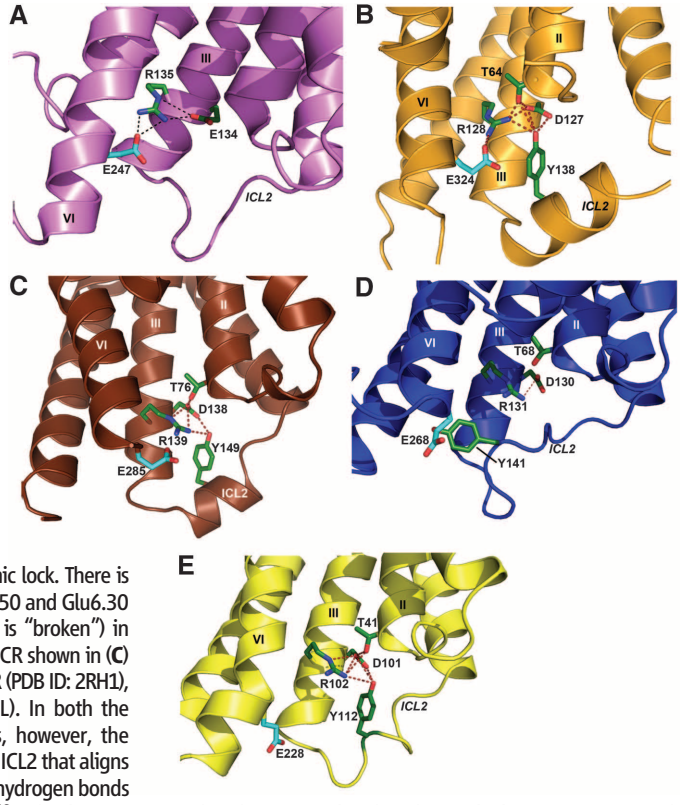

Fig. 2. Conformation of ICL2 and ionic lock motif in D3R and other GPCR structures. As also seen in (**A**) the inactive Rhodopsin structure (PDB ID: 1U19), the conserved ionic lock motif D[E]RY is in a "locked" conformation in (**B**) the D3R structure, i.e., with a salt bridge formed between Arg128$^{3.50}$ and Glu324$^{6.30}$. In addition, the side chain of Tyr138 in the ICL2 α helix of the D3R is inserted into the seven-TM bundle forming hydrogen bonds with Thr64$^{2.39}$, Arg128$^{3.50}$, and Asp127$^{3.49}$ (distances of 3.0, 3.2, and 3.2 Å, respectively), potentially stabilizing the ionic lock. There is no salt bridge between Arg3.50 and Glu6.30 (and hence the "ionic lock" is "broken") in other crystal structures of GPCR shown in (**C**) β_1AR (PDB ID: 2VT4), (**D**) β_2AR (PDB ID: 2RH1), and (**E**) A_{2A}AR (PDB ID: 3EML). In both the β_1AR and A_{2A}AR structures, however, the corresponding Tyr residue in ICL2 that aligns to Tyr138 in D3R forms two hydrogen bonds with the Asp$^{3.49}$ and Arg$^{3.50}$ side chains even in the absence of the closed ionic lock conformation. Salt bridges and hydrogen bond interactions are shown as dashed lines.

helix in only one copy of the receptor may be due to the conformational dynamics of ICL2 and the associated regions (*30*), as in chain B, ICL2 is unstructured and the intracellular ends of helices IV and V are shifted ~2.9 Å closer to each other relative to their positions in chain A (fig. S3C). The two different conformational states of ICL2 observed in the D3R structure suggest that this helix is transient, raising the possibility that interactions between ICL2 and the receptor ionic lock may modulate the signaling properties of the D3R and perhaps contribute to the tolerance property in D3R signaling that persists after agonist is removed (*31*).

Strong electron density was observed for eticlopride in the binding cavity (fig. S3, A and B), which is similar to the β_2AR pocket (Fig. 3, C and D), as expected for receptors that bind closely related catecholamine ligands (*32*). The similarity includes a number of conserved side chains in the core binding site deep in the seven-TM bundle (10 of 18 eticlopride contact residues are conserved in the β_2AR) and open access to this site through a crevice from the extracellular side. Compared with the β_2AR, however, a part of the D3R access crevice is blocked by the inward shift of helices V and VI, and access to the ligand binding pocket is controlled by side chains of helices I, II, III, VII, and ECL2.

Eticlopride occupies the part of the binding pocket defined by side chains from helices II, III, V, VI, and VII (Figs. 1 and 3A and table S4) that largely overlaps with the carazolol binding site in the β_2AR (Fig. 1B). The tertiary amine in the ethyl-pyrrolidine ring of eticlopride is likely charged at physiological pH and forms a salt bridge (2.8 Å) to the carboxylate of Asp110$^{3.32}$, which is highly conserved in all aminergic receptors (Fig. 3, A and B). This salt bridge is structurally and pharmacologically critical for high-affinity ligand binding to the aminergic subfamily of GPCRs (*4*, *33*). Another key component of the eticlopride pharmacophore is a substituted aromatic ring connected to the pyrrolidine by an amide bond that fits tightly within a hydrophobic cavity formed by Phe345$^{6.51}$ and Phe346$^{6.52}$ in helix VI; Val189$^{5.39}$, Ser192$^{5.42}$, and Ser193$^{5.43}$ in helix V; and Val111$^{3.33}$ in helix III, as well as Ile183 in ECL2. Polar substituents (e.g., OH, OCH_3) in the phenyl ring form intramolecular hydrogen bonds with both the N and O of the amide, thereby maintaining the compound in an almost planar conformation (Fig. 3, A and B), consistent with the small-molecule crystal structure determination (*13*).

Of the 18 eticlopride contact residues in the D3R structure, 17 are identical in the D2R (Val350$^{6.56}$ is an isoleucine in D2R), whereas 5 differ in the D4R (see fig. S4). Qualitatively, this agrees with the finding that eticlopride, and some of its analogs, share similar affinities for the D2R and D3R with lower binding affinities for D4R. Mutation of four divergent residues in D2R to the aligned D4R residues led to a three-order-of-magnitude enhancement of binding to a D4R-selective antagonist (*34*). Most of the differences in ligand binding specificity between D4R and D2R/D3R can therefore be explained by the differences in physicochemical properties of the contact side chains, as the mutated D2 residues included three of the five nonconserved, eticlopride-contact residues—Val91$^{2.61}$Phe, Phe110$^{3.28}$Leu, and Tyr408$^{7.35}$Val.

The structural determinants of pharmacological specificity in the D3R and D2R are more subtle considering that the residues lining the binding pocket are essentially identical. In accordance with high conservation of the eticlopride binding site between D3R and D2R, the available structure-activity relationship (SAR) data suggest that, to achieve targeted selectivity (>100-fold), the ligand must extend toward the extracellular opening of the binding pocket [reviewed in (*12*)]. The D3R-selective pharmacophore consists of an extended aryl amide connected to an amine-containing scaffold by a relatively flexible four-carbon linker (fig. S1) (*35*). Previous

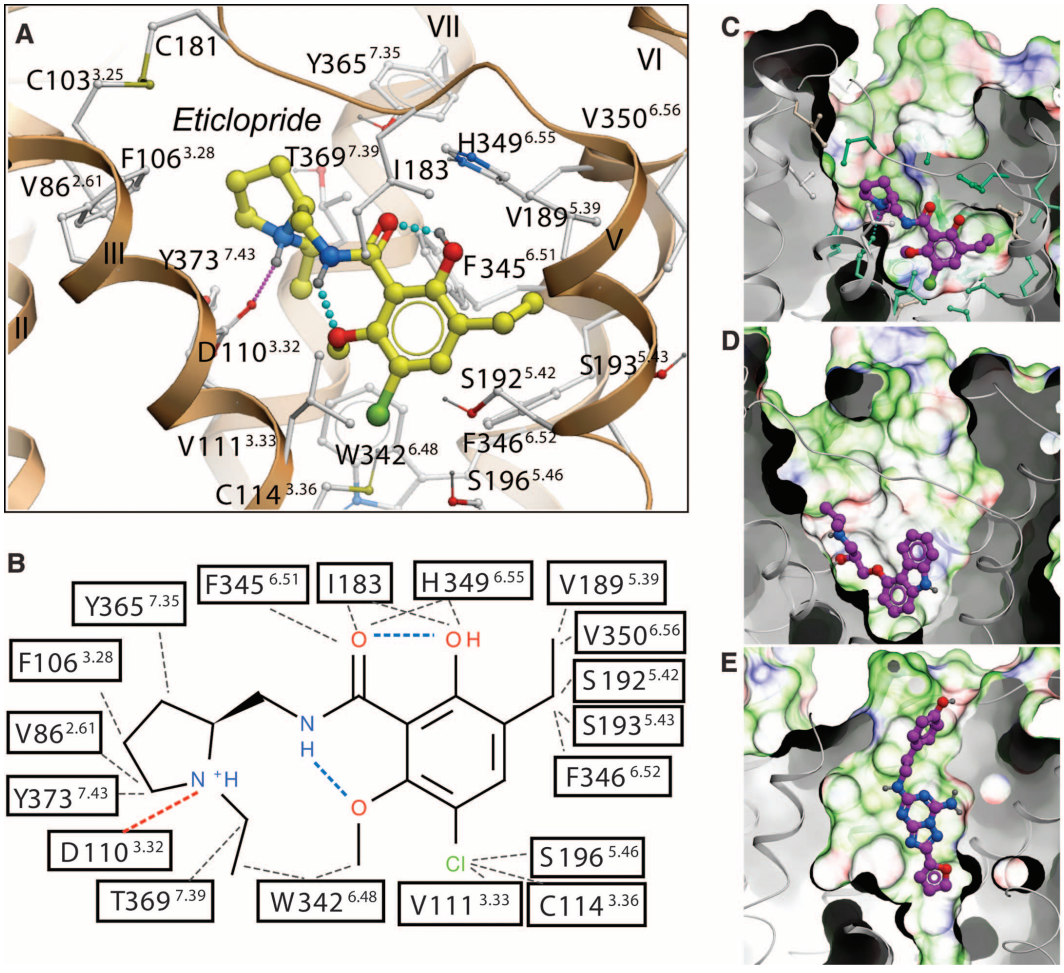

Fig. 3. Structural diversity of ligand binding sites in GPCR structures. (**A**) Close-up of the eticlopride binding site showing the protein-ligand interaction. (**B**) Chemical structure of eticlopride and interactions with the D3R residues; hydrophobic contacts are shown in gray dashed lines, hydrogen bonds in blue, and salt bridges in red. The ligand binding sites in (**C**) D3R, (**D**) β_2AR (PDB ID: 2RH1), and (**E**) A_{2A}AR (PDB ID: 3EML) crystal structures are shown in exactly the same orientation. A semitransparent skin shows the molecular surface of the receptor, colored by the residue properties (green, hydrophobic; red, acidic; and blue, basic). Corresponding ligands (C) eticlopride, (D) carazolol, and (E) ZM241385 are shown with carbon atoms colored magenta. For the D3R pocket, residues conserved between D3R and β_2AR are colored turquoise, and nonconserved residues are in gray.

efforts to rationalize the structural basis of D3R selectivity have naturally focused on regions that are not conserved, with primary attention being given to ECL2, which has previously been implicated in ligand binding to the D2R (*4*, *36*). Indeed, in chimeric studies, ECL2 has been found to play a role in both enantioselectivity and D3R selectivity of a number of compounds in which the butylamide linker is functionalized (*37*). In addition, roles for both ECL2 and ECL1 have been demonstrated for the D3R-selective tetrahydroisoquinoline, SB 269,652 (fig. S1) (*38*).

To explore the structural basis of selectivity, we created a homology model of D2R based on the D3R structure (*18*). Eticlopride could be reproducibly docked to the D3R structure and D2R model in orientations highly similar to that in the crystal structure. However, alignment of residues of the D3R and D2R indicates substantial differences in their extracellular electrostatic surfaces that could affect binding of other longer and bulkier ligands (figs. S5 and S6). Docking studies with the D3R-selective antagonist R-22 (*37*) revealed that the core amine-containing substituent (2,3-diCl-phenylpiperazine) binds in essentially the same binding pocket as eticlopride, whereas the indole-2-carboxamide terminus is oriented toward the extracellular part of the binding pocket consisting of ECL2/ECL1 and the junction of helices I, II, and VII, defining a second extracellular binding pocket (orange ellipse in Fig. 4A) that includes conserved Tyr373$^{7.43}$ and Glu95$^{2.65}$ (Fig. 4B). However, the residue at 1.39, which is spatially positioned between Tyr373$^{7.43}$ and Glu95$^{2.65}$, is divergent (Tyr36$^{1.39}$ in D3R and Leu41$^{1.39}$ in D2R) (Fig. 4, C and D). Moreover, Tyr36$^{1.39}$ is located in a stretch of five nonconserved residues at the extracellular end of helix I. Indeed, 44% of the extracellular half of helix I from 1.35 to 1.50 is not conserved between D2R and D3R (fig. S6), which should lead to functionally relevant changes in packing in D2R at the junction of helices I, II, and VII (Fig. 4, C and D, and fig. S7), consistent with previous structure-function investigations (*39*–*41*). The lack of conservation of Thr368$^{7.38}$ (Phe in D2R), which forms a hydrogen bond with the backbone of the conserved Tyr365$^{7.35}$ in the D3R, may also contribute to a shift in the relative position of helices I and VII (Fig. 4, C and D) (*42*).

Such differences in packing and backbone configuration between the D2R and D3R, even when relatively subtle, are expected to lead to changes in selectivity even without changes in ligand contact side chains in the binding pocket. Indeed, molecular dynamics simulations of the D2R in an explicit lipid bilayer (*18*) suggest a reorganization of ECL3 and helices I, II, and VII that alters the configuration of the second binding pocket (Fig. 4D and fig. S7). Accordingly, the distance between the conserved residues Glu95$^{2.65}$ (in the second binding pocket) and Tyr373$^{7.43}$ (between the orthosteric binding site and the second binding pocket) is ~1 Å greater in the D3R than in the D2R because of distinct 2.65-1.39-7.43 interactions (Fig. 4, C and D, and fig. S7), representing subtle but critical differences in the relative disposition between the orthosteric binding site and the second binding pocket in the D2R and D3R (Fig. 4B).

The crystal structure of the human D3R provides an opportunity to identify subtle structural differences, at the molecular level, between closely related GPCRs that can be exploited for novel drug design. In particular, the structural observation of an extracellular binding pocket, which may interact with bitopic or allosteric ligands, highlights the importance of the extracellular loops that were once thought to only provide superficial definition to ligand binding. Highly D2R and D3R subtype-selective molecules will provide the tools necessary to parse behavioral actions associated with individual subtypes and identify mechanisms underlying side effects, resulting in improved medications for the treatment of neuropsychiatric disorders, including drug abuse.

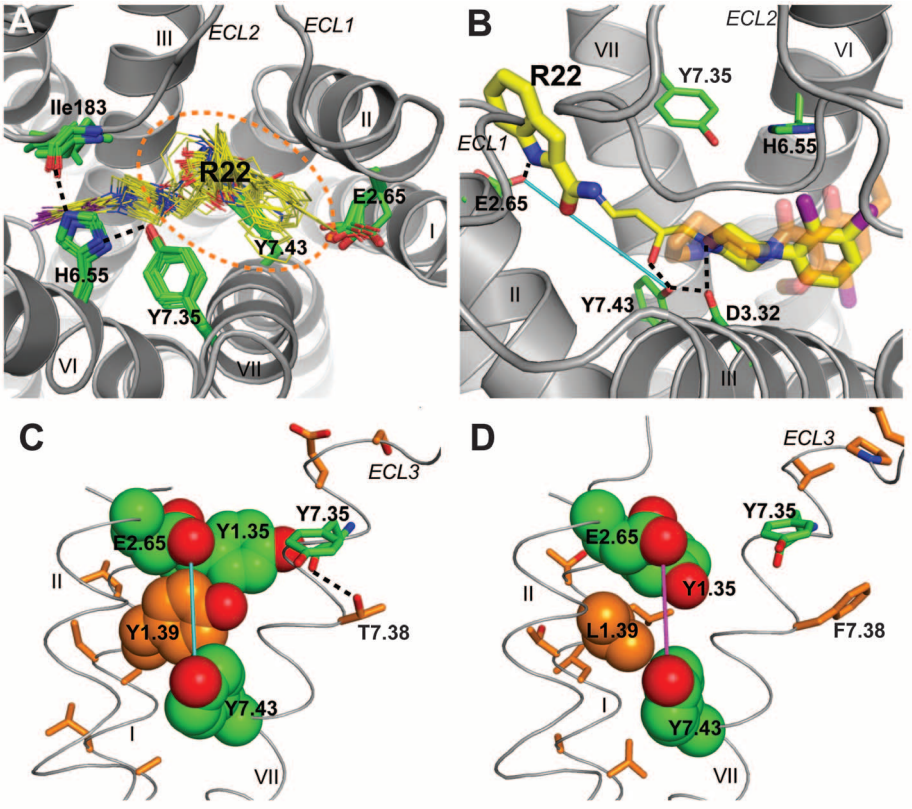

Fig. 4. The second binding pocket defined by R-22 is differentially modulated by nonconserved residues in D3R and D2R. (**A**) In addition to the core binding pocket, which essentially overlaps with that of eticlopride, the potential docking conformations of the core-constrained (see supporting online material) D3R-selective compound R-22 position the extended aryl amide within a second binding pocket comprising the junction of ECL1 and ECL2 and the interface of helices II, VII and I [dotted orange ellipse in (A)]. (**B**) In the docking pose with the most extended conformation of R-22 (yellow), the ligand makes contact with several key conserved residues, including Asp110$^{3.32}$, Tyr373$^{7.43}$, and Glu90$^{2.65}$. The linker region of R-22 connecting the aryl amide and phenylpiperazine moieties (see fig. S1) is in a thinner representation. The 2,3-diCl-phenylpiperazine occupies essentially the same space as bound eticlopride (orange). (**C** and **D**) Close-up view of the interface of helices II, VII, and I of the D3R (C) and D2R (D) showing the results of molecular dynamics simulations indicating that the nonconserved regions of helix I and position 7.38 (orange) may orient key conserved contact residues differently and alter the shape of the second binding pocket, as reflected by the simulated distances between Glu90$^{2.65}$ and Tyr373$^{7.43}$ in D3R (cyan) and D2R (magenta) (see fig. S7).

References and Notes

1. O. Civelli, in *Psychopharmacology: The Fourth Generation of Progress*, F. Bloom, D. Kufper, Eds. (Raven, NY, 1995), pp. 155–161.
2. B. Levant, *Pharmacol. Rev.* **49**, 231 (1997).
3. P. Sokoloff, B. Giros, M. P. Martres, M. L. Bouthenet, J. C. Schwartz, *Nature* **347**, 146 (1990).
4. L. Shi, J. A. Javitch, *Annu. Rev. Pharmacol. Toxicol.* **42**, 437 (2002).
5. P. Sokoloff *et al.*, *Eur. J. Pharmacol.* **225**, 331 (1992).
6. A. Holmes, J. E. Lachowicz, D. R. Sibley, *Neuropharmacology* **47**, 1117 (2004).
7. J. G. Gilbert *et al.*, *Synapse* **57**, 17 (2005).
8. M. Pilla *et al.*, *Nature* **400**, 371 (1999).
9. K. Spiller *et al.*, *Psychopharmacology (Berl.)* **196**, 533 (2008).
10. S. R. Vorel *et al.*, *J. Neurosci.* **22**, 9595 (2002).
11. Z. X. Xi *et al.*, *Neuropsychopharmacology* **31**, 1393 (2006).

12. C. A. Heidbreder, A. H. Newman, *Ann. N. Y. Acad. Sci.* **1187**, 4 (2010).
13. T. DePaulis, H. Hall, S. Ogren, *Eur. J. Med. Chem. Chim. Ther.* **20**, 273 (1985).
14. N. Griffon, C. Pilon, F. Sautel, J. C. Schwartz, P. Sokoloff, *J. Neural Transm.* **103**, 1163 (1996).
15. In Ballesteros-Weinstein numbering, a single most conserved residue among the class A GPCRs is designated x.50, where x is the transmembrane helix number. All other residues on that helix are numbered relative to this conserved position.
16. C. B. Roth, M. A. Hanson, R. C. Stevens, *J. Mol. Biol.* **376**, 1305 (2008).
17. D. M. Rosenbaum *et al.*, *Science* **318**, 1266 (2007).
18. Materials and methods are available as supporting material on *Science* online.
19. V. Cherezov *et al.*, *Science* **318**, 1258 (2007).
20. M. A. Hanson *et al.*, *Structure* **16**, 897 (2008).
21. V. P. Jaakola *et al.*, *Science* **322**, 1211 (2008).
22. T. Warne *et al.*, *Nature* **454**, 486 (2008).
23. J. M. Baldwin, *EMBO J.* **12**, 1693 (1993).
24. T. H. Ji, M. Grossmann, I. Ji, *J. Biol. Chem.* **273**, 17299 (1998).
25. A similar intraloop disulfide bond is present in the A_{2A}AR structure and likewise is thought to constrain the position of ECL3 and orients His359 at the top of the ligand binding site.
26. T. Okada *et al.*, *J. Mol. Biol.* **342**, 571 (2004).
27. K. Palczewski *et al.*, *Science* **289**, 739 (2000).
28. J. A. Ballesteros *et al.*, *J. Biol. Chem.* **276**, 29171 (2001).
29. R. Vogel *et al.*, *J. Mol. Biol.* **380**, 648 (2008).
30. R. O. Dror *et al.*, *Proc. Natl. Acad. Sci. U.S.A.* **106**, 4689 (2009).
31. E. V. Kuzhikandathil, L. Westrich, S. Bakhos, J. Pasuit, *Mol. Cell. Neurosci.* **26**, 144 (2004).
32. R. Duman, E. J. Nestler, in *Psychopharmacology: The Fourth Generation of Progress*, F. Bloom, D. Kupfer, Eds. (Raven, NY, 1995), pp. 303–320.
33. C. D. Strader *et al.*, *J. Biol. Chem.* **266**, 5 (1991).
34. M. M. Simpson *et al.*, *Mol. Pharmacol.* **56**, 1116 (1999).
35. F. Boeckler, P. Gmeiner, *Pharmacol. Ther.* **112**, 281 (2006).
36. L. Shi, J. A. Javitch, *Proc. Natl. Acad. Sci. U.S.A.* **101**, 440 (2004).
37. A. H. Newman *et al.*, *J. Med. Chem.* **52**, 2559 (2009).
38. E. Silvano *et al.*, *Mol. Pharmacol.* **78**, 925 (2010).
39. W. Guo *et al.*, *EMBO J.* **27**, 2293 (2008).
40. L. Shi, M. M. Simpson, J. A. Ballesteros, J. A. Javitch, *Biochemistry (Mosc.)* **40**, 12339 (2001).
41. G. L. Alberts, J. F. Pregenzer, W. B. Im, *Mol. Pharmacol.* **54**, 379 (1998).
42. J. A. Ballesteros, X. Deupi, M. Olivella, E. E. Haaksma, L. Pardo, *Biophys. J.* **79**, 2574 (2000).
43. This work was supported in part by Protein Structure Initiative (PSI) grant U54 GM074961 and PSI:Biology grant U54 GM094618 for structure production, NIH Roadmap grant P50 GM073197 for technology development, NIH grant R21 RR025336 (V.C.), and Pfizer. Additional support was provided by the National Institute on Drug Abuse Intramural Research Program (A.H.N.), grants DA022413 and MH54137 (J.A.J.), and grant DA023694 (L.S.). The content is solely the responsibility of the authors and does not necessarily represent the official views of the National Institute of General Medical Science or the NIH. We thank J. Velasquez for help with molecular biology, T. Trinh and K. Allin for help with baculovirus expression, D. Gray for assistance with eticlopride synthesis, M. Griffor for large-scale production of the receptor, X. Qiu for suggestions, and A. Walker for assistance with manuscript preparation. We acknowledge Y. Zheng, The Ohio State University and M. Caffrey, Trinity College (Dublin, Ireland), for the generous loan of the in meso robot (built with support from NIH grant GM075915), the National Science Foundation (grant IIS0308078), and Science Foundation Ireland (grant 02-IN1-B266); and J. Smith, R. Fischetti, and N. Sanishvili at the GM/CA-CAT beamline at the Advanced Photon Source, for assistance in development and use of the minibeam and beamtime. The GM/CA-CAT beamline (23-ID) is supported by the National Cancer Institute (grant Y1-CO-1020) and the National Institute of General Medical Sciences (grant Y1-GM-1104). Atomic coordinates and structure factors have been deposited in the Protein Data Bank with identification code 3PBL. A.H.N. is an inventor on a patent application from the National Institutes of Health that covers the use of R-22 and analogs as D3 receptor selective agents. R.C.S. is on the Board of Directors of Receptos, which does structure-directed drug discovery on GPCRs.

Supporting Online Material

www.sciencemag.org/cgi/content/full/330/6007/1091/DC1
Materials and Methods
Figs. S1 to S8
Tables S1 to S4
References

6 September 2010; accepted 21 October 2010
10.1126/science.1197410

Mcl-1 Is Essential for Germinal Center Formation and B Cell Memory

Ingela Vikstrom,[1] Sebastian Carotta,[1] Katja Lüthje,[1] Victor Peperzak,[1] Philipp J. Jost,[1] Stefan Glaser,[1] Meinrad Busslinger,[2] Philippe Bouillet,[1,3] Andreas Strasser,[1,3] Stephen L. Nutt,[1,3] David M. Tarlinton[1,3]*

Lymphocyte survival during immune responses is controlled by the relative expression of pro- and anti-apoptotic molecules, regulating the magnitude, quality, and duration of the response. We investigated the consequences of deleting genes encoding the anti-apoptotic molecules Mcl1 and Bcl2l1 (Bcl-x_L) from B cells using an inducible system synchronized with expression of activation-induced cytidine deaminase (Aicda) after immunization. This revealed Mcl1 and not Bcl2l1 to be indispensable for the formation and persistence of germinal centers (GCs). Limiting Mcl1 expression reduced the magnitude of the GC response with an equivalent, but not greater, effect on memory B cell formation and no effect on persistence. Our results identify Mcl1 as the main anti-apoptotic regulator of activated B cell survival and suggest distinct mechanisms controlling survival of GC and memory B cells.

Vertebrate immune responses are characterized by the clonal expansion of antigen-specific lymphocytes, by their differentiation into effector cells, and by the production of small, persistent populations of memory cells. An added feature of B cell immunity is the increasing affinity of the antibody response with time, with B cells expressing high-affinity antigen receptors (BCRs) preferentially recruited into the effector and memory compartments (*1*). The processes underpinning changes in affinity of immunoglobulin receptors occur within germinal centers (GCs), which are transient structures that arise after T cell–dependent immunization (*2*–*4*). Thus, the factors governing the survival of GC B cells will determine the qualitative and quantitative attributes of the effector cells—which in this case are plasma cells—and memory B cells. Survival of GC B cells is mediated by both the intrinsic and extrinsic apoptotic cell death pathways (*5*), with roles proposed for Fas ligand (CD95L)/Fas (CD95) (*6*, *7*), Bcl2l1 (Bclx_L) (*8*), Bcl2 (*9*, *10*), and Bim (*11*). These studies, however, do not identify the prosurvival molecules that are physiologically relevant within the GC.

To address the components of the intrinsic apoptotic pathway regulating GC B cell behavior, we first measured the expression of relevant proteins, comparing GC and follicular B cells (Fig. 1) (*12*). Besides Bcl2l1 and Bim expression being up-regulated and Bcl2 down-regulated as previously reported (*6*, *13*, *14*), Mcl1 protein was increased in GC B cells (Fig. 1).

Increases in Bcl2l1 and Mcl1 expression in GC B cells prompted us to examine the contribution of these prosurvival proteins to the production of memory B cells, plasma cells, and affinity maturation. We therefore conditionally deleted loxP-flanked alleles of *Bcl2l1* or *Mcl1* in B cells after antigen activation using a transgene-encoded Cre recombinase expressed concurrently with the activation-induced cytidine deaminase (*Aicda*) locus (*15*). The loxP-flanked alleles should therefore be deleted in B cells, initiating somatic hypermutation (SHM) or class-switch recombination (CSR), which are processes requiring activation-induced cytidine deaminase (AID) (*16*).

Bcl2l1$^{fl/-}$*Aicda*-Cre mice, with one *Bcl2l1* allele deleted (*17*) and one flanked by LoxP (fl) sites (*18*), were immunized with a T cell–dependent antigen composed of the 4-hydroxy-3-nitrophenyl (NP) hapten conjugated to keyhole limpet hemocyanin (NP-KLH). Cellular responses were analyzed 21 days later in *Bcl2l1*$^{fl/-}$*Aicda*-Cre and control mice, when GC and memory B cells coexist (*6*, *19*). No significant difference in the frequency or number of antigen-specific (NP^+IgG1^+) B cells was observed in the spleens of *Bcl2l1*$^{fl/-}$*Aicda*-Cre mice as compared with controls, both in total and after subdivision into GC ($CD38^-$) and memory ($CD38^+$) compartments (Fig. 2, A and B). Similarly, no differences were seen 7 and 14 days after immunization, excluding the possibility of an early deficit being masked by compensation as

[1]Walter and Eliza Hall Institute of Medical Research, 1G Royal Parade, Parkville, Victoria 3052, Australia. [2]Research Institute of Molecular Pathology, Vienna Biocenter, Dr. Bohr-Gasse 7, A-1030 Vienna, Austria. [3]Department of Medical Biology, University of Melbourne, Parkville, Victoria 3050, Australia.

*To whom correspondence should be addressed. E-mail: tarlinto@wehi.edu.au

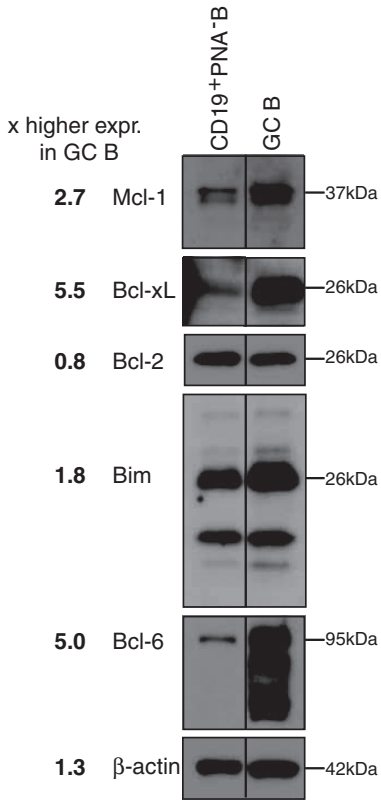

Fig. 1. Expression of anti- and pro-apoptotic proteins in GC B cells. Shown are immunoblots of lysates from sorted CD19$^+$PNA$^-$ follicular B cells and CD19$^+$PNA$^+$ germinal center B (GC B) cells. The presence and absence of Bcl6 was used to ascertain the efficiency of cell sorting. Blots were probed with antibodies to Mcl1, Bcl2l1, Bcl2, Bim, Bcl6, and β-actin. Intensities are expressed as fold change relative to follicular B cells. Values from one of two independent experiments are shown. Duplicate lanes were removed from the original image, with the solid line indicating the point of rejoining.

the response progressed (fig. S1). Immunofluorescent staining of spleen sections confirmed the presence of physical GC (Fig. 2C). Other explanations for a lack of difference, such as incomplete deletion or a failure to appropriately express the Cre recombinase, were excluded (figs. S2 and S3). Conditional deletion of *Bcl2l1* did, however, affect the bone marrow plasma cell compartment, which is itself a product of the GC (*20*, *21*). Although the representation of NP-specific immunoglobulin G1 (IgG1) antibody secreting cells (ASCs) in the spleen was normal at day 21, the frequency in bone marrow was reduced (Fig. 2D)—a difference that was significant at 14 days after immunization (fig. S4A). Consistent with this, serum titers of antibody-to-NP IgG1 in *Bcl2l1*$^{fl/-}$*Aicda*-Cre mice at day 21 were significantly diminished as compared with those of controls (fig. S4B). Collectively, these results demonstrate that Bcl2l1 is dispensable for GC formation, the expansion of antigen-specific B cells, and the formation of B cell memory but functions in establishing or maintaining emigrant populations of ASC (*22*).

Mcl1 was another candidate for the mediation of B cell survival within GC (Fig. 1). Although Mcl1 and Bcl2l1 function in the same apoptotic pathway (*23*), they differ substantially in their ability to bind members of the pro-apoptotic

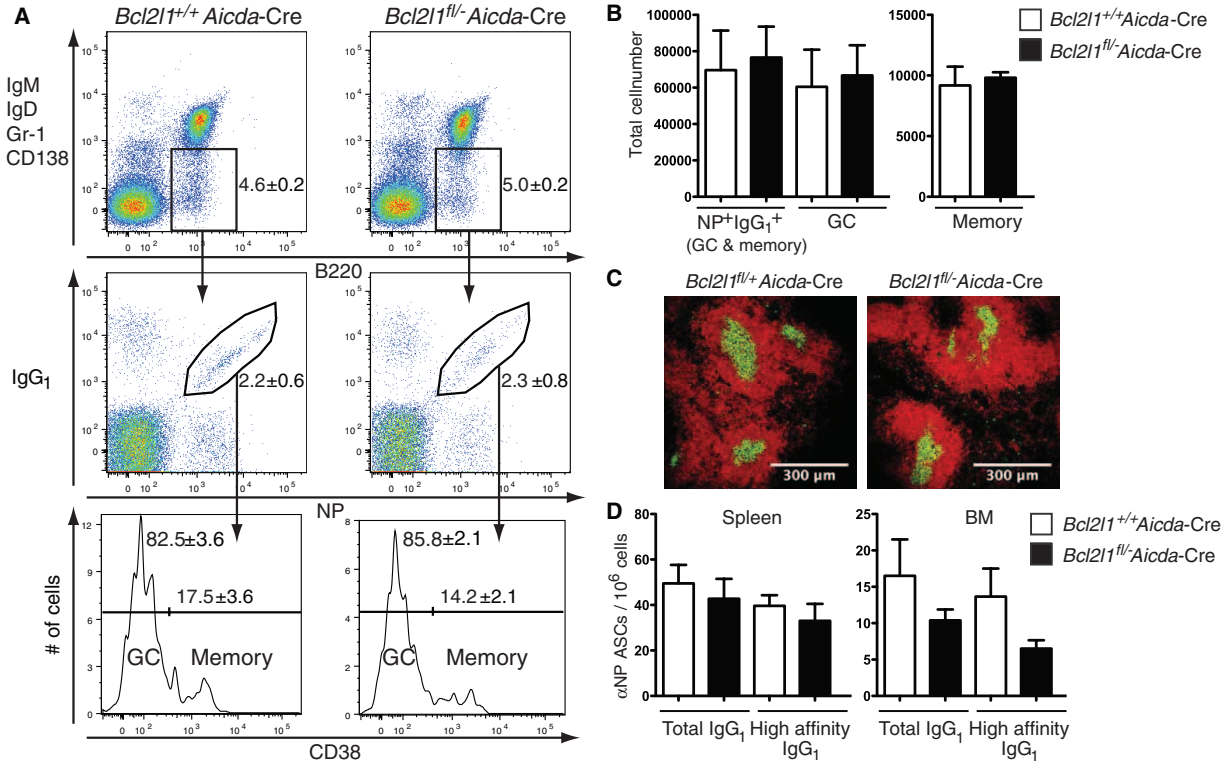

Fig. 2. Bcl2l1 is dispensable for GC formation and the subsequent development of NP-specific IgG1 B cells and memory B cells. (**A**) Flow cytometric analysis of splenocytes day 21 after intraperitoneal immunization with NP-KLH in alum. Isotype-switched B cells (IgM$^-$ IgD$^-$ Gr-1$^-$CD138$^-$ B220$^+$) were analyzed for NP$^+$IgG1$^+$ status with NP$^+$IgG1$^+$ cells being subdivided into GC (CD38$^-$) and memory (CD38$^+$) B cells. Numbers in plots and histograms represent mean percentage ± SEM of all mice examined. (**B**) Absolute cell numbers of the populations identified in (A) are graphed as mean ± SEM of between four and six mice in each group and summarize two experiments. (**C**) Frozen spleen sections from *Bcl2l1*$^{fl/+}$*Aicda*-Cre and *Bcl2l1*$^{fl/-}$*Aicda*-Cre mice, 14 days after immunization, stained with antibodies to B220 to identify follicles (red) and GL7 for germinal centers (green). Original magnification is ×20 with scale indicated. (**D**) Frequencies of total and high-affinity NP-specific IgG1-secreting ASCs in spleen and bone marrow. Data are the mean ± SEM of replicate wells, with between four and six mice in each group, and summarize two experiments.

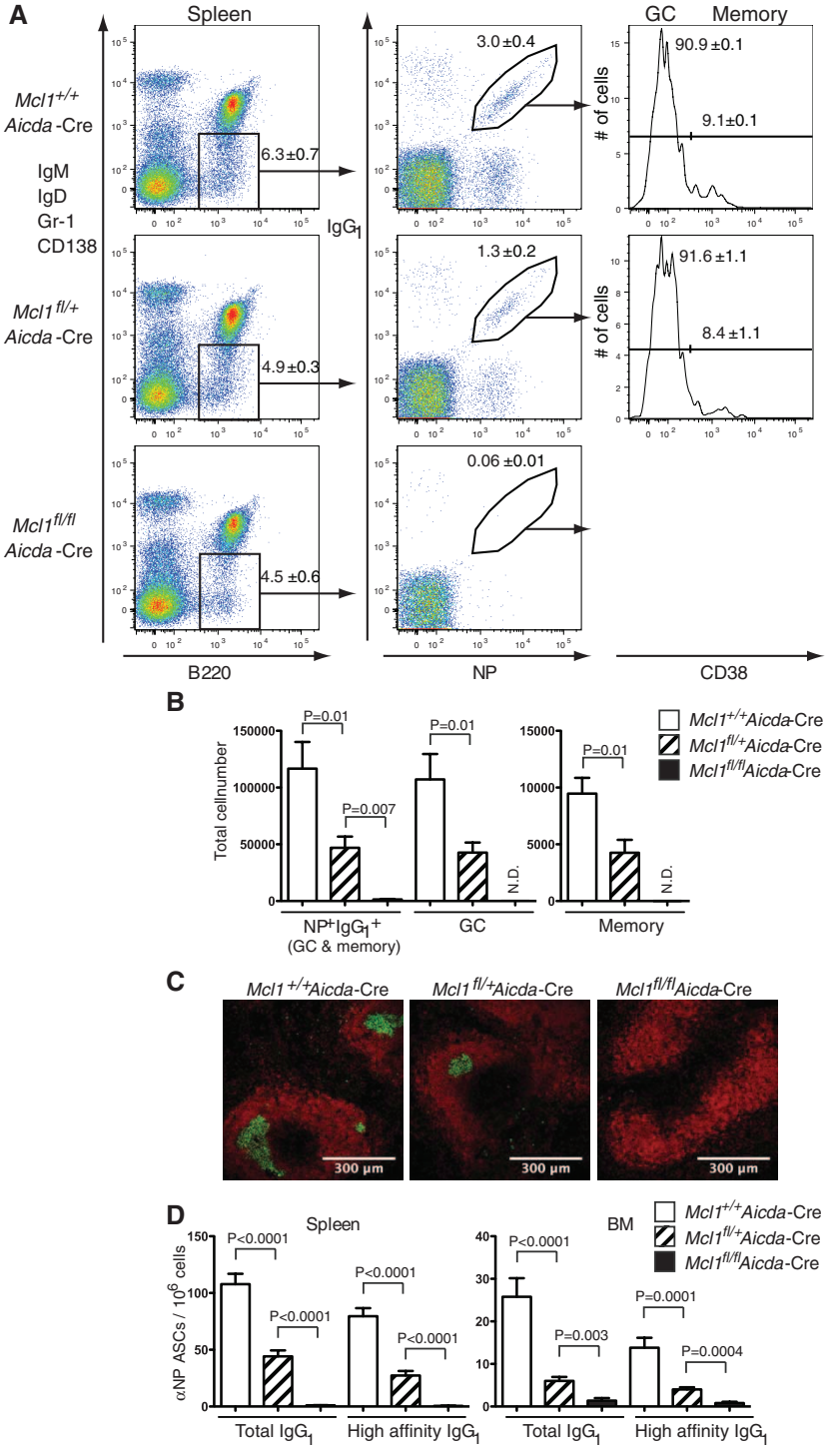

Fig. 3. Conditional deletion of *Mcl1* abrogates the GC response and the formation of NP-specific memory B cells. (**A**) Flow cytometric analysis of splenocytes 14 days after intraperitoneal immunization with NP-KLH in alum. Isotype-switched B cells (IgM$^-$IgD$^-$Gr-1$^-$CD138$^-$ B220$^+$) were analyzed for NP$^+$IgG1$^+$ status. NP$^+$IgG1$^+$ cells were further subdivided into GC (CD38$^-$) or memory (CD38$^+$) B cells. Numbers in dotplots and histograms represent mean percentage ± SEM of all mice examined. (**B**) Absolute cell numbers of the populations identified in (A) are shown in the graphs as the mean ± SEM of between five and 10 mice in each group, summarizing four experiments. (**C**) Frozen spleen sections from *Mcl1*$^{+/+}$*Aicda*-Cre, *Mcl1*$^{fl/+}$*Aicda*-Cre, and *Mcl1*$^{fl/fl}$*Aicda*-Cre mice, 14 days after immunization, stained with antibodies to B220 to show B cell follicles (red) and GL7 to show germinal centers (green). Original magnification is ×20, with scale indicated. (**D**) Frequencies of total and high-affinity NP-specific IgG1 ASCs in spleen and bone marrow. Data are the mean ± SEM of replicate wells from between five and 10 mice in each group and summarize four experiments. Significant differences in (B) and (D), determined with Student's *t* test, are indicated.

BH3-only and Bax/Bak-like proteins (*24*) and could thus have distinct roles. We therefore generated mice with *Mcl1* alleles flanked by LoxP sites (*25*) and carrying the *Aicda*-Cre transgene (*15*). Analysis of spleens of *Mcl1*$^{fl/fl}$*Aicda*-Cre mice 14 days after immunization revealed the absence of NP$^+$IgG1$^+$ B cells when both alleles of *Mcl1* were conditionally deleted, whereas deleting one *Mcl1* allele produced a partial reduction in antigen-specific B cells, with the GC and memory compartments affected equally (Fig. 3, A and B). Thus, Mcl1 is essential for the generation of antigen-specific IgG1 B cells and appears to be a limiting determinant in the magnitude of the GC response. Moreover, GC could not be observed with histology in the spleens of immunized *Mcl1*$^{fl/fl}$*Aicda*-Cre mice, and those seen in *Mcl1*$^{fl/+}$*Aicda*-Cre mice were reduced in size and frequency (Fig. 3C). The frequency of NP-specific IgG1 ASC in both spleen and bone marrow was severely diminished in homozygous *Mcl1*-deleted mice with a corresponding reduction in heterozygous *Mcl1*-deleted mice (Fig. 3D). Serum titers of antibody-to-NP IgG1, but not IgM, were correspondingly and significantly reduced (fig. S5). To determine when Mcl1 became critical for the survival of activated B cells, we examined *Mcl1*$^{fl/fl}$*Aicda*-Cre mice on day 5 (fig. S6) and day 7 (fig. S7) after immunization with NP-KLH in alum. Although an immune response was detected at both times, no antigen-specific, isotype-switched, or GC phenotype B cells were detected in the *Mcl1*$^{fl/fl}$*Aicda*-Cre mice, indicating that the dependence on Mcl1 precedes GC formation.

The effects of Mcl1 deletion in GC formation extended beyond the NP response because the number of GC-phenotype B cells (CD19$^+$PNA$^+$IgD^{lo}) in *Mcl1*$^{fl/+}$*Aicda*-Cre mice was reduced, and in *Mcl-1*$^{fl/fl}$*Aicda*-Cre mice, no hCD2t$^+$ (and therefore Cre-expressing) GC B cells were found (fig. S8, A and B). Furthermore, analysis of Peyer's patches in the *Mcl1* strains revealed the absence of GC-phenotype B cells in *Mcl-1*$^{fl/fl}$*Aicda*-Cre mice and their reduction in *Mcl1*$^{fl/+}$*Aicda*-Cre mice compared with controls (fig. S8C), emphasizing the generality of the requirement for Mcl1 in GC formation. The conditional *Mcl1* allele was constructed so that after deletion of *Mcl1*, hCD4 is expressed on the cell surface under the control of the *Mcl1* regulatory elements, serving as a reporter of *Mcl1* deletion and *Mcl1* expression (fig. S9). The persisting GC and memory B cells in *Mcl1*$^{fl/+}$ *Aicda*-Cre mice were all hCD4$^+$ and had thus deleted one allele of *Mcl1* (fig. S10).

The reduced number of NP$^+$IgG1$^+$ cells in *Mcl1*$^{fl/+}$*Aicda*-Cre mice compared with controls revealed a relationship between the *Mcl1* gene dosage and the survival of antigen-reactive B cells, suggesting that amounts of Mcl1 could underpin B cell competition within the GC or affect persistence in the memory B cell compartment. To determine whether this was the case, lethally irradiated Ly5.1 recipients were reconstituted with an equal mixture of bone marrow from

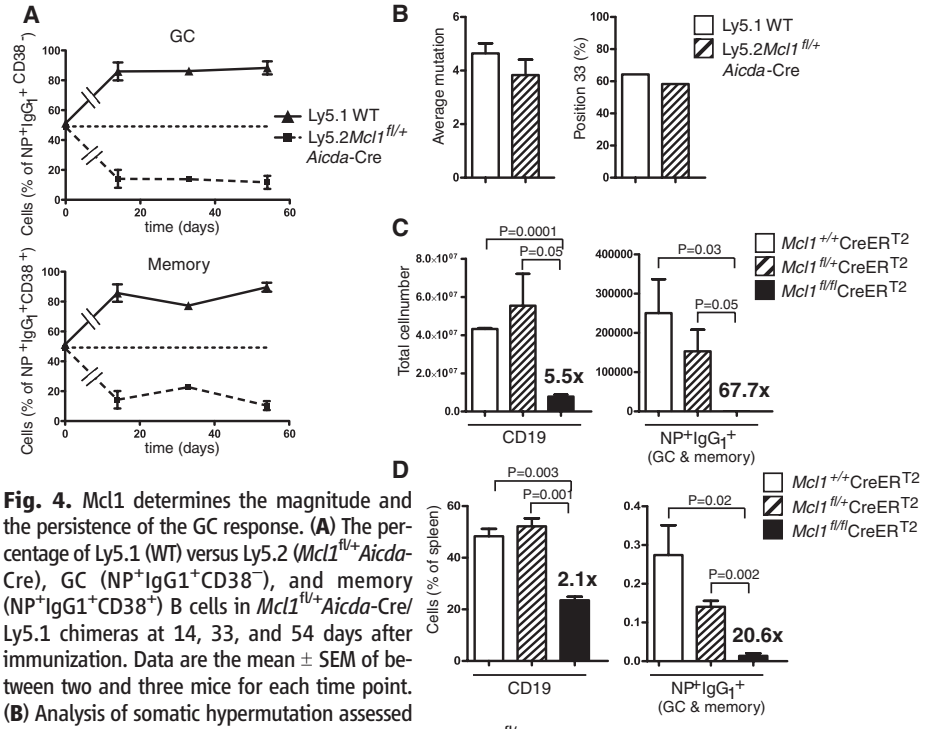

Fig. 4. Mcl1 determines the magnitude and the persistence of the GC response. (**A**) The percentage of Ly5.1 (WT) versus Ly5.2 (*Mcl1*$^{fl/+}$*Aicda*-Cre), GC (NP$^+$IgG1$^+$CD38$^-$), and memory (NP$^+$IgG1$^+$CD38$^+$) B cells in *Mcl1*$^{fl/+}$*Aicda*-Cre/Ly5.1 chimeras at 14, 33, and 54 days after immunization. Data are the mean ± SEM of between two and three mice for each time point. (**B**) Analysis of somatic hypermutation assessed by comparing the V_H186.2 genes of single NP$^+$IgG$_1^+$ *Mcl1*$^{fl/+}$*Aicda*-Cre B cells with those in Ly5.1 control B cells, sorted 14 days after immunization of the chimeric mice described in (A). Average mutation per V_H186.2 gene segment compares the region encoding amino acids 10 to 96 with the germline sequence from 12 *Mcl1*$^{fl/-}$ NP$^+$IgG$_1^+$ B cells and 14 control cells. Position 33 (percent) measures the frequency of the Trp-to-Leu exchange within CDR1 of V_H186.2 that alone confers a 10-fold increase in affinity of binding NP (*35*). (**C**) Absolute number of B cells and NP$^+$IgG1$^+$ B cells after Tamoxifen treatment of chimeric mice in which Mcl1 is amenable to deletion only in B cells. Mice, immunized with NP-KLH in alum intraperitoneally, were treated with Tamoxifen on days 7 and 8 and analyzed on day 9 for B cells (CD19$^+$) and NP$^+$IgG1$^+$ cells among isotype-switched B cells (IgM$^-$IgD$^-$Gr-1$^-$CD138$^-$ B220$^+$). Status of the *Mcl1* alleles in B cells is indicated. (**D**) Proportion of B cells (CD19$^+$) and NP$^+$IgG1$^+$ B cells in the spleens of the mice described in (C). Fold changes between the indicated B cell compartments in Tamoxifen-treated *Mcl1*$^{+/+}$ and *Mcl1*$^{fl/fl}$ mice are shown. Significant differences in (C) and (D), determined with Student's *t* test, are indicated.

Mcl1$^{fl/+}$*Aicda*-Cre (Ly5.2) and WT (Ly5.1) mice and were then immunized with NP-KLH in alum and analyzed 14, 33, and 54 days later. The representation of antigen-reactive B cells with one allele of *Mcl1* deleted upon activation (Ly5.2) was reduced significantly in day 14 GC as compared with parity in the naïve B cell populations and remained constant thereafter (Fig. 4A), which suggested a disadvantage in initiation but not persistence. The decreased representation of *Mcl1*$^{fl/+}$ B cells within the GC was reflected in an identical fold reduction among memory B cells at all time points measured (Fig. 4A and fig. S11), suggesting that entry into and persistence within the GC-derived memory compartment are not influenced by amounts of Mcl1. Other routes of memory B cell formation may have distinct survival requirements (*26*).

It was possible that GC B cells lacking either Bcl2l1 or Mcl1 had compensated for a survival disadvantage by acquiring higher-than-normal affinity, permitting their persistence in the plasma cell and memory B cell compartments. Affinity amongst antigen-specific ASC, measured by using the ratio of high affinity:total binding (*21*, *27*), was unaffected in both cases (fig. S12, A and B), indicating no change in selection into this compartment. Affinity among NP memory B cells was determined by means of sequence analysis of the immunoglobulin V_H186.2 genes (*28*, *29*). The distribution, frequency, and nature of somatic mutations in the V_H186.2 genes (*28*, *29*) of sorted, single NP$^+$IgG1$^+$CD38^{hi} memory B cells 21 days after immunization of *Bcl2l1*$^{fl/+}$*Aicda*-Cre mice were similar to controls (fig. S12C). The same analysis of NP$^+$IgG1$^+$ B cells from *Mcl1*$^{fl/+}$*Aicda*-Cre (Ly5.2) and WT (Ly5.1) chimeric mice, 14 days after immunization, also revealed no differences in distribution or frequency of somatic mutations (Fig. 4B), indicating that there was no compensation for reduced Mcl1 protein in GC B cells through enhanced selection.

Lastly, we examined whether survival of GC B cells after formation also required Mcl1. We created groups of mice through bone marrow reconstitution in which B cells were *Mcl1*$^{fl/fl}$, *Mcl1*$^{fl/+}$, or *Mcl1*$^{+/+}$, in each case with *Rosa26*-CreER^{T2} (fig. S13). Deletion of *Mcl1* in these mice was thus Tamoxifen (Tam)–inducible and restricted to B cells. These mice were immunized with NP-KLH in alum, treated with Tam on days 7 and 8, and analyzed on day 9 for the presence of NP$^+$IgG1$^+$ B cells. Relative to *Rosa26*-CreER^{T2} controls, NP$^+$IgG1$^+$ cells were deleted from the *Mcl1*$^{fl/fl}$ *Rosa26*-CreER^{T2} B cell group and reduced in the Mcl1$^{fl/+}$ *Rosa26*-CreER^{T2} group (Fig. 4, C and D). Although Tam treatment of *Mcl1*$^{fl/fl}$ Cre-ErT2 mice affected the survival of naïve B cells in spleen (fig. S13), reducing their number by greater than a factor of five, the reduction of NP$^+$IgG1$^+$ B cells was considerably greater, with 1/68 that of the controls remaining (Fig. 4, C and D). The 50% reduction in frequency of NP$^+$IgG1$^+$ B cells in the spleens of Tam-treated *Mcl1*$^{fl/+}$ Cre-ErT2 mice in the context of no change in overall B cell representation (Fig. 4D) emphasizes the sensitivity of GC B cells to changes in amounts of Mcl1. Immunohistology of the spleens of the Tam-treated immunized mice revealed IgM$^+$ blasts as clusters in control spleens but only as rare, single cells in spleens from *Mcl1*$^{fl/fl}$ *Rosa26*-CreER^{T2} mice (fig. S14), indicating that the survival of activated, unswitched B cells also depends on Mcl1. Thus, in addition to a role in naïve B cells (*30*), Mcl1 is required for the survival of activated B cells, for the formation of GC, and for the persistence of GC once established.

Differential cell survival is central to regulating the quality and quantity of lymphocyte responses to antigen (*31*, *32*). Previous experiments modulating expression of Bcl-2 family member proteins in B cells (*6*, *9*–*11*) led to models of GC function in which affinity for antigen enhances B cell survival and therefore representation through modulation of those Bcl-2 family member proteins (*31*, *32*). The data presented here show unequivocally that Mcl-1 has a distinct role in maintaining antigen-reactive B cells after their initial exposure and then within the GC. This dependency of GC B cells on Mcl1 is distinguished from that of naïve B cells by two features. First, the sensitivity of GC B cells to reduced amounts of Mcl1 is greater than that of naïve B cells. Second, compounds that specifically antagonize Bcl2 and Bcl2l1 (*33*) diminish naïve B cells in spleen but leave GC B cells unaffected (*22*), which is a result complementary to the data presented here. These results, showing that particular prosurvival proteins can become limiting at particular stages of immune responses, are further exemplified by the differential sensitivity of post-GC plasma cells to altered Bcl2 and Bcl2l1 (*22*); these cells are sensitive en route but resistant once established in their survival niches in the bone marrow (*20*, *22*). Collectively, our results challenge the current view of what regulates GC survival, offer insights into the formation and maintenance of B cell memory, and also suggest Mcl1 as a potential target in GC-derived lymphomas that do not overexpress *Bcl2l1* (*34*).

References and Notes

1. K. Rajewsky, *Nature* **381**, 751 (1996).
2. A. M. Haberman, M. J. Shlomchik, *Nat. Rev. Immunol.* **3**, 757 (2003).

3. A. Lanzavecchia, F. Sallusto, *Nat. Rev. Immunol.* **2**, 982 (2002).
4. I. C. MacLennan, *Annu. Rev. Immunol.* **12**, 117 (1994).
5. A. Strasser, P. J. Jost, S. Nagata, *Immunity* **30**, 180 (2009).
6. Y. Takahashi, H. Ohta, T. Takemori, *Immunity* **14**, 181 (2001).
7. Z. Hao *et al.*, *Immunity* **29**, 615 (2008).
8. Y. Takahashi *et al.*, *J. Exp. Med.* **190**, 399 (1999).
9. K. G. Smith, U. Weiss, K. Rajewsky, G. J. Nossal, D. M. Tarlinton, *Immunity* **1**, 803 (1994).
10. K. G. Smith *et al.*, *J. Exp. Med.* **191**, 475 (2000).
11. S. F. Fischer *et al.*, *Blood* **110**, 3978 (2007).
12. Materials and methods are available as supporting material on *Science* Online.
13. U. Klein *et al.*, *Proc. Natl. Acad. Sci. U.S.A.* **100**, 2639 (2003).
14. T. Yokoyama *et al.*, *Immunol. Lett.* **81**, 107 (2002).
15. K. Kwon *et al.*, *Immunity* **28**, 751 (2008).
16. M. Muramatsu *et al.*, *Cell* **102**, 553 (2000).
17. N. Motoyama *et al.*, *Science* **267**, 1506 (1995).
18. K. U. Wagner *et al.*, *Development* **127**, 4949 (2000).
19. A. Ridderstad, D. M. Tarlinton, *J. Immunol.* **160**, 4688 (1998).
20. A. Radbruch *et al.*, *Nat. Rev. Immunol.* **6**, 741 (2006).
21. K. G. Smith, A. Light, G. J. Nossal, D. M. Tarlinton, *EMBO J.* **16**, 2996 (1997).
22. E. M. Carrington *et al.*, *Proc. Natl. Acad. Sci. U.S.A.* **107**, 10967 (2010).
23. J. M. Adams, S. Cory, *Oncogene* **26**, 1324 (2007).
24. L. Chen *et al.*, *Mol. Cell* **17**, 393 (2005).
25. S. N. Willis *et al.*, *Science* **315**, 856 (2007).
26. H. Toyama *et al.*, *Immunity* **17**, 329 (2002).
27. J. Roes, K. Rajewsky, *J. Exp. Med.* **177**, 45 (1993).
28. D. Allen, T. Simon, F. Sablitzky, K. Rajewsky, A. Cumano, *EMBO J.* **7**, 1995 (1988).
29. A. Cumano, K. Rajewsky, *EMBO J.* **5**, 2459 (1986).
30. J. T. Opferman *et al.*, *Nature* **426**, 671 (2003).
31. C. D. Allen, T. Okada, J. G. Cyster, *Immunity* **27**, 190 (2007).
32. D. Tarlinton, *Nat. Rev. Immunol.* **6**, 785 (2006).
33. T. Oltersdorf *et al.*, *Nature* **435**, 677 (2005).
34. J. H. Cho-Vega *et al.*, *Hum. Pathol.* **35**, 1095 (2004).
35. D. Allen *et al.*, *Immunol. Rev.* **96**, 5 (1987).

36. This work was supported in part by grants from the National Health and Medical Research Council (NHMRC) Australia (356202 to D.M.T. and S.L.N. and 461221 to P.B. and A.S.), the Leukemia and Lymphoma Society (SCOR grant 7413), and the NIH (CA43540 and CA80188). D.M.T. and A.S. are supported by fellowships from the NHMRC; S.L.N. by a Pfizer Australia Research Fellowship; I.V. by the Olle Engkvist Byggmastare and Wenner-Gren Foundations; K.L. by a fellowship from the German Academic Exchange Service; P.B. by the Charles and Sylvia Viertel Charitable Foundation; and M.B. by Boehringer Ingelheim. DNA sequence data are available in GenBank (accession number HM804028-HM804084). We are indebted to the facilities of our respective institutes, particularly those responsible for animal husbandry and flow cytometry. We also acknowledge the assistance of L. O'Reilly for Western blot antibodies and the many helpful discussions with members of the Walter and Eliza Hall Institute B Cell Program. Author contributions are as follows: I.V. and D.M.T. designed the research; I.V., K.L., S.G., V.P., S.C., and P.J. performed experiments and contributed to interpretation and discussion; M.B., P.B., A.S., and S.L.N. contributed to the design of experiments, interpretation of results, and drafting the manuscript; I.V., K.L., and V.P. analyzed data and prepared figures; and I.V. and D.M.T. wrote the manuscript.

Supporting Online Material

www.sciencemag.org/cgi/content/full/science.1191793/DC1
Materials and Methods
SOM Text
Figs. S1 to S14
References

3 May 2010; accepted 7 September 2010
Published online 7 October 2010;
10.1126/science.1191793

Interdependence of Cell Growth and Gene Expression: Origins and Consequences

Matthew Scott,[1]*† Carl W. Gunderson,[2]* Eduard M. Mateescu,[1] Zhongge Zhang,[2] Terence Hwa[1,2]‡

In bacteria, the rate of cell proliferation and the level of gene expression are intimately intertwined. Elucidating these relations is important both for understanding the physiological functions of endogenous genetic circuits and for designing robust synthetic systems. We describe a phenomenological study that reveals intrinsic constraints governing the allocation of resources toward protein synthesis and other aspects of cell growth. A theory incorporating these constraints can accurately predict how cell proliferation and gene expression affect one another, quantitatively accounting for the effect of translation-inhibiting antibiotics on gene expression and the effect of gratuitous protein expression on cell growth. The use of such empirical relations, analogous to phenomenological laws, may facilitate our understanding and manipulation of complex biological systems before underlying regulatory circuits are elucidated.

Systems biology is as an integrative approach to connect molecular-level mechanisms to cell-level behavior (*1*). Many studies have characterized the impact of molecular circuits and networks on cellular physiology (*1*, *2*), but less is known about the impact of cellular physiology on the functions of molecular networks (*3*–*5*). Endogenous and synthetic genetic circuits can be strongly affected by the physiological states of the organism, resulting in unpredictable outcomes (*4*, *6*–*8*). Consequently, both the understanding and implementation of molecular control are predicated on distinguishing global physiological constraints from specific regulatory interactions.

For bacterial cells under steady-state exponential growth, the rate of cell proliferation (the "growth rate") is an important characteristic of the physiological state. It is well known that the macromolecular composition (e.g., the mass fractions of protein, RNA, and DNA) of bacterial cells under exponential growth depends on the growth medium predominantly through the growth rate allowed by the nutritional content of the medium (*9*, *10*). Such growth rate dependencies inevitably affect the expression of individual genes (*4*, *11*) because protein synthesis is directly dependent on the cell's ribosome content. The latter is reflected by the RNA/protein ratio. In *Escherichia coli*, most of the RNA (~85%) is rRNA folded in ribosomes (*10*, *11*). A predictive understanding of the impact of growth physiology on gene expression therefore first requires an understanding of the cell's allocation of cellular resources to ribosome synthesis (manifested by the RNA/protein ratio) at different growth rates.

For exponentially growing *E. coli* cells (*10*, *12*), the RNA/protein ratio r is linearly correlated with the specific growth rate λ [= (ln 2)/doubling time] (Fig. 1A). The correlation is described mathematically as

$$r = r_0 + \frac{\lambda}{\kappa_t} \quad (1)$$

where r_0 is the vertical intercept and κ_t is the inverse of the slope (table S1). This linear correlation holds for various *E. coli* strains growing in medium that supports fast to moderately slow growth [e.g., 20 min to ~2 hours per doubling (*11*)], and it appears to be quite universal; similar linear correlations have been observed in many other microbes, including slow-growing unicellular eukaryotes (fig. S1). As suggested long ago from mass-balance considerations (*11*) and elaborated in (*13*), this linear correlation is expected if the ribosomes are growth-limiting and are engaged in translation at a constant rate, with the phenomenological parameter κ_t predicted to be proportional to the rate of protein synthesis. Consistent with the prediction, data on RNA/protein ratios from slow-translation mutants of *E. coli* K-12 (triangles in Fig. 1B) also exhibited linear correlations with the growth rate λ, but with steeper slopes than the parent strain (circles), which have smaller κ_t. Moreover, the corresponding κ_t values correlated linearly with the directly measured speed of translational elongation (*14*) (Fig. 1B, inset). Consequently, we call κ_t the "translational capacity" of the organism.

Translation can be inhibited in a graded manner by exposing cells to sublethal doses of a translation-inhibiting antibiotic. The RNA/protein ratios obtained for wild-type cells grown in medium with a fixed nutrient source and various

[1]Center for Theoretical Biological Physics, Department of Physics, University of California, San Diego, La Jolla, CA 92093, USA. [2]Section of Molecular Biology, Division of Biological Sciences, University of California, San Diego, La Jolla, CA 92093, USA.

*These authors contributed equally to this work.
†Present address: Department of Applied Mathematics, University of Waterloo, Waterloo, Ontario N2L 3G1, Canada.
‡To whom correspondence should be addressed. E-mail: hwa@ucsd.edu

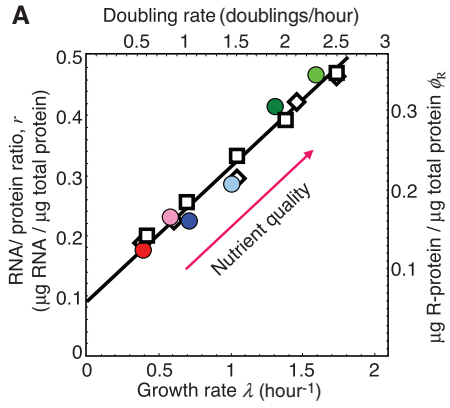

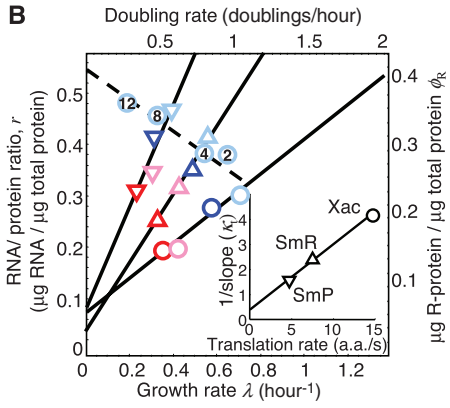

Strain / Medium	EQ2	Xac	SmR	SmP	Xac in cAA+glc Cm conc. (μM)	
M63+glyc	●	○	△	▽	2	2
M63+gluc	●	○	△	▽	4	4
cAA+glyc	●	○	△	▽	8	8
cAA+gluc	●	○	△	▽	12	12
RDM+glyc	●	Historical data: □ Strain B/r; Ref. (*10*) ◇ Strain 15τ-bar; Ref. (*12*)				
RDM+gluc	●					

Fig. 1. Correlation of the RNA/protein ratio r with growth rate λ for various strains of *E. coli*. (**A**) Comparison among *E. coli* strains grown in minimal medium: Strain B/r [(*10*), squares], 15τ-bar [(*12*), diamonds], and EQ2 (this work, solid circles). The growth rate is modulated by changing the quality of nutrients as indicated in the key at lower left. The fraction of total protein devoted to ribosome-affiliated proteins (ϕ_R) is given by the RNA/protein ratio as $\phi_R = \rho \cdot r$ (table S1). (**B**) The RNA/protein ratio for a family of translational mutants SmR (triangles) and SmP (inverted triangles) and their parent strain Xac (circles) (*27*), grown with various nutrients (see key at lower left) (table S2). Translational inhibition of the parent Xac strain via exposure to sublethal doses of chloramphenicol (circled numbers; see legend table) gave RNA/protein ratios similar to those of the mutant strains grown in medium with the same nutrient but without chloramphenicol (light blue symbols). Dashed line is a fit to Eq. 2. Inset: Linear correlation of κ_t values obtained for the Xac, SmR, and SmP strains (table S2) with the measured translation rate of the respective strains (*14*) ($r^2 = 0.99$).

amounts of chloramphenicol (Fig. 1B, light blue circles) were consistent with data obtained for the isogenic translational mutants grown in medium with the same nutrient but no antibiotic (light blue triangles). Surprisingly, these data revealed another linear correlation between r and λ (Fig. 1B, dashed line), given by

$$r = r_{max} - \frac{\lambda}{\kappa_n} \qquad (2)$$

where r_{max} is the vertical intercept and κ_n is the inverse slope. Such a linear correlation was obtained for cells grown with each of the six nutrient sources studied (Fig. 2A and table S3). The correlation described by Eq. 2 has been observed in cells subjected to numerous other means of imposing translational limitation (fig. S2).

From Fig. 2A and the best-fit values of the parameters r_{max} and κ_n (table S4), we observed that the parameter κ_n exhibited a strong, positive correlation with the growth rate of cells in drug-free medium (fig. S3A). Thus, κ_n reflects the nutrient quality and is referred to as the "nutritional capacity" of the organism in a medium [see eq. S18 in (*13*) for a molecular interpretation of κ_n]. In contrast, the vertical intercept r_{max} depended only weakly on the composition of the growth medium (fig. S3B). Qualitatively, the increase of the RNA/protein ratio r with increasing degree of translational inhibition can be seen as a compensation for the reduced translational capacity, implemented possibly through the relief of repression of rRNA synthesis by the alarmone ppGpp (*15*), in response to the buildup of intracellular amino acid pools resulting from slow translation. Because r_{max} is the (extrapolated) maximal RNA/protein ratio as translation capacity is reduced toward zero, its weak dependence on the quality of the nutrients suggests a common

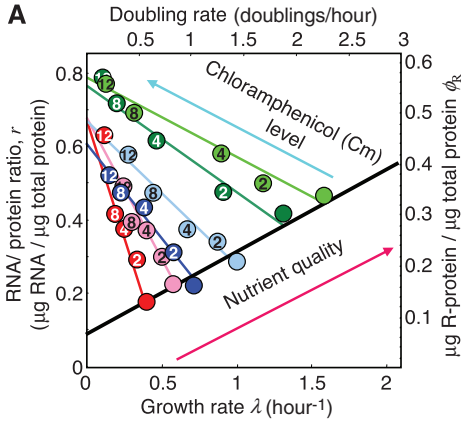

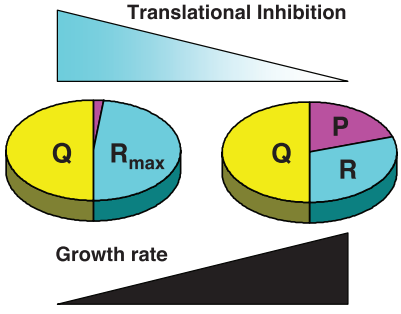

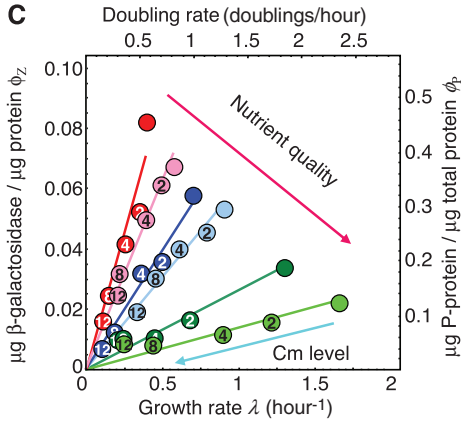

Strain / Medium	EQ2/EQ3 Chloramphenicol conc. (μM) 0	2	4	8	12
M63+glyc	●	2	4	8	12
M63+gluc	●	2	4	8	12
cAA+glyc	●	2	4	8	12
cAA+gluc	●	2	4	8	12
RDM+glyc	●	2	4	8	12
RDM+gluc	●	2	4	8	12

Fig. 2. Effect of translational inhibition. (**A**) RNA/protein ratio for strain EQ2 grown in different media, each with various levels of chloramphenicol (see key at lower right) (table S3). Solid lines were obtained from fitting data of the same color to Eq. 2. The black line describes the data in the absence of chloramphenicol (as in Fig. 1A). (**B**) Translational inhibition results in an increased synthesis of R-class proteins (cyan), effectively decreasing the fraction allocable to the P-class (magenta). (**C**) Mass fraction of constitutively expressed β-galactosidase (strain EQ3) plotted as a function of growth rate. The lines were fit according to Eq. 4. The growth rate dependence of constitutive gene expression due to nutrient limitation found in (*4*) is also well described by the theory (fig. S5C).

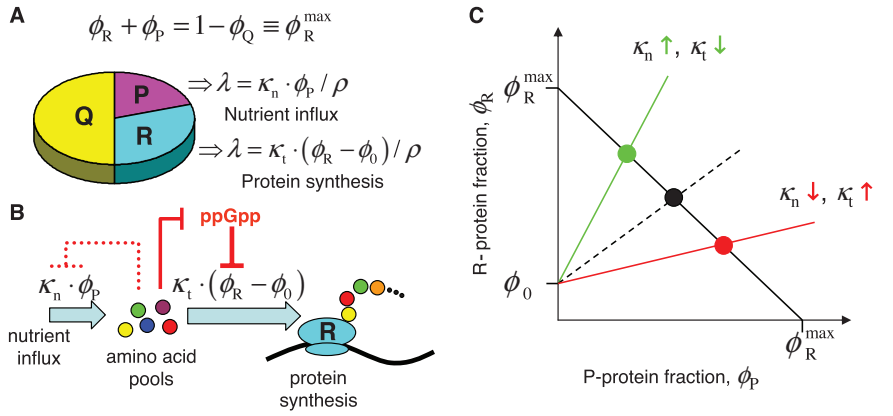

Fig. 3. A phenomenological theory of bacterial growth. (**A**) The growth theory comprises three key ingredients: (i) a three-component partition of the proteome, consisting of a fixed core sector (Q) and two adjustable sectors (R and P) whose fractions (ϕ_R and ϕ_P) must add up to a constant ($\phi_R^{max} = 1 - \phi_Q$); (ii) a ribosomal fraction ϕ_R containing all the ribosomal proteins and their affiliates and exerting a positive effect on growth (with growth rate $\lambda \propto \phi_R - \phi_0$, where $\phi_0 = \rho \cdot r_0$ corresponds to the vertical intercept in Fig. 1A); (iii) a remaining fraction ϕ_P exerting a similarly positive effect on growth (with growth rate $\lambda \propto \phi_P$) by providing an influx of nutrients (*13*). (**B**) During steady-state exponential growth, efficient resource allocation requires that the nutrient influx ($\kappa_n \cdot \phi_P$) be flux-matched to the amino acid outflux $\kappa_t \cdot (\phi_R - \phi_0)$. This can be coordinated by ppGpp, which up-regulates ribosome synthesis and hence amino acid outflux in response to increase in the amino acid pools, and has the opposite effect (down-regulating ribosome synthesis and hence amino acid outflux) in response to decrease in the amino acid pools (*15*). Changes in ϕ_R also indirectly regulate nutrient influx through the constraint of Eq. 3, in addition to direct regulatory mechanisms (dashed line). (**C**) Balancing the demands of protein synthesis and nutrient influx leads to the constraint $(\phi_R - \phi_0)/\phi_P = \kappa_n/\kappa_t$, sketched as the dashed black line. The other constraint (Eq. 3) is shown as the solid black line. The unique combination (ϕ_P, ϕ_R) satisfying both constraints is shown as the solid black circle. Upon increasing κ_n and/or decreasing κ_t, ϕ_R needs to be increased and ϕ_P decreased to maintain the balance (green line and circle), whereas with decreasing κ_n and/or increasing κ_t, ϕ_P needs to be increased and ϕ_R decreased (red line and symbols).

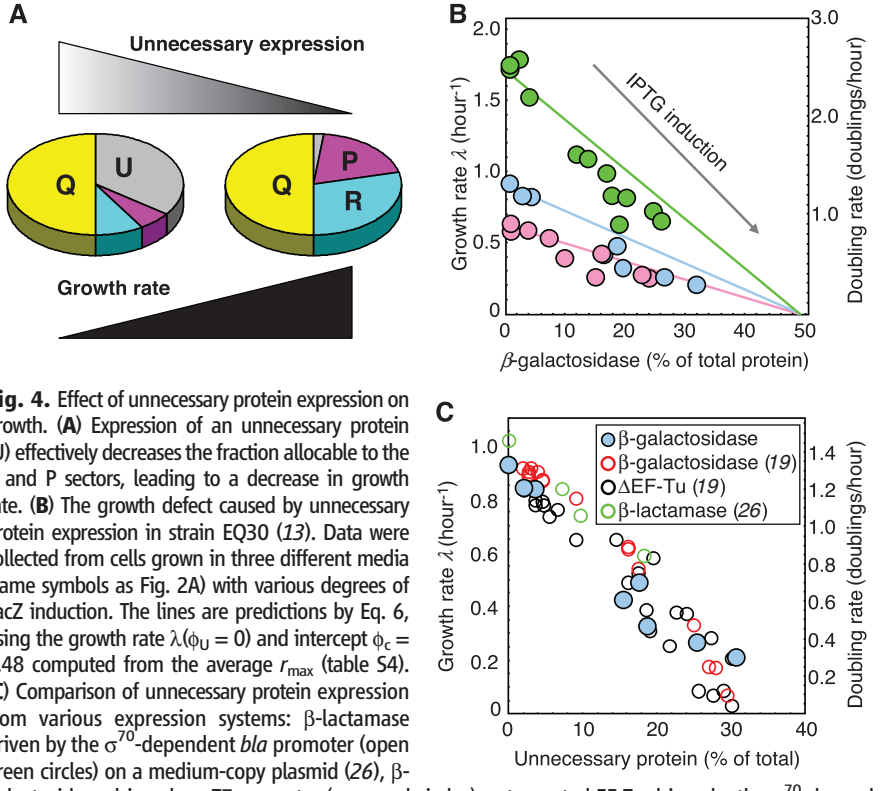

Fig. 4. Effect of unnecessary protein expression on growth. (**A**) Expression of an unnecessary protein (U) effectively decreases the fraction allocable to the R and P sectors, leading to a decrease in growth rate. (**B**) The growth defect caused by unnecessary protein expression in strain EQ30 (*13*). Data were collected from cells grown in three different media (same symbols as Fig. 2A) with various degrees of LacZ induction. The lines are predictions by Eq. 6, using the growth rate $\lambda(\phi_U = 0)$ and intercept $\phi_c = 0.48$ computed from the average r_{max} (table S4). (**C**) Comparison of unnecessary protein expression from various expression systems: β-lactamase driven by the σ^{70}-dependent *bla* promoter (open green circles) on a medium-copy plasmid (*26*), β-galactosidase driven by a T7 promoter (open red circles) or truncated EF-Tu driven by the σ^{70}-dependent *tac* promoter (open black circles), both on high-copy plasmids (*19*). β-Galactosidase driven by the σ^{54}-dependent P*u* promoter (solid blue circles) on a medium-copy plasmid [as in (B)] is shown for comparison.

limit in the allocation of cellular resources toward ribosome synthesis.

The simplest model connecting ribosome abundance to gene expression assumes that the total protein content of the cell (called the proteome) is composed of two classes: ribosome-affiliated "class R" proteins (with mass fraction ϕ_R), and "others" (with mass fraction $1 - \phi_R$) (*5*, *16*). But the maximum allocation to the R-class proteins as derived from the value of r_{max}, $\phi_R^{max} = \rho \cdot r_{max} \approx 0.55$, is well below 1 [see (*13*) for the conversion factor ρ]. This suggests that the "other" proteins can be further subdivided minimally into two classes (Fig. 2B): "class Q" of mass fraction ϕ_Q, which is not affected translational inhibition, and the remainder, "class P" of mass fraction ϕ_P, with $\phi_P \to 0$ as $\phi_R \to \phi_R^{max}$ (*17*). Because $\phi_P + \phi_Q + \phi_R = 1$, we must have $\phi_R^{max} = 1 - \phi_Q$, with

$$\phi_P = \phi_R^{max} - \phi_R = \rho \cdot (r_{max} - r) \qquad (3)$$

representing an important constraint between ϕ_P and ϕ_R. Together with Eq. 2, the model predicts

$$\phi_P = \rho \cdot \lambda / \kappa_n \qquad (4)$$

which describes a linear relation between the abundance of the P-class proteins and the growth rate λ for a fixed nutritional capacity κ_n. The growth rate independence of protein abundance may be maintained through negative autoregulation (*4*) (fig. S4). Unregulated (or "constitutively expressed") proteins belong instead to the P-class and can be used to test the prediction of Eq. 4: Expression of β-galactosidase driven by a constitutive promoter (ϕ_Z, mass of β-galactosidase per total protein mass) in cells grown under different degrees of chloramphenicol inhibition indeed correlated linearly with λ for each nutrient source studied (Fig. 2C), and the slopes of these correlations (colored lines) agree quantitatively with the nutritional capacity κ_n (fig. S5, A and B) as predicted by Eq. 4.

Although the correlations (Eqs. 2 and 4) were revealed by growth with antibiotics, their forms do not pertain specifically to translational inhibition. Equation 4 may be interpreted as a manifestation of P-class proteins providing the nutrients needed for growth [eqs. S15 to S18 in (*13*)], just as Eq. 1 is a reflection of R-class proteins providing the protein synthesis needed for growth (Fig. 3A). For different combinations of the nutritional and translational capacities (κ_n, κ_t), efficient resource allocation requires that the abundance of P- and R-class proteins be adjusted so that the rate of nutrient influx provided by P (via import or biosynthesis) matches the rate of protein synthesis achievable by R (Fig. 3B), while simultaneously satisfying the constraint of Eq. 3 (Fig. 3C). We can derive the resulting allocation mathematically by postulating that λ, ϕ_R (or *r*), and ϕ_P are analytical functions of the variables κ_t and κ_n that respectively capture all molecular details of translation and nutrition (analogous to state variables in thermodynamics). The mathematics

is identical to the description of an electric circuit with two resistors (fig. S6), with Eqs. 1 and 4 being analogous to Ohm's law. Solving these equations simultaneously leads to the Michaelis-Menten relation known empirically for the dependence of cell growth on nutrient level (*18*)

$$\lambda(\kappa_t, \kappa_n) = \lambda_c(\kappa_t) \cdot \frac{\kappa_n}{\kappa_t + \kappa_n} \quad (5)$$

The value of the maximal growth rate $\lambda_c(\kappa_t) = \kappa_t \cdot (r_{max} - r_0) \approx 2.85\ hour^{-1}$ (based on the average r_{max}) corresponds well to the doubling time of ~20 min for typical *E. coli* strains in rich media. Moreover, Eq. 5 quantitatively accounts for the correlation observed between growth rate λ and nutritional capacity κ_n (fig. S3A).

This theory can be inverted to predict the effect of protein expression on cell growth. Unnecessary protein expression leads to diminished growth (*19*). Understanding the origin of this growth inhibition is of value in efforts to increase the yield of heterologous protein in bacteria (*20*) and to understand the fitness benefit of gene regulation (*21*, *22*). Aside from protein-specific toxicity, several general causes of growth inhibition have been suggested, including diversion of metabolites (*23*), competition among sigma factors for RNA polymerases (*24*), and competition among mRNA for ribosomes (*19*, *25*).

We modeled the expression of unnecessary protein (of mass fraction ϕ_U) as an additional (neutral) component of the proteome that effectively causes a reduction of r_{max} to $r_{max} - \phi_U/\rho$ (Fig. 4A). Equation 5 then predicts a linear reduction of the growth rate,

$$\lambda(\phi_U) = \lambda(\phi_U = 0) \cdot [1 - (\phi_U/\phi_c)] \quad (6)$$

extrapolating toward zero growth at $\phi_c = \rho \cdot (r_{max} - r_0) \approx 0.48$. The prediction quantitatively described the observed growth defect caused by inducible expression of β-galactosidase (Fig. 4B), as well as previous results obtained for various proteins and expression vectors (Fig. 4C) (*19*, *26*), without any adjustable parameters. These results suggest that growth reduction is a simple consequence of ribosome allocation subject to the constraints of Eqs. 1, 3, and 4.

Robust empirical correlations of the RNA/protein ratio with the growth rate (Figs. 1A and 2A and figs. S1 and S2) revealed underlying constraints of cellular resource allocation and led to the formulation of a simple growth theory that provided quantitative predictions and unifying descriptions of many important but seemingly unrelated aspects of bacterial physiology. Like Ohm's law, which greatly expedited the design of electrical circuits well before electricity was understood microscopically, the empirical correlations described here may be viewed as microbial "growth laws," the use of which may facilitate our understanding of the operation and design of complex biological systems well before all the underlying regulatory circuits are elucidated at the molecular level.

References and Notes

1. N. J. Guido *et al.*, *Nature* **439**, 856 (2006).
2. H. Youk, A. van Oudenaarden, *Nature* **462**, 875 (2009).
3. E. M. Airoldi *et al.*, *PLOS Comput. Biol.* **5**, e1000257 (2009).
4. S. Klumpp, Z. Zhang, T. Hwa, *Cell* **139**, 1366 (2009).
5. A. Zaslaver *et al.*, *PLOS Comput. Biol.* **5**, e1000545 (2009).
6. A. P. Arkin, D. A. Fletcher, *Genome Biol.* **7**, 114 (2006).
7. C. Tan, P. Marguet, L. You, *Nat. Chem. Biol.* **5**, 842 (2009).
8. R. Kwok, *Nature* **463**, 288 (2010).
9. M. Schaechter, O. Maaloe, N. O. Kjeldgaard, *J. Gen. Microbiol.* **19**, 592 (1958).
10. H. Bremer, P. P. Dennis, in Escherichia coli *and* Salmonella, F. C. Neidhardt, Ed. (ASM Press, Washington, DC, 1996), pp. 1553–1569.
11. O. Maaløe, in *Biological Regulation and Development*, R. F. Goldberger, Ed. (Plenum, New York, 1979), pp. 487–542.
12. J. Forchhammer, L. Lindahl, *J. Mol. Biol.* **55**, 563 (1971).
13. See supporting material on *Science* Online.
14. T. Ruusala, D. Andersson, M. Ehrenberg, C. G. Kurland, *EMBO J.* **3**, 2575 (1984).
15. B. J. Paul, W. Ross, T. Gaal, R. L. Gourse, *Annu. Rev. Genet.* **38**, 749 (2004).
16. A. L. Koch, *Can. J. Microbiol.* **34**, 421 (1988).
17. A particular protein species may belong to multiple classes; sometimes this is a result of expression from multiple promoters that are differently regulated.
18. J. Monod, *Annu. Rev. Microbiol.* **3**, 371 (1949).
19. H. Dong, L. Nilsson, C. G. Kurland, *J. Bacteriol.* **177**, 1497 (1995).
20. C. P. Chou, *Appl. Microbiol. Biotechnol.* **76**, 521 (2007).
21. E. Dekel, U. Alon, *Nature* **436**, 588 (2005).
22. D. M. Stoebel, A. M. Dean, D. E. Dykhuizen, *Genetics* **178**, 1653 (2008).
23. B. R. Glick, *Biotechnol. Adv.* **13**, 247 (1995).
24. A. Farewell, K. Kvint, T. Nyström, *Mol. Microbiol.* **29**, 1039 (1998).
25. J. Vind, M. A. Sørensen, M. D. Rasmussen, S. Pedersen, *J. Mol. Biol.* **231**, 678 (1993).
26. W. E. Bentley, N. Mirjalili, D. C. Andersen, R. H. Davis, D. S. Kompala, *Biotechnol. Bioeng.* **35**, 668 (1990).
27. R. Mikkola, C. G. Kurland, *Biochimie* **73**, 1551 (1991).

28. We thank H. Bremer, L. Csonka, P. Dennis, M. Ehrenberg, P. Geiduschek, M. Schaechter, A. Tadmor, and members of the Hwa lab for suggestions and discussions; D. Hughes for the Sm mutant strains; and P.-h. Lee and B. Willumsen for the use of unpublished data. Supported by NIH grant RO1GM77298, NSF grant MCB0746581, and the NSF-supported Center for Theoretical Biological Physics (grant PHY0822283). M.S. was supported by a Natural Sciences and Engineering Research Council of Canada fellowship.

Supporting Online Material

www.sciencemag.org/cgi/content/full/330/6007/1099/DC1
Materials and Methods
SOM Text
Figs. S1 to S6
Tables S1 to S7
References

20 May 2010; accepted 6 October 2010
10.1126/science.1192588

Symbiotic Bacterium Modifies Aphid Body Color

Tsutomu Tsuchida,[1]*† Ryuichi Koga,[2]† Mitsuyo Horikawa,[3] Tetsuto Tsunoda,[3] Takashi Maoka,[4] Shogo Matsumoto,[1] Jean-Christophe Simon,[5] Takema Fukatsu[2]*

Color variation within populations of the pea aphid influences relative susceptibility to predators and parasites. We have discovered that infection with a facultative endosymbiont of the genus *Rickettsiella* changes the insects' body color from red to green in natural populations. Approximately 8% of pea aphids collected in Western Europe carried the *Rickettsiella* infection. The infection increased amounts of blue-green polycyclic quinones, whereas it had less of an effect on yellow-red carotenoid pigments. The effect of the endosymbiont on body color is expected to influence prey-predator interactions, as well as interactions with other endosymbionts.

The world is full of colors, and many animals have color vision, recognizing their environment, habitat, food, enemies, rivals, and mates by visual cues. Body color is thus an ecologically important trait, often involved in species recognition, sexual selection, mimicry, aposematism, and crypsis (*1*, *2*). In the pea aphid *Acyrthosiphon pisum*, red and green color morphs are found in the same populations. Early work has shown that the aphid body color is genetically determined, with red being dominant over green (*3*). Ecological studies show that ladybird beetles tend to consume red aphids on green plants (*4*), and parasitoid wasps preferentially attack green aphids (*5*). The predation and parasitism pressures appear to maintain the color variation in natural aphid populations (*1*, *4*). An unexpected recent discovery showed that the aphid genome contains several genes for carotenoid synthesis not found in animal genomes. The genes are of fungal origin and appear to have been acquired in the evolutionary history of aphids via ancient lateral transfer. One of the genes is involved in synthesis of red color pigments, and the presence or absence of the gene is responsible for the red or green coloration of the aphids (*6*). Here, we report another factor affecting aphid color polymorphism: a previously unrecognized endosymbiont that modifies insect body color in natural populations.

While screening pea aphid strains from natural populations collected in France, we found several strains of green aphids producing red nymphs. As the nymphs grew, their body color changed from reddish to greenish, and the adults became

[1]Molecular Entomology Laboratory, RIKEN Advanced Science Institute, Wako 351-0198, Japan. [2]National Institute of Advanced Industrial Science and Technology (AIST), Tsukuba 305-8566, Japan. [3]Faculty of Pharmaceutical Sciences, Tokushima Bunri University, Tokushima 770-8514, Japan. [4]Research Institute for Production Development, Kyoto 606-0805, Japan. [5]Institut National de la Recherche Agronomique, UMR 1099 BiO3P, Institut National de la Recherche Agronomique (INRA)/Agrocampus Ouest/Université Rennes 1, BP 35327, 35653 Le Rheu Cedex, France.

*To whom correspondence should be addressed. E-mail: t-tsuchida@riken.jp (T.T.); t-fukatsu@aist.go.jp (T.F.)
†These authors contributed equally to this work.

green (Fig. 1A and table S1). A survey of endosymbiotic microbiota in these aphid strains from distinct geographic origins and bearing different genotypes (*7*) identified γ-proteobacterial facultative endosymbionts (one of which is a *Hamiltonella*- or *Serratia*-like organism) that confer protection to their host aphids against parasitoid wasps (*8*). In addition, we found a previously unrecognized aphid endosymbiont of the genus *Rickettsiella*, whose members are insect pathogens that are phylogenetically related to the human pathogens *Coxiella* and *Legionella* (Fig. 2A) (*9*).

By antibiotic treatments (*7*), we successfully eliminated the *Hamiltonella*/*Serratia* infection from the aphids without affecting *Rickettsiella* and *Buchnera* infections. Their body-coloring patterns did not change after the treatments (Fig. 1B). When we injected diverse aphid strains, which harbored only *Buchnera*, with hemolymph from the *Rickettsiella*-infected strains (*7*), the aphids produced both *Rickettsiella*-infected and -uninfected offspring. Notably, *Rickettsiella*-infected red aphids of distinct genotypes consistently changed body color to green as they developed, whereas neither uninfected red aphids nor originally green aphids were affected (Fig. 1, fig. S1, and table S1). The body-coloring patterns in the experimentally infected aphid strains were similar to those in the naturally *Rickettsiella*-infected strains (Fig. 1). Quantitative polymerase chain reaction (PCR) analyses revealed that the intensity of green color was positively correlated with the infection density of *Rickettsiella* for different host and endosymbiont genotypes (fig. S1). These results indicate that the *Rickettsiella* infection is responsible for green body color in at least some green pea aphids in natural populations.

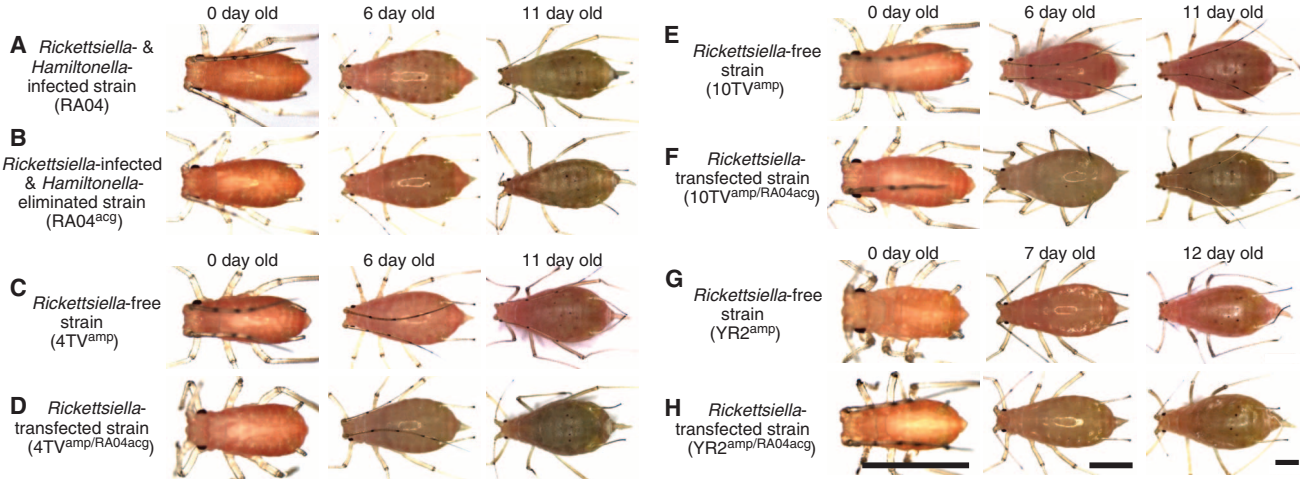

Fig. 1. (**A** to **H**) *Rickettsiella*-induced body-color change in pea aphids of different genetic backgrounds. Scale bars, 1 mm. For details of the aphid strains, see table S1.

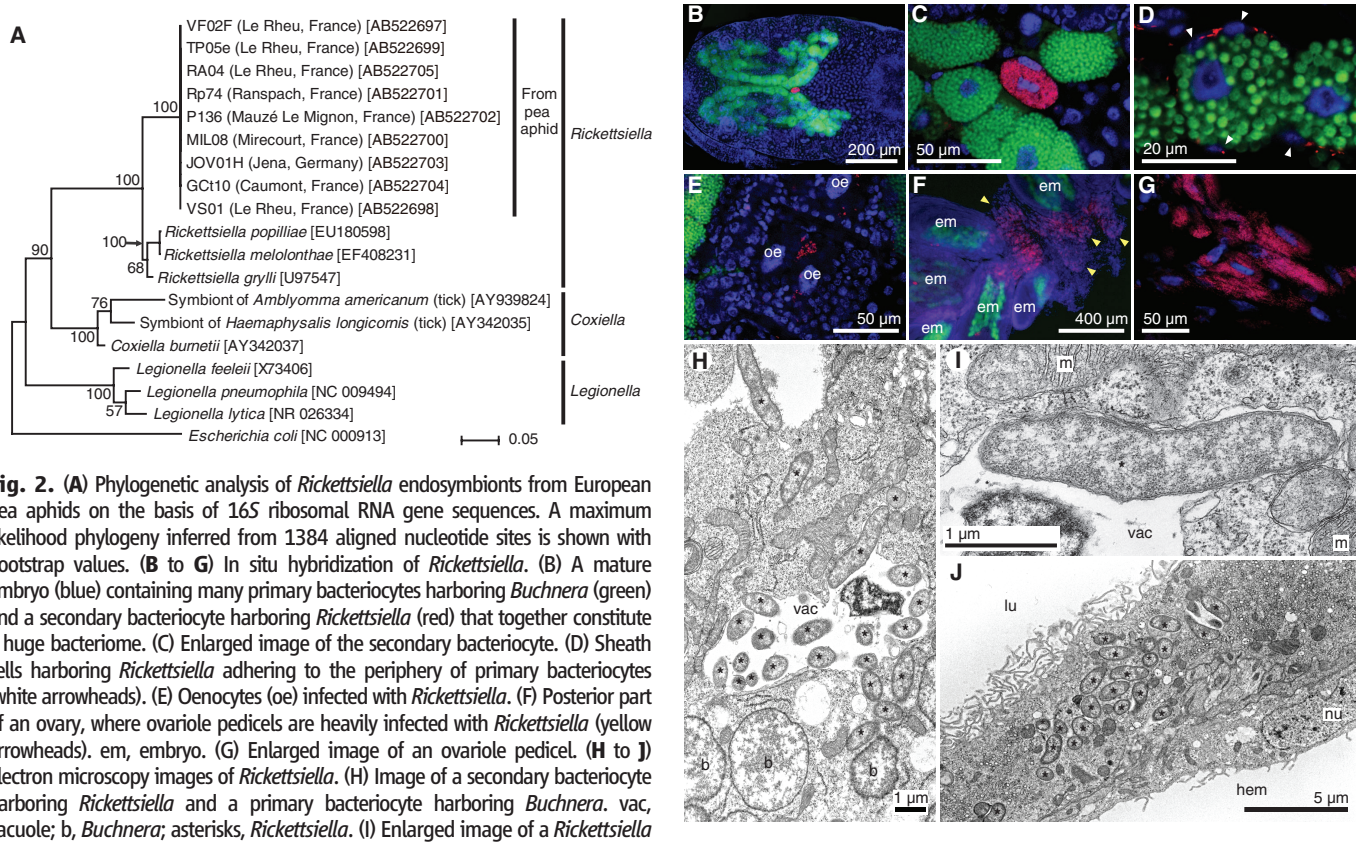

Fig. 2. (**A**) Phylogenetic analysis of *Rickettsiella* endosymbionts from European pea aphids on the basis of 16*S* ribosomal RNA gene sequences. A maximum likelihood phylogeny inferred from 1384 aligned nucleotide sites is shown with bootstrap values. (**B** to **G**) In situ hybridization of *Rickettsiella*. (B) A mature embryo (blue) containing many primary bacteriocytes harboring *Buchnera* (green) and a secondary bacteriocyte harboring *Rickettsiella* (red) that together constitute a huge bacteriome. (C) Enlarged image of the secondary bacteriocyte. (D) Sheath cells harboring *Rickettsiella* adhering to the periphery of primary bacteriocytes (white arrowheads). (E) Oenocytes (oe) infected with *Rickettsiella*. (F) Posterior part of an ovary, where ovariole pedicels are heavily infected with *Rickettsiella* (yellow arrowheads). em, embryo. (G) Enlarged image of an ovariole pedicel. (**H** to **J**) Electron microscopy images of *Rickettsiella*. (H) Image of a secondary bacteriocyte harboring *Rickettsiella* and a primary bacteriocyte harboring *Buchnera*. vac, vacuole; b, *Buchnera*; asterisks, *Rickettsiella*. (I) Enlarged image of a *Rickettsiella* cell. m, mitochondrion. (J) Image of the wall of an ovariole pedicel infected with *Rickettsiella*. hem, hemocoel; lu, lumen of ovariole pedicel; nu, nucleus.

Diagnostic PCR surveys detected 7.9% [28 of 353 insects (28/353)] *Rickettsiella* infection in Western European populations of *A. pisum* (fig. S2A). Fitness measurements revealed that infection status did not affect growth rate and body size for two aphid genotypes, although we observed significantly larger body size and faster growth with *Rickettsiella* infection for one aphid genotype (fig. S3). Similarly to *Hamiltonella* and *Serratia* (*10*, *11*), *Rickettsiella* resided in secondary bacteriocytes and sheath cells in vivo and was also found intracellularly and extracellularly in various tissues and the hemolymph (Fig. 2, B to J). In natural populations, not all green aphids were infected with *Rickettsiella*, and some strains of red aphids were found with *Rickettsiella* infection (fig. S2, B and C). It appears that the combination of aphid genotype and the endosymbiont contribute to body color (*3*, *6*): Some endosymbiont genotypes may fail to induce green coloration, whereas some host genotypes may attenuate or inhibit the activity of *Rickettsiella*. Similar interactions have been documented for other facultative endosymbionts in the pea aphid (*12*, *13*).

Aphid body color mainly consists of two major groups of pigment molecules: (i) yellow-red colors from carotenoid pigments such as β-carotene, lycopene, and torulene (*6*, *14*) and (ii) blue-green and other pigments from structurally complex polycyclic quinones and their glycosides, called aphins or aphinins (*14*, *15*). When the naturally red aphid strain was infected with *Rickettsiella* and became green, we observed some changes in carotenoid compositions, but the differences were not sufficient to account for the degree of green pigmentation (fig. S4). Moran and Jarvik (*6*) have found that a fungus-derived carotenoid desaturase gene, *tor*, is present in red aphid clones but is absent in green aphid clones and is responsible for production of the red carotenoids. Our quantitative reverse transcription–PCR assay showed that expression levels of the *tor* gene were not significantly affected by the *Rickettsiella* infection (fig. S5).

We recovered almost all of the green pigments into the butanol fraction by water-butanol extraction of the aphids (*7*). Thin-layer chromatography of the extracts separated one major and several minor green bands, which presumably represented polycyclic quinone glycosides like aphinins (*14*), although their exact structures were not determined (*7*). The intensity of the green bands was greater in the *Rickettsiella*-infected green-aphid strains than in the original red-aphid strains (fig. S6A). Densitometric quantification of the major band revealed a 2.4- to 4.6-fold increase of the green pigment in the *Rickettsiella*-infected aphid strains compared with the uninfected strains (fig. S6B). We presume that *Rickettsiella* does not synthesize new green pigments for itself but stimulates aphid metabolism to increase green-pigment production (fig. S7). The murky hue of the *Rickettsiella*-induced green aphids (Fig. 1 and fig. S1) is probably a result of the combination of the green pigments and the reddish carotenoid pigments. Genome sequencing of the *Rickettsiella* endosymbiont and transcriptomic analysis of the infected and uninfected aphid hosts should provide insights into the molecular and metabolic interactions between host and endosymbiont that lead to the body-color change.

Previous studies have identified a variety of biological roles for facultative endosymbionts in the pea aphid, including tolerance to high temperature, resistance against natural enemies, and plant adaptation (*8*, *16*–*19*). We have added another endosymbiont relationship that potentially affects a host trait of ecological importance in ways that have yet to be verified. For example, the induced green color may reduce the predation risk by ladybird beetles. Notably, *Rickettsiella* is frequently found in co-infections with either *Hamiltonella* [55.6% (35/63)] or *Serratia* [20.6% (13/63)] endosymbionts (fig. S2D), both of which are protective against parasitoid wasps (*8*) and may act to offset the risk of green aphids attracting parasitoids.

References and Notes

1. G. D. Ruxton, T. N. Sherratt, M. P. Speed, *Avoiding Attack: The Evolutionary Ecology of Crypsis, Warning Signals and Mimicry* (Oxford Univ. Press, Oxford, 2005).
2. J. Leonard, A. Cordoba-Aquilar, *The Evolution of Primary Sexual Characters in Animals* (Oxford Univ. Press, Oxford, 2010).
3. F. P. Müller, *Z. Pflanzenkr.* **69**, 129 (1962).
4. J. E. Losey, J. Harmon, F. Ballantyne, C. Brown, *Nature* **388**, 269 (1997).
5. R. Libbrecht, D. M. Gwynn, M. D. E. Fellowes, *J. Insect Behav.* **20**, 25 (2007).
6. N. A. Moran, T. Jarvik, *Science* **328**, 624 (2010).
7. Materials and methods are available as supporting material on *Science* Online.
8. K. M. Oliver, J. A. Russell, N. A. Moran, M. S. Hunter, *Proc. Natl. Acad. Sci. U.S.A.* **100**, 1803 (2003).
9. R. Cordaux *et al.*, *Appl. Environ. Microbiol.* **73**, 5045 (2007).
10. R. Koga, T. Tsuchida, T. Fukatsu, *Proc. Biol. Sci.* **270**, 2543 (2003).
11. N. A. Moran, J. A. Russell, R. Koga, T. Fukatsu, *Appl. Environ. Microbiol.* **71**, 3302 (2005).
12. K. M. Oliver, N. A. Moran, M. S. Hunter, *Proc. Natl. Acad. Sci. U.S.A.* **102**, 12795 (2005).
13. J. A. Russell, N. A. Moran, *Proc. Biol. Sci.* **273**, 603 (2006).
14. K. S. Brown, *Chem. Soc. Rev.* **4**, 263 (1975).
15. J. H. Bowie, D. W. Cameron, J. A. Findlay, J. A. K. Quartey, *Nature* **210**, 395 (1966).
16. C. B. Montllor, A. Maxmen, A. H. Purcell, *Ecol. Entomol.* **27**, 189 (2002).
17. T. Tsuchida, R. Koga, T. Fukatsu, *Science* **303**, 1989 (2004).
18. C. L. Scarborough, J. Ferrari, H. C. J. Godfray, *Science* **310**, 1781 (2005).
19. K. M. Oliver, P. H. Degnan, G. R. Burke, N. A. Moran, *Annu. Rev. Entomol.* **55**, 247 (2010).

20. We thank J. Peccoud, Y. Outreman, S. Stoeckel, L. Mieuzet, J. Jaquiéry, and W. Weisser for aphid sampling; J. Bonhomme, L. Mieuzet, and J. Makino for aphid rearing and genotyping; and X.-Y. Meng and S. Hanada for help with electron microscopy. This work was supported by the Japan-France Integrated Action Program SAKURA of the Japan Society for the Promotion of Science (to T.F. and J.-C.S.); the Grant-in-Aid for Scientific Research on Innovative Areas (22128007) of the Ministry of Education, Culture, Sports, Science and Technology, Japan (to T.F.); and funds from INRA AIP Bioresources (to J.-C.S.). T.T. was supported by a RIKEN special postdoctoral research fellowship.

Supporting Online Material

www.sciencemag.org/cgi/content/full/330/6007/1102/DC1
Materials and Methods
Figs. S1 to S7
Table S1
References

22 July 2010; accepted 8 October 2010
10.1126/science.1195463

PiggyBac Transposon Mutagenesis: A Tool for Cancer Gene Discovery in Mice

Roland Rad,[1] Lena Rad,[1] Wei Wang,[1] Juan Cadinanos,[1,2] George Vassiliou,[1] Stephen Rice,[1] Lia S. Campos,[1] Kosuke Yusa,[1] Ruby Banerjee,[1] Meng Amy Li,[1] Jorge de la Rosa,[2] Alexander Strong,[1] Dong Lu,[1] Peter Ellis,[1] Nathalie Conte,[1] Fang Tang Yang,[1] Pentao Liu,[1] Allan Bradley[1]*

Transposons are mobile DNA segments that can disrupt gene function by inserting in or near genes. Here, we show that insertional mutagenesis by the *PiggyBac* transposon can be used for cancer gene discovery in mice. *PiggyBac* transposition in genetically engineered transposon-transposase mice induced cancers whose type (hematopoietic versus solid) and latency were dependent on the regulatory elements introduced into transposons. Analysis of 63 hematopoietic tumors revealed that *PiggyBac* is capable of genome-wide mutagenesis. The *PiggyBac* screen uncovered many cancer genes not identified in previous retroviral or *Sleeping Beauty* transposon screens, including *Spic*, which encodes a PU.1-related transcription factor, and *Hdac7*, a histone deacetylase gene. *PiggyBac* and *Sleeping Beauty* have different integration preferences. To maximize the utility of the tool, we engineered 21 mouse lines to be compatible with both transposon systems in constitutive, tissue- or temporal-specific mutagenesis. Mice with different transposon types, copy numbers, and chromosomal locations support wide applicability.

Genetic screening in higher organisms has been hampered for decades by the lack of efficient insertional mutagenesis tools. Retroviruses have been used for cancer gene discovery in mice, but their application has been limited to the study of hematopoietic and mammary tumors because of viral tropism for these tissues (*1*). DNA transposons, which are the key insertional mutagens in lower organisms, were inactivated in vertebrate genomes millions of years

ago. Only recently have new transposons been engineered to be active in mammalian cells, a development that provides opportunities for their use as genetic tools in higher organisms (*2*). *Sleeping Beauty* (*SB*), a TC1/mariner transposon, was reconstructed from dormant elements in fish genomes and optimized to transpose in multiple cell types (*3*), including mouse embryonic stem cells (*4*). Further improvements of *SB* led to its successful application for somatic mutagenesis in mice (*5*, *6*). Another transposon, *PiggyBac* (*PB*) from the cabbage looper moth *Trichoplusia ni*, was recently engineered to be highly active in mammalian cells (*7*) and has been shown to have biological properties distinct from those of *SB* (*2*, *7*–*9*). *PB* can move larger DNA fragments (allowing complex transgene designs to be incorporated into the transposon), and it has a weaker tendency for local hopping in vitro (which makes it an attractive candidate for genome-wide mutagenesis). Furthermore, in contrast to *SB*, *PB* does not leave undesired footprint mutations after transposition. Lastly, *PB* and *SB* have different integration preferences.

To deploy *PB* for genetic screening in mice, we generated *PB* transposase knockin mice (*RosaPB*) and 19 mouse lines carrying different types of transposons (Fig. 1 and fig. S1) (*10*). All transposons possess *PB* and *SB* inverted terminal repeats (ITRs), allowing mobilization with both transposases. Promoter and enhancer elements, a splice donor, bidirectional SV40 polyadenylation signals, and two splice acceptors were introduced in between the ITRs to allow gain- or loss-of-function mutations, depending on the transposon orientation and its spatial relation to genes. Transgenic mice were generated with three variants of these bifunctional activating and inactivating transposons (ATP1, ATP2, and ATP3), which carry different promoter/enhancer elements (CAG, MSCV, and PGK). The chromosomal location and copy number of transposons were determined for each line by fluorescence in situ hybridization (FISH) and quantitative real-time polymerase chain reaction (QPCR) (figs. S2 and S3). Nineteen transgenic mouse lines were established, with transposon arrays on 14 different chromosomes and 2 to 150 transposon copies (Fig. 1).

To analyze the biology of *PB* transposition in vivo, we intercrossed *RosaPB* mice with 14 ATP lines and assessed nearly 900 progeny. When "low copy" ATP lines (<20 copies) were used, double-transgenic offspring were born at Mendelian frequency or close to it, whereas "high copy" ATP mice (e.g., *ATP1-H39*) did not produce live-born double-positive progeny (Fig. 2A). However, double-transgenic *RosaPB;ATP1-H39* embryos

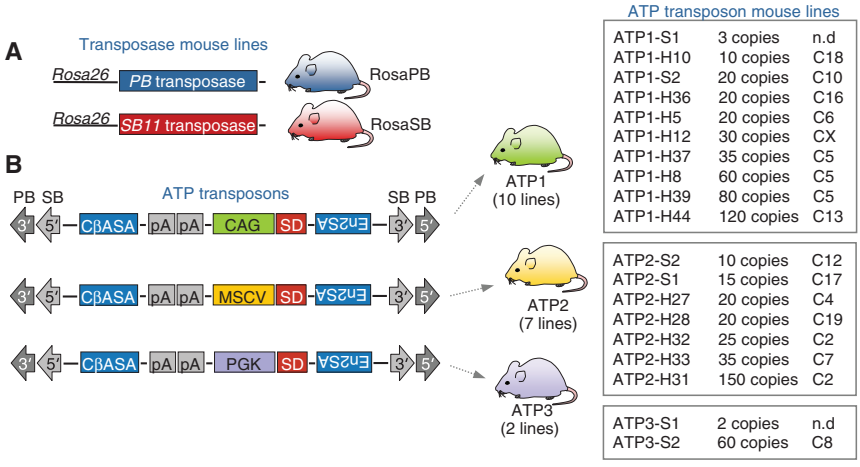

Fig. 1. Mouse lines carrying the genetic components of the transposon systems. (**A**) *RosaPB* and *RosaSB* knockin mice express *PiggyBac* or *Sleeping Beauty* transposase under control of the constitutively active *Rosa26* promoter. (**B**) Transposon design and transposon mouse lines. (Left) Three transposon constructs were designed, which differ in their promoter and enhancer. All three transposons have *PB* as well as *SB* ITRs and can therefore be mobilized with both transposases. (Right) Three types of transposon mouse lines (*ATP1*, *ATP2*, and *ATP3*) were generated by using these constructs. A total of 19 ATP lines were developed and are listed in the tables on the right. For each line, the chromosome harboring the transposon donor locus and the transposon copy number in the donor concatemer are indicated. n.d, not determined; CβASA, Carp β-actin splice acceptor; En2SA, *Engrailed-2* exon-2 splice acceptor; SD, *Foxf2* exon-1 splice donor; pA, bidirectional SV40 polyadenylation signal; CAG, cytomegalovirus enhancer and chicken beta-actin promoter; MSCV, murine stem cell virus long terminal repeat; PGK, phosphoglycerate-kinase promoter.

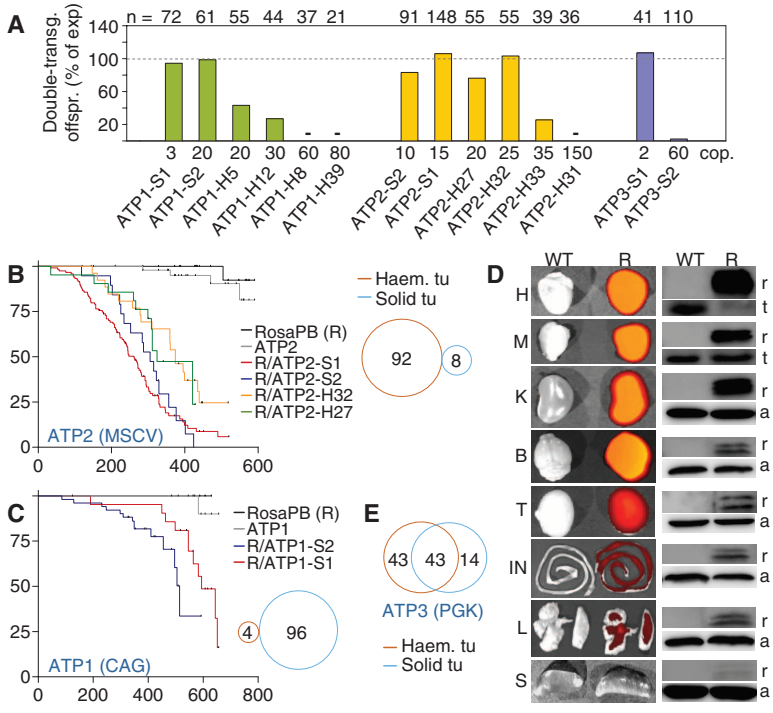

Fig. 2. Embryonic lethality, tumor spectrum, and latency in different ATP mouse lines upon *PiggyBac* mobilization. (**A**) Embryonic lethality in offspring from *RosaPB;ATP* intercrosses. 14 ATP mouse lines were used. Each line's transposon copy number is indicated below the graph. The number of mice born in each colony is shown above the graph. Bars represent double transgenic progeny as a percentage of expected. (**B**, **C**, and **E**) Tumor spectrum and latency in different ATP mouse lines upon *PB* transposon mobilization. The percentage of mice with hematopoietic or solid tumors is indicated for *RosaPB;ATP2* (B), *RosaPB;ATP1* (C), and *RosaPB/ATP3* mice (E). Kaplan-Meier survival curves are shown for indicated genotypes. (**D**) CAG promoter–driven DsRed expression in mouse tissues. (Left) Red fluorescence detection in organs from wild-type (WT) and *hprt*$^{CAG\text{-}DsRed}$ (R) male mice. H, heart; M, skeletal muscle; K, kidney; B, brain; T, testicle; IN, small intestine; L, lung; S, spleen. (Right) Western blot analysis of the same organs using a DsRed-specific antibody (r) or control antibodies (t, α-tubulin; a, β-actin).

[1]Wellcome Trust Sanger Institute, Genome Campus, Hinxton-Cambridge CB10 1SA, UK. [2]Instituto de Medicina Oncológica y Molecular de Asturias (IMOMA), Avenida Richard Grandío s/n, Oviedo, 33193, Spain.

*To whom correspondence should be addressed. E-mail: abradley@sanger.ac.uk

were identified, suggesting extensive transposition-induced embryonic lethality (fig. S4). Less pronounced was the effect of the transposon type and donor location on embryonic lethality, although weak positional effects could be observed for some lines (e.g., *ATP1-H5*). Further characteristics of *PB* mobilization in vivo are shown in fig. S4.

We next investigated whether *PB*-based mutagenesis induced cancer in the mice. We monitored 393 animals from multiple cohorts and found that beginning at 2 months of age, double-transgenic *RosaPB;ATP* mice, but not single-transgenic animals, developed cancers. The tumor type and latency were profoundly influenced by the transposon type. Mobilization of ATP2 transposons resulted in highly penetrant hematopoietic cancer formation. More than 90% of *RosaPB;ATP2* mice developed aggressive leukemias and lymphomas (Fig. 2B and fig. S5). In contrast, *RosaPB;ATP1* animals had almost exclusively solid tumors, including sarcomas and various carcinomas with poor differentiation and metastasis (Fig. 2C, fig. S6, and tables S1 and S2).

To explore whether the lack of hematopoietic carcinogenesis in A*TP1* mice is related to tissue specificity of the CAG promoter, we generated reporter mice expressing DsRed constitutively under control of CAG from the *Hprt* locus. This knockin line has two major advantages over conventional transgenic reporter mice: (i) Promoters inserted into *Hprt* are not subject to epigenetic silencing and drive gene expression in all tissues (*11*) and (ii) only one copy of the promoter/reporter is used, which accurately reflects the effect of one ATP1-CAG-transposon. The analysis of *Hprt-Cag-DsRed* mice revealed robust DsRed expression in most organs but not in the spleen (Fig. 2E), suggesting low CAG activity in the hematopoietic compartment.

Lastly, we analyzed *RosaPB;ATP3* mice, which developed solid and/or hematopoietic tumors, with a high percentage of mice having both (Fig. 2D and fig. S7). Further characterization of *PB*-induced tumors is shown in the supporting online material (SOM), including immunohistochemical subtype analysis of hematologic cancers (fig. S8), evidence for lack of generalized transposon-induced genomic instability (fig. S9), proof of clonality of insertions in tumors (fig. S10), analysis of transposase expression and transposon copy numbers in tumors (fig. S11), and the distribution pattern of different transposon types in genes (table S3).

SB has a strong tendency for local hopping, with 32 to 45% of all integrations mapping to the donor chromosome in *SB*-induced tumors (*12*, *13*). To examine the potential of *PB* for genome-wide mutagenesis, we cloned more than 50,000 transposon integration sites in 63 hematopoietic tumors originating from three transposon mouse lines. A total of 5590 nonredundant insertions were identified. Figure 3 and table S4 show that *PB* integrations were uniformly distributed across the genome and correlated with the size and the TTAA frequency (the *PB* integration site) of individual chromosomes. There was a slightly increased insertion density on chromosomes 2, 9, 11, and 19 in all three groups of mice, which might be related to the high gene density (table S5) or the high number of oncogenic insertions (fig. S12) on those chromosomes. On donor chromosomes, the number of integrations was as expected or only slightly higher, and local hopping was confined to a small region (1 to 3 Mb) around the donor locus (Fig. 3). Together these results demonstrate the unique qualities of *PB* for genome-wide mutagenesis.

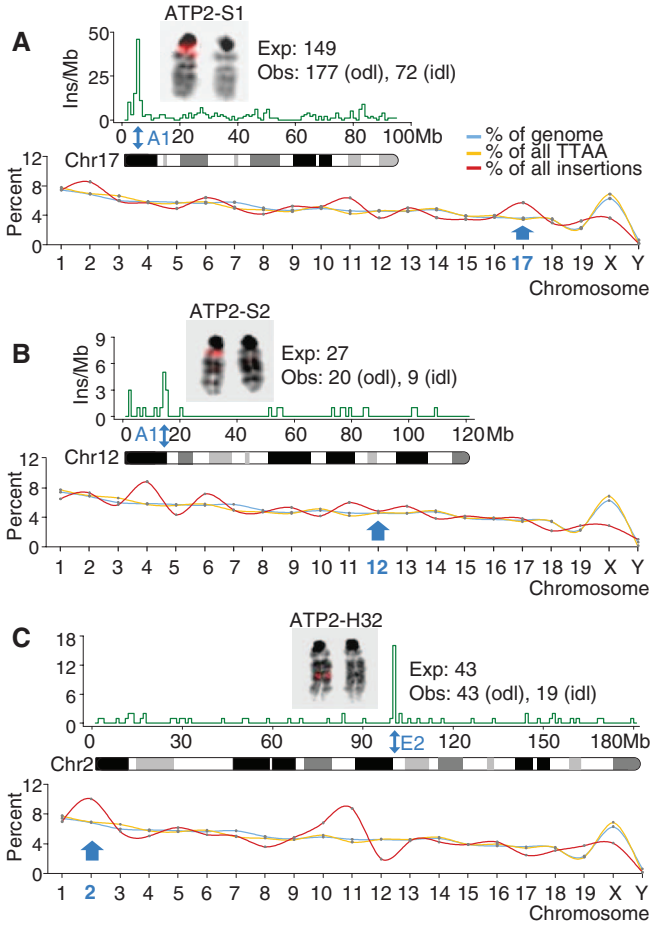

Fig. 3. *PB* integration pattern in tumors from different *ATP2* mouse lines. (**A**) Analysis of tumors from *RosaPB;ATP2-S1* mice (50 tumors, 4379 insertions). The bottom graph compares the percentage of transposon insertions to the size and TTAA frequency on individual chromosomes. The donor chromosome and locus were identified by FISH and are indicated by blue arrows. The top graph shows the distribution of insertions on Chr17 at a 1-Mb resolution. The numbers of expected (exp) and observed insertions outside (odl) and inside (idl) a 3-Mb interval surrounding the donor locus are indicated. Results from (**B**) *RosaPB;ATP2-S2* mice (seven tumors; 594 insertions; donor Chr12) and (**C**) *RosaPB;ATP2-H32* mice (six tumors; 618 insertions; donor Chr2) are presented accordingly.

To discover candidate cancer genes, we used a statistical framework based on Gaussian kernel convolution (*14*), which identified 72 unique common integration sites (CISs) at 67 independent loci (Fig. 4 and table S6). Figure S12 visualizes the global transposon integration pattern for each chromosome at a 1-Mb resolution and indicates all significant CISs. A search in the Retrovirus Tagged Cancer Gene Database (*15*) and in recent large-scale insertional mutagenesis studies (*13*, *16*) revealed, as expected, that some of these CISs (or genes within CISs) have also been identified in earlier retroviral or *SB* screens (Fig. 4A). However, 42% of the CISs have not been reported before our study. Given that thousands of murine hematologic cancers have been generated and analyzed earlier by using retroviral or *SB* mutagenesis, this high number of novel CISs was unexpected and underscores the potential of *PB* for genetic screening.

The integration pattern in oncogenes suggests a high selective pressure for insertions in specific regions where transposons cause gene activation. All *Nras* or *Evi1* integrations, for example, were upstream of the translation start site, and transposons were sense-oriented, supporting gene expression from the unidirectional murine stem cell virus (MSCV) promoter (Fig. 4B and fig. S13). Some oncogenes had more complex integration patterns. *Notch1*, for example, had one insertion cluster in intron 27, leading to overexpression of an intracellular Notch1 domain like in human T-ALL with t(7;9) translocations (*17*), and a second cluster of truncating integrations in intron 2, leading to a "decoupled" intracellular domain that can be expressed from a cryptic *Notch1* promoter (*18*).

In contrast to oncogene insertions, hits in tumor suppressor genes (TSGs) were randomly distributed throughout genes (e.g., *Ikzf1* or *Pten*; Fig. 4B) and were either sense- or antisense-oriented, suggesting that gene disruption is the disease-causing mechanism. In some tumors multiple integrations in TSGs occurred, leading to trapping of both alleles (fig. S14). *Pten* was frequently hit in this screen but not in previous

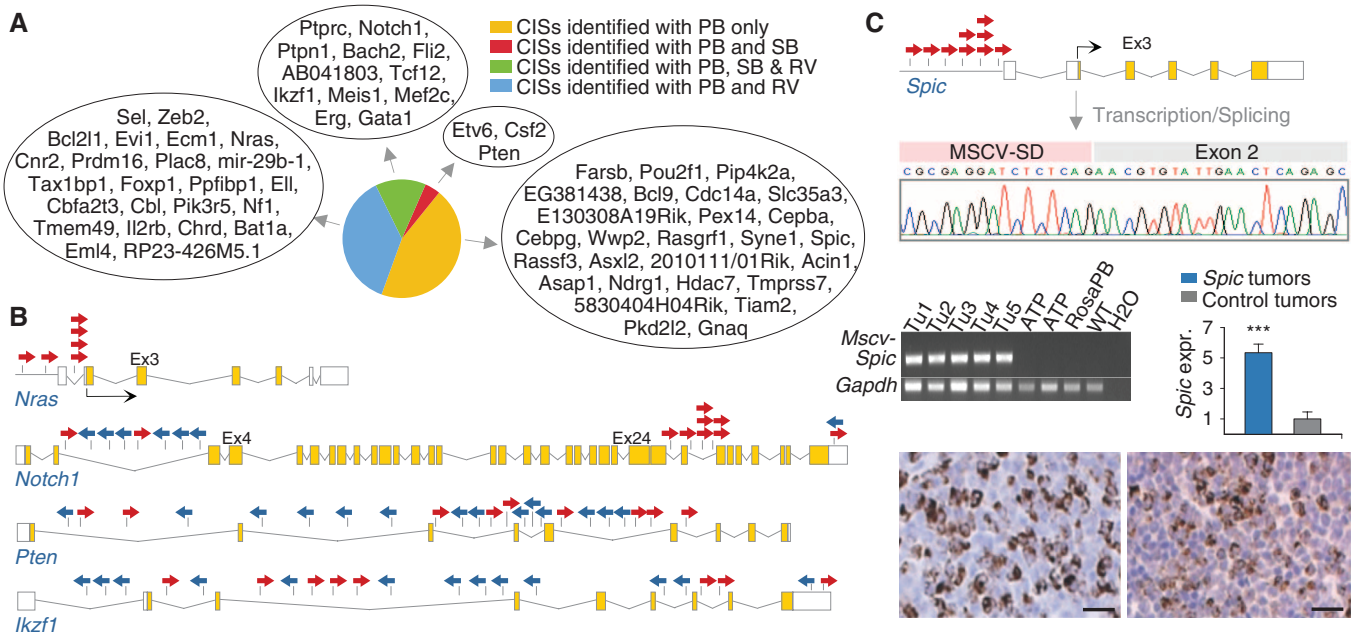

Fig. 4. Identification of CISs in *PiggyBac*-induced hematopoietic tumors. (**A**) Pie chart representing all CISs identified: Some were reported in earlier screens that used retroviruses (RV, 36%), *Sleeping Beauty* (SB, 4%), or both (18%). Forty-two percent have not been identified in earlier screens. (**B**) Insertion pattern in known oncogenes and TSGs. Arrows indicate individual insertions and their orientation (red or blue, sense or antisense orientation of the transposon's promoter to genes, respectively). (**C**) Promoter insertions in *Spic* in nine tumors. MSCV-*Spic* fusion transcripts were detected by reverse transcription PCR and sequencing. *Spic* expression was analyzed by QPCR and normalized to *Gapdh* expression. Tumors with *Spic* integrations are myeloid leukemias, as shown by immunohistochemical myeloperoxidase staining (left, spleen; right, lymph node from one mouse). Scale bars, 25 μm; error bars, SEM. ***$P < 0.001$.

retroviral screens, highlighting the different integration preferences of these insertional mutagens.

Examples of novel candidate cancer genes with promoter insertions identified in this screen are the PU.1-related transcription factor *Spic*, the histone deacetylase *Hdac7*, the Wnt pathway component *Bcl9*, and the cell cycle regulatory phosphatase *Cdc14* (Fig. 4 and fig. S13). *Spic* was hit in nine tumors, which were all myeloperoxidase (MPO)-positive myeloid leukemias. In all tumors, transposons were sense-oriented and located within a narrow region [760 base pairs (bp)] upstream of the translation start site. *MSCV-Spic* fusion transcripts were confirmed by sequencing, and *Spic* overexpression was shown by QPCR (Fig. 4C). Little is known about the biological function of *Spic*, but a recent study has suggested its role in myelomonocytic development (*19*), which further supports our findings. *HDAC7* is specifically expressed in CD4/CD8 double-positive human thymocytes (*20*), but its role in hematopoietic tumorigenesis has not been studied so far. The β-catenin cofactor Bcl9 is a rare translocation partner in human hematopoietic malignancies (*21*), and a recent study revealed frequent amplifications of a chromosomal region that includes *BCL9* in various human malignancies (*22*).

The mouse is a major model organism for the study of human physiology and disease. Our study adds an efficient and versatile tool kit for genetic screening in mice that can be exploited for a wide range of applications, including constitutive, tissue-specific, or spatiotemporally controlled somatic mutagenesis, using conditional and tamoxifen-inducible *PB* (*23*). In tissue-specific screens, we were able to induce aggressive metastatic solid tumors, which in principle will facilitate future studies of tumor initiation, progression, and metastasis, as well as the genetic basis of various histological subtypes of individual cancers. *PB* can be used alone for genome-wide mutagenesis, but the ATP lines described here with donor loci on 14 different chromosomes can also be used in combination with *SB* [e.g., to exploit its local hopping tendency (*24*) for chromosome-specific screens in known cancer susceptibility regions]. These transposon tool kits in mice have the potential to increase the speed and efficiency with which cancer genes and oncogenic signaling networks are discovered and should likewise facilitate functional analysis of these genes.

References and Notes

1. J. Kool, A. Berns, *Nat. Rev. Cancer* **9**, 389 (2009).
2. Z. Ivics *et al.*, *Nat. Methods* **6**, 415 (2009).
3. Z. Ivics, P. B. Hackett, R. H. Plasterk, Z. Izsvák, *Cell* **91**, 501 (1997).
4. G. Luo, Z. Ivics, Z. Izsvák, A. Bradley, *Proc. Natl. Acad. Sci. U.S.A.* **95**, 10769 (1998).
5. A. J. Dupuy, K. Akagi, D. A. Largaespada, N. G. Copeland, N. A. Jenkins, *Nature* **436**, 221 (2005).
6. L. S. Collier, C. M. Carlson, S. Ravimohan, A. J. Dupuy, D. A. Largaespada, *Nature* **436**, 272 (2005).
7. S. Ding *et al.*, *Cell* **122**, 473 (2005).
8. W. Wang *et al.*, *Proc. Natl. Acad. Sci. U.S.A.* **105**, 9290 (2008).
9. Q. Liang, J. Kong, J. Stalker, A. Bradley, *Genesis* **47**, 404 (2009).
10. Materials and methods are available as supporting material on *Science* Online.
11. S. K. Bronson *et al.*, *Proc. Natl. Acad. Sci. U.S.A.* **93**, 9067 (1996).
12. T. K. Starr *et al.*, *Science* **323**, 1747 (2009); 10.1126/science.1163040.
13. L. S. Collier *et al.*, *Cancer Res.* **69**, 8429 (2009).
14. J. de Ridder, A. Uren, J. Kool, M. Reinders, L. Wessels, *PLoS Comput. Biol.* **2**, e166 (2006).
15. K. Akagi, T. Suzuki, R. M. Stephens, N. A. Jenkins, N. G. Copeland, *Nucleic Acids Res.* **32**, D523 (2004).
16. A. G. Uren *et al.*, *Cell* **133**, 727 (2008).
17. L. W. Ellisen *et al.*, *Cell* **66**, 649 (1991).
18. C. D. Hoemann, N. Beaulieu, L. Girard, N. Rebai, P. Jolicoeur, *Mol. Cell. Biol.* **20**, 3831 (2000).
19. M. Kohyama *et al.*, *Nature* **457**, 318 (2009).
20. F. Dequiedt *et al.*, *Immunity* **18**, 687 (2003).
21. T. G. Willis *et al.*, *Blood* **91**, 1873 (1998).
22. R. Beroukhim *et al.*, *Nature* **463**, 899 (2010).
23. J. Cadiñanos, A. Bradley, *Nucleic Acids Res.* **35**, e87 (2007).
24. V. W. Keng *et al.*, *Nat. Methods* **2**, 763 (2005).

25. We thank the research support facility team, B.L. Ng, B. Fu, and Y. Hooks for technical assistance; N. Carter and C. Lopez-Otin for experimental resources; L. Wessels, J. ten Hoeve, and J. de Ridder for software used in data analysis; D. Saur for technical advice; and H. Prosser for reagents. The work was supported by the Wellcome Trust. R.R. and J.R. are recipients of a fellowship from the Deutsche Forschungsgemeinschaft and the Fundación Maria Cristina Masaveu Peterson, respectively.

Supporting Online Material

www.sciencemag.org/cgi/content/full/science.1193004/DC1
Materials and Methods
Figs. S1 to S14
Tables S1 to S7
References

28 May 2010; accepted 20 September 2010
Published online 14 October 2010;
10.1126/science.1193004

Calcium-Permeable AMPA Receptor Dynamics Mediate Fear Memory Erasure

Roger L. Clem and Richard L. Huganir*

Traumatic fear memories can be inhibited by behavioral therapy for humans, or by extinction training in rodent models, but are prone to recur. Under some conditions, however, these treatments generate a permanent effect on behavior, which suggests that emotional memory erasure has occurred. The neural basis for such disparate outcomes is unknown. We found that a central component of extinction-induced erasure is the synaptic removal of calcium-permeable α-amino-3-hydroxyl-5-methyl-4-isoxazole-propionate receptors (AMPARs) in the lateral amygdala. A transient up-regulation of this form of plasticity, which involves phosphorylation of the glutamate receptor 1 subunit of the AMPA receptor, defines a temporal window in which fear memory can be degraded by behavioral experience. These results reveal a molecular mechanism for fear erasure and the relative instability of recent memory.

Fear conditioning is the development of a fearful emotional response to a neutral cue [a conditioned stimulus (CS)] that occurs together with an unpleasant event [an unconditioned stimulus (US)]. Fear memories present as defensive reactions to the CS for a period of up to many months after learning (*1*). However, when conditioned subjects repeatedly encounter a CS without a reinforcing US, responses to a CS that no longer predicts harm are diminished in a process known as extinction. This paradigm is analogous to human exposure-based therapy for traumatic memories (*2*), in which maladaptive fear is suppressed by exposure to stimuli that were present at the time of trauma. However, because fear can recur after these treatments, extinction probably does not affect emotional memory, which can later be reactivated by specific cues (*3*, *4*).

A number of studies indicate that a more lasting reduction of fear can be dependent on the conditions at the time of extinction, such as the age of the subjects (*5*), the intertrial spacing of stimuli (*6*–*8*), or the time elapsed since initial learning (*9*, *10*). Because even strong reminder cues do not trigger the recurrence of conditioned fear in some cases (*5*–*8*), an intriguing possibility is that, under the right conditions, permanent erasure of fear memory occurs during the course of extinction. Such techniques could be useful in the treatment of emotional disorders. However, maximizing this approach requires an understanding of the cellular and molecular mechanisms underlying this fear erasure, which at present remain obscure.

Overwhelming evidence indicates that plasticity within amygdala circuits underlies fear conditioning in animals and humans (*11*, *12*). Cue-dependent fear conditioning is thought to be mediated by the potentiation of glutamatergic synaptic transmission in the lateral amygdala (LA) (*13*, *14*). Correspondingly, we observed an enhancement of α-amino-3-hydroxyl-5-methyl-4-isoxazole-propionate receptor (AMPAR) excitatory postsynaptic currents (AMPAR-EPSCs) at thalamic afferents to LA neurons after auditory fear conditioning in mice. This enhancement was evident as both an increase in the ratio of evoked AMPAR- to *N*-methyl-D-aspartate receptor (NMDAR)–mediated currents (Fig. 1, A and B, and fig. S1), as well as larger AMPAR miniature EPSC amplitudes (mEPSCs, Fig. 1, C and D, and fig. S2). These enhancements lasted for 7 days, suggesting that this potentiation may underlie the long-term maintenance of fear memory.

In principal neurons throughout the adult brain, AMPARs containing the glutamate receptor 2 subunit (GluA2) predominate (*15*). However, in vivo experience induces in other brain areas a switch from GluA2-containing to GluA2-lacking AMPARs (*16*–*18*), which are known as calcium-permeable (CP-AMPARs). We therefore assayed for CP-AMPARs at thalamic synapses before and after fear conditioning in mice. In naïve animals, current-voltage plots of AMPAR-EPSCs revealed a slight degree of inward rectification (fig. S3), which is a signature of CP-AMPARs, and rectification was eliminated by the CP-AMPAR antagonist 1-naphthylacetyl spermine (NASPM). Our examination of responses after fear conditioning revealed a slowly developing enhancement of rectification (Fig. 1, E and F, and figs. S4 and S5), mirroring an increase in AMPAR-EPSC inhibition by NASPM (fig. S6). Both increased rectification and NASPM sensitivity appeared within hours after conditioning, peaked at 24 hours, and disappeared by day 7. Thus, synapses were modified by the transient addition of CP-AMPARs even as transmission strength remained stable.

Long-term depression (LTD), an in vitro model of experience-dependent synaptic weakening, has been associated with the trafficking of CP-AMPARs in other systems (*16*, *19*–*21*). We therefore examined the effect of the presence of CP-AMPARs on LTD in mouse brain slices before and after fear conditioning. In naïve animals, LTD could be induced when LA neurons were mildly depolarized (–50 mV) in conjunction with paired-pulse low-frequency stimulation (ppLFS pairing) (Fig. 1G). The induction of this form of LTD was mediated by NMDARs and metabotropic glutamate receptor 1 (mGluR1) but not mGluR5 (fig. S7). When treated with NASPM after ppLFS pairing, neurons exhibited no further decrease in EPSC amplitude except when LTD had been blocked by inhibition of mGluR1 (Fig. 1G), indicating that LTD was expressed by selective removal of CP-AMPARs. At 24 hours after fear conditioning, when CP-AMPARs are elevated, LTD was of much greater magnitude (Fig. 1H). Synaptic removal of CP-AMPARs also mediated LTD at this time, because AMPAR rectification (fig. S8) and sensitivity to NASPM (Fig. 1H) were both eliminated by ppLFS pairing. These results suggest that CP-AMPAR incorporation after fear conditioning increases the capacity for synaptic weakening through mGluR1-dependent LTD.

Because synaptic CP-AMPARs reach their peak level at 1 day after fear conditioning, we hypothesized that the reversal of fear-dependent synaptic potentiation by removal of CP-AMPARs, and thus fear erasure, might be more easily achieved at this time by using specific extinction protocols. An extinction protocol that can fully eliminate fear, here referred to as reconsolidation update, has recently been described (*6*). This protocol targets a labile period after memory retrieval, when treatment with amnesic drugs leads to complete memory loss (*22*). Similarly, extinction training in this window permanently attenuates fear. The critical requirement for this effect is exposure to a single isolated CS (retrieval) between 10 min and 6 hours before extinction.

Thus, we subjected our mice to retrieval 30 min before extinction (Fig. 2A), and after extinction, fear relapse was examined in spontaneous recovery and renewal tests (Fig. 2, D to F). Spontaneous recovery develops passively with time and is measured in the extinction context, whereas renewal can be triggered at any time by exposure to the CS in the training context. As a negative control, we examined mice treated identically to retrieval subjects, except that retrieval was omitted and one additional CS was delivered during extinction to balance total CS exposure (Fig. 2, A to C, no retrieval). When extinction was performed on day 1 after conditioning (day 0), neither group exhibited spontaneous recovery on day 2 (Fig. 2D). However, no-retrieval controls exhibited significant renewal on day 2, and by day 7 they exhibited spontaneous recovery in addition to renewal after extinction on day 1 (Fig. 2E). In contrast, retrieval mice extinguished on day 1 displayed no fear relapse under any condition (Fig. 2, D and E), which is consistent with memory erasure. To determine whether reconsolidation update, like

Department of Neuroscience and Howard Hughes Medical Institute, Johns Hopkins University School of Medicine, Baltimore, MD, USA.

*To whom correspondence should be addressed. E-mail: rhuganir@jhmi.edu

LTD-induced removal of CP-AMPARs (Fig. 1G), requires the activation of mGluR1, we examined fear relapse in mice that were treated systemically with 1-aminoindan-1,5-dicarboxylic acid [AIDA, 2 mg per kilogram of body weight (mg/kg)] 1 hour before retrieval extinction (Fig. 2G). AIDA-injected mice, but not saline controls, exhibited significant recurrence of fear in spontaneous recovery and renewal tests on day 7. Thus, reconsolidation update and CP-AMPAR–mediated LTD share a requirement for mGluR activation.

We next examined whether synaptic depression underlies fear memory erasure in mouse brain slices prepared after reconsolidation update on day 1. Here we included two additional controls to determine how retrieval and no-retrieval extinction might differentially affect synaptic properties (Fig. 3A). Unpaired controls experienced CS/US cues that were explicitly unpaired to control for stimulus effects unrelated to memory formation. Context-only controls underwent paired conditioning and were exposed to the extinction arena without any tones. As expected, context-only mice displayed high tone-evoked freezing 2 hours after context exposure (Fig. 3B). Although no-retrieval controls showed significantly less freezing than context-only mice in the test of spontaneous recovery, fear renewal in the conditioning context eliminated this difference. Conversely, under both test conditions, retrieval mice displayed lower freezing than context-only controls (Fig. 3B), and when tested on day 7, this difference was still present (fig. S9).

Electrophysiological recordings 2 hours after reconsolidation update revealed a significant decrease in AMPAR-mediated transmission in the retrieval group as compared to context-only and no-retrieval controls (Fig. 3, C and D, and fig. S9), demonstrating that reconsolidation update reverses fear-related synaptic strengthening. This reversal was accompanied by the selective removal of synaptic CP-AMPARs, because rectification of AMPAR-EPSCs and sensitivity to NASPM was greatly reduced after reconsolidation update (Fig. 3, E and F). Because no effect of extinction on AMPAR-EPSCs was seen in no-retrieval animals, as compared to context-only controls, we conclude that reconsolidation update reduces transmission by removing CP-AMPARs.

Furthermore, ppLFS pairing revealed that LTD was significantly enhanced in context-only and no-retrieval animals (Fig. 3G), indicating that CP-AMPAR incorporation had increased the capacity for synaptic weakening. Conversely, because of prior synaptic removal of CP-AMPARs in retrieval animals, further synaptic depression was occluded. NASPM had no effect after LTD, which indicates that changes in LTD could not

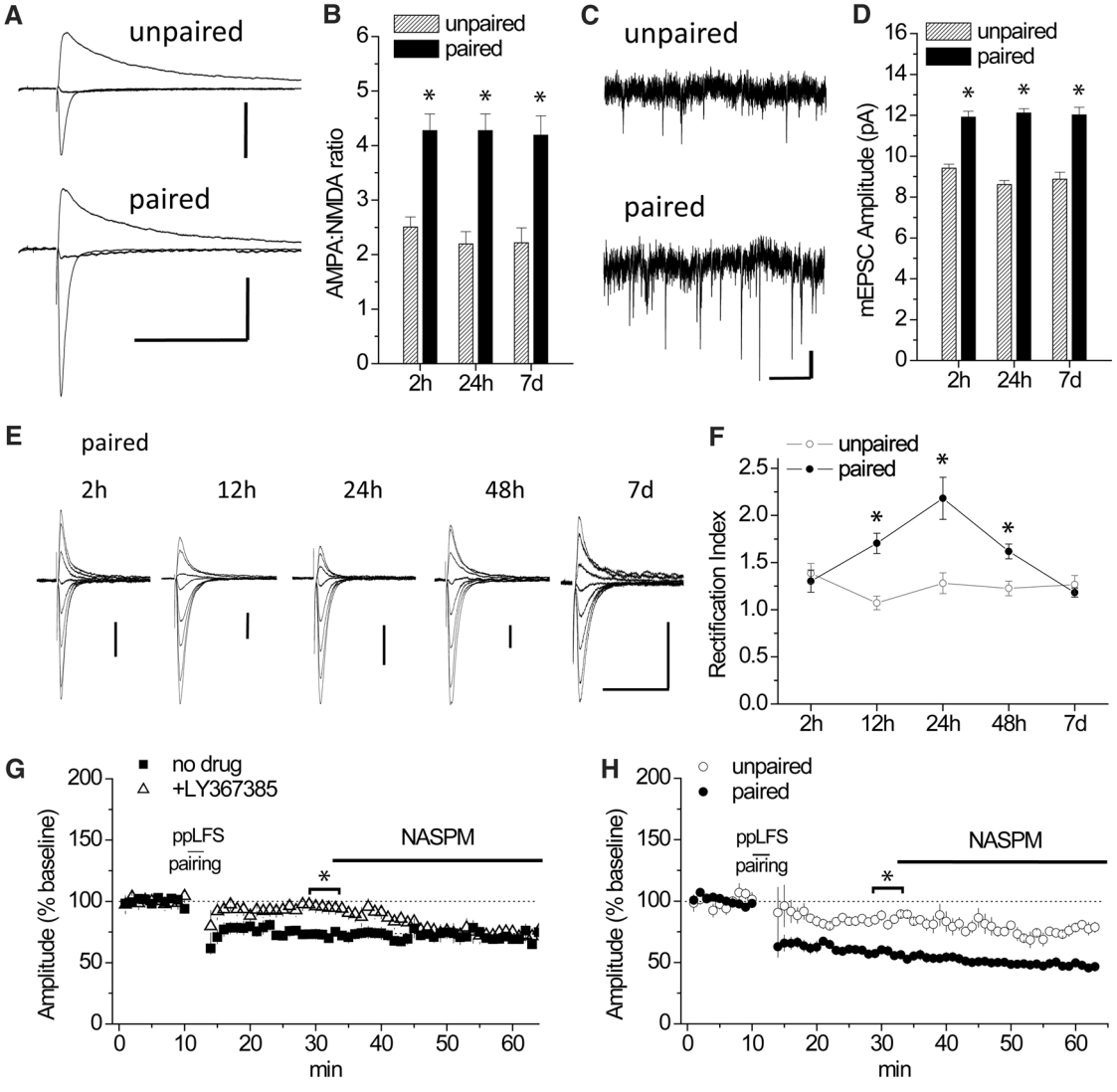

Fig. 1. Fear conditioning alters AMPAR subunit composition and LTD at thalamo-LA synapses. Training entailed six CSs (auditory tones) and USs (footshocks) delivered in a paired or unpaired configuration. (**A**) EPSCs at membrane holding potential (V_h) = −70, 0, and +40 mV, scaled to peak amplitude at +40 mV, at 24 hours after conditioning. Scale bars, 100 pA × 200 ms. (**B**) AMPA:NMDA ratio as a function of time after conditioning. *P < 0.01 analysis of variance (ANOVA); Tukey's post-hoc test for paired (n = 11 to 12 cells) versus unpaired (n = 7 to 10 cells) configuration. h, hours; d, days. (**C**) mEPSCs at 24 hours after conditioning. Scale bar, 5 pA × 1 s. (**D**) mEPSC amplitude as a function of time after conditioning. *P < 0.0001 ANOVA; Tukey's post-hoc paired versus unpaired cells. (**E**) AMPAR-EPSCs after paired conditioning at V_h = −70, −60, −40, −20, 0, +20, +40, and +50 mV, normalized to peak amplitude at −70 mV. Scale bars, 50 pA × 40 ms. (**F**) Rectification index. *P < 0.05 ANOVA; Tukey's post-hoc for paired (n = 6 to 9 cells) versus unpaired (n = 5 to 7 cells) configuration. (**G**) In slices from naïve mice, LTD induction by ppLFS pairing (with a 3-Hz paired-pulse stimulation at a 50-ms interpulse interval, for 3 min at −50 mV) without drug (n = 6 cells) or in the presence of LY367385 (100 μM, n = 6 cells), followed by normalization of EPSC amplitude by NASPM. (**H**) Enhanced LTD 24 hours after conditioning. Paired (n = 6 cells) and unpaired (n = 5 cells) configurations are shown. *P < 0.05, Student's t test.

be explained by reduced coupling of synaptic activity to CP-AMPAR trafficking.

In the above experiments, reconsolidation update was performed on day 1 after fear conditioning, when CP-AMPARs are transiently elevated and susceptible to removal by reconsolidation update. To examine whether erasure is effective after CP-AMPARs have subsided, we performed reconsolidation update on day 7. In that case, we observed significant recurrence of fear in both no-retrieval and retrieval groups on day 14 (Fig. 2F). Furthermore, on day 7, reconsolidation update conferred no benefit over no-retrieval extinction in the reduction of fear, suggesting that an abundance of CP-AMPARs at the time of extinction enables erasure.

Having established a role for CP-AMPARs in reconsolidation update, we next investigated the molecular requirements for their synaptic delivery. Conditioned fear requires glutamate receptor 1 (GluA1)–containing AMPARs (*23*, *24*), whose phosphorylation-dependent trafficking underlies synaptic plasticity (*25*–*27*). Phosphorylation of the protein kinase A (PKA) target serine-845 (S845A) in GluA1 has also been shown to regulate the stability of CP-AMPARs (*19*). We therefore examined CP-AMPAR dynamics in GluA1 phosphorylation site knockin (KI) mutant mice. Alanine substitution of the protein kinase C (PKC)/calcium-calmodulin–dependent kinase II target residue serine-831 (S831A) did not prevent an increase in rectification 24 hours after conditioning (Fig. 4, A and B). However, mutation of the PKA site S845A abolished fear-induced enhancement of CP-AMPAR currents (Fig. 4, A to C). Despite their failure to accumulate CP-AMPARs, however, S845A synapses were nevertheless potentiated by fear conditioning (Fig. 4, D to F). However, because of the absence of CP-AMPAR dynamics, LTD was unaffected by fear conditioning or extinction in S845A mutants (Fig. 4G).

Because CP-AMPAR synaptic removal underlies reconsolidation update, we next examined fear memory erasure in GluA1 mutants. Freezing in S845A animals was equivalent to that in wild-type littermates during conditioning on day 0 and reconsolidation update on day

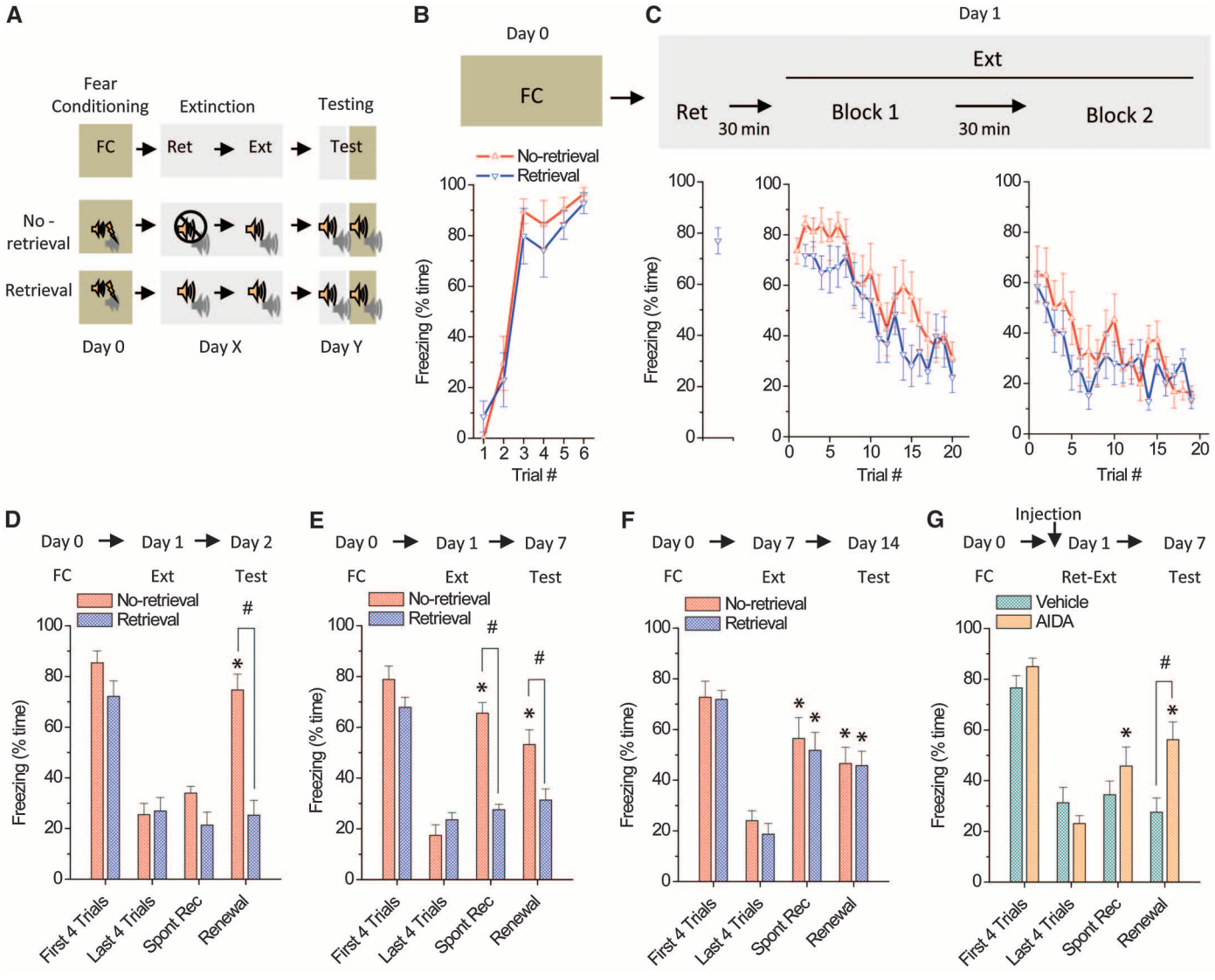

Fig. 2. Reconsolidation update performed soon after fear conditioning (FC) erases fear. (**A**) Experimental groups. Ret, retrieval; Ext, extinction. (**B** and **C**) CS-evoked freezing during conditioning and extinction. (**D** to **F**) Freezing was averaged for the first and last four trials of extinction. Spontaneous recovery (Spont Rec) and renewal were assessed by test comparison with the last four trials of extinction. Repeated-measures ANOVA revealed a significant group × test interaction in (D) [$F_{3,39} = 10.1$, $P < 0.0001$ ($n = 7$ to 8 mice)] and (E) [$F_{3,36} = 9.6$, $P < 0.0001$ ($n = 7$ to 8 mice)] but not in (F) [$F_{3,36} = 0.34$, $P = 0.80$ ($n = 6$ to 8 mice)]. *$P < 0.001$, Tukey's post-hoc comparison with the last four trials. #$P < 0.0001$. (**G**) Effect of systemic AIDA 1 hour before retrieval extinction (Ret-Ext). Repeated-measures ANOVA, treatment × test: $F_{3,48} = 4.95$, $P < 0.01$ ($n = 8$ to 10 mice). *$P < 0.01$, Tukey's post-hoc comparison with the last four trials. #$P < 0.01$.

1 (Fig. 4, H and I, and fig. S10). However, retrieval extinction was accompanied by significant renewal of fear on day 2 in S845A mutants but not in wild-type littermates (Fig. 4H). In addition, on day 7 after reconsolidation update on day 1, S845A retrieval mice displayed fear recurrence in both spontaneous recovery and renewal tests (Fig. 4I), whereas wild-type littermates did not. Conversely, S831A mutants did not relapse under these conditions (fig. S11), indicating that serine-845 phosphorylation is a specific prerequisite for memory erasure during reconsolidation update. These results do not rule out effects of S845A mutation in brain regions beyond the amygdala. However, a wealth of data illustrates the requirement for LA synaptic plasticity in conditioned fear (*11*, *12*), supporting our conclusion that the reversal of synaptic strengthening by CP-AMPAR trafficking (Fig. 3) mediates fear erasure.

Our data reveal that even as fear memories are maintained by persistent increases in excitatory transmission, underlying changes in the molecular composition of AMPARs make these imprints vulnerable to erasure. These effects demonstrate the behavioral significance of GluA1 serine-845 phosphorylation and CP-AMPAR dynamics, which occur in several brain regions after in vivo experience (*15*), and suggest that this form of metaplasticity may loosen constraints on behavioral reversals in other models. In particular, a switch from GluA2-containing to GluA2-lacking AMPARs occurs in the ventral tegmental area (*16*) and nucleus accumbens (*18*) after cocaine experience. Thus, CP-AMPAR trafficking may also constitute a strategy for the erasure of drug memories. Indeed, it is also possible that CP-AMPARs regulate memory erasure and editing through their accumulation at additional sites throughout the brain.

Coactivation of NMDARs and mGluR1, which removes synaptic CP-AMPARs during in vitro LTD, may distinguish reconsolidation update from conventional extinction. Interestingly, pharmacological enhancement of NMDAR currents alleviates the recurrence of fear after extinction (*28*, *29*). Our results suggest that this effect may be attributable to CP-AMPAR synaptic removal. Similarly, mGluR1 may also be an effective drug target for improving the long-term success of extinction, or exposure-based therapy, in preventing the return of emotional responses.

Extinction-induced erasure has been interpreted as interference with the reconsolidation

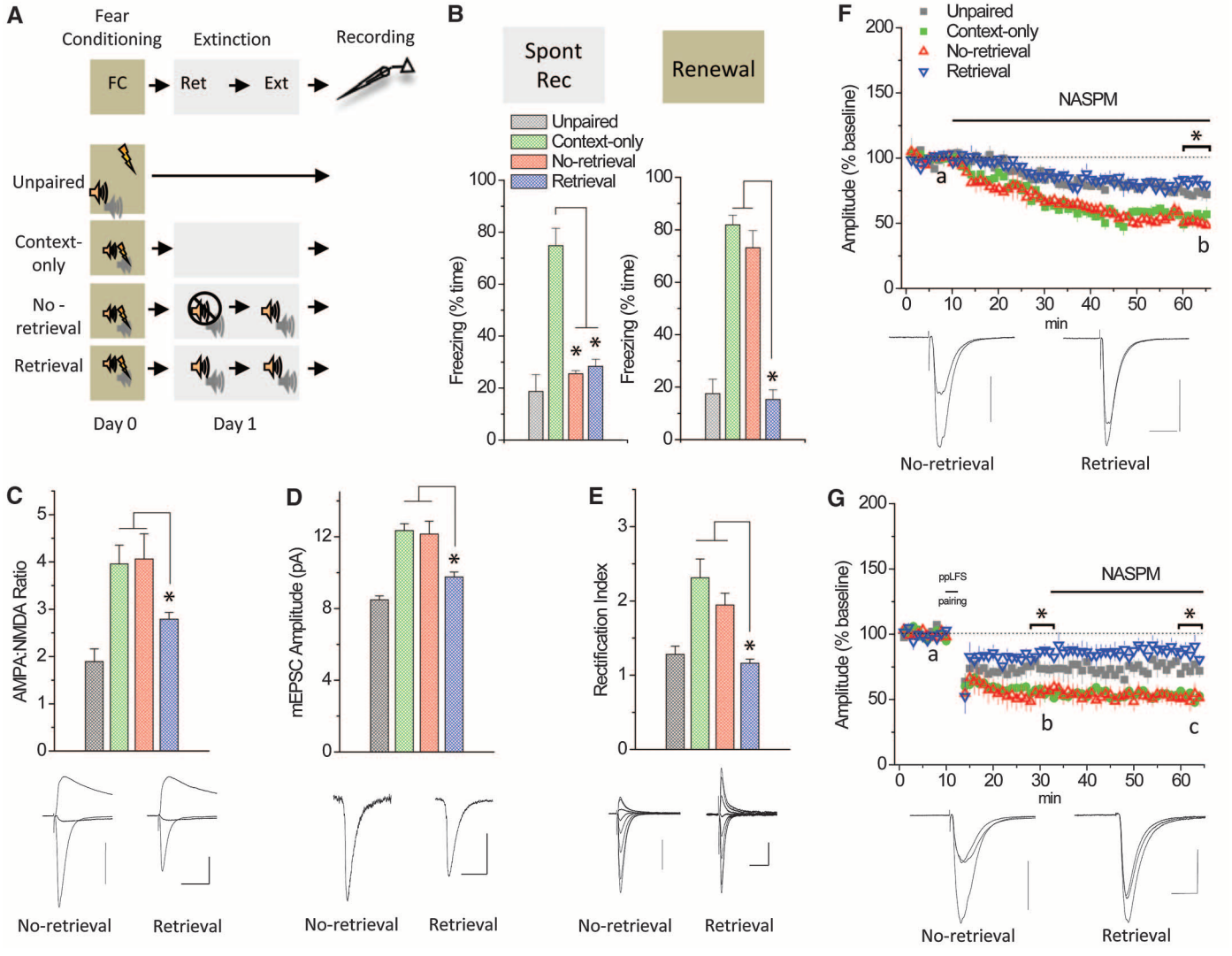

Fig. 3. Reconsolidation update dampens amygdala transmission via removal of synaptic CP-AMPARs. (**A**) Treatment groups for synaptic physiology. (**B**) Freezing during spontaneous recovery and renewal tests 2 hours after extinction. *$P < 0.01$ ANOVA, Tukey's post-hoc test ($n = 6$ mice each). (**C** to **F**) AMPAR properties 2 hours after extinction, including AMPA:NMDA ratio [(C), $n =$ 7 to 9 cells], AMPAR-mEPSC amplitude [(D), $n = 8$ to 18 cells], AMPAR-EPSC rectification index [(E), $n = 7$ to 13 cells], and AMPAR-EPSC sensitivity to NASPM [(F), $n = 5$ to 6 cells]. *$P < 0.01$ ANOVA, Tukey's post-hoc test. Scale bars for (C) to (E) are as follows: (C) 100 pA × 40 ms, (D) 5 pA × 20 ms, (E) 50 pA × 40 ms. (F) Representative traces from time points a and b; scale bars, 100 pA × 20 ms. (**G**) ppLFS pairing LTD followed by test for CP-AMPARs by NASPM (50 μM). *$P < 0.01$ ANOVA followed by Tukey's post-hoc comparison of retrieval with context-only and no-retrieval. Representative traces from time points a, b, and c are shown; scale bars, 100 pA × 20 ms.

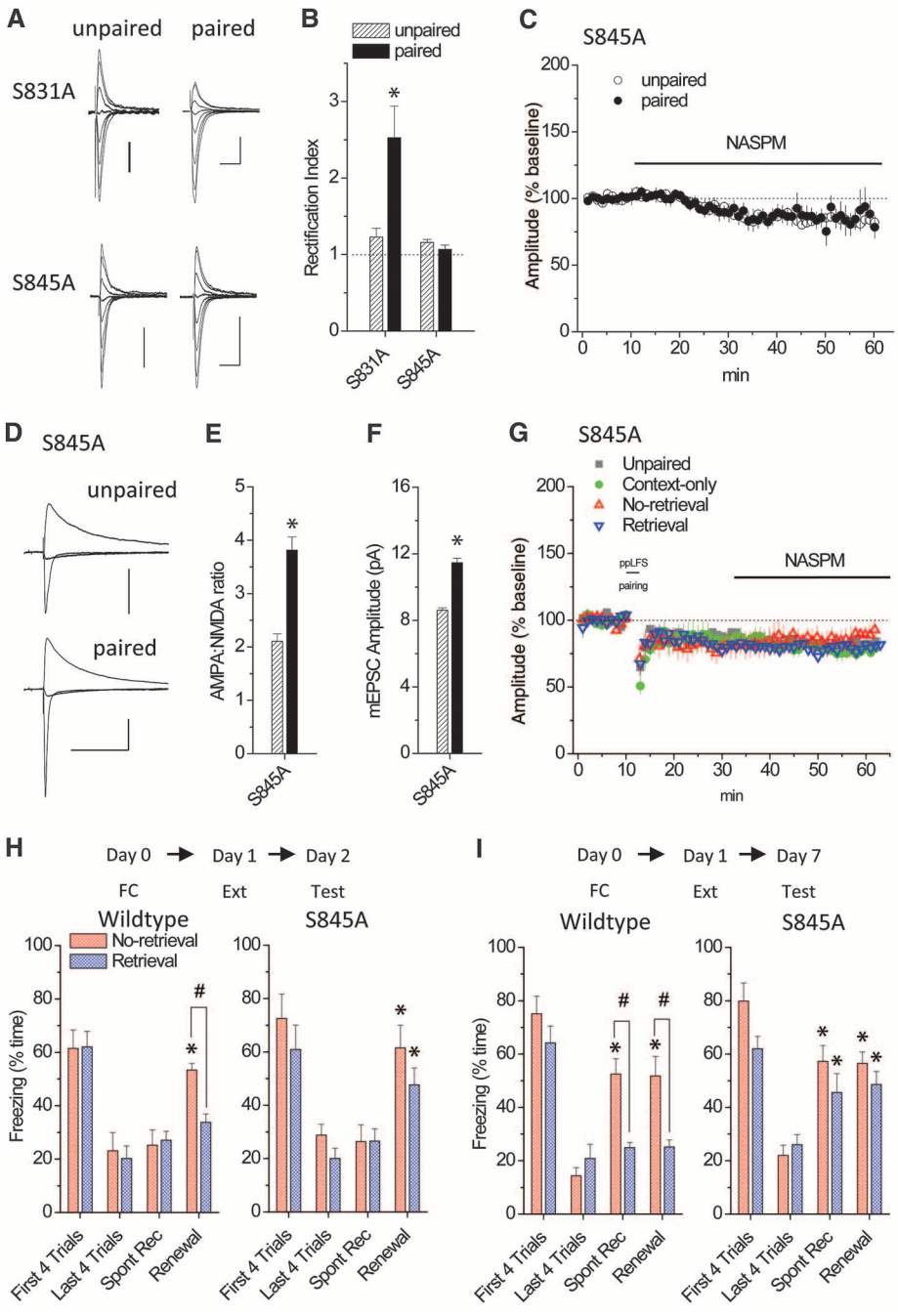

Fig. 4. GluA1 phosphorylation regulates LTD and fear erasure by controlling synaptic CP-AMPAR levels. (**A**) AMPAR-EPSCs at V_h = −70, −60, −40, −20, 0, +20, +40, and +50 mV, scaled to peak amplitude at −70 mV, in homozygous GluA1 S831A mice (n = 6 each) and S845A knockin mutant mice (n = 6 to 8) 24 hours after conditioning. Scale bars, 100 pA × 40 ms. (**B**) Rectification index 24 hours after conditioning. *P < 0.02, Student's t test. (**C** to **F**) For S845A mutants 24 hours after conditioning, the NASPM sensitivity of AMPAR-EPSCs [(C), n = 5 to 6 cells], the AMPA:NMDA ratio [(D) and (E), n = 9 to 14 cells], and the AMPAR-mEPSC amplitude [(F), n = 7 to 8 cells] are shown. *P < 0.001, Student's t test. Scale bars in (D), 100 pA × 200 ms. (**G**) ppLFS pairing in S845A knockin mice 2 hours after reconsolidation update on day 1 (as in Fig. 2). (**H** and **I**) Spontaneous recovery and renewal in S845A knockin mice and wild-type littermates after reconsolidation update. (H) Repeated measures ANOVA, group × test interaction: for the wild type, $F_{3,33}$ = 3.29, P < 0.05 (n = 5 to 8 mice); for S845A mice, $F_{3,33}$ = 1.69, P = 0.19 (n = 5 to 8 mice). (I) Repeated measures ANOVA, group × test interaction: for the wild type, $F_{3,36}$ = 4.72, P < 0.01 (n = 6 to 8 mice); for S845A mice, $F_{3,36}$ = 0.54, P = 0.66 (n = 6 to 8 mice). *P < 0.01 Tukey's post-hoc comparison with the last four trials. #P < 0.01.

of memory by CS exposure (*6*). The progressive consolidation of memories onto new substrates, or even their translocation to different brain areas (*30*), may dictate that recent and remote memories undergo different forms of editing. Our data indicate that soon after initial consolidation, changes in synaptic properties render the permanence of recent memory highly reversible. This period may be important for the fine-tuning of information stored by the fear system, as well as a useful point for intervention in alleviating traumatic memories.

References and Notes

1. G. D. Gale *et al.*, *J. Neurosci.* **24**, 3810 (2004).
2. R. J. McNally, *Clin. Psychol. Rev.* **27**, 750 (2007).
3. C. Herry *et al.*, *Eur. J. Neurosci.* **31**, 599 (2010).
4. H. C. Pape, D. Pare, *Physiol. Rev.* **90**, 419 (2010).
5. N. Gogolla, P. Caroni, A. Lüthi, C. Herry, *Science* **325**, 1258 (2009).
6. M. H. Monfils, K. K. Cowansage, E. Klann, J. E. LeDoux, *Science* **324**, 951 (2009).
7. D. Schiller *et al.*, *Nature* **463**, 49 (2010).
8. G. P. Urcelay, D. S. Wheeler, R. R. Miller, *Learn. Behav.* **37**, 60 (2009).
9. N. C. Huff, J. A. Hernandez, N. Q. Blanding, K. S. LaBar, *Behav. Neurosci.* **123**, 834 (2009).
10. S. Maren, C. H. Chang, *Proc. Natl. Acad. Sci. U.S.A.* **103**, 18020 (2006).
11. S. M. Rodrigues, G. E. Schafe, J. E. LeDoux, *Neuron* **44**, 75 (2004).
12. E. A. Phelps, J. E. LeDoux, *Neuron* **48**, 175 (2005).
13. M. G. McKernan, P. Shinnick-Gallagher, *Nature* **390**, 607 (1997).
14. M. T. Rogan, U. V. Stäubli, J. E. LeDoux, *Nature* **390**, 604 (1997).
15. S. J. Liu, R. S. Zukin, *Trends Neurosci.* **30**, 126 (2007).
16. C. Bellone, C. Lüscher, *Nat. Neurosci.* **9**, 636 (2006).
17. R. L. Clem, A. Barth, *Neuron* **49**, 663 (2006).
18. K. L. Conrad *et al.*, *Nature* **454**, 118 (2008).
19. K. He *et al.*, *Proc. Natl. Acad. Sci. U.S.A.* **106**, 20033 (2009).
20. M. T. Ho *et al.*, *J. Neurosci.* **27**, 11651 (2007).
21. S. Q. Liu, S. G. Cull-Candy, *Nature* **405**, 454 (2000).
22. K. Nader, O. Hardt, *Nat. Rev. Neurosci.* **10**, 224 (2009).
23. Y. Humeau *et al.*, *J. Neurosci.* **27**, 10947 (2007).
24. S. Rumpel, J. LeDoux, A. Zador, R. Malinow, *Science* **308**, 83 (2005).
25. J. Boehm *et al.*, *Neuron* **51**, 213 (2006).
26. H. K. Lee, M. Barbarosie, K. Kameyama, M. F. Bear, R. L. Huganir, *Nature* **405**, 955 (2000).
27. H. K. Lee *et al.*, *Cell* **112**, 631 (2003).
28. S. C. Mao, Y. H. Hsiao, P. W. Gean, *J. Neurosci.* **26**, 8892 (2006).
29. D. L. Walker, K. J. Ressler, K. T. Lu, M. Davis, *J. Neurosci.* **22**, 2343 (2002).
30. T. Sacco, B. Sacchetti, *Science* **329**, 649 (2010).

31. Supported by grants from NIH (R01NS036715) and the Howard Hughes Medical Institute. R.L.C. was supported by a postdoctoral fellowship from NIH (F32 MH087037-01). We thank G. Thomas, D. Linden, L. Volk, and A. Lade for helpful comments.

Supporting Online Material

www.sciencemag.org/cgi/content/full/science.1195298/DC1
Materials and Methods
Figs. S1 to S11
References

19 July 2010; accepted 15 October 2010
Published online 28 October 2010;
10.1126/science.1195298

Universality in the Evolution of Orientation Columns in the Visual Cortex

Matthias Kaschube,[1,2]* Michael Schnabel,[1,3] Siegrid Löwel,[4,5,6] David M. Coppola,[7] Leonard E. White,[8] Fred Wolf[1,5]*

The brain's visual cortex processes information concerning form, pattern, and motion within functional maps that reflect the layout of neuronal circuits. We analyzed functional maps of orientation preference in the ferret, tree shrew, and galago—three species separated since the basal radiation of placental mammals more than 65 million years ago—and found a common organizing principle. A symmetry-based class of models for the self-organization of cortical networks predicts all essential features of the layout of these neuronal circuits, but only if suppressive long-range interactions dominate development. We show mathematically that orientation-selective long-range connectivity can mediate the required interactions. Our results suggest that self-organization has canalized the evolution of the neuronal circuitry underlying orientation preference maps into a single common design.

In the visual cortex of carnivores and primates, neurons selective for the orientation of visual edges are organized in orientation columns, which are vertical arrays of neurons that prefer the same orientation (*1*–*5*). Not all mammals have orientation columns (*4*). Mammalian taxa that do have been on separate evolutionary paths for more than 65 million years (Fig. 1A) (*6*–*8*), colonizing disparate ecological niches and evolving disparate cortical architectures (*9*). Nevertheless, these taxa share an architecture of orientation columns arranged around numerous singularities, called pinwheel centers (*2*, *3*, *5*, *10*, *11*). Around each singularity, the neuronal preferences for stimulus orientation are circularly arranged, ascending, as in a spiral staircase, either clockwise or counterclockwise from 0° to 180°. Pinwheel organization is similar across disparate mammalian taxa; it is, however, unknown whether this qualitative similarity is imposed by evolutionary history, ecological or developmental constraints, or neural function. To address these issues, we analyzed the arrangement of pinwheels in the visual cortex of three phylogenetically and ecologically diverse species (*6*–*8*, *12*): the tree shrew (*Tupaia belangeri*), galago (*Otolemur crassicaudatus*), and ferret (*Mustela putorius*). Tree shrews and galagos are more closely related to rodents and lagomorphs, which lack orientation columns (*4*, *9*), than to carnivores (*6*–*8*). This taxonomic sample allowed us to compare mammals diverging from the primate lineage either before (ferrets) or after (tree shrews) the supraprimate ancestor (Fig. 1A).

We developed a statistical approach based on the concept of pinwheel density ρ (*13*), which we define as the mean number of pinwheels per orientation-hypercolumn area (*1*). For geometrically defined subregions of each map, we calculated independent estimates of local column spacing Λ (*14*) and pinwheel number, defined the area of an orientation hypercolumn as Λ^2 (*14*), and estimated the pinwheel density ρ in each subregion (*12*). This definition does not presuppose the existence of a discrete set of orientation hypercolumns and is consistent with the original notion (*1*, *13*). Pinwheel density characterizes the layout of orientation columns independently of their absolute size and can differentiate between different column layouts (Fig. 1B) (*13*, *15*–*17*) that may occur even in directly adjacent cortical regions (Fig. 1, C and D).

We first examined the mean pinwheel density averaged over entire hemispheres. Whereas hypercolumn sizes varied substantially between individuals and species, the number of pinwheels occurring per square millimeter scaled with hypercolumn size so that the average pinwheel density was virtually identical (Fig. 2, A and B): 3.12 [3.06, 3.18] {mean [2.5, 97.5] percentiles of bootstrap confidence interval (BCI) (fig. S7) (*12*) in tree shrew, 3.15 [2.97, 3.30] in galago, and 3.15 [3.08, 3.22] in ferret (values were confirmed with automated analysis) (fig. S4) (*12*)}.

Second, we assessed intramap heterogeneity and local arrangement of neighboring pinwheels. We characterized the variability of pinwheel densities by its standard deviation (SD) in subregions of size A between one and 30 hypercolumns (Fig. 2, C and D). SDs of pinwheel densities were very similar for tree shrew, galago, and ferret and different from values characterizing a distribution of randomly positioned pinwheels (fig. S6) (*12*). Analyzing histograms of nearest-neighbor (NN) distances in units of local column spacing of the respective cortical region for the three species, we observed virtually identical distributions (Fig. 2E). Histograms were also similar when calculated for pairs of same or opposite topological charges (Fig. 2F), where charge denotes whether preferred orientations increase clockwise or anti-clockwise around a pinwheel center (Fig. 1F).

These observations suggest that orientation column layouts follow a common design characterized by the virtual identity of (i) pinwheel density, (ii) pinwheel density fluctuations as a function of subregion size, and (iii) NN distance distributions. An objective quantitative assessment of pinwheel density and its fluctuations and of the NN distance statistics confirmed this concept. To quantitatively compare pinwheel density fluctuations, we defined a variability exponent, γ, and a variability coefficient, *c*, and estimated them by fitting the SD(A) curves with $c(\rho/A)^{\gamma}$ (figs. S6, S10) (*12*), where A is the subregion size. To assess the similarity of the NN distance statistics, we used the average distances of NN pinwheels, d, and of pinwheels of same or opposite topological charges, d^{+-} and d^{+-} (fig. S11) (*12*). Relative differences in all parameters were on average below 9%, with one exception below 5% (tables S1 and S2) (*12*). Furthermore, almost all confidence intervals for the considered parameters overlapped for different species (fig. S7) (*12*). Thus, in quantitative terms, differences between species were typically very small, confirming the concept of a common design for the layout of orientation columns.

How can this common design observed among species long-separated in mammalian evolution be explained? Recognizing that ancestral eutheria were small-brained nocturnal mammals, with modest visual abilities and a small neocortex that was already subdivided into several cortical areas (*6*), and that orientation hypercolumns in extant species are relatively large, it is unlikely that orientation columns and the common design are retained from stem eutheria (*12*). The phylogenetic relations depicted in Fig. lA would then indicate that systems of orientation columns evolved independently in laurasiatheria (such as carnivores) and in euarchonta (such as tree shrews and primates). Alternatively, one might hypothesize that ancestral mammals in the cretaceous already possessed a primitive system of few or miniaturized orientation columns. Even assuming such a homology scenario, the precision with which orientation column layout follows the common design in disparate mammalian lineages implicates a common, constraining developmental mechanism (*12*).

As the formation and maintenance of orientation-preference maps is activity-dependent (*18*), we thus examined orientation maps generated by models involving activity-dependent self-organization. In many models, maps reminiscent of the common

[1]Max-Planck-Institute for Dynamics and Self-Organization, Bernstein Center for Computational Neuroscience, Faculty of Physics, Göttingen University, D-37073 Göttingen, Germany; and Kavli Institute for Theoretical Physics, Santa Barbara, CA 93106–4030, USA. [2]Lewis-Sigler Institute for Integrative Genomics, Department of Physics, Princeton University, Princeton, NJ 08544, USA. [3]Physical Sciences–Oncology Center, Northwestern Institute on Complex Systems, Departments of Applied Mathematics and Physics, Northwestern University, Evanston, IL 60208, USA. [4]Institute for General Zoology and Animal Physiology, University of Jena, D-07743 Jena, Germany. [5]Bernstein Focus for Neurotechnology, Göttingen University, D-37073 Göttingen, Germany. [6]School of Biology, Göttingen University, D-37073 Göttingen, Germany. [7]Department of Biology, Randolph-Macon College, Ashland, VA 23005, USA. [8]Department of Community and Family Medicine, Duke Institute for Brain Sciences, Duke University, Durham, NC 27710, USA.

*To whom correspondence should be addressed. E-mail: kaschube@princeton.edu (M.K.); fred-wl@nld.ds.mpg.de (F.W.)

design transiently appeared but—in agreement with previous reports—subsequently broke down either by pinwheel annihilation producing pinwheel-sparse maps (*12*, *13*, *16*, *17*) or by crystallization of pinwheels into a regular lattice (*12*, *16*, *19*, *20*). However, in a model in which pinwheels are stabilized through long-range neuronal interactions (*12*, *17*, *21*) we found that theoretically predicted maps exhibited all essential features of the common design in a dynamically stable and robust fashion (Figs. 1B, quasi-periodic map, and 3) (*12*). In this long-range interaction model, only orientation preference and selectivity are mathematically specified for simplicity. Patterns of orientation columns of a given spatial wavelength Λ develop with an effective growth rate r. Whether long-range or short-range interactions stabilize the orientation map is determined by an effective coupling parameter, g (*17*). Long-range interactions dominate for $\sigma > \Lambda$ and $g < 1$. As we show in (*12*), this model can be derived from biologically plausible assumptions about the structure of long-range connectivity in the visual cortex.

The mathematical properties of the long-range interaction model suggest an explanation for the emergence of the common design in disparate evolutionary branches (laurasiatherian and euarchontan). Near the instability threshold ($r \ll 1$), a large set of stationary solutions of this model exhibit the property of universality; they are the common solutions of an entire class of models. This class is defined by four symmetry principles that guarantee that maps that are translated or rotated across the cortical surface or for which receptive fields are rotated by a fixed angle can occur with equal probability and that all orientations are represented by the visual cortex (*17*). Pinwheel configurations in these universal solutions exhibit universal pinwheel statistics, and when the interaction range is substantially larger than one column spacing, these statistics are very similar to the common design (Fig. 3, C and E to H) (*12*). In fact, apart from a slightly smaller variability coefficient c average differences between pinwheel statistics in representative maps (eq. S20, $n = 20$ active modes) (*12*) and in experimental observations were below 5% (tables S1 and S2) (*12*). It is thus not required that exactly the same mechanisms underly map development in disparate lineages as long as they are described by models from the same universality class as the long-range interaction model. Our analyses suggest that such mechanisms of network development include suppressive long-range interactions (*12*) that extend beyond a single hypercolumn (*12*) and stabilize the orientation map (*12*, *15*). In numerical simulations of the long-range interaction model, we found that realistic pinwheel statistics can already occur in transient states and farther away from the instability threshold and for interaction ranges between one and two hypercolumns (Fig. 3D) (*12*). These results suggest that the robust emergence of the common design in mammalian evolution is explained by selection for self-organizing cortical networks dominated by long-range interactions.

To assess this apparent robustness experimentally, we analyzed properties of orientation maps in ferrets reared in darkness beginning about 1 week before eye opening and the emergence of orientation maps (*22*). Dark-rearing alters the spatiotemporal pattern of activity in the afferent visual pathway, induces abnormal receptive field properties in the lateral geniculate nucleus (*23*) and visual cortex (*24*), but does not prevent the formation of orientation maps (Fig. 4, A and B) (*22*). The average pinwheel density in dark-reared ferrets was 3.22 [3.13, 3.30] and thus indistinguishable from normal ferrets ($P = 0.14$) (Fig. 4C and table S3) (*12*). Moreover, both pinwheel-density variability and NN distances in dark-reared ferrets were similar to those of normal ferrets, with overlapping confidence intervals for all assessed statistics (*12*).

For large interaction ranges, the mean pinwheel density predicted by the universal pinwheel statistics rapidly approaches an asymptotic constant equal to π (*21*). This raises the possibility that the pinwheel density in the common design is a mathematical constant. In support of this possibility, the grand average pinwheel density 3.14 [3.08, 3.20] in all three species was statistically indistinguishable from π. To assess whether our analysis methods might bias mean pinwheel densities toward π, we analyzed randomly generated orientation maps (*13*) by randomizing the phases of the original measurements in the Fourier domain and then subjected the randomized maps to the same pre-

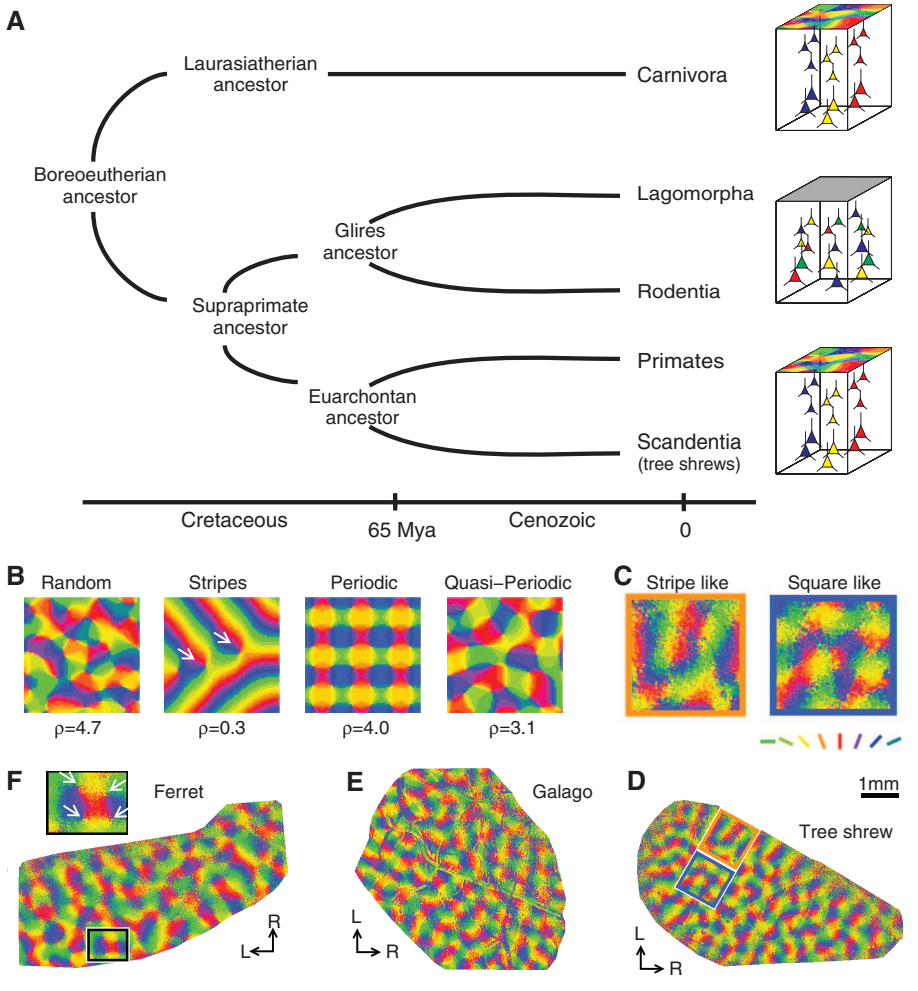

Fig. 1. Orientation selectivity in the visual cortex of diverse boreoeutherian mammals. (**A**) phylogenetic relationships (*6*–*8*) between mammalian ancestors, the three species examined, and rodents and lagomorphs. (Right) Arrangement of orientation-selective neurons in these species. Rodents and lagomorphs show salt-and-pepper arrangement of preferred orientations (ORs). Carnivores, primates, and tree shrews show columnar arrangement of preferred ORs. (**B**) Synthetic orientation maps of equal column spacing Λ but widely different pinwheel densities ρ. From left to right are the solutions of different models (*13*, *15*–*17*). Colors code preferred ORs as indicated by the bars in (C). (**C**) High (blue frame) and low (orange frame) pinwheel density regions in tree shrew visual cortex. (**D** to **F**) Optically recorded orientation maps in (D) tree shrew, (E) galago, and (F) ferret visual cortex. Regions shown in (C) are marked in (D). White arrows in (F) mark selected pinwheel centers. Framed regions in (C) and (F) are magnified.

processing and analyses as the original data (Fig. 4, D and E). Randomized maps exhibited significantly higher pinwheel densities {between 3.15 and 3.9, mean = 3.50 [3.41, 3.59]} than what we found in any of the species ($P < 10^{-4}$) (Fig. 4F and tables S1 and S3) (*12*). For several other statistics, randomized maps differed considerably more from the three analyzed species than the species did from one another (tables S1 to S3) (*12*).

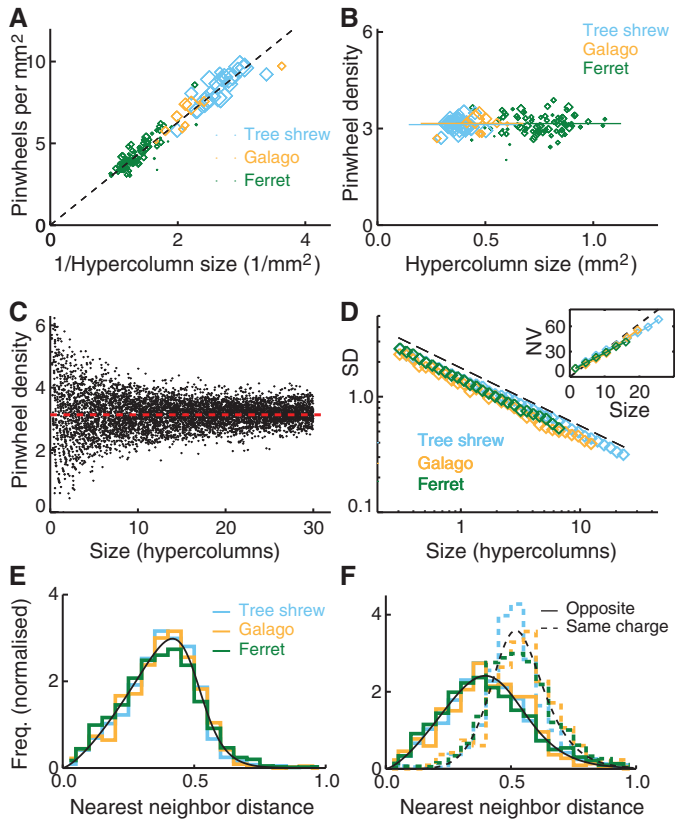

Fig. 2. Common design of orientation maps and pinwheels in ferret, tree shrew, and galago. (**A**) The mean number of pinwheels per square millimeter, r, scales with the inverse of hypercolumn size Λ^2 in individuals of the three species (tree shrew, n = 26 hemispheres; galago, n = 9 hemispheres; ferret, n = 82 hemispheres; symbol size proportional to map size in units of Λ^2). Dashed line indicates $r = \langle\rho\rangle/\Lambda^2$ (where $\langle\rho\rangle = 3.14$ grand average pinwheel density). (**B**) Dimensionless pinwheel densities ρ versus hypercolumn size. Solid lines indicate average pinwheel densities of the three species. (**C**) Pinwheel densities estimated for regions of up to 30 hypercolumns randomly selected from tree shrew orientation maps (*12*). Red dashed line indicates average pinwheel density in tree shrew. (**D**) SDs of pinwheel densities estimated from randomly selected regions for the three species. Black dashed curve indicates SD for a two-dimensional Poisson process of equal density. (Inset) Number variance (NV) for tree shrew, ferret, and galago and for the Poisson process. (**E** and **F**) NN distances for pinwheels of (E) arbitrary and (F) opposite and equal topological charge (*12*). Black curves indicate $f(x) = ax^n/\{1 + \exp[(x - x_0)/b)]\}$ [(E) $n = 1.2$, $x_0 = 0.48$, $b = 0.047$], [(F) solid curve, $n = 1.2$, $x_0 = 0.46$, $b = 0.08$; dashed curve, $n = 4.5$, $x_0 = 0.5$, $b = 0.05$]. Distances are in units of Λ.

Our empirical results and theoretical analyses suggest that the precise spatial organization of pinwheels in the visual cortex reflects cortical network self-organization rather than genetic prespecification or environmental instruction of neuronal circuit development. Our theory reveals that dynamical network self-organization can robustly constrain the spatial organization of cortical circuitry to a specific design. Currently, only one alternative arrangement has been observed in nature: the columnless, apparently random, salt-and-pepper organization of rodent visual cortex (*4*, *9*). Because a complete lack of local order appears to be its key feature, we expect that fundamental properties of local rather than long-range circuit formation are essential for its self-organization. It is possible that this fundamentally different organization can also be derived from a dynamical theory of network self-organization. If so, the principles of network self-organization operating on a local order would account for the presence or absence of orientation columns, whereas long-ranging interactions would explain the organization of orientation columns into pinwheels, with a spatial layout conforming to the common design.

Our analysis of the long-range interaction model predicts that spatial range and an overall suppressive nature of nonlocal interactions are essential for the formation of the pinwheel layout in carnivores and primates. These requirements are consistent with the physiological action of nonlocal influences in the visual cortex (*12*, *25*) but hard to reconcile with the notion that pinwheels are quasi-isolated local circuit elements. The relevant genes controlling their formation are thus expected to concern the regulation of lateral axon outgrowth and the setting of overall synaptic input balance (*14*, *25*). Genetic or

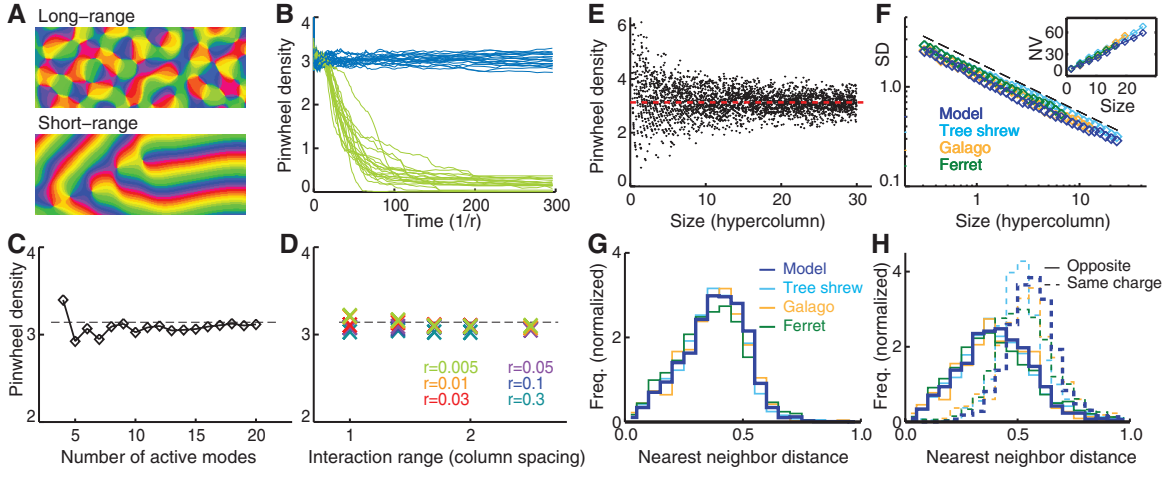

Fig. 3. Self-organization of orientation columns dominated by long-range interactions explains the common design. (**A**) Nearly stationary solutions of the long-range interaction model (eqs. S10 to S13) (*12*) are pinwheel-rich when long-range interactions dominate and pinwheel-sparse when they are absent. (**B**) Pinwheel densities as a function of time without long-range interactions (green, $r = 0.1$, $g = 2$, $n = 30$ different random initial conditions) and when long-range interactions dominate (blue, $r = 0.1$, $\sigma = 1.7$, $g = 0.98$, $n = 30$ different random initial conditions). (**C**) Average pinwheel densities $\langle\rho\rangle$ of closed-form solutions for $r << 1$ (eq. S20) (*12*). Solutions consists of n active modes (Fourier components; error bars are smaller than symbol size). In the long-range interaction model, n scales linearly with interaction range σ (*12*). (**D**) Average densities $\langle\rho\rangle$ in numerical solutions for different r at $t = 300$ ($g = 0.98$, $\sigma = 1.7$). (**E** to **H**) Spatial statistics of pinwheels (as in Fig. 2) for $n = 26$ randomly chosen closed-form solutions (eq. S20, $n = 20$ active modes) (*12*).

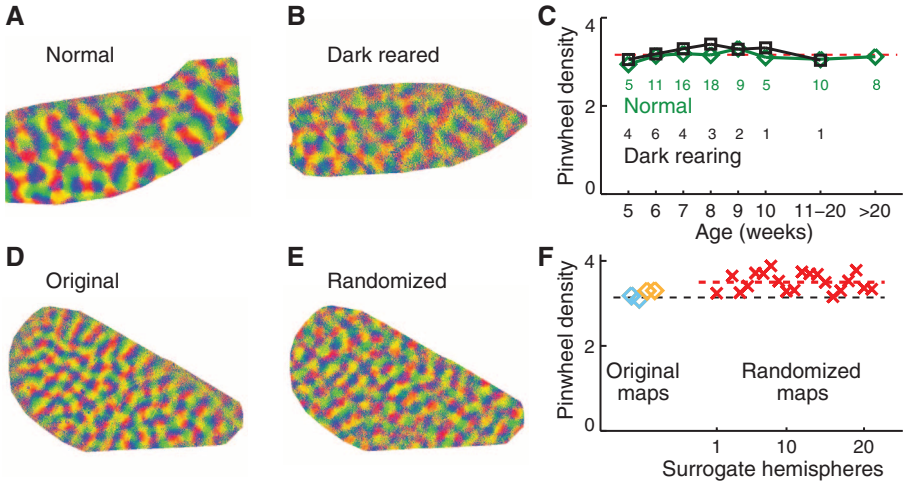

Fig. 4. The common design persists under dark-rearing (**A** to **C**) but not under phase randomization (**D** to **F**) and is attained early during development (C). Orientation maps from (A) a normal and (B) a dark-reared ferret. (C) Pinwheel densities for dark-reared (n = 21) and normal ferrets (n = 82) versus postnatal age (numbers are the sample sizes). Random orientation maps (E) generated from the tree shrew orientation map (D) by phase shuffling in the Fourier domain (*12*). (F) Pinwheel densities of randomized maps (crosses, n = 20 randomized maps) and of original maps [diamonds, n = 4 (tree shrew, n = 2; galago, n = 2); five random maps were generated from each original map]. Red dashed line indicates average pinwheel density of randomized maps. Black dashed line indicates 3.14.

experimental perturbations that restrict neuronal interactions in the visual cortex to the range of an individual hypercolumn are predicted to induce the breakdown of spatially complex orientation maps into pinwheel sparse or crystal-like patterns. Verification of this prediction would confirm that building cortical networks by self-organization imposes discrete design alternatives. Evolutionary selective pressure could then only drive a switching between discrete circuit types but could not gradually transform one into the other.

Already in 1942, Waddington (*26*) suggested that robustness of developmental processes may play an adaptive role in evolution, protecting developing organisms from both genetic and environmental perturbations by canalizing the physiological and anatomical organization of organisms into a much narrower range than might be expected from their genetic diversity (*27*–*29*). If our explanation of the common design is correct, its evolution represents a genuine example of such canalization through an emergent property of complex cortical networks expressed in long-separated mammalian lineages. We conclude that wherever such complex biological systems unfold, especially in the mammalian brain where they are likely to abound, the principles of dynamical network self-organization may design and constrain system behavior as powerfully as an organism's genetic endowment or early life experiences.

References and Notes

1. D. H. Hubel, T. N. Wiesel, *Proc. R. Soc. London Ser. B Biol. Sci.* **198**, 1 (1977).
2. G. G. Blasdel, G. Salama, *Nature* **321**, 579 (1986).
3. T. Bonhoeffer, A. Grinvald, *Nature* **353**, 429 (1991).
4. K. Ohki, S. Chung, Y. H. Ch'ng, P. Kara, R. C. Reid, *Nature* **433**, 597 (2005).
5. K. Ohki *et al.*, *Nature* **442**, 925 (2006).
6. J. H. Kaas, *Brain Res. Bull.* **75**, 384 (2008).
7. J. O. Kriegs *et al.*, *PLoS Biol.* **4**, e91 (2006).
8. J. O. Kriegs *et al.*, *Trends Genet.* **24**, 156 (2007).
9. S. D. Van Hooser, *Neuroscientist* **13**, 639 (2007).
10. K. Obermayer, G. G. Blasdel, *Neural Comput.* **9**, 555 (1997).
11. W. H. Bosking, Y. Zhang, B. Schofield, D. Fitzpatrick, *J. Neurosci.* **17**, 2112 (1997).
12. Materials and methods are available as supporting material on *Science* Online.
13. F. Wolf, T. Geisel, *Nature* **395**, 73 (1998).
14. M. Kaschube, F. Wolf, T. Geisel, S. Löwel, *J. Neurosci.* **22**, 7206 (2002).
15. R. Durbin, G. Mitchison, *Nature* **343**, 644 (1990).
16. H. Y. Lee, M. Yahyanejad, M. Kardar, *Proc. Natl. Acad. Sci. U.S.A.* **100**, 16036 (2003).
17. F. Wolf, *Phys. Rev. Lett.* **95**, 208701 (2005).
18. L. E. White, D. Fitzpatrick, *Neuron* **56**, 327 (2007).
19. N. Mayer, J. M. Herrmann, T. Geisel, *Neurocomputing* **44-46**, 533 (2002).
20. L. Reichl, S. Löwel, F. Wolf, *Phys. Rev. Lett.* **102**, 208101 (2009).
21. M. Kaschube, M. Schnabel, F. Wolf, *N. J. Phys.* **10**, 015009 (2008).
22. L. E. White, D. M. Coppola, D. Fitzpatrick, *Nature* **411**, 1049 (2001).
23. C. J. Akerman, D. Smyth, I. D. Thompson, *Neuron* **36**, 869 (2002).
24. Y. Li, D. Fitzpatrick, L. E. White, *Nat. Neurosci.* **9**, 676 (2006).
25. M. Kaschube, M. Schnabel, F. Wolf, S. Löwel, *Proc. Natl. Acad. Sci. U.S.A.* **106**, 117205 (2009).
26. C. H. Waddington, *Nature* **150**, 563 (1942).
27. J. Maynard Smith *et al.*, *Q. Rev. Biol.* **60**, 265 (1985).
28. T. Flatt, *Q. Rev. Biol.* **80**, 287 (2005).
29. J. E. Niven, *PLoS Biol.* **2**, e19 (2005).

30. We thank J. Crowley, J. Fischer, T. Geisel, H. Greenside, A. Grinvald, M. Gutnick, J. Kaas, T. Kottos, T. Moser, and J. Schmitz for discussions; B. Bosking for acquiring and processing imaging data; W. Keil and L. Reichl for calculations; B. Goetze for graphics; D. Fitzpatrick for support of imaging experiments (NIH/National Eye Institute (NEI) EY06821 and EY11488); and the Kavli Institute for Theoretical Physics for its hospitality. This work was funded by grants from the Human Frontier Science Program and Bundesministerium für Bildung, Wissenschaft, Forschung und Technologie to S.L. and F.W. (01GQ0430 and 01GQ0922); NSF to D.M.C. (0641433); NIH/National Institute of General Medical Sciences to M.K. (P50 GM071508); and the Whitehall Foundation to L.E.W. and was supported in part by the National Science Foundation (NSF PHY05-51164).

Supporting Online Material

www.sciencemag.org/cgi/content/full/science.1194869/DC1
Materials and Methods
SOM Text
Figs. S1 to S24
Tables S1 to S5
References

9 July 2010; accepted 5 October 2010
Published online 4 November 2010;
10.1126/science.1194869

NEW PRODUCTS FOCUS: ESSENTIAL LAB EQUIPMENT

MANUAL AND ELECTRONIC PIPETTES

The comprehensive range of Sarpette M manual and Sarpette E electronic pipettes come in single-, eight-, and 12-channel configurations. Sarpette M pipettes feature continuously adjustable volumes from either the dispenser button or thumbwheel and offer exceptional accuracy and precision. Lightweight and well balanced for comfortable pipetting, Sarpette M pipettes require low dispensing and tip ejection forces. Multichannel options feature a curved ejector bar and an individual shaft suspension system to further reduce hand strain. Sarpette M pipettes are fully autoclavable. Sarpette E electronic pipettes are controlled by a high-precision motor and microprocessor to ensure smooth and accurate pipetting. Practical, user-friendly operation modes include various mixing, multiple dispensing, and sequential aspirating/dispensing options as well as five speeds and nine memory programs. Sarpette E pipettes feature a large, angled LCD display, an extremely lightweight ergonomic design, and a long-lasting rechargeable lithium ion battery. High-quality pipette tips are offered in a wide-range of packaging and purity options as well as corresponding carousel and linear stands to compliment the Sarpette pipettes.

Sarstedt, Inc.

For info: 800-257-5101 | www.sarstedt.com

MINI CENTRIFUGE

The compact, economical Scie-Plas Mini Centrifuge comes with three different rotors for use in a wide-range of bioscience research applications. Designed with a small footprint to fit easily even where space is limited, this centrifuge model is very easy to use. An on/off switch enables the lid to be closed without starting the unit and when the lid is opened, the centrifuge stops automatically. For added value and versatility, the Scie-Plas Mini Centrifuge includes three rotors: a six-place rotor for 1.5 ml tubes, a 0.2 ml PCR strip rotor, and a 1- by 3-inch slide rotor. A maximum speed of 6,000 rpm/2,000 x g is perfect for quickly spinning down samples, in microgel filtration applications and for microvolume centrifugation.

Scie-Plas

For info: +44-1223-427888 | www.scie-plas.com

SPECTROMETER

FT-IR spectrometer, Nicolet iS5, is designed for users seeking no-compromise, affordable, and compact FT-IR spectroscopy to assist in their product assurance testing, basic troubleshooting, and chemistry teaching. The Nicolet iS5 establishes a new benchmark in small-footprint laboratory FT-IR spectroscopy. Delivering comparable performance to full-size spectrometers, the instrument has an open-architecture sample compartment that accepts a wide variety of sampling accessories. The spectrometer incorporates the award-winning OMNIC software, widely adopted by major industrial manufacturers and forensic laboratories around the world. The Nicolet iS5 spectrometer, its new iD sampling accessories, and OMNIC software solutions for raw materials, impurities, and mixtures identification, create a unique user experience "from sample-in to answer-out."

Thermo Fisher Scientific

For info: 800-532-4752 | www.thermoscientific.com/ftir

MICROPLATE SEALING FILM

The revolutionary microencapsulated clear sealing film for microplates, MicroBurst, circumvents the use of adhesive seals that can easily stick to your glove rather than your microplate. MicroBurst sealing films have been developed to eliminate this problem. With its adhesive encapsulated in millions of tiny spheroids, MicroBurst sealing film is not sticky when first handled and can be quickly and easily moved into position. Only when you are satisfied that the film is in the correct place do you press down hard to burst and activate the MicroBurst adhesive microcapsules. No more mess, no more incorrectly positioned adhesive seals. The clear film has excellent optical properties and once activated, produces a very firm seal which quickly strengths to form a near-permanent seal on your plates. MicroBurst film can be pierced by pipette tips or robot liquid handlers and is temperature stable, making it ideal for PCR work.

Porvair Sciences Ltd.

For info: +44-1372-824290 | www.porvair-sciences.com

LIGHT-SHIELDING GLASSWARE

The new VITLAB light-shielding volumetric flasks are made of a specially pigmented polymethyl pentene (PMP) plastic that provides excellent absorption of light. In particular, absorption in the ultraviolet range—below 280 nm and the upper visible range above 580 nm—yet provides sufficient translucency to verify contents and volume, in most applications superior to amber glass. It provides a sunlight protection factor of nearly 20. Flasks are lightweight and break resistant, and provide a cost-effective alternative to glass. Screw-on caps help protect flask contents better than traditional stoppers. Flasks are available in sizes from 10 ml to 1000 ml. All volumes are Class A per DIN EN ISO 1042.

BrandTech Scientific, Inc.

For info: 888-522-2726 | www.brandtech.com

Electronically submit your new product description! Go to **www.sciencemag.org/products/newproducts.dtl** for more information.

Newly offered instrumentation, apparatus, and laboratory materials of interest to researchers in all disciplines in academic, industrial, and governmental organizations are featured in this space. Emphasis is given to purpose, chief characteristics, and availability of products and materials. Endorsement by *Science* or AAAS of any products or materials mentioned is not implied. When you seek additional information from the manufacturer or supplier, tell them you saw it here.

If you enjoy reading *Science*, you will relish the AAAS Annual Meeting

Join Us in Washington, DC

Attend sessions on the implications of finding other worlds, the next steps in brain-computer interfaces, frontiers in chemistry, the next big solar storm, and more. Talk to leaders in science, technology, engineering, education, and policy-making. Mingle with colleagues at receptions and social events. It's all available at the world's largest interdisciplinary science gathering.

Get program details and take advantage of early-bird registration and hotel discounts at:
http://www.aaas.org/meetings

Follow us in cyberspace at: http://www.facebook.com/AAAS.Science. **Get regular updates at Twitter.com, #AAASmtg**

Reporters: The EurekAlert! Web site hosts the AAAS Meeting Newsroom. Reporters can obtain details and register at:
www.eurekalert.org/aaasnewsroom

AAAS
ADVANCING SCIENCE, SERVING SOCIETY

AAAS, publisher of *Science*, presents the

2011 Annual Meeting

Science Without Borders

17—21 February • Washington, DC

Alice S. Huang, Ph.D.
AAAS President and
2011 Program Chair

Dear Colleagues,

On behalf of the AAAS Board of Directors, it is my distinct honor to invite you to the 177th Meeting of the American Association for the Advancement of Science (AAAS).

The Annual Meeting is one of the most widely recognized pan-science events, with hundreds of networking opportunities and broad global media coverage. An exceptional array of speakers and attendees will gather at the Walter E. Washington Convention Center in Washington, DC. **You will have the opportunity to interact with an exceptional array of scientists, engineers, educators, and policy-makers who will present the latest thinking and developments in the areas of science, technology, engineering, education, and policy-making.**

The meeting's theme — ***Science Without Borders*** — integrates interdisciplinary science, both across research and teaching, that utilizes diverse approaches as well as the diversity of its practitioners. The program will highlight science and teaching that cross conventional borders or break out from silos, especially in ground-breaking areas of research that highlight new and exciting developments in support of science, technology, and education. Sessions will feature strong scientific content to illustrate the interface of different disciplines or will exemplify a multidisciplinary approach to problem solving.

Everyone is welcome at the AAAS Annual Meeting. Those who join us will choose among a broad range of activities, including plenary and topical lectures by some of the world's leading scientists and engineers, multidisciplinary symposia, cutting-edge seminars, career development workshops, an international exhibition, and a host of networking opportunities.

The Annual Meeting reflects contributions from the AAAS sections, which I gratefully acknowledge. I also extend a personal thanks to the Scientific Program Committee for assembling this outstanding meeting and to our local co-chairs, **Freeman A. Hrabowski III**, president, University of Maryland, Baltimore County; **Ray O. Johnson**, vice president and chief technology officer, Lockheed Martin; and **Robert Tjian**, president, Howard Hughes Medical Institute.

I look forward to seeing you in Washington, DC,

Alice S. Huang
AAAS President and
Senior Faculty Associate in Biology
California Institute of Technology

President's Address

Thursday, 17 February

Alice S. Huang

AAAS President and Senior Faculty Associate in Biology, California Institute of Technology

Dr. Huang is a distinguished virologist and proponent for women in science. She was previously a professor of microbiology and molecular genetics at Harvard Medical School and subsequently dean for science at New York University. She is particularly interested in interdisciplinary research, the organization of higher educational institutions, and in policy issues related to education, science, and technology. She was the first to purify and characterize defective interfering viral particles. Her suggestion that these particles play a major role in viral pathogenesis stimulated work on many viral systems including plant viruses, and has led to the possibility of using these particles for disease prevention.

Friday, 18 February

John P. Holdren

Assistant to the President for Science and Technology, Director of the White House Office of Science and Technology, and Co-Chair of the President's Council of Advisors on Science and Technology

Dr. Holdren is highly regarded for his work on energy technology and policy, global climate change, and nuclear arms control and nonproliferation. A former AAAS president, he is a member of the National Academy of Sciences, the National Academy of Engineering, and the American Academy of Arts and Sciences as well as foreign member of the Royal Society of London. Prior to joining the Obama administration, Dr. Holdren was Teresa and John Heinz Professor of Environmental Policy and Director of the Program on Science, Technology, and Public Policy at Harvard University's Kennedy School of Government as well as professor in Harvard's Department of Earth and Planetary Sciences and Director of the independent, nonprofit Woods Hole Research Center.

Saturday, 19 February

Frances H. Arnold

Dick and Barbara Dickinson Professor of Chemical Engineering and Biochemistry, California Institute of Technology

Frances Arnold is a pioneer in the use of methods of laboratory evolution to generate novel and useful enzymes and organisms for applications in medicine and in alternative energy. Her multidisciplinary approach reveals insight into the way natural evolution might have occurred. She holds more than 20 patents and patent applications, has co-authored 220 scientific publications, and edited several books on protein engineering and laboratory protein evolution. Dr. Arnold is a member of the National Academy of Sciences, the National Academy of Engineering, and the Institute of Medicine. Recent awards and honors include the Linnaeus Lectureship at Uppsala University in Sweden and the Genencor Award in Enzyme Engineering.

Sunday, 20 February

Plenary Panel on Biosecurity

Rita R. Colwell

Distinguished University Professor, University of Maryland, College Park, and Johns Hopkins University Bloomberg School of Public Health

Dr. Colwell recently chaired a study committee of the U.S. National Research Council that wrote, *Responsible Research with Biological Select Agents and Toxins*. A former AAAS president, she has held many advisory positions in the U.S. government, nonprofit science policy organizations, and private foundations as well as in the international scientific research community.

Anthony S. Fauci

Director, National Institute of Allergy and Infectious Diseases (NIAID), National Institutes of Health

Dr. Fauci oversees an extensive research portfolio of basic and applied research to prevent, diagnose, and treat infectious diseases such as HIV/AIDS and other sexually transmitted infections, influenza, tuberculosis, malaria and illness from potential agents of bioterrorism. He is also a member of the National Science Advisory Board for Biosecurity, which deals with such questions as how to prevent published research in biotechnology from aiding terrorism without slowing scientific progress.

Claire M. Fraser-Liggett

Director of the Institute for Genome Sciences and Professor of Medicine, University of Maryland School of Medicine, Baltimore

Dr. Fraser-Liggett was previously the president and director of The Institute for Genomic Research, and has played a role in the sequencing and analysis of human, animal, plant, and microbial genomes to better understand the role that genes play in development, evolution, physiology, and disease. She led the teams that sequenced the genomes of several microbial organisms, including important human and animal pathogens, and as a consequence helped to initiate the era of comparative genomics. She has served on a number of National Research Council's committees on counterbioterrorism, domestic animal genomics, polar biology, and metagenomics.

The Honorable Rush Holt

U.S. Congressman

Prior to his election in 1998 to represent New Jersey's 12th District, Dr. Holt, a physicist, worked as an educator, scientist, and arms control expert. At the U.S. State Department, he monitored the nuclear programs of countries such as Iraq, Iran, North Korea, and the former Soviet Union. Permanent Select Committee on Intelligence, its only scientist. He also chairs the Select Intelligence Oversight Panel.

Moderator: Jeanne Guillemin

Senior Advisor, MIT Security Studies Program, Research Professor, Boston College, Chestnut Hill, MA

Dr. Guillemin has long been involved in issues regarding medicine, infectious diseases, and biological weapons. She wrote *Anthrax: The Investigation of a Deadly Outbreak*, which documents the U.S.-Russian inquiry into the contested cause of the 1979 Sverdlovsk anthrax outbreak. She also investigated the "yellow rain" controversy of the 1980s. Her latest book is *Biological Weapons: From the Invention of State-Sponsored Programs to Contemporary Bioterrorism*.

Topical Lecture Series

G. Wayne Clough

Secretary, Smithsonian Institution

Scientific Literacy – Where Are Our Forçados When We Need Them?

Regina E. Dugan

Director, Defense Advanced Research Projects Agency

Topic To Be Announced

Robert M. Hazen

Senior Staff Scientist, Geophysical Laboratory, Carnegie Institution for Science, and Clarence Robinson Professor of Earth Science, George Mason University

The Deep Carbon Observatory

Samantha B. Joye

Professor of Marine Sciences, University of Georgia, Athens

Offshore Ocean Aspects of the Gulf Oil Well Blowout

Gerard Karsenty

Paul A. Marks Professor and Chair, Department of Genetics and Development, Columbia University Medical Center

Biology Without Walls: The Novel Endocrinology of Bone

Colin Phillips

Professor of Linguistics, Neuroscience, and Cognitive Science, University of Maryland, College Park

Linguistic Illusions: Where You See Them, Where You Don't

Lisa Randall

Frank B. Baird, Jr. Professor of Science, Harvard University

String Theory and New Physics

Sean C. Solomon

Director, Department of Terrestrial Magnetism, Carnegie Institution for Science

Exploring the Planet Mercury: The MESSENGER Mission

George M. Whitesides

Woodford L. and Ann A. Flowers University Professor, Harvard University

Changing the Paradigms of Science

George Sarton Memorial Lecture in the History and Philosophy of Science

Lawrence M. Principe

Drew Professor of the Humanities, Johns Hopkins University

Revealing the Secrets of Alchemy

John P. McGovern Lecture in the Behavioral Sciences

Linda M. Bartoshuk

Bushnell Professor of Community Dentistry and Behavioral Science, University of Florida, Gainesville

We Live in Different Taste Worlds: How Do We Know and What Does It Mean?

Seminars

Body and Machine

Friday, 18 February

No border is more fundamental than the one between humans and the external world. The limits of our body are defined by our brain—how we grasp an object or move around in a room is determined by how the brain perceives where the body is in space and time. These limits can be manipulated, extended, and explored when traditional scientific disciplines work together.

Linking Mechanics, Robotics, and Neuroscience: Novel Insights from Novel Systems

Organized by Mitra J.Z. Hartmann, Northwestern University, Evanston, IL

SPEAKERS

Jérôme Casas, University of Tours, France; B. Bathellier, Institute for Molecular Pathology
Air-Flow Sensing Hairs in Crickets and Biomimetic Micro-Electro-Mechanical Systems (MEMS) Sensors

Peter M. Narins, University of California, Los Angeles
Mostly Malleus: Ground Sound Detection by the Golden Mole

Mitra J.Z. Hartmann, Northwestern University, Evanston, IL
Characterizing the Complete Mechanosensory Input to the Rat Vibrissal Array

Danica Kragic, Center for Autonomous Systems, Stockholm
Attention, Segmentation, and Learning for Object Manipulation

Francisco J. Valero-Cuevas, University of Southern California, Los Angeles
A Systems-Based Engineering Approach to Sensorimotor Control of the Human Hand

Mind and Machine: The Next Step in Neuroprosthetics and Brain-Computer Interfaces

Organized by Michael D. Mitchell, Ecole Polytechnique Fédérale de Lausanne (EPFL), Switzerland; Christian Simm, Swissnex San Francisco, CA

SPEAKERS

Daniel Moran, Washington University, St. Louis, MO
Electrocorticographic Brain-Computer Interfaces

José del R. Millan, EPFL, Lausanne, Switzerland
Multitasking with Non-Invasive Neuroprosthetics

Christa Neuper, Graz University of Technology, Austria
Future Directions in Hybrid Brain-Computer Interfaces

Andrew Schwartz, University of Pittsburgh, PA
Useful Signals from the Motor Cortex

Jonathan R. Wolpaw, New York State Department of Health and State University of New York
Brain-Computer Interfaces: Traditional Assumptions Meet Emerging Realities

Other Worlds

Saturday, 19 February

Speakers will represent multidisciplinary and multinational initiatives that are closely coordinated at national and international levels. The Kepler Mission will do something that no other mission can do: determine the frequency of Earth-like planets in our galaxy and begin to constrain the prevalence of life in our universe. Other efforts are engaged in searching for evidence of extraterrestrial life. The world's largest dedicated, full-time astronomical instrument — the Very Long Baseline Array — spans more than 5,000 miles, providing astronomers with the sharpest vision of any telescope on Earth or in space.

Kepler: Looking for Other Earths

Organized by Alan P. Boss, Carnegie Institution for Science, Washington, DC; William J. Borucki, NASA Ames Research Center, Moffet Field, CA

SPEAKERS

William J. Borucki, NASA Ames Research Center, Moffet Field, CA
Kepler Mission Overview and Planet Discoveries

Matthew J. Holman, Harvard–Smithsonian Center for Astrophysics, Cambridge, MA
Searching for Planets by Transit Timing Variations

Sara Seager, Massachusetts Institute of Technology, Cambridge
Planet Discoveries in a Physical Context

William Chaplin, University of Birmingham, United Kingdom
Results for Solar-Like Oscillators Observed by Kepler

Conny Aerts, Instituut voor Sterrenkunde, Leuven, Belgium

Asteroseismology Across the Hertzsprung–Russell Diagram
Martin D. Still, NASA Ames Research Center, Moffet Field, CA
The Kepler Guest Observer Program

Seeking Signs of (ET) Life: The Search Steps Up on Mars and Beyond

Organized by Linda Billings, George Washington University, Washington, DC

SPEAKERS
Mary A. Voytek, NASA, Washington, DC
Greatest Hits and Grand Challenges in Astrobiology
Cassie Conley, NASA, Washington, DC
Preserving the Planets— Ours and Others: Planetary Protection in Space Exploration
Andrew Steele, Carnegie Institution for Science
The Search for Life on Mars: Mars Science Laboratory and Mars Sample Return

The Universe Revealed by High-Resolution, High-Precision Astronomy

Organized by Mark T. Adams, National Radio Astronomy Observatory (NRAO), Charlottesville, VA

SPEAKERS
Geoffrey C. Bower, University of California, Berkeley
Seeking New Planets at Radio Wavelengths
Mark J. Reid, Harvard–Smithsonian Center for Astrophysics, Cambridge, MA
Mapping Our Galaxy in 3D
James A. Braatz, NRAO, Charlottesville, VA
Supermassive Black Holes and Precision Cosmology with Megamasers

Frontiers in Chemistry

Sunday, 20 February

AAAS is celebrating the International Year of Chemistry to acknowledge the achievements of chemistry, its contributions to the well-being of humankind, and what the future may hold. Research and teaching in these fields involves multidisciplinary approaches and diverse, international investigators. This seminar will disclose cutting-edge research across a variety of scientific disciplines, thereby exemplifying a multidisciplinary approach to scientific exploration.

Frontiers in Organic Materials for Information Processing, Energy, and Sensors

Organized by Seth R. Marder and Jean-Luc Bredas, Georgia Institute of Technology, Atlanta; Tobin J. Marks, Northwestern University, Evanston, IL

SPEAKERS
Alan Heeger, University of California, Santa Barbara
Plastic Solar Cells and Photodetectors: Self-Assembly by Spontaneous Phase Separation
Richard Friend, University of Cambridge, United Kingdom
Current and Future Scientific and Commercial Opportunities for Organic Electronics
Zhenan Bao, Stanford University, CA
Organic Materials Based Flexible Electronic Sensors
Larry Dalton, University of Washington, Seattle
Electro-Optic Technology: Implications for Telecommunications, Computing, and Sensing
Joseph W. Perry, Georgia Institute of Technology, Atlanta
Organic Photonic Materials for All-Optical Signal Processing
Mark E. Thompson, University of Southern California, Los Angeles
New Molecular Materials for Energy-Based Optoelectronics: Solar Energy and Lighting

Molecular Self-Assembly and Artificial Molecular Machines

Organized by Miguel A. Garcia-Garibay, University of California, Los Angeles; Bruce E. Maryanoff, The Scripps Research Institute, La Jolla, CA

SPEAKERS
J. Fraser Stoddart, Northwestern University, Evanston, IL
Fashioning Functional Materials with Integrated Mechanostereochemical Systems
Josef Michl, University of Colorado, Boulder
Artificial Surface-Mounted Molecular Rotors
Nadrian C. Seeman, New York University, New York City
DNA: Not Merely the Secret of Life
Stacey F. Bent, Stanford University, CA
Nanostructuring for Efficient Energy Conversion
M. Reza Ghadiri, The Scripps Research Institute, La Jolla, CA
Toward Single-Molecule DNA Sequencing with Engineered Nanopores
Ben L. Feringa, University of Groningen, The Netherlands
Molecular Motors: In Control of Molecular Motion

DISCUSSANT
Miguel A. Garcia-Garibay, University of California, Los Angeles

Special Sessions

AAAS Community College Forum: Lessons Learned About Biotechnology Education

Thursday, 17 February

Organized by Yolanda S. George, AAAS Education and Human Resources, Washington, DC, and Elaine Johnson, City College of San Francisco, CA

The Forum will highlight cutting-edge curriculum for use in biotechnology post-secondary education as well as innovative industry partnerships. Community college based biotechnology programs and educators play a vital role in preparing post-secondary students for careers in the biotechnology industries including research and development, diagnostics, regulatory affairs, homeland security, and sustainable energy production and management. Biotechnology education curriculum areas include laboratory techniques, industrial biotechnology, green biotechnology, nanotechnology, homeland security, agriculture, and bioenergy and biofuels. The Forum will include presentations about vision and change in undergraduate biology education, exemplary curriculum in biotechnology education, and partnerships with industry. For more information, contact Yolanda George at ygeorge@aaas.org.

Symposium Tracks

Brain and Behavior

Chronic Illness Management and Cognitive Science: Translation Beyond Genes?

Organized by Howard Leventhal, Rutgers University, New Brunswick, NJ

Crossing Borders in Language Science: What Bilinguals Tell Us About Mind and Brain

Organized by Judith F. Kroll, Pennsylvania State University, University Park

Cultural Evolutionary Dynamics of Cooperation

Organized by David M. Carballo, Boston University, MA

From Artificial Limbs to Virtual Reality: How the Brain Represents the Body

Organized by Michael D. Mitchell, Ecole Polytechnique Fédérale de Lausanne, Switzerland; Christian Simm, swissnex San Francisco, CA

From Freud to fMRI: Untangling the Mystery of Stuttering

Organized by Nan Ratner, University of Maryland, College Park

Hunter-Gatherers and Language Change

Organized by Claire Bowern, Yale University, New Haven, CT

Molecules to Mind: Challenges for the 21st Century

Organized by Bruce Altevogt, Institute of Medicine, Washington, DC

Nature, Nurture, and Antisocial Behavior: Biological and Biosocial Research on Crime

Organized by William Alex Pridemore, Indiana University, Bloomington

Neurodegenerative Diseases: A Need for Multidisciplinary and Global Approaches

Organized by Elmar Nimmesgern, European Commission, Brussels, Belgium; Philippe Amouyel, Institut Pasteur de Lille, France

Science Behind Improved Foreign Language Expertise: Meeting the Global Challenge
Organized by Amy S. Weinberg, University of Maryland, College Park

Scientific and Ethical Issues for the Surgical Treatment of Psychiatric Disorders
Organized by Mahlon DeLong, Emory University School of Medicine, Atlanta, GA

The Science of Eating: Perception and Preference in Human Taste
Organized by Albert H. Teich and Rieko Yajima, AAAS Science and Policy Programs, Washington, DC; Jill Pace, American College of Real Estate Lawyers, Rockville, MD

Thinking About Thinking: How Do We Know What We Know?
Organized by Eva Hoogland and Chloe Kembery, European Science Foundation, Strasbourg, France

Transatlantic Synergies To Promote Effective Traumatic Brain Injury Research
Organized by Ramona Hicks, National Institute of Neurological Disorders and Stroke, Bethesda, MD; Patrizia Tosetti, European Commission, Direcorate General-Research/Health, Brussels, Belgium

Climate Change

Adapting to a Clear and Present Danger: Climate Change and Ocean Ecosystems
Organized by Chad English, Communication Partnership for Science and the Sea, Silver Spring, MD; Mary Ruckelshaus, National Oceanic and Atmospheric Administration (NOAA) Northwest Fisheries Science Center, Seattle, WA ; Scott Doney, Woods Hole Oceanographic Institution, MA

Can Reef Fisheries Take the Heat? Ecological and Economic Impacts of Climate Change
Organized by Joshua E. Cinner, Australian Research Center, Townsville

Changing Climate, Changing Approaches: Conservation in the Face of Climate Change
Organized by Michelle M. McClure, NOAA Northwest Fisheries Science Center, Seattle, WA

Climate Change: Altering the Physics, Ecology, and Socioeconomics of Fisheries
Organized by Rashid Sumaila, University of British Columbia, Vancouver, Canada; William W.L Cheung, University of East Anglia, Norwich, United Kingdom

Comparing National Responses to Climate Change: Networks of Debate and Contention
Organized by Jeffrey P. Broadbent, University of Minnesota, Minneapolis

How Climate Change Affects the Safety of the World's Food Supply
Organized by Ewen C. Todd, Michigan State University, East Lansing

In Hot Water: Rising Public Health Concerns from Changing Ocean Conditions
Organized by Carolyn Sotka, NOAA Oceans and Human Health Initiative, Charleston, SC; Paul Sandifer, NOAA, Washington, DC

Limiting Climate Change: Reducing Black Carbon and Tropospheric Ozone Precursors
Organized by Frank Raes, European Commission, Joint Research Council (JRC) Institute for Environment and Sustainability, Ispra, Italy; Geraldine Barry, European Commission, JRC, Brussels, Belgium

Research Infrastructures: The Emergence of Key Players for Environmental Research
Organized by Janine Delahaut and Elena Righi-Steele, European Commission, Brussels, Belgium

Rethinking Adaptation to a Changing Global Environment
Organized by Gregory P. Dietl, Paleontological Research Institution, Ithaca, NY

Where Ocean Meets Land: Dynamic Shorelines in a Warming World
Organized by Gregory S. Mountain, Rutgers University, Piscataway, NJ; Charna Meth, Consortium for Ocean Leadership, Washington, DC

Education

Aiming for Scientific Literacy by Teaching the Process, Nature, and Limits of Science
Organized by Jay B. Labov, National Academy of Sciences, Washington, DC; Judy Scotchmoor, University of California Museum of Paleontology, Berkeley

Celebrating Marie Curie's 100th Anniversary of Her Nobel Prize in Chemistry
Organized by Penny J. Gilmer, Florida State University, Tallahassee; Alan Rocke, Case Western Reserve University, Cleveland, OH

Engaging Students in Undergraduate STEM Education with a Focus on Global Stewardship
Organized by Jay B. Labov, National Academy of Sciences, Washington, DC; Melvin D. George, University of Missouri, Columbia; Catherine Middlecamp, University of Wisconsin, Madison

Implementing the Vision and Change Report on Undergraduate Biology Education
Organized by Michael M. Cox, University of Wisconsin, Madison; Barbara Illman, U.S. Forest Service, Madison, WI

Invisible Men? Addressing the Participation of Minority Males in Science and Engineering
Organized by Catherine Didion, National Academy of Engineering, Washington, DC

Just-in-Time Support for Science Teaching: Web-Based Approaches
Organized by Nancy P. Moreno and Deanne B. Erdmann, Baylor College of Medicine, Houston, TX

Learning Research and Educational Practice: How Can We Make Better Connections?
Organized by Janice Earle and Soo-Siang Lim, National Science Foundation (NSF), Arlington, VA

Science Without Borders: Learning from TIMSS Advanced 2008
Organized by Patsy Wang-Iverson, Gabriella and Paul Rosenbaum Foundation, Stockton, NJ

Teaching and Learning in the Digital Age: Reliable Resources Across the Disciplines
Organized by Linda N. Fanis, Chemical Education Digital Library, Madison, WI

The Challenge of Teaching Evolution in the Islamic World
Organized by Eugenie C. Scott, National Center for Science Education, Oakland, CA

The University of the Future
Organized by Robert M. Nerem, Georgia Institute of Technology, Atlanta; James J. Duderstadt, University of Michigan, Ann Arbor

Transcending Gender and Ethnic Barriers to Full STEM Participation
Organized by Nicole M. Else-Quest, Villanova University, PA

Emerging Science and Technology

Aeroecology: Transcending Boundaries Among Ecology, Meteorology, and Physics
Organized by Winifred F. Frick, University of

California, Santa Cruz; Phillip B. Chilson, University of Oklahoma, Norman

Biological Role and Consequences of Intrinsic Protein Disorder
Organized by H. Jane Dyson and Peter E. Wright, The Scripps Research Institute, La Jolla, CA

Bioprinting: A Future of Regenerative Medicine
Organized by Vladimir Mironov, Medical University of South Carolina, Charleston

Chemically Speaking: How Organisms Talk to Each Other
Organized by Barbara Illman, U.S. Forest Service, Madison, WI; Jerrold Meinwald, Cornell University, Ithaca, NY

Explaining Phase Transitions
Organized by David Lightfoot, Georgetown University, Washington, DC

First Physics from the Large Hadron Collider
Organized by James Gillies, European Organization for Nuclear Research (CERN), Geneva, Switzerland; Katie Yurkewicz, Fermi National Accelerator Laboratory, Batavia, IL

Growth and Form in Mathematics, Physics, and Biology
Organized by L. Mahadevan, Harvard University, Cambridge, MA; Edward Aboufadel, Grand Valley State University, Allendale, MI

Inspiring Researchers: Building on the Legacy of Marie Curie
Organized by Louise Byrne, Research Executive Agency, Brussels, Belgium

Mathematics and Collective Behavior
Organized by Warren Page, City University of New York (Retired), Larchmont, NY

Matter Wave Magic and Technology
Organized by Charles W. Clark, National Institute of Standards and Technology, Gaithersburg, MD

Nanoworld, Megaproblems? The Impact of Nanotechnology on the Environment and Society
Organized by Alberto Pimpinelli, Science and Technology Office of the French Embassy in the United States, Houston, TX

Sharper Images in Astronomy, Microscopy, and Vision Science Using Adaptive Optics
Organized by Christopher Dainty, National University of Ireland, Galway

Superconductivity: From 1911 to 2021
Organized by David Pines, University of California, Davis

Through the Looking Glass: Recent Adventures in Antimatter
Organized by Charles W. Clark, National Institute of Standards and Technology, Gaithersburg, MD

Use of Lasers in Surgery, Regenerative Medicine, and Medical Device Fabrication
Organized by Roger Narayan, University of North Carolina, Chapel Hill

Energy

Biorefinery: Toward an Industrial Metabolism
Organized by Daniel Thomas, University of Technology of Compiegne, France; Adele Martial, Consulate General of France, Chicago, IL

Deepwater Drilling: A Risk Worth Taking?
Organized by Richard D'Souza, Granherne Global Operations, Houston, TX

Energy Efficiency in Europe and the United States: Success Stories and Future Potentials
Organized by Katja Stempfle-Eberl, Baden-Württemberg International, Stuttgart, Germany

Fractures Developing: The Science, Policy, and Perception of Shale Gas Development
Organized by John P. Martin, New York State Energy Research and Development Authority, Albany; Michele L. Aldrich, California Academy of Sciences, San Francisco

If Termites Can Do It, Why Can't Humans?
Organized by Lakshmi N. Reddi and Eduardo Divo, University of Central Florida, Orlando

Mathematics and Our Energy Future
Organized by Mary Lou Zeeman, Bowdoin College, Brunswick, ME; Russel E. Caflisch, Institute for Pure and Applied Mathematics, Los Angeles, CA

Pillars, Polymers, and Computers: Creative Approaches to Electrical Energy Storage
Organized by Ashley Predith, University of Maryland, College Park

Portraits of the California Energy System in 2050: Cutting Emissions by 80 Percent
Organized by Jane C.S. Long, Lawrence Livermore National Laboratory, CA; Susan Hackwood and Miriam John, California Council on Science and Technology, Riverside

Powering the Planet: Generation of Clean Fuels from Sunlight and Water
Organized by Harry B. Gray, Bruce B. Brunschwig, and Jay R. Winkler, California Institute of Technology, Pasadena

The Energy and Water Nexus: Turning a Double Problem into a Solution
Organized by Estathios Peteves, European Commission, JRC Institute for Energy, Petten, Netherlands; Geraldine Barry, European Commission, JRC, Brussels, Belgium

Waste Not, Want Not: Waste As the World's Most Abundant Renewable Resource
Organized by Michael Webber, University of Texas, Austin

Global Collaboration

Bridging Nations and Fields: East Asian Approaches to Science and Technology Policy
Organized by Asuka Hoshikoshi, National Institute of Science and Technology Policy, Tokyo, Japan

Bringing Innovation to International Development: New Actors, New Mechanisms
Organized by Alex Dehgan and Ticora V. Jones, U.S. Agency for International Development, Washington, DC; Mark Doyle, NSF, Arlington, VA

Can Global Science Solve Global Challenges?
Organized by Tracey Elliott, The Royal Society, London, United Kingdom

Cross-Border Responses to Global Challenges: Can Everybody Win?
Organized by David Wilkinson and Geraldine Barry, European Commission, JRC, Brussels, Belgium

Crossing Boundaries and Opening Borders: The European Research Council as Innovation
Organized by Samantha Christey, European Research Council, Brussels, Belgium

Education, Science, and Innovation as Tools for New Engagement with the Islamic World
Organized by Ben Koppelman, The Royal Society, London, United Kingdom

Europe, Africa, and Asia: Rising on the Same Tide
Organized by Geraldine Barry, European Commission, JRC, Brussels, Belgium

Foreign Participation in National Technology Development Programs

Organized by Christopher Hill, George Mason University, Arlington, VA; George R. Heaton, Technology Policy International, Newton Center, MA; David Cheney, SRI International, Arlington, VA

International Territory: Science at Sea, Science in Space, and Science at the Poles
Organized by Susan Humphris, Woods Hole Oceanographic Institution, MA; Charna Meth, Consortium for Ocean Leadership, Washington, DC

Joining Global Efforts in Post-Disaster Recovery and Reconstruction
Organized by Delilah Al Khudhairy, European Commission, JRC Institute for the Protection and Security of the Citizen, Ispra, Italy; Geraldine Barry, European Commission, JRC, Brussels, Belgium

Networks, Collaboration, and Research in a Non-Western Context: The Role of Technology
Organized by B. Paige Miller, University of Wisconsin, River Falls; Ricardo B. Duque, University of Vienna, Austria

Research Integrity in the Global Perspective
Organized by Melissa S. Anderson, University of Minnesota, Minneapolis

Role of U.S. Federal Agencies in Building Scientific Capacity in Developing Countries
Organized by Pallavi Phartiyal, AAAS Science and Policy Programs, Washington, DC

The Crowd and the Cloud: The Future of Online Collaboration
Organized by Michael R. Nelson, Georgetown University, Washington, DC

The Practice of Science Diplomacy in the Earth Sciences
Organized by Thomas J. Casadevall, U.S. Geological Survey, Denver, CO; Ester Sztein, The National Academies, Washington, DC; Melody Brown Burkins, University of Vermont, Burlington

Human Biology and Health

Anthropology and Global Health: Genes, Biology, and Culture
Organized by Cynthia M. Beall, Case Western Reserve University, Cleveland, OH

Diseases Without Borders: TB and AIDS
Organized by Anne E. Goldfeld, Harvard Medical School, Boston, MA

Epigenetic Processes in Development: Gene-Environment Interplay
Organized by Jeanne Brooks-Gunn, Columbia University, New York City; Stephen J. Suomi, National Institutes of Health, Bethesda, MD

Evolutionary Personalized Medicine
Organized by Turkan K. Gardenier, Pragmatica Corp., Vienna, VA

Global Health Care: Advances and Challenges
Organized by Metin Akay, University of Houston, TX

Humans Without Borders: Evolutionary Processes at Work in Humans and Their Relatives
Organized by James J. Smith, Michigan State University, East Lansing; Robin Smith, National Evolutionary Synthesis Center, Durham, NC

Interfering with Gene Expression and Interfering with Disease
Organized by Judy Lieberman, Harvard Medical School, Boston, MA

Medicine Safety in a World of Science Without Borders
Organized by William T. Beck, University of Illinois, Chicago; Guill Wientjes, Ohio State University, Columbus

One Health: From Ideas to Implementation, Rhetoric to Reality
Organized by Barbara Hyde, American Society for Microbiology, Washington, DC
Oral Clefts: Equal Opportunity Disorders
Organized by Margarita Zeichner-David, University of Southern California, Los Angeles

Oral Sex Is Sex and Can Lead to Cancer
Organized by Margarita Zeichner-David, University of Southern California, Los Angeles

Personalized Medicine: Moving Forward or Backward?
Organized by Jennie C. Hunter-Cevera, RTI International, Research Triangle Park, SC; Anice Anderson, Private Consultant, Terre Haute, IN

Reducing the Cost of Health Care Through Science and Engineering
Organized by Raphael C. Lee, University of Chicago, IL; Anice Anderson, Private Consultant, Terre Haute, IN

The Human Body as Supra-Organism, Microbial Observatory, and Ecosystem at Risk
Organized by David A. Relman, Stanford University, Palo Alto, CA; Jeffrey I. Gordon, Washington University School of Medicine, St. Louis

The Surprising Influenza H1N1 Pandemic, Waves I and II: The Race to Vaccinate
Organized by M. Elizabeth Halloran, University of Washington, Seattle

Land and Oceans

2050: Will There Be Fish in the Ocean?
Organized by Villy Christensen, University of British Columbia, Vancouver, Canada

A New Vision for Research: Goals for the National Institute of Food and Agriculture
Organized by Brian A. Larkins, University of Arizona, Tucson; Roger Beachy, U.S. Department of Agriculture, Washington, DC

Beyond Lines on Maps: Marine Spatial Planning for a Dynamic World
Organized by Donald F. Boesch, University of Maryland Center for Environmental Science, Cambridge, MD; Karen L. McLeod, Oregon State University, Corvallis

Borlaug's Impact on World Agriculture: Will There Be a Second Green Revolution?
Organized by Ronald L. Phillips, University of Minnesota, St. Paul; Edward Runge, Texas A&M University, College Station

Fishing for Solutions: Community Institutions for Effective Resource Management
Organized by Astrid J. Scholz, Ecotrust, Portland, OR

From Practice to Theory and Back: Ecosystem Services and Marine Spatial Planning
Organized by Anne Guerry, Stanford University, CA; Mary Ruckelshaus, NOAA Northwest Fisheries Science Center, Seattle, WA ; Paul Sandifer, NOAA, Washington, DC

Global Agricultural History: Mapping the Past for Modeling the Future
Organized by William E. Doolittle, University of Texas, Austin; Mats Widgren, Stockholm University, Sweden

Global and Local Responses to the Nitrogen Challenge: Science, Practice, and Policy
Organized by Todd S. Rosenstock and Thomas P. Tomich, University of California, Davis

GM Crop Regulations: Safety Net or Insurmountable Obstacle?"
Organized by Wayne Parrott, University of Georgia, Athens; Alan McHughen, University of California, Riverside; Donald P. Weeks, University of Nebraska, Lincoln

Invasive Species: What Harm Do They Do?
Organized by Peter Alpert, Invasive Species Advisory Committee, Amherst, MA

Lost at Sea: Where Are the Humans in Marine Ecosystem Management?
Organized by Rebecca Gruby, Larry Crowder,

and Morgan Gopnik, Duke University Marine Laboratory, Beaufort, NC

Marine Spatial Planning: A Science-Based Tool for Conservation and the Economy

Organized by Elliott A. Norse, Marine Conservation Biology Institute, Bellevue, WA

Plant Breeding Today: Genomics and Computing Advances Bring Speed and Precision

Organized by Ian Graham and Elspeth Bartlet, University of York, United Kingdom

Science and Society

Astronomical Pioneering: The Implications of Finding Other Worlds

Organized by Jennifer Wiseman and Peyton West, AAAS Science and Policy Programs, Washington, DC

Communicating Diversity in Science: Implications for Climate Change Denial

Organized by Prajwal Kulkarni, U.S. Environmental Protection Agency, Washington, DC

Communication Outside the Box

Organized by Michel Claessens, European Commission, Brussels, Belgium; David Bennett, Delft University of Technology, Netherlands; Richard Jennings, University of Cambridge, United Kingdom

Crossing Boundaries with Citizen Science

Organized by Janis L. Dickinson, The Cornell Lab of Ornithology, Ithaca, NY; Bart Selman, Cornell University, Ithaca, NY

Doing Good with Good OR: Applying Operations Research for Societal Impact

Organized by Karen Smilowitz, Northwestern University, Evanston, IL; Ozlem Ergun, Georgia Institute of Technology, Atlanta

Earth Science and Evolution

Organized by Jere H. Lipps, University of California, Berkeley

Earthwatch and the HSBC Climate Partnership: A Unique Citizen Science Model

Organized by Kristen Kusek, Earthwatch Institute, Boston, MA

Evangelicals, Science, and Policy: Toward a Constructive Engagement

Organized by Peyton West and Jennifer Wiseman, AAAS Science and Policy Programs, Washington, DC

Innovative Strategies for Ensuring Access to the Benefits of Scientific Progress

Organized by Jessica M. Wyndham, AAAS Science and Human Rights Program, Washington, DC; Joseph G. Perpich, JG Perpich, Bethesda, MD

Reaching Out to People in East Asia on Green Issues: Policies and Practices

Organized by Sook-Kyoung Cho, Korea Foundation for the Advancement of Science and Creativity, Seoul; Masataka Watanabe, Japan Science and Technology Agency, Tokyo; Sun Mengxin, China Association for Science and Technology, Beijing

Science Without Borders and Media Unbounded: What Comes Next?

Organized by Bud Ward, *Yale Forum on Climate Change and the Media*, White Stone, VA

Surprise...It's Science! Reaching New Audiences in Unconventional Ways with Festivals

Organized by Jan Riise, European Science Events Association, Onsala, Sweden; Ben Wiehe, MIT Museum, Cambridge, MA

Techno-Optimism or Pessimism? Media Coverage of Quick Fixes for Global Climate Change

Organized by Cristine Russell, Harvard Kennedy School, Cambridge, MA

TV Meteorologists Communicating Climate Change

Organized by Katherine E. Rowan, George Mason University, Fairfax, VA

When Pollution Gets Personal: Ethics of Reporting on Human Exposures

Organized by Julia G. Brody, Silent Spring Institute, Newton, MA

The Science Endeavor

As Borders Dissolve, Which Standards and Mechanisms Prevail?

Organized by Mary Kavanagh, European Commission, Directorate-General for Research, Brussels, Belgium

Crisis Averted? How a Critical Shortage in Helium-3 Was Good and Bad for Science

Organized by Benn Tannenbaum, AAAS Center for Science, Technology, and Security Policy, Washington, DC

Design Thinking To Mobilize Science, Technology, and Innovation for Social Challenges

Organized by Yoko Nitta, Tateo Arimoto, and Suguru Ishiguro, Japan Science and Technology Agency, Tokyo

It Is Unethical Not To Do Research with Animals

Organized by Stuart Zola, Emory University, Atlanta, GA

Measurements as a Cornerstone of Global Trade and Quality of Life

Organized by David Anderson, European Commission, JRC Institute for Reference Materials and Measurements, Geel, Belgium; Geraldine Barry, European Commission, JRC, Brussels, Belgium

Modeling Across Millennia: Interdisciplinary Paths to Ancient Socionatural Systems

Organized by Timothy A. Kohler and Stefani A. Crabtree, Washington State University, Pullman

Networks and Culture of Scientific and Technological Communities in Global Policy

Organized by Denis F. Simon and Darryl Farber, Pennsylvania State University, University Park

Perspectives on Research and Development in the President's FY 2012 Budget Request

Organized by Patrick J. Clemins, AAAS Science and Policy Programs, Washington, DC

Publication Without Borders: Spanning Countries, Disciplines, Audiences, and Roles

Organized by Barbara Gastel, Texas A&M University, College Station

Reaching a Global Standard in Research Integrity

Organized by Chloe Kembery and Vanessa Campo-Ruiz, European Science Foundation, Strasbourg, France

Solving the Weight of Evidence Problem: A Way Forward?

Organized by Heather E. Douglas, University of Tennessee, Knoxville

The Digitization of Science: Reproducibility and Interdisciplinary Knowledge Transfer

Organized by Victoria C. Stodden, Columbia University, New York City

Security

Atomic Detectives: Science Behind International Efforts To Combat Nuclear Terrorism

Organized by Klaus Mayer, European Commission, JRC Institute for Transuranium Elements, Karlsruhe, Germany; Geraldine Barry, European Commission, JRC, Brussels, Belgium

International Neighborhood Watch: Citizen Scientists and International Security

Organized by Gerald L. Epstein, AAAS Center for Science, Technology, and Security Policy, Washington, DC

New START and Nuclear Winter: Climatic Consequences of the Nuclear Weapons Agreement

Organized by Alan Robock, Rutgers University, New Brunswick, NJ; Richard Turco, University of California, Los Angeles

Promoting Security and Sustaining Privacy: How Do We Find the Right Balance?

Organized by Christopher Hankin, Imperial College London, United Kingdom; Benn Tannenbaum, AAAS Center for Science, Technology, and Security Policy, Washington, DC

Reconciling National Security Requirements with Research and Education

Organized by Kavita M. Berger, AAAS Center for Science, Technology, and Security Policy, Washington, DC; Tobin L. Smith, Association of American Universities, Washington, DC

Science and Policy for Environmental Security in the Asia-Pacific Region

Organized by James Scott Hauger and Virginia Watson, Asia-Pacific Center for Security Studies, Honolulu, HI

Space Weather: The Next Big Solar Storm Could Be a Global Katrina

Organized by Thomas J. Bogdan and Terrance Onsager, NOAA, Boulder, CO; Stephan Lechner, European Commission, JRC Institute for Protection and Security of the Citizen, Ispra, Italy

Using Quantitative Content Analysis To Assess the Likelihood of Terrorist Violence

Organized by Allison G. Smith, U.S. Department of Homeland Security, Washington, DC

White-Blue Arctic: Promoting Cooperation and Preventing Conflict in the Arctic Ocean

Organized by Paul Arthur Berkman, University of Cambridge, United Kingdom; Oran Young, University of California, Santa Barbara

Sustainability

Data Cocktails for Biodiversity: Protected Area Management Without the Hangover

Organized by Alan Belward, European Commission, JRC Institute for Environment and Sustainability, Ispra, Italy; Geraldine Barry, European Commission, JRC, Brussels, Belgium

Estimating Earth's Human Carrying Capacity

Organized by Kenneth G. Cassman, University of Nebraska, Lincoln; Ruth Cooper, The Royal Society, London, United Kingdom; David Tilman, University of Minnesota, St. Paul

How Can the World Feed 9 Billion People by 2050 Sustainably and Equitably?

Organized by Kate Von Holle, British Embassy, Washington, DC; Jon Parke, Foresight Program, U.K. Government Office of Science, London

If a Culture of Growth Is Unsustainable, What Should Change?

Organized by Paul H. Reitan, University at Buffalo, NY; Ward Chesworth, University of Guelph, Canada

Mapping and Disentangling Human Decisions in Complex Human-Nature Systems

Organized by Li An, San Diego State University, CA; Stuart Aitken, San Diego State University, CA; Janet Silbernagel, University of Wisconsin, Madison

Research Frontiers in Sustainability Science: Bridging Disciplines and Practices

Organized by William C. Clark, Harvard Kennedy School of Government, Cambridge, MA; Simon A. Levin, Princeton University, NJ

Resource Use and Ecological Resilience in a Tropical Socio-Ecological System

Organized by Oskar Burger and Jose M.V. Fragoso, Stanford University, CA

Social Networks and Sustainability

Organized by Thomas Dietz, Michigan State University, East Lansing; Adam D. Henry, West Virginia University, Morgantown

Telecoupling of Human and Natural Systems

Organized by Jianguo (Jack) Liu and William McConnell, Michigan State University, East Lansing; Thomas J. Baerwald, NSF, Arlington, VA

The Challenge of Measuring Sustainability

Organized by Eugene A. Rosa, Washington State University, Pullman; Thomas Dietz, Michigan State University, East Lansing

Act Now ... Rates Go Up in January

Registration

Discounted advance registration rates are available until Thursday, 27 January 2011.

Take advantage of unlimited access to all symposia, seminars, topical lectures, plenary events, career workshops, the International Exhibition, and a variety of networking opportunities.

Professional
$295 Members/$375 New Members/
$399 Non-Members

Postdoc
$235 Members/$315 New Members/
$335 Non-Members

K-12 Teacher
$235 Members/$315 New Members/
$335 Non-Members

Emeritus
$235 Members/$315 New Members/
$335 Non-Members

Student
$60 Members/$70 New Members/
$90 Non-Members

After 27 January 2011, on-site rates apply. For more information visit http://www.aaas.org/meetings.

Housing

Special room rates and benefits are available to Annual Meeting registrants.

Renaissance Downtown
(Headquarters Hotel)
Rate: $232 Single/$252 Double

Embassy Suites Convention Center
Rate: $234 Single/$259 Double

Grand Hyatt Washington
Rate: $239 Single/$264 Double

Hampton Inn Convention Center
Rate: $209 Single/Double

Rooms are available on a first-come, first-served basis until 16 January 2011 for the Grand Hyatt and 23 January for the Renaissance, Embassy Suites, and Hampton Inn.

More Ways To Save

Discount Travel to Washington, DC

For details about discounts on airfare and rail, visit www.aaas.org/meetings and click on "Hotel and Travel" then "Travel Discounts."

To browse the updated program, register, and reserve hotel rooms, visit **www.aaas.org/meetings.**

AAAS, publisher of *Science*,
thanks the sponsors and supporters of the

2011 Annual Meeting

Presenting Sponsor

Canada

SUBARU

HELMHOLTZ ASSOCIATION

EUROPEAN RESEARCH
SUCCESS THROUGH COOPERATION

Johnson & Johnson
PHARMACEUTICAL RESEARCH & DEVELOPMENT, L.L.C.

NSF

THE KAVLI FOUNDATION

AAAS
ADVANCING SCIENCE, SERVING SOCIETY

AAAS ANNUAL MEETING | 17-21 February 2011 | Washington, D.C.

Bioperfection.

Sigma's Prestige Antibodies® could prove priceless to your research.

Sigma now offers over 10,000 Prestige Antibodies powered by Atlas Antibodies.

1,700 new Prestige Antibodies are now available! Developed through the Human Protein Atlas Project, Prestige Antibodies are standardized in universal protocols to enhance the efficiency and effectiveness of your research. Each antibody is supported with over 700 immunohistochemistry, immunofluorescence and Western blot images that are all publicly available on the Human Protein Atlas website.

Prestige Antibodies® Powered by ATLAS ANTIBODIES

wherebiobegins.com/biomolecules

SIGMA-ALDRICH®

SIGMA® Life Science Where bio begins™

Cancer
Development
Endocrinology
Glycobiology
Immunology
Neuroscience
Proteases
Signal Transduction
Stem Cells

R&D Systems Products for Neuroscience Research

R&D Systems offers a wide range of high quality products for neuroscience research. In addition to high performance **antibodies**, we offer the most referenced collection of premium quality **proteins** and **ELISA kits** in the industry. Our catalog also includes primary rat and mouse cortical **stem cells**, and kits for the expansion, differentiation, and identification of neural stem cells.

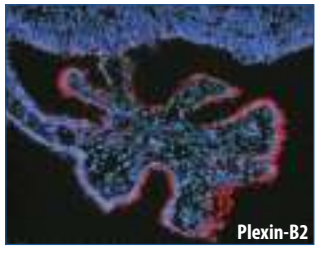

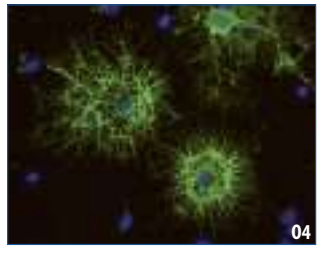

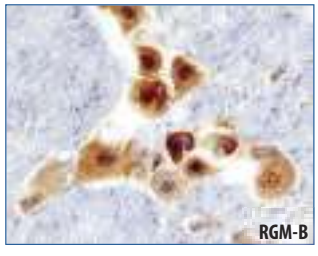

Performance.
Results.
Progress.

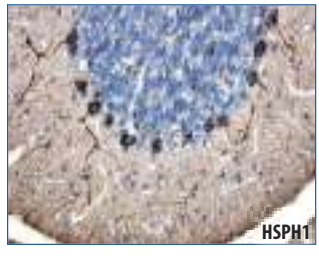

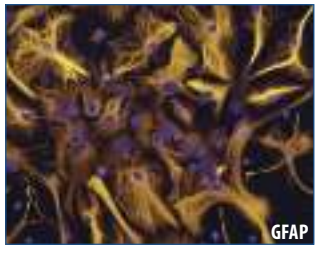

For more information visit our website at www.RnDSystems.com/go/Neuroscience

For research use only. Not for use in diagnostic procedures.

R&D Systems, Inc. www.RnDSystems.com

R&D Systems Europe, Ltd. www.RnDSystems.co.uk

R&D Systems China Co., Ltd. www.RnDSystemsChina.com.cn

R&D SYSTEMS®

GE Healthcare
Life Sciences

Thank you ECL™ Plus, you've been great.

For every success there's a successor. It's called progress. So while we knew we had something special in Amersham™ ECL Plus, our Western blotting team was quietly working on the next generation of detection reagent. The result: a new substrate that operates with superior levels of sensitivity, signal intensity and stability than even its famous predecessor, making it an excellent choice for CCD imagers. **Welcome to ECL Prime.**

Signal intensity sustained at higher antibody dilutions

Ab dilution		Amersham ECL Prime		Amersham ECL Plus	
Primary	**Secondary**	10 µg	156 ng	10 µg	156 ng
1:3000	1:300 000				
1:10 000	1:500 000				

Comparison of Amersham ECL Prime and Amersham ECL Plus detection of ß-catenin in NIH 3T3 whole cell lysates using different dilutions of rabbit anti-ß-catenin and HRP-conjugated anti-rabbit IgG.

Find out more about Amersham ECL Prime at www.gelifesciences.com/eclprime

imagination at work

Any sample, any application — no limits

Maximize success with QIAGEN sample technologies

- Innovative, room-temperature sample collection and stabilization
- DNA, RNA, and protein purification from any sample
- Hands-free automated sample preparation
- Reliable genetic, epigenetic, and gene expression analysis from FFPE samples
- Whole genome and transcriptome amplification to overcome sample limitations

Contact QIAGEN today or visit www.qiagen.com/sample-technologies

QIAGEN®

Sample & Assay Technologies

ADNASamplePort0910S1WW

Dedication to Science
How is the light wavelength of knowledge calculated? Leica Microsystems has mapped its corporate values.
For more information, visit our website.

Professor Tanke, why is curiosity a building block of life?

Hans Tanke, a researcher and pioneer of digital fluorescence microscopy, is driven by passionate curiosity. He is Head of the Department of Molecular Cell Biology at Leiden University Medical Center, Netherlands, where he gives young scientists creative freedom: this enables them to develop the ethically responsible dedication with which he himself keeps tracking down the building blocks of life.

www.leica-microsystems.com

Living up to Life

Leica
MICROSYSTEMS

GS Junior Sequencing System

A *NEW* Scale of Sequencing –

Amplicon Sequencing on Your Benchtop

Amplicon Assay	Samples per Run
HIV Drug Targets (*e.g.,* 16 amplicons covering 5 regions at 1500X [Protease, RT, Integrase, Envelope V3, gp41 heptad repeats])	8
Gene Sequencing (*e.g.,* CFTR, 34 amplicons covering 27 exons at 50X)	48
HLA Sequencing (*e.g.,* high-resolution genotyping at 7 loci)	16
VDJ Sequencing (*e.g.,* for vaccine response or minimal residue detection for known clonality)	8

Figure 1: Get the right depth and coverage for your amplicon project. You can customize your experimental design to maximize data throughput for optimal sample coverage per sequencing run. Examples of various applications and optimum sample number per run are shown for the GS Junior System.

Bring the power of 454 pyrosequencing to your amplicon projects. Now available, the new small-footprint **GS Junior System** generates 70,000 reads per run, and delivers the performance and long reads (up to 500 base pairs) of the GS FLX Titanium chemistry to your benchtop.

- **Detect SNPs, insertions, and deletions.**
- **Discover rare somatic mutations in complex samples based on ultra-deep sequencing of amplicons.**
- **Sequence and analyze collections of human exons for identifications of rare alleles.**
- **Find viral quasispecies present within infected populations.**
- **Identify rare alleles associated with diseases.**

For complete information on the GS Junior System and all of the Roche sequencing solutions, visit ***www.454.com*** or contact your local Roche representative today.

For life science research only.
Not for use in diagnostic procedures.

454 SEQUENCING

Roche Diagnostics Corporation
Roche Applied Science
Indianapolis, Indiana

Roche

eppendorf advantage

New Promotion, Sept. 1–Dec. 31, 2010
www.eppendorf.com/advantage

- **Limited offer:**
  Centrifuges 5430 and 5424
  with free standard rotor!

- **New promotion:**
  Centrifuge 5418
  with 20 % off!

- **Save big**
  with Eppendorf's
  Cell Culture Bundles!

- **Buy 3 get 4:**
  Eppendorf DNA LoBind
  and Protein LoBind Tubes
  in a special promotion pack!

Limited offer
Sept. 1–Dec. 31,
2010

Top Performance!

Save big with Centrifuge Bundles and Eppendorf LoBind™ Tubes

Get top performance!

- **Eppendorf centrifuges** provide top performance in the lab. They are strong, reliable, durable and long lasting. Best results are ensured by tried and trusted technology and latest safety features.

- **Eppendorf DNA LoBind and Protein LoBind Tubes** ensure top performance in terms of highest recovery rates.They provide maximum protection from sample loss – thus improving the results of your assays!

Enjoy great savings!

With our new **Eppendorf Advantage** offers you can get top performance and enjoy great savings on micro-centrifuges, multipurpose centrifuges and LoBind Tubes.

Take advantage now!

Check out our new limited offers and contact your participating Eppendorf Partner today.
For full details and dealer contact information, please visit **www.eppendorf.com/advantage**.

eppendorf
In touch with life

Your local distributor www.eppendorf.com/worldwide · **Application Support** E-mail: support@eppendorf.com
Eppendorf AG · Hamburg · Germany · Tel: +49 40 538 01-0 · Eppendorf North America, Inc. · USA · Tel: +1 800 645 3050 menu option 2

Need to assess the novelty of substances?
SciFinder is the answer.

It includes CAS REGISTRY,[SM] the most comprehensive substance information available, integrated with relevant journal articles and patents.

Give your research team the highest quality and most timely scientific information resource.

Make SciFinder an essential part of your research process.

For more information about SciFinder, visit www.cas.org or e-mail help@cas.org.

SciFinder®—an essential Part of the process.™

CAS | SciFinder®

www.cas.org

CAS is a division of the American Chemical Society

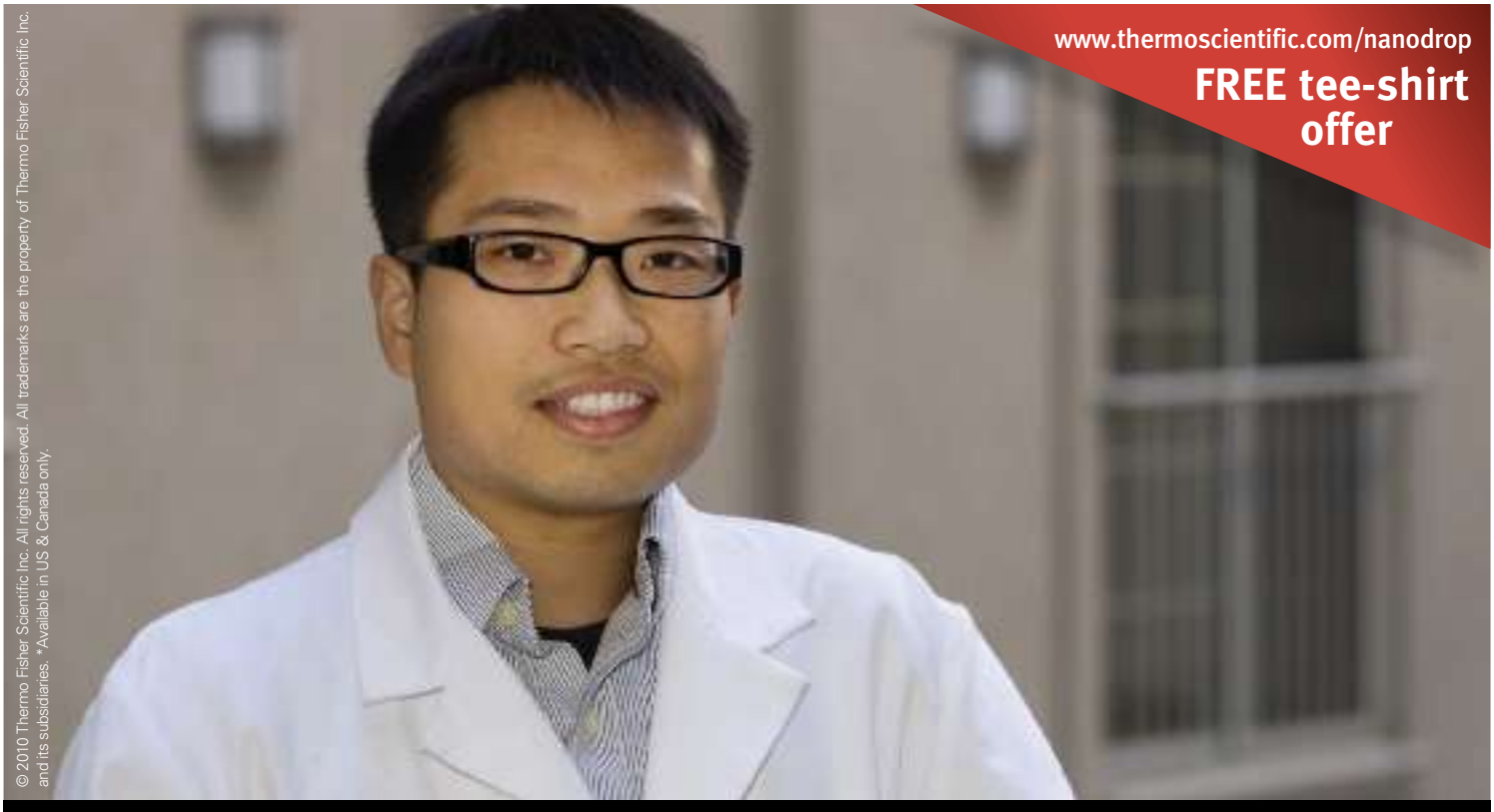

www.thermoscientific.com/nanodrop

FREE tee-shirt offer

"I really like this instrument! Reliability and reproducibility are so important." —Hing Cheong (Henry) Lee, Ph.D.

Emotional reactions to instrumentation from scientists are rare. Yet with Thermo Scientific NanoDrop Spectrophotometers, they are becoming commonplace. That's because scientists who own a NanoDrop™ are passionate about its simplicity. These instruments reduce analysis time and minimize sample waste with fast, easy and accurate micro-volume nucleic acid and protein sample quantitation. Just ask Dr. Lee:

"With NanoDrop I use less sample. Reproducibility of results is much higher—and I get them in a few seconds. The previous machine I used to measure DNA took much longer, and the results weren't nearly as reliable. NanoDrop is much faster. It is small, quick and convenient."

Learn about our special offers including a FREE tee-shirt promotion
www.thermoscientific.com/nanodrop

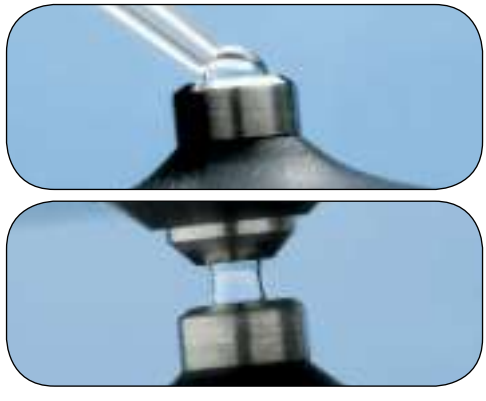

Thermo Scientific NanoDrop UV-Vis Spectrophotometers offer easy, reliable micro-volume analysis, with sample size as low as 0.5 µl and measurement time of less than 5 seconds—no dilutions.

Moving science forward

Thermo SCIENTIFIC

Part of Thermo Fisher Scientific

INTRODUCING

AAAS **Member**Central

The exclusive new website for the AAAS member community.

AAAS MemberCentral is a new website focused on helping you — the scientists, engineers, educators, students, policymakers, and concerned citizens who make up the AAAS community — connect like never before.

On MemberCentral you can contribute to discussion groups or blogs, participate in a webinar, or share photos of your field research. You can exchange ideas, learn about your fellow members, and gain fresh insights into issues that matter to you the most. MemberCentral is also an easy access point for a wide variety of other AAAS membership benefits, like discounts on cars and books, travel opportunities, and more.

Experience MemberCentral for yourself. Visit MemberCentral.aaas.org today and log in using your *Science* online username and password.

AAAS

MemberCentral.aaas.org

ATCGATCG

TruSeq™

The most accurate next-gen sequencing technology available.

Every Illumina sequencer is powered by TruSeq—the technology that delivers the most accurate human genome at any coverage. TruSeq produces the highest yield of error-free reads. The most bases over Q30. The greatest number of peer-reviewed publications—more than 1,000 in the past three years.

That's Tru data quality.

Get the proof. Go to
www.illumina.com/TruSeq

HiSeq™ 2000 | HiSeq™ 1000 | HiScan™ SQ | Genome Analyzer$_{IIx}$

illumina®

NEW PRODUCTS FOCUS: ESSENTIAL LAB EQUIPMENT

MANUAL AND ELECTRONIC PIPETTES

The comprehensive range of Sarpette M manual and Sarpette E electronic pipettes come in single-, eight-, and 12-channel configurations. Sarpette M pipettes feature continuously adjustable volumes from either the dispenser button or thumbwheel and offer exceptional accuracy and precision. Lightweight and well balanced for comfortable pipetting, Sarpette M pipettes require low dispensing and tip ejection forces. Multichannel options feature a curved ejector bar and an individual shaft suspension system to further reduce hand strain. Sarpette M pipettes are fully autoclavable. Sarpette E electronic pipettes are controlled by a high-precision motor and microprocessor to ensure smooth and accurate pipetting. Practical, user-friendly operation modes include various mixing, multiple dispensing, and sequential aspirating/dispensing options as well as five speeds and nine memory programs. Sarpette E pipettes feature a large, angled LCD display, an extremely lightweight ergonomic design, and a long-lasting rechargeable lithium ion battery. High-quality pipette tips are offered in a wide-range of packaging and purity options as well as corresponding carousel and linear stands to compliment the Sarpette pipettes.

Sarstedt, Inc.

For info: 800-257-5101 | www.sarstedt.com

MINI CENTRIFUGE

The compact, economical Scie-Plas Mini Centrifuge comes with three different rotors for use in a wide-range of bioscience research applications. Designed with a small footprint to fit easily even where space is limited, this centrifuge model is very easy to use. An on/off switch enables the lid to be closed without starting the unit and when the lid is opened, the centrifuge stops automatically. For added value and versatility, the Scie-Plas Mini Centrifuge includes three rotors: a six-place rotor for 1.5 ml tubes, a 0.2 ml PCR strip rotor, and a 1- by 3-inch slide rotor. A maximum speed of 6,000 rpm/2,000 x g is perfect for quickly spinning down samples, in microgel filtration applications and for microvolume centrifugation.

Scie-Plas

For info: +44-1223-427888 | www.scie-plas.com

SPECTROMETER

FT-IR spectrometer, Nicolet iS5, is designed for users seeking no-compromise, affordable, and compact FT-IR spectroscopy to assist in their product assurance testing, basic troubleshooting, and chemistry teaching. The Nicolet iS5 establishes a new benchmark in small-footprint laboratory FT-IR spectroscopy. Delivering comparable performance to full-size spectrometers, the instrument has an open-architecture sample compartment that accepts a wide variety of sampling accessories. The spectrometer incorporates the award-winning OMNIC software, widely adopted by major industrial manufacturers and forensic laboratories around the world. The Nicolet iS5 spectrometer, its new iD sampling accessories, and OMNIC software solutions for raw materials, impurities, and mixtures identification, create a unique user experience "from sample-in to answer-out."

Thermo Fisher Scientific

For info: 800-532-4752 | www.thermoscientific.com/ftir

MICROPLATE SEALING FILM

The revolutionary microencapsulated clear sealing film for microplates, MicroBurst, circumvents the use of adhesive seals that can easily stick to your glove rather than your microplate. MicroBurst sealing films have been developed to eliminate this problem. With its adhesive encapsulated in millions of tiny spheroids, MicroBurst sealing film is not sticky when first handled and can be quickly and easily moved into position. Only when you are satisfied that the film is in the correct place do you press down hard to burst and activate the MicroBurst adhesive microcapsules. No more mess, no more incorrectly positioned adhesive seals. The clear film has excellent optical properties and once activated, produces a very firm seal which quickly strengths to form a near-permanent seal on your plates. MicroBurst film can be pierced by pipette tips or robot liquid handlers and is temperature stable, making it ideal for PCR work.

Porvair Sciences Ltd.

For info: +44-1372-824290 | www.porvair-sciences.com

LIGHT-SHIELDING GLASSWARE

The new VITLAB light-shielding volumetric flasks are made of a specially pigmented polymethyl pentene (PMP) plastic that provides excellent absorption of light. In particular, absorption in the ultraviolet range—below 280 nm and the upper visible range above 580 nm—yet provides sufficient translucency to verify contents and volume, in most applications superior to amber glass. It provides a sunlight protection factor of nearly 20. Flasks are lightweight and break resistant, and provide a cost-effective alternative to glass. Screw-on caps help protect flask contents better than traditional stoppers. Flasks are available in sizes from 10 ml to 1000 ml. All volumes are Class A per DIN EN ISO 1042.

BrandTech Scientific, Inc.

For info: 888-522-2726 | www.brandtech.com

Electronically submit your new product description! Go to **www.sciencemag.org/products/newproducts.dtl** for more information.

Newly offered instrumentation, apparatus, and laboratory materials of interest to researchers in all disciplines in academic, industrial, and governmental organizations are featured in this space. Emphasis is given to purpose, chief characteristics, and availability of products and materials. Endorsement by *Science* or AAAS of any products or materials mentioned is not implied. When you seek additional information from the manufacturer or supplier, tell them you saw it here.

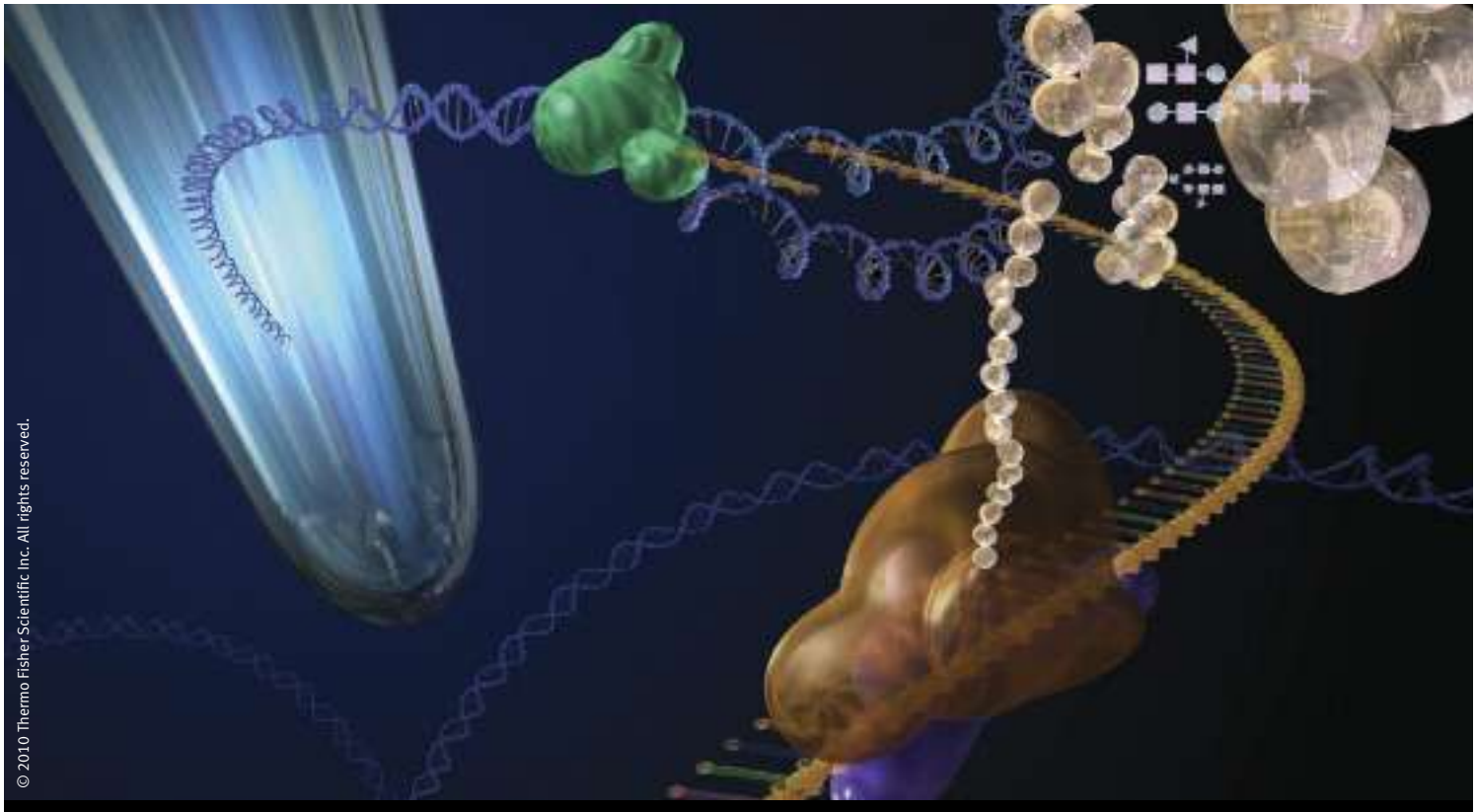

Synthesize functional proteins *in vitro* with human cell-free extracts.

Now there is an alternative for your *in vitro* protein synthesis. The Thermo Scientific Pierce *In Vitro* Translation Systems use human cell-free extracts to produce proteins with post-translational modifications such as glycoproteins. In 90 minutes, our systems produce more protein than rabbit reticulocyte systems.

- Express functional protein from any organism in 90 minutes
- Optimized system for glycoprotein expression available
- Achieve proper post-translational modifications
- Successfully express proteins up to 250 kDa
- Used for IP/co-IP, EMSA, protein labeling or mutant screening

Visit *thermoscientific.com/pierce* to learn why human cell-free extracts produce better *in vitro* translation results for a variety of applications.

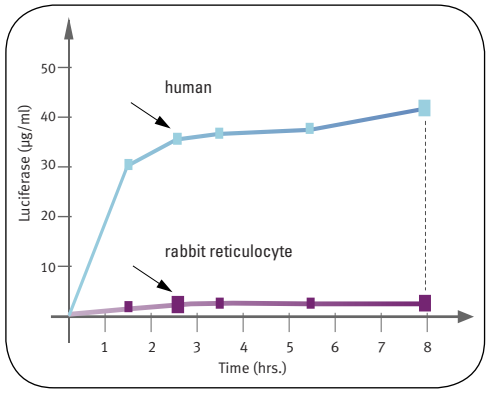

Comparison of luciferase expression in human cell-free extracts and rabbit reticulocyte lysates. The Pierce Human *In Vitro* Protein Expression System improves protein yield up to 15 times greater than rabbit-based systems.

Moving science forward

Thermo SCIENTIFIC

Part of Thermo Fisher Scientific

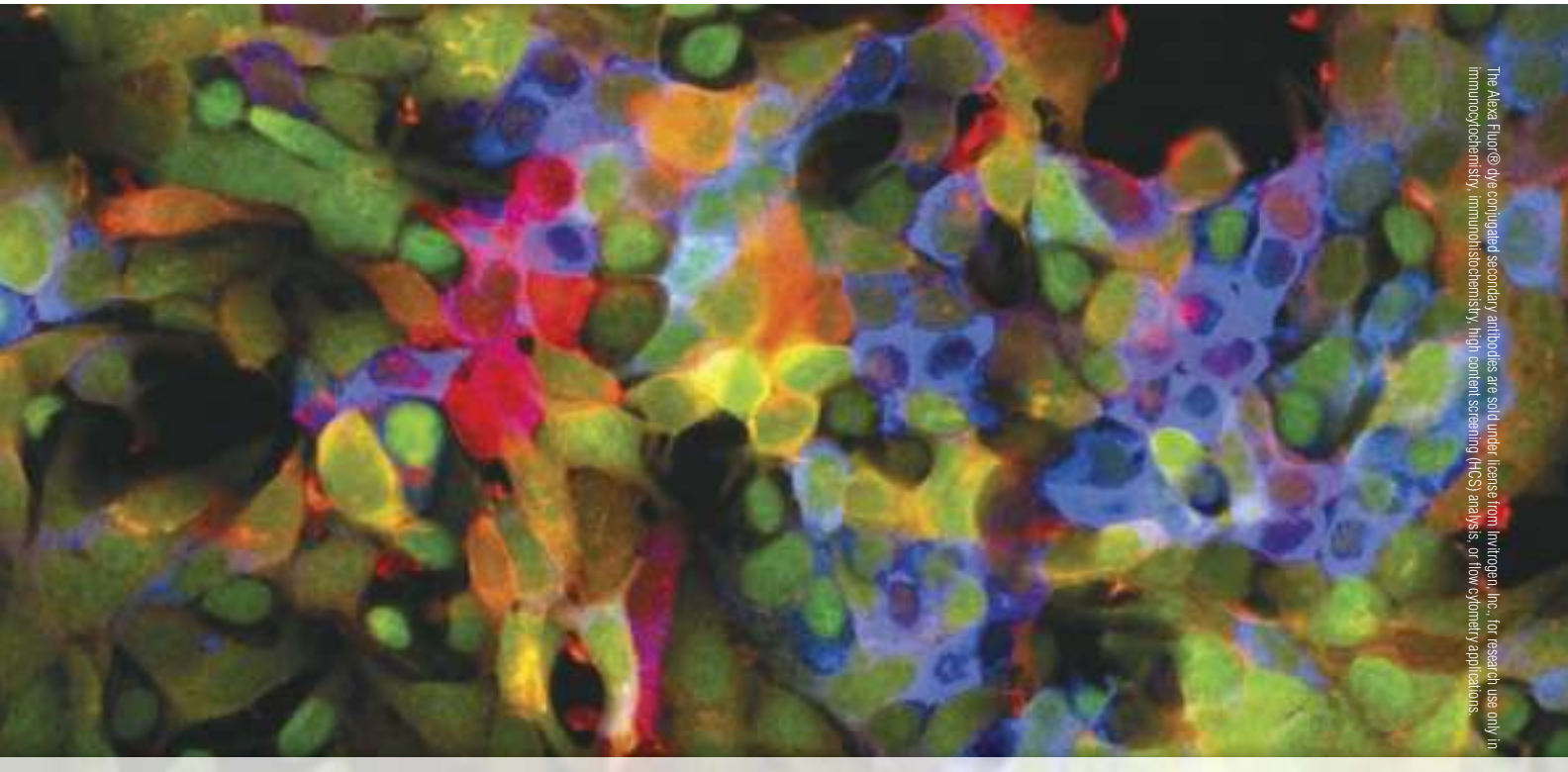

PathScan® Signaling Nodes Multiplex IF Kit

from Cell Signaling Technology

Immunofluorescent analysis of MCF7 (human breast adenocarcinoma) cells insulin-treated for 5 minutes, using PathScan® Signaling Nodes Multiplex IF Kit #8999.

PathScan® Signaling Nodes Multiplex IF Kit #8999 from Cell Signaling Technology provides a novel multiplex assay to simultaneously assess signaling through key pathway nodes (activated-Akt, p44/42, and S6 Ribosomal Protein) using automated imaging or laser scanning high content platforms, or manual immunofluorescence microscopy. The kit provides reagents necessary to perform 100 assays (based on 100 µl assay volume).

- The kit allows the analysis of multiple pathway endpoints within a single sample, saving time and reagents.
- The kit is produced and optimized in-house with the highest quality antibodies, providing you with the greatest possible specificity and sensitivity.
- Technical support is provided by our in house IF group who developed the product and knows it best.

#8999 Kit Targets	Detection Dye	$Ex_{(max)}$ (nm)	$Em_{(max)}$ (nm)
Phospho-Akt (Ser473)	Alexa Fluor® 555	555	565
Phospho-p44/42 (Erk1/2) (Thr202/Tyr204)	Alexa Fluor® 488	495	519
Phospho-S6 Ribosomal Protein (Ser235/236)	Alexa Fluor® 647	650	665

for quality products you can trust...

www.cellsignal.com

Cell Signaling TECHNOLOGY®

Orders (toll-free) 1-877-616-2355 | **Technical support** (toll-free) 1-877-678-8324 support@cellsignal.com | **Inquiries** info@cellsignal.com | **Environmental Commitment** eco.cellsignal.com

Early Independent Scientists in the NIH Intramural Research Program

The National Institutes of Health, the nation's premier agency for biomedical and behavioral research, is pleased to announce a new program for Early Independent Scientists in the NIH Intramural Research Program (IRP). We are looking for new Ph.D., M.D., D.D.S. and equivalent doctoral researchers who have the creativity, intellect and maturity to flourish in an independent research position.

The IRP is home to approximately 1,200 tenured and tenure-track investigators and 5,000 trainees. We provide an environment that encourages and supports innovative, high-impact research. To enhance the development and early-stage careers of exceptional investigators, the NIH has developed this new program to support recent doctoral graduates in independent positions without the need to perform a post-doctoral career fellowship. Thus, the graduate can immediately start an independent career after graduation.

Early Independent Scientists will be provided the resources to establish an independent research program, including salary and benefits, support for lab personnel, lab space, supplies, and start-up equipment. At the time of application, candidates must be within 12 months of completing their Ph.D., M.D. or D.D.S. degree, or for clinician-scientists within twelve months of completing their core clinical residency program. The NIH will support up to five Early Independent Scientists per year, with each scientist receiving up to five years of support. Successful candidates also will be eligible to apply for funds from the NIH Common Fund Early Independent Investigator program.

Complete applications must be received by **December 20, 2010**. Candidates should submit electronically a **cover letter, curriculum vitae, and a 3-page statement of research interests and future plans, and arrange to have 3 to 5 letters of reference sent to: Charles Dearolf, Ph.D., Assistant Director for Intramural Research, National Institutes of Health, Email: dearolfc@od.nih.gov**

The NIH recognizes a unique and compelling need to promote diversity in the biomedical, behavioral, clinical and social sciences research workforce. The NIH expects its efforts to diversify the workforce to lead to the recruitment of the most talented researchers from all groups. We encourage applications from talented researchers from diverse backgrounds underrepresented in biomedical research, including underrepresented racial and ethnic groups, persons with disabilities, and women for participation in all NIH-funded research opportunities.

Research Fellow
Medical Oncology Branch, NCI
(deadline: December 30)

The National Cancer Institute (NCI) Center for Cancer Research (CCR), Medical Oncology Branch, Office of the Medical Director is seeking bioinformaticist candidates for a Research Fellow (FTE and/or contract researcher). The position is located on the campus of the National Institutes of Health (NIH) in Bethesda, Maryland. The person will be responsible for bioinformatics analysis of data generated in the MOB labs. The person's work will focus on, but not limited to: next-generation sequence analysis, genomics data (CGH, SNP array data etc.), transcriptome data (gene expression profiling, clustering, feature extraction etc.), epigenetics data, proteomics (mass-spec) data, synthetic DNA sequences design, data integration, network analysis and high-level database mining.

The successful candidate must have a Ph.D. degree and at least three (3) years of research experience in bioinformatics. The candidate must have a strong technical background and excellent communication skills. Individuals who are interested in pursuing a career in basic and translational investigation and cancer drug development are encouraged to apply. For further information about the Medical Oncology Branch, the NCI programs, faculty and training, or the NIH, please visit our respective web sites: http://ccr.cancer.gov/labs/lab.asp?labid=753, http://bethesdatrials.cancer.gov/clinical-programs/theraputics/default.aspx , http://ccr.nci.nih.gov/, and http://www.nih.gov/

Position Requirements: Candidates must have a Ph.D. degree and be experienced in a broad array of bioinformatics tools and techniques. Salary will be commensurate with experience on this renewable, time-limited federal position. Applications should include: a personal statement of clinical and research experience and interests; a career synopsis, a current curriculum vitae and complete bibliography; and the names, addresses and phone numbers of three (3) references. Applications must be postmarked or received by email at **coleta@mail.nih.gov by December 30, 2010**. **Send applications to: Mrs. Tammy Cole, Medical Oncology Branch, C/o of Dr. Giuseppe Giaccone, Bldg. 10, Room 12N-226, 10 Center Drive, Bethesda, MD, 20892-1906**.

National Institute on Aging

Health Scientist Administrator (Branch Chief), GS-601-15
Division of Aging Biology

The National Institute on Aging (NIA), a major research component of the National Institutes of Health (NIH) and the Department of Health and Human Services (DHHS), is seeking an individual to help plan and direct the Institute's research programs in the field of genetics and cell biology and provide independent leadership in research of national and international significance. The selectee will join a team of professionals responsible for advancing basic and translational research, research training, and information programs supporting research that addresses the biological underpinnings of health issues and needs of the elderly.

Candidates should have a PhD or an equivalent doctoral degree, training in a relevant biomedical research field, at least two years of direct experience in the independent planning, design, administration and performance of research projects, experience in scientific grant application writing or review; and demonstrated skills in administration and communication.

Salary is commensurate with professional experience and qualifications, and it includes a full Federal benefits package (i.e., retirement, health, life and long-term care insurance, Thrift Savings Plan participation, etc.).

To apply and review qualifications, evaluation criteria, application instructions, salary and benefits information, please visit http://www.nia.nih.gov/AboutNIA/Jobs.htm. For additional information on application procedures and announcement posting dates, please contact Erika Meares at 301 594-2316. National Institute on Aging, http://www.nia.nih.gov/

CMU
CENTRAL MICHIGAN UNIVERSITY

Great Lakes Research (Tenure-Track, Open Rank)

Position Summary: Central Michigan University invites applications for three tenure-track positions in the newly-created CMU Institute for Great Lakes Research (CMU-IGLR). Appointments will be considered at the rank of Assistant, Associate or full Professor depending on prior experience. Applicants should have established research programs on some aspect of Great Lakes research or possess expertise that will allow them to develop such a program. Those with expertise in areas including, but not limited to: toxicology, hydrology, GIS and remote sensing, environmental analysis and modeling, climate change, biogeochemistry, aquatic chemistry, or aquatic biology are especially encouraged to apply. Applicants should be qualified to hold a tenure track position in a department within the College of Science and Technology (Biology, Chemistry, Computer Science, Geography, Geology and Meteorology, Mathematics, Physics, and the School of Engineering and Technology). Successful candidates will be expected to develop and maintain a rigorous externally-funded research program involving undergraduate and graduate students and post-doctoral researchers and to participate in the activities of IGLR, including involvement in, and where appropriate, leading multidisciplinary research projects and proposals. Additional responsibilities include teaching one course per semester and university and departmental service.

Required Qualifications: Ph.D.; prior success in obtaining, or the demonstrated potential to obtain, external funding; demonstrated effective communication skills; a commitment to excellence in undergraduate teaching and graduate education.

Preferred Qualifications: Preference will be given to candidates with expertise that complements that of existing CMU faculty working on the Great Lakes, to individuals who will strengthen the research programs at the Central Michigan University Biological Station on Beaver Island, and to those with post-doctoral experience.

Applications: Applications should include a CV, cover letter, statement of research interests and the names and contact information for 3 referees and must be submitted electronically through **www.jobs.cmich.edu**. Requests for further information may be addressed to the Director of CMU-IGLR, Dr. Donald Uzarski (uzars1dg@cmich.edu).

About the Department: CMU's Institute for Great Lakes Research occupies spacious and modern laboratories in the Center for Applied Research and Technology (CART). Available resources include field and laboratory equipment, technicians, and graduate assistantships. CMU-IGLR faculty are currently conducting international Great Lakes research in collaboration with universities and government agencies across the basin on projects ranging from Great Lakes coastal wetland chemistry and ecology to hydrology. IGLR faculty also utilize research facilities at the CMU Biological Station **http://cmich.edu/beaverisland** located on Beaver Island, Lake Michigan, approximately 30 miles northwest of Charlevoix, Michigan. Classified by the Carnegie Foundation as a doctoral research university, CMU is recognized for strong undergraduate education and a range of focused graduate and research programs. CMU is a student-focused university with opportunities for leadership, internships, and off-campus volunteer programs.

CMU, an AA/EO institution, strongly and actively strives to increase diversity within its community (see www.cmich.edu/aaeo/).

Assistant/Associate/Professor in Immunology

FIU is a multi-campus public research university located in Miami, a vibrant, international city. FIU offers more than 180 baccalaureate, masters, professional, and doctoral degree programs to over 42,000 students. As one of South Florida's anchor institutions, FIU is worlds ahead in its local and global engagement and is committed to finding solutions to the most challenging problems of our times.

Florida's newly accredited College of Medicine at Florida International University (FIU) is seeking candidates with PhD, MD, MD/PhD degrees for tenure track/tenured Assistant /Associate or Full Professorial position in the Immunology Department. Selected candidate will also have a joint appointment with the Institute for Neuro-Immune Pharmacology, and is expected to work closely with Center Directors. Applicants must bring or show evidence of mobility and have significant external funding for their independent research. Candidates with significant expertise in Molecular Immunology, Neuro-Immune Pharmacology, Nanotechnology and Drug Targeting in Drugs Abuse Research areas and HIV infections is preferred.

For more information or to apply, please visit us on-line at **http://www.fiujobs.org** and reference position number **42296/42295**. Qualified applicants must submit a letter of interest accompanying their curriculum vitae with names and addresses of three professional references.

FIU | FLORIDA INTERNATIONAL UNIVERSITY

FIU is a member of the State University System of Florida and is an Equal Opportunity, Equal Access Affirmative Action Employer.

THE UNIVERSITY of TENNESSEE HEALTH SCIENCE CENTER

Director of Regional Biocontainment Laboratory

The University of Tennessee Health Science Center (UTHSC) is seeking applications and nominations for Director of the UTHSC Regional Biocontainment Laboratory (RBL). The UTHSC RBL is a new, fully equipped, select agent approved, state-of-the-art 30,000 square foot facility designed for work requiring BSL-3 and ABSL-3 (animal biosafety level 3) containment. The successful candidate will be an established scientist with extramural funding, a robust publication record, and a strong reputation in research involving microbial pathogenesis, and infectious diseases with an emphasis on biosafety level 3 (BSL-3) policies and practices. Administrative experience is desired as the Director will be charged with continuing the growth and development of research at the UTHSC RBL. The Director will report to the Vice-Chancellor for Research and also hold a tenure track position in a department consistent with their expertise.

Interested candidates should submit curriculum vitae, statement of research interests and the names of three references to:

Gerald I. Byrne, Ph.D.
Chair, Department of Microbiology,
Immunology and Biochemistry
UTHSC College of Medicine
PO Box 63647, Memphis, TN 38163
Or
e-mail rdonald@uthsc.edu

Review of applications will begin immediately and continue until the position is filled.

The University of Tennessee is an EEO/AA/Title VI/Title IX/Section 504 ADA/ADEA institution in the provision of its education and employment programs and services.

MARINE POPULATION DYNAMICS FACULTY POSITION SCRIPPS INSTITUTION OF OCEANOGRAPHY UNIVERSITY OF CALIFORNIA, SAN DIEGO

Scripps Institution of Oceanography (SIO) at the University of California in San Diego (**http://scripps.ucsd.edu**) is committed to academic excellence and diversity within the faculty, staff, and student body. We invite faculty applications to fill the marine population dynamics faculty position listed below. In addition to having demonstrated the highest standards of scholarship and professional activity, the preferred candidates will have experience in the arena of equity and diversity such as leadership in teaching, mentoring, research or service towards building an equitable and diverse scholarly environment. SIO is a world renowned center of marine research with approximately 200 principal investigators leading research programs on all aspects of earth, ocean and atmospheric sciences.

Successful candidates will be expected to teach classes and supervise research at both the graduate and undergraduate level. The position requires a PhD degree and a competitive record of publication, as well as evidence of the ability to conduct and fund an active research program consistent with the opportunity to have done so at this career level. Applicants are encouraged to submit all materials by **December 31, 2010. All applications and related materials should be submitted electronically via Academic Personnel Online RECRUIT at: https://apol-recruit.ucsd.edu/**. Applicants should send a letter including descriptions of their teaching experience, research interests, past experience and leadership in equity and diversity, a list of publications, immigration status, and the names of three potential referees, along with their complete institution address, e-mail address, phone and fax numbers.

Applicants should clearly indicate that they are applying for the marine population dynamics position. Questions about submission of applications may be addressed to **Leslie Costi at 858-822-1800, (lcosti@ucsd.edu)**. Salary will depend on the experience of the successful applicant and will be based on the UCSD pay scales.

Marine Population Dynamics (#10-230): We invite applications to fill a faculty position in marine population dynamics for fisheries and protected species. Research areas of special interest include population dynamics and stock assessment, management strategy evaluation, climate effects, and ecosystem and food web modeling. This key appointment builds upon a long record of accomplishment and collaboration between Scripps Institution of Oceanography and NOAA Fisheries Service. The successful candidate is expected to play a major role in training future practitioners in the science of population assessment and development of enhanced assessment methods that incorporate environmental variability, food web linkages and spatial heterogeneity. Preference will be given to scholars at the rank of Assistant Professor, but excellent candidates at other levels and in other specific areas will also be seriously considered.

UCSD is an Affirmative Action/Equal Opportunity Employer with a strong institutional commitment to excellence through diversity.

UNIVERSITY OF MARYLAND

Dean, College of Computer, Mathematical, and Natural Sciences University of Maryland, College Park

The University of Maryland, College Park invites applications and nominations for the position of Dean of the recently formed College of Computer, Mathematical, and Natural Sciences (**www.cmns.umd.edu**). A member of the Association of American Universities (AAU) and the flagship of the University System of Maryland, the University is located in the Baltimore-Washington corridor within nine miles of the nation's capital. The University ranks among the top 20 public universities, with nationally-ranked programs and innovative undergraduate programs.

The search for new knowledge, with its transformative effect on society, is increasingly becoming an interdisciplinary endeavor. For this reason, the University established the College of Computer, Mathematical, and Natural Sciences (CMNS) by integrating the former colleges of Chemical and Life Sciences (CLFS) and Computer, Mathematical, and Physical Sciences (CMPS). This integration will facilitate and encourage the rapid development of collaborations among faculty from across the two former colleges. This newly formed College includes the following Departments: Astronomy, Atmospheric and Oceanic Science, Biology, Cell Biology and Molecular Genetics, Chemistry and Biochemistry, Computer Science, Entomology, Geology, Mathematics, and Physics. CMNS also has a number of prestigious research Institutes and Centers that are highly interdisciplinary.

Nationally recognized for education and research, many programs in CMNS are ranked among the top ten of US public research universities. The College offers every student a high quality, innovative and cross-disciplinary educational experience, and a degree that commands respect around the world.

The Dean reports to the Senior Vice President for Academic Affairs and Provost, and is the chief academic officer and executive officer of the College, which has a full-time tenured/tenure-track faculty of 340 who are internationally respected and highly accomplished scholars. The College also employs more than 400 non-tenure-track research faculty and postdoctoral fellows. The College has over 5,000 undergraduate students and over 1,500 master and doctoral students. In addition, research awards for fiscal 2010 exceeded $200M.

We seek a leader who, in collaboration with the College chairs and directors, will play a major role in fostering continuous improvement in the standards, accomplishments, and international prestige of the faculty and students in the College. This includes strengthening the strong partnerships that exist between the College and nearby federal agencies and laboratories, as well as encouraging engagement with other regional, national, and international organizations. The Dean is expected to provide dynamic leadership toward achieving excellence in research, teaching, and service to the community and profession, in strategic planning, and in fundraising. The Dean must be able to lead a complex organization, and be dedicated to fostering the goals of diversity and affirmative action to enhance the College's integrative and intellectual mission. The Dean must demonstrate an understanding of contemporary issues in computer, mathematical, and natural sciences research and education, and must possess the ability to anticipate and address future challenges and opportunities. Qualified applicants must merit appointment at the rank of Professor with tenure in a CMNS unit, and have successful administrative experience. Salary will be competitive and commensurate with experience. The appointment date is open, with a start date of July 2011 preferred.

Applicants and nominees should submit a letter of interest; curriculum vitae; and the names, addresses, and telephone numbers of at least four persons who can be contacted by the search committee for reference. Nominations are encouraged and will be received at any time. Confidential review of nominations and applications for this position will begin **December 1, 2010**, and continue until the position is filled. Please send all materials to:

Search Committee for Dean, College of Computer, Mathematical, and Natural Sciences
Attention: Ms. Sandra Davis
1119 Main Administration Building
University of Maryland
College Park, MD 20742-5031
Tel (301)405-6813 Fax (301)405-8195

Electronic applications should be e-mailed to: **sandyd@umd.edu** followed by hard copies mailed to the above address.

The University of Maryland, College Park is an Equal Opportunity Employer; women and minority candidates are encouraged to apply.

UNC
LINEBERGER COMPREHENSIVE CANCER CENTER
N.C. CANCER HOSPITAL

HEMATOLOGY/ONCOLOGY ENDOWED PROFESSOR
UNIVERSITY OF NORTH CAROLINA AT CHAPEL HILL

The UNC-Chapel Hill Division of Hematology/Oncology, the Department of Medicine and the UNC Lineberger Comprehensive Cancer Center are recruiting for a senior faculty member at the level of Professor with tenure for an endowed and named chair.

The Wellcome Professorship will be awarded to a qualified physician or PhD researcher whose program is based in the laboratory and/or clinic with a focus on an improved understanding of the pathophysiology, molecular mechanisms, etiology, or treatment of hematologic malignancies. Candidates are expected to have an established basic, translational or clinical research program with a track record of peer reviewed funding and publications.

Clinical activity will be performed in the new 290,000 sq ft North Carolina Cancer Hospital which houses the inpatient units and outpatient clinics for the Division of Hematology/Oncology. Additionally, candidates will be eligible for membership in the UNC Lineberger Comprehensive Cancer Center, one of forty NCI Comprehensive Cancer Centers. UNC is home to exceptional physicians and scientists whose work has fueled significant growth in basic, translational and clinical research. .

Candidates with an MD degree must have completed a fellowship in Hematology or Medical Oncology, and be BC/BE in Internal Medicine and Hematology or Oncology. Interested individuals should apply online at **http://jobs.unc.edu/2500490** and attach a letter of interest and current CV. (For questions or additional information regarding the position you can contact: **Dr. Jonathan Serody, MD, Chair, Search Committee, Division of Hematology/Oncology, Department of Medicine, University of North Carolina at Chapel Hill, CB# 7305, Chapel Hill, NC 27599-7305**.)

UNC-CH is an Equal Opportunity Employer.

American University
College of Arts and Sciences
Department of Biology
Endocrinology

The Department of Biology at American University invites applications for a tenured position at the advanced Associate or Full Professor level, to begin fall 2011. A PhD in Endocrinology or a closely related field; an established record of research including evidence of significant external funding and a strong publication record; and substantial teaching experience are required. Responsibilities will include maintaining a strong externally funded research program, recruiting new faculty, mentoring junior faculty and graduate students, teaching undergraduate and graduate courses, including advanced courses in endocrinology, and providing university service. The primary appointment will be in the Department of Biology, with possible joint appointment in the Department of Psychology depending on experience and research interests. Applicants should submit a letter of application, curriculum vitae, an overview of their research program, and the names of at least 3 references to: **Dr. Victoria Connaughton, Endocrinology Search Committee Chair, Department of Biology, American University, 4400 Massachusetts Ave, NW, Washington, DC 20016**. To submit electronically (preferred), send applications to **biology@american.edu**. Review of applicants will begin on **November 15, 2010**, and continue until the position is filled.

American University is an Affirmative Action Equal Opportunity Employer, committed to a diverse faculty, staff and student body. Women and minority candidates are strongly encouraged to apply.

Brain Science Institute RIKEN

FACULTY POSITION
in Computational Neuroscience
RIKEN Brain Science Institute

The Brain Science Institute (BSI) of RIKEN in Wako, Japan, invites applications from candidates for a tenure-track Team Leader position (equivalent to a U.S. Assistant or Associate Professor) in Computational Neuroscience.

Candidates must have earned a Doctorate in a related field and demonstrated research expertise in any of the broad areas related to computational neuroscience, such as mathematical neuroscience, models for neural information processing, mathematical analysis of neural data, simulation of large-scale neural systems, and brain-inspired technology for real-world applicants. The candidate will be expected to conduct an independent research program.

A generous annual research fund and startup package will be provided, in addition to an apartment/condo rental allowance and other employee benefits.

The Search Committee will begin reviewing applications immediately. The search will continue until the position is filled. Interested applicants should submit a curriculum vitae, a summary of current and proposed research, and arrange for three letters of recommendation, all to be sent to:

Search Committee 2, RIKEN Brain Science Institute
2-1 Hirosawa, Wako, Saitama 351-0198, Japan
Fax: +81-48-467-9683; Email: **search20102@brain.riken.jp**
http://www.brain.riken.jp

RIKEN-BSI is an Equal Employment Opportunity Employer. Women are strongly encouraged to apply.

Faculty Positions in Bioengineering

Temple University's College of Engineering is forming a new department of Bioengineering and searching for outstanding individuals to occupy faculty positions in the department and college. Department growth will be accommodated in state-of-the-art facilities located in the new research tower immediately adjacent to the present Engineering building. This development is coupled with aggressive hiring in all departments in the College.

Although candidates in all traditional Bioengineering areas are welcome to apply, we are particularly interested in leveraging existing strengths in Engineering, Medicine, and the Basic Sciences. Accordingly, individuals with backgrounds in Cardiovascular research, Regenerative Medicine, Targeted Drug Delivery, and Biomaterials are particularly encouraged to apply.

Faculty is being sought at all academic ranks. Senior candidates should have a record of externally funded research, and junior faculty candidates should have significant postdoctoral experience with evidence of independent contributions.

Interested persons should submit an up-to-date copy of their CV, a statement of research goals and teaching philosophy, and the names and contact information for three references to:

George Baran, Ph.D.
Associate Dean
College of Engineering, Temple University
GRBaran@Temple.edu

Temple University is an Equal Opportunity/Affirmative Action Employer. Applications from women and minorities are especially encouraged.

ASSISTANT PROFESSOR

Department of Biological Sciences

The University of Alabama is among the top academic research institutions in the southeastern United States, and the Department of Biological Sciences is committed to maintaining this tradition of excellence. We currently seek applicants for tenure-track faculty positions at the rank of **Assistant Professor** in (1) **Computational Biology,** and (2) **Landscape/Spatial Ecology.**

Computational Biology

All areas of computational biology and bioinformatics will be considered. Applications from candidates with a demonstrated record of developing and/or applying computational approaches to study biological questions in areas including (prokaryotic and eukaryotic) genomics, evolutionary genomics, genetics, cell and molecular biology, and systems biology and a demonstrated interest in collaborative research are especially encouraged to apply. Candidates must have a Ph.D. in the biological sciences or quantitative discipline and postdoctoral experience. The successful applicant will be expected to participate in undergraduate and graduate education and training, and establish an active, externally funded research program. Applicants may contact the chair of the computational biology search committee, Dr. Julie Olson at **jolson@bama.ua.edu** or 205-348-2633, if additional information is required.

Landscape/Spatial Ecology

All areas of landscape and spatial ecology will be considered. Applications from candidates who use quantitative techniques, and/or modeling to study the relationship between spatial heterogeneity and ecological patterns, and with interests in aquatic ecology (freshwater, marine), biodiversity, microbial ecology, ecosystem studies, evolution, or linkages between terrestrial and aquatic systems are especially encouraged to apply. Candidates must have a Ph.D. and postdoctoral research experience and are expected to develop an active, externally funded research program and participate in undergraduate and graduate education and training. Applicants may contact the chair of the landscape/spatial ecology search committee, Dr. Robert Findlay at **rfindlay@bama.ua.edu** or 205-348-4167, if additional information is required.

To apply, go to **https://facultyjobs.ua.edu**, complete the online application (Job # 0804423 COMPBIO) or (Job # 0804424 LANDSCAPE), and upload (1) an application letter with a list of at least four references (including contact information); (2) CV; (3) statement of research interests and goals; and (4) statement of teaching interests and philosophy.

Consideration of applications will begin December 15 2010, and continues until the position is filled. Prior to the hiring, the final candidate(s) may be required to successfully pass a pre-employment background investigation.

Additional information on the Biological Sciences Department and the available positions can be found on our webpage at **http://bsc.ua.edu**

The University of Alabama is an Equal Opportunity/Equal Access Employer and actively seeks diversity among its employees.

touching lives
THE UNIVERSITY OF ALABAMA

Roche

Research Leader Tumor Immunology

Who we are
At Roche, 80,000 people across 150 countries are pushing back the frontiers of healthcare. Working together, we've become one of the world's leading research-focused healthcare groups. Our success is built on innovation, curiosity and diversity, and on seeing each other's differences as an advantage. To innovate healthcare, Roche has ambitious plans to keep learning and growing – and is seeking people who have the same goals for themselves.

The Position
Roche Glycart AG, a 100% affiliate of Roche Pharmaceuticals, is active in the research, development of new engineered antibody-based products for the treatment of cancer and autoimmune disease. We offer a stimulating and truly international environment. Roche Glycart AG is located in Schlieren/Zurich.
Lead Scientific and Drug Discovery Projects focusing on the characterization and optimization of a new generation of engineered, antibody-based molecules for cancer immunotherapy.

- The position is based at the Oncology Discovery and Translational Area at Roche Glycart in Schlieren, Zurich and projects will be conducted in collaboration with additional groups at Roche Glycart, both in the Discovery and in Translational Medicine areas, as well as with additional Roche research and development functions globally and with academic institutions.

Who you are
You're someone who wants to influence your own development. You're looking for a company where you have the opportunity to pursue your interests across functions and geographies, and where a job title is not considered the final definition of who you are, but the starting point.

- We are seeking candidates with a PhD in immunology and ample postdoctoral research experience in tumor immunology, with a strong tumor immunology scientific background and track record, being an active and recognized member of the international tumor immunology research community and having excellent written and verbal skills in English
- The candidate should have experience with animal work (mice) and be proficient with state-of-the art immunoprofiling techniques to characterize tumor infiltrating lymphocytes and anti-tumoral immune responses
- You have a high degree of self-motivation, flexibility and are able to independently conduct experiments. You are also inquisitive and strive for continuous process improvement. In addition you interact effectively with a truly multinational team of scientists.

Job ID No.: 367740
Contact HR: W. Kinzy, Phone: +41 61 687 94 03

The next step is yours. To apply online for this position visit www.careers.roche.ch

UNIVERSITY of NEW HAMPSHIRE

Two Tenure Track Faculty Positions in Sustainable Agriculture and Ecosystem Science

The University of New Hampshire seeks to expand on its cluster of five recent hires in the areas of Sustainable Agriculture and Sustainable Ecosystem Science and management, by filling two new positions at the Assistant Professor level. Detailed descriptions of these two positions are provided at **http://www.colsa.unh.edu/employment/**

- **Landscape Ecology** - Understanding how spatial patterns interact with ecological processes is a central component of ecology and is critical for developing sustainable land use strategies. The successful candidate will have expertise in quantitative spatial analyses, possibly including the use of remote sensing, GIS, and/or spatial statistics to address ecological problems and processes.
- **Specialty Crop Improvement** - The future of farming and other agricultural enterprises in the northeastern U.S. is tied to their economic, environmental, and social sustainability. The successful candidate will focus on the breeding of specialty crops (fruits, vegetables, or ornamental crops) adapted to sustainable production practices aimed at increasing the viability of small farms.

Applicants must have a Ph.D. in a relevant field. Preference will be given to those candidates displaying an interest and ability in working across traditional disciplinary/departmental boundaries. These new faculty are expected to establish vibrant, collaborative research programs, and to enhance the university's prominence in interdisciplinary research, teaching, and outreach. Our new faculty colleagues will be expected to train graduate students, to offer outstanding courses at the undergraduate and graduate levels, and demonstrate a commitment to diversity and inclusivity in research and education. These positions will be located within the College of Life Sciences and Agriculture (COLSA) and successful candidates will be matched with the department that best suits their interests and expertise. UNH is a Research-I, Land, Sea and Space Grant University that has been recognized both nationally and internationally for research excellence and a commitment to sustainability and public engagement.

Application Process: Information, including detailed position descriptions, is available at **http://www.colsa.unh.edu/employment/** All applicants will be required to apply online at **https://jobs.usnh.edu** Review of applications will begin on December 15, 2010 and will continue until the positions are filled.

The University actively seeks excellence through diversity among its administrators, faculty, staff and students and prohibits discrimination on the basis of race, color, religion, sex, age, national origin, sexual orientation, gender identity or expression, disability, veteran status, or marital status. Application by members of all underrepresented groups is encouraged.

The University of Luxembourg
is a multilingual, international research university

The University of Luxembourg invites applications for the following vacancy in its Faculty of Science, Technology and Communication:

Professor or Associate Professor in Computational Biology (m/f)

focus on stochastics, probabilistics and biostatistics

Ref.: F1-100038 • Employee status, full-time • Start date: 01/09/2011

Further information can be found on "More jobs" under
www.uni.lu

The University of Luxembourg is an equal opportunity employer.

uni.lu
UNIVERSITÉ DU LUXEMBOURG

Applications with clear reference to the position should be sent in printed form until March 30th, 2011 to the following address:

University of Luxembourg • Professor Paul Heuschling
Dean of the Faculty of Science, Technology and Communication
6, rue Coudenhove Kalergi • L-1359 Luxembourg

Applications will be handled in strict confidence.

DePaul University
Assistant Professors of Biology

Two tenure-track openings at the Assistant Professor level are available in the Department of Biological Sciences at DePaul University. The Department is housed in spacious and well-equipped teaching, research and support facilities, including a confocal microscope and a 2,000 sq. ft. state-of-the-art staffed animal care facility. Visit **http://las.depaul.edu/bio/** for more departmental information. Review of applications will begin **December 15, 2010**, and will continue until position is filled. Applicants should apply online with a cover letter, curriculum vitae, statement of research interests (2 page maximum), statement of teaching interests with educational philosophy (2 page maximum), and general list of equipment and supply needs with cost estimates. We also request three letters of reference (please supply the online system with the e-mail addresses of these three individuals).

Assistant Professor Neurobiology

A tenure-track opening for a neurobiologist is available in the Department of Biological Sciences at DePaul University starting September 2011. Successful candidate will be broadly trained in neurobiology with a strong commitment to undergraduate education. We especially encourage applications from neuroanatomists, neurophysiologists, and neurobiologists using cell/molecular approaches to study neuroscience. Ph.D. required; postdoctoral and previous teaching experience preferred. Teaching responsibilities to include some combination of: introductory biology for non-majors; co-teaching one quarter of introductory biology for majors; anatomy; core courses for our neurobiology concentration; and graduate/advanced undergraduate course in candidate's area of expertise. Startup funds are provided. E-mail **Dr. Talitha Rajah** at **trajah@depaul.edu** for additional inquiries. To apply, please submit application online at: **facultyopportunities.depaul.edu/applicants/Central?quickFind=50729**

Assistant Professor Ecology

A tenure-track opening for an ecologist is available in the Department of Biological Sciences at DePaul University starting September 2011. The successful candidate will be broadly trained in ecology with a strong commitment to undergraduate education. We encourage applications from candidates in all areas of ecology, using any plant or other organismal system, and any modern approach including population biology or cell/molecular analysis. Ph.D. required; postdoctoral and previous teaching experience preferred. Teaching responsibilities to include some combination of: introductory biology for non-majors; introductory biology for majors; sophomore level ecology; and graduate/advanced undergraduate course in candidate's area of expertise. Startup funds are provided. E-mail **Dr. Stanley Cohn** at **scohn@depaul.edu** for additional inquiries. To apply, please submit application online at: **facultyopportunities.depaul.edu/applicants/Central?quickFind=50730**

As an Equal Employment Opportunity (EEO) Employer, DePaul University provides job opportunities to qualified individuals without regard to race, color, ethnicity, religion, sex, sexual orientation, national origin, age, marital status, physical or mental disability, parental status, housing status, source of income or military status, in accordance with applicable federal, state and local EEO laws.

Faculty Position in Autonomous Robotics

at the Ecole polytechnique fédérale de Lausanne (EPFL)

ÉCOLE POLYTECHNIQUE
FÉDÉRALE DE LAUSANNE

The School of Engineering at EPFL invites applications for the position of **tenure-track assistant professor** in the area of **Autonomous Robotics** for the newly launched Swiss National Center of Competence in Research (NCCR) for Robotics. This is a broad search in all areas of autonomous robotics, with relevant fields including **materials and components** (e.g. soft bodies, artificial muscles, intelligent material), **manipulation** (dexterous and compliant manipulation, grasping, interaction with humans), **field robotics** (outdoor robots, intelligent vehicles, system design and integration, energy harvesting) and **medical microrobotics** (inner body monitoring, drug delivery, surgery).

As a faculty member of the School of Engineering, the successful candidate will be expected to initiate independent, creative research programs and participate in undergraduate and graduate teaching. Internationally competitive salaries, start-up resources and benefits are offered.

EPFL has a long-standing tradition in robotics, with special emphasis on the science and engineering of autonomous, intelligent, and bio-mimetic systems. EPFL has been selected by the Swiss Federal Government to house the NCCR for Robotics, a multi-year center of excellence federating and promoting robotics research in Switzerland. A new building on campus with laboratory space, prototyping and educational facilities for all robotics researchers will be completed in 2013.

The EPFL, located in Lausanne, Switzerland, is a dynamically growing and well-funded institution fostering excellence and diversity. It has a highly international campus at an exceptionally attractive location boasting first-class infrastructure. As a technical university covering computer and communication sciences, engineering, environment, basic and life sciences, management of technology and financial engineering, EPFL offers a fertile environment for research cooperation between different disciplines. The EPFL environment is multi-lingual and multi-cultural, with English often serving as a common interface.

Applications should include a curriculum vitae with a list of publications, a concise statement of research and teaching interests, and the names of at least five referees. Applications should be uploaded in PDF format to the recruitment web site: **robotics-search10.epfl.ch**

Evaluation of candidates will begin on **15 January 2011**, and will continue until the position is filled.

Further questions can be addressed to:
Prof. Auke Ijspeert, Search Chairman
e-mail: **hiring.robotics@epfl.ch**

For additional information on EPFL, please consult the web sites **www.epfl.ch, sti.epfl.ch** and **www.nccr-robotics.ch**.

EPFL is committed to increasing the diversity of its faculty, and strongly encourages women to apply.

Duke University Cluster Hire at the Intersection Between Ecology and Hydrology

NICHOLAS SCHOOL
OF THE ENVIRONMENT
DUKE UNIVERSITY

forging a sustainable future

The Nicholas School of the Environment (NSOE) at Duke University is continuing a search to develop a cross-disciplinary area of excellence at the interface between ecology and hydrology, two disciplines of longstanding strength at Duke. NSOE anticipates hiring a cluster of tenure-track professors in the coming year.

Given the School's current expertise in earth system processes at subcontinental to global scales and in terrestrial and aquatic systems at regional and local scales, individuals able to integrate across global patterns of variability in climate and the water cycle and the smaller-scale dynamics of terrestrial, freshwater, wetlands, or coastal ecosystems are encouraged to apply.

The successful candidate(s) will contribute to the Nicholas School's curriculum at the undergraduate, professional Master's and Doctoral level. Further, we seek scholars with interest in collaborating with other units on campus.

Consideration of applications will begin **January 1, 2011**, and will continue until all positions are filled. Applications should include a full CV, statement of research and teaching goals, and names of three references. In addition, we ask that applicants provide a one-page vision statement describing how their research is generating new insights at an important confluence of ecology and hydrology. Applications should be sent electronically as a single PDF to **Ms. Beatriz Martin** at **cabrera@duke.edu**.

The Nicholas School and Duke University are committed to equal opportunity in employment. Applications are strongly encouraged from members of under-represented populations.

NUS National University of Singapore

Faculty Position
Assistant Professor
at the
National University of Singapore
Department of Anatomy

The National University of Singapore (NUS) invites applications for a full-time tenure-track position in the Department of Anatomy. The Department is currently engaged in the following research programs: (a) Neuroscience, (b) Cancer Biology and (c) Toxinology. Candidates should hold a Ph.D. degree, with post-doctoral research experience preferably in Developmental Biology or Neuroscience. Research interest and experience with special focus on translational aspects of the above two fields would be advantageous.

Candidates are expected to have competent knowledge of Human Anatomy and Histology / Embryology. The successful appointee must be able to compete for independent research funding and is required to participate in undergraduate level teaching of medical and life science students.

Remuneration will commensurate with qualifications and experience.

Interested candidates should send their resume, research plan and names of six referees to: Professor BAY Boon-Huat, Head, Department of Anatomy, Yong Loo Lin School of Medicine, Block MD10, 4 Medical Drive, Singapore 117597 Email: antteov@nus.edu.sg Fax: (65) 67787643 Website: **http://www.med.nus.edu.sg/ant/**

Department of Anatomy
NUS Yong Loo Lin School of Medicine
A member of the National University Health System

POSITIONS OPEN

ASSOCIATE DIRECTOR
Center for Vascular Biology Research
Department of Pathology
Beth Israel Deaconess Medical Center
Harvard Medical School

The Department of Pathology at Beth Israel Deaconess Medical Center is seeking a full-time biomedical scientist in the area of vascular biology to serve as Associate Director of the Center for Vascular Biology Research (CVBR). The CVBR is an interdepartmental consortium of over 25 core investigators working in contiguous research space with expertise in pulmonary vascular disease, sepsis, translational medicine, diabetes, structural biology, atherosclerosis, and angiogenesis.

We are seeking candidates with leadership and mentoring skills, and strong records of research creativity and productivity in basic or translational research in vascular biology and angiogenesis. The research should involve fundamental mechanisms of vascular cell function in health and disease. It may also involve the use of model organisms or the development of new technologies and strategies for the study of tumor angiogenesis.

The successful candidate will receive a highly competitive startup package and an appointment to the faculty of Harvard Medical School at a rank that is commensurate with his/her qualifications. The Department of Pathology and the CVBR strongly encourage interactions between research and clinical faculty and provide opportunities to access an extraordinary human tissue resource through its Divisions of Anatomic Pathology and Laboratory Medicine. We also provide unparalleled opportunities for collaborative interactions within the basic and applied vascular biology research community at Harvard Medical School and its affiliated teaching hospitals.

Applicants must hold a Ph.D. and/or M.D. degree. *Beth Israel Deaconess Medical Center is committed to increasing the representation of women and members of minority groups on its faculty and we particularly encourage applications from such candidates.*

Interested applicants should submit curriculum vitae, a statement outlining existing and planned research activities and career goals, and the names of three professional references to:

Dr. Jack Lawler
Director, Division of Experimental Pathology
Beth Israel Deaconess Medical Center,
Research North Room 270K,
99 Brookline Avenue,
Boston, MA 02215

POSTDOCTORAL SCIENTIST
ROCKEFELLER UNIVERSITY
Mass Spectrometry, Proteomics, Nanotechnology

The Laboratory of Mass Spectrometry and Gaseous Ion Chemistry (**Professor Brian Chait**) and the Laboratory of Cellular and Structural Biology (**Professor Michael Rout**) are looking for a postdoctoral scientist. The joint project continues recent work on the nuclear pore complex and its biotechnological use (*Nature* **457:**1023, 2009). This involves a broad range of methods including mass spectrometry, protein production and purification, super-resolution fluorescence microscopy and nanotechnology.

Position available immediately.

Interested scientists should send curriculum vitae and three references to: **Beth Anne Hatton, Administrative Assistant, e-mail: hattonb@mail.rockefeller.edu.**

The Rockefeller University is an Affirmative Action/Equal Opportunity/VEVRAA Employer and solicits applications from women and underrepresented minorities.

POSITIONS OPEN

FACULTY POSITION IN IMMUNOLOGY
Massachusetts General Hospital
Harvard Medical School

The Center for Immunology and Inflammatory Diseases and the Division of Rheumatology, Allergy, and Immunology at the Massachusetts General Hospital (MGH) is seeking an outstanding scientist to develop a rigorous independent research program in immunology. Applicants whose programs address any area of basic experimental immunology or translational human immunology are encouraged to apply. Areas of particular interest include autoimmunity, B cell biology, tolerance, and immune mechanisms of rheumatologic diseases. Laboratory space is within the MGH Center for Immunology and Inflammatory Diseases, a diverse interactive research center interested in basic mechanisms of immune-mediated diseases. Applicants may have an M.D., Ph.D., or M.D.-Ph.D. degrees. Academic appointment at the **ASSISTANT** or **ASSOCIATE PROFESSOR** level will be at Harvard Medical School and a generous startup package will be provided. Applicants should submit curriculum vitae, research plan, and the names of three references to **Dr. Andrew Luster** c/o **e-mail: ciidsearch@mgh.harvard.edu.**

Women and minority applicants are particularly encouraged to apply.

ASSISTANT PROFESSOR
Biology
Georgetown University

The Department of Biology, Georgetown University, invites applications for a tenure-track position at the assistant professor level commencing in January 2012. We seek applicants whose research efforts are in an area of global health, with a focus on infectious disease. This work is expected to complement ongoing research and teaching efforts in global health at Georgetown University, including a new Center for Global Health, a Center for Infectious Disease, a graduate program in Global Infectious Disease, and an undergraduate major in the Biology of Global Health. The successful candidate will be expected to teach one course per semester, mentor undergraduates, graduate students, and postdoctoral fellows, and maintain an active, extramurally funded research program. Department information can be found at **website: http://biology.georgetown.edu/.** Candidates should submit a letter of application, curriculum vitae, a detailed description of previous research accomplishments and future research plans, a statement of teaching philosophy, and the names and contact information for three or more references. Application materials should be submitted electronically in PDF format (preferred) to **e-mail: biology@georgetown.edu** with "BGH Application" as subject. Application materials must be received by January 14, 2011. *Georgetown University is an Affirmative Action/Equal Opportunity Employer.*

UNIVERSITY OF COLORADO—website: http://mse.colorado.edu. The interdisciplinary Materials Science and Engineering program at the University of Colorado seeks to hire exceptional candidates as **ASSISTANT PROFESSORS,** with higher levels also considered. This program offers tenure-track appointments in science and engineering departments across the campus to candidates with interests in materials research. Candidates with interests in all materials research areas will be considered. Applicants should go to **website: http://www.jobsatcu.com** (**posting #811675**) for information on submitting their applications. Review of applications will begin in December 2010. *The University of Colorado is committed to diversity and equality in education and employment. The University of Colorado at Boulder conducts background checks for all final applicants.*

POSITIONS OPEN

XEUS

MICROBIOLOGIST

XEUS in Boston, Massachusetts seeks a Microbiologist. Position requires an exceptional understanding of microbial fermentation, along with a solid working knowledge of common organisms utilized in the biofuels area.

Applicant will team with Bio-Processing Engineers in the scaling and commercialization our cellulosic biofuels technology. The candidate preferably has a Ph.D. in Microbiology or the equivalent. The ideal candidate should have a minimum of five years of relevant industrial experience. Send curriculum vitae to **e-mail: microbiologist@xeus.info.**

FACULTY POSITIONS IN ZOOLOGY
Assistant Professor of Zoology

The Department of Zoology at the University of Hawaii (**website: http://www.hawaii.edu/zoology**) is hiring two tenure-track faculty at the rank of assistant professor in the fields of evolutionary biology and genetics. These new colleagues will join the department in a newly renovated research building during a major phase of growth aimed at building strength in evolutionary biology. We are particularly interested in individuals with expertise in phylogenetics or population/quantitative genetics. The study system is open to any biological kingdom. Of particular interest are colleagues whose research programs will capitalize on Hawaii's unique evolutionary legacy or position in the Pacific Rim, as well as individuals who can successfully collaborate across research fields. Teaching responsibilities will include an advanced undergraduate course in either evolution or genetics and a graduate course in the individual's specialty. Applicants must have a Ph.D., a strong publication record and potential for extramural funding. To apply, please send PDF formatted documents that include a curriculum vitae, statement of research interests and plans, teaching statement, two publications, and names and contact information (including e-mail address) of three professional references to **e-mail: zsearch@hawaii.edu.** For a complete job announcement, please refer to **website: http://workatuh.hawaii.edu.** Review of applications will begin on December 1 and continue until positions filled. *The University of Hawaii is an Equal Opportunity/Affirmative Action Institution and encourages applications from women and minority candidates.*

West Virginia University invites applications for a tenure-track position at the **ASSISTANT PROFESSOR** level in the Department of Biology beginning August 2011. We are especially interested in enhancing our strengths in the areas of chemical ecology, developmental biology, neurobiology, reproductive physiology/endocrinology, or molecular genetics, but outstanding candidates in any area of biochemistry are encouraged to apply. We seek an individual with a broad biology background and strong biochemistry skills to develop an externally funded, independent research program. The candidate may participate in existing programs in the Department of Biology and in institution-wide multidisciplinary research initiatives (**website: http://researchoffice.wvu.edu/centers/centers_listing**). Postdoctoral experience, excellent written and oral communication/teaching skills, and the potential to secure external funding are required. Preference will be given to candidates with a record of scholarly publications, and the expertise to teach biochemistry courses at the undergraduate and graduate levels. Qualified applicants should prepare research and teaching statements, curriculum vitae, and arrange for three letters of reference to be sent to **e-mail: wvubiology@mail.wvu.edu.** Review of applications will commence on December 6 and continue until the position is filled. For more information visit **website: http://www.as.wvu.edu/biology/faculty/positions.htm.** *West Virginia University is an Equal Opportunity/Affirmative Action Employer and does not discriminate on the basis of race, color, religion, sex, age, marital status, disability, veteran status, national origin, or sexual orientation.*

POSITIONS OPEN

TENURE-TRACK ASSISTANT PROFESSOR of Entomology-Apiculture—The Department of Entomology at Texas A&M University and the Texas AgriLIFE Research seek qualified applicants for this position with a 67 percent research and 33 percent teaching appointment. Applicants should possess a Ph.D. in Entomology or related field, and must have demonstrated knowledge of honeybees or other pollinators. The candidate should have insights or experiences in linking broad, new scientific discoveries with technologies and applications valuable to end-user groups. The incumbent will provide training for graduate students and classroom responsibilities will include an undergraduate course in Honeybee biology and participate in graduate education program. See details at **website: http://insects.tamu.edu** for a full description and instructions for submission of application materials. The closing date for applications is January 4, 2011. *Texas A&M University seeks individuals who are able to work with diverse students and colleagues, who have experience with a variety of teaching methods and curricular perspectives, and who will contribute to the diversity efforts of the University.*

YALE UNIVERSITY
Microbial Diversity Institute

Yale University, to further the development of its West Campus research enterprise, is seeking faculty at both junior and senior ranks to join its multidisciplinary Microbial Diversity Institute. Faculty associated with this Institute will have primary appointments in any of several life science and physical science departments within the Faculty of Arts and Sciences, the School of Engineering and Applied Science, the School of Forestry and Environmental Studies, or the School of Medicine. Candidates must have a Ph.D. or equivalent degree in a relevant discipline and a record of research that demonstrates originality in addressing significant questions in the broad area of microbial sciences. Relevant research areas include, among others, environmental microbiology; microbial interactions with other organisms; geomicrobiology; functional, comparative, or evolutionary genomics; and microbial genetics, physiology, or pathogenesis; and may focus on any group of microorganisms, including viruses, bacteria, archaea, or eukaryotes. To apply, please submit the following materials as PDF files to **e-mail: kelly.locke@yale.edu** under the subject heading "Microbial Diversity Faculty Search": a statement of research interests, complete curriculum vitae and up to five reprints of published work, and arrange for three letters of recommendation. Applications may also be addressed to: **Microbial Diversity Search Committee, c/o Howard Ochman, Director, Microbial Diversity Institute, Yale University West Campus, PO Box 27388, West Haven, CT 06516.** The review of applications will begin on December 15, 2010. *Yale University is an Affirmative Action/Equal Opportunity Employer. Yale values diversity among its faculty, students and staff, and strongly encourages applications from women and underrepresented minorities.*

POSTDOCTORAL POSITIONS are available to study molecular mechanisms of estrogen receptor (ER) action. One project is to study the role of transcriptional coactivators and corepressors in controlling ER function in breast cancer and a second project is in the area of molecular mechanisms regulating ER-dependent gene expression. Projects utilize molecular cellular biology and high throughput genomics approaches. For details of the laboratory's research, see **website: http://www.bcm.edu/mcb/index.cfm?pmid=7708.**

Required Qualifications: Recent Ph.D. with strong background in molecular biology and/or cell biology. Salary commensurate with experience. To apply send a letter of application including a short description of research experience and interests, a curriculum vitae, and names and contact information for three references to **Carolyn Smith, Ph.D.** (**e-mail: carolyns@bcm.edu**). *Baylor College of Medicine is an Equal Opportunity, Affirmative Action, and Equal Access Employer.*

POSITIONS OPEN

Southern Illinois University
School of Dental Medicine
TENURE-TRACK FACULTY POSITIONS
Section of Anatomy

The Section of Anatomy at Southern Illinois University School of Dental Medicine is seeking applicants for two full time (12-month) tenure-track faculty positions at the **ASSISTANT/ASSOCIATE PROFESSOR** level. Applicants must have a Ph.D., postdoctoral training, and prior teaching experience in one of the anatomical sciences below are desirable. Teaching duties are shared within the Section and include courses in Gross Anatomy, Neuroanatomy, Histology, and Oral Biology. Candidates are expected to direct one course, participate in additional teaching, and are expected to actively participate and collaborate in current ongoing dental research areas supported by the School. Academic rank and salary are commensurate with experience and qualifications. The school is located on a historic campus in Alton, 30 minutes from St. Louis. Review of applications will begin immediately. Applicants should submit a letter of application that describes teaching experience, topic preferences and research experience related to dental medicine, curriculum vitae, and three letters of reference to: **Dr. Ann Boyle, Dean, SIU-SDM, 2800 College Avenue, Alton, Illinois 62002-4900** or by **e-mail: aboyle@siue.edu.** *SIU-SDM is an Equal Employment Opportunity/Affirmative Action Employer. Women and minorities are encouraged to apply. SIUE is a state university—benefits under state sponsored plans will not be available to holders of F-1 or J-1 visas.*

TENURE-TRACK FACULTY POSITION
IMMUNOLOGY/VIROLOGY
Department of Biological Sciences
The University of Southern Mississippi

The Department of Biological Sciences at The University of Southern Mississippi (**website: http://www.usm.edu/biology/**) invites applications for a tenure-track **ASSISTANT PROFESSOR** position in immunology and/or virology. The successful candidate will join our rapidly growing and collaborative microbiology/molecular biology group. We are seeking outstanding candidates taking innovative, molecular, and cellular approaches to the study of immunology and/or virology. This area is broadly defined and would include the study of immunology, immunopathology, virology, or host-pathogen interactions. Applicants will be expected to establish an active, extramurally funded research program, mentor graduate students, and participate in undergraduate/graduate teaching in their area of expertise. Applicants must hold an earned Ph.D. in immunology, virology, microbiology, or related area and have relevant postdoctoral experience. A competitive salary commensurate with qualifications and experience, competitive startup package, laboratory space, and state-of-the-art facilities will be provided. The position will begin August 2011, and is contingent on available funding. Applications must be submitted online at **website: https://jobs.usm.edu.** Review of applications will begin February 1, 2011, and will continue until the position is filled. For inquiries about the position, contact **Dr. Mohamed Elasri, Search Committee Chair,** at **telephone: 601-266-6916** or **e-mail: mohamed.elasri@usm.edu.** *Affirmative Action/Equal Opportunity Act/ADAI.*

A POSDOCTORAL POSITION is available in the Department of Obstetrics, Gynecology and Reproductive Sciences, University of Pittsburgh School of Medicine to study the neurobiology of energy homeostasis with emphasis on leptin and insulin signaling in the hypothalamus using knockout mouse models. The qualified person with a recent Ph.D. or M.D.-Ph.D. degree should have experience with molecular and biochemical techniques and a strong interest in neuroendocrinology. Please send curriculum vitae and contact information of three references to **Dr. Abhiram Sahu** (**e-mail: asahu@pitt.edu**).

POSITIONS OPEN

SMITHSONIAN INSTITUTION
FELLOWSHIP PROGRAM

GRADUATE STUDENT, PREDOCTORAL, POSTDOCTORAL, and **SENIOR FELLOWSHIPS** in animal behavior, ecology, and environmental science; including an emphasis on the tropics; Earth sciences and paleobiology; Evolutionary and systematic biology; History of science and technology. Tenable in residence at the Smithsonian facilities. Stipends and tenure vary. Awards are contingent upon the availability of funds.

Deadline: January 15 annually. Contact: **Office of Fellowships, Smithsonian Institution, Desk S, P.O. Box 37012, L'Enfant 7102 MRC 902, Washington, D.C. 20013-7012, telephone: 202-633-7070, e-mail: siofg@si.edu, website: http://www.si.edu/research+study.** *An Equal Opportunity Employer.*

FULL-TIME FACULTY POSITION
University of Maryland School of Medicine
Department of Pathology

The Department of Pathology, University of Maryland School of Medicine invites applicants with a M.D. or Ph.D. degree to apply for a full-time faculty position focused on independent translational research in the area of molecular biology. The applicant should have evidence of scholarly achievement, to include a history of funded research and current research funding and have experience in developing and translating their discoveries into novel clinical applications. The applicant will be expected to be active in the School of Medicine's teaching programs. Academic appointment and salary will be commensurate with experience.

The University of Maryland School of Medicine is the first public and fifth oldest medical school in the United States. On the University of Maryland Baltimore campus, the School of Medicine serves as the foundation for a large academic health center that combines medical education, biomedical research, patient care, and community service. The School of Medicine ranks in the top tier of U.S. medical schools and in fiscal year 2010 external research funding exceeded $479 million.

Please forward curriculum vitae, a brief statement of research interests, funding, teaching experience, and the names of three references to:

Sanford A. Stass, M.D.
Professor and Chair
C/o Pati Butler (e-mail: pabutler@som.umaryland.edu)
Department of Pathology
University of Maryland School of Medicine
10 S. Pine Street, Room 700A, MSTF
Baltimore, MD 21201

The University of Maryland is an Affirmative Action/Equal Employment Opportunity/ADA Equal Opportunity Employer. Minorities and women are encouraged to apply.

MICROBIOLOGIST—Applications are invited for a tenure-track **ASSISTANT PROFESSOR** position to begin August 2011. Teaching responsibilities will include undergraduate courses in microbiology, general biology, and an upper division/graduate class in area of expertise. Establishment of a funded research program involving M.S. graduate students and undergraduates is expected. Area of research in any branch of microbiology will be considered. Postdoctoral experience expected. Applicants should submit a letter of application, curriculum vitae, selected recent reprints, statements of research and teaching interests and have three letters of recommendation sent by January 10, 2011 to: **Dr. Frank Paladino, Search Committee Chair, Department of Biology, Indiana-Purdue University Fort Wayne, 2101 E. Coliseum Boulevard, Fort Wayne, IN 46805-1499** or electronically to **e-mail: paladino@ipfw.edu. Website: http://www.ipfw.edu/bio/.** Employment is contingent on a satisfactory background records history check. *IPFW is an Affirmative Action/Equal Access Employer fully committed to a diverse workforce.*

SCHOOL OF MEDICINE & DENTISTRY
UNIVERSITY of ROCHESTER MEDICAL CENTER

Faculty Position in Environmental Health Sciences

Applications are invited for a tenure-track faculty position at the Assistant or Associate Professor level in the Department of Environmental Medicine at the University of Rochester. We are especially interested in applicants that apply cutting-edge approaches to fundamental questions in neurotoxicology and/or epigenetics that examine the relationship between environmental chemical exposures and human diseases and disorders, with a particular emphasis on fetal/neonatal exposures, but other areas of environmental health sciences will also be considered. We seek an outstanding individual with a strong commitment to excellence in research, scholarship and teaching.

The successful candidate will be part of a highly interactive environment with faculty research interests and programs spanning neurotoxicology, cardiopulmonary and developmental toxicology, osteotoxicology, immunotoxicology and the molecular biology of xenobiotic receptors and transporters. These programs include both animal models and human research. The Department of Environmental Medicine, site of the successful applicant's primary appointment, has been a long-standing home to an NIEHS Environmental Health Sciences Center of Excellence and an NIEHS Toxicology Graduate Training Program (**http://www2.envmed.rochester.edu/envmed/index.html**). In addition, the University of Rochester recently was ranked as one of the top 15 Best Places to Work in Academia of 2010 (The Scientist, July 2010).

Competitive salary, startup packages and access to the many Facility Cores of the NIEHS Center and the Medical Center are provided. The University of Rochester Medical Center is undergoing a major expansion of its research facilities and infrastructure, with an emphasis on the areas of neuromedicine, cancer, cardiovascular disease, immunology and infectious disease and musculoskeletal disease.

Applicants should send a CV, a statement of research interests including future plans, and the names of 3-5 references to: **Dr. Deborah A. Cory-Slechta, Search Committee Co-Chair, Box EHSC, Department of Environmental Medicine, University of Rochester School of Medicine, Rochester, NY 14642 (deborah_cory-slechta@urmc.rochester.edu)**.

The University of Rochester is an Equal Opportunity Employer.

AWARDS

McGill

The Louis and Artur Lucian Award For Research in Circulatory Diseases

Each year a Committee from the McGill University Faculty of Medicine confers the Louis and Artur Lucian Award ($60,000 CDN) for outstanding research in the field of circulatory diseases. The purpose of this Award is to honour a scientific investigator or group of investigators whose current contribution to knowledge in this field is deemed worthy of special recognition. The successful recipient is invited to spend a period of time at McGill University to give a formal Lucian Lecture and to have interchanges with members of the McGill community. Submissions should be received on or before **March 25, 2011**.

For further information and to download the nomination form, please check the following website, **http://www.mcgill.ca/lucianaward** or contact:

Dr. Jacques Genest, Chair
The Louis and Artur Lucian Award Committee
Royal Victoria Hospital
McGill University Health Centre
Cardiovascular Research Laboratories, H7.14
687 Pine Avenue West
Montreal, Quebec, CANADA H3A 1A1
Tel: (514) 934-1934, Ext. 34630
FAX: (514) 843-2843

utmb Health

Working together to work wonders.

Faculty Positions in Vaccine Development for Cancer, Addiction and Neurodegenerative Diseases

Chronic diseases are an increasing major public health issue of the 21st century. In response, the University of Texas Medical Branch at Galveston (UTMB Health) has established the "Vaccines for Chronic Diseases" initiative to encompass research at all stages of vaccine development, from basic science/discovery through clinical studies. We seek highly motivated researchers with an established record of extramural funding, or the potential to establish a robust research program, as well as a willingness to work in a highly collaborative and interdisciplinary environment. Currently, areas of particular interest are: **addiction, cancer, and neurodegenerative diseases**. We are recruiting individuals holding MD, PhD, and/or DVM degrees at the Assistant, Associate or Full Professor level, including tenure-track positions for suitably qualified individuals.

UTMB Health provides a rich environment for research, with a number of highly interactive centers of excellence and biomedical institutes. The "Vaccines for Chronic Diseases" initiative is led by the Sealy Center for Vaccine Development (www.utmb.edu/scvd) in conjunction with the UTMB Cancer Center (www.utmb.edu/cancer), the Center for Addiction Research (http://www.utmb.edu/addiction), and the Mitchell Center for Neurodegenerative Diseases (http://www.utmb.edu/neuro/MitchellCenter.htm). Additional UTMB centers of excellence involved in this initiative include:

- Center for Interdisciplinary Research in Women's Health (http://www.utmb.edu/cirwh)
- Clinical Proteomics Center (https://bioinfo.utmb.edu/CPC)
- Institute for Human Infections and Immunity (http://www.utmb.edu/ihii)
- Institute for Translational Science (http://www.its.utmb.edu)
- Sealy Center on Aging (http://www.utmb.edu/scoa/index.html)
- Sealy Center for Molecular Medicine (http://scmm.utmb.edu)
- Sealy Center for Structural Biology and Molecular Biophysics (http://www.scsb.utmb.edu)
- Stark Diabetes Center (http://www.stark-diabetes.org)

Each of these centers/institutes has interests in vaccine development. With this wealth of expertise and our state-of-the-art core facilities, UTMB offers outstanding opportunities for collaboration and multidisciplinary research.

UTMB is home to the oldest medical school in Texas. The city of Galveston is a popular tourist and cruise ship destination that includes beaches, museums, historical architecture, a vibrant arts scene, and excellent restaurants; all located only 45 minutes away from Houston, the nation's fourth largest city.

Interested candidates should send a C.V., outline of research interests and names of four references electronically to **behawkin@utmb.edu**, or by mail to: **Vaccines for Chronic Diseases Search Committee C/O Dr. Bridget Hawkins, UTMB SCVD, 301 University Blvd, Galveston, TX, 77555-0436. For additional information, contact Dr. Alan Barrett, (abarrett@utmb.edu; phone 409-772-6662)**.

UTMB Health is an Equal Opportunity, Affirmative Action Institution, which proudly values diversity. Candidates of all backgrounds, including persons with disabilities, are encouraged to apply.

POSITIONS OPEN

TENURE-TRACK FACULTY POSITION in Molecular Biology

The Department of Molecular Biology at the University of Wyoming seeks an outstanding scientist to fill a tenure-track faculty position in molecular/cellular biology at the **ASSISTANT PROFESSOR** level. The successful candidate will establish an extramurally funded research program, participate in undergraduate teaching in the core molecular biology curriculum, and contribute to Departmental (Molecular Biology) and Interdepartmental (Molecular and Cellular Life Sciences) graduate education programs (see links at **website: http://uwacadweb.uwyo.edu/UWmolecbio/**). Salary and startup package will be competitive. Candidates must have a Ph.D. degree or equivalent, postdoctoral research experience, and clear evidence of research productivity. Applications must be sent electronically to **e-mail: molecularbiology@uwyo.edu** as a single PDF file labeled with your last name and first initial that includes a cover letter, curriculum vitae, description of research interests, and description of teaching interests and philosophy. In addition, please have three letters of recommendation sent electronically to **e-mail: molecularbiology@uwyo.edu** or by regular mail to: **Search Committee Chair, Department of Molecular Biology, University of Wyoming, 1000 E. University Avenue, Department 3944, Laramie, WY 82071.** The Department of Molecular Biology includes 17 faculty with diverse research interests and significant extramural support. The University of Wyoming enrolls approximately 13,500 students, including about 2,900 graduate students. Laramie is located in the Rocky Mountain region of southeastern Wyoming, about 120 miles from Denver. In addition to opportunities for academic excellence, the University of Wyoming and Laramie offer a college-town environment, extraordinary outdoor recreational opportunities, and daily conveniences that contribute to our quality of life. Screening of applications will begin on December 20, 2010, and continue until a suitable candidate is identified.

The University of Wyoming is committed to diversity and endorses principles of affirmative action. We acknowledge that diversity enriches and sustains our scholarship and promotes equal access to our educational mission. We seek and welcome applications from individuals of all backgrounds, experiences, and perspectives. The University of Wyoming is dedicated to ensuring a safe and secure environment for our faculty, staff, students, and visitors. To achieve that goal, we will conduct a background investigation on the successful candidate.

ASSISTANT OR ASSOCIATE PROFESSOR Arthritis Center/Rheumatology

The Arthritis Center at the Boston University School of Medicine invites applications for a position at the rank of Assistant or Associate Professor in the areas of immunology relevant to autoimmune disorders. Outstanding candidates working in all areas of immunology are invited to apply. We particularly encourage applications from candidates working in the field of innate immunity and lymphocyte function. Preference will be given to applicants with research interest and experience in areas that complement and enhance the existing programs (**website: http://www.bumc.bu.edu/rheumatology/**).

Successful candidates for this position are expected to develop and maintain a competitively funded research program. The minimum requirements for an Assistant Professor position include a M.D., Ph.D., or M.D.-Ph.D. with at least three years postdoctoral experience. Appointment at the Associate Professor level requires a minimum of five years experience at the Assistant Professor level or equivalent, and a nationally recognized and federally funded research program.

Arthritis Center offers competitive startup package, excellent core facilities, and collegial atmosphere. Interested candidates should electronically submit curriculum vitae, a brief summary of research interest and plans, and the contact information for three references to: **Maria Trojanowska, Ph.D.** (**e-mail: trojanme@bu.edu**), **Director, Arthritis Center, 72 East Concord Street, E-5, Boston, MA 02118.**

Boston University is an Equal Opportunity Employer and actively seeks applications from women and underrepresented groups.

POSITIONS OPEN

FACULTY POSITION

Brown University School of Engineering seeks applicants in the field of Biomedical Engineering. Positions are open at all levels. See full listing at **website: http://www.engin.brown.edu.**

Anubhav Tripathi - Search Committee Chair
School of Engineering
184 Hope Street
Providence, RI 02912
E-mail: anubhav_tripathi@brown.edu

Brown University is an Equal Opportunity/Affirmative Action Educator and Employer.

TENURE-TRACK FACULTY POSITION in Bioinformatics, Genomics, and Computational Biology

The Department of Biochemistry and Molecular Biology at The George Washington University Medical Center invites applications for a tenure-track **ASSISTANT/ASSOCIATE PROFESSOR.**

Basic qualifications: Applicants must have a strong biology background and demonstrated excellence in comparative proteomics and genomics, sequence-structure analysis, and function prediction as evidenced by publications, prior teaching experience, and related funding. Applicants must hold a Ph.D. degree in an appropriate discipline, and a demonstrated interest in fostering collaboration and commitment to teaching while having a research program in Bioinformatics in the interface of Genomics and Proteomics. Experience teaching graduate level bioinformatics and workshops is also required.

Preferred qualifications: Preference will be given to candidates with experience in the development of bioinformatics resources, collaborative interaction with other bioinformatics and molecular biology databases, and the potential to build an extramural funded research program or bring a funded research program. Excellent communication skills are also desirable.

Application process: The GW University will provide a competitive startup package to successful candidates. Interested applicants must send a complete curriculum vitae, a statement of current and future research interests (limited to three pages), and the names and addresses of three references to: **Rakesh Kumar, Ph.D., Professor and Chair, Department of Biochemistry and Molecular Biology, Faculty Search, The George Washington University Medical Center, Suite 530, 2300 Eye St. NW, Washington, DC 20037;** or electronically to **e-mail: bcmkdc@gwumc.edu.** Review of applications by the Search Committee will begin on February 1, 2011, and will continue until the position has been filled. Only complete applications will be considered.

The George Washington University is an Affirmative Action/Equal Opportunity Employer.

POSTDOCTORAL ASSOCIATE

The Lillehei Heart Institute is a premier institute at the University of Minnesota in Minneapolis with state-of-the-art technologies and core facilities focused on the molecular regulation of myogenesis, stem cell, and regenerative biology. We are accepting applications for highly motivated postdoctoral associates to work on NIH-funded research pertaining to the role of transcription factor mediated networks to direct the fate of stem and iPS cells to a mesodermal fate (i.e. cardiac, endothelial, skeletal muscle). Ph.D. and expertise with molecular biological-biochemistry techniques as well as the use of transgenesis and knockout technologies will be required for this position. Interested applicants should apply online to: **Daniel J. Garry, M.D.-Ph.D., Director of Lillehei Heart Institute, University of Minnesota** at **website: http://employment.umn.edu** (**reference job search #166342**) and include curriculum vitae, statement of interest, and names of three references. *Candidates must be able to demonstrate authorization to work in the United States at the University of Minnesota by the start date. The University Of Minnesota is an Affirmative Action/Equal Opportunity Employer.*

POSITIONS OPEN

NASA AMES RESEARCH CENTER Synthetic Biology Innovation Laboratory

NASA Ames Research Center has an established track record in biotechnology and fundamental biology research, with applications in astrobiology, radiation biology, biosensors, biofuels, bionanotechnology, human health, and bioregenerative life support. Ames is seeking to infuse synthetic biology into these and other applications.

Two positions are available for **RESEARCH FELLOWS** in the newly established Synthetic Biology Innovation Laboratory, a cross-disciplinary research group formed to create new technologies that meet NASA needs. Fellows will be expected to develop research projects in collaboration with NASA scientists, engineers, and outside experts with the intention of demonstrating, publishing, and/or patenting relevant new technologies and applying them to NASA missions. Research will create both enabling technologies for space exploration and foundational tools to make biological systems easier to engineer. Projects taking advantage of flight opportunities on the International Space Station and aboard small satellites are encouraged. Fellows may also participate in mentoring a student team to take part in the International Genetically Engineered Machine Competition (iGEM).

Applicants should have a Ph.D., substantial experience in molecular biology, and a strong drive to bring synthetic biology concepts to space exploration. Applications will include one-page outlines of two potential NASA relevant research projects, one high risk and one low risk. Technology areas include, but are not limited to: biomaterials, biosensors, long term habitation, closed loop life support, food and fuel production, high value chemicals, biological in situ resource utilization (ISRU), and biomining as well as air, water, and waste processing.

Appointments will be for two years with the potential for two one-year extensions. Stipend will be competitive and commensurate with experience. Please apply online at **website: http://syntheticbiology.arc.nasa.gov/** follow the link for research fellows. Applications must be received by January 21, 2011.

FACULTY POITIONS

MOLECULAR BIOLOGIST, three-year visiting position, to teach introductory biology, introductory cellular and molecular biology, and upper level courses in cellular and molecular biology. Will also direct undergraduate research in the College's required Independent Study Program. Applicants should have a Ph.D.; postdoctoral research and/or teaching experience preferred. Send curriculum vitae, statements of research and teaching philosophy, transcripts, and three letters of recommendation to: **Dr. M. D. Loveless, Chair of Biology, The College of Wooster, Wooster, OH** (**e-mail: mloveless@wooster.edu**). Electronic applications are preferred, and should be received by February 4, 2011, for full consideration.

ECOLOGIST/CONSERVATION BIOLOGIST, ECOLOGIST and **CONSERVATION BIOLOGIST**, one-year position, to teach introductory biology and upper level courses in general ecology and conservation biology, and to direct undergraduate research in the College's required Independent Study Program. Applicants should have a Ph.D.; postdoctoral research and/or teaching experience preferred. Send curriculum vitae, statements of research and teaching philosophy, transcripts, and three letters of recommendation to: **Dr. M. D. Loveless, Chair of Biology, The College of Wooster, Wooster, OH** (**e-mail: mloveless@wooster.edu**). Electronic applications are preferred, and should be received by March 25, 2011, for full consideration.

Wooster seeks to ensure diversity by its policy of employing persons without regard to age, sex, color, race, creed, religion, national origin, disability, veteran status, sexual orientation, or political affiliation. The College of Wooster is an Equal Opportunity/Affirmative Action Employer.

AAAS is here – helping scientists achieve career success.

Every month, over 400,000 students and scientists visit ScienceCareers.org in search of the information, advice, and opportunities they need to take the next step in their careers.

A complete career resource, free to the public, *Science* Careers offers a suite of tools and services developed specifically for scientists. With hundreds of career development articles, a grants and scholarships database, webinars and downloadable booklets filled with practical advice, a community forum providing real-time answers to career questions, and thousands of job listings in academia, government, and industry, *Science* Careers has helped countless individuals prepare themselves for successful careers.

As a AAAS member, your dues help AAAS make this service freely available to the scientific community. If you're not a member, join us. Together we can make a difference.

To learn more, visit **aaas.org/plusyou/sciencecareers**

AAAS + U = Δ

POSITIONS OPEN

AQUATIC ECOLOGIST

Loyola University Chicago (LUC), College of Arts and Sciences, Department of Biology, invites applications for a full-time, tenure-track position in Aquatic Ecology at the rank of **ASSISTANT PROFESSOR,** beginning August, 2011. We are a large department that serves more than 1500 undergraduate majors and 25 M.S. students. We have modern laboratory facilities and a 2100 square-foot artificial stream facility. For an overview of the department visit **website: http://www.luc.edu/biology/.** Candidates must have a Ph.D. and postdoctoral experience, and will be expected to establish a vigorous, externally funded research program involving undergraduates and M.S. students. Preference will be given to candidates working in freshwater ecology with research expertise complementing existing research strengths in the department. Teaching responsibilities shall include general biology, general ecology, and an advanced course in the candidate's area of specialization. Candidates for the position must clearly demonstrate the potential for excellence in research and teaching and have a record of (or clear potential for) distinguished scholarship, grant-funded research, and student mentorship. Candidates should complete the online application in full at **website: http://www.careers.luc.edu** with cover letter, curriculum vitae, research plan, teaching philosophy statement, and names and contact information for three references. Review of applications will begin on December 10, 2010, and continue until the position is filled. Written inquiries about the position can be sent to: **Aquatic Ecologist Search Committee, Loyola University Chicago, Department of Biology, 1032 West Sheridan Road, Chicago, IL 60660.** *Loyola University Chicago is an Equal Opportunity/Affirmative Action Employer with a strong commitment to diversifying its faculty. Applications from women and minority candidates are especially encouraged.* For information about LUC, visit **website: http://www.luc.edu.**

FACULTY POSITION in MICROBIAL BIOLOGY
Department of Biology, University of Utah

The Department of Biology at the University of Utah invites applications for a tenure-track faculty position in Microbial Biology. We encourage applicants who are investigating any area of microbial biology, including eukaryotic microbes and microbial interactions with higher organisms. For an overview of the department, please visit **website: http://www.biology.utah.edu/.** Applicants should submit in PDF format curriculum vitae, up to five representative publications, descriptions of current and future research interests (up to two pages each), statement of teaching interests, and the names of three references to **e-mail: microsearch@biology.utah.edu.** Please also arrange for three letters of reference to be sent directly to: **The Microbial Biology Search Committee, Department of Biology, University of Utah, 257 South 1400 East, Rm. 201, Salt Lake City, UT 84112-0840, USA.** Review of applications will begin on January 15, 2011, and continue until the position is filled. *The University of Utah values candidates who have experience working in settings with students from diverse backgrounds, and possess a strong commitment to improving access to higher education for historically underrepresented students. The University of Utah is fully committed to affirmative action and to its policies of nondiscrimination and equal opportunity in all programs, activities, and employment. Employment decisions are made without regard to race, color, national origin, sex, age, status as a person with a disability, religion, sexual orientation, gender identity or expression, and status as a protected veteran. The University seeks to provide equal access for people with disabilities. Reasonable prior notice is needed to arrange accommodations. Evidence of practices not consistent with these policies should be reported to:* ***Director, Office of Equal Opportunity and Affirmative Action, telephone: 801-581-8365 (V/TDD).***

POSITIONS OPEN

POSTDOCTORAL FELLOW POSITIONS

Several NIH-supported postdoctoral positions are available in the laboratories of **Drs. David Busija** and **Prasad Katakam** in the Department of Pharmacology at Tulane University Medical School in New Orleans, Louisiana United States to study cerebral and coronary vascular control mechanisms starting January 1, 2011. Research focuses on (1) mitochondrial influences on arteries; (2) effects of disease processes such as insulin resistance or ischemic stress on the vasculature; and (3) therapeutic approaches to protect or restore vascular responsiveness during insulin resistance or ischemia. The research will involve a variety of approaches including videomicroscopic dimensional analysis of pressurized arterioles, confocal microscopy imaging calcium, reactive oxygen species and membrane potential, immunofluorescence, western blotting, and RT-PCR. Applicants should have a Ph.D. or M.D. and a background in cardiovascular sciences. Preference will be given to individuals with experience handling isolated arteries, confocal microscopy, and/or in vivo myocardial ischemia-reperfusion technique. Successful applicants will join an active research program in vascular biology supported in part by an NHLBI-funded grants. Stipend levels are in accordance with NIH guidelines; however, applications are not restricted to U.S. citizens.

Applicants should send curriculum vitae, description of their research experience/interests, and the names and contact information of two to three references to:

Dr. David Busija
Professor and Chairman
Department of Pharmacology
Tulane University Medical School
In care of: Debbie Sanders, Office Manager,
E-mail: dsanders@tulane.edu

Tulane University is an Affirmative Action and Equal Opportunity Employer. We invite Women and Minorities to apply.

VERTEBRATE WILDLIFE ECOLOGIST
University of North Dakota

The Department of Biology at the University of North Dakota invites applications for a tenure-track **ASSISTANT** or **ASSOCIATE PROFESSOR** of Vertebrate Wildlife Ecology. The Department offers graduate degrees through the Ph.D. and the campus environment is conducive for building a competitive research program including University owned field stations in the region. The position is integral to the Department's undergraduate degree in fisheries and wildlife biology and will also strengthen the Department's program in ecology, evolution, and conservation biology. We will consider vertebrate wildlife ecologists with a broad range of interests, but especially those able to work with state and federal agencies and whose research will benefit from our location in the prairie pothole region of the northern Great Plains. The successful candidate will establish a productive, extramurally funded research program and actively train M.S. and Ph.D. students. Teaching expectations will not exceed two courses per year for the first several years. Courses taught will include wildlife management and other upper level courses depending on the candidate's area of expertise. Position will begin 16 August 2011, and a Ph.D. is required, with postdoctoral experience desired. Review of applicants will begin 15 December 2010 and continue until the position is filled. Send curriculum vitae, three representative reprints, statements of teaching philosophy and research interest, and names with contact information for three references to: **Dr. Brett Goodwin, Department of Biology, 10 Cornell Street, Stop 9019, University of North Dakota, Grand Forks, ND 58202-9019.** For more information visit **website: http://www.und.edu/dept/biology/jobs.htm.** *The University of North Dakota is an Equal Opportunity/Affirmative Action Employer and we strongly encourage applications from women and underrepresented groups.*

POSITIONS OPEN

POSTDOCTORAL RESEARCH ASSOCIATE

Immediate openings are available for several **POSTDOCTORAL ASSOCIATE, RESEARCH ASSOCIATE,** and **SENIOR RESEARCH ASSOCIATE** positions to work on Genetics/Aging projects in the laboratory of **Dr. Eugenia Wang,** an internationally known specialist in how genetics affects aging. A strong background in Biochemistry and Molecular Biology with experience in genomic biology, methylation, and molecular cloning are desired as evidenced by research publications. Work is carried out using both cell culture and mouse models. The ideal candidate will be highly motivated, ambitious, and enthusiastic about working in a fully equipped, modern laboratory with research scientists at all levels of training. The successful candidate will have a strong verbal and written background in English. Salary is commensurate with experience.

The University of Louisville is a state supported research university established in 1798 and located in Kentucky's largest metropolitan area. The University has three campuses and is accredited by the commission on Colleges of the Southern Association of Colleges and Schools to award Associate's, Bachelor's, Master's, specialist, Doctoral, and first-professional degrees. It has a student body of approximately 20,000, faculty and staff of approximately 5,900, and an operating budget of $680.3 million.

Interested candidates should submit curriculum vitae and the names of three references to:

Dr. Eugenia Wang in care of Cathi Lyninger,
Unit Business Manager
Gheens Center on Aging
University of Louisville School of Medicine;
e-mail: cathi.lyninger@louisville.edu.

The University of Louisville is an Equal Opportunities Employer.

RESEARCH SCIENTIST

The R&D Department of ChemGen Corp., in Gaithersburg, Maryland is recruiting a research scientist to work on the development of microbial strains for the production of industrial enzymes. The projects use the application of mutagenesis and high throughput screening to guide the directed evolution of certain improved enzyme properties. Also involved is the construction of Gram-positive bacterial host strains with high-level gene expression and protein secretion. The work requires a Ph.D. or equivalent, and ideally expertise in molecular biology, enzymology, microbiology, and microbial genetics. Candidates should have a strong record of achievement and innovation, and interest to participate in collaborative work. ChemGen is a growing biotechnology company with worldwide sales focused on the development of novel products for animal feed applications. We provide a comprehensive benefits package that includes health, dental, life, FSAs, and 401k. Please send your resume to **e-mail: hr@chemgen.com** or to **fax: 301-948-5866.** *ChemGen Corp. is an Equal Opportunity Employer.*

MARKETPLACE